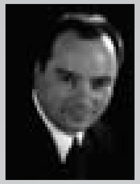

Professor Dr. rer. nat. Thorsten M. Buzug

Director of the Institute of Medical Engineering, University of Luebeck

Buzug was born in Lübeck, Germany in 1963. He received his PhD in 1993 in Applied Physics from the University of Kiel. After a postdoctoral position at the German Federal Armed Forces Underwater Acoustics and Marine Geophysics Research Institute where he worked on signal processing for SONAR systems he joined the Philips Research Laboratories Hamburg in the end of 1994. As leader of the Philips research cluster Medical Image Processing he was responsible for several projects in that field. In 1998 Buzug has been appointed as Professor of Physics and Medical Engineering at RheinAhrCampus Remagen. In 2006 he has been appointed as director of the Institute of Medical Engineering at the University of Lübeck.

Professor Dr. rer. nat. Jens Bongartz

Bongartz studied Physics at the Heinrich-Heine-University of Duesseldorf and „Medical Physics and Engineering“ at the University of Kaiserslautern. In 2002 he received his doctoral degree from the University of Duesseldorf with a thesis about holographic facial measurement. He worked for the Institute of Laser Medicine at the University of Duesseldorf and the *center for advanced european studies and research (caesar)* in Bonn as a rearch fellow. Since beginning of 2004 he is Professor for Medical Engineering at the RheinAhrCampus in Remagen,

Various approaches for face reconstruction on a skeletonized skull of an unknown individual have been presented since the 19th century. Recently, tremendous advances in information technology lead to significant further developments and refinements of the reconstruction methods. In combination with modern imaging technology, 3D simulation methods have been applied that create facial expressions. An international conference series on reconstruction of soft facial parts (RSFP) has been initiated to inform police officers and international scientists about this complex scientific branch and to simultaneously encourage future international cooperative networks of the involved disciplines. This book includes contributions of the multi-faceted status quo of scientific developments in reconstruction of soft facial parts.

www.luchterhand-fachverlag.de
www.wolterskluwer.de

Facial Reconstruction Gesichtsrekonstruktion

Buzug/Sigl/Bongartz/ Prüfer (Eds.)

Bundeskriminalamt

T. M. Buzug
K.-M. Sigl
J. Bongartz
K. Prüfer (Eds.)

Facial Reconstruction

Gesichts-rekonstruktion

Luchterhand

Facial Reconstruction
Gesichtsrekonstruktion

Polizei + Forschung
Bd. 35
herausgegeben vom
Bundeskriminalamt (BKA)
Kriminalistisches Institut

Bundeskriminalamt

Thorsten M. Buzug
Karl-Michael Sigl
Jens Bongartz
Klaus Prüfer (Eds.)

Facial Reconstruction

Forensic, Medical and Archeological Methods of the Reconstruction of Soft Facial Parts

Gesichtsrekonstruktion

Forensische, medizinische und archäologische Methoden der Gesichtsweichteilrekonstruktion

BKA

Luchterhand

Bibliografische Information Der Deutschen Bibliothek
Die Deutsche Bibliothek verzeichnet diese Publikation in der Deutschen Nationalbibliografie; detaillierte bibliografische Daten sind im Internet über http://dnb.ddb.de abrufbar.

Alle Publikationen der BKA-Reihe *Polizei + Forschung* (ausgenommen VS-NfD-eingestufte Bände) sind im Internet im PDF-Format unter www.bka.de (Kriminalwissenschaften/Kriminalistisches Institut) eingestellt.

Die Beiträge wurden von den Autoren im Nachgang zur 2. Internationalen Konferenz zur Gesichtsweichteil-Rekonstruktion am 17./18.03.2005 in Remagen zugeliefert. Die Aufsätze sind entweder in englisch, deutsch und/oder englisch/deutsch veröffentlicht. Für Text und Inhalt ist der jeweilige Autor verantwortlich.

Redaktion:

Heinrich Schielke

Bundeskriminalamt
Kriminalistisches Institut

Umschlaggestaltung: arttec grafik simon & wagner, St. Goar
Satz: Satzoffizin Hümmer, Waldbüttelbrunn
Druck: Drukkerij Wilco, Amersfoort

∞ Gedruckt auf säurefreiem, alterungsbeständigem und chlorfreiem Papier

Grußwort und Dank

Auf Initiative des Bundeskriminalamtes und in Kooperation mit dem Landeskriminalamt Brandenburg, dem Niederländischen Forensischen Institut, dem Kriminalistischen Institut in Prag und mit finanzieller Unterstützung des AGIS-Programms der Europäischen Union – Generaldirektion Justiz und Innere fand im November 2003 die 1. internationale Konferenz zur Gesichtsweichteil-Rekonstruktion für Polizeibeamte, Wissenschaftler und Techniker in Potsdam/D statt.

Ausschlaggebend für die Aktivitäten des Bundeskriminalamtes war das vermehrte Aufkommen von Anfragen durch die Polizeien der Bundesländer zur Gesichtsweichteil-Rekonstruktion. Um sowohl national als auch international einen Überblick über wissenschaftliche Erkenntnisse und anerkannte Experten zu erhalten, wurde eine Fragebogenaktion im europäischen Raum durchgeführt. Die Auswertung ließ einen großen Bedarf an einem Informationsaustausch über Forschungsergebnisse erkennen. Damit war der Grundstein für eine internationale Konferenz zur Gesichtsweichteil-Rekonstruktion gelegt.

Die 1. Konferenz erwies sich als Erfolg. Die gesetzten Ziele „Initiativfunktion im Bereich eines technisch geprägten, bisher nicht ausschließlich von der Polizei fokussierten Themas", „Förderung der internationalen Zusammenarbeit" und „Schaffung eines Forums für Wissenschaftler, Techniker und Polizeibeamte" wurden übertroffen. Dazu trugen nicht nur 17 internationale Experten von Universitäten, Instituten und Polizeien mit ihren Präsentationen zur Gesichtsweichteil-Rekonstruktion, sondern auch die Diskussionen im großen Teilnehmerkreis von ca. 70 wissenschaftlichen Kollegen und Polizeibeamten bei.

Der hohe Stellenwert dieses speziellen Wissenschaftszweiges und dessen Relevanz für die kriminalistische Praxis wurden erkannt, der weitergehende intensive Erfahrungsaustausch für notwendig empfunden.

Spontan wurde noch während der 1. Konferenz durch die anwesenden Vertreter des RheinAhrCampus Remagen, der Heinrich Heine Universität in Düsseldorf und der Stiftung ceasar (Center of Advanced European Studies and Research) in Bonn an die Organisatoren der Wunsch herangetragen, den wissenschaftlichen Informationsaustausch auf dem Gebiet der Gesichtsweichteil-Rekonstruktion zu vertiefen.

Damit war der Startschuss für eine zeitnahe Folgeveranstaltung gefallen. Noch in Potsdam wurden die Rahmenbedingungen für diese abgesteckt.

So organisierte das Bundeskriminalamt zum zweiten Mal, diesmal in Zusammenarbeit mit dem RheinAhrCampus Remagen, der katholischen Universität Leuven/Belgien, der Heinrich Heine Universität Düsseldorf sowie caesar Bonn, eine internationale Konferenz zur Gesichtsweichteil-Rekonstruktion. Als Ko-Partner konnten erneut das Kriminalistische Institut in Prag, das Forensische Institut der Niederlande, das Landeskriminalamt Brandenburg, des weiteren IEEE Joint Chapter EMB (German Section), NEC Europe Ltd., C&C Research Lab und die Universität in Freiburg gewonnen werden. Als Veranstaltungsort wurde der RheinAhrCampus in Remagen gewählt. Eine Einladung zu diesem Meeting erfolgte weltweit. So erweiterte sich nicht nur der Teilnehmerkreis, sondern auch die Anzahl der Referenten um ein Vielfaches. Erstmals konnten Wissenschaftler, Techniker und Polizeibeamte aus China, Indien, Neuseeland und Australien begrüßt werden.

Basierend auf den Erkenntnissen aus der traditionellen Gesichtsrekonstruktion umfasste das Spektrum der Präsentationen modernste Methoden, die durch Anwendung komplexer Softwareprogramme, in Kombination mit Lasertechnologie und unter Berücksichtigung kiefer- und gesichtsmedizinischer sowie anthropologischer Forschungsergebnisse zur Rekonstruktion menschlicher Gesichter eingesetzt werden. So bekommen mittels 3D-Bildtechnik blanke Schädelknochen im wahrsten Sinne des Wortes ein neues Gesicht. Damit kann für die polizeiliche Verbrechensaufklärung, zum Beispiel bei Gewaltverbrechen wie Mord und Totschlag, ein bedeutender Schritt zur Identifizierung unbekannter Toter geleistet werden.

Auf diese Weise kann aber nicht nur die Identität von Opfern ermittelt werden, sondern auch jene der Täter, die bei Begehung der Straftat selbst ums Leben kamen. So können bei Selbstmordattentaten wertvolle Erkenntnisse über die Hintergründe der Tat gewonnen werden.

Aber auch bei schweren Naturkatastrophen, wie z. B. der Tsunami in Südostasien, trägt die Gesichtsweichteil-Rekonstruktion dazu bei, aufgefundene unbekannte Tote zu identifizieren.

Die Gesichtsweichteil-Rekonstruktion ist somit in jeder Beziehung ein äußerst wichtiges Hilfsmittel bei der Identifizierung unbekannter Toter. Aber selbst wenn nicht unmittelbar eine Person eindeutig zu identifizieren ist, so stellt sie vor allem im Zusammenhang mit den sonstigen Personenmerkmalen, am Fundort aufgefundenen persönlichen Gegenständen, den bei der rechtsmedizinischen Obduktion ermittelten individuellen Daten und einem anthropologisch-forensischen Gutachten eine wertvolle Hilfe dar.

Im Rahmen der Konferenz wurden erstmals auch die Ergebnisse einer wissenschaftlichen Vergleichsstudie vorgestellt. Wissenschaftler aus aller Welt erhielten die Möglichkeit die verschiedensten Methoden der Weichteilrekonstruktion zur praktischen Anwendung zu bringen. Den Teilnehmern wurde eine Replik eines Schädels zur Verfügung gestellt, dem sie unter Anwendung ihrer wissenschaftlichen Erkenntnisse ein menschliches Antlitz verleihen konnten.

Damit konnten sie möglicherweise wertvolle Hinweise zur Klärung der Identität des Toten bzw. zur Aufklärung einer Straftat oder eines Unglücksfalles beisteuern.

Hintergrund ist ein bisher ungelöster Fall der Polizeiinspektion Celle, in deren Bereich im Jahr 2003 ein Schädel gefunden wurde.

Eine ausführliche Analyse der Studien wurde im Nachgang der Veranstaltung durch Prof. Dr. Bongartz vom RheinAhrCampus in Remagen erstellt.

Im Namen der Amtsleitung des Bundeskriminalamtes darf ich mich an dieser Stelle recht herzlich bei allen bedanken, die zum Gelingen der Veranstaltung beigetragen haben.

In erster Linie spreche ich meinen Dank gegenüber den Kooperationspartnern, der fachlichen Leitung, den Referenten, den Teilnehmern und nicht zuletzt dem Organisationsteam aus.

Das Bundeskriminalamt unterstreicht nicht zuletzt durch die Veröffentlichung dieses speziellen Bandes zur Gesichtsweichteil-Rekonstruktion in der BKA-Schriftenreihe „Polizei und Forschung“ den Stellenwert des Themas für die polizeiliche Arbeit.

In seiner Funktion als Zentralstelle der deutschen Polizei hat das Bundeskriminalamt die erforderliche Initialzündung für dieses wichtige Hilfsmittel geleistet und nebenbei auch ein Netzwerk zwischen Wissenschaftlern, Technikern und Polizeibeamten in unterschiedlichsten wissenschaftlichen Fachrichtungen und Sparten, die mit der Gesichtsweichteil-Rekonstruktion in Verbindung zu bringen sind, ins Leben gerufen. Der Grundstein für ein breites Diskussionsforum, das zur Weiterentwicklung der Technik zweifellos beitragen wird, ist damit geschaffen.

Jörg Ziercke
Präsident des Bundeskriminalamtes

Foreword and Acknowledgements

This book presents recent results in the field of facial soft-tissue reconstruction presented on the 2nd International Conference on Reconstruction of Soft Facial Parts. The meeting was focused on new face reconstruction procedures in all forensic, anthropologic and medical application areas and brought together scientific, medical, anthropologic and forensic experts from university and clinical departments as well as criminal divisions and commercial sites.

Facial reconstruction is important in several scientific areas, especially in forensic science, archaeology and craniofacial surgery. In the first two areas the basis of all work is a skull find of a dead person where the soft tissue should be reconstructed. This helps with the identification of a skeleton from an open case of death or the comparison of facial features between modern and ancient human beings. In the case of craniofacial surgery a face must be reconstructed after, for example, cancer surgery.

Traditionally, manual techniques employing clay or plasticine modeled onto the skull are used. The principal goals of this kind of work are twofold. On the one hand, anthropologists are interested in giving an impression of the appearance of famous persons in history – the Stoertebecker face reproduction is an example of such work or giving an idea of a Neanderthaler's visage as a artwork for a museum's exhibition. On the other hand, forensic anthropologists are working hand in hand with criminal departments to identify a person by means of a soft-facial reconstruction to be published.

While the first goal offers some artistic freedom to the sculptor, the latter restricts him or her to the information that has been assembled within the criminal investigation. If the sculptor, for example, has been supplied with the skull only, without any indication of the structure and color of hair, it is recommended to leave the hair away and to show the reproduction of the face only.

Nevertheless, one requirement is the same for both goals. Manual face reconstruction requires profound know-how in material preparation, a deep understanding of anatomy and anthropology as well as artistic talents and handicraft skills. It is therefore apparent that only a small community of anthropologic scientists is able to perform adequate face reconstructions. However, even very experienced anthropologic or forensic sculptors need weeks for this very complicated reconstructive work. For that reason computer assisted facial reconstruction is becoming more and more important to facilitate and speed up the process of finding the appropriate reproduction of an individual's facial appearance.

"Mystery of dead woman in Winkeler Bay solved" – After ten years, a female body found mutilated beyond recognition has been identified thanks to a technique known as facial reconstruction. Thanks to the information obtained as a result of the reconstruction, searches for the potential murderer have now been initiated. – Reports of this type were rare in the past. Today, however, a revolutionary progress in computer-aided methods has also made its way into the reconstruction of the soft tissues of the human face.

The main goal of computer-based craniofacial reconstructions is to simplify and fasten the process of finding the appropriate reproduction of a subject's facial appearance corresponding to forensic findings or the modeling and prediction of the appearance after a surgical intervention. The recent developments in the IT-sector and the implicated improvement of computing power and progress in technologies for visualization, lead to novel ways for computer-aided forensical, archaeological as well as surgical facial reconstruction.

Based on the findings of traditional facial reconstruction, more and more complex software programs are being designed and applied. In combination with state-of-the-art medical imaging and laser scanning technology, detailed 3D-images can be created with different facial expressions. The conventional, manual 4-step approach of

i. examination of the skull,

ii. development of a reconstruction plan,

iii. practical sculpturing and

iv. mask design is very time consuming.

However, even with the use of modern imaging and computer tools, the general workflow has not been changed. It is still a 4-step approach of

i. Computed Tomography or Laser Scanning of the Skull Find

This step includes the taking of skull measurements. The methods may use above all anatomical landmarks, which first have to be selected and entered into the computer. Digitalisation by the computer tomograph offers the advantage that further, and even very complex marks of the skull form, e. g. so-called "crest lines" or other structural features defined by differential geometry, may be determined.

ii. Selection of a Soft-Tissue Template or a Landmark Set

The development of a reconstruction plan aims at identifying the "correct" soft tissue template in a (magnetic resonance, computed tomography, ultrasound or laser scanning) database or selecting appropriate landmarks. Additional information which should originate from the results of the forensic and anthropological examination and CID (*criminal investigation division*) finds at the place where the body was discovered (e. g. hair fragments) is still indispensable and is also used in preparation of step *iv.*

iii. Warping or Morphing a Skin onto the Skull-Find CT Data

In this step the computer carries out an elastic warping of the soft-tissue template from a database onto the skull find or uses the landmarks as basis for a surface spline reconstruction. Usually, subsequent interactive corrections of individual parts of the face are necessary.

iv. Texture Mapping

Texture mapping includes the application of patterns, shading and colours to surfaces. Today, computers are very well able to carry out this task. The real problem is rather the scope for artistic design. As for the manual method the decisions in this field are still left to the medicolegal expert and the anthropologist. But decision-making can be supported by the computer, and wrong decisions can be easily corrected.

These basic steps aim at supplementing and above all at accelerating traditional procedures.

There is a difference between the objectives of craniofacial or facial plastic surgery on the one hand and forensic or anthropologic face reconstruction on the other. In the case of the latter two application, fields the reconstruction of facial soft tissue must be performed without any knowledge of the exact target face. The main goal is to identify an unknown individual in the forensic case or at least to give an impression of the visual appearance of historic persons in the anthropologic case. As mentioned above, the latter type of problems leaves some degree of artistic freedom to the sculptor.

As chair of the conference I would like to thank the institutional co-organizers, partners and their representatives: German Federal Criminal Department, Bundeskriminalamt, BKA (Prof. Dr. Jürgen Stock, Vice Predident; Klaus Prüfer; Karl Sigl; Dr. Bernd Rieger); Caesar Bonn and University Düsseldorf (Prof. Dr. Peter Hering); Katholieke Universiteit Leuven, Departments of Orthodontics and Forensic Odontology (Prof. Dr. Guy Willems); Institute of Criminalistics Prague (Dr. Hana Eliasova); IEEE Joint Chapter EMB – German Section (Dr. Thomas Lehmann); NEC Europe Ltd., C&C Research Lab (Dr. Guy Lonsdale); Nederlands Forensisch Instituut, Rijswijk (Prof. Dr. George J. R. Maat); Landeskriminalamt Brandenburg (Dr. Bernd-Ulrich Straube); University of Freiburg (Prof. Dr. Ursula Wittwer-Backofen).

Many thanks go to the members of the program committee for the selection of works included in this book of abstracts. Members of the program committee in alphabetical order are

Jens Bongartz	RheinAhrCampus Remagen
Thorsten M. Buzug	University of Lübeck
Martin P. Evison	University of Sheffield

Ulrich Hartmann	RheinAhrCampus Remagen
Richard P. Helmer	Institute of Applied Medical Forensic Remagen
Peter Hering	University of Düsseldorf
Dietrich Holz	RheinAhrCampus Remagen
Om Parkash Jasuja	University of Punjabi
George J. R. Maat	Nederlands Forensisch Instituut, Rijswijk
Bernd Rieger	Bundeskriminalamt Wiesbaden
Georg Schmitz	University of Bochum
Bernd-Ulrich Straube	Landeskriminalamt Brandenburg
Wolfgang J. Spitzer	University Clinic of Saarland
Jean-Noel Vignal	Institute of Criminal Research of the French Gendarmerie
Ursula Wittwer-Backofen	University of Freiburg
Christoph P. E. Zollikofer	University of Zuerich

I would like to thank all partners organizing the comparative study. I thank Prof. Dr. Jens Bongartz (RheinAhrCampus Remagen) for organizing and chairing the study. Especially, my thanks go to Prof. Dr. Richard P. Helmer (Institute of Applied Medical Forensics Remagen) for taking over the Study Jury Chair. Last but not least I have to thank Dr. Carsten Tille and Dr. Hermann Seitz (Caesar Bonn, rapid prototyping group) for producing the skull casts.

For producing the proceedings in cooperation with Luchterhand Publishers I would like to thank German Federal Criminal Department (Bundeskriminalamt BKA), especially Karl-Michael Sigl and Klaus Prüfer. Further, I would like to thank the translator team of the Bundeskriminalamt.

For supporting the conference I have to thank the Wirtschaftsförderung Kreis Ahrweiler and Förderverein des RheinAhrCampus Remagen as well as NEC (St. Augustin), the German Society of Biomedical Engineering (DGBMT) and the German Section of IEEE.

Finally, warm thanks go to the members of the local organization team: Tobias Bildhauer, Holger Dörle, Susanne Dröppelmann, Dieter Gruschinski, Dr. Anke Hülster, Elvira Kluge, Birgit Lentz, Dr. Kerstin Lüdtke-Buzug, Volker Luy, Gisela Niedzwetzki, Waltraud Ott and Dirk Thomsen. Without their help the 2nd International Conference on Reconstruction of Soft Facial Parts would not have been possible.

Prof. Dr. Thorsten M. Buzug
Institute of Medical Engineering
University of Lübeck

Einführung

Der technologische Fortschritt nimmt in allen öffentlichen und privaten Lebensbereichen in immer größerem Maße Einfluss. „Neue Technologien“ eröffnen dabei sowohl Chancen als auch Risiken. Dies gilt auch für die Arbeit der Strafverfolgungsbehörden. Sie sind aufgefordert „Neue Technologien“ für mögliche präventive und repressive Nutzung zu analysieren. Doch gleichzeitig eröffnet die dynamische Entwicklung vor allem im Bereich der Informations- und Kommunikationstechnologien auch den Straftätern eine Plattform für bisher unbekannte Begehungsformen und konfrontiert die deutsche Polizei mit teils schwerwiegenden Ermittlungshemmnissen. Im Bundeskriminalamt stellt sich der Fachbereich KI 21 des Kriminalistischen Institutes dieser Aufgabe. Hier werden „Neue Technologien“ durch gezielte Beobachtung des Marktes identifiziert, analysiert, bewertet und etwaiger Handlungsbedarf erarbeitet. Dabei beruhen sicherheitspolitische Gesetzesinitiativen nicht selten auf den Ergebnissen der Fachbereichsarbeit.

Die Palette der Arbeitsthemen reicht von Kryptografie über Miniaturdrohnen, Telekommunikation, Weltraumtechnik bis zur Gesichtsweichteil-Rekonstruktion. Ein interdisziplinäres Team aus Kriminalbeamten, Wissenschaftlern und Technikern an der Schnittstelle „Neue Technologien und Polizei“ bildet die Basis für eine Erfolg versprechende Auftragserledigung.

Im Sinne dieser Aufgabenstellung und der allgemeinen Zentralstellenfunktion, polizeiliche Methoden und Arbeitsweisen der Kriminalitätsbekämpfung zu erforschen und zu entwickeln, begann sich der Fachbereich im Jahr 1999 mit der Thematik der Gesichtsweichteil-Rekonstruktion eingehender zu befassen. Dabei war vor dem Hintergrund der Komplexität dieses Wissenschaftszweiges (Human- und Rechtsmedizin, Holografie, Kommunikationstechnologie, Anthropologie, Archäologie, Odonthologie, Sozialwissenschaften usw.) und den damit notwendigerweise verbundenen Ressourcen in technischer, personeller und finanzieller Hinsicht von Anfang an beabsichtigt, ein Netzwerk zu initiieren, das Wissen und Kenntnisse über Techniken und Experten zusammenfasst.

Eine nationale und internationale Abfrage über den jeweils aktuellen Wissensstand führte sehr schnell zu der Erkenntnis, dass allgemein ein großes Interesse an einem gemeinsamen, interdisziplinären Informations- und Erfahrungsaustausch zum Thema „Gesichtsweichteil-Rekonstruktion“ sowohl bei Polizeibeamten als auch bei Wissenschaftlern und Technikern vorhanden war. Daher erfolgte die Einladung zur 1. Internationalen Konferenz nach Potsdam in Deutschland. Es gelang, die polizeilichen Bedürfnisse einerseits und die bereits vorhandenen wissenschaftlichen Forschungsergebnisse andererseits im Rahmen dieser Veranstaltung darzulegen. Es wurde aber auch deutlich, dass dies lediglich der Grundstein für eine gewinnbringende, künftige Zusammenarbeit sein konnte.

Dies wurde auch in einem gemeinsamen Schlusskommunique zum Ausdruck gebracht, dessen Kernaussagen wie folgt lauten:

– Weitergehender Erfahrungsaustausch und Forschungskooperationen zur Gesichtsweichteil-Rekonstruktion sind anzuregen und differenziert zu verwirklichen. Dabei ist beabsichtigt, sowohl internationale als auch nationale Ressourcen zu erschließen.
– Bündeln, Koordinieren und Intensivieren der Aufgaben und Ziele der Gesichtsweichteil-Rekonstruktion mindestens in Europa, verbunden mit dem Steigern der Effizienz der Methoden und Verfahren, sowie dem Entwickeln von Standards und europaweiter Versuchsserien.
– Entwickeln der Methoden der Gesichtsweichteil-Rekonstruktion zu einem praktischen Arbeitsinstrument und wissenschaftliche Anerkennung als eine Methode kriminalistischer Identifizierung.
– Aufgreifen, Weiterverfolgen und Institutionalisieren der Ergebnisse und Signale in internationalen sowie nationalen Gremien und Arbeitsgruppen.
– Erschließung von Publikationsmöglichkeiten, um die Ergebnisse in breiter Form der Fachwelt zugänglich zu machen.

Als die Idee geboren wurde, sich im Fachbereich eingehender mit der Gesichtsweichteil-Rekonstruktion zu beschäftigen, war nicht abzusehen, welche internationale Initialzündung zu einer intensiven Zusammenarbeit zwischen Polizei und Wissenschaft damit ausgelöst wurde. Auch die doch sehr ehrgeizigen Zielsetzungen des Schlusskommuniques erweckten eher Zweifel als Hoffnung, dass sie gänzlich umgesetzt würden.

Allen Zweifeln zum Trotz, sind mittlerweile alle Aussagen erfolgreich umgesetzt, auch wenn die eine oder andere Ankündigung mehr Zeit und Kosten in Anspruch genommen hat, als zu Beginn abzusehen war.

Als Initiatoren für die Konferenzreihe sind wir zuversichtlich, dass diese fortgeführt wird und bedanken uns an dieser Stelle bei all jenen, die uns tatkräftig bei den Planungen, Durchführungen und Nachbereitungen unterstützt haben. In erster Linie gilt der Dank den Referenten und Teilnehmern sowie den Organisatoren für die künftigen Konferenzen.

Als Fazit halten wir fest, dass die Technik der Gesichtsweichteil-Rekonstruktion immer noch sehr aufwendig ist. In der Reihe der Identifizierungsmöglichkeiten, wie Finger-/Handabdrücke, Zahnstati, DNA-Analysen oder Effektenauswertung besitzt sie dennoch einen erheblichen Stellenwert bei der Aufklärung von Straftaten und der Identifizierung der Opfer von Naturkatastrophen. Sie ist und bleibt nach wie vor, der „letzte Strohhalm“, das letzte Mittel für die Polizei, unbekannte Tote zu identifizieren.

Karl-Michael Sigl
Bundeskriminalamt, KI 21–1

Contents • Inhaltsverzeichnis

1.

Invited Contributions
Eingeladene Beiträge

Reconstructing hominids: hard and soft evidence

Christoph P.E. Zollikofer and Marcia S. Ponce de León

Anthropological Institute, University of Zurich, Winterthurerstrasse 190,
CH-8057 Zürich, Switzerland

Abstract

Paleoanthropologists investigate human evolution on the basis of the preserved skeletal evidence that documents morphologic change over the past 7 million years. However, the hominid fossil record is extremely scarce, so reconstructing the evolutionary path from ape-like ancestors to humans and Neanderthals is a real challenge. Here, we ask how we can reconstruct three-dimensional fossil morphologies, and how we can go beyond the skeletal scaffold of our ancestors and explore how they might have looked like. It turns out that this question has many different answers, which depend on the aims and purpose of soft tissue reconstruction. This leads to a comparison of methods and issues of soft tissue reconstruction in paleoanthropology and in forensics, which exhibit interesting differences, but also major commonalities.

Introduction

The major difficulties that arise during the analysis of human fossils are the dearth of material evidence and the incompleteness of individual specimens. Even by paleontological standards, hominid fossils are extremely rare objects. This can be illustrated by a simple calculation: the last 7 million years of human evolution are documented, at best, by about 700 individual fossil individuals (counting only those that consist of several fragments representing, at least, part of the skull, trunk and limb anatomy). Assuming even distribution over time (which is not the case in reality), this results in an average of one individual per 10'000 years, or per 400 generations.

It is easy to see that the principal difficulties encountered during the analysis of incomplete and distorted fossil bones will multiply in this special case. Nevertheless, human fossils have a special attraction – not only to scientists, but also to a wider public interested in such basic questions as to how we evolved and where we came from. Given the need to gain a maximum of information from a minimum of material evidence, one of the main challenges of paleoanthropology is to enhance the investigative power of methods for reconstruction and analysis, while minimizing the invasiveness of methods used for data acquisition.

Reconstructing fossils on the computer screen

Over past years, we developed and implemented an extensive set of methods to tackle these problems that can be subsumed under the notion of Computer-assisted Paleoanthropology (CAP) [1], [2]. One important feature of CAP is that it permits non-invasive virtual reconstruction of fossil specimens. The first step is the acquisition of three-dimensional data volumes from the original specimen.

Computed tomography (CT) is the method of choice, as it provides cross-sectional images revealing internal structures of solid objects in a noninvasive manner. Modern multislice medical CT devices permit rapid acquisition of volume data sets at a resolution of about 0.3mm per isotropic voxel. However, many fossils are heavily mineralized and exhibit corresponding higher densities, such that medical scanners fail to retrieve detailed information about internal structures. In such cases, industrial tomography is a feasible alternative, while microCT technology can be used to acquire data from small specimens, with a spatial resolution in the micrometer range.

Once volumetric data of fossil specimens have been acquired, data segmentation procedures are applied to extract relevant object structures from the data set. For example, it is possible to free a fossil fragment embedded in sediment with an electronic chisel. After data segmentation, geometric descriptions and graphical representations of the fossil fragments are created through 3D reconstruction procedures. Up to this point, CAP essentially follows a reverse engineering approach, i. e., a preexisting physical object is converted into a virtual object .

Manipulating fossil fragments on a computer screen as virtual objects instead of handling the real fossil specimens is of great benefit. Whereas physical preparation and reconstruction are highly invasive and potentially destructive processes, the analogous computer-assisted manipulations are completely noninvasive. Furthermore, CT data permit inspection of both external and internal anatomic structures.

In the following step, fossils are reconstructed from isolated and partially distorted fragments in virtual reality. This task can be compared to the assembly of a three-dimensional puzzle in which important pieces are unavailable. An example is given in Figure 1, which shows the virtual reconstruction of a Neanderthal child skull from 5 isolated original fragments [3]. The underlying reconstructive goals are to correct distortions that occurred during fossilization, to re-establish anatomic connections between preserved parts, and to replace missing parts by mirror-imaging preserved antimeres. To avoid a "reconstructional bias" toward preconceived morphologies, each reconstructive step follows predefined anatomic criteria that represent general biologic constraints [4]. In other words: virtual reconstruction of a set of cranial fragments of, for example, a supposed Neanderthal observes constraints imposed by the cranial anatomy of a generalized hominid, not that of a (specialized) Neanderthal.

In the following steps of CAP, the finalized virtual fossil reconstruction can be submitted to comparative morphometric analysis, used as a guide during physical preparation, and, last but not least, transformed into physical hard copies using rapid prototyping technologies.

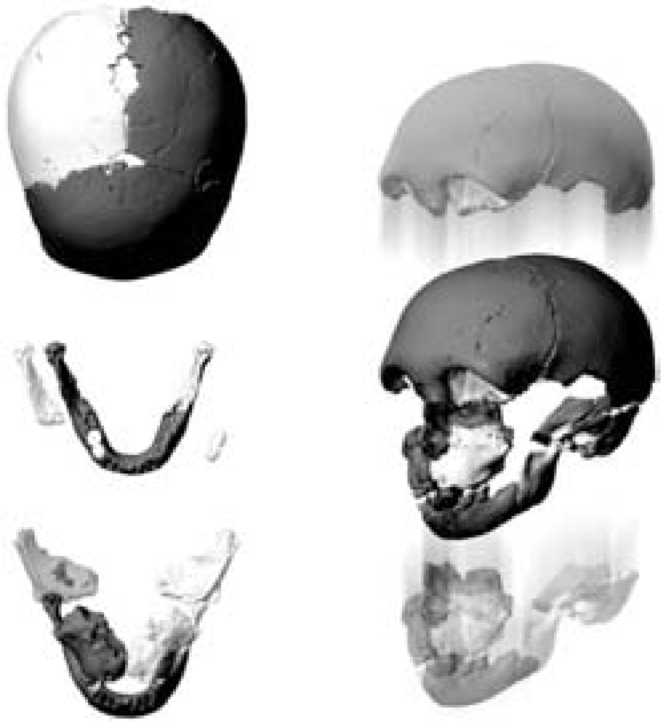

Fig. 1 Virtual fossil reconstruction of the Neanderthal Child from Devil's Tower (Gibraltar) from isolated fragments (original parts: dark grey; parts completed with mirror-imaging techniques: white). Left side: independent reconstruction of the cranial vault, the mandible, and the midface. Right side: Docking of neurocranial and viscerocranial parts. Note inner ear structure in right temporal bone.

Skeletal reconstruction and soft tissue reconstruction

In its essence, virtual fossil reconstruction attempts at recovery of the state of an individual at the time of its death. This is the starting point for comparative analyses, which themselves aim at recovery of the fossil individual's evolutionary, developmental and life history. Here, clear parallels arise between fossil reconstruction and forensic analysis of skeletal remains. Indeed, methods of forensics and paleopathology can be applied to analyze fossilized human remains.

However, paleoanthropology faces difficulties that forensic analysis does not. Most notably, paleoanthropologists are dealing with "individuals" that belong to paleopopulations of extinct species. Unfortunately, relatively little is known about these populations in terms of interindividual skeletal variation, such that it is difficult to discern between sex-, age-, and size-related traits, and between features that discriminate species and/or populations, and features that express individuality.

These difficulties are epitomized during reconstruction of fossil soft tissue parts. Why, after all, do paleoanthropologists not content themselves with the reconstruction of hard tissues but attempt at inference of soft tissue structures? There are two answers to this question, a strictly scientific/biological one, and a museological one.

The first issue concerns the relation between hard and soft tissue. Although the skeletal elements of the human body appear to constitute the "hard" evidence, developmental studies show that, in many respects, it is the soft tissue that ultimately determines the formation of skeletal parts. This is exemplified with the developmental matrix hypothesis [5] that states that bone deposition and resorption in the craniofacial skeleton is mediated by the surrounding and/or enclosed soft tissue structures. This is best seen during brain development, where cranial vault bones essentially follow the pattern of growth of the cortical surface rather than vice versa. Along another line of argument, structure-function relationships exert additional constraints on musculoskeletal shape. For example, evidence from the human masticatory system shows that the size of the jaws relative to other facial skeletal elements depends not only on genetic factors, but also on masticatory loads exerted during an individual's lifetime [6]. Likewise, it is well known that locomotor specialization and physical activity greatly influences the shape of the long bones via differential loading through muscular forces [7]. Accordingly, it makes sense to state that, at least to some extent, skeletal shape reflects soft tissue shape and that, during reconstruction of fossil skeletal morphology, hypotheses about soft tissue constitution must therefore be stated explicitly.

In the following sections, we consider the principles and methods used to reconstruct fossil soft tissue and illustrate the respective approaches with examples.

Reconstructing external soft tissue: the face

Museological issues of fossil soft tissue reconstruction concern perceptual rather than anatomic/morphologic issues. Soft tissue reconstructions in museum exhibits can be as informative as skeletal reconstructions. The human visual system is tuned to "classify" human faces with respect to various features, such as sex, age, ethnicity, and personal acquaintance. For a non-professional museum visitor, therefore, it is easier to recognize species and age differences on fleshed-out faces than on skulls. This is because assessing facial appearance belongs to everybody's daily experience, while assessment of skeletal structures is a professional task.

For example, the soft tissue reconstruction of the 4-year-old Neanderthal child intuitively looks "older" than a modern human of the same age (Fig. 2). Drawing on the human ability to estimate age from facial appearance leads museum visitors to think about differences in developmental timing between species that are hard to conceive on a purely skeletal basis.

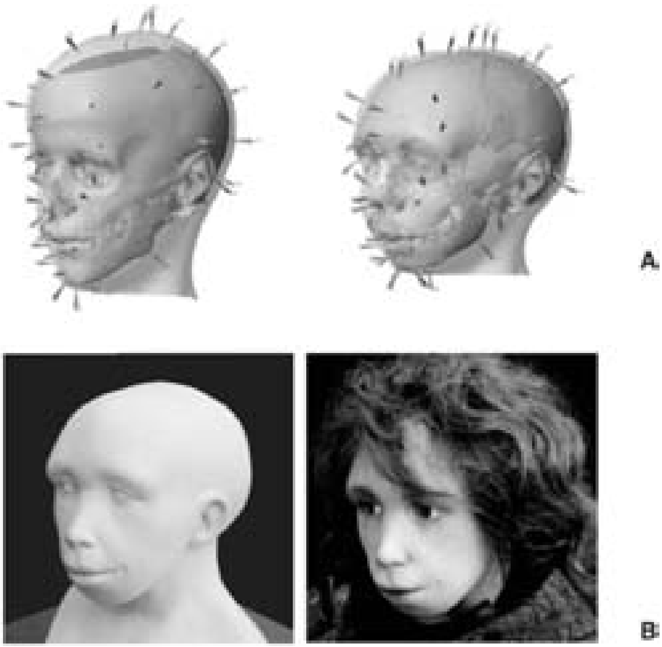

Fig. 2 Facial reconstruction of the Devil's Tower Neanderthal child. **A:** Corresponding anatomic landmarks on a modern human child skull (left; clinical CT data from two subjects) and the Neanderthal child skull (right) were used to morph modern soft tissues onto the Neanderthal skull. **B:** Plaster reconstruction based on stereolithographic replica (left) and finished model (right) of the Neanderthal child.

While forensic reconstruction aims at inference of individual facial parameters and draws on our recognition and classifying skills, the same classifying mechanisms often interfere with the aims of fossil soft tissue reconstruction. For example, we tend to perceive a reconstructed Neanderthal face as an individual rather than as a specimen representing the species *Homo neanderthalensis*. Likewise, the question of whether this individual's skin color represents suntan or genetic disposition typically occupies museum visitors more than the question what makes the anatomical difference between a Neanderthal and a modern human.

How can we find a balance between soft tissue reconstructions representing an individual versus representing a fossil species? There is no unique solution to this issue; here, we will outline a statistical morphing-based approach to the problem. As an example, we continue with the reconstruction of the Neanderthal child portrayed in Fig. 2. As a reference sample, we used composite clinical CT data sets of two 4-year-old modern human children to determine a set of anatomic landmarks on the skeletal surface. The same set of landmarks was determined for the Neanderthal skull. To transfer the modern soft tissue thickness data onto the Neanderthal child skull, we used a three-dimensional thin-plate spline (TPS) interpolation function [8], whose nodes were defined at 120 anatomical landmarks, approximately evenly distributed over the craniofacial surfaces. Based on the modern-to-Neanderthal skeletal landmark homology, the TPS function morphs the entire modern average cranial skeleton into the Neanderthal cranial skeleton. During this process, the modern average soft tissue is allowed to "flow" together with the skeletal data and is transformed into the inferred Neanderthal facial morphology. A similar approach, based on an alternative volume morphing method [9], has been proposed for forensic reconstruction [10]. The resulting soft tissue reconstruction is "parsimonious" in the sense that no specific assumptions were made about Neanderthal soft tissue peculiarities; it is based on the hypothesis that the relation between skeletal and soft tissue structures was essentially the same in Neanderthals as in modern humans. Parsimony results in a trend toward "modern humanness," but leaving open intentionally any questions regarding the inference of "archaic" features distinguishes this reconstruction from classic approaches.

Reconstructing internal soft tissue: the brain

While facial reconstruction is the most widespread application, paleoanthropology is involved in the reconstruction of another soft tissue structure that is less visible than, but equally prominent as the face: the brain. During brain reconstruction, the situation is reverse, because the form of an internal organ is inferred from the form of the bony case including it.

Endocranial capacity has long been used as a proxy of brain size in human evolutionary studies and the surface structure of endocranial casts (so-called endocasts) as an indicator of brain structure. The fundamental question of how endocranial structures are related to actual brain structures was considered in one important monograph [11] but has received comparatively little attention in subsequent evolutionary studies. Medical imaging techniques now permit a new approach to this question, as it is possible to quantify the brain-bone interface in living subjects. A preliminary study using "morphologic brain mapping" shows that this relation is highly ambiguous [12]. Small-scale sulci and gyri that exhibit large interindividual variability are well-represented, whereas large-scale features such as the Sylvian fissure that characterize interindividual homologies tend to be underrepresented. As a consequence, the interpretation of endocranial fine structure in terms of cortical surface structure and, ultimately, in terms of behavioral/cognitive performance must be carried out with caution.

Conclusion

Soft tissue reconstruction in human fossils has both its biological and museological benefits. It drives scientists to think of skeletal remains as part of an integrated evolutionary, developmental and functional system and to consider skeletal morphology as expressing soft tissue morphology. On the other side, it forces museum visitors to re-think their own attitude towards "humanness", i. e. how human beings have changed over evolutionary times, how they might have looked like, and how different and/or similar they are to present-day humans.

References

[1] C. P. E. Zollikofer, M. S. Ponce de León, *Virtual Reconstruction: A Primer in Computer-assisted Paleontology and Biomedicine*, New York: Wiley, in press.

[2] C. P. E. Zollikofer, M. S. Ponce de León, R. D. Martin, "Computer-assisted paleoanthropology," *Evolutionary Anthropology,* vol. 6, 41–54, 1998.

[3] C. P. E. Zollikofer, M. S. Ponce de León, R. D. Martin, P. Stucki, "Neanderthal computer skulls," *Nature*, vol. 375, 283–285, 1995.

[4] M. S. Ponce de León, C. P. E. Zollikofer, *Anat. Rec.*, vol. 254, 474–489, 1999.

[5] M. L. Moss, *Nova acta Leopoldina NF*, vol. 58, 17–25, 1986.

[6] S. Kiliaridis, "Masticatory muscle influence on craniofacial growth," *Acta Odontologica Scandinavica*, vol. 53, 196–202, 1995.

[7] E. Trinkaus, S. E. Churchill, C. B. Ruff, "Postcranial robusticity in Homo: II. Humeral bilateral asymmetry and bone plasticity", *American Journal of Physical Anthropology* vol. 93, 1–34, 1994.

[8] F. L. Bookstein, *Morphometric Tools for Landmark Data*, Cambridge: Cambridge University Press, 1991.

[9] M. Chen, M. W. Jones, P. Townsend, "Volume distortion and morphing using disk fields," *Comput. Graph.* vol. 20, 567–575, 1996.

[10] L. A. Nelson, S. D. Michael, "The application of volume deformation to three-dimensional facial reconstruction: a comparison with previous techniques," *Forensic Sci. Int.* 94, 167–181, 1998.

[11] C. J. Connolly, *External morphology of the primate brain*. Illinois: Thomas Springfield, 1950.

[12] C. P. E. Zollikofer, M. S. Ponce de León, "The brain and its case: computer-based case studies on the relation between software and hardware in living and fossil hominids," in *Humanity from African Naissance to Coming Millennia* P. V. Tobias, M. A. Raath, J. Moggi-Cecchi, G. A. Doyle, Eds. Florence: Florence University Press, 2001, pp. 379–384.

The Facial Reconstruction: Past, Present and Future

Jean-Noel Vignal, Anthropologist Phd, Paleopathologist Phd

Head of the department of anthropology-thanatology-odontology Institut of criminal research of the french gendarmerie, France

Introduction

This paper aims initially to plunge us in a brief and not exhaustive history of the facial reconstruction. In first, I will propose a travel to you through the time, which will enable us to remind ourselves the great stages of this history.

Then, I will stop a few moments to give a progress report on the current techniques. I will give you my point of view on what I consider as the only goal of the facial reconstruction. I will benefit from it to show you some actual facial reconstructions.

And, I will finish this paper with a projection in the future. Difficult exercise but which appears essential to me to target our respective research orientations.

Lichtenberg said "The most exciting surface of the world, it is, for us, the human face."

If the face has a relationship with the vision, it is however what always overflows the representation, the "chosification" like said Jean-Paul Sartre. "It is when you see a nose, eyes, a forehead, a chin, and that you can describe them, that you turn to others like worms an object. The best way of meeting others, it is not to even notice the color of its eyes!" Levinas writing.

But, forensic ambition is different from philosophy ambition. When you reconstruct a face, you must describe eyes, nose, forehead, chin, lips and so on to be able identify the person. The facial reconstruction must be able to find the features most characteristic of a face like those of an object. But it cannot find the heart which animated this face.

Past

Paul Broca (1824–1880) is often considered to be the first who had begin searches in the field of correlations between shape of the skull and shape of the face. He thus was the first to scientifically consider the concept of individuality in the human face. He described the different proportions of the skull and proportions of the face for several type of populations.

Although we need to use with precautions the results of his observations not to fall into racist wandering. It should nevertheless be admitted that face architecture is correlated with skull architecture.

And when we observe several skulls, we see several different faces. We are all differents.

The shape of the skull determine the shape of the face.

If we have both eyes, a nose, lips, a face. Those present between them ratio of proportions and ratios of distances which make that each face is different from the different one. Sometimes it can happen that this subtle arrangement reproduces and then we are opposite doubles or twins. But it is well the subjacent cranium which determines the shape of the face.

Soft tissue thicknesses have been collected since the nineteenth century by Welcker (1883).

He studied tissue depth measurements on thirtheen males cadavers onto nine median anthropological points.

W. His was one of the first researchers to obtain informations about tissue depth measurements. In 1895, he examined twenty eight cadavers using a double-edged knife technique. A sharp needle was inserted into the facial tissue at nine anthropological points in the median plane and six lateral points on the profile of the face. The distance between the needle point and a special rubber disc fitted onto the needle was measured to obtain facial thickness depths.

His used this data to make the facial reconstruction of Johann Sebastien Bach. The presumed skull provided of skeletal remains exhumed with other skeletons during renovations at the Church of St John in Leipzig.

In a second study, he shown some correlations between soft tissue thicknesses and the stoutness. His sample was composed of 24 men of normal stoutness and 9 male of thin stoutness.

To model the faces, HIS positionned reference marks plasters on the median and side points. Then he connected them by clay to obtain the shape of the face.

In 1898, Kollmann and Buchly looked further into work of his by establishing more precise measurements of soft tissues thicknesses and by interpreting them by statistical studies.

They added additionnal points to those of his. To measure depth tissue, they used a needle passed to the flame of a candle. By penetring soft tissues thicknesses, the blackened part was then unobtrusive on all the depth.

Their sample associated with those of his and Welcker, increased the number total of subjects to 45 men and 4 women.

At the same time, Merkel reconstructed the face of an individual using muscular insertions. It then imagined the shape of the muscles and the possible soft tissues thicknesses. It was the first to use for modelling a new material, the plasteline.

At the beginning of the XX° century, Czekanowski developped a graduated needle what allowed the direct reading of the soft tissue thickness before retire the needle. The precision of measurements improved.

In 1913, Doctor Henri-Martin decides to put a face on cranium of the Neanderthal woman discovered by him on the site of La Quina (France). From a cast of the skull, with the sculptor Charles Bousquet, he reconstituted the musculature step by step, then the skin was illustrated by a fine layer of ground. Elements are largely interpreted by the prehistorian: he said "the eyes, the nose and the ears not having traces were inspired of the traits observed on the chimpazee".

When he finished his facial reconstruction, Henri-Martin said:

"I estimated that at the mousterian period, the evolution of the intelligence was sufficient to translate in the eyes the reflection of the thougt.

Affined feature, long hair added on the face increase the female character.

In 1908 a near-complete skeleton established as belonging to Neanderthal man was discovered in the La Chapelle-aux-Saints (France). The bones were assembled by Marcellin Boule, a famous palaeontologist and geologist of the time.

The Neanderthal Man which emerged as a result of that assembly had a stooped posture and a protruding skull. Moreover, its limbs remained locked at the joints, making it unable to stand fully erect.

This ape-like appearance fixed the Neanderthals as primitive creatures in peoples' minds. They were depicted as primitive ape-men in pictures.

And in 1921, Marcellin Boule, with the sculptor Joanny Durand, try to rebuild the head of the man of Neanderthal of the Chapelle aux Saints. Their work is limited to the positionning of the muscle of cranium. The eyes, the skin and the hair were not represented.

But with their subjectivity they reconstruct a bad face of Neanderthal, this face has a primate appearance like the facial reconstruction of Doctor Henri-Martin.

In fact this facial reconstruction was in agreement with the idea of the time which placed neanderthal among the primates and not among the men.

It was not a scientifc facial reconstruction but a philosophical rebuilding!

It was in Russian, where the technique of forensic sculpture was more fully developped."

Mikhail Gerasimov was an anthropologist, archeologist and ethnologist.

He headed the department of archeology at a museum and he experimented facial reconstruction with the skulls in his care.

In 1935, he had become fairly adept at taking a skull and reforming it into a face that people recognized. Four years later, he helped to solve a murder. In 1950, the USSR established the Laboratory for Plastic Reconstruction.

Gerasimov's work was an eccentric combination of paleontology, archaeology, anthropology, and forensic science. It was a way to gaze on the faces of those long dead, he wrote in his 1968 memoir, "The face finder."

At the beginning of the "eighties", Rhine and Campbell and Rhine and Moore have been instrumental in the collection of tissue measurements from the different sexes and races (American negroid, American caucasoid, Soutwestern American indian). The measurements collected by Rhine and colleagues take into consideration the thickness of the muscle, fatty and connective tissue, and skin thickness all in one calculated measurement at a particular morphological landmark. The data of all of Rhine's table are divided by emaciated, normal and obese groupings.

Present

Before to talk about the present, I would like to give my my point of view about the goal of the facial reconstruction into forensic investigations.

Facial reconstruction is only justified when traditional forensic investigations cannot end up to the identification of the body.

It's not a method of positive identification like dental, medical, fingerprints or DNA identification.

The unique ambition of the facial reconstruction is to propose the most coherent caricature of the face of a person in order to release witnesses' calls. And only after, when we have the name of a potential victim we can make a positive identification by comparative methods like dental, DNA and so on.

Currently, there are three different ways from the facial reconstructrion according to the team and countries.

These three ways are:

- Drawing method
- Sculpture method
- 2D and 3D computed methods

I will not detail you these various methods because we will see these during this congress but I will show you the technique used by the Institute of criminal research of the french gendarmerie.

Whatever the method is, working on facial reconstruction necessitates first an anthropological study to determine sex, age at death and skull characteristics of the deceased.

After, we calculated soft tissues thicknesses according to our data bank coming from CT-scan made on living people.

We make a Skull acquisition by numeric camera. Then we elaborate a composite face with a forensic software.

After we deform the composite face on the picture of the skull by a warping software.

And in last we put on the face reconstructed: hairs, mustache, beard, and so on in function of remains discovery.

Our sample is made of 41 males hospitalized patients and 34 females, all of the leucoderm group and without pathology of the head. Mean age is 49 and stoutness index has a mean value of 2,38 for male and mean age is 62 and stoutness index has a mean value of 2,23 for female.

In this study, the appreciation of stoutness focused on the Davenport's index also called Kaup's index with weight divided by the square of the size

On a mathematical point of view, this ratio is not a constant since weight and square of the size are not similar fonctions. However, as relative weight is not constant in scale of size, this ratio is sufficient to characterize stoutness of individuals whatever, big or small, statures are.

The scale of Davenport gives the following results:

very thin	1,40 to 1,80
thin	1,81 to 2,14
medium	2,15 to 2,56
corpulent	2,57 to 3,05
obese	3,05 and more

For us CT-scan represents a tool choice to visualize and measure soft tissue thicknesses in order to extract suitable data for face reconstruction.

The number of sections and their thicknesses can be determined and checked with convenience. Similarly locating craniometric points is easier using CT-scan rather than radiographies. Thus, points difficult to localize such as gonions are easily seen on profile reconstruction associating six or seven sections. When these points are indexed, they are automatically noticed by computer in coronal view and soft tissue thicknesses are measured with a great precision. At that time, recording and storage of images using magnetic supports allow a 3D facial reconstruction.

On each point, minimal and maximal value of soft tissue thicknesses are defined with a confidence interval of 95 %. Using the regression equations calculated on the populations we studied, differences between these maximum and minimum values correspond to the possible variation of soft tissue thickness at a point with reference to stoutness. These limits correspond to the freedom the operator has to define regions, the algorithm of warping will distort. It allows to match, in the limits we fixed, the different soft tissue thicknesses on the face giving a coherent and balanced shape. In practice, this calculated interval reduces subjectivity due to the operator, leaving him up to a point of managing the statistical tool quantifies.

Here you have equations for the male. Each soft tissue thickness is calculated with the best correlation factor (age, stoutness' other correlated point). In this way, the values of the soft tissues are specific to each studied cranium and they are not taken in arbitrary choice in fixed databases.

The cranium is digitalized using a numeric camera.Then, with the help of a specific software, soft tissue thicknesses coming from our data bank and calculated according to age, sex and stoutness we defined, are put on the digital image of the cranium.

According to height and width of the head, probable pattern of the nose and of the line of eyebrows, a virtual face is built by means of the composite picture software. The interest of this step lies on building a shape of a face and limiting abnormal distortions due to warping. In fact, principe of image deformation lies on successive rotations, translations and displacements on the scale which, when in a great number, cause interferences on image.

When soft tissue thicknesses are materialized on the digitalized cranium, outline of face and image of the cranium can be exported on the warping software. The operator has only to delimit the regions of the skull he want to warp taking in account calculated soft tissue thicknesses and anatomical landmarks.

In our example, we decided to consider the shape of the face, the ocular, nasal, and oral region in order to define the craniometric points with accuracy. In these conditions, the algorithm of warping will distort the first face to match it with the cranium image, the soft tissue thicknesses placed on.

When we proceed to a media diffusion we give the face reconstructed with different hairstyle to increase the recognition.

Combining actual scientific approach with the talent of an artist like Elisabeth Daynes, we be able to produce new vision of the past.

It's an other finality of the facial reconstruction. Here the most probable caricature of the face is not sufficient for the public to understand our past. It's necessary to give them a realist face reconstructed and for this an artistic worker is essential.

On this actual facial reconstruction of a Neandertal, you can appreciate the difference with a past approach.

On the facial reconstruction of the Man of Cromagnon by Elisabeth Daynes according to the forensic computer method, in the right part of the frontal, there is the mark of the pathology founded on the skull, that is probably actinomycosis.

When people see this facial reconstruction and the modern reconstruction of neandhertal, they can understand better their living together.

An other actual facial reconstruction has been made on the skull discovered into one of the ships of Monsieur de Lapérouse by the SALOMON new-caledonian association, in the coral reef of La Faille, in two thousand three.

There is a difference between the forencic facial reconstruction based on the caricature and the more realistic and beautifull artistic face sculpted in function of the forensic reconstruction by Elisabeth Daynes.

In last, there is the facial reconstruction of the famous german pirate Klaus Störtebecker by Elisabeh Daynes.

Klaus Störtebecker, captain of the Vitalienbrüder, was beheaded to Hambourg in 1400 with one hundred of his friends .

The skul was discovered in 1878.

I let to you appreciate the realism of this face.

Future

The future developments of the facial reconstruction will be able to make in research associating the disciplines also differents that anthropology, medicine, mathematics, physics and computer science. Indeed, if we want to exploit information that us progress of the medical imagery gives, we must be able to treat them from a mathematical point of view in order to obtain a good 3D modeling of the face.

One of the resarch orientations which we think important consists in generating a numerical 3D library of the muscles or groups of muscles of the face. Indeed, this library would make it possible to equip cranium with its muscular masses. Then, with the physical parameters of some muscular groups, we could reproduce on the face of the dynamic feature of the facial expresssion.

In the same way, It seem important to us to undertake research in the space relations in 3D between the components of the face (the eyes, nose, lips and so on) and subjacent osseous volumes. This approach will not have to be satisfied with correlations points to points as until now but it will have to take from a space point of view these relations. That implies the implementation of complex mathematics starting from sources of medical imagery.

Here, you have our near future. We developp in collaboration with the University of Marne la Vallée a 3D software for the facial reconstruction.

This software will be able to generate 3D face on the same principe of our 2D protocol. The aim will to propose for the investigators a 3D caricature of the victim face.

Another way of the reflexion would consist in proposing starting from the same cranium a thin, average and large face and to compare them automatically with the data bases of the missing people or with the photography of the victims of a mass disaster.

Lastly, in a more remote future, we can imagine to associate information resulting from the decoding of the human DNA with the 3D facial reconstruction, in order to restore without error or subjective interpertation the face of the dead person.

But it's probably and certainly an utopia.

Conclusion

The facial reconstruction is a discipline in full expanding. And the sucess of this second conference lets predict many developments of quality which will be able to benefit this branch of the anthropology.

2.

Tissue-Depth Measurements and Markers

Weichteildickenmessungen und anatomische Marker

Computer-Aided Measurement of the Tissue Thickness of Deceased Persons with Computer Tomography Scans of the Head

D. Bellmann[1], Th. Fuchs[2], A. Weidenbusch[1], J. Haber[2], K. M. Stein[3], T. Georg[4] und J. Wilske[1]

[1] Institute of Legal Medicine, University of Saarland/Homburg
[2] Max Planck Institute for Computer Science, Saarbrücken
[3] Institute of Legal Medicine, University of Heidelberg
[4] Institute for Medical Biometrics, Epidemiology and Medical Computer Science

1 Summary

The facial reconstruction of the skelettonized human skull for the identification of unknown persons with manual or computer-aided methods is based on known soft-tissue values in the face area. The already known soft tissue values vary with each used method and material. Furthermore, due to the noticed change and enhancement of alimentation of the population in middle Europe, particularly in the last decades, we have to bargain with a noncorectness of the already known values of the soft-tissue thickness.

Because of this, we aspired a measurement of the facial thickness with a newly developed computer-aided method that allows a reproducible, orthogonal to the skull realisable method.

Our material consists of 135 CT-Scans of deceased persons of Caucasoid origin.

The initial point of the development of the here presented measure method is the fact that measuring the range from the skin to the underneath bony structures from CT-Scans is possible. While doing so, using a commercial program, the surface of the skin and skull are displayed separately and projected on each other in anatomically correct positions. The measurement of the range at any point on the skull with a computer program made specially for this purpose, can be done in the so far common method of using the right angle, or can be made in others ways.

The measurement results of the facial soft-tissues are slightly influenced by the intra individual error of the examiner and his choice of the landmark range.

External factors have greater influence on the results, like the early post mortal change of the facial soft tissue thickness and the post mortal movement of the facial soft-tissue depending on the body posture and stocking. This might require the use of a correction factor when evaluating the measurement.

2 Introduction

A facial reconstruction in forensic medicine is needed if the identity of an unknown deceased with partially or complete skelettonized skull is not possible through dental identification or DNA-Examination. At present such reconstructions are made with Plastilin, Clay or Wax [1], [2], a procedure that demands a large amount of time as well as some artistic skill. In contrast, computer-aided methods save much time [3], [4], [5], [6], [7]. They make operability easy as well. The possibilty to fit different variations with regards to constitution and facial expression in an existing facial reconstruction is another advantage of computer-aided methods.

Such software is based on facial soft-thickness values of persons of different ethnical origin, different constitution types and different age classes. Already existing data for the facial soft-thickness were made predominant by means of manual methods [8], [9], [10] or with hardcopies from digital imaging methods [11], [12]. Using these methods, an accurate orientation and orthogonal direction is not always possible. Beyond this, it seems that due to different and better alimentation in the last decades, the existing soft-tissue tables are not up to date. Because of this, the development of a computer-aided measure method of the facial soft-thickness was aspired.

3 Method and material

3.1 Material

From the Institute of Legal Medicine Heidelberg, 135 CT-Scans of deceased persons with Caucasoid origin between 16 and 89 years were chosen. Overall, the group consists of 77 men and 58 women, with a body-mass-index between 16 and 42.

The used computertomograph is a Siemens Somatom Plus S, constructed in 1989. The data-scan of the head is raised with spiral technics with a layer thickness between 3 and 5mm.

The examined person-subgroups were differed after Sex and Body-mass-index into six groups (Tab. 1).

3.1.1 Selection criteria of the CT-Scans

For the selection of the CT-Scans, we used the following criteria:

1) As little as possible appearance of radiological artefacts, for instance noisy patterns or overlaying of bony structures through dental works.
2) Little body idle period before the CT-Scan as well as an exact placement of the head in the middle line. Bodies with beginning decomposition, bloating of the facial soft-tissue or asymmetric placement of the head with displacement of the facial soft-tissue were not used in the examination. The estimates of these conditions were done with the 3d-illustration of the skin surface of the corresponding skull surface with the help of our computer program AMIRA®.
3) Completeness of the bony skull and the facial soft-thickness. In case of multiple traumas, cranio cerebral-injury, maximal trauma, homicide, gunshot wound and the like, the heads were not included in our examination. Furthermore, CT-Scans of heads with substance defects, cracks, deformations, breaking-up of the bone matrix, asymmetry of the skin surface or foreign bodies etc. were not used.

3.2 Method

3.2.1 Processing of the data set

The data set is totally anonymously presented in the DICOM-Format and is imported in the AMIRA® Program. There, it is possible to create a 3-dimensionall display of the skin and skull surface, a so-called isosurface, which can be arranged digital. The optimal threshold for the density is usually around the value of ±300 and has to be adjusted manually for each skin- and skull processing (Fig. 1 and 2).

AMIRA®2005-Mercury Computer Systems www.mc.com/tgs

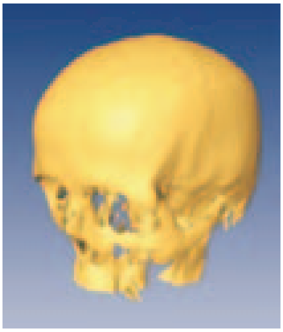

Fig. 1 Skull surface

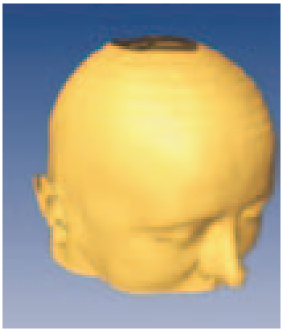

Fig. 2 Skin surface

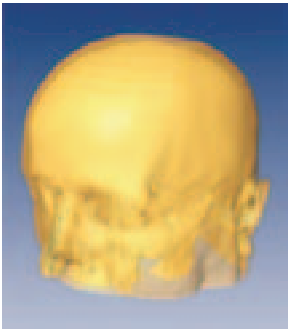

Fig. 3 Semitransparent overlay

After the making of the 3-D image from skin and skull on the base of the above described selection criteria, the adequate data sets are chosen.

To reduce the amount of data, all bony structures and soft-tissue parts that are not necessary for the later measurement were digitally deleted. These are mainly parts of the base of the skull, the inner ear and the air sinus. Possible appearance of radiological artefacts or foreign bodies is left out as well.

Subsequently, the data sets are saved separately in skin- and skull surface in the "iv-Format" of the AMIRA® program. To allow an easy access to the data sets, they are encoded.

3.2.2 Encoding of the data set

The used code consists of abbreviations for sex, age, body-mass-index, ethnical origin, place of the data collection, represented part of the skull as well as the information, if it is an in vivo or post mortal data set. At the last position, there is an abbreviation that tells us if it is a skin surface or skull surface data set.

3.2.3 Measurement of the soft-tissue thickness

To measure the soft-tissue thickness at a specific landmark position, we employ a measure program developed at the Max-Planck-Institute for Computer Science.

After loading the complete data set (consisting of skin and skull surface) into the measure program, a 3-D model of skin and skull are displayed in superposition in a graphics window. The complete head model is aligned to an underlying coordinate system in the following way:

– The yz-plane coordinate system is the median or sagittal plane of the model of the head

– The origin of the coordinate system coincides with the landmark "Nasion" (n)

Next, the user interactively specifies the position of the landmarks on the skull model. The program asks for each landmark to be specified by selecting its position on the skull through a mouse click. Landmarks can be placed anywhere on the skull model, and their position can be modified or corrected at any time later on. For incomplete data sets, i. e. partial or fragmented skulls, the placement of individual landmarks can be skipped, if the corresponding bone structure is not present in the data set.

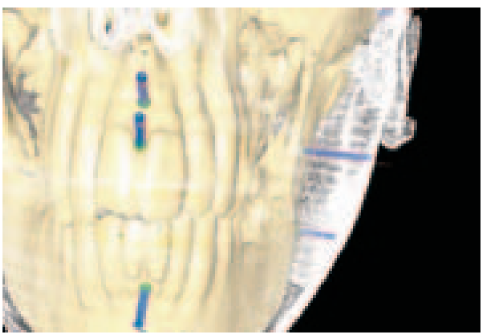

Fig. 4 Semitransparent overlaying of skull and skin

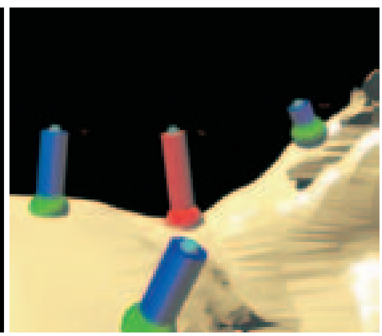

Fig. 5 Positioning of the landmarks

For each landmark specified by the user, the program automatically computes the distance between the landmark (on the skull) and the skin surface above. This distance is measured orthogonaly to the skull surface. In practice, the determination of the orthogonal direction (and hence the distance) is not always well defined. Both noisy data, e. g. the typical rippling pattern visible at the boundaries of layers from CT scans, and pathological causes, e. g. tumours, may affect the exact computation of the orthogonal direction in a specific landmark position. Hence, we use an averaged orthogonal direction computed from the local neighbourhood of the skull surface around the landmark position. The user can set the size of this neighbourhood. In our measure program, this neighbourhood is called range. The smaller this range is chosen, the better does the computed orthogonal direction represent local surface detail, but also the more vulnerable is the computation to noisy or pathological data. The larger the range is chosen, the more robust is the computation of the orthogonal direction. After the orthogonal direction is computed, the distance along this direction between the landmark and the skin surface above is calculated using a ray tracing approach. In this technique, a virtual ray is "shot" from the landmark position L on the skull along the orthogonal direction computed before. The intersection point P of this virtual ray with the skin surface is used to compute the soft-tissue thickness $d := ||P - L||_2$

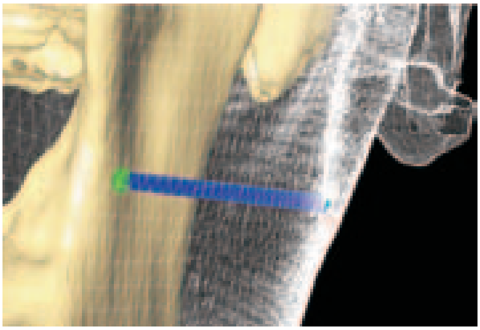

Fig. 6 Measurement of the orthogonal distance between skin and skull

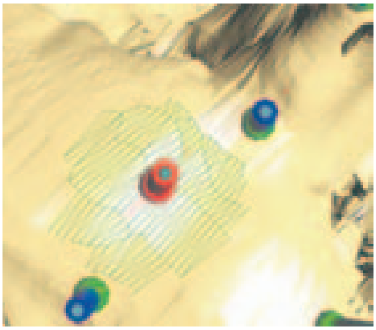

Fig. 7 Illustration of the range

The complete set of landmark positions is saved with the corresponding soft-tissue thickness values and additional meta data (e. g., gender, age . . .) for each data set (fig. 8 and 9)

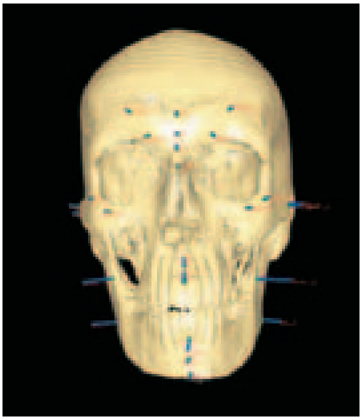

Fig. 8 Skull with landmarks frontal

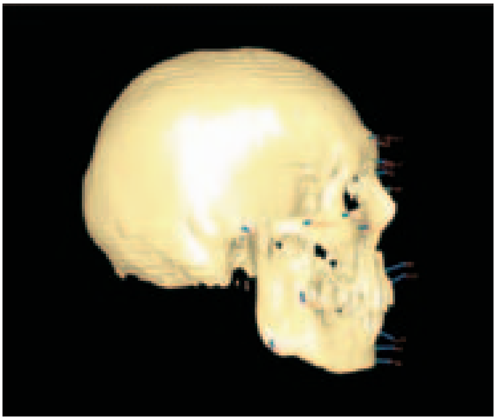

Fig. 9 Skull with landmarks lateral

In addition to that "classic" method of measuring soft-tissue thickness values along an orthogonal direction at each landmark position, we are currently investigating the applicability of other measuring paradigms. To avoid the vulnerable computation of orthogonal directions, it might be useful to measure soft-tissue thickness values, for instance, at all grid points of a uniform, volumetric grid that encloses the complete data set. The resulting data, however, would not be comparable directly to data obtained in the traditional way. Nevertheless it might be beneficial to use the data obtained from such a volumetric measuring technique in automated facial reconstructions, if the reconstruction algorithm is adapted to this new type of data

3.2.4 Selection of the landmarks

We consider 10 unilateral and 8 bilateral landmarks. Because there is a strong variation in naming, choosing and localisation of measure points, we chose to use measure points according to K. T. TAYLOR [13] and RHINE [10]. Regardless, we were forced to modify those measure points to our methods.

3.2.4.1 Unilateral landmarks

Supraglabella:	Above the Glabella, on a level with the frontal eminence
Glabella:	The most prominent point between the supraorbital ridges in the midsagittal plane
Nasion:	The midpoint of the suture between the frontal ridges and the two nasal bones
End of Nasals:	The anterior tip or the farthest point out on the nasal bones. If the structure cannot be displayed exactly with AMIRA®, we used the most distal point of the nasal bone.
Mid-Philtrum:	The midline of the maxilla, placed as high as possible before the curvature of the anterior nasal spine begins.
Upper Lip Margin:	Centred between the mandibular central incisions at the level of the cementum enamel junction. If the structure cannot be displayed exactly with AMIRA®, we used a point some millimetres above the Cementum Enamel Junction.
Lower Lip Margin:	Centred between the mandibular central incisors at the level of the Cementum Enamel Junction. If the structure cannot be displayed exactly with AMIRA®, we used a point some millimetres under the Cementum Enamel Junction
Chin-lip Fold:	The deepest midline point of indentation on the mandible between the teeth and the chin protrusion.
Mental Eminence:	The most anterior or projecting point in the midline on the chin
Beneath Chin:	The lowest point on the mandible

3.2.4.2 Bilateral landmarks

Frontal Eminence:	Place on the projections at both sides of the forehead. If the structure is not visible, we chose a point in projection on the vertical orbita mid-line lifted halfway of the orbit height above the orbit.
Supraorbitale:	Above the orbit. Centred on the upper most margin or border
Suborbitale:	Below the orbit, centred on the lower most margin or border
Lateral Orbit:	Drop a line from the outer margin of the orbit and place the marker about 10 mm below.
Zygomatic Arch:	Halfway along the Zygomatic arch
Supraglenoid:	Above and slightly forward of the external auditory meatus
Gonion:	The most lateral point on the mandibular angle
Occlusal Line:	On the mandible in alignment with the line where the teeth bite

3.3 Error Analysis

3.3.1 Investigation for reproducibility

For quantification of the variability, which is resulting out of the localisation of the separate landmarks with a single investigator, a random skull is measured ten times after the above-mentioned method.

3.3.2 Influence of different ranges on facial tissue thickness

As above-mentioned, we use an averaged orthogonal direction, which is measured out of the local neighbourhood of the landmark. In our measure program, it is marked as “range”. The range has the metric unit millimetre and can be chosen freely by the user. For our measurements, we use a range between 2 and 3 millimetres. For estimate of the influence of different ranges on the facial thickness, we measured all landmarks on a random skull with the ranges 2 and 3 to calculate the range of the facial tissue thickness.

3.3.3 Investigation of facial thickness movement in lying and standing body posture

The determination of the facial soft-tissue thickness in our experiment as in other experiments before is done with lying persons and with deceased lying person respectively. Whereas the reconstruction of the face and head should be image a head in an erectly position. So, it is a question in which dimension a soft tissue movement takes place with a lying and standing person, depending to age, BMI and sex and which effects can be expected. If a clear dislocation of the facial tissue thickness appears, we have to discuss a use of a correction factor.

Due to these facts, we started a test series at living persons in cooperation with the Institute of Dermatology, Venerology and Allergology of the University of Saarland to measure the facial soft tissue thickness based on ultra-sound.

At present time there are only measurements of three probands, two men and one woman, available.

3.3.4 Investigation of the influence of post mortal changing on facial soft tissue thickness

Only because of the possibility of a facial measurement with data out of imaging methods an inclusion of living persons is possible. The measures made with manual methods with use of a needle or dental drill were carried out only on deceased persons.

For investigation of the influence of the early post mortal change on facial soft tissue thickness, we started a second test series. We determined the facial soft tissue thickness of three deceased persons until the fourth post mortal day with a soot-blackened needle at the above mentioned landmarks.

It is about three women aged between 22 and 65 years with a nutritional status between slim and corpulent. The deceased persons were transported directly to the Institute of Pathology at the University of Saarland and were cooled the whole period at four degree Celsius.

4 Results

4.1 Frequency Distribution

In the classification of the probands by sex and BMI there are resulting six different groups with the following distribution (Tab. 1).

Tab. 1: Frequency distribution of the researched individuals with partition after Sex and BMI

Group	1.1	1.2	1.3	2.1	2.2	2.3
Definition	Men with a BMI until 19	Men with a BMI between 20 and 25	Men with a BMI of 26 or larger	Women with a BMI until 19	Women with a BMI between 20 and 25	Women with a BMI of 26 or larger
Number	4	35	38	9	31	18

The facial soft tissue thickness above all landmarks of all 135 data-scans is measured separately by the above-mentioned method. The individual measure point is only included if the anatomical position on the skull is correctly displayed. This leads to the fact, that some measure points were measured infrequently or were even not measured as the measure points SubM2 and SupraM2. The resulting frequency distribution is shown in table 2.

Tab. 2: Frequency distribution of the measured landmarks in all groups

		Group 1.1	Group 1.2	Group 1.3	Group 2.1	Group 2.2	Group 2.3
Unilateral							
Supraglabella		4	34	35	9	31	15
Glabella		4	33	38	9	31	18
Nasion		4	35	36	9	30	18
End of Nasals		1	21	17	4	13	7
Mid-Philtrum		4	19	21	2	15	5
Upper-Lip-Margin		0	5	6	1	5	1
Lower-Lip-Margin		1	5	3	0	3	1
Chin-lip Fold		1	5	4	0	4	1
Mental Eminence		0	3	4	0	2	1
Beneath Chin		0	1	1	0	2	1
Bilateral							
Frontal Eminence	Right	3	33	35	9	31	18
	Left	4	34	36	9	31	18
Supraorbitale	Right	4	34	36	9	29	18
	Left	4	35	38	9	30	18
Suborbitale	Right	4	31	34	7	24	15
	Left	4	31	34	7	25	16
Lateral Orbit	Right	4	31	38	9	27	17
	Left	4	32	38	9	27	17
Zeugmatic Arch	Right	4	32	37	9	28	17
	Left	4	30	38	9	29	18
Supraglenoid	Right	4	30	38	9	29	16
	Left	4	29	37	9	29	18
Gonion	Right	0	5	3	0	4	1
	Left	0	5	3	0	4	1
Occlusial Line	Right	0	7	6	1	5	0
	Left	0	7	6	1	5	0

In doing so, in **group 1.1** the soft tissue thickness above the unilateral landmarks Upper Lip Margin, Mental Eminence, Beneath Chin as well as above the bilateral landmarks Gonion and Occlusial Line on both sides could not be measured. All other landmarks were measured between one and four times. In **group 1.2** and **group 1.3** the measurement above all landmarks is possible at which the frequency varies between 1 and 35 in **group 1.2** and between 1 and 38 in **group 1.3**

In **group 2.1** the soft tissue thickness above the unilateral landmarks Lower Lip Margin, Chin-Lip Fold as well as the bilateral landmark above the Gonion on both sides could not be measured. In **group 2.3** the soft tissue thickness above the bilateral point Occlusial Line is not applicable on both sides. **In group 2.1** all other landmarks were measured between 1 and 9 times and in group 2.3 between one and eighteen times. In **group 2.3** the measurement above all landmarks is possible, at which the frequency varies between 2 and 31 measurements.

4.2 Soft tissue thickness values

The facial soft tissue thickness is ascertained in the above-mentioned method at all possible landmarks of the 135 heads with a choice of range between two and three millimetres. The metric unit of the facial soft tissue thickness is also millimetre. Mean values, standard derivation as well as minimal- and maximalvalues are ascertained (Tab. 3).

Tab. 3: Facial soft tissue thickness in millimetre of all groups

Group **Landmark**	**1.1** Mean value Standard deviation Min.-max.	**1.2** Mean value Standard deviation Min.-max.	**1.3** Mean value Standard deviation Min.-max.	**2.1** Mean value Standard deviation Min.-max.	**2.2** Mean value Standard deviation Min.-max.	**2.3** Mean value Standard deviation Min.-max.
Unilateral						
Supraglabella	**3,35** 0,59 2,73–4,15	**3,82** 0,92 1,86–5,71	**4,64** 1,19 2,06–6,77	**3,77** 1,11 1,91–5,55	**4,37** 0,80 3,07–6,26	**5,65** 1,46 3,17–9,73
Glabella	**5,23** 0,14 5,03–5,36	**5,09** 0,95 2,99–6,9	**5,97** 1,39 2,76–8,66	**4,63** 1,20 2,65–6,02	**5,13** 0,75 2,98–6,62	**6,18** 1,79 3,50–11,47
Nasion	**6,16** 1,65 4,89–8,49	**6,42** 1,22 3,91–9,95	**7,06** 1,59 3,32–10,31	**5,33** 1,63 3,00–7,35	**5,76** 0,98 2,49–7,11	**6,60** 1,89 4,56–12,04
End of Nasals	**1,26** 0 1,26–1,26	**2,28** 0,53 1,34–3,19	**2,14** 0,46 1,53–3,15	**1,93** 0,76 1,29–2,93	**2,19** 0,78 1,45–4,27	**2,92** 1,03 1,90–4,32
Mid-Philtrum	**12,74** 2,60 9,16–15,42	**13,06** 2,80 8,74–19,92	**14,80** 1,82 11,54–19,49	**12,55** 3,15 10,32–14,79	**13,53** 4,39 8,38–26,96	**13,39** 1,62 11,54–15,24
Upper Lip Margin		**11,45** 2,32 9,04–14,15	**13,96** 2,62 11,16–18,93	**11,66** 0 11,66–11,66	**11,01** 2,09 7,74–13,00	**12,48** 0 12,49–12,49

Group **Landmark**	**1.1** Mean value Standard de- viation Min.-max.	**1.2** Mean value Standard de- viation Min.-max.	**1.3** Mean value Standard de- viation Min.-max.	**2.1** Mean value Standard de- viation Min.-max.	**2.2** Mean value Standard de- viation Min.-max.	**2.3** Mean value Standard de- viation Min.-max.
Lower Lip Margin	**12,70** 0 12,71–12,71	**10,79** 1,09 9,45–12,46	**12,83** 0,86 11,95–13,69		**11,16** 2,50 9,08–13,95	**11,75** 0 11,75–11,75
Chin-Lip Fold	**12,95** 0 12,96–12,96	**11,46** 1,09 10,30–12,77	**14,10** 1,73 11,89–16,11		**10,19** 1,99 8,69–13,09	**12,15** 0 12,16–12,16
Mental Eminence		**7,64** 1,18 6,48–8,85	**12,16** 1,31 10,29–13,36		**8,71** 3,73 6,07–11,35	**10,62** 0 10,63–10,63
Beneath Chin		**3,41** 0 3,41–3,41	**9,72** 0 9,72–9,72		**5,80** 4,47 2,64–8,97	**9,15** 0 9,15–9,15
Bilateral						
Frontal Eminence Left	**3,77** 0,43 3,44–4,39	**4,17** 1,12 1,89–6,89	**5,29** 1,47 1,77–8,73	**4,54** 1,46 2,41–7,05	**4,64** 0,93 2,72–6,47	**6,08** 1,60 4,24–10,89
Frontal Eminence Right	**3,93** 0,88 3,02–4,80+	**4,21** 1,13 2,18–6,83	**5,28** 1,45 1,98–8,66	**4,31** 1,21 2,19–6,63	**4,76** 0,77 3,12–6,67	**6,02** 1,57 3,92–9,59
Supraorbitale Left	**5,64** 0,86 4,64–6,67	**5,59** 1,29 2,99–8,78	**6,51** 1,39 2,54–9,29	**5,09** 1,34 3,31–7,39	**5,45** 1,15 3,21–8,01	**6,28** 1,93 3,14–11,71
Supraorbitale Right	**5,60** 0,43 5,16–6,18	**5,57** 1,88 3,93–8,45	**6,71** 1,38 3,62–10,18	**5,02** 1,19 3,54–7,08	**5,44** 1,10 3,27–8,45	**6,60** 2,08 3,41–12,93
Suborbitale Left	**4,44** 2,04 2,45–7,31	**5,13** 2,51 1,55–11,18	**7,08** 2,39 1,68–12,25	**5,72** 2,16 2,09–8,06	**5,73** 2,20 2,45–10,25	**11,16** 5,19 4,51–26,47
Suborbitale Right	**4,22** 1,61 2,74–6,46	**4,86** 2,16 2,04–10,18	**7,30** 2,46 1,60–13,64	**5,52** 1,96 1,90–7,60	**5,92** 2,33 2,17–10,05	**10,88** 5,31 4,39–26,52
Lateral Orbit Left	**5,24** 1,39 3,38–6,42	**5,45** 2,15 2,8–11,0	**7,55** 2,73 2,08–15,63	**6,00** 1,81 3,44–8,54	**6,21** 2,00 2,75–11,37	**10,65** 4,30 5,79–25,45
Lateral Orbit Right	**5,21** 1,07 3,68–6,2	**5,18** 1,85 3,01–9,84	**7,32** 2,11 1,85–11,08	**6,20** 1,59 4,11–8,34	**6,38** 1,95 2,80–9,99	**10,33** 4,28 5,14–24,78
Zygomatic Arch Left	**8,27** 0,49 7,79–8,96	**7,47** 1,83 4,74–12,28	**11,38** 3,98 4,44–24,56	**7,65** 2,23 5,18–11,98	**8,04** 2,03 3,57–11,19	**15,34** 6,04 9,67–33,20
Zygomatic Arch Right	**8,01** 0,73 7,38–8,91	**7,63** 1,89 4,78–12-75	**11,01** 2,93 4,21–16,17	**7,28** 1,88 4,69–10,19	**8,23** 2,00 3,51–13,11	**14,45** 6,84 7,67–34,81
Supraglenoid Left	**12,31** 1,73 10,07–13,94	**13,06** 2,01 8,37–17,31	**17,23** 3,83 8,37–28,54	**10,77** 3,04 6,34–15,88	**10,95** 2,06 7,06–15,98	**19,60** 8,08 12,17–47,21
Supraglenoid Right	**11,55** 2,25 9,48–14,01	**14,11** 2,78 7,79–20,53	**17,38** 2,97 10,11–23,23	**10,09** 2,94 5,43–15,54	**12,25** 2,15 8,10–17,50	**20,06** 7,28 11,33–42,41

Group **Landmark**	**1.1** Mean value Standard de- viation Min.-max.	**1.2** Mean value Standard de- viation Min.-max.	**1.3** Mean value Standard de- viation Min.-max.	**2.1** Mean value Standard de- viation Min.-max.	**2.2** Mean value Standard de- viation Min.-max.	**2.3** Mean value Standard de- viation Min.-max.
Gonion Left		**13,14** 2,01 11,08–16,48	**29,25** 4,39 25,69–34,16		**12,15** 2,13 9,80–14,64	**18,32** 18,32–18,32
Gonion Right		**13,62** 3,36 9,96–17,62	**34,17** 6,34 26,95–38,85		**13,86** 1,84 11,65–16.00	**19,35** 19,36–19,36
Occlusial Line Left		**20,66** 3,46 15,06–25,43	**28,82** 4,09 21,07–31,72	**18,09** 18,10–18,10	**20,64** 3,11 17,05–24,26	
Occlusial Line Right		**22,55** 3,60 16,60–25,81	**29,63** 5,40 20,53–35,93	**17,28** 17,29–17,29	**23,17** 2,10 20,96–25,58	

The facial soft tissue thickness is measured four-digits after the comma that results in an accuracy of $^{1}/_{10000}$ millimetre.

The standard deviation of the separate measure points lies between 0,14451 mm above the landmark Glabella and 8,08569 mm above the landmark Supraglenoid left. Thus, most of the values have a standard deviation between 0,14451 mm and 4,47944 mm.

Outliers result in **group 3.2** for the following measure points: Suborbitale left (5,19957 mm) and right (5,31968 mm), Zygomatic Arch left (6,04319 mm) and right (6,84023 mm) as well as Supraglenoid left (8,08569 mm) and right (7,28922 mm). In **group 1.3** the measure point Occlusial Line right (5,40143 mm) and Gonion right (6,34615 mm) shows a higher standard deviation.

4.3 Error Analysis

4.3.1 Investigation of the reproducibility

To ascertain the reproducibility of our method, we measured a skull ten times with a single investigator. Out of this test series, we calculated the mean value, standard deviation and minimal- and maximal values (Tab. 4).

Tab. 4: Reproducibility of the facial soft tissue thickness in mm

Landmark	Mean value	Standard deviation	Minimum	Maximum
Unilateral				
Supraglabella	3,49	0,17	3,28	3,76
Glabella	6,28	0,18	6,03	6,68
Nasion	6,80	0,07	6,70	6,87
End of Nasals	2,57	0,03	2,54	2,65
Mid-Philtrum	15,20	0,35	14,55	15,82

Landmark	Mean value	Standard deviation	Minimum	Maximum
Upper Lip Margin	12,17	0,37	11,58	12,79
Lower Lip Margin	12,71	0,22	12,29	12,92
Chin-Lip Fold	12,75	0,03	12,70	12,79
Mental Eminence	10,58	0,26	10,20	10,96
Bilateral				
Frontal Eminence Left	3,63	0,22	3,44	4,16
Frontal Eminence Right	4,33	0,07	4,25	4,47
Supraorbitale Left	5,11	0,21	4,73	5,42
Supraorbitale Right	5,08	0,24	4,58	5,46
Suborbitale Left	5,08	0,13	4,90	5,35
Suborbitale Right	3,27	0,12	3,14	3,58
Lateral Orbit Left	5,46	0,14	5,24	5,62
Lateral Orbit Right	5,04	0,37	4,46	5,38
Zygomatic Arch Left	8,06	0,06	7,98	8,17
Zygomatic Arch Right	7,33	0,14	7,21	7,72
Supraglenoid Left	11,65	0,03	11,59	11,70
Supraglenoid Right	11,28	0,13	11,15	11,52
Gonion Left	22,26	0,03	22,19	22,30
Gonion Right	19,07	0,18	18,79	19,54
Occlusial Line Left	12,26	0,35	11,87	13,05

Thus, a maximal standard deviation of 0,37688504 mm above the landmark Upper Lip Margin appears. The minimal standard deviation appears above the landmark Chin-Lip Fold with 0,03018451 mm.

4.3.2 Influence of different ranges on facial tissue thickness

The influence of the usage of different ranges on facial soft tissue thickness is shown in table 5. Here, the difference between the minimum range at two millimetres and the maximum range at three millimetres is ascertained as the range.

Tab. 5: Influence of different ranges on facial soft tissue values

Landmark	Range 2,0 mm	Range 3,0 mm	Difference
Unilateral			
Supraglabella	3,65	3,64	0,01
Glabella	6,34	6,29	0,04
Nasion	6,71	6,75	0,03
End of Nasals	2,60	2,54	0,06
Mid-Philtrum	11,23	11,29	0,05
Upper Lip Margin	12,33	12,12	0,21
Lower Lip Margin	11,58	11,65	0,06
Chin-Lip Fold	12,68	12,69	0,00
Mental Eminence	9,58	9,56	0,01
Bilateral			
Frontal Eminence Left	4,37	4,36	0,00
Frontal Eminence Right	4,40	4,39	0,00
Supraorbitale Left	5,28	5,38	0,09
Supraorbitale Right	4,88	4,84	0,04
Suborbitale Left	4,87	4,91	0,03
Suborbitale Right	3,26	3,28	0,02
Lateral Orbit Left	6,12	5,90	0,22
Lateral Orbit Right	5,38	5,47	0,08
Zygomatic Arch Left	7,97	7,95	0,02
Zygomatic Arch Right	7,23	7,24	0,01
Supraglenoid Left	11,59	11,59	0,00
Supraglenoid Right	11,44	11,57	0,13
Gonion Left	22,29	22,30	0,01
Gonion Right	19,11	19,05	0,06
Occlusial Line Left	12,38	12,35	0,03
Occlusial Line Right	17,31	17,56	0,24

Therefore, a maximal difference is resulting with 0,2493 mm between a range of 2 millimetres and a range of 3 millimetres.

4.3.3 Investigation of the influence of early post-mortal change on facial thickness

Due to our small sample size it is impossible for us to give any significant evidence for the influence of early post mortal change on facial thickness. But, relating to our already measured values of facial soft tissue thickness it can be shown that most of the measured soft tissue thickness is increasing and only a few of those are declining.

4.3.4 Investigation of facial thickness movement in lying and standing body posture

Due to our small sample size it is impossible for us to give any significant evidence for the influence of facial thickness movement in lying and standing body posture. But, depending to our already measured values of the facial soft tissue thickness it can be shown that there is a clear trend for bilateral measure points to move depending on body posture. As in point 4.3.3., further investigations have to follow to give a significant statistical conclusion.

5 Discussion

For a long time the attempt was made to identify an unknown person with the help of the reconstructed face [13], [14]. The facial soft tissue thickness is the base for every manual or virtual facial reconstruction [3], [5]. So, a broad, in age, sex and constitution type separated data collection seems to be an important point. Due to the constant changing influences on the middle European population in consequence of the changing alimentation and working practice, it makes sense for us, to collect again data about the facial tissue thickness.

So we started a new test series with the objective to develop a measure method that is able to create on every bony structure the exactly orthogonal distance from skull to skin, based on virtual data.

The preparation of our data to the measure program, the separated display of the skin and skull surface and the reduction of data by deleting all non-needed structures were carried out with the computer program AMIRA®. With the help of this program, most of the current Ct-Scans can be arranged.

The disadvantage of using data from Ct-Scans is the exposure of radiation for living probands. Hence, we recommend to use post mortal scans of deceased persons, or better, already existing scans made for diagnostic purposes of living persons. If done so, one has to mind that the data scans made for diagnostic purposes do not show the whole skull, but rather parts of the skull, which is examined. These are usually the calotte, the Para nasal sinus and the soft parts of the throat. This can lead to problems in the statistical analysis later.

Due to this, we used in our initially solely data of post mortal Ct-Scans test series. The strict selection criteria of the Ct-Scans make assure that changing or movement of the facial soft tissue thickness through external influence or foreign bodies are nearly impossible.

A further problem in using this method is the incomplete display of the boundaries of the layers that are resulting from the layer thickness of the Ct-Scans. Hence, it was impossible for us to locate every measure point on every skull. This leads to an unsteady frequency distribution and even more, forced us to renounce the measure points Sub M_2 and Supra M_2 because we only recognized measure points that ensure a safe measurement.

The selection of the measure points occurs according to the landmarks described by K. T. Taylor [13]. In line with the analysis of the literature a lot of different measure points for ascertainment of the facial soft tissue thickness can be found [8], [9], [10], [14], at which K. T. Taylor [13] gives a well and balanced assortment. Due to the virtual mode of operation, we had to modify some landmarks as Supraglabella, Nasion, End of Nasals, Upper Lip Margin, Lower Lip Margin, Frontal Eminence, Supraorbitale, Suborbitale, Lateral Orbit and Zygomatic Arch.

To label our measure points we use the same landmark names as K. T. Taylor [13] does. This guarantees a good multidisciplinary communication.

The examined persons are separated according to K. T. Taylor [13] depending on sex, ethnical origin and nutritional condition to allow a comparison to other authors. A classification depending on age is possible [9], [11], but is not discussed here. Some authors abandon the classification depending on nutritional condition [10], others give weight classes [9], [11] or a classification according to the constitution type [14].

The classification into BMI groups seems the best way for us to represent the nutritional condition. As shown in Tab. 1, men and women with a BMI under 20 are underrepresented in our study. If this frequency distribution represents the middle European population or if it is influenced by other factors, like the small sample size, this cannot be answered clearly.

The measure values are ascertained with an accuracy of $^1/_{10.000}$ mm. Because such a high accuracy is not necessary in facial reconstruction, we recommend rounding the values to $^1/_{100}$ mm.

The standard deviation of most of the points varies between 0,14 mm and 4,48 mm. Outliers can be found mainly in the group of corpulent women as well as in the group of corpulent men, but there in smaller numbers. The fact that these groups include extremely corpulent probands, with a BMI of 46 for example, could be the answer to this question. Due to this, a classification of the BMI above 25 would make sense.

To estimate the influence of the error to our measurement values we analyse the source of error in conjunction with our measure program. This analysis concerns the intra individual variability in multiple measurements with a single investigator and the method-relating variability that is resulting from the small variation of the range.

Thus, one has to consider that only source of error inside the measure program is the small deviation in choosing the measure points. All other sources of error are mostly eliminated by the independent program sequence. Furthermore, due to the independent program sequence, the appearing errors are independent from the length of the measurement distance.

Because the user can choose the range freely, differences in the measure values developed from choosing different ranges are not measurement errors narrower sense. During our measurements, we used ranges between 2 mm and 3 mm according to the bony structures of the landmark. The smaller this range is chosen, the better does the computed orthogonal direction represent local surface detail, but also the more vulnerable is the computation to noisy or pathological data. The larger the range is chosen, the more robust is the computation of the orthogonal direction, but also the less the measure point represents the landmark. In consideration of this aspect, the range was ascertained for each individual landmark. An example of this estimation shows figure 10 and 11.

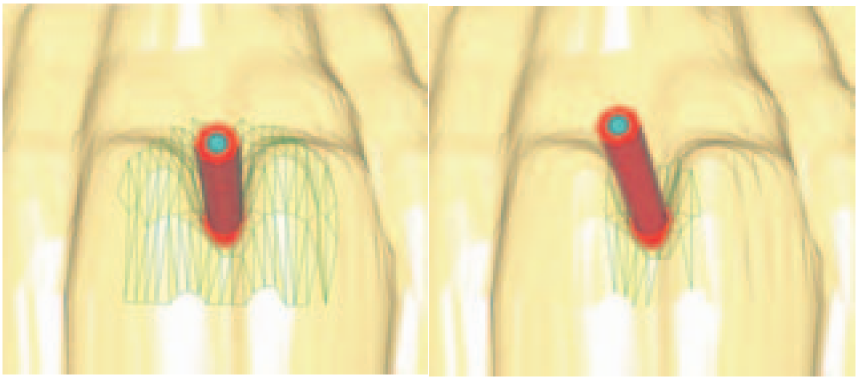

Fig. 10 and **11** Ascertaining the range on rough surfaces

To estimate the error depending on the use of slightly different ranges, the facial tissue thickness above all landmarks is ascertained with a range of 2 mm and 3 mm. There, a maximal difference of 0,25 mm results which lies in the lower area of the standard deviation of the original measure values and maximal standard deviation of the intra individual error.

Among other sources of error depending on the measure program, external factors influence the resulting measure values as well. This concerns the early post mortal change of the facial tissue thickness and the posture depending movement of facial tissue thickness. It is too early to give any clear statement about these two parameters. So, we confine ourselves to give tendencies for these parameters. In the early post mortal days, the facial tissue thickness seems to increase for which the reason is not clear. Due to the exsiccosis and the absence of the muscle tonus we rather expected a decrease [1], [15].

Like other authors we found a posture depending on the movement of the facial tissue thickness especially on the bilateral measure points [1]. Thereby, corpulent bodies are showing a bigger sensitivity than normal or slender bodies. A sure indicator for that is the pre auricular bulge in combination with a descent of the jowls to the base. Due to this, in further test series when using lying probands, a correction factor should be used.

Altogether, the presented measure method is a good, reproducible, orthogonal and only lightly influenced method, which allows a measurement to all bony structures and the depending tissue thickness. It just needs an accurate choice and preparation of the data.

Additionally, we are developing other methods of measuring the facial soft tissue thickness with the program.

Bibliography

[1] C. Wilkinson, Forensic Facial Reconstruction. Cambridge: University Press, 2004.

[2] Krogman W. M., The Human Skeleton in Forensic Medicine. Springfield: Charles C. Thomas, 1986.

[3] V. M. Phillips, N. A. Smuts, Facial reconstruction: Utilization of computerized tomography to measure facial tissue thickness in a mixed racial population. Forensic Science International, vol. 83, pp. 51–59, 1996.

[4] G. F. Walker, The Computer and the Law: Coordinate Analysis of Skull Shape and Possible Methods of post mortem Identification, Journal of forensic science, vol. 20, pp. 357–366,1975.

[5] P. Vanezis, M. Vanezis, G. McCombe, Facial Reconstruction using 3-D Computer Graphics, Forensic science international, vol. 108, pp. 81–95,1999.

[6] R. M. George, The lateral craniographic method of facial reconstruction. Journal of Forensic Sciences, vol. 32, pp. 1305–1330, 1987.

[7] K. Kähler, J. Haber, H. P. Seidel, Reanimating the Dead: Reconstruction of expressive Faces from Skull Data, ACM SIGGRAPH Conference Proceedings.

[8] K. Suzuki, On the Thickness of the Soft Parts of the Japanese Face. Journal of Anthropological society of Nippon, vol. 60, pp. 7–11,1948.

[9] I. Robetti, M. Iorio, V. Mascaro, Die Stärke des Weichgewebes des Gesichtes zur Personenidentifizierung. Zeitung für Rechtsmedizin, vol. 89, pp. 119–124, 1982.

[10] J. S. Rhine, H. R. Campell, Thickness of Facial Tissues in American Blacks. Journal of Forensic Sciences, vol. 25, pp 847–858, 1980.

[11] R. P. Helmer, Schädelidentifizierung durch elektronische Bildmischung. Heidelberg: Kriminalistik Verlag, 1984.

[12] R. P. Helmer, F. Koschorek, B. Terwey, T. Frauen, Dickenmessung der Gesichtsweichteile mit Hilfe der Kernspin-Tomographie zum Zwecke der Identifizierung. Archiv für Kriminologie, vol. 177/178, pp. 139–150, 1986.

[13] K. T. Taylor, Forensic Art and Illustration. Boca Raton, London, New York, Washington D. C.: CRC Press, 2001.

[14] M. Y. Iscan, R. P. Helmer, Forensic Analysis of the Skull. New York, Chichester, Brisbane, Toronto, Singapore: Wiley-Liss, 1993.

[15] W. Weber, K. Munzert, Postmortale Exsikkation der Fingerbeeren – Ergebnisse systematischer quantitativer und qualitativer experimenteller Untersuchungen, Zeitschrift für Rechtsmedizin, vol. 96, pp. 279–289, 1986.

Computergestützte Weichteildickenmessung an CT-Aufnahmen des Schädels von verstorbenen Personen

D. Bellmann[1], Th. Fuchs[2], A. Weidenbusch[1], J. Haber[2], Th. Georg[3], K. M. Stein[4] und J. Wilske[1]

[1] Institut für Rechtsmedizin der Univ. des Saarlandes, Homburg
[2] Max Planck Institut für Informatik, Saarbrücken
[3] Institut für Medizinische Biometrie, Epidemiologie und Medizinische Informatik, Universität des Saarlandes, Homburg
[4] Institut für Rechtsmedizin der Universität Heidelberg

1 Zusammenfassung

Die Gesichtsrekonstruktion an skelettierten Schädeln zur Identifikation unbekannter Personen stützt sich sowohl bei manuellen als auch bei computergestützen Verfahren auf bekannte Weichteildickenwerte im Gesichtsbereich. Die in der Literatur bereits vorhandenen Weichteildicken unterliegen dabei z. T. großen Schwankungen. Des Weiteren muss damit gerechnet werden, dass auf Grund der insbesondere in den letzten Jahrzehnten zu beobachtenden Veränderungen in der Ernährung der Bevölkerung in Mitteleuropa die bereits vorliegenden Weichteildicken die Gegebenheiten nicht mehr korrekt widerspiegeln.

Aus diesem Grund wurde eine Bestimmung der Gesichtsweichteildicke unter Einsatz eines neu entwickelten computergestützten Messverfahrens angestrebt, welches eine reproduzierbare, senkrecht zur knöchernen Oberfläche durchführbare Messung erlaubt.

Als Untersuchungsgut dienen 135 CT-Datensätze verstorbener Personen des kaukasoiden Formenkreises.

Ausgangspunkt der Entwicklung der hier vorgestellten Messmethode ist die Tatsache, dass eine Messung des Abstandes von der Hautoberfläche zu darunter befindlichen knöchernen Strukturen aus CCT-Datensätzen möglich ist. Hierbei können unter Verwendung eines handelsüblichen Programms die Oberflächen der Haut und des Knochens getrennt dargestellt und in anatomisch korrekter Position aufeinander projiziert werden. Die Messung des jeweiligen Abstandes an beliebigen Punkten kann dann durch ein eigens dafür hergestelltes Programm entweder auf die bisher übliche Art und Weise senkrecht zur Knochenoberfläche oder in anderweitiger Form erfolgen.

Die sich anhand dieser Messmethode ergebenden Weichteildickenwerte werden durch intraindividuelle Fehler des Untersuchers bei der Lokalisation der „Landmarks“ und durch die unterschiedliche Auswahl programmintern wählbarer „Ranges“ nur gering beeinflusst.

Größeren Einfluss haben externe Faktoren wie die Veränderung der Weichteildicke in der frühen postmortalen Phase und die Verschiebung der Weichteile infolge einer Lageänderung, was evtl. die Einführung von Korrekturfaktoren bedingen könnte.

2 Einleitung

Eine Gesichtsrekonstruktion wird in der forensischen Arbeit immer dann nötig, wenn die Identität eines unbekannten Toten mit teilweise oder vollständig skelettiertem Schädel weder durch den Zahnstatus noch durch DNA-Untersuchungen verifiziert werden kann. Derartige Rekonstruktionen werden auch international noch oft durch Auftragen von Plastilin, Ton [1], [2] oder Wachs vorgenommen.

Dieses Vorgehen erfordert neben künstlerischem Verständnis einen hohen Zeitaufwand. Computergestütze Verfahren [3], [4], [5], [6] zeichnen sich demgegenüber durch eine weitestgehend einfache Bedienbarkeit sowie durch einen deutlich reduzierten Zeitaufwand aus. Bei einigen Verfahren, wie bei dem durch das Max-Planck-Institut entwickelte Programm [7], besteht die Möglichkeit, jederzeit verschiedene Variationen hinsichtlich Konstitutionstyp und Mimik in eine bereits fertiggestellte Rekonstruktion rasch einzufügen.

Die Basis einer derartigen Software bilden die Weichteildickenwerte von Personen unterschiedlicher ethnischer Herkunft, unterschiedlicher Konstitutionstypen sowie verschiedener Altersklassen. Bereits vorhandene Angaben zu den Weichteildicken wurden zum überwiegenden Teil mittels manueller Methoden [8], [9], [10] erhoben oder an Hardcopies bildgebender digitaler Verfahren [11], [12] ausgemessen. Eine vollständige und genaue Orientierung sowie senkrechte Ausrichtung der Messstrecke zur knöchernen Oberfläche bereitet hier immer wieder Schwierigkeiten. Weiterhin erscheint es uns möglich, dass die bereits vorliegenden Weichteildicken die Gegebenheiten nicht mehr korrekt widerspiegeln, nachdem auf Grund der insbesondere in den letzten Jahrzehnten zu beobachtenden Verbesserung der Ernährung der Bevölkerung in Mitteleuropa mit Veränderung gerechnet werden muss. Aus diesen beiden Gründen wurde die Entwicklung eines computergestützten Messverfahrens der Gesichtsweichteildicke angestrebt, welches eine reproduzierbare, senkrecht zur knöchernen Oberfläche durchführbare Messung erlaubt.

3 Untersuchungsgut und Methodik

3.1 Untersuchungsgut

Es werden aus dem Institut für Rechtsmedizin in Heidelberg CT-Datensätze von 135 Köpfen verstorbener Personen des kaukasoiden Formenkreises im Alter von 16 bis 89 Jahren ausgewählt. Darunter befinden sich 58 Frauen und 77 Männer mit einem Body-Mass-Index zwischen 16 und 46.

Bei dem Computertomographen handelt es sich um das Gerät Somatom Plus S der Firma Siemens, Baujahr 1989. Die Datenerfassung im Kopfbereich erfolgt in Spiral-Technik mit einer Schichtdicke zwischen 3 mm und 5 mm.

Der von uns untersuchte Personenkreis wird zunächst nach Geschlecht und BMI in insgesamt 6 Gruppen unterteilt. (Tab. 1).

3.1.1 Auswahlkriterien der Datensätze

Zur Auswahl der 135 Datensätze werden folgende Kriterien verwendet:

1.) Möglichst geringes Auftreten von radiologischen Artefakten, insbesondere Überlagerungen von knöchernen Strukturen durch zahntechnische Arbeiten.

2.) Geringe Leichenliegezeit vor der CT-Erfassung des Kopfes sowie möglichst exakte Lagerung der Köpfe auf der Hinterhauptsmitte. Leichen mit beginnender Dunsung der Gesichtsweichteile oder Fäulnis sowie mit unsymmetrischer Lagerung des Kopfes oder mit Verformung der Gesichtsweichteile durch anliegende Fremdkörper (wie Kopfhörer, Kopfstützen etc.) und dadurch verursachter Verschiebung der Gesichtsweichteile zu einer Seite werden nicht in die Untersuchung einbezogen. Die Abschätzung dieser Gegebenheiten erfolgt anhand der dreidimensionalen Darstellung der Hautoberfläche in dem von uns verwendeten Programm AMIRA.

3.) Vollständigkeit des knöchernen Schädels und der Weichteilstrukturen. In Fällen von Polytrauma, Schädel-Hirn-Trauma, Maximaltrauma, Tötungsdelikten, Schussverletzungen u. ä. werden die Köpfe ebenfalls nicht in die Untersuchung einbezogen. Gleiches gilt für Datensätze von Köpfen mit Substanzdefekten, Rissen, Deformationen, Auflockerungen der Knochenmatrix, Asymmetrie der Hautoberfläche, an- oder einliegenden Fremdkörpern etc.

3.2 Methodik

3.2.1 Bearbeitung der Datensätze

Die CT-Datensätze liegen vollständig anonymisiert im Dicom-Format vor und werden im Programm AMIRA eingelesen. Im Programm selbst kann über eine Justierung des Dichtewertes für Haut und Knochen eine getrennte 3-dimensionale Darstellung der Hautoberfläche und des knöchernen Schädels – Isosurface – erreicht, und somit einer digitalen Bearbeitung zugänglich gemacht werden (Abb. 1 und Abb. 2).

amira®2005-Mercury Computer Systems www.mc.com/tgs

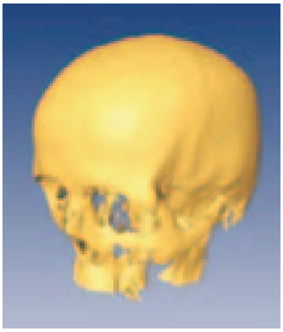

Abb. 1: Schädeloberfläche

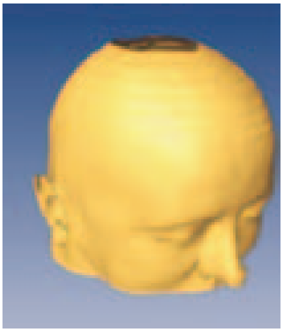

Abb. 2: Hautoberfläche

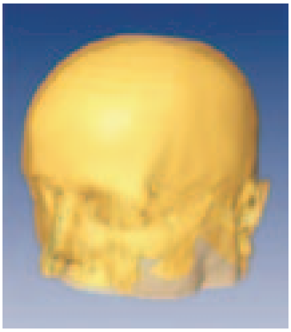

Abb. 3: Semitransparente Überlagerung

Die Dichtewerte zur optimalen Darstellung der Haut- und Knochenoberflächen variieren in einem geringen Umfang und werden durch manuelle Anpassung für jeden einzelnen Fall erneut bestimmt.

Nach Herstellung der 3-dimensionalen Abbilder von Haut und Knochen werden anhand der oben beschriebenen Auswahlkriterien die zur weiteren Verwendung geeigneten Datensätze ausgewählt. Eine Erleichterung dabei bildet die Möglichkeit der semitransparenten Überlagerung beider Oberflächen (Abb. 3).

Um einen für die weitere Bearbeitung geeigneten Umfang der Datensätze zu erreichen, werden alle knöchernen Strukturen und Weichteilanteile, die nicht zur späteren Messung der Weichteildicke benötigt werden, digital entfernt. Hierbei handelt es sich am häufigsten um Anteile der Schädelbasis, des Innenohres und der Nasennebenhöhlen. Eventuell auftretende radiologische Artefakte oder Fremdkörper werden ebenfalls verworfen.

Im Anschluss erfolgt eine Speicherung der einzelnen Datensätze nach Haut- und Knochenoberfläche getrennt im iv- („open-inventor") Format von AMIRA. Um einen einfachen Zugriff auf die Datensätze zu ermöglichen, werden diese codiert.

3.2.2 Codierung der Datensätze

Der von uns verwendete Code besteht aus Kürzeln für Geschlecht, Alter, Body-Mass-Index, die ethnische Herkunft, den Ort der CT-Datenerhebung, die abgebildeten Anteile des Schädels sowie die Erhebung postmortem, da für andere Studien auch intravital erhobene Datensätze zur Verfügung stehen. An letzter Stelle befindet sich ein Kürzel, aus welchem hervorgeht, ob es sich um einen Datensatz für die Haut oder für die knöchernen Schädelanteile handelt.

3.2.3 Messung der Weichteildicke

Zur Messung der Weichteildicke an spezifischen Messpunkten verwenden wir ein vom Max-Plank-Institut für Informatik entwickeltes Computerprogramm. Nach dem Laden des kompletten Datensatzes, bestehend aus Haut- und Knochenoberfläche, werden Haut und Knochen übereinander liegend in einem Graphikfenster angezeigt (Abb. 4). Das komplette Kopfmodell wird auf folgende Weise in ein zugrunde liegendes Koordinatensystem eingepasst:

– die yz-Ebene des Koordinatensystems ist die Sagittalebene des Kopfmodells,

– der Ursprung des Koordinatensystems fällt zusammen mit dem Landmark „Nasion".

Als nächstes spezifiziert der Benutzer die Position der Landmarks auf dem Schädelmodell (Abb. 5). Die Landmarks können überall auf dem Schädel aufgesetzt und ihre Position jederzeit korrigiert oder verändert werden. Für unvollständige Datensätze, etwa bei Schädelfragmenten, kann die Platzierung individueller Landmarks übersprungen werden, falls der dazugehörige Knochen im Datensatz nicht vorhanden ist.

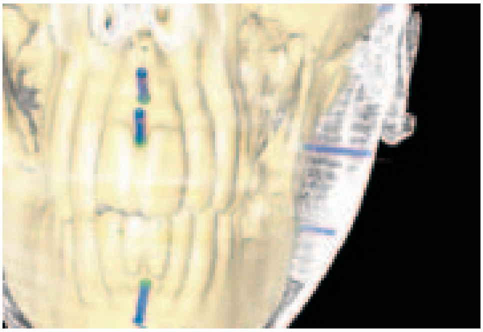

Abb. 4: Semitransparente Darstellung von Haut und Knochen

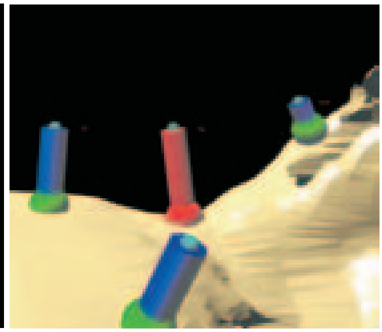

Abb. 5: Positionierung der Landmarks

Für jeden vom Benutzer spezifizierten Landmark misst das Programm die Distanz zwischen knöchernem Schädel und Haut (Abb. 6). Dabei wird die Distanz orthogonal zur Knochenoberfläche gemessen. In der Praxis ist die Bestimmung der orthogonalen Richtung (und die daraus resultierende Distanz) nicht immer hinreichend definiert. Sowohl verrauschte Eingabedaten, wie sie z. B. an den Schichtgrenzen bei CT-Scans vorliegen, als auch pathologische Fälle, wie z. B. Tumore, können die robuste Berechnung der orthogonalen Richtung an speziellen Landmarks beeinträchtigen. Daher verwenden wir eine gemittelte orthogonale Richtung, die über eine lokale Umgebung des Landmarks (im Bild grün dargestellt) auf der Schädeloberfläche berechnet wird (Abb. 7). Im Programm wird diese lokale Umgebung als „Range" in Millimetern angegeben. Dabei kann die Größe der Umgebung durch den Benutzer vorgegeben werden. Je kleiner die Umgebung gewählt wird, desto besser repräsentiert die errechnete orthogonale Richtung die lokale Oberfläche, aber auch desto anfälliger ist die Berechnung gegenüber verrauschten oder pathologischen Daten. Je größer die Umgebung gewählt wird, desto stabiler ist die Berechnung der orthogonalen Richtung. Nachdem die orthogonale Richtung berechnet wurde, wird der Abstand zwischen Knochen und Haut entlang dieser Richtung mit Hilfe eines Strahlenverfolgungsverfahrens (ray tracing) bestimmt. Bei dieser Technik wird ein virtueller Strahl von der Landmarkposition L auf dem knöchernen Schädel entlang der zuvor errechneten orthogonalen Richtung zur Haut „geschossen". Der Schnittpunkt P dieses virtuellen Strahls mit der Hautoberfläche wird benutzt, um die Weichteildicke d zu errechnen: $d := ||P - L||_2$.

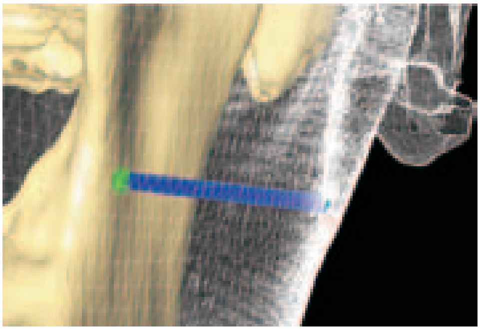

Abb. 6: Messung der orthogonalen Distanz zwischen Haut- und Knochenoberfläche

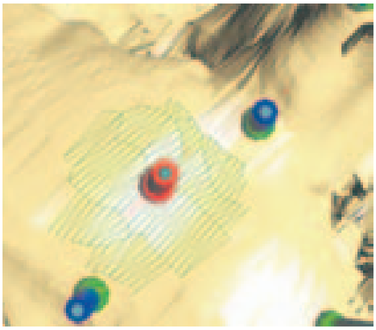

Abb. 7: Darstellung der Range

Der komplette Satz der Landmarks kann zusammen mit den korrespondierenden Weichteildicken und zusätzlichen Metadaten wie z. B. Geschlecht oder Alter für jeden Datensatz abgespeichert werden (Abb. 8, Abb. 9).

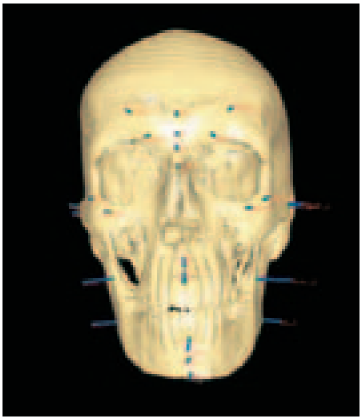

Abb. 8: Schädel mit Landmarks frontal

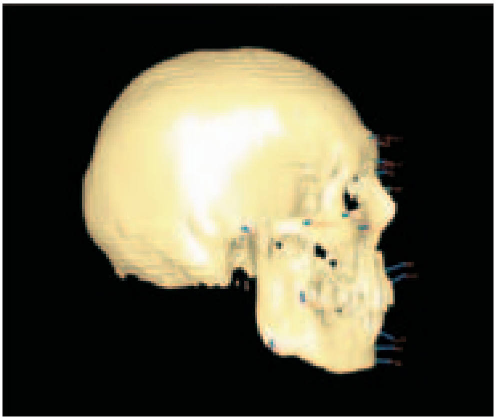

Abb. 9: Schädel mit Landmarks seitlich

Zusätzlich zu dieser „klassischen" Methode der Weichteildickenmessung entlang der orthogonalen Richtung in jedem Landmark, untersuchen wir zur Zeit die Anwendbarkeit anderer Messmethoden. Um die anfällige Berechnung der orthogonalen Richtung zu umgehen, könnte man die Weichteildicken z. B. an allen Gitterpunkten eines uniformen Volumengitters bestimmen, welches den kompletten Datensatz umfasst. Die resultierenden Daten lassen sich dabei jedoch nicht direkt mit traditionell gemessenen Daten vergleichen. Dennoch könnte es sich als vorteilhaft erweisen, die so gemessenen Daten für automatisierte Gesichtsrekonstruktionen zu verwenden, nachdem der Rekonstruktionsalgorithmus an diesen Datentyp angepasst wurde.

3.2.4 Auswahl der Landmarks

Bei der Auswahl der Landmarks werden 10 unilaterale und 8 bilaterale Landmarks berücksichtigt. In der Literatur trifft man hier auf eine stark variierende Auswahl, Benennung und Lokalisation von Messpunkten. In unserer Untersuchung werden die Landmarks in Anlehnung an das Buch von K. T. TAYLOR [13] „Forensic Art“ gewählt, wobei die Autorin als Quelle die Datensammlung nach RHINE [10] angibt. Die Messpunkte werden hinsichtlich ihrer Lokalisation entsprechend den Gegebenheiten leicht modifiziert.

3.2.4.1 Unilaterale Landmarks

Supraglabella: Über der Glabella, etwa auf Höhe der Frontal Eminence.

Glabella: Der prominenteste Punkt in der Mitte zwischen den Augenbrauenwülsten.

Nasion: Der Mittelpunkt der Sutur an der Grenze zwischen Os frontale und beiden Ossa nasalia. Da diese Sutur auch nach Aufarbeitung und 3 dimensionaler Darstellung des Schädels in AMIRA nicht sicher zu erkennen ist, wird hier der im Profil am weitesten zurückliegende Punkt des Nasensattels in der vorderen Körpermittellinie gewählt.

End of Nasals: Die vorderste Spitze beider Ossa nasalia. Da diese Struktur meist nur unvollständig zur Darstellung kommt, wird hier der am weitesten distal liegende Punkt beider Nasenbeine verwendet.

Mid-Philtrum: Direkt unterhalb der Spina nasalis anterior.

UpperLip Margin: Zwischen den beiden vorderen Schneidezähnen des Oberkiefers an der Zement-Zahnschmelz-Grenze. Da die Zement-Zahnschmelz-Grenze in AMIRA nicht mit ausreichender Deutlichkeit zur Darstellung kommt, wird dieser Landmark meist wenige Millimeter oberhalb der Zement-Zahnschmelz-Grenze gesetzt.

Lower Lip Margin: Zwischen den vorderen unteren Schneidezähnen, auf Höhe der Zement-Zahnschmelz-Grenze. Da die Zement-Zahnschmelz-Grenze in AMIRA auch hier nicht mit ausreichender Deutlichkeit zur Darstellung kommt, wird dieser Landmark meist wenige Millimeter unterhalb der Zement-Zahnschmelz-Grenze gesetzt.

Chin-Lip Fold: In der am weitesten zurückliegenden Einziehung der Profillinie zwischen Unterlippe und Kinnvorsprung in der vorderen Körpermittellinie.

Mental Eminence:	Der am weitesten vorspringende Punkt des Unterkiefers.
Beneath Chin:	Der am weitesten nach unten weisende Punkt des Unterkiefers in der vorderen Körpermittellinie.

3.2.4.2 Bilaterale Landmarks

Frontal Eminence:	Frontalhöcker auf beiden Stirnseiten. Auf Grund der unterschiedlichen Ausbildung dieser anatomischen Struktur und der nicht immer sicheren Lokalisation wird der Landmark in Projektion auf die vertikale Orbitamittellinie um die Hälfte der Orbitahöhe über dem oberen Orbitarand gesetzt.
Supraorbitale:	Über der höchsten Stelle des knöchernen Orbitadaches.
Suborbitale:	An der tiefsten Stelle des knöchernen Orbitadaches.
Lateral Orbit:	Unterhalb des lateralsten Punktes der Orbita hier auf Höhe des Oberrandes des Jochbogens.
Zygomatic Arch:	Die Mitte des Jochbogens.
Supraglenoid:	Über und vor dem Eingang des äußeren Gehörgangs.
Gonion:	Der am weitesten lateral gelegene Punkt am Unterkieferwinkel.
Occlusal Line:	Über dem Unterkieferast in Höhe der Bisslinie der Zähne.

3.3 Fehleranalyse

3.3.1 Untersuchung zur Reproduzierbarkeit

Zur Quantifizierung der Schwankungen, die sich bei der Lokalisation der einzelnen Landmarks und der daraus resultierenden Weichteildickenwerte bei einem Untersucher ergeben, wird ein zufällig ausgewählter Kopf insgesamt 10-mal von einem Untersucher nach der oben aufgeführten Methode vermessen.

3.3.2 Einfluss unterschiedlicher Ranges auf die Weichteildickenwerte

Wie bereits oben ausgeführt, verwenden wir eine gemittelte orthogonale Richtung, die über einer lokalen Umgebung des Landmarks auf der Schädeloberfläche berechnet wird. Im Programm wird diese lokale Umgebung als „Range“ in Millimetern angegeben und kann vom Untersucher frei gewählt werden. Die Weichteildicken in unserer Versuchsreihe werden mit einer Range zwischen 2 und 3 mm bestimmt. Zur Abschätzung der Beeinflussung der Weichteildickenwerte durch Änderungen der Range werden an einem Schädel alle Weichteildickenwerte für eine Range von 2 mm und von 3 mm gemessen und die Differenz berechnet.

3.3.3 Untersuchung zu Gesichtsweichteilverschiebungen in liegender und aufrechter Körperposition

Die Bestimmung der Gesichtsweichteildicke erfolgt in unserem Versuch wie auch bei einigen anderen Versuchsreihen in der Literatur [10], [9] an der liegenden Person bzw. aus Datensätzen, die an liegenden Personen erhoben wurden. Die Rekonstruktion der Gesichter an skelettierten Schädeln hingegen soll anhand der so gewonnenen Dickenwerte einen Kopf in aufrechter Position abbilden. Es stellt sich die Frage, in welchem Maße unter Berücksichtigung weiterer Einflussfaktoren wie Alter, BMI und Geschlecht eine Verschiebung der Weichteile bei liegenden Personen erfolgt und welche Auswirkungen sich daraus auf die Rekonstruktion „aufrecht stehender" Köpfe ergeben. Bei deutlichen Verlagerungen wäre die Einführung eines Korrekturfaktors zu diskutieren.

Auf Grund dieser Tatsache wurde eine Untersuchungsreihe an lebenden Personen begonnen, wobei in Zusammenarbeit mit der Klinik für Dermatologie, Venerologie und Allergologie der Universität des Saarlandes Ultraschalluntersuchungen der Gesichtsweichteildicken an den oben aufgeführten Messpunkten in liegender und aufrechter Position durchgeführt wurden. Zur Untersuchung wird eine Breitbandmultifrequenzsonde des Gerätes Siemens Elegra sowie das Standardgel der Fa. Siemens verwendet.

Zum gegenwärtigen Zeitpunkt liegen erst Messungen an 3 Probanden vor. Es handelt sich dabei um 2 Männer und 1 Frau im Alter zwischen 40 und 89 Jahren mit einem BMI zwischen 19 und 28.

3.3.4 Untersuchungen zum Einfluss der postmortalen Leichenveränderungen auf die Gesichtsweichteildicke

Erst seit der Möglichkeit der Weichteildickenmessungen anhand der Daten bildgebender Verfahren ist eine Einbeziehung lebender Personen zur Erhebung der Werte möglich. Die vor einigen Jahren noch übliche Messung der Gesichtsweichteildicke mittels manueller Methoden (z. B. unter Verwendung einer Nadel [10] oder eines Bohrers [9]) erfolgt ausschließlich an verstorbenen Personen. Trotzdem ist es gegenwärtig noch häufiger nötig, z. B. aus Gründen der Strahlenbelastung beim CT, auch bei Verfügbarkeit bildgebender Verfahren auf verstorbene Personen zurückzugreifen. Verfahren ohne nennenswerte Strahlenbelastung der untersuchten Person, wie die Kernspintomographie, sind davon natürlich nicht betroffen.

Zur Untersuchung des Einflusses der frühen Leichenveränderungen auf die Weichteildickenwerte wurde eine zweite Versuchsreihe begonnen. Dabei werden bei zunächst drei Probanden bis zum vierten postmortalen Tag durch Einstiche mittels einer rußgeschwärzten Nadel die Weichteildicken an den oben aufgeführten Messpunkten ermittelt.

Es handelt sich hier um 3 Frauen in einem Alter zwischen 22 und 65 Jahren mit einem Ernährungszustand zwischen schlank und adipös. Die Probanden werden sofort nach Versterben in das Institut für Pathologie der Universitätskliniken des Saarlandes überführt und dort über den gesamten Zeitraum bei 4,0˚C gelagert.

4 Ergebnisse

4.1 Häufigkeitsverteilungen

Bei der Unterteilung der untersuchten Personen nach Geschlecht und BMI ergaben sich 6 Gruppen mit folgender Verteilung der Probanden (Tab. 1):

Tab. 1: Häufigkeitsverteilungen der untersuchten Personen bei Aufteilung nach Geschlecht und BMI

Gruppe	1.1	1.2	1.3	2.1	2.2	2.3
Definition	Männer mit einem BMI bis einschließlich 19	Männer mit einem BMI zwischen 20 und 25	Männer mit einem BMI von 26 oder darüber	Frauen mit einem BMI bis einschließlich 19	Frauen mit einem BMI zwischen 20 und 25	Frauen mit einem BMI von 26 oder darüber
Personenanzahl	4	35	38	9	31	18

Die Gesichtsweichteildicken über den Landmarks aller 135 Datensätze werden mit dem oben angegebenen Verfahren vermessen und getrennt nach diesen Gruppen ausgewertet. Die einzelnen Messpunkte werden nur dann in diese Untersuchung mit einbezogen, wenn die anatomische Position auf dem knöchernen Schädel korrekt darstellbar ist, was dazu führt, dass einige Messpunkte nur selten bzw. gar nicht untersucht werden können. Auf die bei Taylor [13] aufgeführten Punkte Sub M_2 und Supra M_2 wird aus diesem Grund vollständig verzichtet. Dabei ergibt sich eine Häufigkeitsverteilungen der Messungen über den einzelnen Landmarks wie in Tab. 2 dargestellt.

Tab. 2: Häufigkeitsverteilung der gemessenen Landmarks in den Gruppen

	Gruppe 1.1	Gruppe 1.2	Gruppe 1.3	Gruppe 2.1	Gruppe 2.2	Gruppe 2.3
Unilateral						
Supraglabella	4	34	35	9	31	15
Glabella	4	33	38	9	31	18
Nasion	4	35	36	9	30	18
End of Nasals	1	21	17	4	13	7

	Gruppe 1.1	**Gruppe 1.2**	**Gruppe 1.3**	**Gruppe 2.1**	**Gruppe 2.2**	**Gruppe 2.3**
Mid-Philtrum	4	19	21	2	15	5
Upper Lip Margin	0	5	6	1	5	1
Lower Lip Margin	1	5	3	0	3	1
Chin-Lip Fold	1	5	4	0	4	1
Mental Eminence	0	3	4	0	2	1
Beneath Chin	0	1	1	0	2	1
Bilateral						
Frontal Eminence rechts	3	33	35	9	31	18
Frontal Eminence links	4	34	36	9	31	18
Supraorbitale rechts	4	34	36	9	29	18
Supraorbitale links	4	35	38	9	30	18
Suborbitale rechts	4	31	34	7	24	15
Suborbitale links	4	31	34	7	25	16
Lateral Orbit rechts	4	31	38	9	27	17
Lateral Orbit links	4	32	38	9	27	17
Zygomatic Arch rechts	4	32	37	9	28	17
Zygomatic Arch links	4	30	38	9	29	18
Supraglenoid rechts	4	30	38	9	29	16
Supraglenoid links	4	29	37	9	29	18
Gonion rechts	0	5	3	0	4	1
Gonion links	0	5	3	0	4	1
Occlusial Line rechts	0	7	6	1	5	0
Occlusial Line links	0	7	6	1	5	0

Dabei können bei den Männern in der **Gruppe 1.1** die Weichteildicken über den unilateralen Landmarks Upper Lip Margin, Mental Eminence, Beneath Chin, sowie über den bilateralen Landmarks Gonion und Occlusial Line beidseits nicht bestimmt werden. Alle anderen Landmarks werden zwischen ein- und viermal vermessen. In den **Gruppen 1.2**. und **1.3**. ist die Vermessung über allen Landmarks möglich, wobei die Häufigkeit in **Gruppe 1.2** zwischen einer und 35 und in der **Gruppe 1.3** zwischen einer und 38 Vermessungen schwankt.

Bei den Frauen können in der **Gruppe 2.1** die Weichteildicken über den Landmarks unilateral Lower Lip Margin, Chin-Lip Fold, Mental Eminence, Beneath Chin sowie bilateral über Gonion beidseits nicht bestimmt werden, in der **Gruppe 2.3** entfällt die Weichteildickenbestimmung über dem bilateralen Punkt Occlusial Line beidseits. Alle anderen Landmarks werden in der Gruppe **2.1** zwischen ein- und neunmal und in der Gruppe **2.3** zwischen ein- und achtzehnmal vermessen. In der **Gruppe 2.2**. ist die Vermessung über allen Landmarks möglich, wobei die Häufigkeit zwischen zwei und 31 Vermessungen schwankt.

4.2 Weichteildickenwerte

Die Weichteildickenwerte werden entsprechend der oben ausgeführten Methode an allen lokalisierbaren Landmarks der 135 Köpfe mit einer Range zwischen 2 und 3 mm bestimmt. Die Einheit der Weichteildicken beträgt ebenfalls Millimeter. Es werden Mittelwerte, Standardabweichungen sowie Minimal- und Maximalwerte bestimmt (Tab. 3).

Tab. 3: Weichteildickenwerte in mm über den Landmarks in allen Gruppen

Gruppe **Landmark**	**1.1** Mittelwert Stdabw. Min.-Max.	**1.2** Mittelwert Stdabw. Min.-Max.	**1.3** Mittelwert Stdabw. Min.-Max.	**2.1** Mittelwert Stdabw. Min.-Max.	**2.2** Mittelwert Stdabw. Min.-Max.	**2.3** Mittelwert Stdabw. Min.-Max.
Unilateral						
Supraglabella	**3,35** 0,59 2,73–4,15	**3,82** 0,92 1,86–5,71	**4,64** 1,19 2,06–6,77	**3,77** 1,11 1,91–5,55	**4,37** 0,80 3,07–6,26	**5,65** 1,46 3,17–9,73
Glabella	**5,23** 0,14 5,03–5,36	**5,09** 0,95 2,99–6,9	**5,97** 1,39 2,76–8,66	**4,63** 1,20 2,65–6,02	**5,13** 0,75 2,98–6,62	**6,18** 1,79 3,50–11,47
Nasion	**6,16** 1,65 4,89–8,49	**6,42** 1,22 3,91–9,95	**7,06** 1,59 3,32–10,31	**5,33** 1,63 3,00–7,35	**5,76** 0,98 2,49–7,11	**6,60** 1,89 4,56–12,04
End of Nasals	**1,26** 0 1,26–1,26	**2,28** 0,53 1,34–3,19	**2,14** 0,46 1,53–3,15	**1,93** 0,76 1,29–2,93	**2,19** 0,78 1,45–4,27	**2,92** 1,03 1,90–4,32
Mid-Philtrum	**12,74** 2,60 9,16–15,42	**13,06** 2,80 8,74–19,92	**14,80** 1,82 11,54–19,49	**12,55** 3,15 10,32–14,79	**13,53** 4,39 8,38–26,96	**13,39** 1,62 11,54–15,24
Upper Lip Margin		**11,45** 2,32 9,04–14,15	**13,96** 2,62 11,16–18,93	**11,66** 0 11,66–11,66	**11,01** 2,09 7,74–13,00	**12,48** 0 12,49–12,49
Lower Lip Margin	**12,70** 0 12,71–12,71	**10,79** 1,09 9,45–12,46	**12,83** 0,86 11,95–13,69		**11,16** 2,50 9,08–13,95	**11,75** 0 11,75–11,75
Chin-Lip Fold	**12,95** 0 12,96–12,96	**11,46** 1,09 10,30–12,77	**14,10** 1,73 11,89–16,11		**10,19** 1,99 8,69–13,09	**12,15** 0 12,16–12,16

Gruppe **Landmark**	**1.1** Mittelwert Stdabw. Min.-Max.	**1.2** Mittelwert Stdabw. Min.-Max.	**1.3** Mittelwert Stdabw. Min.-Max.	**2.1** Mittelwert Stdabw. Min.-Max.	**2.2** Mittelwert Stdabw. Min.-Max.	**2.3** Mittelwert Stdabw. Min.-Max.
Mental Eminence		**7,64** 1,18 6,48–8,85	**12,16** 1,31 10,29–13,36		**8,71** 3,73 6,07–11,35	**10,62** 0 10,63–10,63
Beneath Chin		**3,41** 0 3,41–3,41	**9,72** 0 9,72–9,72		**5,80** 4,47 2,64–8,97	**9,15** 0 9,15–9,15
Bilateral						
Frontal Eminence links	**3,77** 0,43 3,44–4,39	**4,17** 1,12 1,89–6,89	**5,29** 1,47 1,77–8,73	**4,54** 1,46 2,41–7,05	**4,64** 0,93 2,72–6,47	**6,08** 1,60 4,24–10,89
Frontal Eminence rechts	**3,93** 0,88 3,02–4,80+	**4,21** 1,13 2,18–6,83	**5,28** 1,45 1,98–8,66	**4,31** 1,21 2,19–6,63	**4,76** 0,77 3,12–6,67	**6,02** 1,57 3,92–9,59
Supraorbitale links	**5,64** 0,86 4,64–6,67	**5,59** 1,29 2,99–8,78	**6,51** 1,39 2,54–9,29	**5,09** 1,34 3,31–7,39	**5,45** 1,15 3,21–8,01	**6,28** 1,93 3,14–11,71
Supraorbitale rechts	**5,60** 0,43 5,16–6,18	**5,57** 1,88 3,93–8,45	**6,71** 1,38 3,62–10,18	**5,02** 1,19 3,54–7,08	**5,44** 1,10 3,27–8,45	**6,60** 2,08 3,41–12,93
Suborbitale links	**4,44** 2,04 2,45–7,31	**5,13** 2,51 1,55–11,18	**7,08** 2,39 1,68–12,25	**5,72** 2,16 2,09–8,06	**5,73** 2,20 2,45–10,25	**11,16** 5,19 4,51–26,47
Suborbitale rechts	**4,22** 1,61 2,74–6,46	**4,86** 2,16 2,04–10,18	**7,30** 2,46 1,60–13,64	**5,52** 1,96 1,90–7,60	**5,92** 2,33 2,17–10,05	**10,88** 5,31 4,39–26,52
Lateral Orbit links	**5,24** 1,39 3,38–6,42	**5,45** 2,15 2,8–11,0	**7,55** 2,73 2,08–15,63	**6,00** 1,81 3,44–8,54	**6,21** 2,00 2,75–11,37	**10,65** 4,30 5,79–25,45
Lateral Orbit rechts	**5,21** 1,07 3,68–6,2	**5,18** 1,85 3,01–9,84	**7,32** 2,11 1,85–11,08	**6,20** 1,59 4,11–8,34	**6,38** 1,95 2,80–9,99	**10,33** 4,28 5,14–24,78
Zygomatic Arch links	**8,27** 0,49 7,79–8,96	**7,47** 1,83 4,74–12,28	**11,38** 3,98 4,44–24,56	**7,65** 2,23 5,18–11,98	**8,04** 2,03 3,57–11,19	**15,34** 6,04 9,67–33,20
Zygomatic Arch rechts	**8,01** 0,73 7,38–8,91	**7,63** 1,89 4,78–12-75	**11,01** 2,93 4,21–16,17	**7,28** 1,88 4,69–10,19	**8,23** 2,00 3,51–13,11	**14,45** 6,84 7,67–34,81
Supraglenoid links	**12,31** 1,73 10,07–13,94	**13,06** 2,01 8,37–17,31	**17,23** 3,83 8,37–28,54	**10,77** 3,04 6,34–15,88	**10,95** 2,06 7,06–15,98	**19,60** 8,08 12,17–47,21
Supraglenoid rechts	**11,55** 2,25 9,48–14,01	**14,11** 2,78 7,79–20,53	**17,38** 2,97 10,11–23,23	**10,09** 2,94 5,43–15,54	**12,25** 2,15 8,10–17,50	**20,06** 7,28 11,33–42,41
Gonion links		**13,14** 2,01 11,08–16,48	**29,25** 4,39 25,69–34,16		**12,15** 2,13 9,80–14,64	**18,32** 18,32–18,32
Gonion rechts		**13,62** 3,36 9,96–17,62	**34,17** 6,34 26,95–38,85		**13,86** 1,84 11,65–16.00	**19,35** 19,36–19,36

Gruppe **Landmark**	**1.1** Mittelwert Stdabw. Min.-Max.	**1.2** Mittelwert Stdabw. Min.-Max.	**1.3** Mittelwert Stdabw. Min.-Max.	**2.1** Mittelwert Stdabw. Min.-Max.	**2.2** Mittelwert Stdabw. Min.-Max.	**2.3** Mittelwert Stdabw. Min.-Max.
Occlusial Line links		**20,66** 3,46 15,06–25,43	**28,82** 4,09 21,07–31,72	**18,09** 18,10–18,10	**20,64** 3,11 17,05–24,26	
Occlusial Line rechts		**22,55** 3,60 16,60–25,81	**29,63** 5,40 20,53–35,93	**17,28** 17,29–17,29	**23,17** 2,10 20,96–25,58	

Die Weichteildickenwerte werden durch das Messprogramm zunächst hinter dem Komma vierstellig bestimmt, was einer Angabe auf zehntausendstel Millimeter entspricht.

Die Standardabweichungen der einzelnen Punkte liegen bei den Weichteildicken von 135 vermessenen Köpfen zwischen 0,14451 über dem Punkt Glabella und 8,08569 mm über dem Punkt Supraglenoid links. Dabei weisen die meisten Werte eine Standardabweichung zwischen 0,14451 mm und 4,47944 mm auf.

Ausreißer ergeben sich in **Gruppe 3.2** für folgende Punkte: Suborbitale links (5,19957 mm) und rechts (5,31968 mm), Zygomatic Arch links (6,04319 mm) und rechts (6,84023 mm) sowie Supraglenoid links (8,08569mm) und rechts (7,28922mm). In der **Gruppe 1.3** weist der Punkt Occlusial Line rechts (5,40143 mm) und Gonion rechts (6,34615 mm) höhere Standardabweichungen auf.

4.3 Fehleranalyse

4.3.1 Untersuchung zur Reproduzierbarkeit

Um die Frage nach der Reproduzierbarkeit der Methode zu beantworten, wird ein Schädel zehnmal von einem Untersucher vermessen. Aus diesen Messreihen werden ebenfalls Mittelwerte, Standardabweichungen sowie Minimal- und Maximalwerte errechnet (Tab. 4).

Tab. 4: Reproduzierbarkeit der Weichteildickenwerte in mm

Landmark	Mittelwert	Standard-abweichung	Minimum	Maximum
Unilateral				
Supraglabella	3,49	0,17	3,28	3,76
Glabella	6,28	0,18	6,03	6,68
Nasion	6,80	0,07	6,70	6,87
End of Nasals	2,57	0,03	2,54	2,65
Mid-Philtrum	15,20	0,35	14,55	15,82
Upper Lip Margin	12,17	0,37	11,58	12,79

Landmark	Mittelwert	Standard-abweichung	Minimum	Maximum
Lower Lip Margin	12,71	0,22	12,29	12,92
Chin-Lip Fold	12,75	0,03	12,70	12,79
Mental Eminence	10,58	0,26	10,20	10,96
Bilateral				
Frontal Eminence links	3,63	0,22	3,44	4,16
Frontal Eminence rechts	4,33	0,07	4,25	4,47
Supraorbitale links	5,11	0,21	4,73	5,42
Supraorbitale rechts	5,08	0,24	4,58	5,46
Suborbitale links	5,08	0,13	4,90	5,35
Suborbitale rechts	3,27	0,12	3,14	3,58
Lateral Orbit links	5,46	0,14	5,24	5,62
Lateral Orbit rechts	5,04	0,37	4,46	5,38
Zygomatic Arch links	8,06	0,06	7,98	8,17
Zygomatic Arch rechts	7,33	0,14	7,21	7,72
Supraglenoid links	11,65	0,03	11,59	11,70
Supraglenoid rechts	11,28	0,13	11,15	11,52
Gonion links	22,26	0,03	22,19	22,30
Gonion rechts	19,07	0,18	18,79	19,54
Occlusial Line links	12,26	0,35	11,87	13,05
Occlusial Line rechts	17,49	0,36	16,94	18,00

Es ergibt sich hierbei eine maximale Standardabweichung über dem Landmark Upper Lip Margin von 0,37688504 mm.

Die minimale Standardabweichung zeigt sich über dem Landmark Chin-Lip Fold mit 0,03018451 mm.

4.3.2 Einfluss unterschiedlicher Ranges auf die Weichteildickenwerte

Der Einfluss unterschiedlicher von uns verwendeter Ranges auf die Weichteildickenwerte ergibt sich aus der Tab. 5. Hierbei wird die Differenz zwischen der kleinsten verwendeten Range von 2 mm und der größten verwendeten Range von 3 mm als Spannweite bestimmt.

Tab. 5: Einfluss unterschiedlicher Ranges auf die Weichteildickenwerte

Landmarks	Range 2,0 mm	Range 3,0 mm	Differenz
Unilateral			
Supraglabella	3,65	3,64	0,01
Glabella	6,34	6,29	0,04
Nasion	6,71	6,75	0,03
End of Nasals	2,60	2,54	0,06
Mid-Philtrum	11,23	11,29	0,05
Upper Lip Margin	12,33	12,12	0,21
Lower Lip Margin	11,58	11,65	0,06
Chin-Lip Fold	12,68	12,69	0,00
Mental Eminence	9,58	9,56	0,01
Bilateral			
Frontal Eminence links	4,37	4,36	0,00
Frontal Eminence rechts	4,40	4,39	0,00
Supraorbitale links	5,28	5,38	0,09
Supraorbitale rechts	4,88	4,84	0,04
Suborbitale links	4,87	4,91	0,03
Suborbitale rechts	3,26	3,28	0,02
Lateral Orbit links	6,12	5,90	0,22
Lateral Orbit rechts	5,38	5,47	0,08
Zygomatic Arch links	7,97	7,95	0,02
Zygomatic Arch rechts	7,23	7,24	0,01
Supraglenoid links	11,59	11,59	0,00
Supraglenoid rechts	11,44	11,57	0,13
Gonion links	22,29	22,30	0,01
Gonion rechts	19,11	19,05	0,06
Occlusial Line links	12,38	12,35	0,03
Occlusial Line rechts	17,31	17,56	0,24

Dabei ergibt sich eine maximale Differenz zwischen den bei einer Range von 2 mm und 3 mm gemessenen Werten von 0,2493 mm.

4.3.3 Untersuchungen zum Einfluss der postmortalen Leichenveränderungen auf die Gesichtsweichteildicke

Im Rahmen der Versuche hinsichtlich des Einflusses der frühen Leichenveränderungen auf die Gesichtsweichteildicke kann auf Grund der derzeit noch sehr geringen Fallzahl keine wertbare statistische Aussage getroffen werden. Betrachtet man jedoch die gemessenen Werte, so lässt sich erkennen, dass die Weichteildicke über einer Vielzahl von Landmarks ansteigt und lediglich über einer Minderheit von Landmarks abfällt.

4.3.4 Untersuchung zu Gesichtsweichteilverschiebungen in liegender und aufrechter Körperposition

Bei der Betrachtung der Weichteilverschiebung im Rahmen unterschiedlicher Körperpositionen zeigt sich eine auch im Hinblick auf die geringe Fallzahl recht eindeutige Tendenz der Verschiebung insbesondere der bilateralen Gesichtspunkte bei einem Wechsel der Körperposition. Auch hier kommt derzeit eine ernsthafte statistische Auswertung auf Grund der Fallzahl noch nicht in Betracht.

5 Diskussion

Um eine Identifizierung unbekannter skelettierter Leichen zu ermöglichen, versucht man seit langer Zeit Gesichter anhand einer Rekonstruktion der Gesichtsweichteile auf der Basis ihrer knöchernen Überreste zu identifizieren [13], [14]. Gesichtsweichteildicken sind die Basis jeder manuellen oder virtuellen Gesichtsrekonstruktion [3], [5]. Um so wichtiger erscheint eine umfassende und nach Alter, ethnischer Herkunft, Geschlecht und Konstitutionstyp getrennte Erfassung dieser Daten.

Auf Grund der sich ständig ändernden Einflüsse auf den Menschen in Mitteleuropa, zu denen letztendlich auch eine grundlegende Änderung seiner Ernährungs- und Arbeitsgewohnheiten zählt, scheint es sinnvoll, eine nochmalige genaue Erfassung der Weichteildickenwerte mittels eines Messverfahrens exakt orthogonal zur Knochenoberfläche durchzuführen.

Ziel dieses Versuchsabschnittes ist es, ein Messverfahren zu entwickeln, das auf der Grundlage virtueller Daten bildgebender Verfahren imstande ist, auf nahezu jeder knöchernen Struktur exakt senkrecht zur Oberfläche den Abstand zwischen Knochen und Haut, also die Gesichtsweichteildicke, zu ermitteln.

Die Vorbereitung der Datensätze für das eigentliche Messprogramm, die getrennte Darstellung von Knochen und Haut und die Reduzierung der Datensätze durch Entfernen nicht benötigter Strukturen, erfolgt im Programm AMIRA. In diesem Programm können CT-Daten ohne Probleme bearbeitet werden, wohingegen sich bei Daten, die durch einen Kernspintomographen gewonnen worden waren, Schwierigkeiten bei der exakten Darstellung der Knochenoberfläche ergeben. Dies ist durch den geringen Wassergehalt des Knochens und der dadurch bedingten schlechteren Darstellung im MRT bedingt. Aus diesem Grund kann zunächst nur auf CT-Datensätze zurückgegriffen werden.

Der Nachteil der Datengewinnung mittels CT liegt in der Strahlenbelastung des lebenden Probanden. Es erscheint bei lebenden Personen daher lediglich vertretbar, bereits bestehende und zu diagnostischen Zwecken angefertigte Datensätze zu verwenden. Dabei handelt es sich jedoch in den meisten Fällen nicht um eine vollständige Darstellung des Kopfes, sondern lediglich von Teilbereichen, was zu Schwierigkeiten im Rahmen einer späteren statistischen Auswertung führen kann.

Aus diesem Grund werden in dieser Versuchsreihe zunächst ausschließlich postmortal erstellte CT-Datensätze des gesamten Kopfes verwendet. Die bei der Auswahl angewandten strengen Selektionskriterien sollen sicherstellen, dass Änderungen oder Verschiebungen im Bereich der Weichteile durch äußere Einflüsse, wie Fremdkörper, asymmetrische Lagerung etc., nahezu ausgeschlossen sind.

Ein weiteres Problem dieser Methode besteht in der z. T. unvollständigen Darstellung randnaher knöcherner Strukturen, was durch die Schichtdicke der CT-Aufnahmen bedingt ist. Daher ist es nicht an allen Schädeln möglich, jeden Punkt auf der knöchernen Oberfläche zu lokalisieren, was zu den unregelmäßigen Häufigkeitsverteilungen bei der Messung der Gesichtsweichteildicken über den einzelnen Landmarks bzw. sogar zum Verzicht auf die Punkte Sub M_2 und Supra M_2 führt. Es werden hier nur Weichteildicken über wiederholt sicher zu lokalisierenden Landmarks in die Auswertung einbezogen.

Die Auswahl der Messpunkte erfolgt in Anlehnung an die bei K. T. Taylor [13] beschriebenen Landmarks. Im Rahmen der Auswertung der Literatur finden sich vielfältige unterschiedliche Messpunkte zur Bestimmung der Gesichtsweichteildicke [8], [9], [10], [14], wobei die bei K. T. Taylor [13] angegebene Auswahl insbesondere den Gesichtsbereich gut zu repräsentieren scheint. Auf Grund der virtuellen Arbeitsweise müssen einige Lokalisationen der Landmarks leicht modifiziert werden. Zu diesen Messpunkten gehören: Supraglabella, Nasion, End of Nasals, Upper Lip Margin, Lower Lip Margin, Frontal Eminence, Supraorbitale, Suborbitale, Lateral Orbit und Zygomatic Arch. Diese Punkte können auf der virtuellen Schädeloberfläche auf Grund z. T. ungenügender Detaildarstellung oder auf Grund fehlender randständiger Knochenstrukturen nicht in dem Maße sicher wie am Originalschädel oder an einem Abguss lokalisiert werden.

Für die Bezeichnung unserer Messpunkte werden, wenn vorhanden, die bei K. T. Taylor [13] angegebenen englischen Begriffe ausgewählt. In der Literatur existieren eine Vielzahl von Messpunkten, welche selbst bei gleicher Definition ihrer Lokalisation unterschiedliche z. T. aus der Anthropologie oder der Anatomie stammende lateinische oder griechische Benennungen aufweisen. Da eine Gesichtsweichteilrekonstruktion eine fach- und berufsübergreifende Aufgabe darstellt, sind nach unserer Einschätzung auf Grund der weiten Verbreitung der englischen Sprache diese Bezeichnungen am besten geeignet, eine schnelle Verständigung aller beteiligten Personen zu ermöglichen.

Die untersuchten Personen werden in unserer Versuchsreihe zunächst wieder in Anlehnung an Taylor [13] hinsichtlich Geschlecht, ethnischer Herkunft und Ernährungszustand eingeteilt, um einen raschen Vergleich mit diesen bereits existierenden Werten zu ermöglichen. Anderweitige Gruppeneinteilungen, z. B. hinsichtlich verschiedener Altersgruppen, wie sie auch bei anderen Autoren vorgenommen werden [9], [11], sind möglich, sollen hier jedoch nicht besprochen werden. Bei einigen Autoren wird auf eine Einteilung nach Ernährungsstatus vollständig verzichtet [10], bei anderen Autoren werden Gewichtsklassen angegeben [9], [11] oder Einteilungen hinsichtlich des Konstitutionstypes gewählt [14]. Eine Einteilung nach dem BMI scheint aus unserer Sicht das beste Äquivalent zum bestehenden Ernährungszustand zu sein. Männer und Frauen mit einem BMI unter 20 sind, wie aus Tab. 1 ersichtlich, in unserer Studie unterrepräsentiert. Ob diese Häufigkeitsverteilung die Verteilung in der Bevölkerung wiedergibt oder durch andere Faktoren, wie die geringe Fallzahl bedingt ist, kann an dieser Stelle nicht festgestellt werden.

Die von uns ermittelten Messwerte werden durch das Messprogramm mit einer Genauigkeit von bis zu $^{1}/_{10.000}$ mm angegeben. Im Hinblick auf die praktische Arbeit ist es bei der Rekonstruktion von Gesichtern mittels Computer zwar möglich, derartige Werte virtuell auf den knöchernen Schädel aufzutragen, erscheint jedoch nicht sinnvoll. In der Praxis sowie bei der weiteren Betrachtung der Messwerte sowie ihrer statistischen Parameter sollten deshalb Rundungen aller Messwerte auf $^{1}/_{100}$ mm erfolgen.

Die Standardabweichungen der meisten Punkte schwanken zwischen 0,14 mm und 4,48 mm. Ausreißer befinden sich hauptsächlich in der Gruppe der adipösen Frauen sowie in geringerer Anzahl der adipösen Männer was evtl. darauf zurückzuführen sein könnte, dass der BMI in diesen Gruppen nach oben offen ist und sich auch extrem übergewichtige Personen mit einem BMI von bis zu 46 in diesen Gruppen befinden, so dass die Weichteildicken innerhalb dieser Gruppe tatsächlich größeren Schwankungen unterliegen. Dies würde eine weitere Unterteilung des BMI oberhalb von 25 sinnvoll erscheinen lassen.

Zur Einschätzung des Einflusses von Fehlergrößen auf unsere Messergebnisse werden zunächst die Fehlerquellen untersucht, die in einem Zusammenhang mit dem Messprogramm stehen, wie die intraindividuellen Schwankungen bei Mehrfachmessungen durch einen Untersucher sowie die methodenspezifischen Schwankungen bei geringer Variation der Range.

Dabei ist zu berücksichtigen, dass innerhalb des Messprogramms die einzige Fehlerquelle für den Untersucher in geringen Abweichungen in der Lokalisation der Messpunkte auf dem knöchernen Schädel besteht. Alle weiteren Fehlerquellen werden durch den selbstständigen Programmablauf weitgehend eliminiert. Weiterhin ist zu beachten, dass auf Grund des vom Untersucher vollständig unabhängigen Messvorganges die hier besprochenen Fehler unabhängig von der Länge der Strecke sind.

Im Rahmen der Untersuchungen hinsichtlich der intraindividuellen Schwankungen ergibt sich eine Standardabweichung der einzelnen Werte zwischen 0,03 mm und 0,38 mm. Bei einem Vergleich mit den oben angeführten Standardabweichungen der eigentlichen Messwerte zeigt sich, dass sich die durch geringe Verschiebungen in der Lokalisation der einzelnen Landmarks bedingten Schwankungen der Messwerte im unteren Bereich der Abweichungen der Messwerte in den einzelnen Gruppen befinden. Somit scheint die Schwankung der Messwerte in den 6 Gruppen durch tatsächliche Unterschiede der Weichteildicken und nicht durch den intraindividuellen Fehler des Untersuchers bedingt zu sein.

Da die Range vom Untersucher frei gewählt werden kann, sind Unterschiede in den Messwerten, die durch die Auswahl unterschiedlicher Ranges entstanden sind, nicht als Messfehler im engeren Sinne zu werten. Während unserer Messungen werden Ranges zwischen 2 mm und 3 mm verwendet, was von der knöchernen Oberfläche in der Region der jeweiligen Landmarks abhängt. Je kleiner die Umgebung (Range) gewählt wird, desto besser repräsentiert die errechnete orthogonale Richtung die lokale Oberfläche, aber auch desto anfälliger ist die Berechnung gegenüber verrauschten oder pathologischen Daten. Je größer die Umgebung gewählt wird, desto stabiler ist die Berechnung der orthogonalen Richtung, je weniger repräsentiert sie jedoch den räumlich begrenzten Landmark. Die Range wird unter Abwägung beider Gesichtspunkte für jeden einzelnen Landmark individuell bestimmt. Ein Beispiel für die z. T. schwierige Abschätzung zeigen die Abb. 10 und 11.

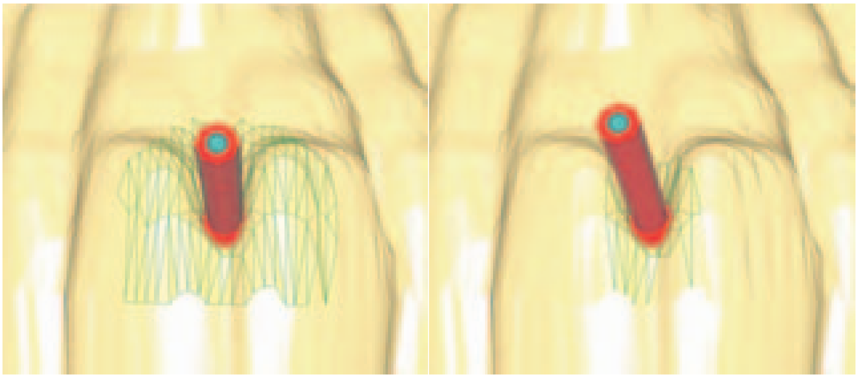

Abb. 10 und **11:** Ermittlung der Range auf sehr unebenen Oberflächen

Zur Abschätzung des durch die Verwendung gering differierender Ranges entstandenen Fehlers werden die Weichteildickenwerte über allen Landmarks eines Schädels bei einer Range von 2 mm im Rahmen der ersten Messung und einer

Range von 3 mm im Rahmen der zweiten Messung bestimmt. Dabei ergibt sich eine maximale Differenz zwischen den beiden Messwerten von 0,25 mm, was ebenfalls eindeutig im unteren Bereich der Standardabweichungen der eigentlichen Messwerte und unterhalb der maximalen Standardabweichung des intraindividuellen Fehlers liegt.

Neben den Fehlerquellen, die in Verbindung mit dem Messprogramm stehen, haben auch externe Faktoren einen Einfluss auf die erhaltenen Messwerte. Dies betrifft zum einen die Veränderung der Weichteildicke durch frühe postmortale Leichenveränderungen zum anderen die Weichteilverschiebungen durch Lageänderungen. Über beide Einflussgrößen existiert für eine statistische Erhebung momentan noch nicht ausreichend Datenmaterial, so dass im Rahmen dieses Teilprojektes nur Tendenzen abgeschätzt werden können.

Die Weichteildicke im Gesicht scheint in den ersten Tagen post mortem eher anzusteigen, wobei die Ursachen hierfür noch unklar sind, da weitaus eher ein Absinken der Weichteildicken auf Grund des einsetzenden Wasserverlustes und des fehlenden Muskeltonus zu erwarten gewesen wäre [1], [15].

Bei der Betrachtung der Lageverschiebung der Gesichtsweichteile in liegender und aufrechter Position zeigt sich eine Verschiebung insbesondere der bilateralen Gesichtspunkte. Auch bei anderen Autoren wird ein Absinken bestimmter Weichteilregionen auf Grund der Gravidität beschrieben [1]. Adipöse Körper weisen dabei eine erhöhte Anfälligkeit für Weichteilverschiebung auf. Ein deutlich sichtbarer Indikator dafür war die präaurikuläre Wulstbildung in Verbindung mit einem Absinken der Wangen zur Liegefläche.

Bei weiteren Erhebungen von Daten zur Gesichtsweichteildicke in liegender Position scheint dadurch die Einführung eines Korrekturfaktors zur besseren Rekonstruktion aufrechter Köpfe geboten.

Insgesamt betrachtet handelt es sich bei der vorliegenden Messmethode um ein nicht oder nur in geringerem Maße durch Fehler beeinflussbares Verfahren, was sicher und gut reproduzierbar in der Lage ist, senkrecht zu jeder beliebigen Knochenoberfläche die darüber liegende Weichteildicke zu erfassen.

Dafür erforderlich sind eine sorgfältige Auswahl des Untersuchungsgutes sowie eine sorgfältige Aufarbeitung und Vorbereitung der Köpfe für das eigentliche Messprogramm.

Zusätzlich zu dieser „klassischen" Methode der Weichteildickenmessung entlang der orthogonalen Richtung an jedem Landmark kann das Messprogramm zu späteren Zeitpunkten auch für andere Messmethoden, wie die Bestimmung der Weichteildicken z. B. an allen Gitterpunkten eines uniformen Volumengitters verwendet werden.

Literaturverzeichnis

[1] C. Wilkinson, Forensic Facial Reconstruction. Cambrigde: University Press, 2004.

[2] W. M. Krogman, The Human Skeleton in Forensic Medicine. Springfield: Charles C. Thomas, 1986.

[3] V. M. Phillips, N. A. Smuts, Facial reconstruction: Utilization of computerized tomography to measure facial tissue thickness in a mixed racial population. Forensic Science International, vol. 83, pp. 51–59, 1996.

[4] G. F. Walker, The Computer and the Law: Coordinate Analysis of Skull Shape and Possible Methods of postmortem Identification, Journal of forensic science, vol. 20, pp. 357–366, 1975.

[5] P. Vanezis, M. Vanezis, G. McCombe, Facial Reconstruction using 3-D Computer Graphics, Forensic science international, vol. 108, pp. 81–95, 1999.

[6] R. M. George, The lateral craniographic method of facial reconstruction. Journal of Forensic Sciences, vol. 32, pp. 1305–1330, 1987.

[7] K. Kähler, J. Haber, H. P. Seidel, Reanimating the Dead: Reconstruction of expressive Faces from Skull Data, ACM SIGGRAPH Conference Proceedings, 2003.

[8] K. Suzuki, On the Thickness of the Soft Parts of the Japanese Face. Journal of Anthropological society of Nippon, vol. 60, pp. 7–11, 1948.

[9] I. Robetti, M. Iorio, V. Mascaro, Die Stärke des Weichgewebes des Gesichtes zur Personenidentifizierung. Zeitung für Rechtsmedizin, vol. 89, pp. 119–124, 1982.

[10] J. S. Rhine, H. R. Campell, Thickness of Facial Tissues in American Blacks. Journal of Forensic Sciences, vol. 25, pp 847–858, 1980.

[11] R. P. Helmer, Schädelidentifizierung durch elektronische Bildmischung. Heidelberg: Kriminalistik Verlag, 1984.

[12] R. P. Helmer, F. Koschorek, B. Terwey, T. Frauen, Dickenmessung der Gesichtsweichteile mit Hilfe der Kernspin-Tomographie zum Zwecke der Identifizierung. Archiv für Kriminologie, vol. 177/178, pp. 139–150, 1986.

[13] K. T. Taylor, Forensic Art and Illustration. Boca Raton, London, New York, Washington D. C.: CRC Press, 2001.

[14] M. Y. Iscan, R. P. Helmer, Forensic Analysis of the Skull. New York, Chichester, Brisbane, Toronto, Singapore: Wiley-Liss, 1993.

[15] W. Weber, K. Munzert, Postmortale Exsikkation der Fingerbeeren – Ergebnisse systematischer quantitativer und qualitativer experimenteller Untersuchungen, Zeitschrift für Rechtsmedizin, vol. 96, pp. 279–289, 1986.

Soft-Tissue Segmentation in Forensic Applications

Andreas Mang, Jan Müller and Thorsten M. Buzug

Institute of Medical Engineering, University of Lübeck,
Ratzeburger Allee 160, 23538 Lübeck, Germany

Abstract

In this paper a new method for extracting a soft facial template from T1 weighted magnetic resonance (MR) images for craniofacial reconstruction is proposed. The reconstruction of the face of dead individuals based on the shape of their skull is for interest in forensic and archaeology as well as in anthropology. Several computational methods have been developed to simplify facial reconstructions. The aim of the presented multimodality approach is to extract a facial template from MR images and register this template on the computed tomography (CT) of the skull of a dead individual. In the following first results of an automatic segmentation strategy to obtain the desired facial template are presented. The approach is based on active contours, introduced by M. Kass et al. [1], which are well known from image processing applications to locate boundary objects. Additionally to the classical formulation their gradient vector flow based version is presented. The resulting flow field leads to a contour, which is capable of entering concave regions. All current results are presented in 2D.

Moreover a brief introduction to the planed mapping of the facial template on the CT cranial bone is proposed in the end.

1 Introduction

Post mortem identification of human remains is a challenging task in forensic science. The main target of computer aided facial reconstructions is to simplify and fasten the process of finding the appropriate reproduction of a subject's facial appearance corresponding to forensic findings.

Three-dimensional facial reconstructions consist of two parts: First of all the depth of the facial soft tissue needs to be determined at any point on the skull. This information usually is withdrawn from different charts (see e. g. [2]) providing tissue depth information at standardized landmark positions according to race, gender, age and body type. Nowadays these measurements are commonly done using Ultrasound or 3D visualization modalities like MR or CT (see [3]) – however, they still suffer from the limited number of anatomical landmarks (about 20 or 30). Second, based on the collected soft tissue depth, the facial shape is produced. For this propose the conventional, manual approach utilizes clay or plasticine. In contradiction to this method that is time consuming, computer based reconstructions depend less on knowledge of anatomy and artistic skills or experience, respectively. Moreover, they provide a greater flexibility, as results are directly available to everybody and modifications on the estimated appearance of the subject can easily be done – especially considering texture mapping, changes on e. g. hair colour can be applied in a fractional amount of time.

In the following some previous work on computerized procedures for 3D reconstruction of facial features are reviewed. The first approach to be described places virtual dowels [4], representing the soft tissue thickness, on a polygonal skull at pre-defined anatomical landmarks (see [5]). According to these standardized landmarks a facial model is produced, by fitting a facial template onto the endpoints of the dowels using hierarchical B-Splines.

The second presented multi-modality approach [6] deals with a landmark based morphing algorithm. It utilizes a 3D extended version of Booksteins Thin-Plate Splines, which are well known from medical registration studies. A set of homologous landmarks needs to be identified in the CT of the cranial bone and in the magnetic resonance tomography (MRT) of a living individual, providing the estimated facial template. According to this set of anatomical landmarks elastic mapping between both datasets is found and the soft tissue template is adjusted to the virtual representation of the forensic skull find.

In contrast to the previous described landmark based approach ([6]) Quatrehomme et al. [7] used so called "crest lines" as features for the deformation of a facial template on a CT scan of the skull. Both datasets – reference and target – are registered before deformation.

Jones [8] introduces an automatic computerized method for facial reconstructions, which is based on two CT scans – one for the virtual representation of the forensic find and another one of a reference head. Between both skulls a correspondence at some feature points is found using cross correlation. Afterwards the facial mapping is applied using distance fields, closed skulls and a distance field work function.

All presented methods simplify the reconstruction but still request much user interaction or depend only on a subset of features. The only approach, being reviewed above, which utilizes the entire information of the soft tissue depth, however, is introduced by Jones [8]. As we propose to extract a facial template directly from the MR data set, the presented method is not dependent on just a view reference points. A facial template is produced, which contains the soft tissue depth for the entire skull. This work relies on the same modalities utilized in [6]. The benefit of using CT for the representation of the skull is that CT yields a virtual representation of the cranial bone that is free of any geometrical distortion. Using MRI to extract the facial template is at hand, as MRI is especially designed to show soft tissues. Thus, one does no longer have to rely on measurements of the soft tissue depth derived from charts and the anthropologist does no longer have to rely just on about 20 or 30 anatomical landmarks.

In the following, first results of a new automatic approach for extracting a facial template from T1 weighted MRI (see fig. 1) in 2D are presented. Furthermore, a brief introduction on the proposed mapping of the extracted facial template is given.

In order to extract the facial template the inner boundary of the soft tissue layer (see fig. 2) needs to be located. In this context, we apply active contours, so called “snakes” [1], which are known from image processing applications to locate boundaries. Due to its efficiency the snake algorithm is widely used in image processing e. g. for edge detection, shape modelling, segmentation and motion tracking [9]. The 3D extension on the snake concept is called balloons – a brief introduction can be found in the conclusion.

Fig. 2 illustrates, that in MR representations of the head, the depth of the facial soft tissue is limited by two clear boundaries. Consequently, we recommend locating the first outer boundary (see fig. 2) using the snake algorithm and afterwards erase the located edge in the Sobel filtered image. The second boundary, which is approached by the snake, is the desired inner boundary of the soft tissue layer. Having located this boundary the facial template might be extracted from the MRI and afterwards mapped onto the CT of the skull.

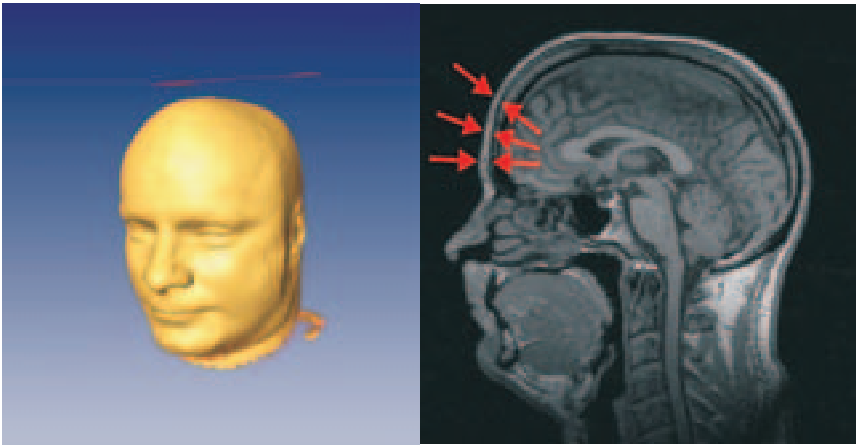

Fig. 1: Surface visualization of the skin from an MRI dataset and the sagittal section through the head. The arrows exemplarily mark the soft tissue depth of the facial template.

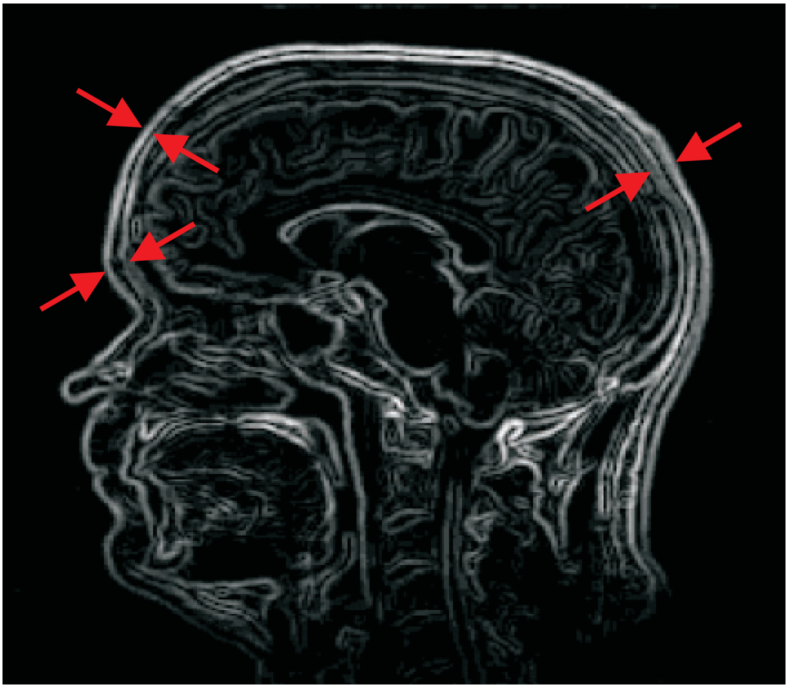

Fig. 2: Sobel filtered mid-sagittal section through the head. The arrows exemplarily mark the first and second edge of the fatty signal, referring to exterior and interior boundary of the facial soft tissue.

In the next section we will review the mathematical background on the classical and the gradient vector flow enhanced active contours, which first were introduced by Xu et al. [9–12].

2 Material and Methods

Snakes, the 2D representation of active contours or deformable models, respectively, are widely used in image processing applications e. g. to locate boundary objects. They move through the image domain to the desired features, usually object boundaries, under the influence of external forces computed directly from the image and internal forces, i. e. intrinsic geometrical properties, the snake contains itself. One drawback to the classical formulation is that the conventional snake algorithm is very sensitive to parameters and noise present in the image. To overcome these problems a specific energy function will be described here.

2.1 Snake Algorithm – Classical Formulation

In literature there are two different versions of active contours, the geometric or implicit and the parametric or explicit deformable models [13]. In contrast to the parametric models, which are local methods based on an energy minimization procedure guided by external forces, the geometric models can be regarded as zero level set of a higher dimensional function, produced in an energy minimizing way. This paper deals with the parametric deformable models.

A snake is a parameterised, planar and dynamic curve C, with physical properties like elasticity and rigidity, defined within an image domain $I : \Re^2 \rightarrow \Re$:

$$C = \{\mathbf{v}(s,t) = (\mathbf{x}(s,t); \mathbf{y}(s,t))/s \in [a; b]\} \tag{1}$$

It can be described as a function

$$C : [a,b] \rightarrow \Re^2. \tag{2}$$

It is moving through the spatial domain of an image $I(x,y)$ by minimizing its own energy (exemplarily shown in figure 3):

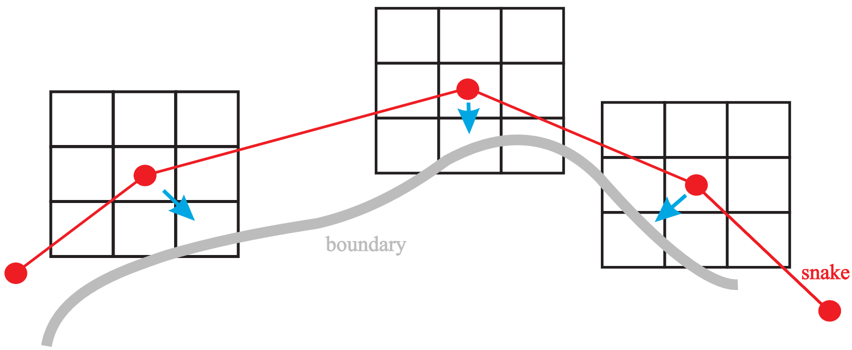

Fig. 3: Schematic illustration of snake movement.

The associated energy function, which controls the physical behaviour of the snake and which has got to be minimized, is given in equation (3). It consists of two terms – the external energy P and the internal energy S:

$$E = \int_a^b S(\mathbf{v}(s))ds + \int_a^b P(\mathbf{v}(s),I)ds \stackrel{!}{=} \min \tag{3}$$

The first term – the internal energy S – is dominated by the geometrical properties of the active contour. For that reason its magnitude depends on the shape of the snake. The second term – the external energy P – is derived directly from the image $I(x,y)$ and its value depends on the position of the snake in the given image.

An active contour minimizing the entire energy function (3) satisfies the following Euler Lagrange equation:

$$\frac{\partial}{\partial s}\left(\alpha(s)\,\frac{\partial \mathbf{v}(s)}{\partial s}\right) - \frac{\partial^2}{\partial s^2}\left(\beta(s)\,\frac{\partial^2 \mathbf{v}(s)}{\partial s^2}\right) - \nabla P(\mathbf{v}(s),I) = 0 \tag{4}$$

Equation (3) simply represents the balance between external and internal forces. In order to find the solution of equation (4) $\mathbf{v}$ must be treated as a function of time t. The partial derivative of $\mathbf{v}$ with respect to t must be set equal to the left hand side of equation (4) [11]. This results in the following energy function:

$$\frac{\partial \mathbf{v}(s,t)}{\partial t} = \alpha(s)\frac{\partial \mathbf{v}^2(s,t)}{\partial s^2} - \beta(s)\frac{\partial^4 \mathbf{v}(s,t)}{\partial s^4} - \nabla P(\mathbf{v}(s,t),I) \quad (5)$$

The solution of equation (5) must be found numerically. When the snake reaches a steady state, all forces are balanced. For that case the Euler Lagrange expression (eq. (4)) disappears, the energy function (eq. 3) is at minimum and the snake has reached the desired feature, e. g. a object boundary, within the given image.

2.1.1 The Internal Energy

The internal energy is composed of two terms, which are dominated by the geometrical properties of the active contour and, for that reason, as mentioned before, controls its physical behaviour:

$$S(\mathbf{v}) = E_{elast}(\mathbf{v}) + E_{rig}(\mathbf{v}) = \int_a^b \alpha(s)\left\|\frac{\partial \mathbf{v}(s,t)}{\partial s}\right\|^2 ds + \int_a^b \beta(s)\left\|\frac{\partial^2 \mathbf{v}(s,t)}{\partial s^2}\right\|^2 ds \quad (6)$$

Consequently, the internal energy tends to preserve the shape of the snake. It could be considered as internal spline energy caused by stretching and bending. Assuming that there is a large gap between two successive points of the snake, the first derivative, representing its elasticity, will have a large value. Therefore, with respect to the minimization of the energy, the first term is responsible for the shrinking of the contour.

The second derivative represents the rigidity and keeps the snake from bending too much. The parameter functions $\alpha(s)$ and $\beta(s)$ determine the elasticity and the rigidity, respectively. For simplicity they commonly are implemented as constant non-negative regularization parameters, which control the weighting between the first and the second derivative. A high α (controlling the elasticity) tends to force the active contour to shrink and a high β (controlling the tension) prevents sharp bending, as mentioned above.

2.1.2 The External Energy

The external energy pushes the snake towards the object boundaries and is computed directly from the image $I\ (x,y)$. It is a potential energy function, which is estimated by integrating the potential energy along the contour:

$$E_{ext} = \int_a^b P(\mathbf{v}(s))ds \quad (7)$$

For a grey level image the most commonly used calculation of the external energy is given by the convolution of the Laplacian of Gaussian (LOG) with the image $I(x,y)$ (see fig. 3):

$$P(x,y) = -\omega\|\nabla[G_\sigma(x,y) \otimes I(x,y)]\|^2, \omega > 0 \quad (8)$$

or via

$$P(x,y) = -\omega\|\nabla I(x,y)\|^2, \omega > 0. \quad (9)$$

∇ donates the Nabla operator and ω (eq. (6)) is a non-negative weighting factor. $I(x,y)$ is the image intensity and $G_\sigma(x,y)$ is a 2D Gaussian function with standard deviation σ. The vectors determined by $\nabla I(x,y)$ point towards the edges of the object and have large magnitudes near its boundaries. In homogenous regions $I(x,y)$ is constant and, consequently, the gradient is zero – for that reason, the snake is not prevented from shrinking.

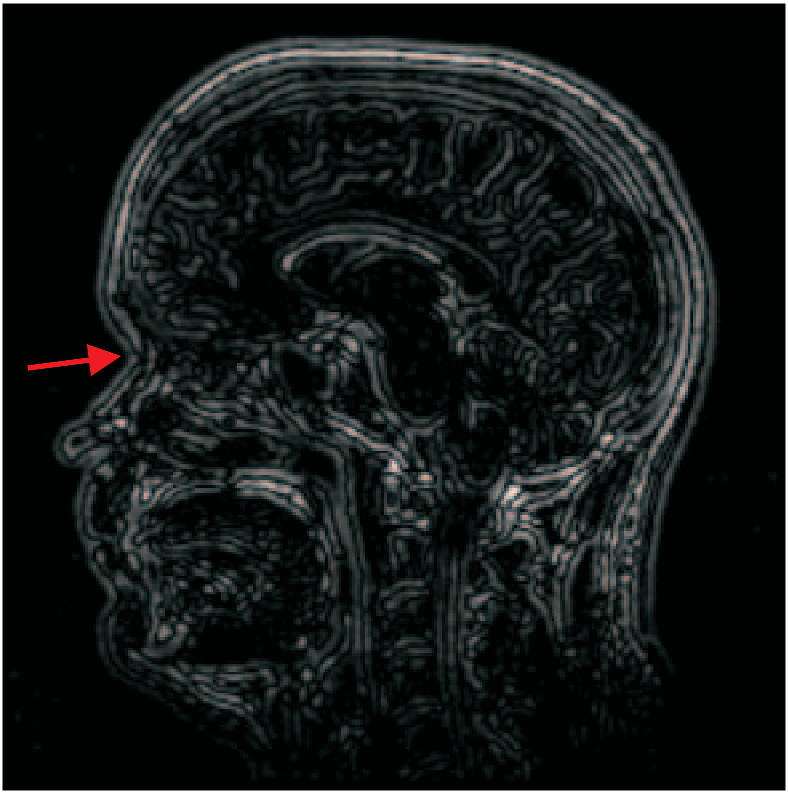

Fig. 4: Attractor image of mid-sagittal section using the LOG operator with 9*9 kernel. The red arrow exemplarily marks the Nasion.

The convergence of the algorithm is mainly dependent on the initial position. In order to extend the capture range of the external energy the so called kernel size of the LOG operator might be enlarged. This might be of interest for points next to the Nasion (see mark fig. 4). On the one hand this leads to better results in some cases. On the other hand enlarging the kernel is not be sufficient in cases, as the shape of the head varies among individuals and, therefore, some features of the face might not be approached using the traditional snake algorithm. Moreover, the traditional snake is very sensitive to noise present in the image. Consequently, it is desired to obtain a new energy function, which does not only contain local information next to boundaries in order to make the snake capable of entering concave regions. This function is presented in the following section.

2.2 Gradient Vector Flow (GVF)

The external energy of the snake algorithm is one of the most discussed topics in the domain of active contours. The energy function described here provides improvements to some drawbacks of the traditional snake algorithm. First of all, the regular snake needs to be initialized close to the object boundaries, as the gradient of the image has a restricted influence range. Another difficulty is that the conventional snake is not capable of entering into concave regions, as the internal energy tends to straighten the snake and rules, in homogenous regions, over the traditional external energy. Moreover, the traditional snake is very sensitive to parameters (see eq. (5) and (6)). To overcome these problems a new external force, the so-called gradient vector flow field, presented by Xu and Prince [9–11], is employed. The result is a new kind of snake, which can be initialised far away from object boundaries, but still tends to move towards the desired object and furthermore is capable of boundary concavities. In addition the snake is less influenced by noise present in the image.

In contrast to the common external energy the GVF field does not only provide local information on the present edges as the gradient information derived from the image does (see eq. (6)). This function P_{GVF} generates a diffusion of the gradient information across the whole domain by generating a vector field $\mathbf{V} = \mathbf{V}(x,y)$. The acquired vectors, just like in the ordinary formulation, point directly to the edges present in the image (see fig. 5). The vector field $\mathbf{V}$ minimizes the following energy function [11]:

$$P_{GVF}(\mathbf{u},\mathbf{v}) = \iint \mu\left(\left(\frac{\partial \mathbf{u}}{\partial x}\right)^2+\left(\frac{\partial \mathbf{u}}{\partial y}\right)^2+\left(\frac{\partial \mathbf{v}}{\partial x}\right)^2+\left(\frac{\partial \mathbf{v}}{\partial y}\right)^2\right) + \|\nabla P\|^2\|\mathbf{V} - \nabla P\|^2 dxdy \quad (10)$$

where μ is a regularization parameter set according to the amount of noise present in the image. $\mathbf{V}(x,y) = [\mathbf{u}(x,y), \mathbf{v}(x,y)]$ denotes the GVF-field; it is also a potential force field, just like the ordinary external energy. In this context P denotes a potential function – it might be computed using a Sobel filter or other edge-emphasizing filters, respectively:

$$P(x,y) = \|\nabla I(x,y)\|^2 \quad (11)$$

Analogous to equation (3) the force balance function of the active contour is given by [14]:

$$\alpha(s)\,\frac{\partial^2 \mathbf{v}(s,t)}{\partial s^2} - \beta(s)\,\frac{\partial^3 \mathbf{v}(s,t)}{\partial s^3} + \gamma\mathbf{V} = 0, \quad (12)$$

where γ denotes a proportional coefficient weighting the external energy against the internal.

The sum of squares of the partial derivates in equation (9) makes the resulting vector flow $\mathbf{V}(x,y)$ varying smoothly. This term is known from the "optical flow" by

Horn and Shunk [15]. The second term represents the difference between the vector flow and its initial status. Hence, if ∇P is small – in homogeneous regions – this formula (eq. (9)) is dominated by the partial derivatives of the vector flow field [14]. This yields to a slowly varying field. When ∇P is large the function is dominated by the second term. The initial value of $\mathbf{V}(x,y)$ is determined by the gradient of the common attractor image $\nabla I(x,y)$ (see eq. (11) and (9)):

$$\mathbf{V}(x,y) = [\mathbf{u}(x,y), \mathbf{v}(x,y)] = \nabla P(x,y) = \nabla(\nabla I(x,y)) \tag{13}$$

Using calculus of variation it can be shown that the GVF $\mathbf{V}(x,y)=[\mathbf{u}(x,y), \mathbf{v}(x,y)]$ is found by solving the following Euler equations [16, 17]:

$$\mu\nabla^2\mathbf{u} - \left(\mathbf{u} - \frac{\partial P}{\partial x}\right)\left(\left(\frac{\partial P}{\partial x}\right)^2 + \left(\frac{\partial P}{\partial y}\right)^2\right) = 0 \tag{14}$$

$$\mu\nabla^2\mathbf{v} - \left(\mathbf{v} - \frac{\partial P}{\partial y}\right)\left(\left(\frac{\partial P}{\partial x}\right)^2 + \left(\frac{\partial P}{\partial y}\right)^2\right) = 0, \tag{15}$$

where $\mathbf{u}(x,y)$ and $\mathbf{v}(x,y)$ denote the partial derivates and ∇^2 the Laplacian operator. In homogeneous regions the second term of the equations above is zero and for that reason $\mathbf{u}(x,y)$ and $\mathbf{v}(x,y)$ are determined by the Laplacian operation. Therefore, the gradient information is diffused into the homogeneous regions [17] (see fig. 5 and fig. 6). These two equations (eq. (13) and eq. (14)) can be solved separately by treating $\mathbf{u}(x,y)$ and $\mathbf{v}(x,y)$ as a function of time:

$$\frac{\partial \mathbf{u}(x,y,t)}{\partial t} = \mu\nabla^2\mathbf{u}(x,y,t) - (\mathbf{u}(x,y,t) - P_x(x,y)) \cdot \left(P_x(x,y)^2 + P_y(x,y)^2\right) \tag{16}$$

$$\frac{\partial \mathbf{v}(x,y,t)}{\partial t} = \mu\nabla^2\mathbf{v}(x,y,t) - \left(\mathbf{v}(x,y,t) - P_y(x,y)\right) \cdot \left(P_x(x,y)^2 + P_y(x,y)^2\right) \tag{17}$$

However, the solution of equation (16) and equation (17) must be found numerically. Solving these equations, leads, with respect to the number of iterations, to a diffusion of the gradient information from the boundaries over the entire image. The resulting vectors point to the object edges (see fig. 6) of the image. The following figures (fig. 5 and fig. 6) compare the results of the classical used external energy compared to the GVF field (left).

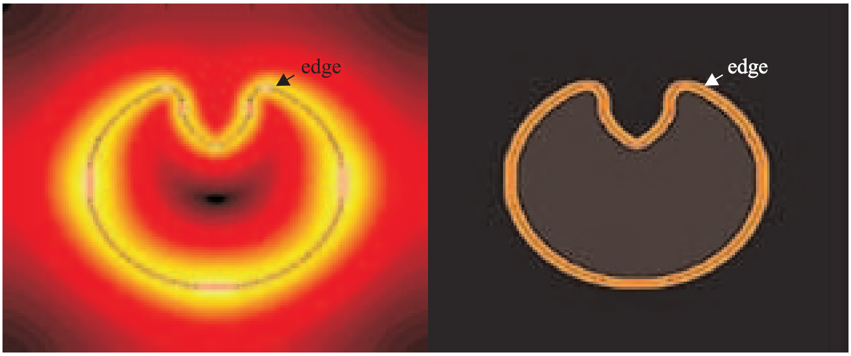

Fig. 5: The diffusion of the gradient information (left) compared to the normal external energy (right).

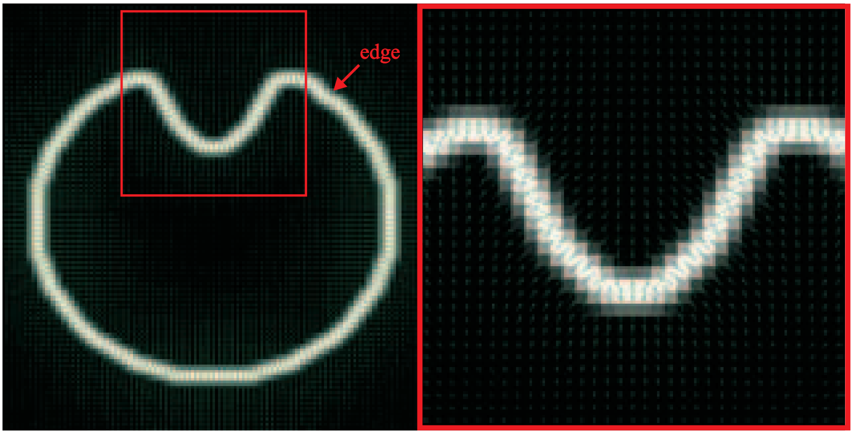

Fig. 6: Global gradient vector field of an edge (left) and close up (right).

3 Results and Discussion

Detecting the inner boundary of the fat signal in MRI data is a challenging task with many problems. The gradient vector flow field was applied to the MR image and results can be seen in figure 7.

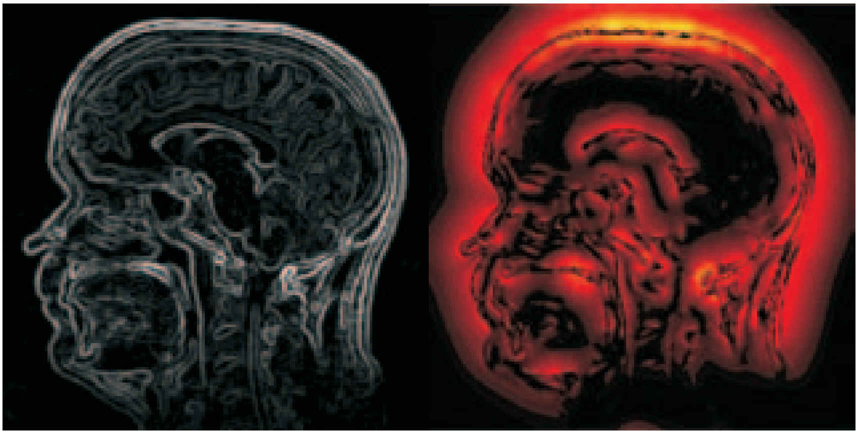

Fig. 7: Comparison between the normal external energy (left) and the gradient vector flow field (right). The pictures show the magnitude of the derived vector fields.

These two pictures emphasize the difference between both energy functions. On the one hand the GVF diffuses the gradient information of the edges and for that reason increases the capture range (see fig. 6). On the other hand applying the GVF to medical images the interior information becomes blurred as there are many structures, which leads to a "noisy" vector field and, thus, there is no clear inner boundary of the fat signal. Small structures in the interior are overwhelmed through the diffusion of the vector field (see fig. 7). On the one hand it might be a benefit for approaching the outer boundary using the gradient vector field. On the other hand the detection of the inner boundary seems to be encumbered using GVF – for this propose the traditional external energy leads to better results.

The next figures (8) and (9) illustrate the first results in 2D of the algorithm described above.

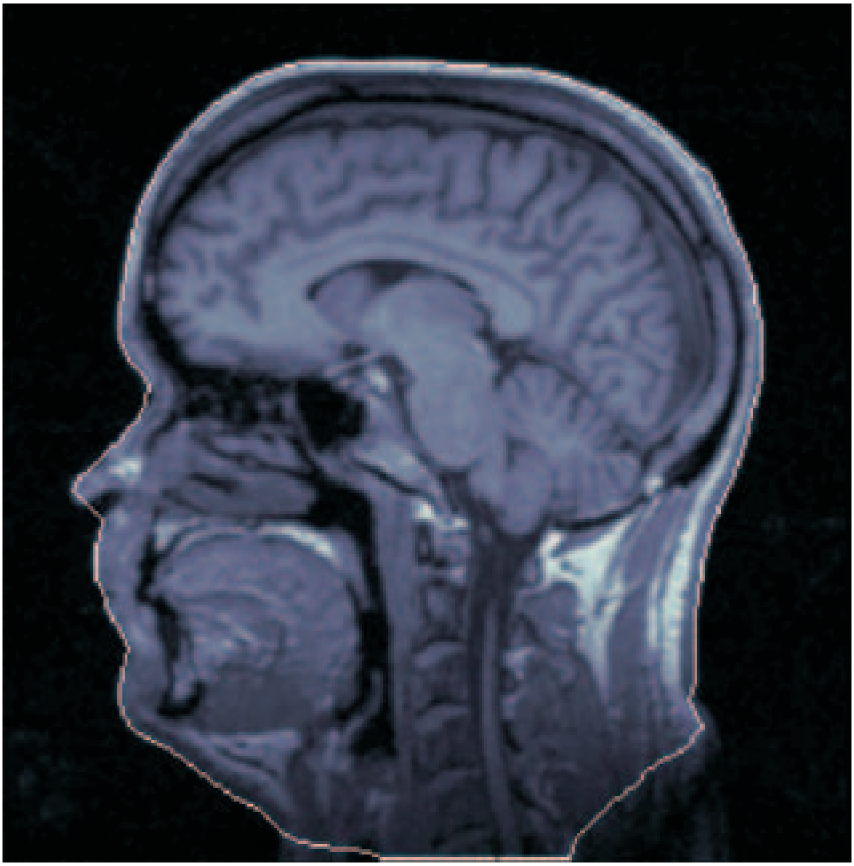

Fig. 8: Snake locating the boarders of the facial template

In order to solve the Euler Lagrange Equation we use a Greedy algorithm. The located outer boundary is deleted in the external energy or Sobel filtered image, respectively, and afterwards the snake is advanced towards the inner boundary of the fat signal. This leads to good results in the upper areas of the MRI. However, around the nose it is quite hard to get adequate results, as in the mid-sagittal slice there is no obvious edge, which could be detected (see fig. 8 and fig. 9).

Fig. 9: First results of the location of the inner soft tissue boundary.

Figure (9) demonstrates that there still are problems in the segmentation, which have to be solved in future. Mainly in the front parts of the face (exemplarily shown with red arrows) it is a challenging problem to locate the inner boundary of the fat signal automatically. Another major problem is that the traditional snake algorithm is, as mentioned in section 2 very sensitive to parameters, which additionally complicates the segmentation of the facial soft tissue template. These results, however, indicate that it is possible to extract the facial template using active contours. We plan to implement the described algorithm in 3D.

Another way to overcome this problem might be to use CT images instead of MRI to get the skin signal information, as CT also contains the desired soft tissue information with less complex structures. However, as it is an aim of this work to build up a database of different facial templates this would be the wrong way, because it is quite hard to get a large number of different CT of the entire head of various subjects.

4 Conclusion and Future Work

In this paper an approach for the segmentation of the facial soft tissue thickness was presented. Further research must be done and other energy functions need to be developed, to use the snake algorithm as a reliable tool for the extraction of facial templates. In literature there are other extensions to the snake concept coping with the drawbacks of the standard gradient vector flow formulation (see e. g. [18]).

Another benefit to the segmentation will result from the 3D implementation. The segmentation of the inner boundary using active contours depends on the boundary information contained in the MR data set. If we use 3D MR images the inner boundary of the soft tissue is not "completely" broken, like in the figured mid-sagittal slice, as we will have further information in the axial direction on the inner boundary. In the following a brief introduction of the 3D extension on the snake concept, the so-called balloons, will be given.

Balloons mainly follow the same idea as the 2D active contours, as they are also propagated through the image domain by an energy minimizing process. The easiest way to initialise balloons is to apply 2D active contours slice by slice on the volumetric data, but the results are often insufficient. Other implementations seem to be more promising as they provide movements in every direction of the three dimensional space.

The internal energy of the surface has to be determined in a different way. The Euler Lagrange equation (eq. (3)), which must be minimized by calculating the values of $\mathbf{v}(r,s)$, must be modified [19]:

$$\begin{aligned} &\nabla E_{ext}(\mathbf{v},I) + \alpha_s \frac{d^2\mathbf{v}(r,s)}{ds^2} + \alpha_r \frac{d^2\mathbf{v}(r,s)}{dr^2} - \dots \\ &\dots - \beta_s \frac{d^4\mathbf{v}(r,s)}{ds^4} - \beta_r \frac{d^4\mathbf{v}(r,s)}{dr^4} - \beta_{sr} \frac{d^4\mathbf{v}(r,s)}{ds^2 dr^2} = 0 \end{aligned} \tag{18}$$

As in 2D this equation means that the internal forces of the active contour will balance the forces extracted from the image data.

The formulation for the internal energy is given by [20]:

$$\begin{aligned} E_{\text{int}} = \iint \alpha_s &\left| \frac{d\mathbf{v}(r,s)}{ds} \right|^2 + \alpha_r \left| \frac{d\mathbf{v}(r,s)}{dr} \right|^2 + \dots \\ &\dots + \beta_s \frac{d^2\mathbf{v}(r,s)}{ds^2} + \beta_r \frac{d^2\mathbf{v}(r,s)}{dr^2} + \beta_{sr} \frac{d^2\mathbf{v}(r,s)}{dsdr}\, dsdr \end{aligned}, \tag{19}$$

where the parameters α_s and α_r define the weighting of the elasticity and the parameters β_s and β_r represent the loading of the rigidity along the corresponding *s*- and the *r*-axis. The last term of each equation (eq. (18) and eq. (19)) is controlled by β_{sr}, defining the inhibition of the rotation.

The segmentation of the facial template is a pre-processing to the actual aim of the entire project. Actually, we want to morph the extracted soft tissue data onto the CT of the skull using the described algorithm. Furthermore, some reference points (see fig. 10, e. g. Nasion, left preauricular point (PAL), right preauricular point (PAR) or Inion and one point on the tip of the nose) need to be set by the user should improve the results. For the mapping it might be possible to use once more active contours. Hence the active contours will need to have – in addition to elasticity and rigidity – one more property, i. e. the soft tissue thickness. The results of this work will show that it is possible to use the snake algorithm not only for segmentation, but also for warping.

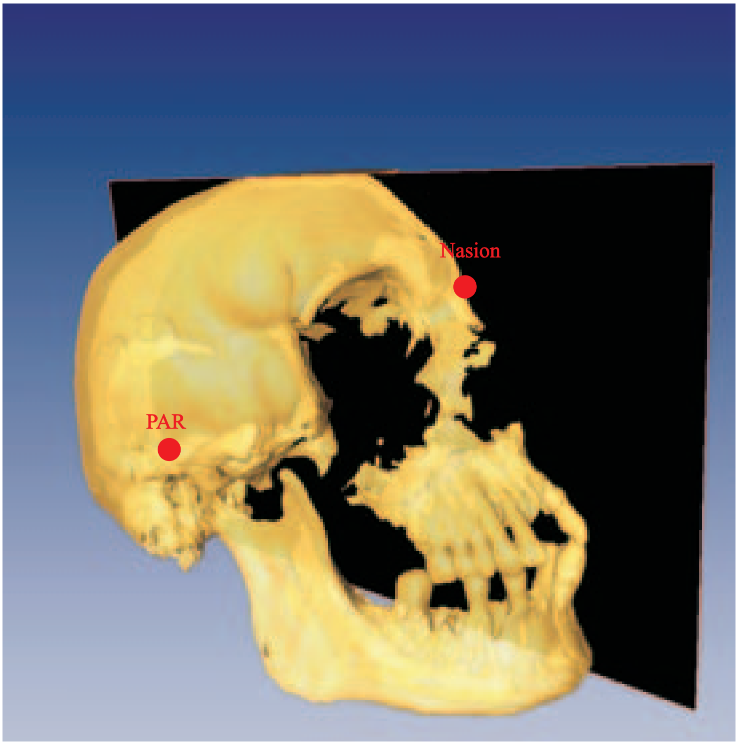

Fig. 10: 3D-CT scan of a skull (Duke of Saxony, Widukind, late 8 century).

5 References

[1] M. Kass, A. Witkin and D. Terzopoulus, "Snakes: Active Contour Models", International Journal of Computer Vision, vol. 1(4), pp. 321–331, 1987.

[2] S. Rhine, "Tissue thickness measures: American Caucasoids, American Blacks, Southwestern Indians", Physical Anthropology Laboratories, Maxwell Museum of Anthropology, University of New Mexico, 1982, 1983, 1984.

[3] V. M. Phillips and N. A. Smuts, "Facial Reconstruction: Utilization of Computerized Tomography to Measure Facial Tissue Thickness in Mixed Racial Population", in J. Forensic Sci., vol. 83, pp. 51–59, 1996.

[4] D. W. Bullock, "Computer Assisted 3D Craniofacial Reconstruction", M. S. thesis, University of British Columbia, Canada, 1999.

[5] R. P. Helmer, S. Rohricht, C. Petersen, and F. Mohr, "Forensic Analysis of the Skull", Chapter 17: Assessment of the Reliability of Facial Reconstruction, Wiley-Liss, 1993, p. 229.

[6] J. Müller, A. Mang, D. Thomsen and T. M. Buzug, "Regularized 3D Thin-Plate Splines for Soft-Tissue Reconstruction", in Proceedings of the BMT 2004, vol. 49, pp. 134–135, February 2004.

[7] G. Quatrehomme, S. Cotin, G. Subsol, H. Delingette, Y. Garidel,G. Grevin, M. Fidrich, P. Bailet and A. Ollier, "A Fully Three-Dimensional Method for Facial Reconstruction Based on Deformable Models", in J. Forensic Sci, vol. 42, p. 649, 1997.

[8] M. W. Jones, "Facial Reconstruction Using Volumetric Data", in Proceedings of the Vision Modelling and Visualization Conference 2001 (VMV 2001), pp. 21–23, 2001.

[9] C. Xu and J. L. Prince, "Snakes, Shapes and Gradient Vector Flow", in IEEE Transactions on Image Processing, vol. 7(3), pp. 359–369, 1998.

[10] C. Xu and J. L. Prince, "Gradient Vector Flow: A New External Force", in Proceedings of the IEEE Conference on Computer Vision an Pattern Recognition (CVPR), pp. 66–71, June 1997.

[11] C. Xu and J. L. Prince, "Generalized Gradient Vector Flow External Forces for Active Contours", in Signal Processing, vol. 71, pp. 131–139, 1998.

[12] C. Xu and D. L. Pham, J. L. Prince, "Medical Image Segmentation using Deformable Models", in Handbook of Medical Imaging – Volume 2: Medical Image Processing and Analysis, J. M. Fitzpatrick and M. Sonka,. SPIE Press, May 2000, pp. 129–174.

[13] K. S. Ntalianis, N. D. Doulamis, A. D. Doulamis, and D. S. Kollias, "Multiresolution Gradient Vector Flow Field, A fast Implementation Towards Video Object Plane Segmentation", in Proceedings of the IEEE International Conference on Multimedia and Exposition (ICME 2001), pp. 1–3, August 2001.

[14] S. Luo, R. Li and S. Ourselin, “A new Deformable Model Using Dynamic Gradient Vector Flow and Adaptive Balloon Forces”, in Proceedings of the APRS Workshop on Digital Image Computing, pp. 9–14, February 2003.

[15] B. K. B. Horn and B. G. Schunk, “Determining Optical Flow”, Artificial Intelligence, vol. 17, pp. 185–203, August 1981.

[16] X. Hang, N. L. Greenberg, and J. D. Thomas, “A Geometric Deformable Model for Echocardiographic Image Segmentation”, Computers in Cardiology, vol. 29, pp. 77–80, September 2002.

[17] M. F. Santarelli, V. Positano, C. Michelassi, M. Lombardi, and L. Landini, “Automated Cardiac MR Image Segmentation: Theory and Measurement Evaluation”, in Medical Engineering and Physics, vol 25(2), pp. 149–159, March 2003.

[18] M. Wei, Y. Zhou, and M. Wan, “A fast Snake Model based on non-linear Diffusion for Medical Image Segmentation”, in Computerized Medical Imaging and Graphics, vol. 28 (3), pp. 109–117, 2004.

[19] J. Ahlberg, “Active Contours in Three Dimensions”, M. S. thesis No. LiTH-ISY-EX-1708, Department of Electrical Engineering, Computer Visions Laboratory, Linköpings University, Sweden, 1996.

[20] C. D. Mansard et. al.: “Qantification of Multicontrast Vascular MR Images with NLSnake, an Active Contour Model: In Vitro Validation and In Vito Evaluation”, Magnetic Resonance in Medicine, vol. 51, pp. 370–379, January 2004.

Weichteil-Segmentierung für forensische Anwendungen

Andreas Mang, Jan Müller und Thorsten M. Buzug

Institut für Medizintechnik, Universität zu Lübeck,
Ratzeburger Allee 160, 23538 Lübeck, Deutschland

Abstract

In dieser Arbeit wird eine neue Methode zur Extraktion von Weichteilen aus T1 gewichteten MR Daten für die Rekonstruktion von Gesichtsmerkmalen von Toten vorgestellt. Nicht nur in der Forensik, sondern auch in der Anthropologie und in der Archäologie werden häufig 3D Gesichtsrekonstruktionen für die postmortale Identifizierung genutzt. Um die Arbeit für die Anthropologen zu erleichtern, wurden in den letzten Jahren einige neue computergestützte Methoden vorgeschlagen. Hier wird eine neue Methode zur Extraktion von Tiefeninformationen der Gesichtshaut aus MR Daten, basierend auf Aktiven Konturen, genauer „Snakes", vorgestellt. Es soll ein Gesichts-Template erzeugt werden, welches später an die virtuelle Repräsentation des Schädels angepasst werden kann.

„Snakes" wurden erstmals von M. Kass et al. [1] vorgestellt. Sie werden in der Bildverarbeitung häufig für die Detektion von Kanten eingesetzt. Neben der klassischen Formulierung wird im Rahmen dieser Arbeit noch auf die *Gradient-Vector-Flow*-Version der so genannten aktiven Konturen eingegangen. Das erzeugte Gradientenfeld führt zu einer Kontur, die in der Lage ist, auch in konkave Regionen einzudringen. Alle bisherigen Ergebnisse werden in 2D präsentiert. Darüber hinaus wird am Ende dieser Arbeit noch ein Ausblick auf das geplante Mappingverfahren für das erzeugte Template, basierend auf dem vorgestellten Segmentierungs-Algorithmus, gegeben.

1 Einführung

Die postmortale Identifizierung stellt eine große Herausforderung an die Forensik dar. Das Hauptziel der computerbasierten Gesichtsrekonstruktion ist es, die Arbeit des Anthropologen zu erleichtern, zu beschleunigen, und eine möglichst genaue Nachbildung des Gesichtes der verstorbenen Person anhand der forensischen Funde zu erreichen. Die dreidimensionale Rekonstruktion besteht im Wesentlichen aus zwei Teilen: Als erstes muss die Schichtdicke des Weichteilgewebes, welche die Grundlage für die Rekonstruktion des Gesichtes liefert, ermittelt werden. Normalerweise wird diese Information aus standartisierten Tabellen (siehe [2]) entnommen, in welchen üblicherweise die Schichtdicke für 20 bis 30 anatomische Landmarken, in Abhängigkeit von Geschlecht, Alter, Rasse und Körperbau, angegeben wird. Heutzutage werden diese Messungen für die Tiefeninformation basierend auf Ultraschall oder anderen 3D Visualisierungs-Modalitäten wie Computer Tomographie (CT) [3] oder Magnetresonanz-Tomographie (MRT) vorgenommen. Dabei ist zu bemerken, dass diese immer noch auf Grund der geringen Datenmenge (20 bis 30 Landmarken) zu ungenauen Ergebnissen führen können. Der zweite Schritt ist die Modellierung des Gesichtes. Die konventionellen, manuellen Verfahren nutzen hierfür Plastiline bzw. Ton. Im Gegensatz dazu erleichtern und beschleunigen computergestützte Verfahren die Rekonstruktion, da sie ein geringeres Maß an künstlerischer Fertigkeit, Erfahrung und geringere Kenntnisse im Bereich der Anatomie von dem Rekonstrukteur verlangen. Zudem wird durch das Erstellen von virtuellen Modellen die Verbreitung der Daten erleichtert und Änderungen, vor allem im Bereich des Texture Mappings, sind sehr einfach und schnell realisierbar – die Änderung der Haarfarbe z. B. erfordert einen Bruchteil des Zeitaufwandes von konventionellen Verfahren.

Im Folgenden sollen einige bisher entwickelte computerbasierte Methoden für die 3D Gesichtsweichteil-Rekonstruktion vorgestellt werden.

Das von Bullock [4] vorgestellte Verfahren basiert auf so genannten B-Splines. Anhand der vorher erwähnten Tabellen werden auf einer virtuellen Repräsentation des Schädels so genannte „dowels“, welche die Tiefeninformation des Weichteilgewebes enthalten, gesetzt. Anschließend wird, basierend auf den an anatomischen Landmarken (siehe [5]) gesetzten Tiefenmarkern, ein vorher erzeugtes Gesichtstemplate mittels hierarchischen B-Splines an den Schädel angepasst.

Ein anderes Verfahren [6] verwendet die 3D Erweiterung von so genannten Thin-Plate-Splines. Es handelt sich um eine multimodale Methode basierend auf einer 3D Computertomographie des Schädels und einem 3D MR-Datensatz, welcher das zu registrierende Gesichtstemplate enthält. In beiden Datensätzen werden korrespondierende Landmarken gesetzt und anhand dieser durch die Bestimmung einer elastischen Transformationsfunktion das Gesichtstemplate auf dem Schädel registriert.

Im Gegensatz zu dem in [6] beschriebenen landmarken-basierten Verfahren verwendet Quaterhomme et al. [7] so genannte „crest-lines“ für das Matching des Gesichttemplates auf die virtuelle Repräsentation des Schädels. Von Jones [8] wird ein weiteres vollautomatisches Verfahren vorgestellt. Es basiert auf einem CT des Schädelfundes und einer CT-Aufnahme eines Referenz-Kopfes einer lebenden Person. In beiden werden korrespondierende markante Punkte über Kreuzkorrelation ermittelt und anschließend wird die Tiefeninformation des gesamten Referenz-Kopfes auf den Schädel übertragen. Damit stellt es das einzige hier vorgestellte Verfahren dar, das die gesamte Tiefeninformation des Templates für die Rekonstruktion ausnutzt, und nicht nur eine Registrierung anhand von wenigen Referenzpunkten, bzw. eine virtuelle Repräsentation des Schädels aus wenigen anatomischen Landmarken, erzeugt.

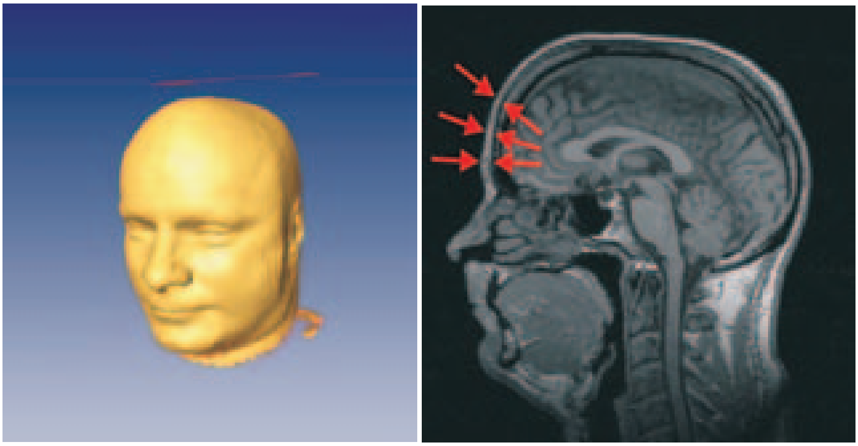

Abb. 1: Oberflächendarstellung der Haut aus einem MRT-Datensatz und der sagittale Schnitt durch den Kopf. Die Pfeile markieren die Dicke des Fettsignals.

Das hier vorgestellte Verfahren setzt genau an dieser Stelle an. Es soll nicht nur die Tiefeninformation an bestimmten Punkten des Referenzschädels für die Rekonstruktion zur Verfügung stellen, sondern an jeder Stelle des Schädels. Es basiert wie [5] auf einem 3D CT-Datensatz und einem 3D MR-Datensatz (siehe Bild 1). Die Nutzung von CT führt zu einer virtuellen Repräsentation des Schädels, die keinerlei geometrische Verzerrungen enthält. Da MRT speziell dafür entwickelt wurde, um Weichteilgewebe darzustellen, liegt es auf der Hand, die Tiefeninformation des Weichteilgewebes aus dieser Modalität zu entnehmen. Dafür muss die innere Grenze des Fettsignals der Haut lokalisiert werden. Unser Ansatz hierfür basiert auf so genannten „Snakes" [1]. Aufgrund der Schnelligkeit und der Effektivität werden Snakes in der Bildverarbeitung häufig zur Kantendetektion, zur Segmentierung und zur Bewegungsverfolgung eingesetzt [9].

Aus Bild 2 geht hervor, dass das Fettsignal der Haut in MR-Aufnahmen durch zwei mehr oder weniger scharfe Kanten begrenzt wird. Die Idee des vorgestellten Verfahrens ist es, die äußere Kante des Kopfes zu detektieren und sie danach zu löschen. Die zweite Kante stellt die Innere Grenze des Fettsignals der Haut dar. Diese Kante wird erneut detektiert und somit als das gesuchte Template aus dem MR Datensatz, welches anschließend auf den CT Schädel registriert werden kann, extrahiert.

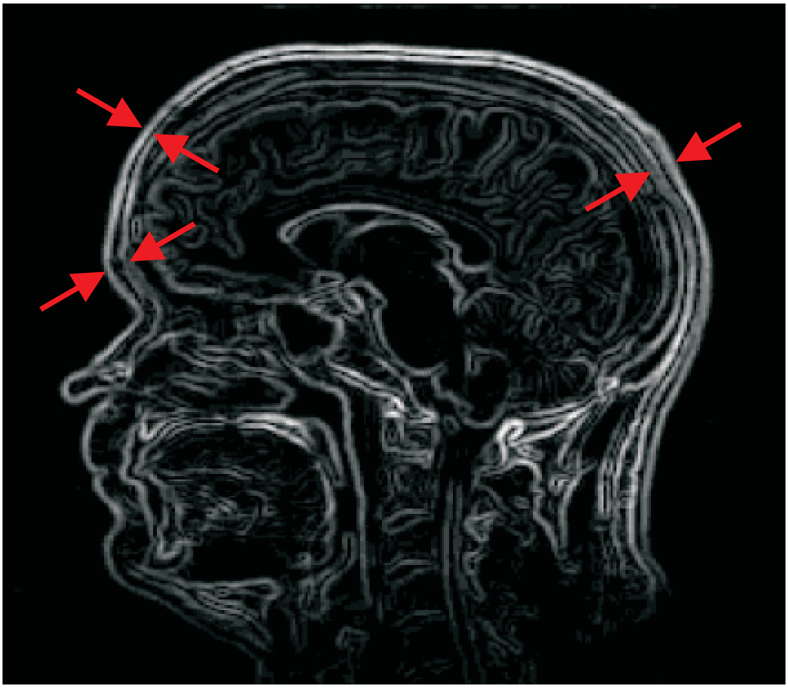

Abb. 2: Sobel-gefiltertes Bild des mid-sagittalen Schnittes durch den MR Datensatzes. Die Pfeile markieren die äußere und die innere Kante des Fettsignals der Haut.

Der folgende Abschnitt beschäftigt sich mit dem mathematischen Hintergrund der klassischen [1] und der Gradient Vector Flow Version der Aktiven Konturen (Xu et. al. [10, 11, 12]).

2 Material und Methoden

Bei Snakes, der 2D Representation von aktiven Konturen oder deformierbaren Modellen, handelt es sich um eine parametrisierte Kurve, die sich unter dem Einfluss von externen und internen Kräften räumlich auf die gesuchten Merkmale – meist Kanten – des Bildes, zubewegt. Ein Nachteil der klassischen Formulierung der Snakes ist deren starke Abhängigkeit von Parametern und die Empfindlichkeit gegenüber den Rauschanteilen im Bild. Im Folgenden wird neben der klassischen Formulierung auch noch eine weitere Energiefunktion vorgestellt, welche die eben angesprochenen Probleme umgeht.

2.1 Snake Algorithmus – Klassische Formulierung

In der Literatur werden zwei verschiedene Versionen von aktiven Konturen vorgestellt. Zum einen die geometrischen bzw. impliziten und zum anderen die parametrischen oder expliziten deformierbaren Modelle [13]. Bei dem parametrischen Modell handelt es sich um eine lokale Methode, die auf einem durch externe Kräfte geleiteten Energie-Minimierungs-Prozess beruht. Im Gegensatz dazu kann das geometrische Modell als Null-Level-Set einer höher dimensionalen Funktion, der durch eine Energie-Minimierung produziert wird, aufgefasst werden. Im Rahmen dieser Arbeit wird nur auf die parametrische Darstellung eingegangen.

Eine Snake ist eine parametrisierte dynamische und planare Kurve, mit physikalischen Eigenschaften, wie Elastizität und Starrheit, die innerhalb der Dimensionen des Bildes $I : \Re^2 \rightarrow \Re$ definiert ist:

$$C = \{\mathbf{v}(s,t) = (\mathbf{x}(s,t); \mathbf{y}(s,t))/s \in [a;b]\}. \quad (1)$$

Sie kann als Funktion

$$C : [a,b] \rightarrow \Re^2 \quad (2)$$

aufgefasst werden, die sich, basierend auf der Minimierung ihrer eigenen Energie, durch das Bild bewegt (siehe Abbildung 3).

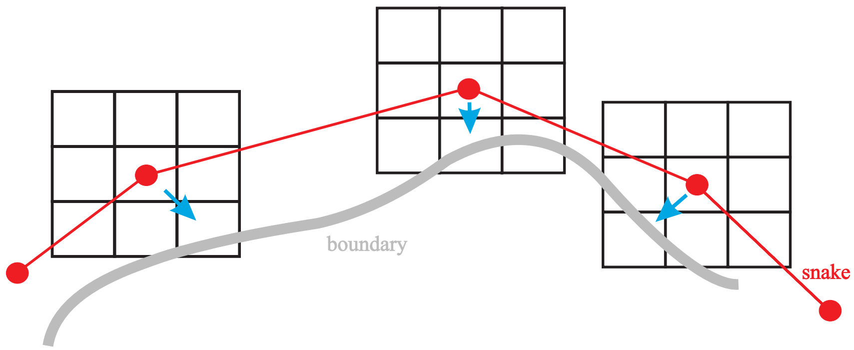

Abb. 3: Schematische Darstellungen der Bewegung der Snake.

Das zu minimierende Energiefunktional kontrolliert das physikalische Verhalten der Snake und ist direkt mit der Kurve verknüpft. Die Funktion besteht aus zwei Termen – der externen und der internen Energie:

$$E = \int_a^b S(\mathbf{v}(s))ds + \int_a^b P(\mathbf{v}(s),I)ds \stackrel{!}{=} \min. \quad (3)$$

Der erste Term – die interne Energie S – wird durch die geometrischen Eigenschaften der Kontur bestimmt und ihr Wert hängt somit von der äußeren Form der Kurve ab. Der zweite Term – die externe Energie P – kann direkt aus dem Bild $I\,(x,y)$ ermittelt werden. Eine Snake, welche die Energiefunktion aus Gleichung (3) minimiert, muss die folgende, aus der Physik bekannte, Euler-Lagrange-Gleichung

$$\frac{\partial}{\partial s}\left(\alpha(s)\,\frac{\partial \mathbf{v}(s)}{\partial s}\right) - \frac{\partial^2}{\partial s^2}\left(\beta(s)\,\frac{\partial^2 \mathbf{v}(s)}{\partial s^2}\right) - \nabla P(\mathbf{v}(s),I) = 0 \quad (4)$$

erfüllen. Gleichung (3) ist eine Darstellung des Gleichgewichtzustandes zwischen den externen und den internen Kräften. Bildet man die partielle Ableitung von $\mathbf{v}(x,y)$ in Bezug auf den Zeitpunkt t erhält man [11]

$$\frac{\partial \mathbf{v}(s,t)}{\partial t} = \alpha(s)\,\frac{\partial \mathbf{v}^2(s,t)}{\partial s^2} - \beta(s)\,\frac{\partial^4 \mathbf{v}(s,t)}{\partial s^4} - \nabla P(\mathbf{v}(s,t),I). \tag{5}$$

Da das Energiefunktional aus Gleichung (3) nicht auf analytischem Wege gelöst werden kann, muss ein numerischer Ansatz gewählt werden. Erreicht die Snake einen statischen Zustand, ist die Lösung von Gleichung (3) gefunden. Folglich verschwindet die Euler-Lagrange-Gleichung (Gl. (4)) und die Snake hat das gesuchte Merkmal, z. B. eine Kante, innerhalb des Bildraumes erreicht.

2.1.1 Die Interne Energie

Die interne Energie

$$S(\mathbf{v}) = E_{elast}(\mathbf{v}) + E_{rig}(\mathbf{v}) = \int_a^b \alpha(s)\left\|\frac{\partial \mathbf{v}(s,t)}{\partial s}\right\|^2 ds + \int_a^b \beta(s)\left\|\frac{\partial^2 \mathbf{v}(s,t)}{\partial s^2}\right\|^2 ds \tag{6}$$

setzt sich aus zwei Termen, die durch geometrische Eigenschaften der aktiven Kontur bestimmt werden, zusammen. Deshalb tendiert die interne Energie dazu, die Form der Kontur zu erhalten. Sie kann somit als interne Spline-Energie aufgefasst werden, die durch Dehnung und Biegung verursacht wird.

Der erste Term stellt die partielle Ableitung nach ds und somit die Krümmung der Kurve dar. Befinden sich zwei benachbarte Punkte in großem Abstand zueinander, ist somit der erste Term, unter Annahme einer Energieminimierung, für die Minimierung der Gesamtlänge der Snake verantwortlich.

Die zweite Ableitung repräsentiert die Starrheit bzw. Glattheit der Kontur und hält die Snake somit davon ab, sich zu sehr zu verbiegen. Die Parameterfunktionen $\alpha(s)$ und $\beta(s)$ bestimmen die Ausprägung der Krümmung bzw. der Glattheit der aktiven Kontur. Zur Vereinfachung können sie auch als konstante positive Regularisierungsparameter, die die Gewichtung zwischen Elastizität und Steifigkeit ermöglichen, aufgefasst werden. Ein großes α (kontrolliert die Elastizität) veranlasst die aktive Kontur dazu, sich zusammen zu ziehen und ein groß gewähltes β (kontrolliert die Spannung) verhindert eine starke Krümmung der Snake.

2.1.2 Die Externe Energie

Die externe Energie P bewegt die Snake auf die Kanten des Objektes zu und wird direkt aus dem Bild ermittelt. Dabei handelt es sich um eine Potential-Energie-Funktion

$$E_{ext} = \int_a^b P(\mathbf{v}(s))ds. \tag{7}$$

Für ein Graustufen Bild sind die meist genutzten Energiefunktionen gegeben durch

$$P(x,y) = -\omega \| \nabla [G_\sigma(x,y) \otimes I(x,y)] \|^2, \omega > 0 \quad (8)$$

oder

$$P(x,y) = -\omega \| \nabla I(x,y) \|^2, \ \omega > 0 \quad (9)$$

∇ bezeichnet dabei den Nabla Operator und ω ist ein positiver Regularisierungsparameter, der die Gewichtung der externen Energie gegenüber der internen Energie erlaubt. $I(x,y)$ ist die Intensität an der Stelle (x,y) des Bildes und $G_\sigma(x,y)$ ist eine 2D Gauß-Funktion mit der Standardabweichung σ. Die durch $\nabla I(x,y)$ bestimmten Vektoren zeigen auf die im Bild enthaltenen Kanten und haben in ihrer Nähe einen großen Betrag. In homogenen Bereichen des Bildes, ist die Intensität $I(x,y)$ konstant und demnach auch der Gradient gleich Null – die Snake kann sich ungehindert fortbewegen.

Durch eine Vergrößerung des Faltungskerns des entsprechenden Operators kann die Reichweite der externen Energie vergrößert werden. Dies ist vor allem von Interesse im Bereich des Nasions (siehe Abb. 4). Dennoch führt dies nicht in allen Fällen zu zufrieden stellenden Ergebnissen. Ein weiterer Nachteil des konventionellen Snake-Algorithmus ist die Empfindlichkeit gegenüber den Parametern, bzw. gegenüber dem im realen Bild immer vorhandenen Rauschen. Deshalb ist es erstrebenswert, eine neue externe Energie einzuführen, die nicht nur die lokalen Informationen des Gradienten in der Nähe der Kanten enthält. Damit wird der Snake ermöglicht, weiter in konkave Regionen vorzudringen. Diese Energie wird im folgenden Absatz vorgestellt.

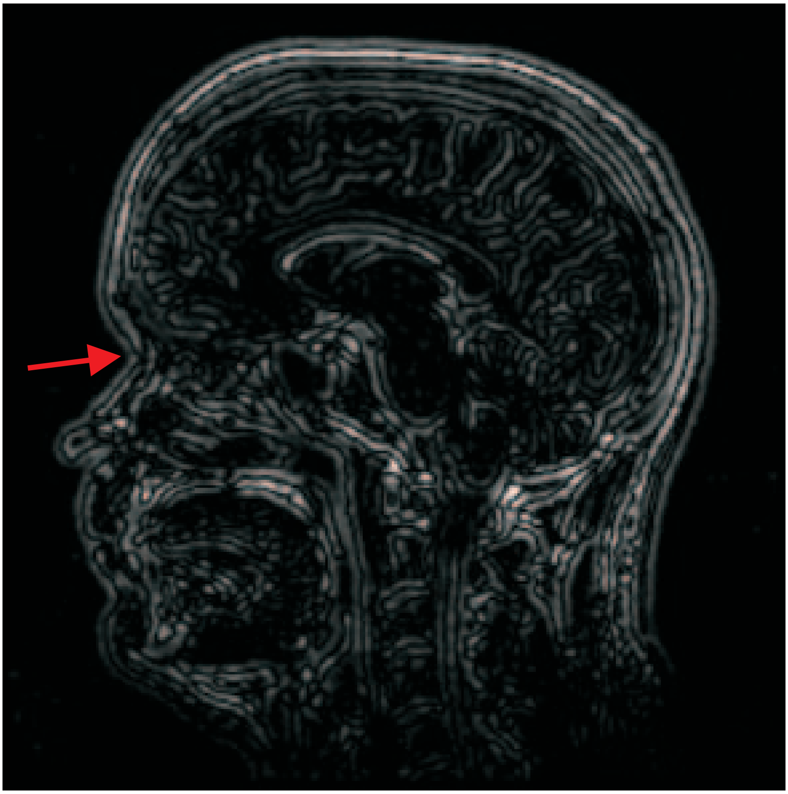

Abb. 4: Edge Map unter Verwendung eines 9x9 Gauß-Kerns. Der rote Pfeil markiert den Bereich des Nasions.

2.2 Gradient-Vector-Flow (GVF)

Die externe Energie ist eine der meist diskutierten Fragestellungen auf dem Gebiet der aktiven Konturen. Die hier vorgestellte Energie beinhaltet einige Verbesserungen gegenüber dem bis jetzt beschriebenen konventionellen Verfahren. Zum einen muss die Snake nicht mehr in der Nähe der Objektkanten initialisiert werden, da die externe Energie nicht mehr nur in direkter Nähe zu den Kanten zur Verfügung steht. Zum andern wird die Empfindlichkeit gegenüber den Parameterfunktionen $\alpha(s)$ und $\beta(s)$ (siehe Gl. (5), Gl. (6)) herabgesetzt. All dies wird ermöglicht durch den Einsatz eines so genannten Gradient-Vector-Flow-Feldes, welches erstmals in diesem Zusammenhang von Xu und Prince [9,10,11] angewendet wurde. Als Resultat ergibt sich eine neue Art von Snake, die, wie eben schon erwähnt, nicht mehr in der Nähe von den Objektkanten initialisiert werden muss. Sie nähert sich immer noch den Objektgrenzen an und außerdem wird der Snake das Vordringen in stark konkave Bereiche des zu segmentierenden Objektes ermöglicht. Die Empfindlichkeit der aktive Kontur gegenüber des im Bild vorhanden Rauschen wird herabgesetzt. Das beschriebene Vektorfeld $\mathbf{V}(x,y)$ minimiert folgende Energiefunktion [11]

$$E(\mathbf{u},\mathbf{v}) = \iint \mu\left(\left(\frac{\partial \mathbf{u}}{\partial x}\right)^2+\left(\frac{\partial \mathbf{u}}{\partial y}\right)^2+\left(\frac{\partial \mathbf{v}}{\partial x}\right)^2+\left(\frac{\partial \mathbf{v}}{\partial y}\right)^2\right) + \|\nabla f\|^2\|\mathbf{V} - \nabla f\|^2 dxdy. \quad (10)$$

μ ist ein Regularisierungsparameter, der von dem im Bild vorhandenen Rauschen abhängt. $\boldsymbol{V}(x,y) = [\mathbf{u}(x,y), \mathbf{v}(x,y)]$ ist das beschreibene GVF Feld; es handelt sich auch hierbei – genau wie in der konventionellen Formulierung der externen Energie – um ein Feld welches durch ein Potential erzeugt wird. In diesem Zusammenhang ist P die Potentialfunktion, welche durch eine Faltung des Bildes I mit dem Sobel-Operator oder mittels anderer kantenhervorhebender Filter berechnet werden kann:

$$P(x,y) = \|\nabla I(x,y)\|^2 \quad (11)$$

Analog zu Gleichung 3 kann auch hier wieder ein Kräftegleichgewicht

$$\alpha \frac{\partial^2 v(s,t)}{\partial s^2} + \beta \frac{\partial^3 v(s,t)}{\partial s^3} + \gamma V = 0, \quad (12)$$

aufgestellt werden [14]. γ bezeichnet hierbei einen Gleichgewichtskoeffizienten zwischen dem Feld $\mathbf{V}(x,y)$ und der internen Energie der Snake.

Die Summe der Quadrate der partiellen Ableitungen aus Gleichung (9) führt dazu, dass sich die aus dem Gradienten des Bildes I errechnete Information (siehe Gl. (6)) über das ganze Bild verteilt. Die Vektoren zeigen wiederum direkt auf die Kanten des Objektes (siehe Abb. 5). Dieser Term ist bekannt aus den Arbeiten zu „Optical Flow“ von Horn and Shunk [15]. Der zweite Term stellt den Unterschied zwischen dem „Vector Flow“ und dem initialen Zustand dar. Daraus ergibt sich, unter der Annahme, dass ∇P klein ist (in homogenen Bereichen), dass Gleichung (9) durch die partiellen Ableitungen des Vektorfeldes dominiert wird [14]. Das führt dazu, dass das Feld in kleinen Bereichen nur wenig variiert. In Bereichen in denen ∇P groß ist, wird die Funktion durch den zweiten Term dominiert. Initialisiert wird das Feld $\mathbf{V}(x,y)$ durch den Gradienten der Potentialfunktion aus Gleichung (10):

$$\mathbf{V}(x,y) = [\mathbf{u}(x,y),\mathbf{v}(x,y)] = \nabla P(x,y) = \nabla(\nabla I(x,y)). \quad (13)$$

Durch die Verwendung von Variatrionsrechnung kann gezeigt werden, dass die Lösung $\mathbf{V}(x,y)=[\mathbf{u}(x,y), \mathbf{v}(x,y)]$ durch folgende Gleichungen gefunden werden kann [16,17]:

$$\mu\nabla^2\mathbf{u} - \left(\mathbf{u} - \frac{\partial P}{\partial x}\right)\left(\left(\frac{\partial P}{\partial x}\right)^2+\left(\frac{\partial P}{\partial y}\right)^2\right) = 0 \quad (14)$$

und

$$\mu\nabla^2\mathbf{v} - \left(\mathbf{v} - \frac{\partial P}{\partial y}\right)\left(\left(\frac{\partial P}{\partial x}\right)^2+\left(\frac{\partial P}{\partial y}\right)^2\right) = 0 \quad (15)$$

Dabei bedeuten $\mathbf{u}(x,y)$ und $\mathbf{v}(x,y)$ die partiellen Ableitungen und ∇^2 stellt den Laplace Operator dar. In homogenen Bereichen ist der zweite Term der obigen Gleichung Null und somit werden $\mathbf{u}(x,y)$ und $\mathbf{v}(x,y)$ allein durch die Laplace-Operation bestimmt. Dadurch wird die Gradienten-Information der Kanten in die homogenen Bereiche des Bildes ausgeweitet [17] (siehe Abb. 5, Abb. 6).

Gleichung (13) und Gleichung (14) können unabhängig voneinander gelöst werden:

$$\frac{\partial \mathbf{u}(x,y,t)}{\partial t} = \mu \nabla^2 \mathbf{u}(x,y,t) - (\mathbf{u}(x,y,t) - P_x(x,y)) \cdot \left(P_x(x,y)^2 + P_y(x,y)^2\right) \quad (16)$$

$$\frac{\partial \mathbf{v}(x,y,t)}{\partial t} = \mu \nabla^2 \mathbf{v}(x,y,t) - \left(\mathbf{v}(x,y,t) - P_y(x,y)\right) \cdot \left(P_x(x,y)^2 + P_y(x,y)^2\right), \quad (17)$$

wobei $\mathbf{u}(x,y)$ und $\mathbf{v}(x,y)$ numerisch zu lösen sind. In Abhängigkeit von der Anzahl der Iterationen erreicht man eine mehr oder weniger große Diffusion des Gradienten über das Bild.

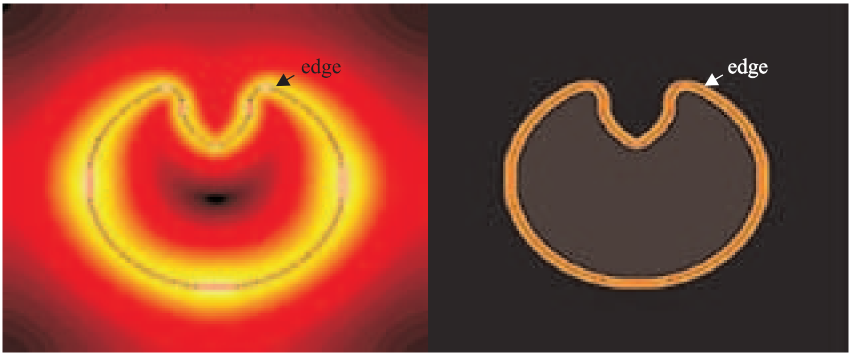

Abb. 5: Vergleich zwischen beiden externen Energien. Dargestellt ist der Absolutwert des GVF (links) und der konventionellen Energie (rechts)

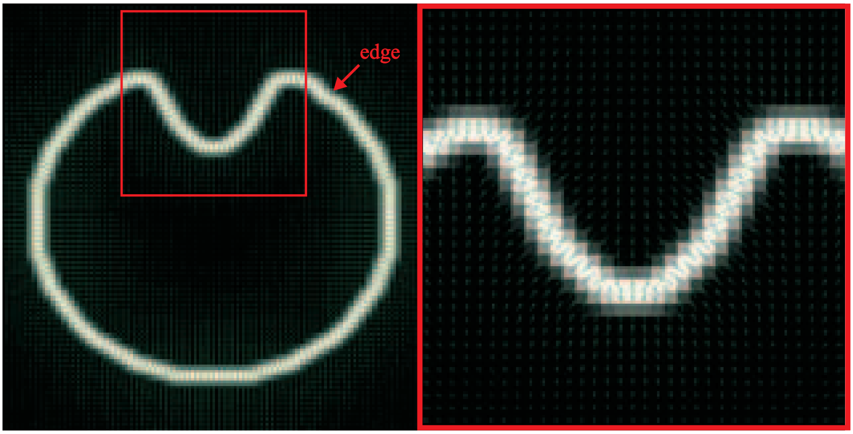

Abb. 6: Vergrößerung des erhaltenen Vektor-Feldes.

3 Resultate und Diskussion

Die Detektion der inneren Kante des Fettsignals der Haut ist eine schwierige Aufgabe. Die Gradient-Vector-Flow-Version wurde auf die MR-Daten angewendet und im Folgenden sollen Vor- und Nachteile für den beschriebenen Anwendungsbereich aufgezeigt werden.

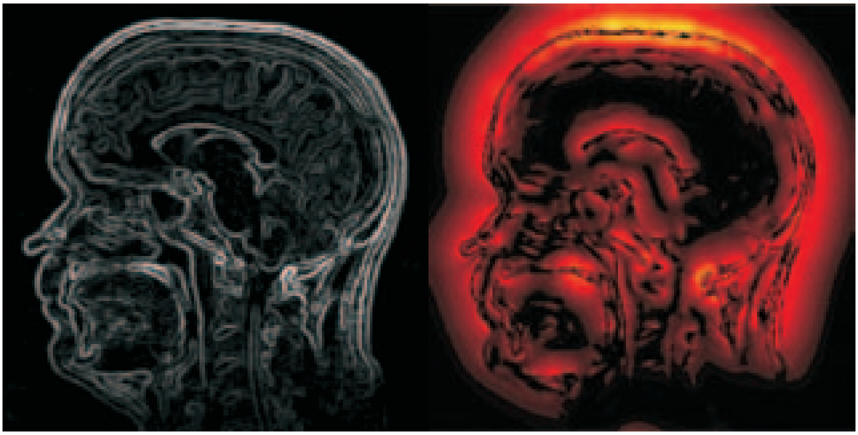

Abb. 7: Vergleich zwischen der normalen externen Energie (links) und Gradient-Vector-Flow-Field (rechts). Dargestellt wird jeweils der Betrag der Energien.

Diese beiden Bilder in Abbildung 7 unterstreichen den Unterschied zwischen beiden Energiefunktionalen. Einerseits wird durch das GVF Feld eine Diffusion der Gradienten-Information der Kanten erreicht und somit der Einflussbereich der externen Energie erhöht. Andererseits wird aber, wie man beim Vergleich der beiden Bilder klar erkennen kann, im Inneren der MR-Daten die Informationen durch Rauschen überlagert – feine Strukturen verschwinden. Dies ist darauf zurück zu führen, dass durch die vielen Strukturen im Inneren des Kopfes die Diffusion des Vektorfeldes zu einem Verschwinden von lokalen Informationen in kleinen Bereichen führt. Deshalb ist dieses Verfahren nur von Vorteil bei der Annäherung an die äußere Kante des Fettsignals der Haut. Bei der Lokalisierung der inneren Kante muss momentan noch auf die traditionelle Formulierung des Snake-Algorithmus zurückgegriffen werden.

In Abbildung 8 werden erste Resultate der Annäherung der Snake an die äußere Kante des Fettsignals gezeigt.

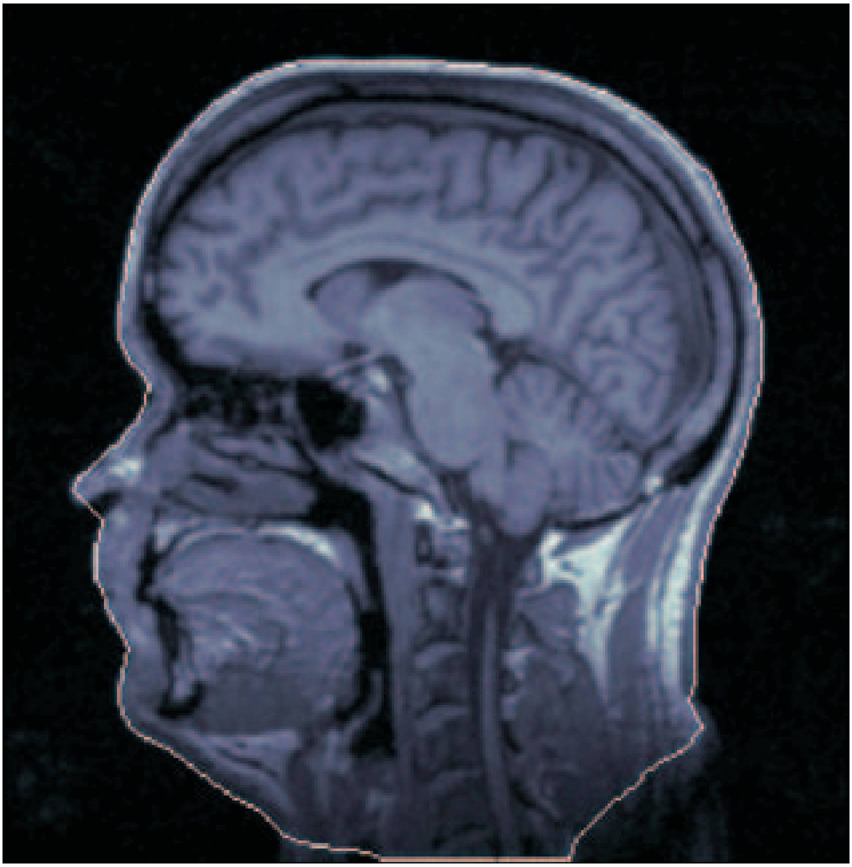

Abb. 8: Lokalisierung der äußeren Kante des Gesichtes

Zur numerischen Lösung der Euler Lagrange Gleichung wurde ein Greedy-Algorithmus eingesetzt. Die äußere Kante wurde in dem Sobel-gefilterten Bild gelöscht. Anschließend wird die innere Kante des Fettsignales detektiert:

Abb. 9: Erste Resultate der Lokalisierung der inneren Kante des Fettsignals der Haut.

Die Bilder zeigen, dass das Verfahren zu sehr guten Ergebnissen im oberen Bereich des Kopfes führt (blaue Pfeile). Im Bereich des Kinns und in der Nähe des Nasions hingegen (rote Pfeile) entsprechen die gezeigten Ergebnisse noch nicht den Erwartungen. Dies liegt daran, dass hier die Kante des Signales unterbrochen wird bzw. keine klar zu segmentierende Kante erkennbar ist (siehe Abb. 9). Vor allem muss noch nach anderen adäquaten Energiefunktionalen gesucht werden, die eine zuverlässige Segmentierung des Fettsignals erlauben (siehe z. B. [18]). Dennoch zeigen die Ergebnisse, dass es möglich ist, das Fettsignal aus MR-Aufnahmen mittels aktiver Konturen zu segmentieren.

Vor allem erhoffen wir uns bessere Resultate bei der Implementierung des Verfahrens in 3D, da somit nicht nur die Informationen einer Schicht zur Verfügung stehen und folglich lokal das Fehlen von Informationen, respektive Kanten, nicht so sehr ins Gewicht fällt.

Eine weitere Möglichkeit wäre, nicht MR-Daten zu nutzen, sondern auf CT Daten zurückzugreifen. Auch diese beinhalten zum Teil Informationen über die Schichtdicke der Haut und dazu weniger komplexe Strukturen. Dies würde die Segmentierung sehr vereinfachen. Unser Ziel ist es aber, eine Datenbank mit verschiedenen Templates zu erzeugen und somit ist die Verwendung von CT Daten eher als problematisch anzusehen, da diese nicht in einer so großen Menge zur Verfügung stehen wie MR-Datensätze. Außerdem werden CT Aufnahmen nur in den seltensten Fällen vom ganzen Kopf gemacht, um die durch die CT Aufnahmen entstehende Strahlenbelastung für den Patienten möglichst minimal zu halten.

4 Zusammenfassung und Ausblick

In diesem Beitrag wurde ein neues Verfahren zum Erstellen eines Gesichtstemplates für forensische Applikationen, welches die komplette Tiefeninformation für das nachzubildende Gesicht liefert, vorgestellt. Es wird gezeigt, dass Snakes ein sehr gutes Mittel für die Segmentierung darstellen, aber dennoch einige Probleme in unserer Implementierung gelöst werden müssen, um zufrieden stellende Ergebnisse zu erhalten. In naher Zukunft soll, wie eben schon kurz angesprochen, das Verfahren auf 3D erweitert werden. Die Erweiterung des Snake-Konzepts auf 3D, die so genannten Balloons, folgt im Allgemeinen derselben Idee wie der vorgestellte 2D Algorithmus. Wiederum bewegt sich eine, diesmal 2-dimensionale, aktive Fläche durch den Raum und nähert sich, basierend auf der Minimierung eines Energiefunktionals, den gesuchten Merkmalen.

Die interne Energie der Oberfläche muss dabei aber auf eine andere Art bestimmt werden. Deshalb wird die durch die Berechnung von $\mathbf{v}(r,s)$ zu minimierende Euler-Lagrange Gleichung (Gl. 3) modifiziert [19]:

$$\begin{aligned}&\nabla E_{ext}(\mathbf{v},I) + \alpha_s \frac{d^2\mathbf{v}(r,s)}{ds^2} + \alpha_r \frac{d^2\mathbf{v}(r,s)}{dr^2} - \dots \\ &\dots - \beta_s \frac{d^4\mathbf{v}(r,s)}{ds^4} - \beta_r \frac{d^4\mathbf{v}(r,s)}{dr^4} - \beta_{sr} \frac{d^4\mathbf{v}(r,s)}{ds^2 dr^2} = 0\end{aligned} \tag{18}$$

Genau wie in 2D ist die Kernaussage dieser Gleichung, dass sich zum Lösen des Problems ein Gleichgewicht zwischen der, aus dem Datensatz errechneten, externen Energie, und der, die flächigen Kontur beschreibenden internen Energie, einstellen muss.

Die interne Energie wird zu [20]:

$$\begin{aligned}E_{\text{int}} = &\iint \alpha_s \left|\frac{d\mathbf{v}(r,s)}{ds}\right|^2 + \alpha_r \left|\frac{d\mathbf{v}(r,s)}{dr}\right|^2 + \dots \\ &\dots + \beta_s \frac{d^2\mathbf{v}(r,s)}{ds^2} + \beta_r \frac{d^2\mathbf{v}(r,s)}{dr^2} + \beta_{sr} \frac{d^2\mathbf{v}(r,s)}{dsdr}\, dsdr\end{aligned} \tag{19}$$

Die Parameter α_s and α_r der beiden Gleichungen (Gl. (18), Gl. (19)) beschreiben die Gewichtung der Parameter für die Elastizität und die Parameter β_s and β_r repräsentieren die Gewichtung der Steifigkeit entlang der korrespondierenden *s*- und *r*-Achse. Der letzte Term, der beiden Energiefunktionale, wird durch β_{sr} kontrolliert, und beschreibt die Unterdrückung der Rotation.

Die Segmentierung des Fettsignals ist nur der erste Schritt in dem vorgestellten Projekt. Das eigentliche Ziel ist es, das segmentierte Template mittels aktiver Konturen auf das Computertomogramm des Schädels zu registrieren. Wenn nötig sollen maximal vier korrespondierende Punkte in den Datensätzen gesetzt werden, wie z. B. Punkte am Nasion, Inion, am linken und am rechten Preauricular Punkt und auf der Nasenspitze, die eine direkte Referenz zwischen der aktiven Kontur und dem Target, respektive dem Schädel, erzeugen. Der Ansatz für das

Mapping ist, dass die verwendete Aktive Kontur neben den ihr innewohnenden physikalischen Eigenschaften Krümmung und Steifigkeit, noch eine weitere Eigenschaft bekommt – die Dicke des Hautsignales. Die Resultate dieser Arbeit werden zeigen ob es möglich ist den Snake Algorithmus nicht nur für die Segmentierung, sondern auch für die Registrierung von Daten zu verwenden.

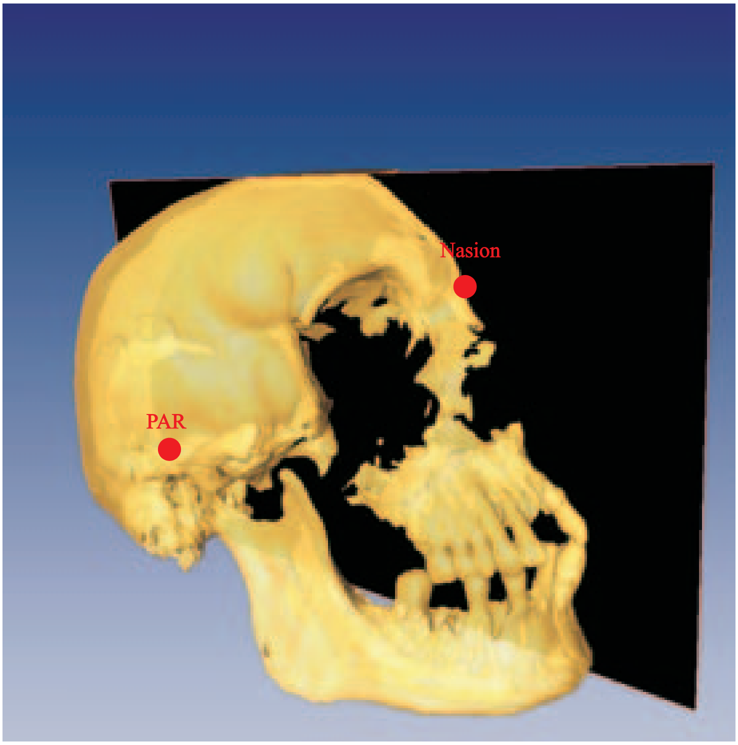

Abb. 10: 3D-CT des Schädels des Herzogs von Sachsen, Widukind, spätes 8. Jahrhundert.

5 Literatur

[1] M. Kass, A. Witkin and D. Terzopoulus, „Snakes: Active Contour Models“, *International Journal of Computer Vision*, vol. 1(4), pp. 321–331, 1987.

[2] S. Rhine, „Tissue thickness measures: American Caucasoids, American Blacks, Southwestern Indians“, Physical Anthropology Laboratories, Maxwell Museum of Anthropology, University of New Mexico, 1982, 1983, 1984.

[3] V. M. Phillips and N. A. Smuts, „Facial Reconstruction: Utilization of Computerized Tomography to Measure Facial Tissue Thickness in Mixed Racial Population“, in *J. Forensic Sci.*, vol. 83, pp. 51–59, 1996.

[4] D. W. Bullock, „Computer Assisted 3D Craniofacial Reconstruction“, M. S. thesis, University of British Columbia, Canada, 1999.

[5] R. P. Helmer, S. Rohricht, C. Petersen, and F. Mohr, „*Forensic Analysis of the Skull*“, Chapter 17: Assessment of the Reliability of Facial Reconstruction, Wiley-Liss, 1993, p. 229.

[6] J. Müller, A. Mang, D. Thomsen and T. M. Buzug, „Regularized 3D Thin-Plate Splines for Soft-Tissue Reconstruction“, in *Proceedings of the BMT 2004*, vol. 49, pp. 134–135, February 2004.

[7] G. Quatrehomme, S. Cotin, G. Subsol, H. Delingette, Y. Garidel,G. Grevin, M. Fidrich, P. Bailet and A. Ollier, „A Fully Three-Dimensional Method for Facial Reconstruction Based on Deformable Models“, in *J. Forensic Sci*, vol. 42, p. 649, 1997.

[8] M. W. Jones, „Facial Reconstruction Using Volumetric Data“, in *Proceedings of the Vision Modelling and Visualization Conference 2001 (VMV 2001),* pp. 21–23, 2001.

[9] C. Xu and J. L. Prince, „Snakes, Shapes and Gradient Vector Flow“, in *IEEE Transactions on Image Processing*, vol. 7(3), pp. 359–369, 1998.

[10] C. Xu and J. L. Prince, „Gradient Vector Flow: A New External Force“, in *Proceedings of the IEEE Conference on Computer Vision an Pattern Recognition (CVPR)*, pp. 66–71, June 1997.

[11] C. Xu and J. L. Prince, „Generalized Gradient Vector Flow External Forces for Active Contours“, in *Signal Processing*, vol. 71, pp. 131–139, 1998.

[12] C. Xu and D. L. Pham, J. L. Prince, „Medical Image Segmentation using Deformable Models“, in *Handbook of Medical Imaging – Volume 2: Medical Image Processing and Analysis*, J. M. Fitzpatrick and M. Sonka,. SPIE Press, May 2000, pp. 129–174.

[13] K. S. Ntalianis, N. D. Doulamis, A. D. Doulamis, and D. S. Kollias, „Multiresolution Gradient Vector Flow Field, A fast Implementation Towards Video Object Plane Segmentation“, in *Proceedings of the IEEE International Conference on Multimedia and Exposition (ICME 2001)*, pp. 1–3, August 2001.

[14] S. Luo, R. Li and S. Ourselin, „A new Deformable Model Using Dynamic Gradient Vector Flow and Adaptive Balloon Forces“, in *Proceedings of the APRS Workshop on Digital Image Computing*, pp. 9–14, February 2003.

[15] B. K. B. Horn and B. G. Schunk, „Determining Optical Flow“, *Artificial Intelligence*, vol. 17, pp. 185–203, August 1981

[16] X. Hang, N. L. Greenberg, and J. D. Thomas, „A Geometric Deformable Model for Echocardiographic Image Segmentation“, *Computers in Cardiology*, vol. 29, pp. 77–80, September 2002.

[17] M. F. Santarelli, V. Positano, C. Michelassi, M. Lombardi, and L. Landini, „Automated Cardiac MR Image Segmentation: Theory and Measurement Evaluation“, in *Medical Engineering and Physics*, vol 25(2), pp. 149–159, March 2003.

[18] M. Wei, Y. Zhou, and M. Wan, „A fast Snake Model based on Non-Linear Diffusion for Medical Image Segmentation“, in *Computerized Medical Imaging and Graphics*, vol. 28 (3), pp. 109–117, 2004.

[19] J. Ahlberg, „Active Contours in Three Dimensions“, M. S. thesis No. LiTH-ISY-EX-1708, Department of Electrical Engineering, Computer Visions Laboratory, Linköpings University, Sweden, 1996.

[20] C. D. Mansard et. al.: „Qantification of Multicontrast Vascular MR Images with NLSnake, an Active Contour Model: In Vitro Validation and In Vito Evaluation“, *Magnetic Resonance in Medicine*, vol. 51, pp. 370–379, January 2004.

Study on the facial tissue thickness of the Finns

Finnish facial tissue thickness

Sirpa Niinimäki,

Hartaantie 11 as 41, 90500 Oulu, Finland
Oulu University, Faculty of Arts, PL 1000, 90014 University of Oulu, Finland

Ari Karttunen

Radiologian klinikka, PL 50, 90029 Oulu, Finland

Abstract

The average tissue thickness of the Finnish face was measured from MRI-scans of adult patients in Oulu University Hospital for facial reconstruction purposes. A total of 31 soft-tissue measurements (49 including paired elements) and 17 cranial measurements were taken from axial, sagittal and coronal scans from 26 normal-weight males and 26 females and 14 over-weight males and 13 females. From this data, average tissue thickness was calculated. Also correlations between soft-tissue thicknesses and cranial measurements were calculated. It was discovered that soft-tissue thicknesses correlated strongly within cheek area and in mid face area, but more strongly in males than females. Cranial dimensions correlated in facial area to cranial length in males and females, but stronger in females. There is some correlation between soft-tissue thicknesses and cranial dimension. These correlations were stronger in males than in females.

Introduction

The main objective was to determine the average facial tissue thickness of the Finns for facial reconstruction purposes. Previous studies of other populations have applied many different methods to measure tissue thickness. For example, with needle from cadavers [1], [2], with the help of x-ray [3], [4], [5], ultrasound [6], [7], [8], computer tomography [9], [10], or magnetic resonance imaging (MRI) [11] from living subjects. All of these methods have advantages and disadvantages. Because needle point method is applied to cadavers, there is a problem with dehydration shrinking and embalming increasing the tissue thickness. Simpson and Henneberg [1] recommend using cadavers that have been embalmed for some period of time so that the excess amount of embalming fluids has had time to drain out. Because radiographic applications are harmful to living tissue their use is usually limited to cases of medical necessity and x-rays are taken only from few angles [7]. Ultrasound is both inexpensive and harmless to living tissue, which allows the collection of a larger group of volunteers. The problem with this method is difficulties to separate bone from soft-tissue. Magnetic resonance imaging (MRI) gives the most detailed information compared to other medical imaging methods, but it is also the most expensive one. Therefore Smith and Throckmorton [8] recommend ultrasound over MRI because of its inexpensiveness.

Although soft-tissue thickness measurements have not been standardized, some common measurement points that allows comparisons of measurements. Most researchers use usually a set of about 20 to 25 different measurement points (not including paired elements). The tissue thickness data is usually grouped according to sex, age and nutritional status. One study has grouped the tissue thickness data according to body constitution type [12]. The sample sizes are usually about 20–40 individuals per sex; the study by Lebedinskaya et al. [7] is an exception because a total of 1695 individuals were measured from nine different population groups. They also studied the correlation of soft-tissue measurements from different parts of the face. They found that although there is a high positive correlation between the morphological zones of the face, there was a lack of correlations in oral and nasal areas.

Simpson and Henneberg [1] have addressed some critique towards using average values in facial reconstructions. They tried to find other means to reconstruct tissue thickness by examining correlations between soft-tissue thicknesses and cranial dimensions. While they found that there are strong correlations in soft-tissue thicknesses in different parts of the face, the cranial dimensions did not correlate as strongly with each other. They calculated regression equations to estimate soft-tissue thickness from cranial dimensions. Due to their restricted sample size (17 males and 23 females) they caution against using their study for more than an illustration of a possibility. In this study, we intended to test these preliminary results about the correlations between soft-tissue thicknesses and cranial dimensions.

Materials and Methods

The first choice of method for measuring the tissue thickness in this study was ultrasound for it allows larger sample sizes because it is not restricted to patient information. However, appropriate equipment was not available in the Oulu University Hospital. We decided to use magnetic resonance imaging (MRI) for data collection, for its resolution is the most accurate from all medical imaging devices. The MRI machineries used in Oulu University Hospital were 1.5 Tesla Signa Horizon (GE Medical System) and 1.5 Tesla Signa Twin Speed (GE Medical System). Data received from both of these machines are alike in relation to imaging bone and other tissue. The use of MRI limited the volunteers to normal protocol patients of Oulu University Hospital in need for MRI examination. Viewing of the scans and measuring of the tissues was done with Radworks -program on hospital computer. Patients were scanned according to normal Oulu University Hospital patient protocol, but additional scans were taken to cover the lower jaw. Scans were taken from coronal, sagittal and axial directions. The coronal and sagittal scans were taken directly perpendicular to the face, and the axial scans were taken parallel to corpus callosum. The axial scans were not therefore directly horizontal, but with a slight tilt from front to back. The scanning sequence for each direction was 5 mm thick and scans were taken with 1.5 mm spacing. Patients were scanned in supine position.

A set of 31 different tissue thickness measurement points (49 with paired elements) were chosen (fig. 1). Most of these points are used by other researchers making it possible to compare results [1], [2], [7], [10], [11], [13], [14]. Of these selected measurements, 13 were taken from the sagittal scans, four from the parasagittal scans in the level of outer canthus on both sides (paired measurement), nine paired measurements from the axial scans, and five paired measurements from the coronal scans. A set of 17 cranial measurements were selected for the study of cranial dimension correlations. These cranial measurements and their landmarks are based to [15], [16], [17]. Measuring cranial dimensions from MRI scans presented few limitations, and therefore some of the rudimentary measurements could not be taken. The correct measurement points were pinpointed from each pack of sagittal, axial, and coronal scans.

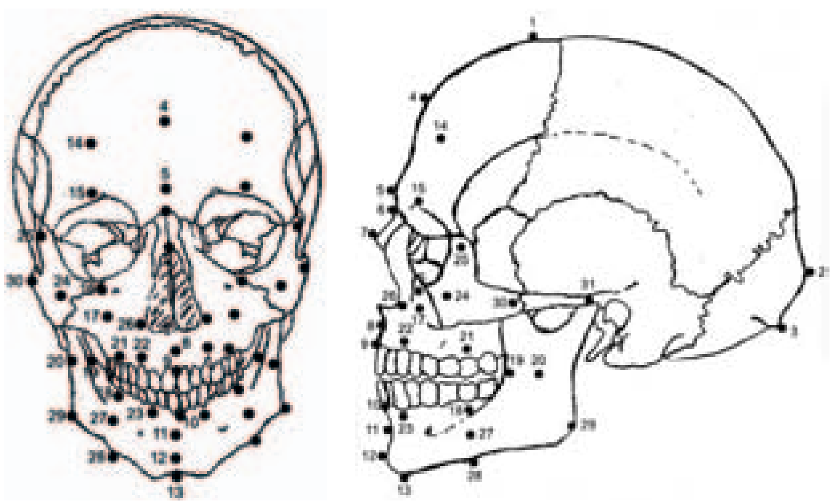

Fig. 1: Measurement points. 1. vertex, 2. inion, 3. opisthocranion, 4. supraglabella, 5. glabella, 6. nasion, 7. rhinion, 8. philtrum, 9. upper lip margin, 10. lower lip margin, 11. chin fissure, 12. pogonion, 13. gnathion, 14. frontal eminence, 15. supraorbital, 16. suborbital, 17. maxilla, 18. second submolar, 19. occlusal line, 20. ramus, 21. second supramolar, 22. subcanine, 23. supracanine, 24. malare, 25. outer canthus, 26. alare, 27. mandibular body, 28. mandibular border, 29. gonion, 30. zygomatic, 31. supraglenoid.

The use of MRI greatly restricted the sample size. It was thus agreed that at least 25 males and 25 females with normal weight should be measured. Normal weight was determined with body mass index (weight in kilograms divided by height in meters squared). A person was considered normal-weight if body mass index was over 18 but under 25. Collection of adult normal weight volunteers proved to be a lengthy process: the collection of volunteers began in the spring of 2003 and the measuring was completed in the fall of 2004. In the end, a total of 40 males and 39 females were measured. Of these 26 males and 26 females was normal-weight. Cranial measurements were taken from 29 females and 29 males. For the normal-weight female patients average body mass index was 22.04 (SD 1.56) with range of 19.43–24.98 and for normal weight males 22.66 (SD 1.78) with range of 18.99–24.97 (Tab. 1). The measured patients also had to be between the ages of 18 and 50, and with no medication or other condition that would affect the tissue thickness. The average age for normal-weight females was 36 years (SD 9.2) with range of 18–49 years and for males 32 years (SD 9.4) with range of 19–49 years (Tab. 2).

Microsoft Excel XP was used for data analysis. Patients were grouped according to sex and whether they were normal or over weight. Average values were calculated for each group. Standard deviations, minimum and maximum values are provided for the normal-weight groups. Symmetry of paired elements was tested with paired T-test. This test showed statistically significant differences in supraorbital measurements in females and males and frontal eminence in males. This existing asymmetry could be misleading and a result of a relatively small sample. Because the asymmetry existed in this sample, those measurement points that displayed asymmetry were presented separately in tables. Average values were calculated for all paired measurements. Correlations were examined between soft-tissue thicknesses, cranial dimensions and between soft-tissue thicknesses and cranial dimensions.

There may be some measurement error due to variation in soft-tissue and craniometric landmark locations [1]. The measurement error was calculated by re-measuring the tissue thickness from 12 individuals (six males and six females). The re-measured value was subtracted from the original value. This subtraction was first squared and then divided by the number of individuals multiplied by two. Finally, square-root was taken from this result.

$$\text{TEM} \quad \frac{\hat{I}\,D^2_{1;2}}{2N}$$

The tissue thickness of the Finns was compared to the tissue thickness of Russians and Lithuanians [7], African Americans [2], African Caucasians [14], mixed [10], Japanese [13], and North-West Indians [11].

Results

The tissue thickness measurements and the related statistics are in tables 1–8. The thinnest tissues are in the scalp area and in the eye and nose area. The thickest tissues are in the middle cheek area. This is also where there is the most variation within measurement. Male-female comparison indicated that females have clearly thicker tissues in vertex, nasion, gnathion, second supramolar, subcanine, malare, outer canthus, and gonion. Males have thicker tissues in inion, glabella, rhinion, midphiltrum, upper lip margin, suborbital, maxilla, ramus, alare, mandibular body, and supraglenoid representing the mid facial area and the lateral part of lower jaw.

There are stronger correlations in soft-tissue thickness in males than in females. It seems that in males the tissue thicknesses in the mid facial area correlate strongly, also with thicknesses in the upper and lower cheek area. In females there is a soft-tissue correlation between upper cheek, mid part of lower jaw, forehead, and the area around eyes. Also areas that have only thin layer of adipose tissue have similar values (Tables 3–4). In females glabella and in males outer canthus correlates with most of the other soft-tissue thicknesses in various parts of the face.

Tab. 1: Soft-tissue thickness for females. Mean (mm), standard deviation, minimum, maximum (SD), technical error of measurement (TEM) for normal-weight and mean (mm) for over-weight.

							Over-weight	
Variable	**Mean**	**SD**	**Minimum**	**Maximum**	**N**	**TIM**	**Mean**	**N**
age	34,00	9,15	18,00	49,00	26		38,62	13
weight	58,90	6,40	49,00	70,00	26		83,69	13
height	163,70	5,95	151,00	176,00	26		165,46	13
body mass index	22,04	1,56	19,43	24,98	26		30,53	13
vertex	3,49	0,75	1,90	4,82	26	0,35	4,70	13
inion	3,85	1,07	2,06	6,71	26	1,19	5,36	13
opisthocranion	5,47	1,45	2,56	8,01	26	1,19	8,58	13
supraglabella	3,07	0,77	1,91	4,26	26	0,76	3,85	13
glabella	5,17	1,18	3,24	8,16	26	0,57	6,46	13
nasion	6,29	1,61	2,23	10,04	26	2,02	7,75	13
rhinion	2,38	1,09	1,10	6,10	26	1,54	2,58	13
philtrum	11,53	1,32	8,92	14,00	26	1,01	12,31	13
upper lip margin	11,96	2,04	7,51	15,38	25	1,06	12,42	13
lower lip margin	13,75	1,74	10,75	16,56	26	1,24	13,61	13
chin fissure	10,04	1,15	7,79	12,51	26	1,13	11,58	13
pogonion	11,02	1,72	7,63	14,09	26	1,22	12,49	13
gnathion	7,90	2,00	4,06	10,82	25	1,00	10,09	13
frontal eminence	3,79	0,85	2,59	5,85	26	0,56	5,01	13
supraorbital	8,40	1,61	4,45	12,19	26	1,30	9,80	13
left	8,97	1,52	6,17	12,19	26	0,73		

							Over-weight	
Variable	**Mean**	**SD**	**Mini-mum**	**Maxi-mum**	**N**	**TIM**	**Mean**	**N**
right	7,84	1,52	4,45	10,22	26	1,10		
suborbital	5,25	1,59	1,32	8,65	26	0,98	7,13	13
maxilla	19,19	2,66	10,67	24,20	26	1,91	19,71	13
second submolar	16,86	2,96	10,30	22,81	26	0,96	19,60	13
occlusal line	22,24	2,97	15,21	29,01	26	1,40	25,84	13
ramus	20,29	3,57	9,14	27,52	26	1,16	25,70	13
second supramolar	30,48	4,62	8,33	38,69	25	2,88	30,69	13
supracanine	10,90	2,14	5,51	14,78	25	0,90	11,74	11
subcanine	8,88	2,25	5,51	13,16	24	1,34	9,84	13
malare	9,69	2,04	2,31	12,57	26	2,18	12,09	13
outer canthus	3,32	1,52	1,05	9,49	26	1,54	4,46	13
alare	3,38	1,16	1,10	5,78	26	1,30	3,89	13
mandibular body	11,67	4,98	3,22	21,87	26	2,80	15,70	13
mandibular border	13,45	3,59	5,37	20,20	24	2,89	18,10	9
gonion	13,16	3,18	6,36	19,90	26	3,76	20,55	13
zygomatic	8,07	2,18	3,18	14,59	26	1,22	12,68	13
supraglenoid	11,69	2,40	6,67	18,03	26	2,54	15,10	13

Tab. 2: Soft-tissue thickness for males. Mean (mm), standard deviation, minimum, maximum (SD), technical error of measurement (TEM) for normal-weight and mean (mm) for over-weight.

							Over-weight	
Variable	**Mean**	**SD**	**Mini-mum**	**Maxi-mum**	**N**	**TIM**	**Mean**	**N**
age	33	19	49	9,56	26		31,64	14
weight	71	60	82	6,11	26		90,07	14
height	177,1	162	190	6,44	26		177,00	14
body mass index	22,66	18,99	24,97	1,78	26		28,62	14
vertex	4,38	2,32	8,12	1,31	26	2,03	5,27	14
inion	4,58	2,30	7,59	1,06	26	1,17	5,76	14
opisthocranion	7,04	3,67	11,98	2,24	26	1,49	8,68	14
supraglabella	3,44	2,19	4,81	0,82	26	1,37	3,84	14
glabella	5,81	3,94	8,60	1,14	26	1,35	6,65	14

							Over-weight	
Variable	**Mean**	**SD**	**Mini-mum**	**Maxi-mum**	**N**	**TIM**	**Mean**	**N**
nasion	8,37	5,72	11,03	1,42	26	1,23	9,74	14
rhinion	2,57	1,26	4,11	0,69	26	1,33	2,89	14
philtrum	14,80	10,68	22,86	2,57	26	2,17	15,02	14
upper lip margin	14,30	10,83	18,77	1,94	26	2,70	15,14	14
lower lip margin	15,34	10,46	19,57	2,09	26	3,51	16,30	14
chin fissure	11,16	8,65	15,21	1,75	26	0,94	11,93	14
pogonion	12,68	10,51	16,37	1,52	24	0,73	14,17	14
gnathion	9,32	6,40	13,05	1,92	19	1,27	12,00	11
frontal eminence	4,54	2,35	8,87	1,13	26	1,72	4,54	14
left	5,01	3,51	6,49	0,66	26	0,81		
right	4,08	2,35	8,87	1,30	26	1,63		
supraorbital	9,51	6,92	12,52	1,63	26	3,33	10,16	14
left	10,26	7,22	12,52	1,50	26	2,48		
right	8,77	6,92	12,01	1,42	26	2,24		
suborbital	5,37	2,46	9,06	1,32	26	1,60	6,62	14
maxilla	19,73	13,44	27,21	2,75	26	8,58	22,34	14
second submolar	15,67	10,51	23,35	3,62	25	4,97	18,73	14
occlusal line	21,01	10,58	29,42	4,19	25	2,47	26,72	14
ramus	20,53	12,98	27,94	3,48	25	2,62	26,12	14
second supramolar	29,78	18,15	38,28	4,03	26	8,04	33,73	14
subcanine	11,05	8,25	14,25	1,49	25	1,30	12,89	14
supracanine	11,14	8,22	13,70	1,56	25	1,63	12,01	14
malare	8,09	5,41	10,86	1,46	26	1,39	10,22	14
outer canthus	2,80	1,17	5,67	1,17	25	1,59	3,34	14
alare	3,23	1,52	6,56	1,07	26	2,73	3,81	14
mandibular body	14,15	8,18	23,18	3,70	26	4,17	19,85	13
mandibular border	11,94	6,58	19,74	3,47	17	2,05	18,72	8
gonion	11,81	5,03	23,18	4,33	26	3,43	20,27	13
zygomatic	8,54	4.99	15,86	2,59	26	2,76	11,97	14
supraglenoid	13,15	9,38	17,33	1,97	26	1,65	15,67	14

Tab. 3. Soft-tissue to soft-tissue correlation table for normal-weight females.

	1	2	3	4	5	6	7	8	9	10	11	12	13	14	15	16	17	18	19	20	21	22	23	24	25	26	27	28	29	30	31	32	33
1 height	**1**																																
2 BMI		**1**																															
3 vertez		0,33	**1**																														
4 inion			0,39	**1**																													
5 opistho-cranium		0,30		0,37	**1**																												
6 metopion				**0,44**		**1**																											
7 glabella	0,38			**0,43**			**1**																										
8 nasion								**1**																									
9 rhinion	0,34			8,38			**0,63**		**1**																								
10 midphiltrum			– 0,30				**0,41**		0,32	**1**																							
11 upper lip margin				**0,41**		**0,49**	**0,41**		0,32	**0,55**	**1**																						
12 lower lip margin											**0,55**	**1**																					
13 chin fissure					0,34							0,33	**1**																				
14 pogonion		**0,54**	**0,41**											**1**																			
15 gnathion		0,33													**1**																		
16 frontal eminence			**0,67**	**0,44**			**0,42**	**0,43**						0,34		**1**																	
17 supraorbital							**0,55**		0,34	0,36	**0,42**						**1**																

	1	2	3	4	5	6	7	8	9	10	11	12	13	14	15	16	17	18	19	20	21	22	23	24	25	26	27	28	29	30	31	32	33
18 suborbital				0,33		0,32	**0,50**		**0,35**		0,37						**0,49**	**1**															
19 mazilla				**0,54**			0,37									**0,48**			**1**														
20 second submolar		0,30		0,33		0,33	**0,50**		**0,41**	0,32	**0,54**	**0,42**					0,38	0,35		**1**													
21 occlusal line							**0,43**		0,36		**0,45**							**0,41**		**0,63**	**1**												
22 ramus						**–0,55**							**–0,38**								0,35	**1**											
23 second supramolar							**0,44**	0,33		**0,53**	**0,49**							0,35			**0,41**	–0,34	**1**										
24 subcanine				0,39			**0,53**		**0,51**	**0,56**	**0,59**	0,32	0,33				**0,49**	**0,52**	0,38	**0,59**	0,33		**0,42**	**1**									
25 supracanine									**0,46**	0,34									0,31	0,35	0,34			**0,58**	**1**								
26 malare		**0,49**		0,34			**0,49**		0,39		**0,49**				**0,40**		**0,62**		0,30	0,34				0,37		**1**							
27 puter canthus		–0,36				**0,42**									**–0,43**			**0,50**							**0,46**	–0,36	**1**						
28 alare			**0,51**	**0,44**			**0,41**									**0,42**			**0,40**									**1**					
29 mandibular body				0,36		0,35					0,39								0,38	**0,42**								**0,56**	**1**				
30 mandibular border											**0,52**				**0,41**						**0,41**				**0,47**					**1**			
31 gonion		0,35		0,33							0,30		**–0,46**		**0,55**											0,33	–0,33		**0,46**	0,31	**1**		
32 zygomatic		**0,67**							0,34		0,33	0,35		0,37	0,33											**0,56**				**0,42**		**1**	
33 supraglenoid		**0,69**		0,32			**0,44**		**0,48**					**0,41**					0,30	**0,48**	**0,45**	0,37		**0,44**		**0,61**						**0,77**	**1**

Tab. 4: Soft-tissue to soft-tissue correlation table for normal-weight males.

	1	2	3	4	5	6	7	8	9	10	11	12	13	14	15	16	17	18	19	20	21	22	23	24	25	26	27	20	29	30	31	32	33
1 height	**1**																																
2 BMI	**–0,48**	**1**																															
3 vertez			**1**																														
4 inion			**0,80**	**1**																													
5 opistho-cranium		0,33	**0,76**	**0,90**	**1**																												
6 metopion			**0,92**	**0,88**	**0,81**	**1**																											
7 glabella			**0,84**	**0,92**	**0,88**	**0,88**	**1**																										
8 nasion			**0,59**	**0,82**	**0,81**	**0,68**	**0,89**	**1**																									
9 rhinion			**0,91**	**0,83**	**0,76**	**0,93**	**0,84**	**0,62**	**1**																								
10 mid-philtrum	0,31	–0,31	**0,80**	**0,80**	**0,85**	**0,79**	**0,89**	**0,82**	**0,73**	**1**																							
11 upper lip margin			**0,93**	**0,78**	**0,82**	**0,87**	**0,87**	**0,71**	**0,82**	**0,94**	**1**																						
12 lower lip margin			**0,96**	**0,73**	**0,77**	**0,86**	**0,82**	**0,62**	**0,84**	**0,88**	**0,98**	**1**																					
13 chin fissure				**0,49**	**0,45**		**0,52**	**0,75**		**0,59**	0,36		**1**																				
14 pogonion				0,36	0,39		**0,40**	**0,69**		**0,46**			**0,90**	**1**																			
15 gnathion				0,39	**0,49**		**0,48**	**0,71**		**0,56**	0,39		**0,90**	**0,88**	**1**																		
16 frontal eminence	0,33					**0,41**	**0,42**									**1**																	

	1	2	3	4	5	6	7	8	9	10	11	12	13	14	15	16	17	18	19	20	21	22	23	24	25	26	27	20	29	30	31	32	33
17 supra orbital											−0,34						**1**																
18 sub-orbital		0,30		**0,40**	**0,54**			0,33										**1**															
19 mazilla	0,36									**0,43**		0,37							**1**														
20 second submolar					0,30						0,32				0,31	**0,51**				**1**													
21 occlusal line	0,39	0,30			**0,46**															**0,58**	**1**												
22 ramus	0,34	0,34		**0,44**	**0,44**		**0,33**									**0,39**				**0,62**	**0,92**	**1**											
23 second supramolar				0,33	**0,50**													**0,50**		0,37	**0,57**	**0,55**	**1**										
24 sub-canine							0,37				**0,45**	**0,53**		**0,49**	**0,60**									**1**									
25 supra-canine							**0,49**			**0,55**	**0,45**	**0,71**	0,37						**0,52**					**0,41**	**1**								
26 malare	**0,48**														0,36	**0,54**		0,38		**0,62**	**0,58**	**0,56**	**0,52**			**1**							
27 outer canthus	0,30			0,33			**0,39**			0,38				0,31		**0,62**	**0,41**			**0,74**	**0,58**	**0,64**	0,33			**0,60**	**1**						
20 alare				**0,60**	**0,42**													**0,54**		**0,42**		0,30					**0,41**	**1**					
29 mandib-ular body		**0,48**		0,39	0,35			**0,33**						**0,48**	**0,57**			0,33		**0,49**	**0,62**	**0,65**	0,37			0,39	**0,57**	0,34	**1**				
30 mandib-ular border						−0,38	**0,54**	**0,40**	**0,32**	**0,42**		0,35			**0,56**					0,38				0,39	**0,40**				**0,58**	**1**			

	1	2	3	4	5	6	7	8	9	10	11	12	13	14	15	16	17	18	19	20	21	22	23	24	25	26	27	20	29	30	31	32	33
31 gonion		**0,51**		**0,41**	**0,44**		0,38								**0,63**	0,37				**0,67**	**0,67**	**0,74**	0,38			**0,56**	**0,62**		**0,79**	**0,54**	**1**		
32 zigo-matic		**0,45**													**0,44**	**0,48**	0,33			**0,66**	**0,65**	**0,73**	0,37			**0,59**	**0,76**		**0,62**	0,37	**0,76**	**1**	
33 supragle-noid					0,37									0,37	**0,50**	0,37		0,30		**0,49**	**0,41**	**0,54**	0,33			**0,46**	**0,49**	0,33			**0,48**	**0,60**	**1**

Cranial dimensions correlated with each other also with some extent both in males and females (Tables 5–6), but the correlation is stronger in females than males. In females there was a strong correlation within facial area cranial measurements. This tendency could also be found in males but it was not as strong. Some of the correlation in males was negative.

Tab. 5: Cranial dimension correlation table for females.

	g-op	ba-b	ba-v	n-sd	n-ns	n-gn	idi-gn	ba-idi	ba-n	ft-ft	ecm-ecm	enm-enm	ol-ol	eu-eu	zy-zy	go-go	cdl-cdl	height	BMI
g-op	**1**																		
ba-b		**1**																	
ba-v		**0,90**	**1**																
n-sd	**0,45**		0,30	**1**															
n-ns				**0,67**	**1**														
n-gn	**0,65**			**0,82**	**0,54**	**1**													
idi-gn	**0,54**	0,37	**0,43**	**0,41**		**0,64**	**1**												
ba-idi	0,37	**0,50**	0,30	**0,63**	0,31	**0,55**	0,35	**1**											
ba-n	0,33	**0,63**	**0,46**	**0,46**	0,34	**0,53**		**0,82**	**1**										
ft-ft	0,31	**0,54**	**0,56**	**0,57**	**0,51**	**0,45**		0,38	**0,57**	**1**									
ecm-ecm											**1**								
enm-enm		0,35	0,32								**0,53**	**1**							
ol-ol	0,31	**0,49**	**0,43**	0,37		**0,46**	0,37	**0,56**	**0,43**				**1**						
eu-eu			0,31							**0,41**		**0,42**		**1**					
zy-zy										0,38		**0,53**		**0,73**	**1**				
go-go										0,31	0,30				0,32	**1**			
cdl-cdl														**0,42**	**0,49**		**1**		
height		0,30				0,36	**0,44**						**0,59**					**1**	
BMI		**0,51**	**0,44**				**0,41**	0,30	0,31					0,30					**1**

Tab. 6: Cranial dimension correlation table for males.

	g-op	ba-b	ba-v	n-sd	n-ns	n-gn	idi-gn	ba-idi	ba-n	ft-ft	ecm-ecm	enm-enm	ol-ol	eu-eu	zy-zy	go-go	cdl-cdl	height	BMI
g-op	**1**																		
ba-b		**1**																	
ba-v	0,35	**0,55**	**1**																
n-sd	0,31			**1**															
n-ns	0,31			**0,78**	**1**														
n-gn				**0,82**	**0,43**	**1**													
idi-gn						**0,59**	**1**												
ba-idi	**0,49**	–0,38						**1**											
ba-n	**0,44**	**0,47**		**0,69**	**0,60**	**0,65**			**1**										
ft-ft	**0,42**			**0,45**	**0,43**					**1**									
ecm-ecm	**0,47**				0,33			0,38			**1**								
enm-enm									–0,36		**0,67**	**1**							
ol-ol	0,32	–0,49						**0,61**			0,30		**1**						
eu-eu														**1**					
zy-zy				0,35	**0,40**				**0,54**	0,43	0,35				**1**				
go-go																**1**			
cdl-cdl	0,35			0,38				0,34	0,31								**1**		
height			0,33	0,39	0,36	0,30			**0,44**									**1**	
BMI								–0,34										**–0,48**	**1**

Explanation of abbreviations: glabella-opisthocranion, basion-bregma, basion-vertex, nasion-supradentale, nasion-gnathion, infradentale-gnathion, basion-nasion, frontotemporale-frontotemporale, ectomolare-ectomolare, endomolare-endomolare, orale-orale, euryon-euryon, zygion-zygion, gonion-gonion, codylion laterale-condylion laterale.

In females those tissue thickness points that correlate with body mass index are pogonion, malare, gonion, zygomatic, and supraglenoid. In males only three tissue thickness points correlated with body mass index. Those are zygomatic, mandibular body and gonion, representing the posterior part of cheek. This correlation was done with normal-weight groups.

In males the strongest correlations of cranial dimensions to soft-tissue thicknesses were found with basion-bregma height and basion-supradentale length measurements (Tab. 8), the former with lower, middle and upper cheek areas and the latter with upper and lower cheek areas. Palatal length (orale-orale) correlated with upper cheek area. All these three cranial dimensions contribute in prognatism of muzzle area and all these cranial measurements are influenced by the mastication stress of the pterygoid muscles. Maximum breadth of cranium (euryon-euryon), bizygomatic breadth, and nasion-supradentale length had no apparent correlation with any of the measured soft-tissue thickness.

In females notably weaker correlations could be found compared to males (Tab. 7). In males, glabella-opisthocranion length correlated (negatively) only with alare. In females this measurement has the strongest (negative) correlation with tissue thickness. It correlates with six tissue thickness measurements. Second strongest correlation is with basion-bregma height, but it correlated with only three tissue depth measurements. With soft-tissue thickness supracanine had the most (negative) correlations with cranial dimension. In males cranial correlations of each tissue thickness measurement is more evenly distributed. Females had almost no correlation with cranial dimension and the thicknesses in cheek area. It could be that males have stronger facial muscles and these muscles contribute to both cranial bone growth and tissue thickness.

Tab. 7: Soft-tissue correlation to cranial dimension table for females.

	g-op	ba-b	ba-v	n-sd	n-ns	n-gn	idi-gn	ba-idi	ba-n	ft-ft	ecm-ecm	enm-enm	ol-ol	eu-eu	zy-zy	go-go	cdl-cdl	height	BMI
height		0,30				0,36	**0,44**						**0,59**					**1**	
BMI		**0,51**	**0,44**				**0,41**	0,30	0,31					0,30				**0,72**	**1**
vertex					–0,34		**0,54**										0,32	**0,73**	
inion	**–0,41**							–0,32			0,38	0,36		0,30			0,39	**0,42**	
opisthocranium														**0,48**	0,35		0,36	0,35	
metopion	–0,34									–0,34						–0,30		0,34	
glabella																			
nasion		**0,43**	**0,48**			0,30	0,38											0,37	0,38
rhinion				0,32	0,35			0,37											
midphiltrum										**0,40**	0,34							0,33	0,34
upper lip margin	–0,35																		
lower lip margin				0,36				0,30								–0,36			
chin fissure										–0,32	–0,34	–0,37							
pogonion							0,33								**–0,47**	–0,33			
gnathion														0,35				**0,42**	
frontal eminence															–0,32				
supraorbital		**0,41**						0,33	**0,44**										
suborbital	**–0,42**										–0,30							0,33	
maxilla																			
second submolar					**–0,42**														
occlusal line					**–0,43**	–0,38											0,39	0,33	
ramus	**0,43**																		

	g-op	ba-b	ba-v	n-sd	n-ns	n-gn	idi-gn	ba-idi	ba-n	ft-ft	ecm-ecm	enm-enm	ol-ol	eu-eu	zy-zy	go-go	cdl-cdl	height	BMI
second supramolar	**–0,46**	0,32																	
subcanine	**–0,45**												–0,30						
supracanine	**–0,41**	**–0,48**	**–0,48**			**–0,47**	**–0,46**		–0,31										
malare		0,38	0,30				0,31												
outer canthus	**–0,41**		–0,32							–0,34				–0,30				**0,49**	
alare		–0,33					0,36												
mandibular body																	0,34		
mandibular border						**–0,42**	**–0,42**												
gonion			0,32									**0,47**					0,32		
zygomatic		0,34	0,30	**0,41**	0,33	0,30		0,31					0,30						
supraglenoid		**0,40**	0,34					0,36										**0,61**	

Tab. 8: Soft-tissue to cranial dimension correlation table for males.

	g-op	ba-b	ba-v	n-sd	n-ns	n-gn	idi-gn	ba-idi	ba-n	ft-ft	ecm-ecm	enm-enm	ol-ol	eu-eu	zy-zy	go-go	cdl-cdl	height	BMI
height			0,33	0,39	0,36	0,30			**0,44**									**1**	
BMI								–0,34										**–0,48**	**1**
vertex							0,33	**–0,47**											
inion								**–0,41**								**–0,42**	**0,40**		
opisthocranium		0,39			–0,36											–0,34	0,39		0,33
metopion										**–0,42**									
glabella			0,35					**–0,46**								–0,36			
nasion				–0,34	–0,37					–0,35									
rhinion											–0,33								
midphiltrum								0,30	**0,70**			**–0,51**			0,31			0,31	–0,31
upper lip margin																			
lower lip margin																			
chin fissure									**0,59**		**–0,42**	**–0,54**							
pogonion																			
gnathion		0,33					**–0,50**	**–0,40**	0,34				–0,33						
frontal eminence													–0,35					0,33	
supraorbital																			
suborbital											–0,30								0,30
maxilla									0,30				0,35	–0,35		–0,38	0,33	0,36	
second submolar		**0,44**						**–0,51**					**–0,44**						
occlusal line		**0,47**					–0,39											0,39	0,30
ramus		**0,52**														–0,33		0,34	0,34

	g-op	ba-b	ba-v	n-sd	n-ns	n-gn	idi-gn	ba-idi	ba-n	ft-ft	ecm-ecm	enm-enm	ol-ol	eu-eu	zy-zy	go-go	cdl-cdl	height	BMI
second supramolar		**0,41**	0,31							0,33	–0,38								
subcanine							–0,35	**–0,40**	–0,30										
supracanine									0,34		–0,37	–0,35				–0,33			
malare		**0,51**						**–0,45**			–0,35		**–0,44**					**0,48**	
outer canthus		**0,47**						**–0,58**					**–0,41**					0,30	
alare	**–0,41**				**–0,40**		**0,40**		–0,34		–0,36								
mandibular body		**0,40**						**–0,47**					–0,32						**0,48**
mandibular border		0,33	**0,50**				–0,38	**–0,53**	0,36		–0,31								
gonion		**0,56**						**–0,57**					–0,31			–0,39			**0,51**
zygomatic		**0,67**	0,32					**–0,56**					**–0,49**						**0,45**
supraglenoid		**0,44**						–0,38		**0,42**									

In this study it was found that there is a correlation within soft-tissue thicknesses in different parts of the face, but with cranial dimensions only few dimensions correlated with each other. Some correlation also existed between cranial dimensions and soft-tissue thickness. Simpson and Henneberg [1] found stronger correlations between soft-tissue thicknesses than this study which findings are similar to those of Lebedinskaya et al. [7]. Simpson and Henneberg [1] noted that those cranial measurements (that were also used in this study) having the strongest correlations to soft-tissues were maximum cranial breadth (euryon-euryon), minimum frontal breadth (frontotemporale-frontotemporale), bizygomatic breadth, and bigonial breadth. Our study found that these cranial measurements had only few correlations to soft-tissue thickness.

Finnish females have thicker tissues in second supramolar than other populations and in maxilla in comparison to the Russians and Lithuanians (Tab. 9). Finnish females have thinner tissues in supracanine, malare and mandibular body measurements compared to the Russian and Lithuanian females, in gonion compared to African American females, in rhinion compared to African American, American Caucasian, Lithuanian and mixed females, in upper lip margin compared to African American and mixed females, in chin fissure compared to Russian, Lithuanian, African American and mixed females, in mental eminence compared to African American and Russian females. The relative tissue thickness is generally the same in all groups, except in upper lip margin in North-West Indian females, where there is relatively less tissue in comparison to other measurement points in the same group. The tissue thickness in Finnish females is thicker in maxilla and second supramolar and thinner in mandibular body, supracanine and malare as compared to the Russian and Lithuanian females. This indicates that the Finnish females have more tissue in middle cheek area than in Russian and Lithuanian females. Finnish females seem to have thinner tissues in the lower jaw area compared to all other groups.

Tab. 9: Comparison of interpopulation tissue thickness, females.

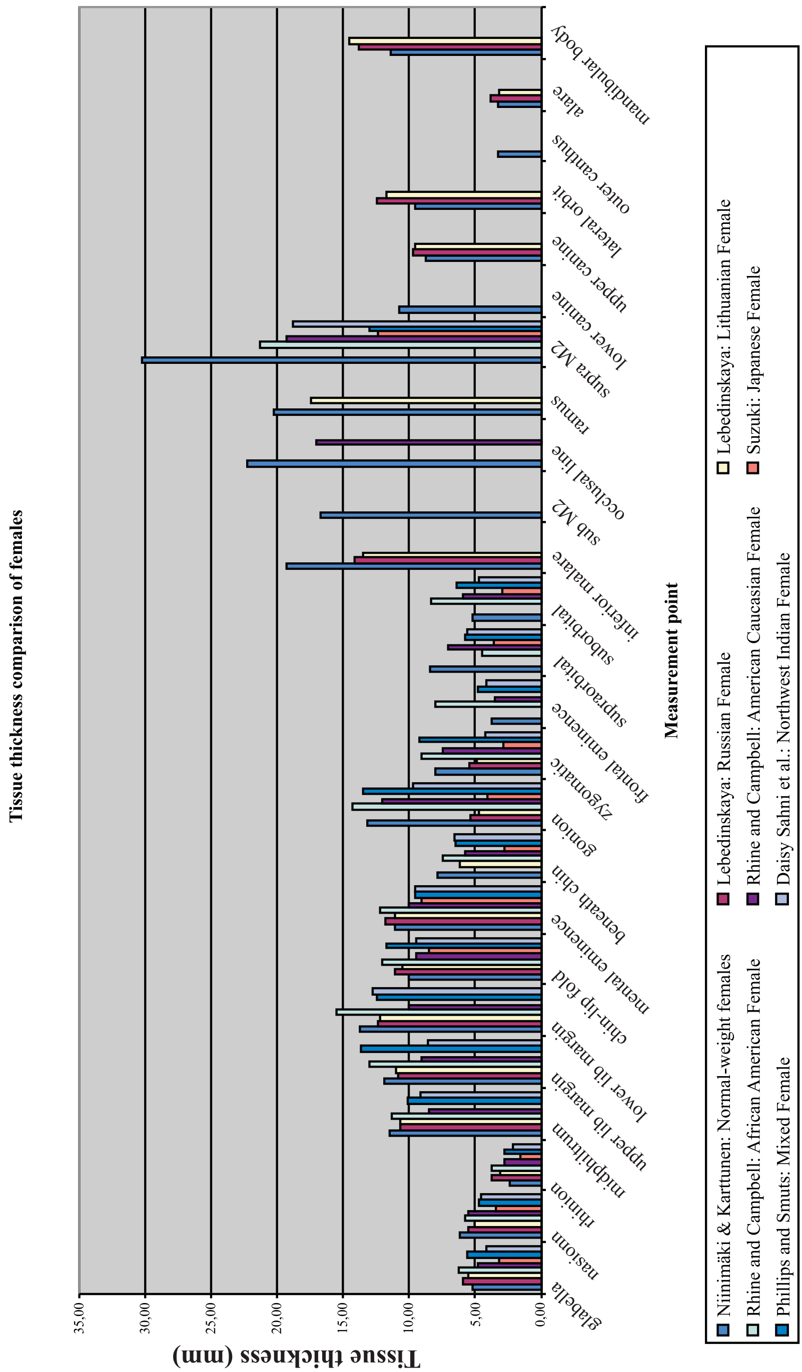

Interpopulation tissue thickness comparison indicates that the Finnish males have thicker tissues compared to those of other populations (Tab. 10). Relative tissue thickness in different parts of the face is generally the same in all population groups, except in African American males with supraorbital, in American White males with second submolar and in North-West Indian males with upper lip margin where the relative thickness of these particular points are not in the same relation as in other groups. Mostly the tissue thicknesses in all populations have the same relative thickness between all of the measured points. Finns seem to have thicker tissues, especially in the points of nasion, midphiltrum, maxilla and second supramolar. Some of the Finnish males tissue thicknesses are smaller than in reference groups, like in suborbital measurements of African American, American White and mixed males, in lateral orbit of Russian, Lithuanian and American White males, in rhinion of African American, American White, Lithuanian males and in chin fissure of African American, Russian, mixed males. These differences would show as thicker middle check area and thinner sub eye area in Finns as compared to the other population groups.

Discussion

There were some differences in interpopulation tissue thicknesses. It seems that Finns have thicker middle cheek area and this appearance is enhanced by the fact that surrounding tissues are relatively thinner. Partly this apparent difference could be a result of different methods employed in measuring the tissue thickness.

The use of average values of tissue thickness in facial reconstructing presents a few problems. Average values ignore individual variation. Especially in the cheek area individual variation is considerable. Other possible sources of error come from the use of anthropometric landmarks because all soft-tissue landmarks are not fixed in relationship to bone. Simpson and Henneberg [1] noted that while tissue thicknesses in cheeks and lower jaw were thick and on forehead and nose were thin, the tissue thickness varies considerably in areas around lips and chin. These measurement points in this study did not display as great variation, but it seems that the measurement points of upper and lower lip margin were influenced not as much with weight but more with occlusion. The thickness of lower lip margin for the over-weight female sample is smaller than in normal-weight females. In the normal-weight sample there were three females with an over-bite of upper incisors. The thickness of the mucosa in lips varies depending on how the lips set on occluded teeth. Cross-bite or malocclusion influence on how the lips set over the teeth and therefore affect the measured thickness in upper and lower lip margin and in very severe cases, also in midphiltrum and chin fissure.

Tab. 10: Comparison of interpopulation tissue thickness, males.

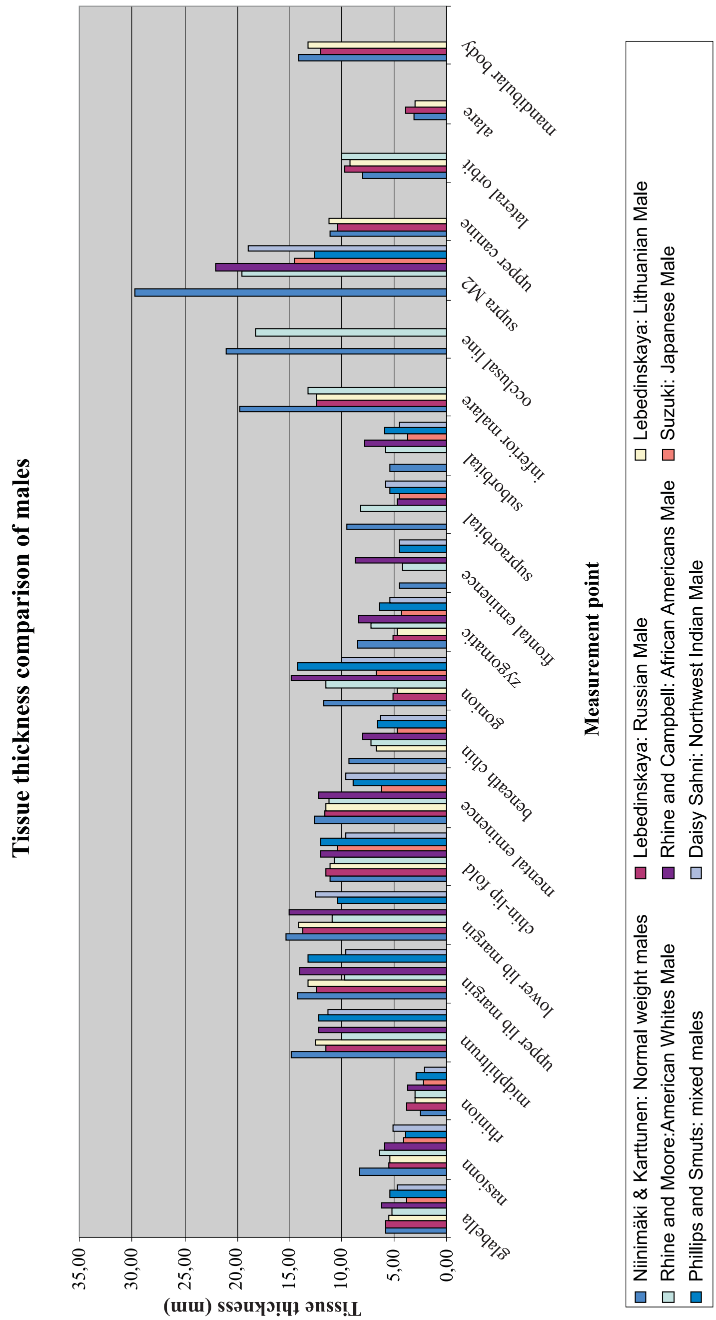

Correlations between soft-tissue thicknesses and cranial dimensions were stronger in males, also soft-tissue thicknesses correlated more strongly with each other. In females cranial dimensions correlated more strongly with each other than in males. Perhaps this is due to mastication muscle stress influencing on tissue thickness and cranial dimensions in males. Simpson and Henneberg found a clear correlation between soft-tissue thickness and cranial dimensions and they presented regression equations for reconstructing certain points for individualized tissue thickness. In this study, however, there was not as strong correlation. Still there are possibilities in trying to individualize the tissue thickness information. One approach could be to study how the strength of mastication muscles influence on the tissue thickness.

Bibliography

[1] E. Simpson, and M. Henneberg, "Variation in soft-tissue thickness on the human face and their relation to craniometric dimensions," *American Journal of Physical Anthropology* vol. 118, pp 121–133, 2002.

[2] J. S. Rhine, and H. R. Campbell, "Thickness of facial tissue on the American Blacks", *Journal of Forensic Sciences*, vol. 25, pp. 847–858, 1980.

[3] T. N. Garlie, and S. R. Saunders, "Midline facial tissue thicknesses of subadults from a longitudinal radiographic study", *Journal of Forensic Sciences*, vol. 44, pp. 61–67, 1999.

[4] S. L. Smith, and P. H. Buschang, "Midsagittal facial tissue thicknesses of children and adolescent from the Montreal growth study," *Journal of Forensic Sciences*, vol 46, No. 6, pp. 1294–1302, 2001.

[5] H. Utsuno, T. Kageyama, T. Deguchi, M. Yoshino, H. Miyazawa, and K. Inoue, "Facial soft tissue thickness in Japanese female children", *Forensic Science International*, article in press, accepted 30 July 2004.

[6] I. H. El-Mehallawi, and E. M. Soliman, "Ultrasonic assessment of facial soft tissue thicknesses in adult Egyptians", *Forensic Science International*, vol. 117, pp. 99–107, 2001.

[7] G. V. Lebedinskaya, T. S. Balueva, and E. V. Veselovskaya, "Principles of facial reconstruction," *Forensic analysis of the skull*, Eds. M. Y. Iscan, and R. P. Helmer, Wiley-Liss, inc. United States, 1993, pp. 183–198.

[8] S. L. Smith, and G. S. Throckmorton, "A new technique for three-dimensional ultrasound scanning of facial tissues," *Journal of Forensic Sciences*, vol 49, No. 3, pp. 1–7, 2004.

[9] W. A. Auselbrook, P. J. Becker, and M. Y. Iscan, "Facial soft-tissue thicknesses in the adult male Zulu," *Forensic Science International*, vol. 79, pp. 83–102, 1996.

[10] V. M. Phillips, and N. A. Smuts, "Facial reconstruction: utilization of computerized tomography to measure facial tissue thickness in a mixed racial population," *Forensic Science International*, vol. 83, pp. 51–59, 1996.

[11] D. Sahni, I. Jit, M. Gupta, p. Singh, and S. Suri, "Preliminary study on facial soft tissue thickness by magnetic resonance imaging in Northwest Indians," *Forensic Science Communications*, vol 4, pp. 1–6, 2002.
[12] R. P. Helmer, S. R. Petersen, F. Möhr, "Assessment of reliability of facial reconstruction," *Forensic analysis of the skull*, Eds. M. Y. Iscan, and R. P. Helmer, Wiley-Liss, inc. United States, 1993, pp. 229–246.
[13] K. Suzuki, "On the thicknesses of the soft parts of the Japanese face," *Journal of Anthropological Society Nippon*, vol. 60, pp. 7–11, 1948.
[14] J. S. Rhine, C. E. Moore, and J. T. Weston, "Facial Reproduction: Tables of Facial Tissue Thickness of American Caucasoids in Forensic Anthropology". Maxwell Museum Technical Series No 1, University of New Mexico, Albuquerque, 1982.
[15] W. M. Bass, "Human Osteology: a Laboratory and Field Manual". Missouri Archaeological Society, 1987.
[16] T. Rakosi, "An Atlas and Manual of Cephalometric Radiography", Wolfe Medical Publications Ltd., 1982.
[17] R. M. George, "Anatomical and artistic guidelines for forensic facial reconstruction," *Forensic analysis of the skull*, Eds. M. Y. Iscan, and R. P. Helmer, Wiley-Liss, inc. United States, 1993, pp. 215–227.

Validated semi-automated ultrasound facial soft tissue depth registration

Sven De Greef[1], Peter Claes[2], Wouter Mollemans, Dirk Vandermeulen[2], Paul Suetens[2], Guy Willems[1].

[1] Centre of Forensic Odontology,
[2] Medical Image Computing (ESAT Radiologie), Faculties of Medicine and Engineering Katholieke Universiteit Leuven, Leuven, Belgium.

Abstract

As part of a project on 3D computer-aided craniofacial reconstruction, facial soft tissue depths of a large group (n=1000) of volunteers had to be measured. A mobile and fast, semi-automatic ultrasound registration system was developed. The system consists of an A-scan ultrasound device, a laptop PC and an interface program controlling data transfer, data storage, landmark specific set-up of the ultrasound device and automatic tissue depth calculation. For 52 landmarks, the system has been tested for repeatability and accuracy. Based on the statistical analysis of the test results, we conclude that the proposed registration system and measurement protocol allows relatively fast, non-invasive, repeatable and accurate acquisition of soft tissue depth measurements.

Introduction

Trying to recreate the face of a deceased individual based on his remains, in the hope recognition would be triggered; researchers developed different two- and three-dimensional, manual or computer-aided facial reconstruction techniques[1]. Apart from some techniques [2]–[4], a majority of the reconstruction techniques use facial soft tissue depth chart data. Concerning the European adult Caucasoid, it should be noticed that, although the first tissue depth registrations were performed by German anatomists at the end of the nineteenth century [5], in vivo studies were until now limited to the study of Helmer [6]. Even today, the soft tissue depth charts from the cadaver study on American Caucasoid of Rhine and Moore [7] are most commonly used for the adult Caucasoid. The aim of the present study is to develop a user-friendly, fast, mobile and carefully validated measuring device to update facial soft tissue depth charts of the contemporary adult Caucasoid.

Materials and method

To the traditional landmarks of Kolmann and Büchly [8] we added an extra 10 bilateral landmarks. Their presence in multiple studies but also the ability to locate these extra landmarks in a standardised way on the face of the volunteer played a mayor role in their selection. This brought the total of landmarks to be measured in this study to 52, 10 landmarks located on the midline and 21 located bilaterally (Fig. 1).

Fig. 1: Skeletal and facial landmarks representation.

Considering the pro's and con's of previous used techniques for tissue depth collection such as puncturing, lateral cephalometric radiography [9]–[12], ultrasound [6], [13]–[18], MRI and CT-scanning [19], [20], ultrasound seemed the most appropriated. In order to reach an as large as possible volunteer group, a mobile "A-scan" ultrasound system was selected and software was developed to minimize overhead in data processing and storage. An "A-scan" ultrasound device was chosen above a "B-scan" for several reasons. The simple curves of the "A-scan"-device, in contrast to the complexity of the "B-scan" image data, required less data transfer time and storage space.Moreover the small "A-scan" transducer appeared to be more indicated for accurately pointing to and analyzing the landmarks. An Epoch 4b® "Panametrics, Waltham, USA) which is a compact, mobile and lightweight industrial ultrasound device with a 0.6 cm small, flat, 10 MHz transducer was chosen.

A Matlab-based (The Mathworks Inc., Natick, MA, US) interface program was created to speed up the registration process by partially automating data transfer, US device setup (gain, gate and range) and depth calculation based on automatic peak-detection.

In order to easily extract specific data and perform statistical analysis, we created a database using MySQL software (MySQL AB, Uppsala, Sweden).

The patient is measured in an upright relaxed position. With the probe as perpendicular as possible to the underlying bone and using a classic neutral coupling echogel, tissue depth is measured taking care not to indent the facial soft tissues. Three measurements are obtained, the highest of which is taken into account for further statistics.

Fig. 2: Set-up

Validation: repeatability and accuracy

For the repeatability evaluation of the US measurements a test group of 33 volunteers, composed of 19 males and 14 females with average age 39.0 years (s. d. 17 years) and average BMI 26.5 (s. d. 6.46), was measured twice, with time intervals varying between 2 days and 2 months. Accuracy was tested comparing ultrasound with CT-scan results. Twelve patients (11 females and 1 male with average age 19.7 years and average BMI 19.5) consented to have their facial soft tissue depths ultrasonically registered before acquisition of a total head CT-scan for preoperative osteotomy planning. Prior to the ultrasound registration, the 52 landmarks were marked on the face using a blue eyeliner pencil and a 3D picture of the face was taken using a 3D portable camera (ShapeCam, Eyetronics, Leuven, Belgium). The skull surface (Fig. 3A) and external surface of the skin (Fig. 3B) were extracted from the CT images by simple thresholding of the CT values. The 3D facial surface obtained with the 3D camera was automatically fitted to the CT-based skin surface (Fig. 3C) in order to determine the CT-coordinates of the exact landmark locations as measured with ultrasound. A software program was developed to perform virtual “A-scan” ultrasonography (Fig. 3D).

Fig. 3: Virtual “A-scan” ultrasonography .

Results

Intra-observer repeatability

A paired t-test and the Wilcoxon paired signed rank test, applied to each landmark separately, showed only 5.8% (n=3) of the landmarks to have a significant difference ($p<0.01$) between the two runs. These apparently very simple landmarks are the left and right supra-orbital and the left frontal eminence.

Accuracy compared to CT

Six of the 52 landmarks showed a statistical difference between the ultrasound and CT measurements using the Wilcoxon paired signed rank test at a significance level $p<0.01$. These landmarks are, bilaterally, the mid-masseter and occlusal line and the right gonion and right supraglenoid.

Discussion

The repeatability study shows very few (n=3) landmarks with a statistically significant ($p<0.01$) difference between the repeated runs. A closer look at the protocol application during this first stage of the project indicated that a slight change of transducer position had occurred between the first and second measurements. Indeed, the position of the supra-orbitalis landmark changed from 'on the eyebrow' to 'just above it' because of the eyebrow interference. This probably explains the significant differences for the left and right supraorbital. Furthermore, the median difference for the left supraorbital is very small (< 0.5 mm) compared to the corresponding average thickness (4.6 mm).

Since the landmarks found to be statistically different between CT and US were all located in the masseter region, we examined whether the differences could be explained by the influence of gravity on the soft tissue thicknesses between the upright position during the US acquisition and the supine position in the CT-scan. This was done by aligning the external skin surface extracted from CT with the 3D facial surface obtained by the 3D camera. The differences for an individual case is visualized in fig. 4 where we see that the larger distances are located precisely at the landmarks in the gonion-, supraglenoid-, and ocllusal line region, substantiating the hypothesis that they are probably due to the gravity effect.

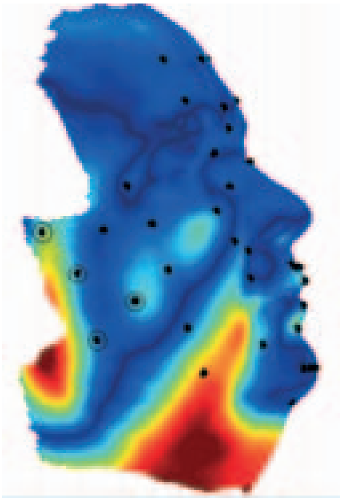

Fig. 4: Difference upright versus supine position.

Conclusion

Thanks to the progress in computer science and medical imaging technology it was possible to create a fast, mobile and user-friendly facial soft tissue depth acquisition system. Statistical analysis of the repeatability and accuracy proved our system to be a reliable and accurate measurement tool. A correct application of the protocol allows in 20 minutes the measurement of 52 facial landmarks in a non-invasive, standardized and repeatable way. It will allow (re)evaluation of older facial soft tissue depth data based on a large group of subjects of different age, sex, race and build.

References

[1] S. De Greef and G. Willems, "Three-dimensional cranio-facial reconstruction in forensic identification: latest progress and new tendencies in the 21st century." J Forensic Sci, vol. 2005.

[2] M. Gerasimov, The Face Finder. Philadelphia: PA: JB Lippencott Co, 1971.

[3] G. Quatrehomme, S. Cotin, G. Subsol, H. Delingette, Y. Garidel, G. Grévin et al., "A fully three- dimensional method for facial reconstruction based on deformable models." J Forensic Sci, vol. 42(4), pp. 649–652, 1997.

[4] L. A. Nelson and S. D. Michael, "The application of volume deformation to three-dimensional facial reconstruction: a comparison with previous techniques." Forensic Sci Int, vol. 94 pp. 167–181, 1998.

[5] W. A. Aulsebrook, M. Y. Iscan, J. H. Slabbert, and P. Becker, "Superimposition and reconstruction in forensic facial identification: a survey." Forensic Sci Int, vol.75 pp. 101–120, 1995.

[6] R. Helmer, Schädelidentifizierung durch Elektronische Bildmischung. Heidelberg: Kriminalistik Verlag GmbH, 1984.

[7] J. S.Rhine JS and C. E. Moore, "Tables of facial tissue thickness of American Caucasoids in forensic anthropology" Maxwell Museum Technical series 1984;1.

[8] J. Kollmann and W. Buchly, "Die persistenz der rassen und die reconstruction der physiognomie prahistorischer schadel." Archiv fur anthropologie, vol. 25, pp. 329–59, 1898.

[9] E. R. Dumont, "Mid-facial tissue depth of white children: An aid in facial feature reconstruction." J Forensic Sci, vol. 31(4), pp. 1463–9, 1986.

[10] T. N. Garlie and S. R. Saunders, "Midline facial tissue thicknesses of subadults from longitudinal radiographic study." J Forensic Sci, vol. 44(1), pp. 61–7, 1999.

[11] S. L. Smith and P. H. Buschang, "Midsagittal facial thicknesses of children and adolescents from the Montreal growth study." J Forensic Sci, vol. 46(6), pp. 1294–1302, 2001.

[12] M. A. Williamson, S. P. Nawrocki, and T. A. Rathburn, "Variation in midfacial tissue thickness of African-american children." J. Forensic Sci, vol. 47(1), pp. 25–31, 2002.

[13] G. V. Lebedinskaya, V. S. Stepia, T. S. Surinina, B. A. Fedosyutkin, and L. A. Tscherbin, "The first experience of application of ultrasound for the studies of the thickness of soft facial tissues." Soviet Ethnogr., vol. 4, pp. 121–131, 1979.

[14] G. Hodson, L. S. Lieberman, and P. Wright, "In vivo measurements of facial tissue thicknesses in American Caucasoid Children." J Forensic Sci, vol. 30(4), pp. 1100–1112, 1985.

[15] W. A. Aulsebrook, P. J. Becker, and M. Y. Iscan, "Facial soft-tissue thicknesses in the adult male Zulu." Forensic Sci Int, vol. 79, pp. 83–102, 1996.

[16] M. H. Manhein, G. A. Listi, R. E. Barsley, R. Musselman, N. E. Barrow, and D. H. Ubelbaker, "In vivo facial tissue depth measurements for children and adults." J Forensic Sci, vol. 45(1), pp. 48–60, 2000.

[17] I. H. El-Mehallawi and E. M. Soliman, "Ultrasonic assessment of facial soft tissue thicknesses in adult Egyptians." Forensic Sci Int, vol. 117, pp. 99–107, 2001.

[18] C. M. Wilkinson, "In vivo facial tissue depth measurements for White Britsh children." J Forensic Sci, vol. 47(3), pp. 459–465, 2002.

[19] V. M. Phillips and N. A. Smuts, "Facial reconstruction: utilization of computerized tomography to measure facial tissue thickness in a mixed racial population." Forensic Sci Int, vol. 83(1), pp. 51–9, 1996.

[20] J. N. Vignal, and Y. Schuliar, "Computer-assisted facial reconstruction. Three years' results and new perspectives." In Proceedings of the Tenth Meeting of the International Association for Craniofacial Identification, 2002, pp. 131.

Low-dose CT based soft tissue modeling for craniofacial reconstruction

D. Vandermeulen[1], M. Loubele[1], P. Claes[1], Q. Wang[1], W. Mollemans[1], S. Srivastava[1], S. De Greef[2], G. Willems[2,], P. Suetens[1]

[1] Medical Image Computing (ESAT-Radiology),
[2] Centre of Forensic Odontology
K. U. Leuven, Faculties of Medicine and Engineering

Abstract

In forensic facial reconstruction, facial features of an unknown individual are approximated based on a mixture of experimentally obtained guidelines on the relationship between soft tissues and the underlying skeleton.

In this paper, we investigate the possibility of using full 3-D cross-sectional CT images for obtaining densely sampled distances between surfaces of the external craniofacial skeleton and skin for automated craniofacial reconstruction.

In order to minimize the radiation dose involved, we determined a low-dose CT acquisition protocol. For each CT image in the reference database, the whole head as well as bone volumes are segmented and transformed into signed distance maps, which are sampled at either (skin/skull) boundary to collect distance values between both surfaces.

These distance measures were compared to manually measured values at specific landmarks (LM) for a set of 7 subject images. The automatically calculated distance values measured on the clinical- and low-dose images (both skull and skin LMs) showed no significant differences (Wilcoxon Rank Sum test, p=0.01). A simplified procedure for reconstructing the skin surfaces was implemented, by warping all reference skull sDT images to the target skull sDT. These warps where subsequently applied to the head sDT's and the zero level set of their arithmetic average was defined as the reconstructed skin surface. Initial results are shown to proof the validity of the concept, but further refinement to the procedures involved and a substantial validation are required.

1 Introduction and related work

In forensic pathology, *craniofacial reconstructions* are sometimes the only way to indirectly infer the identity of a missing person. The purpose of forensic facial reconstruction is to approximate facial features of the unknown individual to aid in recognition and identification. All facial reconstruction techniques are based on the known relationship between the soft tissues and the underlying skull [1], [2]. Traditional 'plastic' methods use modeling clay or plasticine to build up the depth of tissue on the dry skull or a cast of the skull, based on certain principles and a lot of artistic sense. These procedures are extremely time-consuming (limiting their use to exceptional and/or urgent cases), subjective and result in a single facial estimate being produced. The development of software for computerized facial reconstructions of an individual would be of benefit to various law enforcement agencies, by allowing faster, easier and more efficient generation of multiple representations of an individual. These varied likenesses would take into account differences in facial appearance due to body fat content and facial features such as the eyes, nose and lips, which are difficult to reconstruct accurately solely from cranial information.

The majority of current computerized cranio-facial surface reconstruction techniques [3]–[7] are based on fitting a generic skin surface to a set of interactively or automatically placed virtual dowels on a 3D digitized model of the skull. The dowel lengths represent estimates of tissue thickness at a limited number (20–30) of predefined locations on the skull. These tissue thickness estimates are averages over a certain subclass of individuals defined by ancestry, gender and age. Skin surface shape is directly defined at the dowel positions only, and inferred by interpolation in between, possibly in combination with some extra manual modelling of the nose, eyes, e. g. afterwards to improve the result.

In an attempt to increase the number of skull points involved in the estimation of soft tissue thickness, a number of computer-based techniques deform a reference skull surface to a target skull surface [8]–[10]. The calculated skull deformation is extrapolated and applied to the skin surface associated to the reference skull in order to estimate the facial outlook corresponding to the target skull. A reference skull is selected based on similarity in ancestry, gender and age. Reference skulls and corresponding facial surfaces are obtained using CT scanning, which limits its use because of the involved radiation dose.

However, the generic interpolation and extrapolation methods are not face-specific as they don't incorporate knowledge about typical human face variations and correlated differences. All these reconstructions are biased by the generic skin surface or specific best look-alike used. In order to remove this bias, a statistical model of soft tissue thicknesses and facial outlook can be fitted to the individual skull [11], [12], [13]. Our work is similar in spirit to [13] in the use of multiple reference skin and skull surfaces and to [8]–[10] in the concept of warping reference to target skull and applying this warp to the reference skin.

Ideally, one could obtain densely sampled surfaces of the external cranio-facial skeleton and skin very easily from 3-D X-ray CT scans. However, acquisition of such data sets over a sufficiently large normal (!) population is impossible because of the radiation dose involved. Furthermore, metallic teeth filling often disturb the quality of the scans beyond usefulness. The latter point can be solved by proper metal artefact reduction techniques [14].

The former point can be solved by acquiring volumetric images of the head using MRI. The skull, however, cannot be segmented from these data in the same simple manner as from CT images, because its intensity appearance is similar to air and other smaller neighbouring structures. Existing procedures for segmenting bone from MRI head scans [15] are only reliable for the skull bone, not for the maxillar and mandibular part.

Instead we propose to use a low-dose CT protocol with sufficient quality for segmenting the bone and skin surface and possibly also other extracranial soft-tissue structures (fat, muscles), useful for maxillo-facial surgery planning.

For each CT image in the reference database, the whole head as well as bone volumes are segmented using hysteresis intensity thresholding in combination with morphological operations to remove noisy parts and to close the volumes for subsequent operations.

The images corresponding to the volumes encompassed by both surfaces are each transformed into signed distance transform (sDT) maps (representing for each image voxel the closest distance to the nearest object/background border, zero on the surface and positive Euclidean distances inside, negative outside), which are sampled at either (skin/skull) boundary to collect distance values between both surfaces.

These distance measures sampled at a discrete number of manually indicated landmark positions (both on the skin and the skull surface) are compared to manually measured values (mimicking the ultrasound soft tissue measuring procedure) for a set of 7 CT head images. Segmentations obtained from clinical-dose and low-dose protocols were compared using the same methodology.

As a proof of principle, a simplified procedure for reconstructing the skin surfaces was implemented, by warping all reference skull sDT images to the target skull sDT. These warps are subsequently applied to all the associated reference head sDT's. Finally, the zero iso-level set of the arithmetic average of the warped reference head sDT's is defined as the reconstructed skin surface. Other linear combinations such as mixtures of modes of variation (using principal components decompositions) are possible as well, but require a substantially larger reference database.

2 Materials and Methods

Image Acquisition

In order to minimize the radiation dose involved, a low-dose CT acquisition protocol was derived from a clinical multi-slice CT protocol (Siemens Sensation 16 (Erlangen, Germany)) by lowering the X-ray source current and voltage and increasing the pitch (table feed per rotation). The effective radiation dose for the different protocols was measured on a Rando Alderson anthropomorphic head phantom. The image quality for bone segmentation was measured on the European Spine Phantom (ESP [16]) and a skull phantom. The low-dose protocol yielded an effective dose reduction from 1.5 mSv to 0.18 mSv for a multi-slice CT scan of the whole head. The tests on the ESP and the skull phantom indicated that the accuracy of the measurements on the low-dose CT is still acceptable (95% percentile <= 1mm). We refer the reader to [17] for further details.

Seven patients planned for preoperative osteotomy surgery, consented to have this low-dose CT acquisition protocol next to the acquisition of a clinical-dose total head CT-scan.

Image processing and segmentation

All images originally stored in DICOM format are converted to Analyze (Mayo Foundation, Rochester, Minnesota, USA) format and down-sampled by a factor of 2 in each dimension, resulting in image sizes of approximately 256*256*200 unsigned integers. Unfortunately, many of the images contain heavy streak artefacts because of the amalgam teeth fillings. These artefacts are reduced using a simplified version of a projection interpolation method [14]. First, pixels related to high density material are identified using intensity thresholding at 3000 HU. The parallel projection profiles (radon transform) of these high density regions are subtracted from the projection profiles of the original images. Within the ranges along the projection profiles associated to projections of high-density material, the subtracted signal is low-pass filtered (more expensive filtering such as spline smoothing was implemented but with no visible improvement). These processed profiles are then back-projected using a filtered back-projection inverse radon transform.

The head volume is segmented by intensity thresholding at 300 HU, followed by a morphological opening with a sphere (r=2 voxels) to remove isolated artefacts and finally filled to obtain a solid volume. Bone is segmented by hysteresis thresholding in the range [1000 HU,1500 HU], followed by morphological closing with a sphere (r=3 voxels) to close small holes in the skull.

Soft tissue thickness calculation

The images corresponding to the volumes encompassed by skull and skin surfaces are transformed into distance maps using a signed distance transform (sDT). These maps represent for each image voxel the closest distance to the nearest surface point, with a negative sign for voxels outside and positive inside the (closed) surfaces. These distance images are sampled at either (skin/skull) boundary to collect distance values between both surfaces. Note that since the closest point projection used in the distance transform and its associated distance is not a symmetric operation, distances measured at corresponding skull and skin landmarks can be different.

These distance measures sampled at a discrete number (52) of manually indicated landmark positions (both on the skin and the skull surface) were compared to manually measured values (mimicking the ultrasound soft tissue measuring procedure) for a set of 7 patients, planned for maxillofacial surgery for which both low-dose and clinical-dose spiral CT images were acquired. A Wilcoxon signed rank sum test is used for testing statistical similarity.

Surface Reconstruction

Two procedures were implemented to reconstruct the skin surface from a given target skull. Both rely on aligning the implicit surface representations of the skull as implemented by the signed Distance transforms (sDT). They differ in the type of alignment: linear and non-linear. Both use a simple minimum mean squared difference criterion between corresponding voxels in the two images to be registered. The linear transformation is represented by 12 parameters (translation, rotation, anisotropic scaling and shearing), whereas the non-rigid transformation uses a DCT (digital cosine transformation) basis function representation of the non-linear deformation field. The results shown in this paper are obtained using 7*8*7 basis functions with light regularization as implemented in the SPM99 package [18], [19]. Other types of deformation models exist, but this particular one was available, quick and well validated for other applications. Furthermore it represents a good compromise in number of degrees of freedom and extrapolation quality.

Given a target skull, an estimate of the associated skin surface is obtained as follows. The sDTs of the reference skulls in the database are linearly/non-linearly transformed to the sDT of the target skull. These transformations are then applied to the reference skin surface sDTs. After alignment the skin surface sDTs are averaged and the reconstructed surface is defined as the zero value isolevel surface of this average.

We evaluate this procedure using a leave-one-out test. Each subject in the database is selected in turn as the target and reconstructed from the remaining subjects. The reconstructions can then be compared to the real surface, both visually and quantitatively.

3 Results

Image pre-processing and segmentation

Fig. 1 shows an axial cross-section at a level containing severe metal streak artefacts, before and after metal artefact reduction (MAR), together with the associated 3D renderings of the skull surfaces. A successful and a failed case are shown.

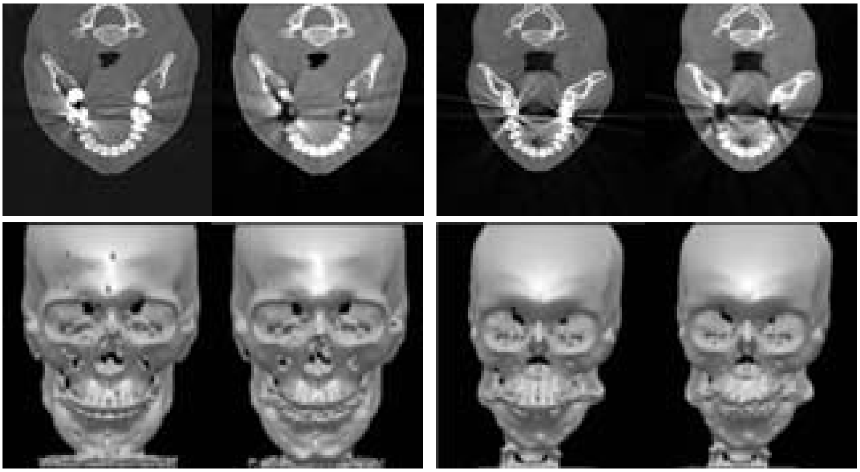

Fig. 1: Metal Artefact Removal (MAR,) successful (left) and failed (right) result. Top row: cross-sections before (left) and after (right) MAR. Bottom row: corresponding 3D surface rendering of bone.

Soft Tissue Thicknesses

The distance values measured at 52 landmarks on the clinical- and low-dose images (both skull and skin LMs) showed no significant differences (Wilcoxon Rank Sum test, p=0.01). 95% Confidence Intervals (CI) on the differences are for all but 4 LMs (maximal CI half size 2.2mm)) smaller than 1mm.

Although the Wilcoxon Rank Sum test did not report any significant differences (p<0.01) between the manually and automatically obtained distances (probably because of the very small (7) sample size), median values of the absolute differences were smaller than 1mm for the skin LMs except for 8 LMs (max diff < 11mm) and ranged typically between 1mm and 2mm (with a bias towards larger automatic measures) for the skull LMs with smaller outliers (max diff < 4mm).

Craniofacial Reconstructions

Figures 2 and 3 show three cases for which the non-linear reconstruction was visibly acceptable. The results for the linear alignment are shown for comparison.

Fig. 4 shows one of the failed cases, but also typical for the failures for the other three. Here the non-linear alignment is severely disturbed by the metal streak artefacts still remaining in the target skull segmentation and, hence, in the target skull sDT.

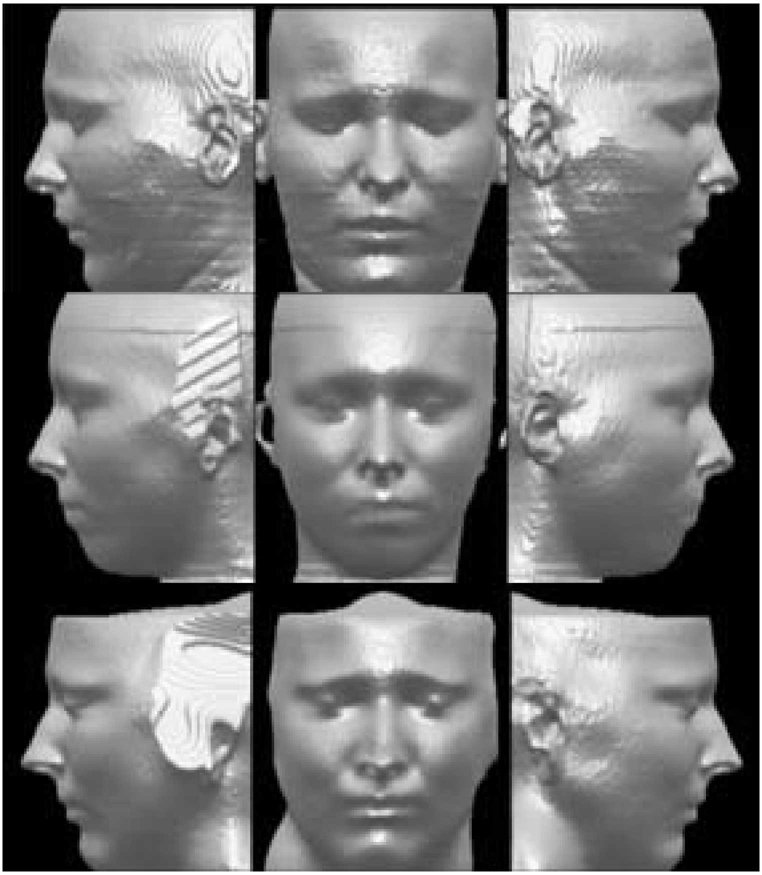

Fig. 2: Cranio-facial reconstruction case 1. Top row: original skin surface. Middle row: skin reconstruction using average of linear alignment of reference skin surfaces. Bottom row: skin reconstruction using average of non-linear alignment of reference skin surfaces.

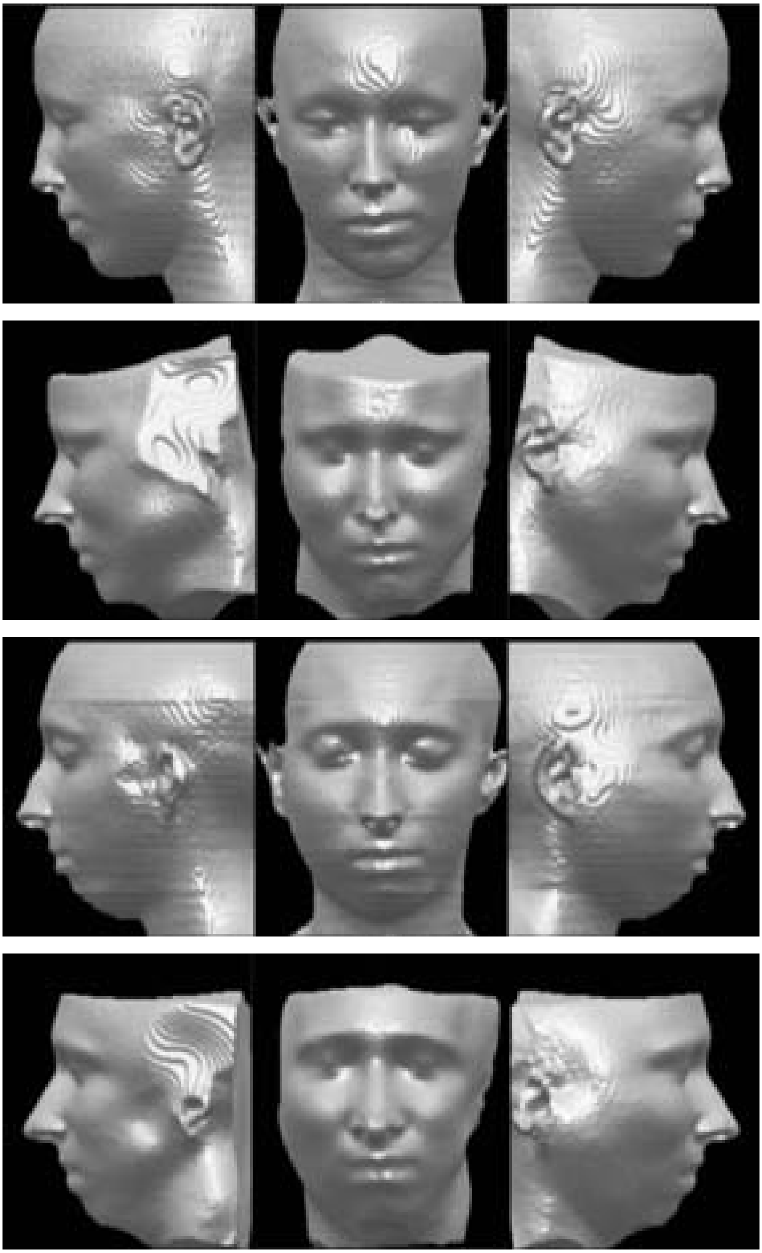

Fig. 3: Cranio-facial reconstruction cases 2 (top 2 rows) and 3 (bottom 2 rows). Top row: original skin surface. Bottom row: skin reconstruction using average of non-linear alignment of reference skin surfaces.

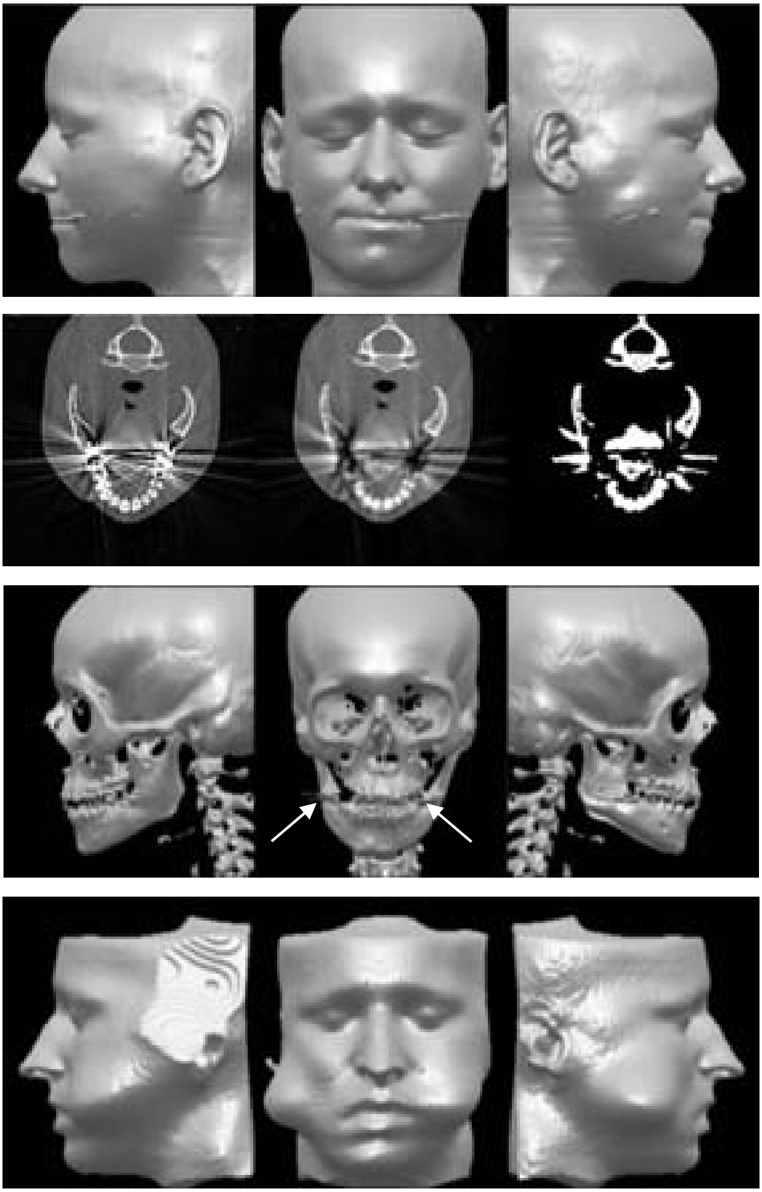

Fig. 4: Failed cranio-facial reconstruction case. First row: original skin surface (before MAR). Second row: cross-section at level of metal artefacts (left: original slice, middle: MAR slice, right: bone segmentation of MAR slice. Third row: bone reconstruction (indications of artefacts). Bottom row: skin reconstruction using average of non-linear alignment of reference skin surfaces. Note the gross deformation due to the metal artefacts in this target image.

4 Discussion

The quality of the proposed low-dose CT protocol is sufficient for segmentation of bone and skin surfaces but needs to be additionally validated for the segmentation of soft tissue into skin, muscle and fat structures as required in maxillofacial surgery planning procedures. The associated dose is hopefully low enough (the equivalent of the effective dose for an X-ray of the head or 4 days of background radiation) to be able to convince an ethical board to sustain the request for CT scanning of a substantially large set of volunteers. In the mean time, we have to rely on a non-selective set of patient image data (with subject consent).

The metal artefact removal procedure is not completely successful in removing the high intensity artefacts that interfere mostly with the intensity thresholding procedures for the bone structures. Although morphological filtering could remove most of these artefacts, we fear that too much of the regular bone structure morphology will change as well. Implementation of more sophisticated MAR procedures is required.

The soft tissue thicknesses determined automatically by sampling the skull sDT at the skin LMs and the skin sDT at the skull LMs are substantially different from the manual measurements at a number of locations because of the following reasons. The manual measurements simulate the Ultrasound measurement procedure [20] by positioning the base of the measurement on the skin landmark and determining the distance along a line projected orthogonal to the skull surface, while not deviating too much from the perpendicular to the skin surface. The automatic measure closest to this procedure is the sampling of the skull sDT at the skin LMs, since this corresponds to the shortest distance being measured along a line orthogonal to the skull. However, at some points on the skin surface, the shortest distance is not the distance measured manually, since other skull structures happen to be closer than the skull LM chosen manually, but at a sharper angle to the skin surface. This occurs specifically at the deeper indentations of the skull surface. Application of the sDTs for surface reconstruction as proposed in this paper, however, does not require these distances to be similar to the manual measures but to be consistent over different subjects.

Comparison of the linear versus non-linear reconstructions shows a marked improvement of the latter procedures, conditioned on a reliable segmentation of the bone structures. This in turn requires a better reduction of the metal streak artefacts. Note also that the current reference database is very small and, hence, still possibly biased by individual facial outlooks in the database. Furthermore, since all images are used for reconstruction, including the ones with severe artefacts, results can still be improved even for the successful cases. Despite these restrictions, reconstructions on good quality target data are visually acceptable.

Registration of the skull sDT's instead of the binary segmentations of the skull has some immediate advantages, especially in the non-linear case, since it uses a spatially extrapolated representation of the skull shapes outside the borders of the skull. Because we apply this transformation to the skin surface (or its implicit sDT representation), a reliable extension of the estimated deformation is required. The use of the implicit representation in combination with a non-linear deformation model with a limited number of degrees of freedom (about 400) seems to result in a relatively acceptable reconstruction procedure. We acknowledge that more test cases need to be processed to examine the joint effect of the surface representation and non-linear registration procedure. A more localized non-linear registration procedure is probably required to fine tune to skeletal surface details.

Linear convex combinations of sDT's have been used in computer graphics applications for continuous morphing the shape of one structure into another. However, the set of sDT's is not closed under linear combinations, meaning that a linear combination of sDTs is not necessarily a true sDT of the embedded surface. Other implicit functions can be suggested (e. g. any monotonic function of the original Euclidean Distance or solutions to variational problems, such as Radial Basis Function representations), but the Euclidean sDT is very simple in implementation and has an intuitive interpretation.

Non-linear warping of an sDT further distorts the representation of true distances to the embedded surface. However, as long as the warping remains smooth and small in magnitude, as is the case in the proposed method, warped sDT's can be assumed to be fair approximations to the sDT of the warped embedded surface. The relationship between surface warping and implicit function representations, however, requires further investigation.

We currently reconstruct only the arithmetic average of the linearly and non-linearly warped skin sDT's. Other combinations can be suggested. For instance, the linear weights for the warped skin sDT's could be made dependent on the similarity of the warped skull to the target skull (for instance relative amount of overlap). Initial experiments on weighted combinations of linearly warped skin sDT's showed only minor changes compared to the simple average, mainly because the similarity measure used was not sensitive enough and not specific for the parts of interest (it measured the relative overlap of bone regions over the whole head).

Following the work of Claes et al. [11], [12] and Tu et al. [13], instead of reporting just the average of all warped skin sDT's, in addition, major modes of variation could be reported as well. This, however, requires a large enough reference dataset for the statistical variations to be representative. Such a dataset would also allow weighing of the combinations towards class-similar surfaces (same gender, age, and body-mass-index).

Finally, weighing is now implemented globally, all points on the surface (or embedding sDT) being considered equal. Local weighing schemes could improve particular features, such as the nose, eyes and lips, by only taking local correlations into account.

5 Conclusion

We have presented a fully automatic procedure for cranio-facial reconstruction, using a database of reference head CT scans. For this purpose, we proposed a low-dose multi-slice CT head-scan protocol with a 90% reduction in effective dose, while still retaining sufficient quality not only for cranio-facial reconstruction purposes but also for maxillo-facial surgery planning. All reference images are automatically segmented into head volumes (enclosed by the external skin surface) and bone/skull volumes, both represented by a signed Distance Transform (sDT) map. The reference skull sDT's are (non)-linearly warped to the target skull sDT and this warping is applied to all reference skin sDT's. A linear combination of the warped reference skin sDT's is proposed as the reconstruction of the external skin surface of the target subject.

Preliminary results show the feasibility of this approach, although further investigations are required. First, metal streak artefacts need to be removed from the images, since they distort the reconstructions to a large extent. Second, the warping procedure needs to be examined more carefully, paying attention on the one hand to better fitting of reference to target skull and smooth extrapolation of the warping on the other hand. Third, other linear combinations besides the mere average need to be explored. Finally, a quantitative validation framework for the reconstructions needs to be set up.

6 Acknowledgements

This work is supported by the Flemish Institute for the Promotion of Innovation by Science and Technology in Flanders (IWT, project IWT/GBOU/020195), by the K. U. Leuven (project /OF/GOA/2004/05) and by the Fund for Scientific Research – Flanders (FWO-Vlaanderen, project FWO/G.0258.02).

References

[1] K. T. Taylor, "Forensic art and illustration." New York: CRC Press, 2001

[2] J. Prag and R. Neave, "Making Faces, using Forensic and Archaeological Evidence." British Museum Press, 1997.

[3] P. Vanezis, "Application of 3-D computer graphics for facial reconstruction and comparison with sculpting techniques." *Forensic Science International* 1989; vol 42: pp. 69–84.

[4] P. Vanezis, M. Vanezis, G. McCombe and T. Niblet, "Facial reconstruction using 3-D computer graphics." *Forensic Science International* 2000; vol 108: pp. 81–95.

[5] R. Evenhouse, M. Rasmussen and L. Sadler, "Computer-aided Forensic facial reconstruction." *Journal of BioCommunication* 1992; vol 19(2): pp. 22–28.

[6] A. W. Shahrom, P. Vanezis, R. C. Chapman, A. Gonzales, C. Blenkinsop and M. L. Rossi, "Techniques in facial identification: computer-aided facial reconstruction using laser scanner and video superimposition." *Int. J. Legal Med*. 1996; vol 108: pp. 194–200.

[7] A. J. Tyrell, M. P. Evison, A. T. Chamberlain and M. A. Green, "Forensic three-dimensional facial reconstruction: historical review and contemporary developments." *Journal of Forensic Science* 1997; vol 42(4): pp. 653–661.

[8] G. Quatrehomme et al., "A fully three-dimensional method for facial reconstruction based on deformable models." *Journal of Forensic Science* 1997; vol 42(4): pp. 649–652.

[9] L. A. Nelson and S. D. Michael, "The application of volume deformation to three-dimensional facial reconstruction: a comparison with previous techniques." *Forensic Science International* 1998; vol 94: pp. 167–181.

[10] M. W. Jones, "Facial reconstruction using volumetric data." *Proceedings of the 6th International Vision Modeling and Visualisation Conference*; 2001 Nov pp. 21–23; Stuttgart.

[11] P. Claes, D. Vandermeulen, P. Suetens, S. De Greef and G. Willems, "Computerized facial approximation using statistical models of tissue depth and 3-D facial outlook," presented at the Conference of the international association for craniofacial identification – IACI'2004, Dailan, China, 2004.

[12] P. Claes, D. Vandermeulen, S. De Greef, G. Willems and P. Suetens, "Combined statistical modeling of tissue depth and 3D facial outlook for computerized facial approximation", these proceedings.

[13] P. Tu, R. Hartley, W. Lorensen, M. Allyassin, R. Gupta and L. Heier, "Face reconstruction using flesh deformation modes," *Forensic Science Communications*, Vol. 2(4), October 2000, http://www.fbi.gov/hq/lab/fsc/current/index.htm

[14] J. Wei, L. Chen. G. A. Sandison, Y. Liang and L. X. Xu, "X-ray CT high-density artefact suppression in the presence of bones," *Physics in Medicine and Biology*, Vol. 40, pp. 5407–5419, November 2004.

[15] H. Rifai, I. Bloch, S. Hutchinson, J. Wiart and L. Garnero, "Segmentation of the skull in MRI volumes using deformable model and taking the partial volume effect into account," *Medical Image Analysis*, Vol. 4, pp. 219–233, 2000.

[16] W. A. Kalender, D. Felsenberg, H. K. Genant, M. Fischer, J. Dequeker and J. Reeve, "The European Spine Phantom – a tool for standardization and quality control in spiral bone mineral measurements by DX and QCT," *European Journal of Radiology*, Vol. 20, pp. 83–92, 1995.

[17] M. Loubele, F. Schutyser, D. Debaveye, R. Jacobs, D. Vandermeulen, G. Marchal and P. Suetens, "Radiation dose versus image quality for low-dose CT protocols of the head for maxillofacial surgery and dental implant planning", presented at International Workshop on Optimisation of Dose and Performance in Interventional and Digital Imaging- DIMOND III, Leuven, Belgium, March 25–27, 2004.

[18] Wellcome Department of Cognitive Neurology. Statistical Parametric Mapping (SPM). http://www._l.ion.ucl.ac.uk/spm/.

[19] J. Ashburner, J. Andersson, and K. J. Friston. "High-Dimensional Nonlinear Image Registration using Symmetric Priors," *NeuroImage*, Vol.9, pp. 619–628, 1999.

[20] S. De Greef, P. Claes, D. Vandermeulen, P. Suetens, G. Willems, "Semi-automated ultrasound facial soft tissue depth registration: Method and preliminary results", presented at 11th Biennial Meeting of the International Association for Craniofacial Identification (IACI 2004), Dalian, China, 2004.

Forensic Assessment on the Multiple Spiral CT (MSCT) in measurement and markers of the Craniofacial Soft-tissue thickness

Wang Li-Jun[1], Liu Chun-Jie[1], LEI Zhen[2], YANG Xiao-Jun[2]

[1] Research Center for Psychology on Scene, Jinzhou Police Department, People's Republic of China, and [2]Jinzhou Medical College, P. R.C)

Abstract

With regard to the measurement and markers of the craniofacial soft-tissue, experts has been carrying out and adopting various kinds of research and methods respectively. In some cases, for the purpose of obtaining the craniofacial soft-tissue thickness for some individuals, many detecting devices and method need to be relied on. In order to seek for a quick and scientifically accurate method in which the craniofacial soft-tissue thickness for different parts, the morphological features and markers of the craniofacial bones can be measured, we carried out the measurement and markers to the craniofacial bones and soft-tissue thickness of Chinese adults of different ages by adopting the Multiple Spiral CT and applying the software AW4.2 in 3D imaging.

In those cases of research measurement, the 3D imaging, the accurate soft-tissue thickness, and craniofacial markers designed can all be shown simultaneously. With implementation of this method, we could measure and collect data of the craniofacial soft-tissue thickness and the morphological features for each of the categorized group of different ethnic races, ages, and genders. This facilitates the forensic craniofacial identification by providing reliable and accurate data evidence.

Introduction

The key in craniofacial reconstruction technology lies in being familiar with and knowing well anatomy of the craniofacial features to accurately measure the craniofacial soft-tissue thickness. With craniofacial reconstruction technology, the key point is to comprehend and grasp anatomy of the craniofacial positions, and to accurately measure and quantify the thickness of the craniofacial soft tissues. And the measuring methods being adopted before by the scholars and experts from various countries are dissection examination on the facial positions of the dead, stylus testing, vivi X-ray testing, ultra sonography, CT scanning, MRI, and recently years' application of the computer technology. This paper elaborates our method of implementing Multiple Spiral CT (MSCT) and the computerized reconstruction system to measure the craniofacial soft tissue thickness for the yellow race in Asia. Comparing with the other methods, it advantageously enjoys simplicity, quickness, and accuracy with the data.

Testing method

1. With the implementation of Multiple Spiral CT scanning method, we adopted with the following parameter: a slice thickness of 0.625–1.2mm, DFOV of 24.6cm, Voltage of 120Kv, mAs of 180mA. And the scanning of all the cranio-

facial parts is completed in 40 seconds with the tested live body on the workstation.

2. To implement AW4.2 software to re-build 3D images.
3. To locate 40 or more different landmarks, as required, on the craniofacial bones imaging that is displayed on the computer screen, and keep those landmarks.
4. To readjust while observing the markers with screen with the display screen of 600 × 40.
5. To measure the thickness of every layer of the soft tissues between the bone surface and the skin at the location of markers, and put them into records.

Results

1. 4 images can be displayed simultaneously within the computer screen – 3D colored stereo-images for the craniofacial bones, 2D transection images, 2D coronary scanning images, and 2D sagittal scanning images.
2. Of the 4 types of images, the 3D colored image is the main one. When moving and re-adjusting the main images showing anatomical locations, the other three images at different projections will change accordingly, displaying the same locations but at different perspectives.
3. Once the window position and width are completed, images for any anatomic components can be derived along with changing the anatomical location of the main images.
4. Apart from the main images, the other three 2D images can indicate the protocols of width, thickness, and density for the soft tissues of bones, muscles, blood vessel, fat, and skin. Meanwhile, CT value for every location can be derived with measurements.
5. From the 29^{th} landmark of the tested live body – lower point of the temporal bone, the 2D transection computer image indicates the soft tissue thickness to be 31.0mm. Even though the 2D coronary image is in different perspective from the aforementioned one, the soft tissue thickness it shows is in line with the one shown by the transection image.

After re-building the images, with converting the skull location to lateral and sagittal section image, it can show clearly and derive measurements of the different layers of soft tissues in terms of their thickness and density for anterior cervical region, submaxilla region, facial complexion, frontoparietal region, occipitalis, fastigial area.

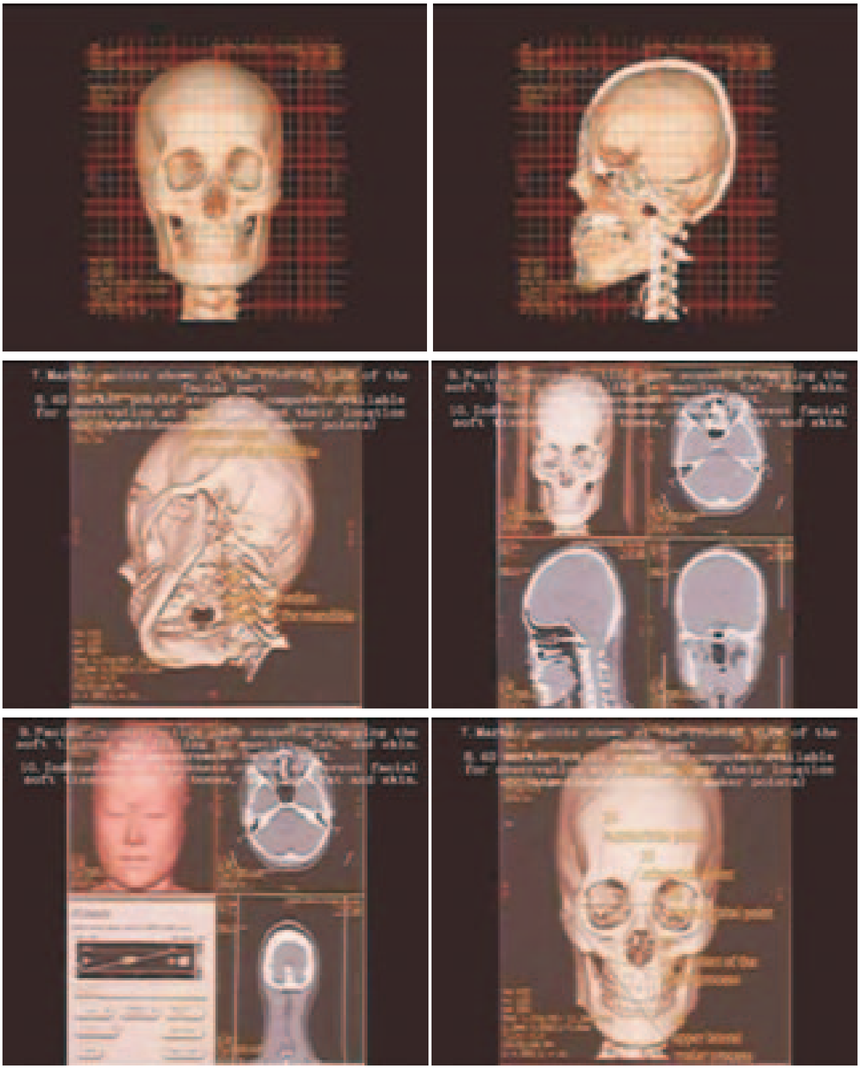

Discussion

The technical methods for identify the unknown skulls are mainly subject to the craniofacial reconstruction identification, whereas the identification relies on derivation of the measurements of the cranium bones and craniofacial soft tissues. We hereby hold the idea that the 3D reconstruction technology of MSCT incorporates more advantages than the aforementioned measurement methods for the cranium bones and facial soft tissues:

1. Upon completion of testing the bodies, all the remaining works can be conducted at the computers, and the re-building of 3D images can be observed dyna-

mically. Also dissection of very complicated articulation can be monitored freely. The other kinds of images in different perspectives and 2D images for the same anatomic positions are displayed simultaneously along with the main image of craniofacial region. The 2D images also can expose the structure and texture of bones and the soft tissues.

2. With this method, adjustment can be made towards the window position and width, and it accurately records morphological features of the bones and thickness of muscles, blood vessels, fat, and soft tissues. It also can indicate accurately and clearly the landmarks previously designed.

3. With the implementation of this method, the whole process of measuring takes only 40 seconds, during which it is pain-free and quick. Those enable craniofacial identification experts and scholars to derive huge amount of measurements within the shortest time. Through statistics management and with the aid of the computer software, those can be utilized in the identification of unknown skulls. Along with invention of modern tools and devices of highly precision, this testing method will be upgraded and perfected. We firmly believe that it will play a critical important role in the identification of unknown bodies by the forensic experts and anthropology scholars.

Improvements in soft tissue data for facial reconstructions

Ursula Wittwer-Backofen[1], Frank Prieels[1], Peter Hering[2]

[1] Department of Human Genetics and Anthropology, University of Freiburg, Albertstr. 9, 79104 Freiburg/Germany
[2] Holography and Laser Technology, caesar Foundation, Ludwig-Erhard-Allee 2, 53175 Bonn/Germany

Abstract

Facial reconstructions are based on soft tissue thickness. Until now, soft tissue thickness data are available for not more than 34 facial landmarks, subdivided by sex and age-decades. Thus, practical work has to model the facial relief between these points manually and, therefore, stays a field for experienced specialists.

Besides age and sex, it is known that facial soft tissue thickness differs between ethnical groups, body constitution, and body weight. The quantitative influence of these variables are not yet known.

We present our project in preparation, which will deliver standard soft tissue data for specified subgroups and to improve the fitting of the reconstruction to the real person, a major aim for the recognition process.

For that purpose, a fairly large number of individual soft tissue datasets are needed for subgroups, which fulfil the requirements of the criteria mentioned above.

This can be reached using CT datasets, acquired from medical departments for the purpose of medical diagnosis. Classical CT scans, however, produced in horizontal position of the patient, deliver distorted soft tissue thickness compared to an upright position. New CT systems, applied in an upright position of the patient can be used instead. To get access to a larger number of individuals in the subgroups, we intend to calculate the quantitative influence of the body orientation by comparing hologram datasets to the horizontal CT datasets. Hologram pictures in upright position will be acquired for a limited number of patients, who have to undergo a CT treatment. If systematic distortions result, a large number of CT datasets can be used to calculate specific soft tissue thickness data.

The role of the skull bone in facial reconstructions

Soft tissue facial reconstructions are based on the knowledge of two different structures: the underlying bone structure and the covering soft tissue. From a large number of studies it is known that both tissue types depend on each other. The hard bone tissue shapes the face in a basic form. However, this hard tissue is not a static structure after reaching adulthood, but underlies the regular bone turnover which varies between 5 and 10years[1], depending on individual factors.

Therefore, the skull might be remodelled significantly in its shape. The major influencing factor is the mechanical stress the bone is exposed to.

A major implication for practical work in forensic facial reconstructions is seen in disparities between the left and right side of a face. This effect may be caused by injuries, tumours, odontological problems, especially tooth decay or tooth loss or just by chewing preferences and may lead to significant side differences within an individual.

This has been widely demonstrated in research fields such as comparative anatomy, developmental biology, biological aging, facial surgery and much more [2], [3].

Anyhow, in forensic case work the skull as a basis for facial soft tissue reconstructions is given as a final snapshot out of a chain of developments during lifetime.

The role of the soft tissue in forensic facial reconstructions

Soft tissue thickness does not depend on the size and shape of the underlying skull bone alone, but on its structure as well. That means, strong muscle attachment areas on the surface of the skull are highly correlated with a high muscle mass, as strong muscle mass leads to mechanical stress of the bone. Therefore, a person with such stress markers on the skull bone possesses enlarged soft tissue thickness compared to a person with moderate or low muscles activity. This can generally be detected by an investigation of the skull surface, with concentration on the masticatory muscles or the muscles of the neck. Actually there is no quantitative correlation of specific bone structures and muscle volume known so far. The minor muscles of the face, which are responsible for the mimic expression of the face, scarcely are accessible for such an approach.

As well, the nutritional status and body constitution of a person shape the face significantly [4], [5]. In forensic case work, if there is no information of a person's nutritional status by using the body mass index of a fresh cadaver, size of clothes or other available personal data, there hardly is a chance of detecting the fat tissue thickness of a face to be reconstructed. In practice, this leaves a broad band of possible solutions and therefore still is a field for specialists in forensic anthropology, well trained in comparative anatomy and artistic illustration.

Compared to the skull bone, the facial soft tissue reacts much faster to physiological conditions as well as to environmental changes. The changes due to the age of a person has a major impact on soft tissue thickness. This has been shown by Helmer in his tables presenting soft tissues thickness by age decades covering the adult age class [6]. However, meanwhile more data are available, which in fact do not include further criteria to separate subgroups showing different soft tissue thickness. Most common in practical forensic use still are the Helmer data.

Males and females differ significantly in soft tissue thickness. These sex specific data are as well provided by Helmer [6].

Thus, besides the already described individual criteria such as sex, age, and nutritional status, soft tissue thickness additionally depends on ecological conditions such as temperature, altitude, UV light exposure and others. Taking into account all influencing criteria for facial soft tissue thickness, a high intra-population as well as a high inter-population variability with a high degree of overlapping between the populations, is expected.

Due to the methods applied so far to gain soft tissue thickness data, the results are limited to well defined anatomical points of the face. Facial parts located between these points are subject to the constructor's forming, guided by her or his experience. Thus, for the soft tissue connections between the Helmer points a high degree of expert knowledge is necessary, no standards of soft tissue data are available for these areas. Such work is limited to anthropologists, experienced in the individual variability of bony structures. From the arguments given it is obvious, that the anthropological profile of the whole skeleton delivers necessary basic data to perform a reliable facial reconstruction, which allows people to recognize a specific missed person.

Requirements for individually adaptable facial soft tissue data

The 2D computer superimposition method for facial reconstruction applied in Freiburg in forensic case work has been described elswhere [7]. The results of this method are virtual faces, composed out of different facial elements of existing persons, thus allowing to present these reconstructions as a realistic photograph to the public. It tries to implement the criteria mentioned above, even though it suffers from the lack of individually adaptable soft tissue data as well as all other methods. From this practical point of view a number of questions have been raised, which may lead to the specification of demands and may help in the project design of facial soft tissue studies: Mostly, soft tissue thickness is observed independently from the bone structure. Is there a correlation between the general size and form of the bony structure and soft tissue thickness? Does this help us to better understand individual variability of soft tissue forming?

This however has not been investigated in a way that would help to understand general correlations. Simpson and Henneberg [8] were the first to show results on these questions in a way that enables us to understand general anatomical interrelations. Only, this has been studied with a small sample of 40 individuals, which does not represent a large variability and does not allow the application of statistical tests. As well, the study has been performed in cadavers, and the measurements have been taken by the manual needle technique, tracing back to the method already applied by His in 1895 [7]. Thus, the resulting data hardly can be helpful in practical use. Anyhow, it has been demonstrated that craniometric-soft tissue correlations exist.

To provide better data sets for soft tissue thickness, it is necessary to represent sufficiently large and well- defined sub- samples which deliver reliable soft tissue data measured in living individuals, not changed by post mortem influences. From these requirements it is obvious, that, if CT or MRI datasets can be used for measuring soft tissues, datasets acquired for medical reasons, can be used. Such datasets are stored in clinics in sufficiently large numbers. They allow to calculate soft tissue thickness at any point of the head.

But this includes severe problems: The medical indications, these CT or MRI scans have been made for may have had significant implications on the change of bony as well as soft tissue structures. Therefore, it is necessary to carefully select the datasets before they are made anonymous.

A second major problem is the position of the patients in the CT and MRI scanning tubes. As they are lying, the soft tissue falls back towards the occipital region and distorts the face of a person, we use to look at in upright position. Thus, the ability to remember a person might be significantly disturbed (Fig. 1).

Fig. 1: Facial soft tissue shift due to the position of the face in two persons, each left side lying position, right side upright position

The shift of soft tissue changes between upright and lying position is not known so far.

At anatomical fixing points the change of soft tissue might be neglectable. These areas, such as the frontal bone, with close fixation of the skin on the bone, or the nose, where the cartilage holds the shape of the nose fixed, are expected to change in a moderate way. In contrast, the area around the mouth and the cheek area, which cover bony structures less fixed, may vary at a higher amount.

This soft tissue shift, depending from the orientation of the head, however, is expected to follow certain regularities. If so, it should be possible to use statistical functions to calculate the soft tissue shift of an upright standing person from his/her measurements taken in lying position. This as well can be calculated depending on age, nutritional status, or other criteria, which are assumed to be major influencing factors.

How can soft tissue thickness be measured in a person of upright position? New cone beam CT scanners could be the solution. Anyhow, this technique exposes the patient to x-rays and for ethical reasons can hardly be used for scientific purpose additionally to conventional CT scans. Here the technique of ultrafast holographic surface topometry can be applied, delivering 3D-data of the facial surface [10]. When a medical indication is given for patients to apply a CT scan, they can be asked to agree to an additional holographic image, which does not include any healthy risks. For a comparison of soft tissue thickness in different positions it is necessary to fix the datasets at marker points, visible in both imaging systems.

Fixed to such matching points, the soft tissue shift between the upright and lying position can be calculated. If such a statistical function can be defined, large amounts of existing CT and MRI datasets might be used to get more precise 3D- soft tissue datasets. The latter can be used for different techniques of facial reconstruction of anatomical modern humans in forensic anthropology, as well as in facial surgery. If there is a basic knowledge on the correlation of craniometric data and soft tissue thickness and if data on the ethnic variability of soft tissue thickness are available, there is as well potential for the facial reconstruction of individuals in paleoanthropological evolutionary context.

References

[1] G. Grupe, S. Christiansen, I. Schröder und U. Wittwer-Backofen, *Anthropologie. Ein einführendes Lehrbuch.* Heidelberg: Springer Verlag, 2004.

[2] G. J. y'Edynak, and M. Y. Iscan, „Craniofacial Evolution and Growth," in *Forensic Analysis of the Skull,* M. Y. Iscan and R. P. Helmer, Eds. New York: Wiley-Liss, 1993, pp. 11–27.

[3] J. B. Schimmler, R. P. Helmer, and J. Rieger, „Craniometric Individuality of Human Skulls," in *Forensic Analysis of the Skull,* M. Y. Iscan and R. P. Helmer, Eds. New York: Wiley-Liss, 1993, pp. 89–96.

[4] D. Leopold, H. J. Hammer, and H. Greil, „Determination of Body Constitution Type from the Face," in *Forensic Analysis of the Skull,* M. Y. Iscan and R. P. Helmer, Eds. New York: Wiley-Liss, 1993, pp. 47–56.

[5] H. Greil, „Anthropologische Grundlagen der Identifikation," in *Identifikation unbekannter Toter,* D. Leopold, Hrsg. Lübeck: Schmidt-Römhild, 1998, S. 53–84.

[6] R. P. Helmer, „Identifizierung unbekannter, unkenntlicher Leichen mittels bildtechnischer oder rekonstruktiver Verfahren," in *Identifikation unbekannter Toter,* D. Leopold, Hrsg. Lübeck: Schmidt-Römhild, 1998, S. 449–501.

[7] U. Wittwer-Backofen, „Gesichtsrekonstruktionen mit Verfahren der Computersuperposition" in *Die Gesichtsweichteil-Rekonstruktion,* Bundeskriminalamt/DE, Landeskriminalamt Brandenburg/DE, Kriminalistisches Institut/CZ und Forensisches Institut/NL, Hrsg. Wiesbaden: Bundeskriminalamt, 2004, S. 57–65.

[8] E. Simpson and M. Henneberg, „Variation in Soft-Tissue Thickness in the Human Face and their Relation to Craniometric Dimensions," *American Journal of Physical Anthropology,* vol. 118, pp. 121–133, 2002.

[9] W. His, „Johann Sebastian Bach. Forschungen über dessen Grabstätte, Gebeine und Antlitz. Bericht an den Rath der Stadt Leipzig," Leipzig: FCW Vogel, 1895.

[10] P. Hering, T. M. Buzug, and R. P. Helmer „Ultraschnelle dreidimensionale Gesichtsprofilvermessung mit gepulster Holographie für forensische Gesichtsrekonstruktion" in *Die Gesichtsweichteil-Rekonstruktion,* Bundeskriminalamt/DE, Landeskriminalamt Brandenburg/DE, Kriminalistisches Institut/CZ und Forensisches Institut/NL, Hrsg. Wiesbaden: Bundeskriminalamt, 2004, S. 123–131.

Verbesserte Weichteildaten für die Gesichtsrekonstruktion

Ursula Wittwer-Backofen[1], Frank Prieels[1], Peter Hering[2]

[1] Institut für Humangenetik und Anthropologie, Universität Freiburg, Albertstr. 9, 79104 Freiburg/Deutschland,
[2] Holographie and Lasertechnik, Stiftung caesar, Ludwig-Erhard-Allee 2, 53175 Bonn/Deutschland

Abstract

Gesichtsrekonstruktionen basieren auf Weichteildicken. Bisher stehen alters- und geschlechtsspezifische Weichteilstärken lediglich für 34 Messpunkte zur Verfügung. Aus diesem Grund muss das Gesichtsrelief durch Verbindung dieser Punkte manuell erarbeitet werden und bleibt daher ein Arbeitsgebiet für erfahrene Spezialisten.

Es ist bekannt, dass Gesichtsweichteilstärken nicht nur mit dem Geschlecht und dem Alter variieren, sondern auch von der Populationszugehörigkeit, der Körperkonstitution und dem Ernährungszustand des Körpers abhängen. Der quantitative Einfluss dieser Faktoren ist jedoch noch unbekannt.

Wir stellen ein Projekt in der Vorbereitungsphase dar, das Standardweichteildaten für definierte Teilgruppen liefert und somit zur Verbesserung der Übereinstimmung von Rekonstruktion und realer Person beitragen kann. Damit kann der Wiedererkennenswert einer Person in einer Gesichtsrekonstruktion verbessert werden

Hierfür wird eine große Individuenzahl benötigt, welche die entsprechende Differenzierung in Teilstichproben erlaubt, die nach den oben genannten Kriterien definiert werden. Derartige Stichproben können durch die Nutzung existierender CT-Datensätze erstellt werden, die in medizinischen Einrichtungen in großer Zahl existieren. Die klassischen CT-Datensätze, die üblicherweise in liegender Position der Patienten aufgenommen werden, liefern jedoch verzerrte Weichteilmaße im Vergleich zu den Werten im aufrechten Stand. Neue CT-Systeme erlauben jedoch auch Aufnahmen im Stand. Um jedoch Zugang zu den zahlreichen benötigten Daten zu erlangen, schlagen wir vor, den quantitativen Einfluss der Körperlageunterschiede zu ermitteln. Zusätzlich zu den üblichen CT- Scans können an einer kleinen Probandengruppe Holographiedatensätze der Oberflächentextur in der aufrechten Position erstellt werden und mit den Weichteildaten der im Liegen erstellten CT-Daten verglichen werden. Ergeben sich dabei systematische Abweichungen, lassen sich große Mengen an CT-Datensätzen zur Ermittlung von Weichteildaten für die Gesichtsrekonstruktion nutzen.

Die Rolle der Schädelknochen bei der Gesichtsrekonstruktion

Die Gesichtsweichteilrekonstruktion basiert auf der Kenntnis von zwei unterschiedlichen Strukturen: Der zugrunde liegenden Knochenstruktur und der bedeckenden Weichteilmasse. Aus zahlreichen Studien ist deren gegenseitige Beeinflussung bekannt. Das harte Knochengewebe formt die Grundstruktur des Gesichtes. Der Knochen stellt dabei auch nach dem Wachstumsabschluss keine statische Einheit dar, sondern ein dynamisches System, in dem alle 5–10 Jahre ein kompletter Substanzumbau stattfindet [1].

In diesem Prozess kann der Schädel auch in seiner Form erheblich in seiner Form verändert werden. Mechanischer Stress kann als ein wesentlicher Einflussfaktor angesehen werden.

Bei der praktischen Arbeit der Gesichtsrekonstruktion spielen insbesondere die Seitenunterschiede eines Gesichtes eine bedeutende Rolle. Diese können durch Störungen wie Verletzungen, Tumore, Probleme des Kauapparates, insbesondere nach Zahnverlust, oder auch bereits durch Seitenpräferenzen beim Kauen entstehen und zu deutlichen Seitenunterschieden führen.

Dies konnte in unterschiedlichen Wissenschaftsfeldern, unter anderem in der vergleichenden Anatomie, der Entwicklungsbiologie, der Alternsforschung, plastischen Gesichtschirurgie, gezeigt werden [2], [3].

In der forensischen Praxis stellt sich der Schädel als das Ergebnis derartiger Prozesse während des Lebenslaufes dar.

Die Rolle der Weichteilgewebe bei der forensischen Gesichtsrekonstruktion

Weichteilstärken hängen nicht nur von der Größe und Form der zugrunde liegenden Schädelknochen ab, sondern auch von dessen Oberflächenstruktur. Ausgeprägte Muskelmarken sind hoch korreliert mit großer Muskelmasse, da ein kräftiger Muskel mechanischen Stress auf den Knochen ausübt und diesen sichtbar gestaltet. Bei einer derartigen Beobachtung an einem Schädel darf man im Vergleich zu geringer Muskelprägung am Knochen verstärkte Weichteildicken erwarten. Zumeist lässt sich dies durch eine Untersuchung der Knochenoberfläche erkennen, insbesondere bei der Kau- und Nackenmuskulatur. Allerdings sind diese Zusammenhänge spezifischer Knochenstrukturen und Muskelvolumen bislang nicht quantifiziert worden. Auch lassen sich feinere Muskeln, wie die mimische Muskulatur, diesbezüglich kaum auswerten.

Weiterhin formen der Ernährungszustand und die Körperkonstitution die Gesichtsweichteile in erheblichem Umfang [4], [5]. Wenn in forensischen Fällen unbekannter Toter keine Informationen zum Ernährungszustand der Person vorliegen, wie etwa der body mass Index eines frischen Leichnams, die Kleidergröße, oder andere hinweisdienliche Daten, sind lediglich sehr feine Strukturmerkmale am Schädel geeignet, die Fettgewebsmasse zu schätzen. In der Praxis bleibt dabei ein weiter Spielraum der Ausgestaltung. Dadurch bleibt dieses Arbeitsfeld speziell ausgebildeten forensischen Anthropologen vorbehalten.

Im Vergleich zu Schädelknochen reagieren die Gesichtsweichteile wesentlich schneller auf Einflussfaktoren. Als eine Begleiterscheinung des Alterns werden ihre Veränderungen am ehesten ersichtlich. Dies wurde von Helmer in seinen nach Altersdekaden differenzierten Weichteildaten berücksichtigt [6]. Wenn auch inzwischen die Weichteildaten weiter ergänzt wurden, so wurden jedoch keine weiteren Kriterien berücksichtigt, nach denen Gesichtsweichteile variieren. In der praktischen forensischen Arbeit bleiben die Daten nach Helmer weiterhin Standard.

In den Gesichtsweichteildaten machen sich auch deutliche Geschlechtsunterschiede bemerkbar, weshalb Helmer auch geschlechtsspezifische Datentabellen liefert [6].

Neben den bereits beschriebenen Kriterien wie Geschlecht, Alter und Ernährungszustand hängen die Weiteilstärken untern anderem auch von Umweltbedingungen wie Temperatur, Höhe oder UV-Licht Exposition ab. Berücksichtigt man alle diese Einflussfaktoren, so kann man hohe Variabilität von Weichteilmaßen innerhalb von Populationen wie auch zwischen Populationen, diese mit großem Überlappungsbereich, erwarten.

Aufgrund der bisher angewandten Methoden sind die Weichteildaten auf gut definierte anatomische Punkte des Gesichtes beschränkt. Gesichtsareale zwischen diesen Punkten unterliegen der Schätzung des Konstrukteurs, der hier gefordert ist, Erfahrungen einfließen zu lassen. Dadurch bleiben vor allem diese Arbeitsschritte aufgrund des Fehlens von Standardweichteilwerten Spezialisten vorbehalten, Anthropologen, die Erfahrung in der individuellen Variabilität von Knochenstrukturen mitbringen. Zusammengefasst lässt sich sagen, dass nur das anthropologische Profil des gesamten Skelettes die Informationen liefert, die notwendig sind, um mit der Rekonstruktion den Wiedererkennenswert einer vermissten Person zu erreichen.

Anforderungen an individuell adaptierbare Weichteildatensätze

Die 2D- Computersuperposition, wie sie in Freiburg angewandt wird [7], liefert Bilder von virtuellen Gesichtern, welche aus realen Gesichtselementen zusammengesetzt sind. Mit der Methode wird versucht, die oben genannten Kriterien zu berücksichtigen, jedoch auch diese Vorgehensweise wird durch das Fehlen von individuell adaptierbaren Weichteildaten limitiert. Anhand dieser Problematik lassen sich einige Desiderate für zukünftige Forschungsansätze formulieren: In bisherigen Studien sind die Weichteilstärken unabhängig von den zugrunde liegenden knöchernen Strukturen erfasst worden. Gibt es eine Korrelation zwischen Weichteilstärke und allgemeinen Form- und Größemerkmalen der knöchernen Struktur? Hilft uns dies zum besseren Verständnis der individuellen Variabilität der individuellen Variabilität der Weichteilgestaltung? Diese Fragen wurden bisher lediglich in wenigen Untersuchungen aufgegriffen. Simpson and Henneberg [8] haben diese Fragen aufgegriffen und in einer Pilotstudie einen Weg aufgezeigt, wie generelle anatomische Zusammenhänge zwischen Gesichtsschädelknochen und Weichteilbedeckung untersucht werden können. Ihre Studie umfasste zwar nur 40 Individuen, die weder in ausreichendem Maße die Variationsbreite wiederspiegelt noch die Anwendung ausreichender Prüfstatistik erlaubt. Problematisch ist ihre Datenerhebung an Leichen und mittels der alten Nadeltechnik, die bereits His 1895 angewandt hat [7]. Aus diesem Grund können die gewonnenen Daten kaum praktische Anwendung erfahren. Die wesentliche Erkenntnis jedoch besteht im aufzeigen genereller Korrelate zwischen kraniometrischen Daten und Weichteildaten.

Um bessere individuell anzupassende Daten für Weichteilstärken zu liefern, müssen umfangreiche und nach Einflusskriterien definierte Stichproben zur Verfügung stehen, die anhand von Messungen Lebender Daten liefern, unbeeinflusst durch postmortale Prozesse. Hier liegt es auf der Hand, CT- oder MRI- Datensätze zu verwenden, die aus medizinischen Indikationen erstellt wurden. Derartige Datensätze sind in medizinischen Institutionen in großer Zahl vorhanden. Sie erlauben die Weichteilbestimmung an jedem beliebigen Punkt des Kopfes.

Dies beinhaltet jedoch auch eine Vielzahl von Problemen: Die Erkrankungen, aufgrund derer die CT- oder MRI- Aufnahmen notwendig wurden, können erheblichen Einfluss sowohl auf die Schädelknochen als auch auf die bedeckenden Weichteile haben. Daher müssen für die hier formulierten weiterführenden Auswertungen die Datensätze vor ihrer Anonymisierung sorgfältig selektiert werden.

Ein zweites Hauptproblem ist die Orientierung der Patienten in den CT- und MRI-Scannerröhren. Da die Personen bei der Aufnahme liegen, fallen die Gesichtsweichteile in Richtung auf die Occipitalregion und verzerren das Gesicht im Vergleich zu der Ansicht in aufrechter Kopfhaltung deutlich. Werden diese Weichteilwerte für Gesichtsrekonstruktionen verwendet, kann der Wiedererkennenswert einer Person erheblich beeinträchtigt werden (Abb. 1).

Abb. 1: Weichteilverlagerung im Gesicht durch Lageunterschiede bei zwei Probanden, jeweils links liegende Position, rechts aufrecht

Das Ausmaß dieser Weichteilverzerrung indes ist nicht bekannt. An anatomischen Punkten, an denen die Weichteile auf dem Knochen gut fixiert sind, ist eine derartige Verzerrung sicherlich gering einzuschätzen und eventuell vernachlässigbar. Dies betrifft am ehesten den Stirnbereich oder die Nase, wobei der Nasenknorpel die Form der Nase weitestgehend fixiert. Im Gegensatz dazu ist zu erwarten, dass im Mund- und Wangenbereich mit deutlich geringerer Fixierung der Weichteile, die Verzerrungen stärker sind.

Unsere Hypothese ist, dass diese Weichteilverzerrungen durch die Lageveränderung gewissen Regelmäßigkeiten folgen. Trifft dies zu, so sollte es möglich sein, das Ausmaß der Verzerrung in Abhängigkeit von der Weichteilstärke zu bestimmen. Dann ließen sich die im Stand zu erwartenden Weichteildicken aus den Liegenddaten berechnen, in Abhängigkeit von den genannten Einflussfaktoren wie Alter oder Ernährungszustand.

Aber wie lassen sich Weichteildaten an einer Person mit aufrechter Kopfhaltung messen? Neue Cone-Beam-CT- Scanner könnten die Lösung sein. Allerdings exponieren auch sie die Probanden mit Röntgenstrahlung und können daher aus ethischen Gründen für eine Untersuchung mit rein wissenschaftlichen Zielen nicht eingesetzt werden. Bisher existiert noch keine entsprechende Datenmenge aus medizinischem Zusammenhang. Wir schlagen den Einsatz ultraschneller Holographieaufnahmen zur dreidimensionalen Darstellung der Oberflächentextur vor [10]. Dies kann als Ergänzung zu einer konventionellen CT-Datenerhebung angewandt werden, da die Methode keine gesundheitlichen Risiken beinhaltet. Weichteilverzerrungen können durch Vergleich des Oberflächenverlaufes aus dem CT-Datensatz (liegend) und den Holographiedaten (aufrecht) berechnet werden. Für den Vergleich können Passpunkte verwendet werden, die auf beiden Aufnahmetechniken sichtbar werden. Lassen sich an einer Stichprobe systematische Verzerrungen erkennen, können existierende CT- oder MRI- Datensätze ohne weiteren zusätzlichen Einsatz holographischer Aufnahmen für die Definition von Weichteilstärken verwendet werden.

Damit kann sich dann Potential für die unterschiedlichen Techniken der Gesichtsrekonstruktion in der forensischen Anthropologie eröffnen. Wenn ausreichende Kenntnisse von Schädel- Weichteil- Korrelaten in Zukunft vorliegen, könnten sich hier auch Möglichkeiten für die Paläanthropologie durch Interpolation aus der Variabilität des anatomisch modernen Menschen aufzeigen.

References

[1] G. Grupe, S. Christiansen, I. Schröder und U. Wittwer-Backofen, *Anthropologie. Ein einführendes Lehrbuch.* Heidelberg: Springer Verlag, 2004.

[2] G. J. y'Edynak, and M. Y. Iscan, „Craniofacial Evolution and Growth," in *Forensic Analysis of the Skull,* M. Y. Iscan and R. P. Helmer, Eds. New York: Wiley-Liss, 1993, pp. 11–27.

[3] J. B. Schimmler, R. P. Helmer, and J. Rieger, „Craniometric Individuality of Human Skulls," in *Forensic Analysis of the Skull,* M. Y. Iscan and R. P. Helmer, Eds. New York: Wiley-Liss, 1993, pp. 89–96.

[4] D. Leopold, H. J. Hammer, and H. Greil, „Determination of Body Constitution Type from the Face," in *Forensic Analysis of the Skull,* M. Y. Iscan and R. P. Helmer, Eds. New York: Wiley-Liss, 1993, pp. 47–56.

[5] H. Greil, „Anthropologische Grundlagen der Identifikation," in *Identifikation unbekannter Toter,* D. Leopold, Hrsg. Lübeck: Schmidt-Römhild, 1998, S. 53–84.

[6] R. P. Helmer, „Identifizierung unbekannter, unkenntlicher Leichen mittels bildtechnischer oder rekonstruktiver Verfahren," in *Identifikation unbekannter Toter,* D. Leopold, Hrsg. Lübeck: Schmidt-Römhild, 1998, S. 449–501.

[7] U. Wittwer-Backofen, „Gesichtsrekonstruktionen mit Verfahren der Computersuperposition" in *Die Gesichtsweichteil-Rekonstruktion,* Bundeskriminalamt/DE, Landeskriminalamt Brandenburg/DE, Kriminalistisches Institut/CZ und Forensisches Institut/NL, Hrsg. Wiesbaden: Bundeskriminalamt, 2004, S. 57–65.

[8] E. Simpson and M. Henneberg, „Variation in Soft-Tissue Thickness in the Human Face and their Relation to Craniometric Dimensions," *American Journal of Physical Anthropology,* vol. 118, pp. 121–133, 2002.

[9] W. His, „Johann Sebastian Bach. Forschungen über dessen Grabstätte, Gebeine und Antlitz. Bericht an den Rath der Stadt Leipzig," Leipzig: FCW Vogel, 1895.

[10] P. Hering, T. M. Buzug, and R. P. Helmer „Ultraschnelle dreidimensionale Gesichtsprofilvermessung mit gepulster Holographie für forensische Gesichtsrekonstruktion" in *Die Gesichtsweichteil-Rekonstruktion,* Bundeskriminalamt/DE, Landeskriminalamt Brandenburg/DE, Kriminalistisches Institut/CZ und Forensisches Institut/NL, Hrsg. Wiesbaden: Bundeskriminalamt, 2004, S. 123–131.

3.

Computer-Aided Facial Reconstruction
Computergestützte Gesichtsrekonstruktion

Radial Basis Functions for 3D Nonlinear Soft-Tissue Warping

Jan Müller, Andreas Mang and Thorsten M. Buzug

Institute of Medical Engineering, University of Lübeck, Ratzeburger Allee 160, 23538 Lübeck, Germany

Abstract

Facial reconstruction is important in several scientific areas, especially in forensic science and archaeology. In both areas the basis of all work is a skull find of a dead person which should be reconstructed. This helps with the identification of a skeleton from an open case of death or the comparison of facial features between modern and ancient human beings. In this paper a new method for forensic facial soft-tissue reconstruction is presented. It is based on a nonlinear warping technique using radial basis functions known as thin-plate splines extended to 3D space. To minimize the amount of errors a regularized thin-plate spline version was implemented. As for the manual facial reconstruction procedure the forensic expert has to attach soft tissue on a skull find. However, since the conventional, manual 4-step approach of i) *examination of the skull*, ii) *development of a reconstruction plan*, iii) *practical sculpturing* and iv) *mask design* is very time consuming, multi-modality elastic matching of 3D MRI soft tissue onto the 3D CT image of a skull find is proposed.

1 Introduction

We deal with an application of a 3D spline method to the problem of identifying an unknown person. It is based on a 3D computed tomography image of the skull find and a 3D magnetic resonance image providing the facial soft-tissue template. Computed tomography (CT) is used, because it yields a 3D scan of the forensic skull find that is free of any geometrical distortion [1]. Generally, there are two possible alternatives to proceed with the 3D CT image stack. As one alternative, which will be described in this article, it is of course conceivable to use the 3D CT dataset as the basis of virtual soft-tissue reconstruction, especially since it is stored in the computer as a representation that can be directly used for further work.

The other alternative employs the CT data as the basis for the so-called rapid prototyping technique [2] that produces plastic copies of the skull in its true size; to these the anthropologist can add the soft tissues with traditional clay without putting the forensic or archaeological find at risk. In fig. 1 a 3D CT visualization and the corresponding rapid-prototyping cast is shown for an archaeological skull find.

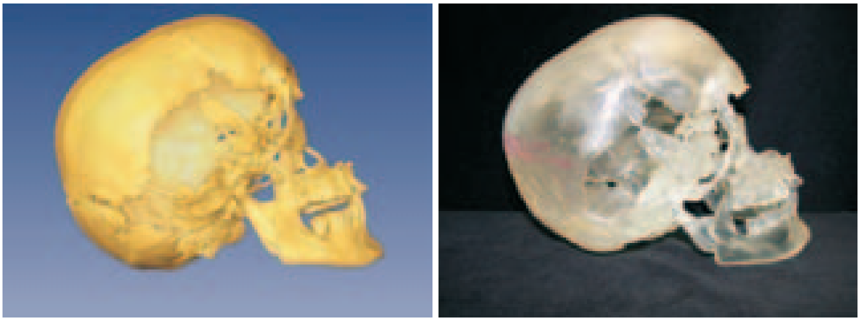

Fig. 1: Left: Translucent side view of the surface rendering of the skull. Right: Reproduced plastic model to which plasticine can be added for soft tissue reconstruction. (Produced by C. Tille and H. Seitz, caesar Rapid Prototyping group [3]).

However, serious shortcomings of this technique are that it is very time consuming and in-depth anatomical and forensic knowledge is necessary to create such a reconstruction.

Therefore, an alternative of a virtual soft-tissue reconstruction is proposed in this paper. In the following sections the methodology for elastic matching of a 3D soft-tissue template with a 3D reconstructed CT skull will be described. According to literature, so-called B-splines are often attached to the 3D skull (see [4] and the papers cited therein); the depth of soft tissue which varies over the skull is defined by standard distances at characteristic anatomical landmarks. Based on these distances, the B-splines so to speak form a soft-tissue tent over the cranial bone. A historical overview over three-dimensional reconstruction methods is given by Tyrell et al. [5].

In our case a novel method is proposed which employs images created by another 3D modality. This multi-modality approach for facial reconstruction is based on the elastic warping of an MRI soft tissue template onto a CT scan of a skull find. Regularized 3D thin-plate splines (TPS) are used for such a topology preserving transformation.

2 Methodology

With the broad availability of computed tomography several new computer based methods for craniofacial reconstruction were created. However, the first step in almost all methods is very similar to the manual approach although it is completely computer based: Virtual dowels, that indicate the spatial distribution of the soft-tissue depth at standard locations, are directly integrated into the 3D CT image via a software user interface and can be edited easily. After dowel placement soft tissue is often simulated by B-Splines attached to all virtual dowels [5]. By adjusting the height of the dowels the appearance of the face can be changed according to the conjectured attributes of the person. This method results in a face which looks somewhat similar to a person but also quite unnatural. This is mainly due to the low number of landmarks with sound height information that are used for reconstruction. Hence, large parts of the face are build upon interpolated height information. To decrease this inaccuracy more dowels could be attached but the result would still show a lack of details. Unfortunately, there is no listed information for a dense distribution of soft-tissue depth landmarks.

Here, a method is proposed that gives a solution to the fundamental problem of dense soft-tissue depth distribution. 3D images produced by magnetic resonance tomographs (MRT) carry the desired information because MRTs are especially designed to show soft tissues (see fig. 2).

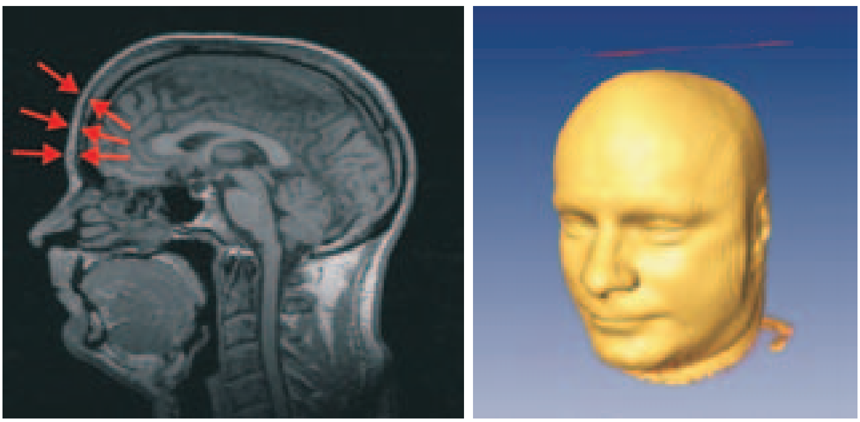

Fig. 2: Sagittal section through the head and surface visualisation of the skin from a 3D MRI dataset. The arrows exemplarily mark the tissue depth of the facial template.

The so-called thin-plate spline method will be used to adjust the MRI soft-tissue template to the CT cranial bone. This landmark-based method is known from registration studies in medicine; in our context we will show the extended 3D implementation of Bookstein's thin-plate spline method [6]. It is essentially a transformation of coordinates using radial basis functions. To avoid errors induced by misplaced landmarks a regularized version of this algorithm is used. In general, the entire computer-aided facial-reconstruction method follows four basic (traditional) steps [7], [8] that aim at supplementing and above all at accelerating traditional procedures:

A. Computed tomography of the skull find

This step includes the taking of skull measurements. The method presented in this article uses above all anatomical landmarks, which first have to be selected and entered into the computer. Digitalisation by the computer tomograph offers the advantage that further, and even very complex marks of the skull form, e. g. so-called "crest lines" or other structural features defined by differential geometry, may be determined later.

B. Matching of a MRI template from a database

The development of a reconstruction plan aims at identifying the "correct" soft-tissue template in a database with the help of additional information. This additional information which should originate from the results of the forensic and anthropological examination and CID (*criminal investigation division*) finds at the place where the body was discovered (e. g. hair fragments) is still indispensable and is also used in preparation of step *D*. Here again, the matching of anatomical landmarks of the MRI soft-tissue template with the anatomical landmarks of the skull find has to be reviewed.

C. Warping of the template to the CT skull find

In a first step the computer carries out the global elastic warping of the MRI template onto the skull find using the landmarks and, if necessary, different interpolation methods. Usually, subsequent interactive corrections of individual parts of the face are necessary.

D. Texture mapping

Texture mapping includes the application of patterns, shading and colours to surfaces. Today, computers are very well able to carry out this task. The real problem is rather the scope for artistic design. As for the manual method the decisions in this field are still left to the medico-legal expert and the anthropologist. But decision making can be supported by the computer, and wrong decisions can be easily corrected. In this contribution we will only deal with step A to C.

2.1 Three-Dimensional Thin-Plate Splines

Starting with a CT scan of the skull a new method for soft-tissue reconstruction is presented in this paper. In contrast to the 3D spline approach described in [4] the soft-tissue thickness is not interpolated through a few single points but all data contained in an MRI scan of a living individual is used for reconstruction. Not being forced to interpolate large areas of the face but being able to use the real thickness of soft tissue should lead to more natural looking reconstructions.

There are two key reasons for combining CT and MRI scans. As described above CT provides a copy of the skull free of geometrical distortion without putting the skull to risk [1]. This modality is chosen as reference or target dataset, respectively, because it makes the bones of the skull clearly visible which is necessary for the following work. Additionally, MR imaging is chosen as an excellent modality for the soft-tissue template datasets of the living individuals because this type of scan is specialized in displaying the skin-fat signal.

The main idea of the new method is not to extract the soft-tissue thickness from the MR image but to directly transform these data in a way that it fits onto the target CT scan, i. e. the skull find. The soft-tissue data – that are warped by thin-plate splines – can be seen as a kind of rubber glove which is wrapped around the skull.

To accomplish this some sort of mathematical transformation algorithm is necessary. In the field of image registration there are two major groups of registration functions which can be used, the affine and the elastic ones. The affine transformations are only capable of applying simple geometrical transformations like translation, rotation and shearing to an object whereas the elastic ones allow much more complex deformations [9].

The affine transformation is a so called collinear or line preserving transformation. This means that points which are collinear before the deformation are still collinear afterwards. Since there is no linear relationship between corresponding points in datasets taken from different individuals the affine transformation is only used for a general global alignment in this application.

For better alignment an elastic transformation must be used, additionally, for local deformations. If necessary, different regions will be deformed in a different way, so the alignment is much more precise as with an purely affine transformation.

Several of these elastic transformations are based upon two sets of corresponding or homologous landmarks (e. g. points, lines, surfaces and volumes), respectively, to influence the degree and the kind of transformation. The process of landmark localization can be done either automatically by software (e. g. edge detection) or manually by the user.

In contrast to Quatrehomme et al. who use a crest-line based algorithm [10] we have chosen to implement a fully point-based method called thin-plate splines (TPS). It was first applied by Bookstein [6] for 2D medical-image applications and is based on two sets of corresponding point landmarks which are set manually in this application. It was decided to employ this non-rigid algorithm as it provides smooth global and local deformations.

The basic version of TPS is an interpolation between the two landmark sets which means that every landmark from one dataset is mapped exactly onto its corresponding counterpart. With perfectly set landmarks this behaviour is desired but in real-world applications errors in landmark localization are very likely to occur. Without any counter measure this would lead to insufficient results. Hence, an extended TPS version which is more an approximation than an interpolation is presented in the next subsection.

2.2 Mathematics in Brief

In this subsection only a brief view onto the algebra of TPS is given, for a comprehensive coverage we refer to Bookstein [6].

The general task is to find a function f which maps all points from the target volume data, i. e. the 3D CT skull find, into their corresponding positions in the source volume data, i. e. the 3D MRI soft-tissue template:

$$f(p^t) = p^s \tag{1}$$

The labels 'target' and 'source' denote from the role of both volume data sets in the actual implementation. The algorithm walks through the entire target data calculating the corresponding point in the source data for each voxel and then copies the grey-value information found at this positions back into the target image.

One of the main concepts behind TPS is the use of a radial basis function (RBF) for the elastic part of the transformation. These functions are called radial because they only depend on the Euclidian distance of their associated data point from their origin. Since we are dealing with a 3D implementation the RBF is as follows:

$$U(r) = f(x,y,z) = \|r\|, \tag{2}$$

where

$$\|r\| = \sqrt{x^2 + y^2 + z^2}. \tag{3}$$

Tab. 1: Radial basis functions for several dimensions and orders. *m* denotes the dimension and M denotes the order.

R^m	D_M	U(x)	Note
R^1	D_2	r^3	
R^1	D_3	r^5	
R^2	D_2	$r^2 \log r$	
R^2	D_3	$r^4 \log r$	
R^3	D_2	r	
R^m	D_α	$r^{2\alpha-m} \log r$	if 2α-m even
R^m	D_α	$r^{2\alpha-m}$	if 2α-m odd

Radial basis functions for other dimensions can be found in table 1 and [11]. A function is in fact a RBF if it solves the so called biharmonic equation

$$\Delta^2 f = 0, \tag{4}$$

i. e. $U(r)$ must satisfy the equation

$$\Delta^2 U(r) = \left(\frac{\partial^4}{\partial x^4} + \frac{\partial^4}{\partial y^4} + \frac{\partial^4}{\partial z^4} + 2\,\frac{\partial^4}{\partial x^2 \partial y^2} + 2\,\frac{\partial^4}{\partial x^2 \partial z^2} + 2\,\frac{\partial^4}{\partial y^2 \partial z^2} \right) \cdot U(r) \propto \delta(x,y,z) \tag{5}$$

where Δ^2 is the two times iterated bilaplacian operator and $\delta(x,y,z)$ is the Dirac distribution.

TPS can be compared in a physical manner with a thin metal plate which is deformed by external forces. The more the plate is bend the higher is the bending energy. Considering only small deviations and ignoring gravitation such a plate will bend in a way that the physical bending energy is minimal [12], [13].

In general this behaviour can be described with one of Duchon's seminorms of appropriate dimension and order (see table 2 and [11], [14]). For the deformation of a volume dataset a seminorm of third dimension and second order is used [15]. Therefore, the bending energy is given by

$$J(f) = \int_{\Re^3} \left(\frac{\partial^2 f}{\partial x^2}\right)^2 + \left(\frac{\partial^2 f}{\partial y^2}\right)^2 + \left(\frac{\partial^2 f}{\partial z^2}\right)^2 + 2\left(\frac{\partial^2 f}{\partial x \partial y}\right)^2 + 2\left(\frac{\partial^2 f}{\partial x \partial z}\right)^2 + 2\left(\frac{\partial^2 f}{\partial y \partial z}\right)^2 dxdydz. \quad (6)$$

In order to minimize this term an appropriate interpolant $f(x,y,z)$ needs to be chosen.

As stated before this function f describes the correspondence between the two sets of landmarks and can be split up into three functions, one for each dimension:

$$f(p_i^t) = \begin{bmatrix} f_x(p_i^t) \\ f_y(p_i^t) \\ f_z(p_i^t) \end{bmatrix} = p_i^s i \in \{1,\ldots,n\} \quad (7)$$

where n denotes the number of landmarks. The interpolation function must be continuously defined and will map each landmark from the target image exactly onto its corresponding landmark in the source image.

Tab. 2: Duchon's Seminorms for several dimensions and orders. *m* denotes the dimension and M denotes the order.

R^m	D_M	$\|f\|^2_{D_M}$ for $f : R^m \to R$
R^1	D_2	$\int_{\Re^1} \left(\frac{\partial^2 f}{\partial x^2}\right)^2 dx$
R^1	D_3	$\int_{\Re^1} \left(\frac{\partial^3 f}{\partial x^3}\right)^2 dx$
R^2	D_2	$\int_{\Re^2} \left(\frac{\partial^2 f}{\partial x^2}\right)^2 + 2\left(\frac{\partial^2 f}{\partial x \partial y}\right)^2 + \left(\frac{\partial^2 f}{\partial y^2}\right)^2 dxdy$
R^2	D_3	$\int_{\Re^2} \left(\frac{\partial^3 f}{\partial x^3}\right)^2 + 3\left(\frac{\partial^3 f}{\partial x^2 \partial y}\right)^2 + 3\left(\frac{\partial^3 f}{\partial x \partial y^2}\right)^2 + \left(\frac{\partial^3 f}{\partial y^3}\right)^2 dxdy$
R^3	D_2	$\int_{\Re^3} \left(\frac{\partial^2 f}{\partial x^2}\right)^2 + \left(\frac{\partial^2 f}{\partial y^2}\right)^2 + \left(\frac{\partial^2 f}{\partial z^2}\right)^2 + 2\left(\frac{\partial^2 f}{\partial x \partial y}\right)^2 + 2\left(\frac{\partial^2 f}{\partial x \partial z}\right)^2 + 2\left(\frac{\partial^2 f}{\partial y \partial z}\right)^2 dxdydz$

As a straightforward extension of Bookstein's warping formula [6]

$$f_\bullet(x,y,z) = a_{0\bullet} + a_{1\bullet}x + a_{2\bullet}y + a_{3\bullet}z + \sum_{k=1}^{n} w_{\bullet k} U(\|P_k - P\|) \quad (8)$$

minimizes $J(f)$. $P=(x,y,z)$ and P_k denote the x, y and z coordinates of the target points. The point denotes the free index for the x-, y- or z-coordinates. The functional consists of two parts, where the first is the 3D version of the normal affine transformation. The second part takes care of the local elastic deformation and contains the previously mentioned radial basis function $U(r)$. The way the volume data is deformed is controlled by the still unknown parameters a and w.

Further investigations on eq. (8) show that the elastic part of the function needs boundary conditions to ensure that local deformations do not affect the whole area:

$$\sum_{k=1}^{n} w_{k\bullet} = 0,\ \sum_{k=1}^{n} w_{k\bullet} x_k = 0,\ \sum_{k=1}^{n} w_{k\bullet} y_k = 0 \text{ and } \sum_{k=1}^{n} w_{k\bullet} z_k = 0. \qquad (9\text{–}12)$$

Again n denotes the number of landmarks and $w_{k\bullet}$ is the set of elastic parameters of eq. 8. These terms limit the translation and rotation of the elastic part. They ensure that terms with a more than linear increase – far away from the landmarks – will not be considered.

The different coefficients a of the affine and w of the elastic part of eq. (8) can be determined by solving the following system of linear equations

$$\begin{aligned} Kw + Pa &= Y \\ P^T w &= 0 \end{aligned} \qquad (13)$$

This can also be written as

$$L^{-1} Y = (W | a_{0\bullet} a_{1\bullet} a_{2\bullet} a_{3\bullet}), \qquad (14)$$

where Y is a matrix containing the source landmarks

$$Y = \begin{bmatrix} x_1^s & y_1^s & z_1^s \\ x_2^s & y_2^s & z_2^s \\ \vdots & \vdots & \vdots \\ x_n^s & y_n^s & z_n^s \end{bmatrix} \text{ and } L = \begin{bmatrix} K & P \\ P^T & 0 \end{bmatrix} \qquad (15,16)$$

K is a matrix containing the values of the radial basis function between each target landmark

$$K = \begin{bmatrix} 0 & U(r_{12}) & \dots & U(r_{1n}) \\ U(r_{21}) & 0 & \dots & U(r_{2n}) \\ \vdots & \vdots & \ddots & \vdots \\ U(r_{n1}) & U(r_{n2}) & \dots & U(r_{nn}) \end{bmatrix} \qquad (17)$$

and P is a matrix containing the target landmarks

$$P = \begin{bmatrix} 1 & x_1^t & y_2^t & z_1^t \\ 1 & x_2^t & y_2^t & z_2^t \\ \vdots & \vdots & \vdots & \vdots \\ 1 & x_n^t & y_n^t & z_n^t \end{bmatrix}. \qquad (18)$$

As mentioned before the problem with this algorithm is that both landmark sets are exactly mapped onto each other. With precisely located landmarks this is not a problem but in a real life application there are always inaccuracies in the landmark placement.

In image data sets of bad quality it is often difficult to decide where to exactly assign a landmark. Therefore, a method is needed that is capable to take these errors into account.

To minimize the influence of errors a regularized TPS version was implemented. Where eq. (1) requires an exact one-to-one correspondence the extended version allows some degree of freedom denoted as ε:

$$\sum_{i=1}^{n} \left\| f(p_i^t) - p_i^s \right\|^2 \leq \varepsilon. \tag{19}$$

The only change that is needed is the addition of a regularization matrix to eq. (13)

$$\begin{aligned} &(K + \lambda I)w + Pa = Y \\ &P^T w = 0 \end{aligned} \tag{20}$$

where I is an identity matrix of appropriate size and λ is the so called regularization parameter. It determines the relative weight between the approximation behaviour and the smoothness of the transformation. For the case $\lambda = 0$ one can see that eq. (20) equals eq. (13), i. e. the transformation is not regularized. For growing λ the elastic part of the transformation becomes weaker. For a very large regularization parameter λ there is only the affine transformation left. In eq. (21) the entire system of equations for the estimation of the transformation parameters is given. It is the explicit form of eq. (20).

$$\begin{pmatrix} x_1^s & y_1^s & z_1^s \\ \vdots & \vdots & \vdots \\ x_n^s & y_n^s & z_n^s \\ 0 & 0 & 0 \\ 0 & 0 & 0 \\ 0 & 0 & 0 \\ 0 & 0 & 0 \end{pmatrix} = \begin{pmatrix} \lambda & \cdots & U(r_{1n}) & 1 & x_1^t & y_1^t & z_1^t \\ \vdots & \ddots & \vdots & \vdots & \vdots & \vdots & \vdots \\ U(r_{n1}) & \cdots & \lambda & 1 & x_n^t & y_n^t & z_n^t \\ 1 & \cdots & 1 & 0 & 0 & 0 & 0 \\ x_1^t & \cdots & x_n^t & 0 & 0 & 0 & 0 \\ y_1^t & \cdots & y_n^t & 0 & 0 & 0 & 0 \\ z_1^t & \cdots & z_n^t & 0 & 0 & 0 & 0 \end{pmatrix} \begin{pmatrix} w_1^x & w_1^y & w_1^z \\ \vdots & \vdots & \vdots \\ w_n^x & w_n^y & w_n^z \\ a_0^x & a_0^y & a_0^z \\ a_1^x & a_1^y & a_1^z \\ a_2^x & a_2^y & a_2^z \\ a_3^x & a_3^y & a_3^z \end{pmatrix} \tag{21}$$

Please note that for $\lambda = 0$ eq. (21) is equivalent to eq. (13).

2.3 Implementation

In the application presented in this paper eq. (8) is implemented for the transformation process and eq. (21) is implemented for determination of the transformation coefficients a and w. The linear system of equations is solved by singular value decomposition. The CT scan of the skull is used as target volume data and the MRI soft-tissue template is used as source data.

To ensure smooth results a trilinear interpolation has been implemented to suppress artifacts which are likely to occur when using a simple nearest neighbor interpolation.

Our current implementation is written in Matlab 6.5 and it takes about 10 minutes to map a typical volume dataset (resolution: 256*256*256, 30 landmarks) on a 2.2 GHz PC.

3 Results

In this section results of the 3D thin-plate spline method described in section 2 are presented. It is a facial soft-tissue reconstruction of an unknown person on the basis of the skull find. The traditional plasticine reconstruction – produced and provided for our experiments by R. P. Helmer [16] – is used as the basis for comparison. Fig. 3 shows the acquisition of the data basis via computed tomography. The plasticine head which contains the original skull is placed at the iso-centre of a Philips Secura spiral CT scanner on a plastic dish (fig. 3, a and b).

As an example four sagittal sections of the plasticine reconstruction seen in fig. 3 b are shown in fig. 4. It is very easy to distinguish between the original skull and the plasticine layer. The metal fixations for the skull used for preparation purposes do not substantially interfere with CT image acquisition.

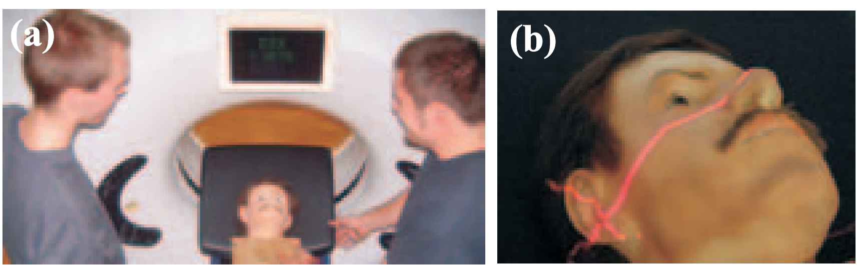

Fig. 3: a) Positioning of the plastic skull reconstruction in the CT scanner on a plastic dish and b) positioning of the head in the iso-centre of the Philips spiral CT scanner.

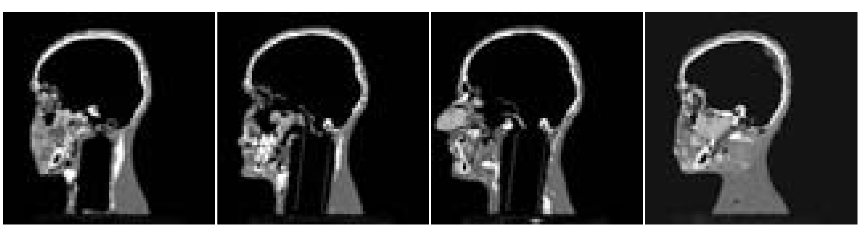

Fig. 4: Representation of sagittal skull sections of the head reconstruction provided by R. P. Helmer [16].

On the basis of the homologous set of landmarks (see fig. 5 left) the set of parameters of the warping spline is estimated. Via the thin-plate spline the entire space is subjected to a nonlinear deformation which is visualized in the right-hand side of fig. 5.

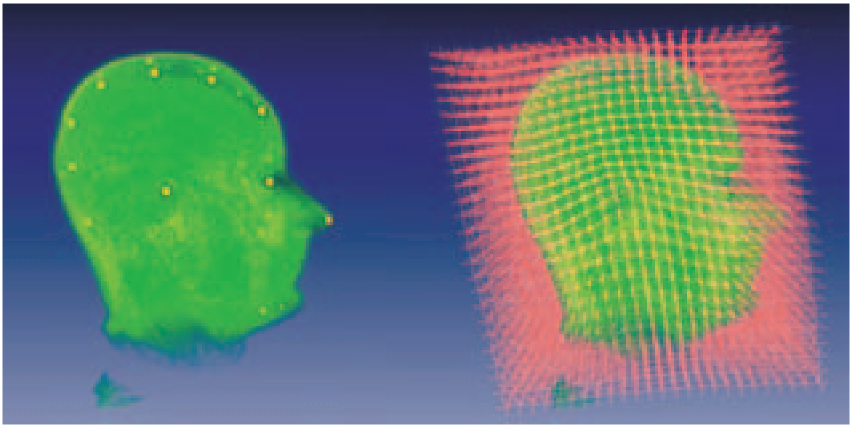

Fig. 5: Visualization of space warping based on regularized thin-plate splines.

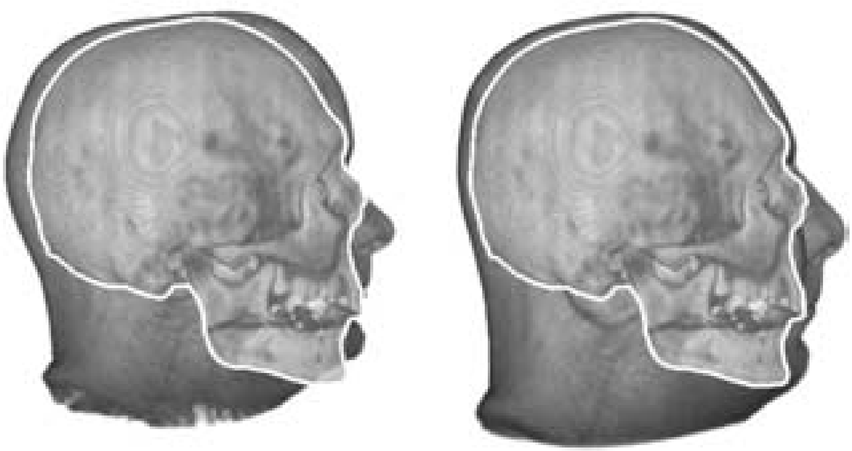

Fig. 6: A skull find is superimposed on the untransformed MR soft-tissue template (left) and on the result of the transformation (right).

The results obtained by this method are encouraging compared to traditional clay-based reconstructions. Fig. 6 shows a case where an arbitrary MRI template was morphed onto the CT scan of a skull find from an unsolved case of murder. It can clearly be seen that after the transformation the MR soft-tissue template matches to the target skull. The region around the nose is an example for the smoothness of the regularized transformation. The two most deformed regions are the forehead and the nose. However, it can also be seen that the nose and lower maxillary needs some refinement because it looks somewhat unnatural.

A comparison between our method and the manual clay-based approach is presented in fig. 7. As demonstrated in the first example the thin-plate spline transformation leads to an acceptable fit between the soft-tissue MR-based template and the CT-based skull find. The displacement of the neck can be explained with the fact that the landmarks are only set upon the skull surface, a few additional virtual soft-tissue landmarks are necessary to correct this error.

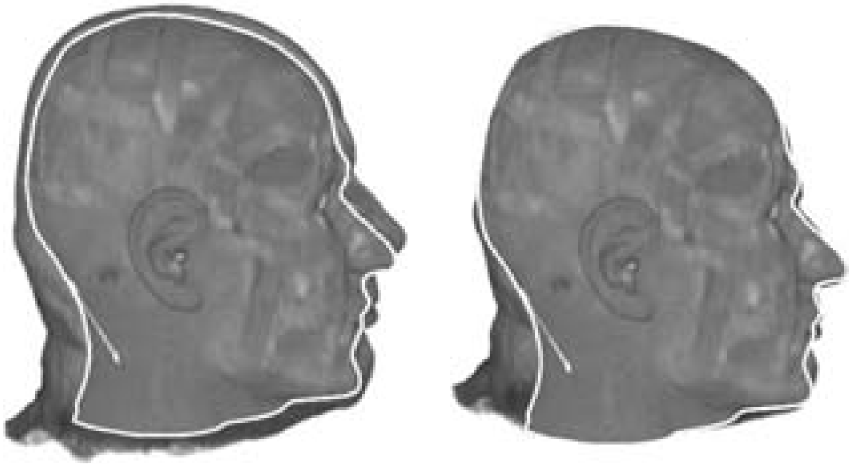

Fig. 7: The work of R. P. Helmer [16] is superimposed on the untransformed MR soft-tissue template (left) and on the result of the transformation (right).

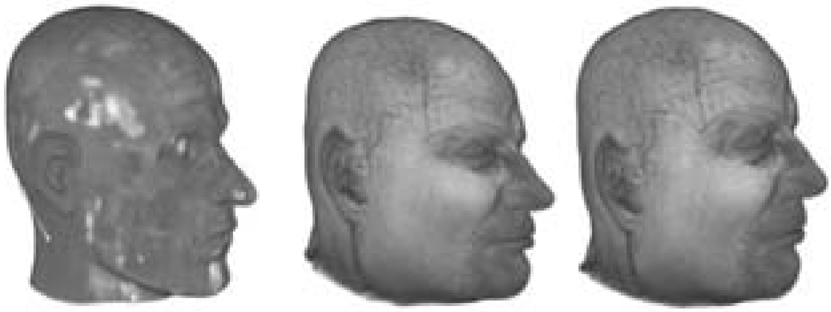

Fig. 8: Comparison between the head produced by R. P. Helmer [16] (first), the result of the transformation (second) and the untransformed template (third).

A direct comparison can be seen in fig. 8. Once again the region around the nose is subjected to large deformation. This comparison also reveals that the selection of an appropriate template is a crucial step of the procedure, because, obviously, for this example case both persons are not assumed to have the same weight. Fig. 8 does not allow a quantitative comparison between both methods because the clay-based work is hypothetical as well.

As demonstrated in fig. 6 and fig. 7, thin-plate spline warping is not capable of all the transformations which are potentially needed because only those transformations which preserve topology are possible. We therefore plan to create an MRI soft-tissue database containing different templates according to ethnic groups, gender, age, weight, physiognomy etc. where appropriate initial templates can be chosen from.

4 Conclusions and Future Work

We have presented results of a 3D thin-plate spline method for forensic facial soft-tissue reconstruction which are based on a CT scan of a skull find and an arbitrarily chosen MRI facial soft-tissue template. In comparison with a traditional plasticine reconstruction the results are encouraging.

The quality of the reconstructed faces is influenced by the choice of an appropriate MRI soft-tissue template. Not all the warping which may be necessary for a perfect fit can be done by 3D thin-plate splines. In particular, only those transformations are possible which preserve topology.

To solve this problem it is planned to build up an MRI soft-tissue template database from which the user can easily select a adequate template based on the age, the gender and other criteria. These templates could have landmark presets such that after the manual landmark setting on the skull-find dataset any appropriate template from the database could be morphed without additional interaction.

A disadvantage of the MRI modality is the acquisition situation in which the individuals for the MRI database are positioned in the scanner. The head is moved into the measuring field of the MRI scanner in a lying and slightly fixed in position. Therefore, pulsed holography will be used for facial measurement in a further step [17]. In the process, the facial template is captured very fast while the individuals are in a normal sitting position, so that a more natural facial expression is generally available for the matching process.

Another direction of future research is the 3D interaction during the process of landmark setting. We are currently working on a new method based on navigation principles of image-guided surgery to simplify this task.

5 Acknowledgements

The authors would like to thank Prof. Richard P. Helmer, Institute of Applied Forensic Medicine and Anthropology, Remagen, Germany, for many critical discussions, manual setting of soft-tissue landmarks, for providing us with the clay-based facial reconstruction, and for overall kind support. Many thanks go to Dr. Carsten Tille and Dr. Herman Seitz, heads of the Rapid Prototyping group at the research centre ceasar Bonn, for providing us with the rapid prototyping skull copy of our CT data. The authors would also like to thank Dirk Thomsen for the kind support in CT image acquisition. Additionally, we would like to thank Prof. Dr. Dr. Jürgen Ruhlmann for providing us with MR images.

6 References

[1] T. M. Buzug, P. Hering, and R. P. Helmer, "3D Tomography as a Basis for Anthropological and Forensic Facial Reconstruction" in *Reconstruction of Soft-Facial Parts, Proceedings of the 1. International Conference RSFP*, 2003, pp. 91–108.

[2] K. Raic, T. Jansen, B. von Rymon-Lipinski, C. Tille, H. Seitz, and E. Keeve, "Fast generation of stereolithographic models" in *Biomed Tech* (Berl). 2002;47 Suppl 1 Pt 1:83–5.

[3] C. Tille and H. Seitz, Private communication, caesar Rapid Prototyping group, Bonn, 2003.

[4] D. W. Bullock, "Computer Assisted 3D craniofacial reconstruction", M. S. thesis, University of British Columbia, 1999.

[5] A. J. Tyrrell, M. P. Evison, A. T. Chamberlain, and M. A. Green, "Forensic Three-dimensional Facial Reconstruction: Historical Review and Contemporary Developments", *Journal Forensic Science*. 1997 Jul;42(4) pp. 653–661.

[6] F. L. Bookstein, "Principal Warps: Thin Plate Splines and the Decomposition of Deformations" *IEEE Transactions on Pattern Analysis and Machine Intelligence*. Volume 11, pp. 567–585, June 1989.

[7] R. P. Helmer, S. Rohricht, D. Petersen, and F. Mohr, "Assessment of the Reliability of Facial Reconstruction" in *Forensic Analysis of the Skull*, Chapter 17, p. 229, Wiley-Liss, 1993.

[8] R. P. Helmer, T. M. Buzug, and P. Hering, "Plastic facial reconstruction on the skull – a transition in Germany from a conventional technique to a new one" in *Reconstruction of Soft-Facial Parts, Proceedings of the 1. International Conference RSFP*; 2003, pp. 77–90.

[9] T. M. Buzug, J. Weese, C. Fassnacht, and C. Lorenz, "Elastic matching based on motion-vector fields obtained with a histogram-based similarity measure for DSA image correction" in *International Conference on Computer Assisted Radiology* pp. 139–144.

[10] G. Quatrehomme et al, "A fully three-dimensional method for facial reconstruction based on deformable models" in Journal Forensic Science., 42(4) pp. 649–652, 1997.

[11] J. Kybic, "Elastic Image Registration using Parametric Deformation Models", Ph. D. dissertation, Ecole Polytechnique Fédérale de Lausanne, Lausanne, Switzerland. 2001.

[12] E. W. Weisstein, "Biharmonic Equation" from MathWorld – A Wolfram Web Resource. http://mathworld.wolfram.com/BiharmonicEquation.html.

[13] E. W. Weisstein, "Thin Plate Spline" from MathWorld – A Wolfram Web Resource. http://mathworld.wolfram.com/ThinPlateSpline.html.

[14] J. Duchon, "Interpolation des fonctions de deux variables suivant le principe de la flexion des plaques minces" in *RAIRO Analyse Numérique* Volume 10, pp. 5–12, 1976.

[15] K. Rohr, H. S. Stiehl, R. Sprengel, T. M. Buzug, J. Weese, and M. H. Kuhn, "Landmark-based elastic registration using approximating thin-plate splines" in *IEEE Transactions on Medical Imaging*, Volume 20, p. 526, 2001.

[16] R. P. Helmer, Private communication, 2004.

[17] P. Hering, T. M. Buzug, and R. P. Helmer, "Ultrafast Holographic 3D Facial Measurement for Forensic Applications" in *Reconstruction of Soft-Facial Parts, Proceedings of the 1. International Conference RSFP*, 2003, pp. 109–117.

Radiale Basisfunktionen für das 3D nichtlineare Weichteil-Warping

Jan Müller, Andreas Mang and Thorsten M. Buzug

Institut für Medizintechnik, Universität zu Lübeck, Ratzeburger Allee 160, 23538 Lübeck

Abstract

Die Rekonstruktion eines Gesichtes anhand eines Schädelfundes spielt vor allem in der Forensik und in der Archäologie eine wichtige Rolle. Zum einen hilft das Rekonstruktionsergebnis bei der Identifizierung eines unbekannten Toten und zum anderen lässt sich so das Aussehen der Menschen früherer Epochen mit dem modernen Menschen vergleichen. Da das konventionelle Vorgehen mit i) *Untersuchung des Schädels* ii) *Planung des weiteren Vorgehens* iii) *die eigentliche Rekonstruktionsarbeit mit Plastilin* und iv.) *Detailarbeit wie Wahl der Augen und Haare* sehr zeitaufwendig ist, wird in diesem Artikel ein neues computergestütztes Verfahren vorgeschlagen. Hierbei wird an einen 3D CT-Scan des Schädels eine 3D MRT-Aufnahme einer lebenden Person mit Hilfe einer elastischen Transformationsfunktion angepasst. Dieses landmarkenbasierte Verfahren ist unter dem Begriff *Thin-Plate Splines* (TPS) bekannt und benutzt für den nichtlinearen Teil der Transformation radiale Basisfunktionen. Um Fehler in der Landmarkenlokalisierung auszugleichen, wird eine regularisierte Variante der TPS benutzt.

1 Einleitung

Da die Gefahr einer Beschädigung des Originalschädels bei der Rekonstruktion zu hoch ist, muss für die Rekonstruktion, egal ob manuell oder computergestützt, eine Kopie des Schädels angefertigt werden. Hierbei hat es sich bewährt, den Schädel mit Hilfe der Computertomographie (CT) zu digitalisieren. Dieses Verfahren bietet sich unter anderem deswegen an, weil es auf die Darstellung von Knochenstrukturen spezialisiert ist. Im resultierenden Datensatz sind die einzelnen Knochen deutlich zu erkennen. Ein anderer Vorteil der CT ist, neben der hohen Auflösung der Bilder, die Tatsache, dass der zu untersuchende Gegenstand verzerrungsfrei abgebildet werden kann [1].

Nachdem nun der Schädel als digitale Kopie vorliegt, gibt es zwei unterschiedliche Möglichkeiten der Rekonstruktion. Die eine, auf die in diesem Artikel später noch näher eingegangen wird, ist ein rein virtueller Ansatz, bei dem alle nötigen Arbeiten direkt am Computer durchgeführt werden können.

Zum anderen kann anhand des Datensatzes mit Hilfe des so genannten Rapid Prototyping [2] eine Kopie des Schädels aus Plastik angefertigt werden. An ihr kann nun die konventionelle Rekonstruktion durchgeführt werden, ohne den Originalschädel einer Gefahr auszusetzen. In Abbildung 1 ist eine Kopie und der dazugehörige Originaldatensatz eines archäologischen Schädelfundes exemplarisch abgebildet.

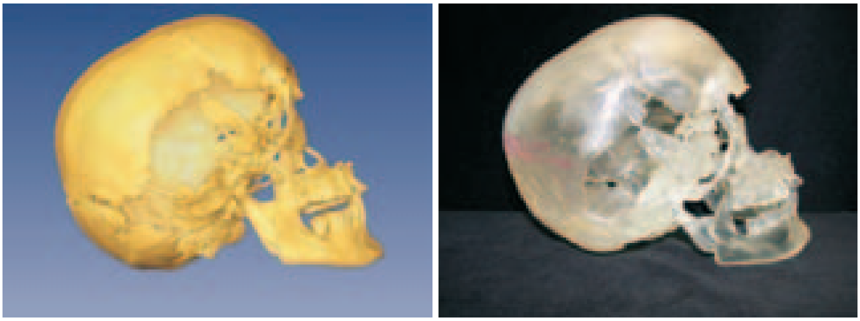

Abb. 1: Links: Transparente Seitenansicht der Schädeloberfläche. Rechts: Das Plastikmodell an welches das Plastilin für die Weichgewebsrekonstruktion angebracht werden kann. (Hergestellt von C. Tille und H. Seitz, caesar Rapid Prototyping Gruppe [3]).

Bei der manuellen Rekonstruktion werden im ersten Schritt die groben Gesichtszüge mit Plastilin oder Wachs nachgebildet. Bei der Dicke der Schichten orientiert man sich an Tabellen, die für verschiedene Punkte im Gesicht typische Gewebetiefen enthalten. Nach und nach werden immer dünnere Schichten aufgetragen und feine Strukturen modelliert. Diese Art der Rekonstruktion führt zwar zu sehr guten Ergebnissen, ist jedoch sehr zeitaufwendig und erfordert ein umfangreiches Wissen auf dem Gebiet der Forensik bzw. der Anatomie.

Ein computerbasiertes Verfahren, das mit einer ähnlichen Technik arbeitet, wird unter anderem in [4] und den darin zitierten Beiträgen vorgestellt. Bei dieser Methode werden im ersten Schritt die Höheninformationen aus den oben beschriebenen Tabellen auf den CT Datensatz des Schädels übertragen. Danach wird mit einer Oberfläche aus B-Splines die Hautoberfläche nachgebildet. Einen historischen Überblick über dreidimensionale Rekonstruktionsmethoden geben Tyrell et al. in [5].

In unserem Fall wird ein neues Verfahren vorgeschlagen, das zusätzlich zu den CT-Aufnahmen Daten einer anderen Modalität benutzt. Hierbei wird mit Hilfe einer elastischen Verformung ein Weichteiltemplate in Form einer MRT-Aufnahme an den CT-Scan des Schädels angepasst. Für diese topologie-erhaltende Transformation wird ein Verfahren namens 3D Thin-Plate Splines benutzt.

2 Beschreibung der Methode

Durch die zunehmende Verbreitung von leistungsfähigen Computern entstanden in den letzten Jahren einige neue computerbasierte Verfahren zur Gesichtsrekonstruktion. Ein Teil dieser Verfahren benutzt, wie schon erwähnt, eine 3D CT-Aufnahme des Schädels als Ausgangsbasis für die Rekonstruktionsarbeit. Die Computertomographie als Aufnahmemodalität hat den Vorteil, dass sie verzerrungsfreie Bilder in hohen Auflösungen des zu untersuchenden Objekts liefert. Ausgehend von diesem Datensatz gibt es mehrere Möglichkeiten, mit Hilfe des Computers, das Gesicht zu rekonstruieren.

Da bei der manuellen Rekonstruktion umfangreiche Listen mit Informationen über die Gewebedicke an markanten Stellen des Gesichtes verwendet werden, liegt es nahe, diese auch für eine computergestützte Rekonstruktion zu benutzen.

Bei einem gängigen Verfahren, das mit diesen Tabellen arbeitet, wird die Hautoberfläche mit B-Splines nachgebildet [4]. Im ersten Schritt werden die Tiefeninformationen aus diesen Tabellen mit Hilfe einer Software auf den Datensatz übertragen. Das spätere Aussehen des Gesichtes lässt sich auf einfache Weise durch eine Änderung dieser Werte steuern. Im zweiten Schritt wird ausgehend von diesen Informationen eine Oberfläche aus B-Splines über dem Schädel aufgespannt. Diese Oberfläche stellt eine Annäherung an das zu rekonstruierende Gesicht dar.

Da jedoch nur die Höheninformationen an ein paar Dutzend Stellen aufgetragen werden, müssen große Teile des Gesichtes interpoliert werden. Die Ergebnisse haben dann zwar Ähnlichkeit mit einem menschlichen Gesicht, sind aber, bedingt durch die Interpolation, recht detailarm. Mit einer größeren Anzahl von anatomischen Landmarken ließe sich dieses Problem abschwächen, aber leider fehlen für solch eine große Anzahl von Punkten die passenden Informationen zu den Gewebedicken.

Im Folgenden wird nun ein Verfahren vorgestellt, das dieses Problem dadurch umgeht, dass es, zusätzlich zu der CT-Aufnahme des Schädels, Informationen einer zweiten Modalität verwendet. In diesem Fall dient eine 3D MRT-Aufnahme einer lebenden Person als zusätzliche Informationsquelle.

Da die Magnetresonanztomographie speziell für die Darstellung von Weichteilen wie z. B. der Haut entwickelt wurde, sind alle für Gesichtsrekonstruktion benötigten Tiefeninformationen in solch einer Aufnahme enthalten. In Abbildung 2 ist ein Schnittbild einer MRT Aufnahme sowie die dazugehörige Darstellung der Hautoberfläche zu sehen.

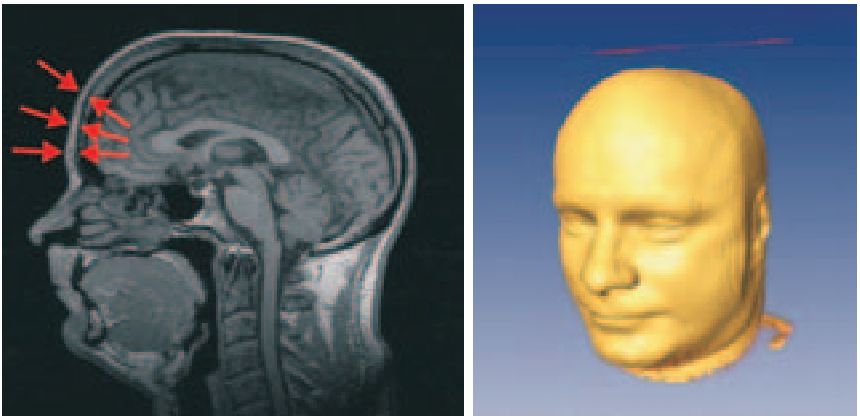

Abb. 2: Links: Sagittaler Schnitt durch den Kopf. Die Pfeile markieren exemplarisch die Weichteildicke an diesen Stellen. Rechts: eine Darstellung der aus einem 3D MRT Datensatz extrahierten Haut.

Bei dem vorgestellten Verfahren werden keine Informationen aus der MRT-Aufnahme extrahiert, vielmehr wird der Datensatz als Weichteiltemplate verwendet und mit Hilfe der so genannten Thin-Plate-Spline-Methode (TPS) vollständig an die virtuelle Repräsentation des Schädels angepasst. Alle im MRT-Datensatz enthaltenen Tiefeninformationen werden so auf die Schädeloberfläche übertragen. Da keine Informationen mehr interpoliert werden müssen, sollte dieses Verfahren detailliertere und natürlichere Resultate als die B-Spline basierten Verfahren liefern.

Diese landmarkenbasierte Methode ist aus mehreren Studien zur medizinischen Bildregistrierung bekannt und wurde zuerst von Bookstein für die Registrierung zweidimensionaler medizinischer Bilder verwendet [6]. In diesem Artikel werden wir näher auf die Mathematik und die praktische Implementierung der dreidimensionalen Variante in einer regularisierten und einer unregularisierten Form eingehen.

Generell orientiert sich dieses computergestützte Verfahren an den vier Schritten der manuellen Rekonstruktion [1], [7], [8]:

A. Arbeiten mit dem Datensatz des Schädels

Um eine Rekonstruktion mit Hilfe der TPS durchführen zu können, müssen im ersten Schritt einige Landmarken an standardisierte Positionen [7], [8] gesetzt werden. Da alle Daten digital vorliegen, können sie auch später noch einfach verändert werden; z. B. können später komplexere Landmarkentypen wie „Crest-Lines“ oder andere Strukturmerkmale, die durch Differentialgeometrie bestimmt werden, verwendet werden.

B. Auswahl eines geeigneten MRT Templates aus einer Datenbank

Da es wenig Sinn macht eine MRT Aufnahme eines 80 kg schweren Mannes auf den Schädel einer 50 kg schweren Frau anzupassen, muss in diesem Schritt ein, für den jeweiligen Fall, passendes Template gewählt werden. Je mehr Daten zu der Person aus vorangegangenen forensischen bzw. anthropologischen Untersuchungen vorliegen, desto genauer kann ein passendes Template gewählt werden. Da die Templates schon mit Landmarken versehen sind, können innerhalb kurzer Zeit verschiedene Templates an den Schädel angepasst werden.

C. Transformation des Templates auf den Schädel

Im einem ersten Schritt passt der Computer nun mit Hilfe der elastischen Transformation und der zuvor festgelegten Landmarken das Template an den Schädel an. Üblicherweise sind danach noch einzelne Korrekturen an einigen Stellen des Gesichts nötig.

D. Texture mapping

Da das zuvor verformte Template keine Farbinformationen aufweist, müssen in diesem letzten Schritt noch Texturen, Farben und Schattierungen aufgebracht werden, um eine möglichst lebensechte Rekonstruktion zu erzeugen. Wie bei der traditionellen Rekonstruktion ist dieser Schritt eher eine künstlerische als eine technische Aufgabe. Die Entscheidungen über das Aussehen sind weitestgehend dem Gerichtsmediziner bzw. dem Anthropologen überlassen, der Computer kann hier nur Hilfestellung leisten. Der Vorteil des neuen Verfahrens liegt darin, dass sich Fehler schnell und einfach korrigieren lassen.

In diesem Beitrag werden nur die Schritte A und C behandelt.

2.1 Dreidimensionale Thin-Plate-Splines

Wie oben schon erwähnt, basiert das hier vorgestellte Verfahren auf der elastischen Verformung eines Volumendatensatzes. Um dies zu ermöglichen, ist eine Transformationsfunktion nötig, mit der die Verformung berechnet werden kann.

Im Bereich der Bildregistrierung werden zwei Arten von Transformationsfunktionen benutzt, die *affinen* und die *elastischen* Transformationen. Die affinen erlauben nur die Anwendung einfacher geometrischer Operationen – Rotationen oder Scherungen – auf ein Objekt. Für komplexere Verformungen muss eine elastische Transformation gewählt werden.

Die affinen Transformationen sind sogenannte kollineare Funktionen, d. h. alle Punkte, die vor der Transformation auf einer Linie lagen, liegen hinterher immer noch auf einer Linie. Dadurch ist das Verfahren recht unflexibel und nicht in der Lage, das MRT-Template perfekt an den Schädel anzupassen.

Für eine bessere Anpassung muss zusätzlich eine elastische Transformation verwendet werden [9]. Durch die Möglichkeit kleinere Teile unabhängig vom Gesamtdatensatz zu deformieren, lässt sich so eine viel höhere Genauigkeit erreichen als dies mit einem rein affinen Verfahren möglich wäre.

Um den Grad der Verformung zu kontrollieren, benutzen ein Teil der elastischen Transformationen so genannte Landmarken. Hierbei werden in den beiden zu verarbeitenden Datensätzen korrespondierende Punkte markiert. Diese Landmarken können verschiedene Formen annehmen, gebräuchlich sind unter anderem Punkte, Linien und Flächen. Die Lokalisierung der Landmarken geschieht entweder durch den Nutzer oder durch ein automatisiertes Verfahren.

Im Gegensatz zu Quatrehomme et al., die einen „Crest-line“ basierten Algorithmus benutzen [10], haben wir uns entschlossen, die Methode der Thin-Plate Splines zu verwenden, die auf punktförmigen Landmarken beruht. Sie wurde als erstes von Bookstein [6] für die Registrierung zweidimensionaler medizinischer Bilder benutzt und ermöglicht sehr glatte und kontinuierliche Ergebnisse. Die Landmarken werden in unserer Anwendung manuell gesetzt, da automatische Verfahren für diesen Zweck noch zu ungenau und zu unzuverlässig sind.

Bei der einfachen Variante der TPS wird jede Landmarke des einen Datensatzes exakt auf das korrespondierende Gegenstück im anderen Datensatz abgebildet. Bei perfekt gesetzten Landmarken ist diese Eigenschaft gewünscht, aber da es in der Praxis leicht zu Fehlern bei der Lokalisation der korrespondierenden Landmarken kommt, würden sich diese Fehler negativ auf die Transformation auswirken. Deswegen wird in dieser Arbeit auch eine regularisierte, und somit flexiblere Variante der TPS vorgestellt, die nicht so empfindlich in Bezug auf fehlerhaft gesetzte Landmarken ist.

2.2 Die Mathematik der TPS

Im Folgenden wird nur ein kurzer Überblick über die Mathematik der Thin-Plate Splines gegeben. Eine ausführliche Beschreibung findet man in [6], [11].

Um eine elastische Transformation durchführen zu können, muss als erstes eine Funktion f gewählt werden, die alle Punkte des Target- oder auch Zielvolumens, d. h. in unserem Fall die CT-Aufnahme des Schädels, auf ihre korrespondierende Positionen im Source- oder auch Quellvolumen, d. h. dem MRT-Template abbildet. Dies kann ganz allgemein als

$$f(p^t) = p^s \tag{1}$$

beschrieben werden. p^t ist ein beliebiger Punkt im Targetvolumen, dessen korrespondierender Punkt p^s im Sourcevolumen mit der Funktion f bestimmt werden kann. Die Bezeichnung ‚Source‘ und ‚Target‘ wurden aufgrund der Implementationsweise des Algorithmus gewählt. Dabei wird für jeden Punkt des Targetvolumens der entsprechende Punkt im Sourcevolumen berechnet und der dort interpolierte Grauwert zurück in das Targetvolumen geschrieben. Dies stellt sicher, dass das Ergebnis der Transformation frei von Löchern ist.

Eines der Hauptkonzepte der TPS ist die Nutzung von radialen Basisfunktionen (RBF) für den elastischen Teil der Transformation. Diese Art von Funktionen werden als radial bezeichnet, weil ihr Wert nur vom euklidischen Abstand des betrachteten Punktes zum Ursprung abhängt, nicht jedoch von seiner absoluten Koordinate. Alle Punkte mit dem selben Abstand zum Ursprung haben den selben Funktionswert.

Die dreidimensionale radiale Basisfunktion 2. Ordnung, die für die hier vorgestellte Anwendung verwendet wird, ist definiert als

$$U(r) = f(x,y,z) = \|r\|, \tag{2}$$

wobei

$$\|r\| = \sqrt{x^2 + y^2 + z^2}. \tag{3}$$

Tab. 1: Radiale Basisfunktionen für verschiedene Dimensionen und Ordnungen. *m* steht für die Dimension und M für die Ordnung [11].

R^m	D_M	U(x)	Bemerkung
R^1	D_2	r^3	
R^1	D_3	r^5	
R^2	D_2	$r^2 \log r$	
R^2	D_3	$r^4 \log r$	
R^3	D_2	r	
R^m	D_α	$r^{2\alpha-m} \log r$	wenn 2α-m gerade
R^m	D_α	$r^{2\alpha-m}$	wenn 2α-m ungerade

Tab. 1 zeigt radiale Basisfunktionen für andere Dimensionen und Ordnungen, siehe dazu auch [11]. Eine Funktion *f* ist immer dann eine radiale Basis Funktion, wenn sie die sogenannte biharmonische Gleichung

$$\Delta^2 f = 0 \tag{4}$$

erfüllt, d. h. $U(r)$ muss im dreidimensionalen Fall eine Lösung der Gleichung

$$\Delta^2 U(r) = \left(\frac{\partial^4}{\partial x^4} + \frac{\partial^4}{\partial y^4} + \frac{\partial^4}{\partial z^4} + 2\,\frac{\partial^4}{\partial x^2 \partial y^2} + 2\,\frac{\partial^4}{\partial x^2 \partial z^2} + 2\,\frac{\partial^4}{\partial y^2 \partial z^2} \right) \cdot U(r) \propto \delta(x,y,z) \tag{5}$$

sein. Δ^2 ist der zweifach angewandte biharmonische Operator und $\delta(x,y,z)$ ist die Delta-Distribution.

TPS lassen sich physikalisch gesehen mit einer dünnen Metallplatte unendlicher Ausdehnung vergleichen, die von externen punktförmigen Kräften verformt wird. Je größer die Verformung dieser Platte, desto größer ist auch ihre interne Biegeenergie. Wird dabei die Gravitation nicht berücksichtigt und handelt es sich nur um kleine Verformungen, so wird sich diese Platte immer dergestalt verformen, dass ihre interne Biegeenergie minimal ist [12], [13].

Tab. 2: Duchon's Seminormen für andere Dimensionen und Ordnungen

R^m	D_M	$\|f\|^2_{D_M}$ für $f : R^m \to R$
R^1	D_2	$\int_{\Re^1} \left(\frac{\partial^2 f}{\partial x^2}\right)^2 dx$
R^1	D_3	$\int_{\Re^1} \left(\frac{\partial^3 f}{\partial x^3}\right)^2 dx$
R^2	D_2	$\int_{\Re^2} \left(\frac{\partial^2 f}{\partial x^2}\right)^2 + 2\left(\frac{\partial^2 f}{\partial x \partial y}\right)^2 + \left(\frac{\partial^2 f}{\partial y^2}\right)^2 dxdy$
R^2	D_3	$\int_{\Re^2} \left(\frac{\partial^3 f}{\partial x^3}\right)^2 + 3\left(\frac{\partial^3 f}{\partial x^2 \partial y}\right)^2 + 3\left(\frac{\partial^3 f}{\partial x \partial y^2}\right)^2 + \left(\frac{\partial^3 f}{\partial y^3}\right)^2 dxdy$
R^3	D_2	$\int_{\Re^3} \left(\frac{\partial^2 f}{\partial x^2}\right)^2 + \left(\frac{\partial^2 f}{\partial y^2}\right)^2 + \left(\frac{\partial^2 f}{\partial z^2}\right)^2 + 2\left(\frac{\partial^2 f}{\partial x \partial y}\right)^2 + 2\left(\frac{\partial^2 f}{\partial x \partial z}\right)^2 + 2\left(\frac{\partial^2 f}{\partial y \partial z}\right)^2 dxdydz$

Dieses Verhalten kann mit einer von Duchon's Halbnormen

$$J(f) = \int_{\Re^3} \left(\frac{\partial^2 f}{\partial x^2}\right)^2 + \left(\frac{\partial^2 f}{\partial y^2}\right)^2 + \left(\frac{\partial^2 f}{\partial z^2}\right)^2 + 2\left(\frac{\partial^2 f}{\partial x \partial y}\right)^2 + 2\left(\frac{\partial^2 f}{\partial x \partial z}\right)^2 + 2\left(\frac{\partial^2 f}{\partial y \partial z}\right)^2 dxdydz. \qquad (6)$$

ausgedrückt werden [14], [15] – genauer gesagt – mit einer Halbnorm der 3. Dimensionen und 2. Ordnung. In Tab. 2 finden sich Formen dieser Gleichung für andere Dimensionen und Ordnungen.

Um die Funktion J in Gleichung (6) zu minimieren, muss eine geeignete Interpolationsfunktion f gewählt werden. f beschreibt im Falle der TPS die Abhängigkeit zwischen korrespondierenden Landmarken und kann für jede Dimension einzeln betrachtet werden:

$$f(p_i^t) = \begin{bmatrix} f_x(p_i^t) \\ f_y(p_i^t) \\ f_z(p_i^t) \end{bmatrix} = p_i^s i \in \{1,\ldots,n\}. \qquad (7)$$

n ist dabei die Anzahl der vorhandenen Landmarkenpaare. Die Interpolationsfunktion muss stetig definiert sein, und jede Landmarke des einen Bildes muss exakt auf die entsprechende Landmarke im anderen Bild abbilden.

Die gesuchte Funktion f, die diese Forderungen erfüllt und gleichzeitig das Energiefunktional J minimiert, ist die dreidimensionale Variante von Bookstein's Transformationsfunktion [6]

$$f_\bullet(x,y,z) = a_{0\bullet} + a_{1\bullet}x + a_{2\bullet}y + a_{3\bullet}z + \sum_{k=1}^{n} w_{\bullet k} U(\|P_k - P\|). \qquad (8)$$

P ist dabei der gerade betrachtete Punkt (x,y,z) und P_k sind die x, y und z Koordinaten einer Landmarke aus dem Zielvolumen. Der Punkt deutet an, dass es sich bei den entsprechenden Variablen um Vektoren der Form (x,y,z) handelt.

Der erste Teil der Funktion ist für die affine Transformation zuständig, der hintere Teil, in dem die radiale Basis Funktion $U(r)$ steht, sorgt zusätzlich für die elastische Transformation. Die bislang unbekannten Parameter a und w steuern dabei die Art und Weise, wie das Volumen verformt wird.

Weitere Untersuchungen der Gleichung (8) zeigen, dass einige Randbedingungen nötig sind, um zu verhindern, dass lokale Verformungen globale Auswirkungen haben:

$$\sum_{k=1}^{n} w_{k\bullet} = 0,\ \sum_{k=1}^{n} w_{k\bullet} x_k = 0,\ \sum_{k=1}^{n} w_{k\bullet} y_k = 0 \text{ and } \sum_{k=1}^{n} w_{k\bullet} z_k = 0 \ldots\ldots\ldots (9\text{–}12)$$

n steht wieder für die Anzahl der Landmarkenpaare und $w_{k\bullet}$ ist ein, aus einer x-, y- und z-Koordinate bestehender Parameter der elastischen Transformation. Diese Terme begrenzen die Translations- und Rotationsbewegungen des elastischen Teils der Funktion und stellen sicher, dass Terme, die weiter weg von den Landmarken und stärker als linear ansteigen nicht berücksichtigt werden.

Die Koeffizienten a und w können durch das Lösen des folgenden linearen Gleichungssystems bestimmt werden. Es setzt sich aus Gleichung (8) und den erwähnten Randbedingungen (9–12) zusammen:

$$\begin{aligned} Kw + Pa &= Y \\ P^T w &= 0 \end{aligned} \qquad (13)$$

Diese Gleichungen können auch als

$$L^{-1} Y = (W | a_{0\bullet} a_{1\bullet} a_{2\bullet} a_{3\bullet}) \qquad (14)$$

geschrieben werden. Y ist dabei eine Matrix, die alle Landmarken des Quellvolumens beinhaltet, also

$$Y = \begin{bmatrix} x_1^s & y_1^s & z_1^s \\ x_2^s & y_2^s & z_2^s \\ \vdots & \vdots & \vdots \\ x_n^s & y_n^s & z_n^s \end{bmatrix} \text{ und } L = \begin{bmatrix} K & P \\ P^T & 0 \end{bmatrix} \qquad (15,16)$$

K ist eine Matrix, in der die Werte der radialen Basisfunktionen für die Abstände zwischen einzelnen Landmarken im Zielvolumen stehen, also

$$K = \begin{bmatrix} 0 & U(r_{12}) & \ldots & U(r_{1n}) \\ U(r_{21}) & 0 & \ldots & U(r_{2n}) \\ \vdots & \vdots & \ddots & \vdots \\ U(r_{n1}) & U(r_{n2}) & \ldots & U(r_{nn}) \end{bmatrix}. \qquad (17)$$

Matrix P enthält alle Landmarken des Zielvolumens, also

$$P = \begin{bmatrix} 1 & x_1^t & y_2^t & z_1^t \\ 1 & x_2^t & y_2^t & z_2^t \\ \vdots & \vdots & \vdots & \vdots \\ 1 & x_n^t & y_n^t & z_n^t \end{bmatrix}. \tag{18}$$

Wie oben schon erwähnt, ist bei diesem Algorithmus problematisch, dass jede Landmarke des einen Bildes exakt auf die entsprechende Landmarke des anderen Bildes abgebildet wird. In der Praxis kommt es jedoch – z. B. aufgrund von verrauschten Bildern oder durch Fehler des Anwenders – zu Ungenauigkeiten beim Setzen der Landmarken.

Um den Einfluss der Fehler auf das Ergebnis zu minimieren, wird im Folgenden die TPS-Methode um eine Regularisierung erweitert. Dabei ist es nicht mehr zwingend notwendig, eine Landmarke exakt auf eine andere zu transformieren. Vielmehr ist hier ein gewisser Fehler erlaubt. Diese Toleranz ist in Gleichung (19) mit ε bezeichnet:

$$\sum_{i=1}^{n} \left\| f(p_i^t) - p_i^s \right\|^2 \leq \varepsilon. \tag{19}$$

Die einzige Änderung, die dafür insgesamt vorgenommen werden muss, betrifft Gleichung (13). Hier muss ein Regularisierungsterm λI addiert werden, so dass

$$\begin{aligned} (K + \lambda I)w + Pa &= Y \\ P^T w &= 0 \end{aligned} \tag{20}$$

I ist eine Einheitsmatrix mit entsprechender Größe, der eigentliche Regularisierungsfaktor wird mit λ bezeichnet. Er bestimmt das Verhältnis zwischen dem Approximationsverhalten und der Glätte der Funktion.

Für den Fall $\lambda{=}0$ sieht man, dass Gleichung (20) exakt der Gleichung (13) entspricht, d. h. die Transformation ist in diesem Fall nicht regularisiert.

Je größer λ ist, desto kleiner ist der Einfluss des elastischen Teils auf die gesamte Transformation. Für sehr große λ bleibt nur noch die affine Abbildung bestehen.

Gleichung (21) zeigt das komplette Gleichungssystem für die Bestimmung der Koeffizienten a und w, sie ist grundsätzlich äquivalent mit Gleichung (20), aber detaillierter aufgeschrieben:

$$\begin{pmatrix} x_1^s & y_1^s & z_1^s \\ \vdots & \vdots & \vdots \\ x_n^s & y_n^s & z_n^s \\ 0 & 0 & 0 \\ 0 & 0 & 0 \\ 0 & 0 & 0 \\ 0 & 0 & 0 \end{pmatrix} = \begin{pmatrix} \lambda & \cdots & U(r_{1n}) & 1 & x_1^t & y_1^t & z_1^t \\ \vdots & \ddots & \vdots & \vdots & \vdots & \vdots & \vdots \\ U(r_{n1}) & \cdots & \lambda & 1 & x_n^t & y_n^t & z_n^t \\ 1 & \cdots & 1 & 0 & 0 & 0 & 0 \\ x_1^t & \cdots & x_n^t & 0 & 0 & 0 & 0 \\ y_1^t & \cdots & y_n^t & 0 & 0 & 0 & 0 \\ z_1^t & \cdots & z_n^t & 0 & 0 & 0 & 0 \end{pmatrix} \begin{pmatrix} w_1^x & w_1^y & w_1^z \\ \vdots & \vdots & \vdots \\ w_n^x & w_n^y & w_n^z \\ a_0^x & a_0^y & a_0^z \\ a_1^x & a_1^y & a_1^z \\ a_2^x & a_2^y & a_2^z \\ a_3^x & a_3^y & a_3^z \end{pmatrix} \tag{21}$$

Gleichung (21) ist für den Fall $\lambda{=}0$ also ebenfalls äquivalent zu Gleichung (13).

2.3 Implementation

Für die in diesem Artikel vorgestellte Anwendung, wurden Gleichung (8) für den Transformationsprozess und Gleichung (21) für die Bestimmung der Transformationskoeffizienten implementiert. Das lineare Gleichungssystem der letzteren Formel wird mit Hilfe der Singulärwertzerlegung gelöst. Die CT-Aufnahme des Schädels ist das Zielvolumen, das MRT-Template wird als Quelldatensatz verwendet.

Als Interpolationsverfahren kommt eine trilineare Interpolation zum Einsatz, da sie wesentlich bessere Ergebnisse als eine einfache Nearest-Neighbour-Interpolation liefert und gleichzeitig schneller als andere Verfahren ist.

Die Anwendung ist in Matlab 6.5 programmiert und benötigt für einen typischen Datensatz mit 256^3 Voxeln und 30 Landmarken auf einem PC mit 2.2 GHz ungefähr 10 Minuten.

3 Ergebnisse

In diesem Abschnitt werden die ersten Ergebnisse der in Abschnitt 2 beschriebenen 3D Thin-Plate-Spline-Methode vorgestellt. Hierbei handelt es sich um ein Verfahren, mit dem das Gesicht eines unbekannten Toten mit Hilfe des Schädels rekonstruiert werden kann. Eine herkömmliche Rekonstruktionsarbeit – angefertigt und zur Verfügung gestellt von R. P. Helmer [16] – wird für Vergleichszwecke benutzt.

Abbildung 3 zeigt Vorbereitungen zur Digitalisierung der Rekonstruktion mit Hilfe eines Computertomographen. Der Plastilinkopf wird samt des darin enthaltenden Originalschädels in das Iso-Zentrum eines Philips Secura Spiral CT-Sanner auf eine Plastikunterlage gelegt (Abbildung 3 a und 3b).

Als Beispiel für eine Rekonstruktion dienen die, in Abbildung 4 gezeigten sagittalen Schnitte, der in Abbildung 3 b erkennbaren Rekonstruktion. Auf diesen Bildern lässt sich der Originalschädel sehr gut von der für Rekonstruktionszwecke aufgetragenen Masse unterscheiden. Die Metallstützen, die den Kopf im Inneren stabilisieren, stören bei der Bildakquisition nur unerheblich.

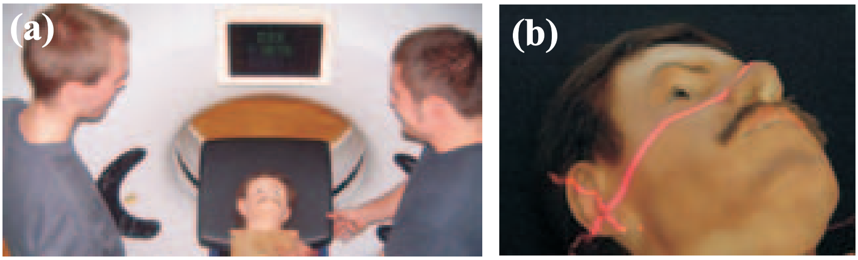

Abb. 3: a) Positionierung des herkömmlich rekonstruierten Kopfes in einem CT Scanner b) Genaue Ausrichtung des Kopfes im Iso-zentrum des Philips Spiral CT Scanners.

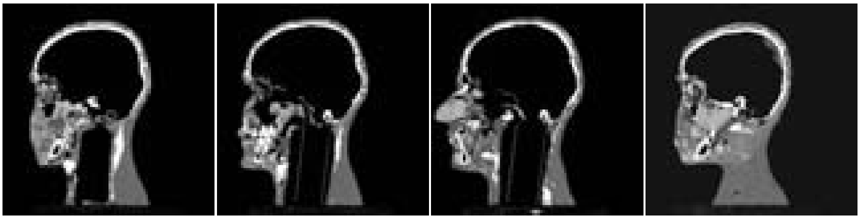

Abb. 4: Darstellung von 4 sagittalen Schnitten der von R. P. Helmer zu Verfügung gestellten Rekonstruktion [16].

Auf Basis der korrespondierenden Landmarken (siehe Abbildung 5 links) können die Parameter der Transformationsfunktion bestimmt werden. Danach wird durch die Thin-Plate-Splines, wie auf der rechten Seite in Abbildung 5 visualisiert, auf den gesamten Datensatz eine nichtlineare Deformation angewandt.

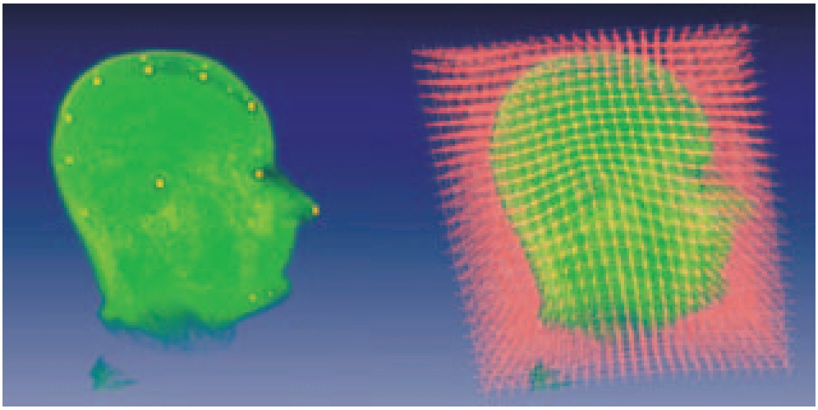

Abb. 5: Visualisierung der durch die Thin-Plate-Splines verursachten Raumkrümmung.

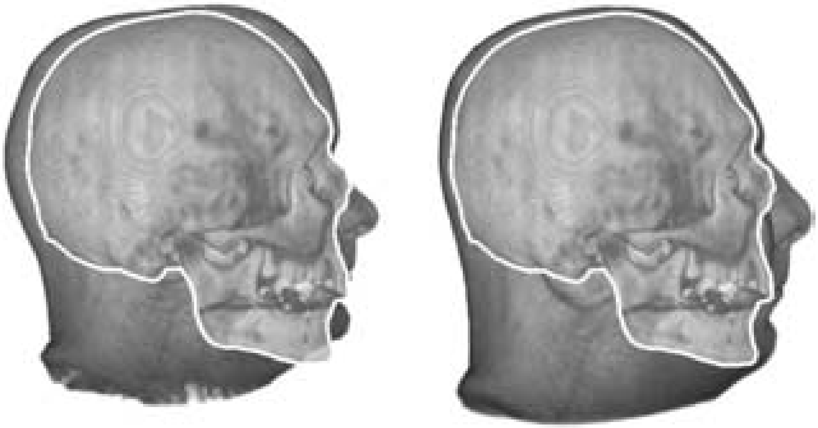

Abb. 6: Ein Schädelfund der über ein untransformiertes MRT Template (links) und das Resultat der Transformation (rechts) gelegt ist.

Verglichen mit der traditionellen, plastilinbasierten Rekonstruktionsmethode sind die Ergebnisse der TPS-basierten Methode ermutigend. Abbildung 6 zeigt eine Rekonstruktion bei der ein willkürlich gewähltes MRT-Template an den Schädel aus einem ungeklärten Mordfall angepasst wurde. Wie klar zu erkennen ist, passt das Template nach der Transformation deutlich besser auf den Schädel. Die Region um die Nase ist dabei ein gutes Beispiel für die Elastizität der regularisierten TPS. Neben der Nase ist die Stirn die mit am stärksten verformte Region. Zu erkennen ist außerdem, dass vor allem die Nase und der Unterkiefer aufgrund ihres recht unnatürlichen Aussehens einer weiteren Bearbeitung bedürfen.

Abb. 7: Die Arbeit von R. P. Helmer [16] überlagert mit dem Ausgangs-MRT-Template (links) und dem Ergebnis der Transformation (rechts).

Abbildung 7 zeigt einen Vergleich zwischen der herkömmlichen und der neuen, hier vorgestellten Methode. Das linke Bild zeigt im Vordergrund den von R. P. Helmer rekonstruierten Kopf, dahinter liegt ein Template in Form einer MRT-Aufnahme einer beliebigen Person. Auf der rechten Seite sieht man im Hintergrund das an den Schädelknochen der Helmer-Rekonstruktion angepasste MRT-Template. Wie schon im ersten Beispiel gezeigt, führt die TPS Methode zu einer akzeptablen Anpassung zwischen dem Template und dem Originaldatensatz.

Die Verschiebung im Nackenbereich lässt sich dadurch erklären, dass nur Landmarken genutzt werden, die direkt auf der Schädeloberfläche liegen. Durch ein paar zusätzliche Landmarken in diesem Bereich lässt sich der Fehler korrigieren.

Ein direkter Vergleich der beiden Verfahren ist in Abbildung 8 zu sehen. Wie beim ersten Beispiel auch, ist die Nase den stärksten Verformungen ausgesetzt. Dieser Vergleich zeigt deutlich, wie wichtig eine sorgfältige Auswahl des Templates ist. Da die beiden Personen offensichtlich ein unterschiedliches Gewicht aufweisen, ähneln sich die Ergebnisse nur bedingt. Abbildung 8 erlaubt keinen qualitativen Vergleich da beide Ergebnisse rein hypothetischer Natur sind.

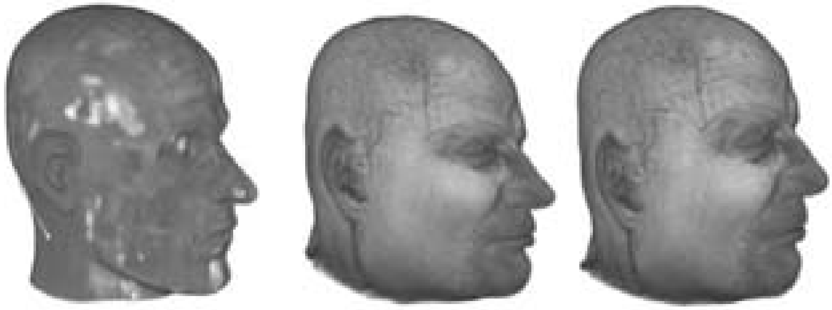

Abb. 8: Vergleich zwischen dem von R. P. Helmer rekonstruierten Kopf [16] (links), dem Ergebnis der TPS Rekonstruktion (Mitte) und dem unbearbeiteten Template (rechts).

Wie in Abbildung 6, 7 und 8 zu sehen ist, ist es nicht möglich, alle potentiell nötigen Transformationen durchzuführen, da die TPS Methode auf Topologie erhaltende Transformationen beschränkt ist. Detailarbeiten z. B. an der Nase und an den Ohren sind so nur beschränkt möglich.

Es ist geplant, eine umfassende Datenbank zu erstellen die MRT-Aufnahmen von Personen mit unterschiedlichsten körperlichen Merkmalen wie Geschlecht, Gewicht, Alter usw. beinhaltet, um eine genauere Auswahl des Templates zu ermöglichen.

4 Zusammenfassung und Ausblick

In diesem Artikel wurden die Ergebnisse einer Anwendung für die forensische Weichteilrekonstruktion vorgestellt. Das Verfahren basiert auf dem dreidimensionalen CT des gefundenen Schädels und einer MRT einer willkürlich gewählten Person als Weichteiltemplate. Im Vergleich zu der traditionellen plastilinbasierten Methode sind die Ergebnisse vielversprechend.

Die Qualität der rekonstruierten Gesichter hängt stark von der Wahl eines geeigneten MRT-Templates ab. Nicht alle für die perfekte Anpassung nötigen Transformationen sind möglich, speziell sind nur solche möglich, die die Topologie erhalten.

Um dies zu umgehen, ist neben diversen Nachbearbeitungsschritten eine Datenbank geplant, aus der ein geeignetes MRT-Template anhand der Personendaten wie Alter, Geschlecht und Größe entsprechend ausgewählt werden kann. Denkbar ist, diese Templates mit standardisierten Landmarken zu versehen, um jedes vorhandene Template schnell und einfach an einen Schädelfund anpassen zu können.

Ein Nachteil von MRT als Aufnahmemodalität ist die Haltung der Personen in der die Aufnahmen durchgeführt werden. Da die Person in einer liegenden Position im MRT-Gerät positioniert und der Kopf leicht fixiert wird, führt dies zu einem unnatürlichen Gesichtsausdruck. Deswegen ist geplant, in einem nächsten Schritt ein gepulstes Holographieverfahren [17] zur Vermessung des Gesichtes zu verwenden. Dabei kann die Person in einer sitzenden Position ohne jede Fixierung aufgenommen werden, was zu einem natürlicheren Gesichtsausdruck führt.

Um die Lokalisierung der Landmarken auf dem Schädel zu vereinfachen, wird grade an der Entwicklung eines neuen Verfahrens mit Mitteln aus der bildgeführten Chirurgie gearbeitet.

5 Danksagungen

Die Autoren bedanken sich bei Prof. Richard P. Helmer, Institute of Applied Forensic Medicine and Anthropology, Remagen, Germany, für die hilfreichen, kritischen Diskussionen sowie für die Hilfe bei der Platzierung der Landmarken und die Zurverfügungstellung der manuellen Gesichtsrekonstruktion. Weiterhin bedanken die Autoren sich bei Dr. Carsten Tille und Dr. Herman Seitz, Leiter der Rapid-Prototyping-Gruppe, Forschungszentrum ceasar Bonn für die Zurverfügungstellung des Fotos einer Rapid-Prototyping-Kopie. Die Autoren bedanken sich auch bei Dirk Thomsen für die Unterstützung bei der CT-Bildakquisition sowie bei Prof. Dr. Dr. Jürgen Ruhlmann, Medical Center Bonn, für den MR-Template-Datensatz.

6 Referenzen

[1] T. M. Buzug, P. Hering, and R. P. Helmer, „3D Tomography as a Basis for Anthropological and Forensic Facial Reconstruction“ in *Reconstruction of Soft-Facial Parts, Proceedings of the 1. International Conference RSFP*, 2003, pp. 91–108.

[2] K. Raic, T. Jansen, B. von Rymon-Lipinski, C. Tille, H. Seitz, and E. Keeve, „Fast generation of stereolithographic models“ in *Biomed Tech* (Berl). 2002;47 Suppl 1 Pt 1:83–5.

[3] C. Tille and H. Seitz, Private communication, caesar Rapid Prototyping group, Bonn, 2003.

[4] D. W. Bullock, „Computer Assisted 3D craniofacial reconstruction“, M. S. thesis, University of British Columbia, 1999.

[5] A. J. Tyrrell, M. P. Evison, A. T. Chamberlain, and M. A. Green, „Forensic Three-dimensional Facial Reconstruction: Historical Review and Contemporary Developments“, *Journal Forensic Science*. 1997 Jul;42(4) pp. 653–661.

[6] F. L. Bookstein, „Principal Warps: Thin Plate Splines and the Decomposition of Deformations“ *IEEE Transactions on Pattern Analysis and Machine Intelligence*. Volume 11, pp. 567–585, June 1989.

[7] R. P. Helmer, S. Rohricht, D. Petersen, and F. Mohr, „Assessment of the Reliability of Facial Reconstruction“ in *Forensic Analysis of the Skull*, Chapter 17, p. 229, Wiley-Liss, 1993.

[8] R. P. Helmer, T. M. Buzug, and P. Hering, „Plastic facial reconstruction on the skull – a transition in Germany from a conventional technique to a new one“ in *Reconstruction of Soft-Facial Parts, Proceedings of the 1. International Conference RSFP*; 2003, pp. 77–90.

[9] T. M. Buzug, J. Weese, C. Fassnacht, and C. Lorenz, „Elastic matching based on motion-vector fields obtained with a histogram-based similarity measure for DSA image correction“ in *International Conference on Computer Assisted Radiology* pp. 139–144.

[10] G. Quatrehomme et al, „A fully three-dimensional method for facial reconstruction based on deformable models“ in Journal Forensic Science., 42(4) pp. 649–652, 1997.

[11] J. Kybic, „Elastic Image Registration using Parametric Deformation Models“, Ph. D. dissertation, Ecole Polytechnique Fédérale de Lausanne, Lausanne, Switzerland. 2001.

[12] E. W. Weisstein, „Biharmonic Equation“ from MathWorld – A Wolfram Web Resource. http://mathworld.wolfram.com/BiharmonicEquation.html.

[13] E. W. Weisstein, „Thin Plate Spline“ from MathWorld – A Wolfram Web Resource. http://mathworld.wolfram.com/ThinPlateSpline.html.

[14] J. Duchon, „Interpolation des fonctions de deux variables suivant le principe de la flexion des plaques minces“ in *RAIRO Analyse Numérique* Volume 10, pp. 5–12, 1976.

[15] K. Rohr, H. S. Stiehl, R. Sprengel, T. M. Buzug, J. Weese, and M. H. Kuhn, „Landmark-based elastic registration using approximating thin-plate splines“ in *IEEE Transactions on Medical Imaging*, Volume 20, p. 526, 2001.

[16] R. P. Helmer, Private communication, 2004.

[17] P. Hering, T. M. Buzug, and R. P. Helmer, „Ultrafast Holographic 3D Facial Measurement for Forensic Applications“ in *Reconstruction of Soft-Facial Parts, Proceedings of the 1. International Conference RSFP*, 2003, pp. 109–117.

Facial image comparison using 3D techniques

Arnout Ruifrok[1], Alize Scheenstra[2], Jurrien Bijhold[a], Remco C. Veltkamp[b]

[1] Netherlands Forensic Institute, Laan van Ypenburg 6, 2497 GB Rijswijk, The Netherlands
[2] Institute of Information and Computing Sciences, Utrecht University, Padualaan 14, 3584 CH Utrecht, The Netherlands

Abstract

In forensic comparison of facial images, preferably reference images are used in which the head is positioned corresponding to the disputed facial image. 3D imaging techniques, together with 3D modeling software, offer the possibility of flexible and reproducible positioning of the head of a person corresponding to the face and camera position of the 2D facial images. We performed an analysis of 3D data from the facial area of 3D whole body scans to find the landmarks that are best suited for automated facial comparison. Eight facial landmarks were manually annotated, and recorded in the scanning process. We measured the absolute distances between these landmarks in the 3D models.

To find a measure of the discriminating value of the distance measurements, we calculated the probability that the measurements of two subjects are not significantly different. If the measurements of a subject are close to the mean (i. e. a 'common' face), there is a probability that the same measurements are found in one of two subjects of the present data. If the measurements of a subject are in the tail of this distribution (i. e. a rare face), the probability that the same measurements are found on another subject is one in twelve subjects. The data set was not geared towards facial recognition however, and used a relative low-resolution scanning system. Therefore, we are currently studying the discriminating value of distance measures in a data set scanned at much higher resolution.

Introduction

In forensic comparison of a facial image with the face of a suspect, preferably reference images are used in which the head is positioned corresponding to the disputed facial image. Techniques using three or more landmark points on the face have been proposed for matching the face and camera positions to the available photographs [1]. However, these methods can be cumbersome, and require the cooperation of the suspect.

3D imaging techniques, together with 3D modeling software, offer the possibility of flexible and reproducible positioning of the head of a person corresponding to the face and camera position of the 2D facial images. Lately, 3D facial models can be more easily acquired since acquisition techniques have been improved. Therefore, some face recognition methods have been extended for 3-dimensional purposes. Using 3D models one can deal with one main problem in 2D face recognition; the pose of the head. Also the surface curvature of the head can now be used to describe a face.

However, a recent study [2] has shown that although useful for positioning, matching of a 3D model with a 2D image cannot be reliably used for identification based on match-point distance statistics. One of the remaining issues in matching

2D images with 3D models is the correct positioning of reference points by the investigators. To study the possibilities of automating the positioning of landmarks, we performed an analysis to find the landmarks that are best suited for automated facial comparison.

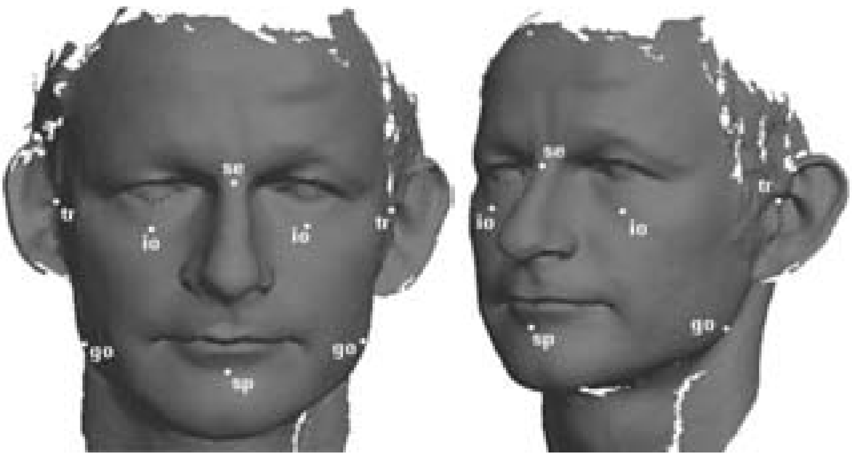

Fig. 1: The positions of the facial landmarks of the CAESAR-survey. These landmarks are manually located.

Materials and Methods

For this study we used the whole body scans of the Dutch and Italian parts of the CAESAR (Civilian American and European Surface Anthropometry Resource) survey [3]. The main goal of the CAESAR-survey was to acquire 3D whole body scans of 5.000 subjects. It took place from December 1997 until December 2001 in America, Italy and the Netherlands. The current study used the 3D body scans of 1127 subjects made in the Netherlands, and 793 scans made in Italy. In the Netherlands a Vitronic 3D body scanner was used to generate the 3D data [4]. In Italy the 3D whole body scans were acquired using a Cyberware 3D body scanner [5]. Of a subset of 20 people in the Netherlands, 18 repeat scans (9 with the Vitronic scanner and 9 with the Cyberware scanner) were made to determine intra-subject variability.

For the data analysis and the 3D face recognition problem we extracted the facial region from each whole body scan using bounding boxes as described in [6]. In this facial region 8 landmarks were defined by the CAESAR-survey:

- *Sellion* (**Se**). Point of greatest indentation of the nasal root depression.
- *Right Infraorbitale* (**r Io**). Lowest point on the inferior margin of the right orbit, marked directly inferior to the pupil.

- *Left Infraorbitale* (**l Io**). Lowest point on the inferior margin of the left orbit, marked directly inferior to the pupil.
- *Supramenton* (**Sp**). Point of greatest indentation of the mandibular symphysus, marked in the midsagittal plane.
- *Right Tragion* (**r Tr**). Notch just above the right tragus (the small cartilaginous flap in front of the ear hole).
- *Left Tragion* (**l Tr**). Notch just above the left tragus (idem).
- *Right Gonion* (**r Go**). Inferior posterior right tip of the gonial angle (the posterior point of the angle of the mandible, or jawbone).
- *Left Gonion* (**l Go**). Inferior posterior left tip of the gonial angle (idem).

The gonion is difficult to find when covered with a lot of tissue.

To indicate the landmarks on the head during scanning, white stickers were used with a diameter of 1 cm. Picking the landmarks in the data set was performed semi-automatically. A program identified the locations of the landmarks based on the white color of the stickers. These locations were presented to the observer to annotate the accurate location in the landmark file. The locations of the landmarks are shown in figure 1.

Results

We determined the absolute distances between the above landmarks in the 3D models. Two datasets were analyzed separately: one dataset with 18 repeat scans from 20 people, and a dataset from scans from 1920 people. From the data set with repeat scans the mean standard-deviation of the measurements per subject was determined (intra-subject variation), as well as the (overall) standard deviation (inter-subject variation), see Tab. 1. As can be seen, the 20 subjects sample is reasonably representative for the larger sample. Also can be seen that the intra-subject variation in this data set is about half the inter-subject variation.

Tab. 1: Mean distance between landmarks, mean standard-deviation of the distance per subject (intra-subject variation) and (overall) standard deviation (inter-subject variation) of landmark distances for the full test-set (N=1920) and a subset (N=20) for which repeated measurements were made.

	Mean standard-deviation per subject	Mean (N=20)	SD (N=20)	Mean (N=1920)	SD (N=1920)
Se_Sp	2.6	97.1	5.8	96.4	7.4
Se_lTr	3.4	117.7	3.8	118.8	7.2
Se_rTr	3.0	124.1	4.8	121.7	7.3
Se_lInfr	2.2	44.7	1.9	45.7	4.9
Se_rInfr	2.1	47.1	2.9	46.2	4.6

	Mean standard-deviation per subject	Mean (N=20)	SD (N=20)	Mean (N=1920)	SD (N=1920)
Se_lGo	3.2	135.7	7.0	131.6	9.9
Se_rGo	3.0	141.0	7.2	135.6	9.8
rInfr_lInfr	3.2	66.4	3.1	66.8	5.5
rInfr_rTr	3.0	92.6	4.5	90.0	5.9
rInfr_Sp	2.6	76.8	4.5	77.2	6.4
rInfr_rGo	3.2	103.3	7.3	96.9	8.0
lInfr_lTr	3.6	86.8	3.6	85.5	5.9
lInfr_lGo	3.8	98.3	6.6	91.3	8.3
lInfr_Sp	2.6	77.9	4.5	77.9	6.3
Sp_lTr	3.2	135.9	5.1	136.6	8.4
Sp_rTr	3.2	140.4	6.0	137.8	9.0
Sp_lGo	3.7	105.3	6.4	98.4	8.4
Sp_rGo	3.6	107.8	7.1	100.8	8.8
rTr_rGo	2.7	68.4	5.6	67.9	9.2
lTr_rTr	2.2	144.7	4.4	148.0	8.4
lTr_lGo	3.1	63.5	5.4	66.6	9.4
rGo_lGo	4.0	111.5	9.5	118.2	11.0

To find a measure of the discriminating value of the distance measurements of the CEASAR data, we calculated the probability that the measurements of two subjects are not significantly different. We assumed that the measurements for all subjects are normal distributed. A problem with the distance data is the high correlation between different distance measures.

Tab. 2: The results of the stepwise discriminant analysis for the landmark set without the gonion.

order	distance	Estimated LR 'mean'	Estimated LR '5%'	variance explained
1	Se – Sp	2.8	19.4	1.000
2	l Tr – r Tr	3.8	26.1	0.994
3	Sp – r Tr	2.8	19.2	0.837
4	Se – r Tr	2.4	16.6	0.695
5	r Io – r Tr	2.0	13.4	0.615
6	Se – r Io	2.2	15.0	0.573
7	Sp – l Tr	2.6	17.9	0.402

order	distance	Estimated LR 'mean'	Estimated LR '5%'	variance explained
8	r Io – Sp	2.5	16.8	0.346
9	Se – l Io	2.2	15.2	0.329
10	r Io – l Io	1.7	11.7	0.205
11	l Io – Sp	2.4	16.5	0.092
12	Se – l Tr	2.1	14.5	0.090
13	l Io – l Tr	1.6	11.2	0.086

For individualization of subjects based on the facial distances, the most identifying distances should be used. To study this problem we used stepwise linear discriminant analysis (LDA). For this analysis we used the same dataset as for the analysis above. The results of the analysis are displayed in figure 2(a) for the landmark set with the gonion and in figure 2(b) for the landmark set without the gonion. In the second set the gonion was excluded, because this landmark is hard to determine accurately based on the facial scans only, and this is the material available for most 3D facial comparison cases. The order of the selection of landmarks for the landmark set without gonion, the estimated LR of each distance, and the fraction of explained variance by each distance are shown in Tab. 2. Using these data, an estimate of the LR of finding the same measurements as those of an 'average' (circles) face can be made, depending on the measurement error (Fig. 3, dashed line).

Another way of estimating the LR of the set of distances was presented by Helmer [7]. He presented a study of the discriminating value of a set of measurements on human skulls. He defined a probability *p(s)* that another skull can be found with the same measurements. In this analysis the complete covariance matrix of the dataset was included. With the probability of finding measurements of a skull at hand being one, *1/p(s)* is equivalent to the Likelihood Ratio (LR), a number indicating the evidential value of an observation. Also with Helmer's formula, it is possible to make estimates of the LR of facial measurement sets. Fig. 3 shows the LR values of the dataset depending on the measurement error (closed symbols).

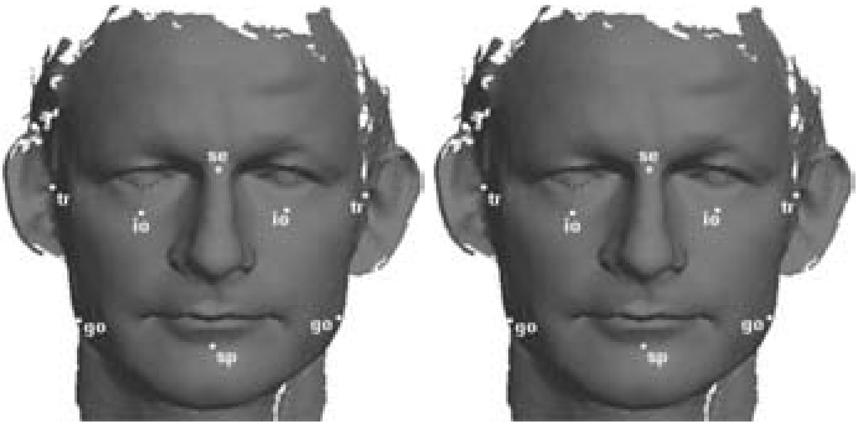

Fig. 2: The landmark sets resulting from the stepwise linear discriminant analysis when started with the complete candidate set (a) and with the candidate set without the distances from and to the gonion (b).

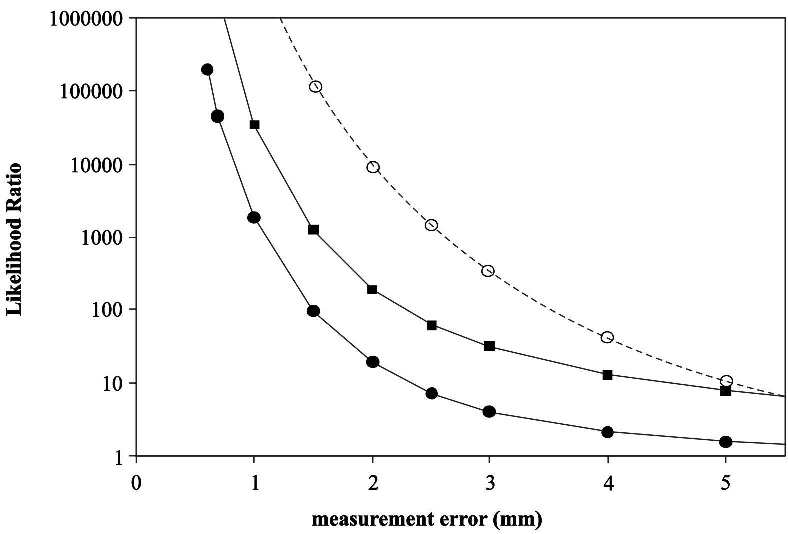

Fig. 3: Estimates of Likelihood ratio of finding the same measurements in an average' (○, ●) or 'rare' (■) face and in a random person of the rest of the sample, as a function of the measurement error, using stepwise LDA (open symbols) or Helmer's formula [6] (closed symbols).

Conclusions

To find a measure of the discriminating value of distances between landmarks on the face, we calculated the probability that the measurements of two subjects in the CEASAR data set are not significantly different. We focused on the dataset without the gonion, because this landmark is hard to detect in facial images. Two models were used to estimate the likelihood ratio of de distance measures:

LDA, and Helmer's formula. The LDA model resulted in more optimistic LR numbers than Helmer's formula by a factor of 10–1000 for measurement result on an 'average' face. However, the message of both models is the same: in the range of measurement errors to be expected in facial comparison image material, i. e. in the range of 1–5mm, the LR is highly dependent on the measurement error.

The CAESAR data set was not geared towards facial recognition however, and used a relative low-resolution scanning system. Therefore, we are currently studying the discriminating value of distance measures in a data set scanned at much higher resolution.

Acknowledgement

This work is partially supported by the AIM@SHAPE Network of Excellence grant 506766 by the European Commission. We thank Hein Daanen of TNO Human Factors in Soesterberg, the Netherlands for the use of their scanned body models.

References

[1] H. van den Heuvel, The positioning of persons or skulls for photo comparison using three point analysis and one-shot-3D photographs. Proceedings of SPIE, Kathleen Higgins, 3576, 203–215, SPIE, Bellingham, 1998.

[2] Goos, M. I. M., Alberink, I. B., Ruifrok, A. C. C. 2D/3D facial comparison using photogrammetry. *Submitted to Forensic Science International.*

[3] CAESAR-survey. The civilian american and european surface anthropometry resource. http://store.sae.org/caesar, oktober 2004.

[4] The Vitus 3D Body Scanner. The Vitronic homepage. http://www.vitronic.com, july 2004.

[5] Whole Body Color 3D Scanner. The yberware homepage. http://www.cyberware.com/products/wbInfo.html, july 2004.

[6] C. A. M. Suikerbuik, J. W. H. Tangelder, H. A. M. Daanen, and A. J. K. Oudenhuijzen. Automatic feature detection in 3D human body scans. In Proceedings of the Digital Human Modelling Conference, 2004.

[7] R. P. Helmer, J. N. Schimmler, and J. Riegler. On the conclusiveness of skull information via the video superimposition technique. Canadian Society of Forensic Science Journal, 22(2):177–197, 1989.

Creating a Three-Dimensional Skull Model from Two-Dimensional Images: Problems and Practicalities in Computerised Facial Reconstruction

Stephanie L. Davy, Damian Schofield, Martin P. Evison

The Research Centre for Human Identification, University of Sheffield, Sheffield United Kingdom. email s.davy@shef.ac.uk

Abstract

Computer graphics technology is constantly evolving; new methods are being developed to assist in the reconstruction of the face of an unidentified person. In the past, an actual skull or cast was needed in order to reconstruct a face using traditional plasticine methods. Most computerised current techniques utilise accurate three-dimensional (3D) models of a skull; however these are often created using expensive laser scanning equipment.

The authors have developed a number of new facial reconstruction techniques, including methods for recreating a computer model of a 3D skull from two-dimensional (2D) photographs. This technique allows the raw skull shape data and measurement information to be transferred electronically, negating the need for highly sensitive or fragile material (such as the skull itself) to be transported; reconstructions can even be performed in another country. The technique has also been applied to create facial reconstructions of recent murder victims and wrapped mummies, based on either skull photographs or radiographs.

This paper does not aim to describe the techniques developed in detail, but to discuss the general practicalities of creating a 3D skull model using only 2D images and explain some of the problems that have been faced. The authors will also briefly give some general guidelines for measuring and photographing a skull which is to be used in a computerised facial reconstruction.

Introduction

Facial reconstruction has been used as a technique to recreate the faces of unknown persons from skulls for decades. Used for both forensic and archaeological skulls, it has traditionally been carried out using either 2D drawing techniques or 3D clay/plasticine sculpturing techniques. Unfortunately, clay reconstructions require the practitioner to have the actual skull or a cast of it in his/her possession. The shipping of human remains, or even plaster casts, can be very difficult due to legal issues and the fragility of the materials. Therefore, practitioners are often chosen simply on the grounds of geographical proximity, or a facial reconstruction may not be considered as an option at all.

For a number of years, the authors have been using modern computer graphics technology to devise novel methods of performing computerised 3D facial reconstructions [1]–[4]. In addition to advantages including speed, reproducibility, and the ability to make rapid alterations, the authors have been able to eliminate the need for possessing the physical skull. In the past, it was only possible to perform a computerised facial reconstruction if one had access to expensive 3D scanning or medical imaging equipment.

Various technologies exist that can be used to capture raw data from a skull for the purpose of a facial reconstruction. These include 3D digital scanners (e. g. laser photogrammetric or structured light based scanners), medical imaging (e. g. Magnetic Resonance Imaging (MRI), Computerised Tomography (CT), radiographs, and photographs). This paper will concentrate mainly on skull reconstruction using photographic methods and by extension, radiographs; however to give a holistic version of the techniques it is necessary to understand the alternative measurement methods available.

Digital 3D scanners are the most accurate and straightforward method of capturing a skull for use in a computerised reconstruction because the entire surface of the skull is scanned and digitised and the image can be exported directly to desktop 3D modelling software for viewing. The authors are currently in involved in a major research project run by the Federal Bureau of Investigation (FBI) in the United States [5] to assess the accuracy of range of different types of 3D digital scanners. However, such scanners can be very expensive and may not be accessible to members of the law enforcement community or museum staff. Similarly, medical imaging is also costly but has the added benefit of enabling the acquisition of a skull image while leaving soft tissues intact. This is useful in cases of mummies or other circumstances where non-invasive measurement techniques are required [6], [7].

The main focus of this paper will be to delineate guidelines for the capture of 2D images to be used in the production of an accurate 3D skull in virtual space. The quality and accuracy of the 3D skull (and therefore of any resulting reconstructions) is reliant upon the data provided by the 2D images and any supporting information. These guidelines have been developed as a direct result of requests for facial reconstructions that have been submitted to the authors. It became apparent that there seemed to be no standard for photographing skulls, as many that were sent to us did not provide adequate information from which we could produce an accurate 3D skull model. Problem factors included improper scaling, lighting, lens distortion, and position/rotation of the specimen (Fig. 1). We will address these issues using a case study to explore the means for achieving the best possible result.

Using 2D Images

The use of photographs (and other 2D images) to loft skulls has several benefits. Firstly, the agency requesting the reconstruction does not need to have access to any specialised equipment such as digital 3D scanners or medical imaging equipment. A standard digital or 35mm camera, along with a few inexpensive lab items and access to email is sufficient. By photographing the skull, there is no need to undergo the expense and inconvenience of casting the skull and physical shipping, nor is there the risk of damage to the original specimen that is inherent in such transport.

The skull must simply be photographed correctly and the resulting 2D digital (or scanned print) files emailed. Images can be sent from the lab or field to anywhere in the world within minutes, (so long a decent connection is provided) as electronic transmission of photographic data can be very rapid. This adds to the potential for facial reconstruction to become more widely used in situations requiring urgency such as mass disasters, mass graves, and crime situations where expensive and specialised equipment is not often available. In such cases, the individual could also be immediately repatriated if the situation required such steps to be taken. Likewise, radiographs can be used in place of photographs. Most mortuary facilities have access to the appropriate equipment, and these images can be used in cases where any remaining soft tissue must be preserved. Digital x-ray equipment is becoming more prevalent, which eliminates any need for scanning the films before transmitting them to the reconstruction practitioner.

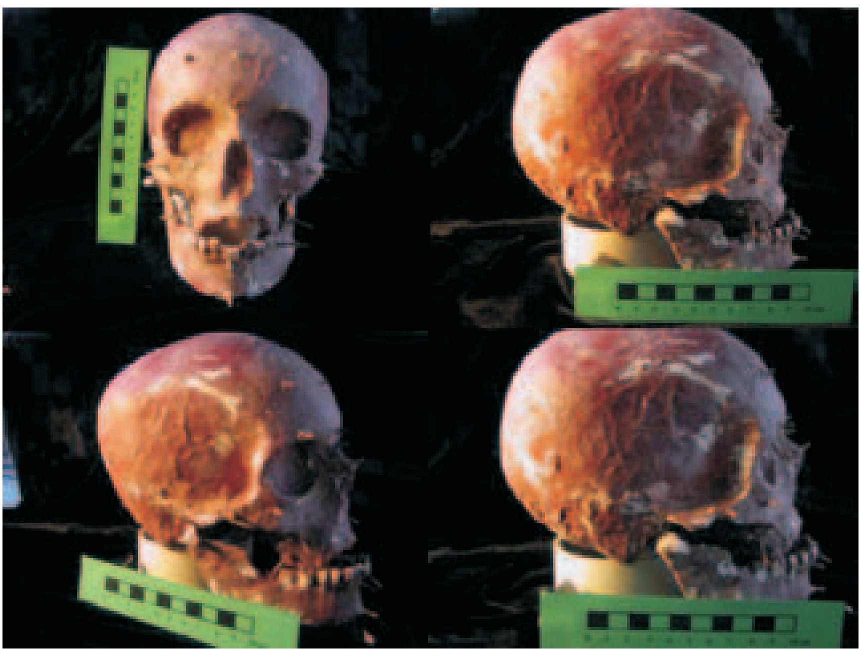

Fig. 1: Examples of factors preventing construction of an accurate 3D model. Clockwise from top left: Improper placement of scale; poor lighting and scale obstructing object; distance from camera; rotation/position of object.

There are, however, disadvantages to the use of 2D images for the reconstruction of a skull. The photographs must be taken following certain guidelines so that the most accurate 3D surface possible can be generated. However, even following these, some detail may still end up being sacrificed using this technique, when compared with other measurement methods. The error ranges encountered will be discussed later in the paper.

Case Study

For this paper, the authors formulated a case study to determine if by following simple guidelines, photographs from a physical skull could be used to create a 3D virtual skull model of sufficient accuracy for use in a facial reconstruction. The techniques developed by the authors to create the 3D skull use a virtual skull model taken from a 3D scanner as a base. This model then undergoes a complex polygonal editing process to match it to scaled images from a target skull in multiple orientations, a process which will be described and expanded upon fully in papers currently being written by the authors. The resulting skull model is then measured against the actual target skull to determine the accuracy of the process.

Materials

For this study, the authors endeavoured to use only equipment that would be accessible to the types of professionals that are likely to possess human remains that require a facial reconstruction. These are usually police, archaeologists, and forensic anthropologists, all of whom are generally subject to limited budgets and resources.

For the photography portion of the study, we used a standard commercially available digital camera (Nikon CoolPix 5700, 5.0 megapixels) to photograph the skull, which was mounted on a tripod for consistency and stability. Blu-tack® adhesive was used to secure the mandible to the cranium, as well as to secure the backdrop. Tape measures and rulers were used to measure distances from the camera, and a cardboard scale indicator was used in the photos. White and Folkens [8] suggest using black velvet for the background in such photographs, hence this was selected as the backdrop in our photographs. Assorted (easily available) materials were used to prop up the skull and to orient it in the Frankfurt Horizontal Plane (FHP). The FHP is an anatomical convention for orienting the skull in which a plane comprised of the left and right porions and the left orbitale is created; the skull is viewed parallel or perpendicular to this plane. With the purpose of keeping a limited budget in mind, we used black velvet skirts purchased from a charity shop for the backdrop and various items such as a roll of masking tape, Lego® building blocks, and cardboard boxes and foam core to create the background and orient the skull. For the lighting, we used an adjustable fluorescent desk lamp and created a reflection panel by covering a piece of cardboard in foil.

Methods

When using 3D modelling software to loft (or extrude) objects from reference images, the scaled photos are projected onto 2D planes which are then oriented to match various key views; the skull model then undergoes a complex set of 3D transformations to be deformed to correlate to the reference images in each view. The greatest accuracy Can be achieved by having reference images (in this case, photographs of the skull) taken at 90˚ perpendicular angles from norma frontalis, norma lateralis left and right, and norma occipitalis. Basic engineering theory tells us that any object can be reconstructed from a 2D images, ideally a plan view and front and side elevations. In order to reduce the error in this process, variables associated with the images such as distance, zoom, rotation and lighting must be eliminated, or at least recorded. By controlling the aforementioned variables and following the methods proposed by the authors, a surface can be derived that is accurate enough to be used in a computerised facial reconstruction.

A plaster cast of a skull was used for the purposes of this case study. We chose a room with indirect natural daylight and turned off all artificial lighting. A small tabletop staging area was created that consisted of a platform for the skull, background, and lighting. Science photography conventions dictate that the light should originate from the upper-left corner relative to the viewer [8], so the lab table was set-up accordingly; the window and the desk lamp were placed to the left of the staging area. Black velvet fabric was draped over a cardboard box to form the rear portion of the background. For the base of the staging area, a square piece of foam core board was covered with another piece of black velvet. The cardboard with foil was placed to the right of the staging to reflect the light from the lamp (Fig. 2).

Fig. 2: The staging area

Once the staging area was completed, the skull cast (Skull A) was propped into the FHP by setting it on the roll of masking tape and securing the skull with Blu-Tack. The skull was placed on the velvet in the approximate centre of the foam core board. The square base provided by the foam core board served as an easy visual reference to ensure that the appropriate angle was photographed. The edge of the board could be aligned parallel to the edge of the lab table (exact alignment can be verified with a spirit level), and then rotated 90˚ for the subsequent shots without moving the skull. In this way, we could keep the rotation between views and the position of the skull constant. Further work is currently being undertaken by the authors to analyze the amount of angular error in the placement of the skull on the foam core.

Skull A was photographed from the anterior, both lateral views, and the posterior. For each orientation the distance between the skull and the camera needed to be kept at a constant, as did the position of the camera. The camera was mounted on a tripod in a position that was in the same plane as the Frankfurt Horizontal relative to the focal plane of the camera. There is no accurate way to absolutely correlate to the FHP; estimating this visually was sufficient for our purposes. Work is currently underway by the authors within the previously mentioned FBI project to assess the extent of this error. The distance between the edge of the foam core platform and the table was measured as a guideline. The distance measurement used to ensure consistency, however, was that between the camera's focal plane and point on the skull nearest to the camera. In the case of the frontal photo, the end of the nasals was used as the primary measuring point. The nearest point to the camera on each side was on the temporal bones. In each orientation, a scale ruler was also included. The ruler was placed parallel to the point on the skull nearest the camera, and not obstructing any portion of the skull. One photo of Skull A from each view was selected to be used as a reference image from which the 3D surface would be generated (Fig. 3).

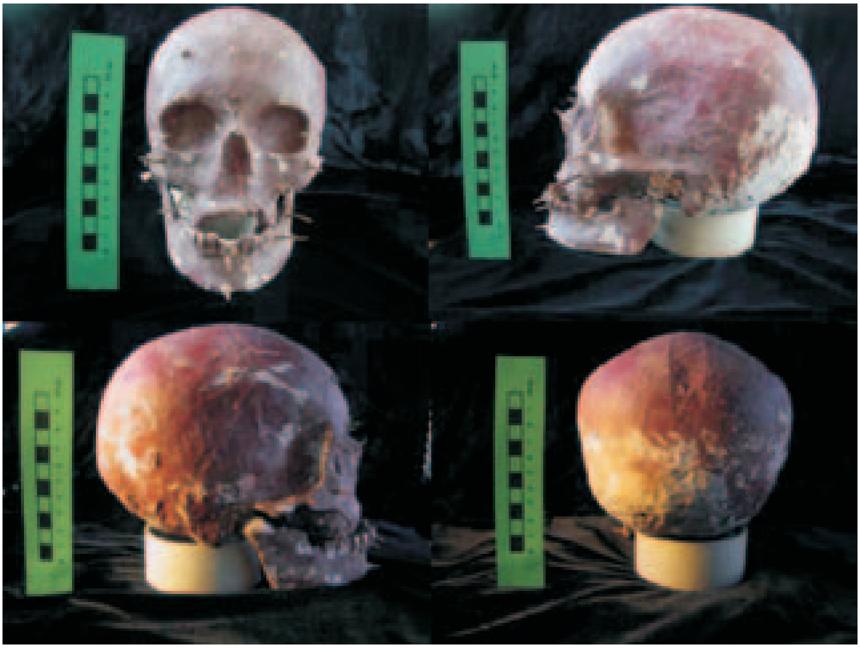

Fig. 3: The skull from the anterior, left lateral, right lateral and posterior (clockwise from top left).

A 3D model of another skull (Skull B) was used as a base model for the reconstruction process. Skull B belonged to an individual of similar ancestry and age, and was scanned using a Cyberware model 3030 Head & Face Color 3D Scanner. The 3D Skull B model was deformed, following the methods defined by the authors, to match the reference photos of Skull A in each view. To create the 3D model, 3ds Max® software by Discreet was used. The image size of each of the four photographs was 16.26 × 21.67 cm. Four 2D planes were created within the 3ds Max® software. These planes matched the dimensions of the photographs. The reference images of the target skull were projected onto the planes; these were then arranged into a box and Skull B imported into the software. Another plane was created to represent the FHP through Skull B so that it could be rotated to match the FHP in the reference images (Fig. 4).

Fig. 4: Skull B with reference planes in 3 orientations (FHP shown in pink).

Although the four images were all taken under controlled conditions, ensuring that controls for distance, position and rotation and were analogous in each image, it becomes immediately apparent that the resulting images within the modelling software are not in a 1:1 ratio with the real-life skull. A scaling factor must be calculated for each image to achieve a true 1:1 ratio. By using the scale ruler positioned in each photograph, the scaling factor can be determined for each image.

Using Adobe Photoshop® desktop image editing software, the resolution of each photo was first set to 300 pixels per inch which allowed exact dimensions to be correlated with pixels measurements within any photographs.

The actual ruler was 10cm long. To determine the scaling factor, the actual height of the ruler (10cm) was divided by the height of the ruler in each image. The resulting value was the factor by which the image must be magnified to achieve a 1:1 ratio between the actual skull size and the image plane within the 3D modelling software.

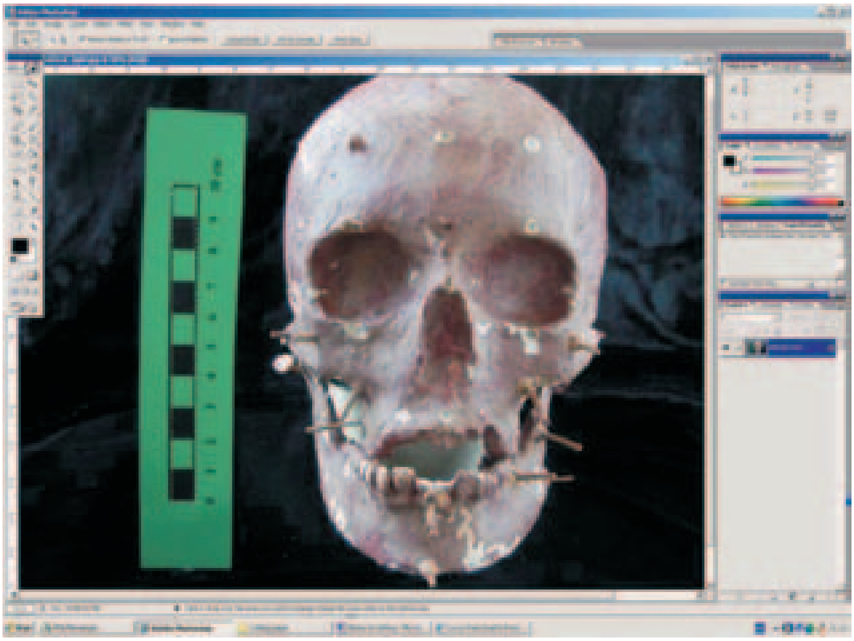

Fig. 5: Cropping the ruler from the reference image to determine scaling factor (image shown at 25% original size), and ruler cropped from image (shown 50% of original image size).

Using the rectangular selection tool and zooming in to each image (usually to approximately 300%), the ruler was outlined and saved as a new image. This action was performed three times for each photo (Fig. 5). For continuity purposes, the ruler edge was determined to be the outer edge of the black outline, beginning at the upper left corner and ending at the lower right. To reduce possible error when cropping the ruler, the action was performed three times for each view, and an average was taken. When photographing the objects, although due care was taken to place the ruler in a 90 degree plane to the camera, slight variations in rotation did occur, introducing some error into the scaling process. The errors carried forward from these measurements will be discussed in the next section.

Tab. 1: Scaling factors

$\frac{\text{Actualmeasurement}}{\text{Image}}$ scaling factor

Photo	Trial 1	Trial 2	Trial 3	Average	Scaling factor
Front view	8.91	8.9	8.91	8.91	1.122
Left view	7.59	7.59	7.59	7.59	1.318
Right view	8.48	8.48	8.47	8.48	1.179
Rear view	8.11	8.11	8.11	8.11	1.233

In the modelling software, each of the planes was scaled using the factors determined above (Tab. 1). However, since the scaling factor for each view was different, common points had to be found between views so that the planes could be aligned. The end of the nasals, and vertex were chosen as points that could be viewed from the front, left and right. Lines intersecting each of these points were drawn perpendicular to each plane. The vertex visible in the rear plane was aligned to the line projecting from the vertex in the front view. The vertex and end of nasals in the 3D model corresponds to the intersection of the lines projecting from the relative point in the reference planes.

Results

Fig. 6: The skull model after scaling and smoothing.

Comparative measurements (Table 2) were taken of both the original skull cast and the lofted skull using standard craniometric landmarks [8]. These landmarks were chosen based on their visibility both on the skull cast and on the lofted skull. Measurements of the skull cast were taken using digital sliding and spreading callipers. Previous work undertaken by the authors has shown that the errors in such measurements is very small, a matter of a few millimetres. The measurements were repeated on the lofted skull using the inbuilt measuring tools within the modelling software.

Tab. 2: Cranial Measurements taken (in mm) from the skull cast and the loftes skull

Cranial Measurements	Skull Cast	Lofted Skull	Difference	Percentage of Error
Maximum Cranial Length	173.64	158.16	15.48	8.91%
Maximum Cranial Breadth	144.3	133.08	11.22	7.76%
Biauricular Breadth	109.35	95.8	13.55	12.39%
Upper Facial Height	60.33	61.84	-1.51	2.50%
Minimum Frontal Breadth	90.73	89.14	1.59	1.75%
Upper Facial Breadth	95.58	95.98	-0.4	.004%
Nasal Height	46.85	51.92	-5.07	10.82%
Nasal Breadth	16.17	17.54	-1.37	8.47%
Orbital Breadth	31.83	28.18	3.65	11.47%
Orbital Height	29.5	31.98	-2.48	8.41%
Biorbital Breadth	84	86.27	-2.27	2.7%
luterorbital Breadth	23.33	25.38	-2.05	8.79%

A range of errors could potentially affect the quality of the lofted skull. Since a plaster cast was used for the purposes of this study, lighting could have a varying effect on image quality when photographing real human bones. Other factors that could have contributed to errors included the use of symmetrical scaling factors in the image reference planes, using a scaling factor which was deduced from a vertical measurement.

The mean error between the original specimen and the lofted skull was 5.1 mm. When comparing the two skulls, errors were generally less than 10%; this was deemed acceptable by the authors. The furthest outlier was the biauricular breadth, which has little effect on the appearance of a facial reconstruction. Due to the broken rami on the skull cast, no mandibular measurements were taken, which could also affect the results. The authors are currently conducting more experiments to further reduce these types of errors and to generate higher definition 3D models.

Guidelines

To obtain the most accurate 3D model possible, the following guidelines must be adhered to when measuring and photographing a skull:

Measurement:

Use standard craniometric measurements and appropriate callipers to measure the skull, and be sure to note which resource was used (i. e. after White [8], Buikstra and Ubelaker [9], or Bass [10]). When recording skull measurements, repeat each one several times and include measurements from more than one qualified observer when possible. Including a list of definitions of the points measured may also be helpful.

Lighting and setup:

It is important to remove as many variables as possible during the photography process. Important factors to consider are those of lighting, position and rotation of the skull, distance from the camera, and scale of the images. The room should be well-lighted, preferably with access to natural daylight as well as artificial lighting. Create a reflection panel to soften shadows (see methods section, above, for details). Disable the camera's flash to avoid overexposure of the image. Black velvet should be used both as a background and beneath the skull so that the only objects showing in the camera view are the skull and ruler. Position the skull in the FHP and align the focal plane of the camera to it.

Photography procedures:

Photograph the skull from norma lateralis, norma frontalis, and norma occipitalis. When photographing the skull, multiple shots of the object in each orientation should be taken with a tripod-mounted camera. Maintain a constant, recorded distance between the camera and the most anterior point on the skull in each orientation. It is important to maintain a constant lens focal distance and zoom in each photograph to remove variables in distance and lens distortion. The skull should be rotated exactly 90˚ between each orientation. To evaluate the rotation, use a rectangular base to rotate the skull; the edges of the base can be aligned to the table edge.

Including a scale:

Include a ruler for scale. Coins, paperclips, or other found objects are not satisfactory. In order to serve as a useful indicator of scale, the ruler must be placed in the same plane as the point on the skull that is nearest the camera. If the ruler is improperly placed, its function is negated. Where possible, include a scale in both the vertical and horizontal axes of the photograph. Also, caution must be taken to ensure that the skull is not obstructed by the ruler.

Further advice:

To highlight unusual features or to include more detail, additional photographs from non-standard angles or using flash and zoom can be included as supplements to the aforementioned photos. The most important tips to remember are to 1) eliminate as many variables as possible, and 2) to make a detailed record of your procedures.

Conclusions

The authors believe that the methods discussed here can be employed to create a 3D skull model from photographs for a facial reconstruction. Although the lofted skull image from our case study was potentially not as detailed as one captured from a 3D scanner or by making a plaster cast, lofting from photographs may be a viable option in cases where scanning and/or casting facilities are not available.

Acknowledgements

Special thanks to Andrew Chamberlain and the University of Sheffield Department of Archaeology for the use of lab space, advice, and various supplies used for the photography portion of this paper.

References:

[1] S. L. Davy, T. Gilbert, D. Schofield, M. P. Evison, "Forensic Facial Reconstruction using Computer Modeling Software," in *Computer-Graphic Facial Reconstruction*. Academic Press, IN PRESS.

[2] M. P. Evison, S. L. Davy, J. March, D. Schofield, "Computational Forensic Facial Reconstruction". In Proceedings of *International Conference of Reconstruction of Soft Facial Parts*, November 2003.

[3] M. P. Evison "Modeling Age, Obesity, and Ethnicity in a Computerized 3-D Facial Reconstruction". *Forensic Science Communications* [Internet]: FBI. (2001).

[4] M. P. Evison and M. A. Green. "Presenting Three-Dimensional Forensic Facial Simulations on the Internet Using VRML" *Journal of Forensic Sciences*, vol. 44, pp. 1216–1220, 1999.

[5] M. P. Evison, D. Schofield, C. Solomon, I. Dryden**, "**Computer Aided Forensic Facial Recognition"**.** The Federal Bureau of Investigation (research grant TSWG – T-216E).

[6] F Cesarani et al, "Facial reconstruction of a wrapped Egyptian mummy using MDCT" *American Journal of Roentgenology*, vol. 183 (3), pp. 755–8, September 2004.

[7] M. Forte et al, "3D facial reconstruction and visualization of ancient Egyptian mummies using spiral CT data," *SIGGRAPH '99*, 1999.

[8] T. D. White, P. A. Folkens, *Human Osteology*. San Diego: Academic Press, 2000.

[9] J. E. Buikstra, D. Ubelaker, eds. "Standards for Data Collection from Human Skeletal Remains," in *Proceedings of a Seminar at the Field Museum of Natural History*. Arkansas Archaeological Survey Press, Fayetteville, (1994).

[10] W. M. Bass, *Human Osteology: a Laboratory and Field Manual*. Missouri Archaeological Society Press, 1995.

4.

Facial Measures and Identification Principles
Gesichtsmerkmale und Identifikationsprinzipien

I know that Face

Mr. Richard Neave[1], Dr. Frank Prieels[2]

[1] RN-DS Partnership, UK,
[2] University of Duesseldorf, Germany

Abstract

The reconstruction of the face of an unknown person, regardless of the technique used, can only be regarded as successful in the event that a subsequently confirmed recognition is forthcoming as a result. The appearance of the final reconstruction when presented to the public will have a major impact upon its success.

A reconstruction based solely on an unknown skull will never be a totally accurate portrait, there being far too many variables. It is essential therefore that only the information, which is likely to trigger a recognition, is shown. The more limited the amount of information that can be used, the less likely it will be for an inaccuracy to adversely influence the outcome.

The purpose of this pilot study was to ascertain how much information could be safely omitted from an image of a known person before they became unrecognisable to those who knew them well. It was also designed in a way that reflects to some extent one of the numerous situations in which a recognition may be forthcoming from a member of the public.

The forensic reconstruction of the face of an unknown person, regardless of the technique used, can only be regarded as successful in the event that a subsequently confirmed recognition is forthcoming as a result. The appearance of the final reconstruction when presented to the public may have a major impact upon its success.

A reconstruction based solely on an unknown skull will never be a totally accurate portrait, there being far too many variables. It is essential therefore that only the information which is likely to trigger a recognition is shown. The more limited the amount of information that can be used, the less likely it will be for an inaccuracy to adversely influence the outcome.

This pilot study was designed to test how much information could be omitted from an image of a known person before the lack of information provided rendered them unrecognisable to those people who might know them well. When such images are presented in the media, the primary targets will be those members of the public who knew the deceased individual well. This would include close friends and, more importantly, members of their own family.

The method chosen was to select an image of one individual from two different families; someone who would be central to the family group. The photographs chosen were not selected because they were either flattering or particularly representative of the features that were central to the individual's appearance. In other words, they were everyday snaps, of the type that most families will have showing people in a very informal situation.

These images were then scanned into the computer, and using the Adobe Photoshop programme were rendered as half-tone images. The image was then progressively reduced in its content by adjusting the contrast and brightness. Initially, the photograph was desaturated, and the median set at 42 pixels. Surrounding information such as glasses and background images were then removed using the air brush tool where necessary. The purpose of this was to eliminate so far as possible any obvious features such as a detailed hairline, which might in turn provide a visual clue which would be unknown in a situation where the face was being constructed from just a skull. The brightness was then adjusted to +58, and the contrast to +73. This image was then duplicated and the brightness again adjusted to +58 and the contrast to +71. This process was carried through to the point at which only the vaguest indication of the shadow indicating the position of the eyes could be seen. All were then adjusted by changing the contrast to +100 (Gausian blur).

Having completed this exercise, five images were selected from each group. This selection of images was then shown to two groups of ten individuals, all of whom were familiar with the subject. Their ages ranged from 7 to 70. The images were shown starting with 1, being that where the least information was available.

In Group 1 (comprising Figures 1–5), Fig. 1 produced no response other than the viewers were looking at a face. Fig. 2 produced an instant recognition from 5 viewers. Fig. 3 produced a recognition from 2 viewers, one being instant, the second being after some three seconds viewing. Fig. 4 produced no response, with the remaining 3 viewers making no recognition until seeing the final Fig. 5, when their response was instant. In percentage terms, we can see that 50% made an instant recognition on image 2, 20% a recognition on image 3, and 30% made no recognition until the final image.

Fig. 1:

Fig. 2:

Fig. 3:

Fig. 4:

Fig. 5:

These results are far from conclusive, but when viewing the initial image of the subject the definition in the region of the chin, the hairline and fine details of the face are very limited. The features that stand out most prominently are the mouth slit, the nostrils and the shadow cast by the upper eyelid, together with the fact that the subject has mid length hair. The reduction of this information in Fig. 4 tends to exaggerate the upper lip, provides very little indication as to the shape of the face and the chin, and gives little indication as to the style of hair. Fig. 3 reduces the contrast of these features further, although it does not reduce the amount of information. Curiously, Fig. 2, although presenting far less information than any of the previous, somehow embodies the character of the subject rather more, although the information itself is extremely limited, featuring a very modest shadow for the upper lip, an almost imperceptible shadow indicating the level of the nostrils, extremely sketchy information about the eyes and virtually nothing of the eyebrows. Details of the hair and the hairline were deliberately disguised, being a feature that cannot be reproduced with much certainty in a reconstruction. Fig. 1 was such as to ensure that without the indication of the position of the nose and something to indicate the outline of the face it could hardly be expected to elicit a recognition.

In Group 2 (comprising Figures 6–10), Fig. 6 was recognised by 4 viewers. Fig. 7 produced a recognition from 2 viewers. Fig. 8 was recognised by 1 viewer; Fig. 9

by 2 viewers, and Fig. 10 by one viewer. In percentage terms, we can see that 40% made a recognition on Fig. 6, 20% a recognition on Fig. 7, 10% on Fig. 8, 20% on Fig. 9 and 10% made no recognition until the final image.

Fig. 6:

Fig. 7:

Fig. 8:

Fig. 9:

Fig. 10:

Again, the results are far from conclusive, although in this case the hair was such a prominent feature that its presence was always going to influence the appearance of all the images. The most prominent other features are the right eye and the upper lip, the shadow cast by the nostrils and the line of the lower jaw. The reduction of this information in Fig. 9 tends to exaggerate the left eye, the hairline and the shape of the upper and lower lip. Fig. 8 further reduces the contrast of all these features, but again, as with Group 1, does not significantly reduce the amount of visual information. Fig. 7 reduces far more the character of the face than Fig. 2 in Group 1, although the line of the hair and the shape of the right eye are still prominent. Fig. 6, although showing relatively little information, still suggests the shape of the lower jaw and the position of the left eye.

From reading the notes made by the authors during the tests, it would appear that amongst the most significant features for recognition to occur is the length and style of hair, the shape and position of the eyes, and the outline of the face, although it appears that none of these features have to be rendered in great detail.

The results of this small study indicate that there are some individuals who will never recognise a reconstruction unless it is a true likeness, and there will be those who recognise it almost instantly, as well as some, of course, who fall somewhere in the middle. What does emerge is that if a person is going to recognise a face, the amount of information that is required can be very limited, and confined largely to the proportions of the face, the expression of the eyes and the size of the mouth. Certainly details indicating nasolabial creases, the mental area of the chin, and indeed the hairline or position of the ears would appear to be far less relevant.

A novel method to train researchers on facial reconstruction sculpture

George. J. Dias[1], Sonia Codinha[2], Russell Barnett[1] and Patricia Mahoney[1]

[1] School of Medical Sciences, University of Otago, Dunedin, New Zealand.
[2] Department of Anthropology, University of Coimbra, Portugal

Abstract

The field of facial recognition is complex and conflicting views exist. A general facial reconstruction, without specific characteristics, may resemble someone known better than a life-like image. A sculptured image provides this general and less suggestive appearance, and considerable refinement will be required before computers mimic sculptures. Facial approximation sculpting methods are: Morphometric, Morphoscopic or Anatomical and Hybrid technique (morphoscopic and morphometric). Currently, there is no standardized method to train new investigators in facial sculpture. Consequently individual artistic perception dictates the final output, with inherent personal interpretation, and wide inter-operator variations. We propose a novel method to train investigators in the science of facial approximation by sculpture. An embalmed cadaveric head was photographed from different profiles, and soft tissue depths at standard points measured. A median skin incision reflected and removed skin from the left side of the face. Tissues from the left side of the nose were excised leaving the nasal septum. The left ear and the left half of orbicularis oris including the intermingling fibers of associated dilator muscles, parotid gland, masseter and temporalis, and the buccal fat pad were excised and preserved. Left orbital contents were enucleated. The remaining soft tissues were removed completely skeletonising the left side of the facial skeleton. Soft tissue depths were demarcated by stainless steel screws, and preserved soft tissues structures placed in correct anatomical orientation on the skull. The face was sculptured using the standard technique with the additional resources of intact right side of the face and original photographs for guidance.

Introduction

The positive identification of human skeletal remains or corpses in an advanced state of decomposition, is the main purpose of Forensic Anthropology. In ideal situations this procedure is based on the similarity between ante-mortem and post-mortem information about the victim, but in the absence of a suspect/victim for comparison, this process becomes impractical. In those situations, a facial approximation procedure is a valuable aid in the creation of an approximate image of the unidentified individual. Although facial approximation in isolation cannot be used for positive identification [1,2], a general reconstruction of facial features may trigger the memory of a viewer to recognize a resemblance with someone they know and, as a consequence, lead to further evidence such as radiographic and/or dental comparisons or DNA analysis [2, 3], which may result in a positive identification. In addition to the medico-legal context, facial approximations have also been used in archaeological context to restore the physiognomies of a number of historical individuals [4, 5]. The three dimensional facial approximation is based on modelling soft tissue structures of the face and head on an unidentified skull, or its replica, with clay, plasticine or wax in an attempt to reproduce the likeliness of the owner [2, 6, 7]. Fundamentally there are three different approaches to the reconstruction of the human face. First, the morphometric method, also known as the American method [1], which makes use of objectivity, measurements and rules. The second is referred to as the Russian morphoscopic or anatomical method, and is based on the modelling of facial muscles, one by one onto the skull [8]. The third method is a hybrid technique developed in the United Kingdom by Neave [4] that combines both the morphoscopic and morphometric methods, and which is also known as the Manchester method).

Although all the methods of three-dimensional facial approximation rely on the use of average soft tissue depths markers at strategic points on the skull [9], there is no standardized method to train new investigators in the expertise of facial sculpture. Frequently, it is the individual artistic perception that dictates the final output, with inherent personal interpretation leading to wide inter-operator variations [10, 11]. This, combined with a lack of consistency in the literature on the relationship between the facial soft tissues and the underlying bone [12], often results in the creation of different faces for the same skull with few resemblances between them [13].

The ideal circumstance would be to incorporate the attributes of a scientist and an artist in the same worker, but this is an infrequent occurrence. Usually the anthropologist works together with a sculptor to model a face. Even in situations where "trained" scientific experts are available, they also need to have some manual dexterity and modelling skills to enable them to reconstruct realistic looking faces [14].

In order to provide the opportunity for both sculptors and scientific experts to gain or improve their modelling skills and, at the same time, expand their practical understanding of head and neck anatomy, we propose a novel method to train investigators in the science of facial approximation by sculpture. This standardized method will minimize artistic license and provide consistency amongst investigators in the final representation of the facial approximation.

Methods

A head and neck was dissected from a cadaver which had been embalmed (Crosado mix) [15, 16] for longer than 6 months. Simpson and Hennenberg [17] demonstrated that soft tissue depths of the face, of cadavers embalmed for longer than 6 months were approximately similar to those that were taken immediately at the time of death [17]. This was then photographed (incorporating a measuring scale) from the following profiles – frontal, lateral (left and right), lateral oblique, superior and inferior (Figures 1–4).

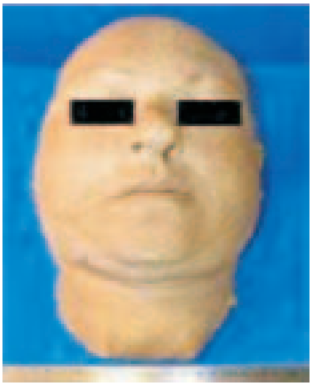

Fig. 1:

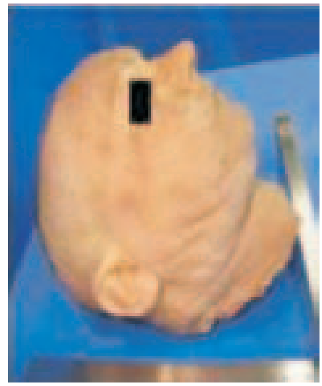

Fig. 2:

Fig. 3:

Fig. 4:

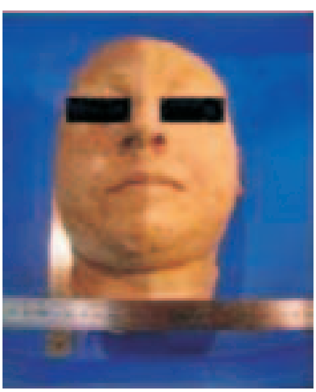

Fig. 5:

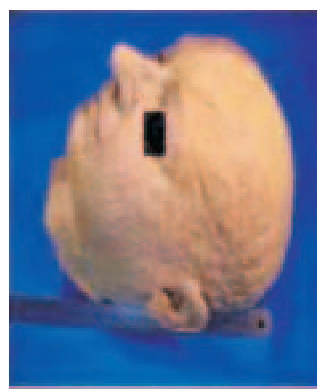

Fig. 6:

Soft tissue depths were measured and recorded at the points detailed in Table 1, using a dental root canal file with a rubber stopper for shorter depths and a spinal needle with a rubber stopper for greater depths. These distances were measured using a high precision stainless steel ruler, calibrated to 0.5mm, and this measurement was confirmed using an electronic caliper (Mitsitoyo, Japan) and recorded. Tissue depths and measurements were then repeated and recorded by a second operator. In instances of discrepancy depths and measurements were repeated independently until the measurements were reconciled.

A median skin incision beginning from the vertex of the head and running anteriorly and posteriorly was made. The anterior incision was carried through the glabella, the nasion and along the mid-line dorsum of the nose to the tip of the nose and continued down bisecting the columella and philtrum to the mid-point of the vermillion border of the upper lip. The incision was carried to the left, laterally along the vermillion border to the commissure of the oral aperture and continued along the vermillion border of the lower lip up to the mid-point. The incision was carried vertically down in the median plane to the mid-point of the chin (symphysis menti), and continued down in the mid-line of the submandibular region until the inferior border of the cadaveric neck was reached. The skin from the left side of the face was carefully reflected from the face and back of the head, excised and discarded (Figures 5 and 6). The mucous membrane of the left upper and lower lips up to the oral aperture was carefully dissected from the underlying oris obicularis muscle and discarded. An impression mould (to make replicas) of the whole head was taken using a silicone/rubber impression material on a resin tray. The mould was made in two halves running through the median plane and once the impression material was cured, the mould was removed from the left half of the head only, leaving the right side of the head within its mould. The remainder of the dissection was carried out keeping the right side of the head within the mould. The subcutaneous fat was carefully dissected from the underlying superficial facial muscles, excised and discarded. An impression of the left side was taken again at this point using the same method described above (Fig. 7).

Tab. 1: Soft Tissue Depths.

Landmark	Reference	Soft tissue depths – (right mm)	Soft tissue depths – (left mm)	Midline tissue depths (mm)
Glabella	9, 22, 23, 24, 25, 26, 27	5.0	5.5	
Trichion	9	3.5	3.2	
Frontal eminence	30	3.5	3.5	
Root of zygoma	29	15	15	
Mid-zygomatic arch	30	10.5	10.5	
Mid-masseteric	25, 29	28.5	28.5	
Zygoma (lateral orbit)	22, 27	10.5	9.5	
Mouth width (ch-ch)	20, 28			53.93

Landmark	Reference	Soft tissue depths – (right mm)	Soft tissue depths – (left mm)	Midline tissue depths (mm)
Greatest lip height	22	15.68	16.68	
Mid-philtrum	22, 25, 26, 27			10.5
Labiale Superius	9, 23, 25, 27			9.5
Labiale Inferius	9, 23, 25, 27			10.5
Supra-labial	29	10	10.5	
Commissural	29	11.5	10	
Supra-commissural	29	22	17.5	
Inferior labial sulcus	9, 22, 23, 25, 26	10	11	
Gonion	9, 22, 27	22.5	22.5	
Menton	9, 24, 25, 26, 27			8.5
Gnathion	9, 23			7.5
Pogonion	9, 25, 27			10
Ectoconchronion	9	4.5	5.5	
Endocanthion	9	4.5	3.5	
Supra M2	30	33	33	
Infra M2	30	19	19	
Mid-supra-orbital	22, 25, 27	7	6	
Mid-infra-orbital	22, 25, 27	6.5	5.5	
Columella	24			36
Alare	9, 23	9.5	9	
Nasion	9, 22, 23, 24, 25, 26, 27			7.5
Nasale	9, 25, 26, 28			3.5
Subnasale	9, 23, 24			16.5
Supradentale	26			11

Fig. 7:

Fig. 8:

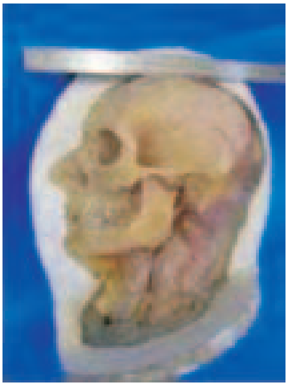

Fig. 9:

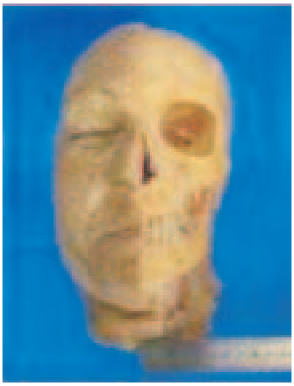

Fig. 10:

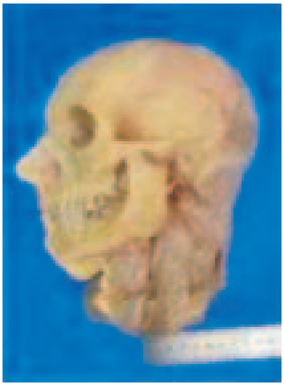

Fig. 11:

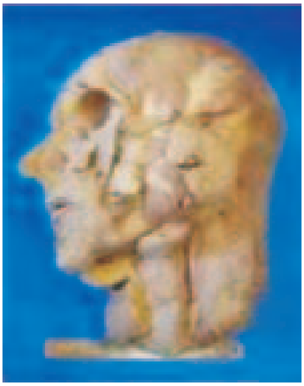

Fig. 12:

The left ear was excised at the junction of the cartilaginous and bony external auditory meatus, and preserved in embalming fluid (Crosado mix) [15, 16]. The temporal fascia was excised exposing the temporalis muscle. The fibrous capsule of the parotid gland was removed and the superficial part of the gland which lies above the masseter muscle, exposed (Fig. 7). At the anterior border of the gland the parotid duct was exposed and followed anteriorly across the masseter muscle. The duct was severed, where it turned medially at the anterior border of the masseter muscle. The deep part of the parotid gland, which extends medially between the masseter muscle and the posterior border of the ramus of the mandible and the mastoid process and sternocleidomastoid muscle was dissected from the surrounding tissues and the entire gland including the duct, was removed intact and preserved in embalming fluid (Crosado mix) [15, 16]. The buccal pad of fat, which lies superficial to the buccinator muscle of the cheek was dissected out intact and preserved in embalming fluid (Crosado mix) [15, 16] (Fig. 8). An impression of the left side was taken again at this point using the same method described above (Fig. 8). The surface of the masseter muscle was cleaned of extraneous tissue, and the superior attachment was detached from the zygomatic arch. The muscle was reflected down and stripped from the lateral surface of the ramus of the mandible by utilizing an osteotome, and finally the muscle was detached form the inferior border of the ramus and the angle of the mandible (Fig. 9, 10 and 11). The muscle was then preserved in embalming fluid (Crosado mix) [15, 16].

The temporalis muscle was stripped from its superior attachment to the temporal fossa of the skull, the muscle reflected down and its tendon running deep to the zygomatic arch identified and detached at the coronoid process, together with the muscle attachment along the anterior border along the anterior border of the ramus of the mandible (Fig. 9, 10 and 11). The muscle was preserved in embalming fluid (Crosado mix).

The left half of the orbicularis oris muscle was completely exposed. (The rhizorious muscle was undeveloped in this cadaver and was not taken into account). The zygomaticus major and minor from their superior attachments to the zygomatic arch and the body of the zygoma respectively were sectioned and the two muscles removed together by detaching their inferior attachment to obicularis oris and preserved in embalming fluid (Crosado mix) [15, 16]. The other dilator muscles associated with obicularis oris (levator labi superioris, levator angular oris, depressor labi inferioris, depressor angular oris, and mentalis) were detached from their respective bony origins. The obicularis oris, in relation to the upper and lower lips was sectioned and excised intact at the mid-line, and it was removed together with the intermingling fibers of the associated dilator muscles (Figures 9, 10 and 11), and preserved in embalming fluid (Crosado mix) [15, 16]. The left upper and lower nasal cartilages together with fibrous ala nasi were excised intact, leaving the nasal septum (Fig. 11). An incision was made through orbicularis occuli muscle along the margins of the bony orbit right down to the bone. The periosteum was stripped with a flat periosteal elevator from the walls of the orbit separating the orbital contents. The optic nerve and associated blood vessels were sectioned at the apex of the bony orbit and the entire left orbital contents enucleated.

The whole of the left side of the face was skeletonised by removing the remaining soft tissue.

Sternocleidomastoid muscle was detached at its superior attachments to the mastoid process and superior nuchal line of the occipital bone and the muscle completely excised. The submandibular gland was exposed by removal of its fibrous capsule and it too was excised and preserved in embalming fluid (Crosado mix) [15, 16]. The subcutaneous fat in the sub-mandibular region was removed exposing the suprahyoid muscles. The carotid sheath and its contents were excised exposing the trachea and the thyroid gland on the left side (Figures 9, 10 and 11). An impression as described above was taken of the whole of the left side of the head and neck (Fig. 9). At each stage where impressions were taken the mould was removed after curing (approximately 6 hours).

Sculpturing

Fine threaded stainless steel screws were screwed at the different soft tissue depth points (Table 1) to indicate the soft tissue depths. Two small bur holes, were drilled in bone using a round half millimeter dental bur– one at the anterior lacrimal crest of the maxilla and the other at the lateral margin of the bony orbit in line with the zygomatic tubercle, to indicate the position of the medial and lateral canthi of the eyelids [18] (Fig. 12).

The preserved soft tissue structures were placed in their correct anatomical orientation on the skull. Where necessary, to get the correct anatomical orientation, the soft tissue structures were supported both underneath and at the sides with modelling clay (Fig. 12). The projection of the globe of the eye was according to Stephan [19]. The nasal projection was calculated according to George [20], and mouth width as described by Stefan [21]. The rest of the face was sculptured over the soft tissue using the soft tissue depth markers, as described by Prag and Neave [4], with the additional resources of intact right side of the face and original photographs for guidance. The ear was sculptured with clay using the excised ear as a reference.

Results and Discussion

Figures 13 and 14 show the resulting approximation of the left side of the face. This facial reconstruction is the first attempt by a new operator having had no previous experience or training in the field of facial reconstruction or in the art of sculpting. The time taken for this first attempt was approximately 8 hours. This procedure should be repeated at regular intervals until operator proficiency is achieved. We believe that after this procedure has been repeated 5 –10 times, the time required will be reduced and the quality of the resulting reconstruction improved.

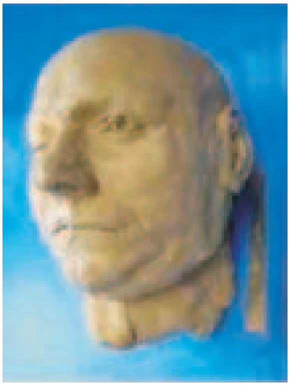

Fig. 13:

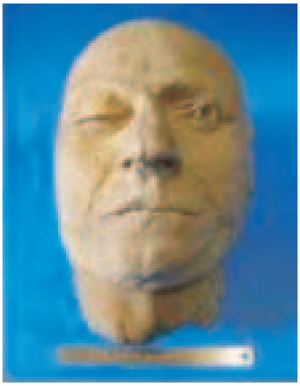

Fig. 14:

Currently there is no standardized and universally accepted method to train new researchers in the science of facial sculpture. Consequently individual artistic perception tends to dictate the final output, with inherent personal interpretation, leading to wide inter-operator variations. This novel method we have proposed, if universally accepted will minimize artistic license and subjectivity and provide consistency amongst investigators in the final representation of the facial approximation.

References

[1] Snow CC. Gatliffe BP. and McWilliams KR. 1970 Reconstruction of facial features from the skull: An evaluation of its usefulness in forensic anthropology. *American Journal. Physical. Anthropology* 33, 221–228.

[2] Tyrrell AJ. Evison MP. Chamberlain AT. Green MA. 1997 Forensic Three-Dimensional Facial Reconstruction: Historical Review and Contemporary Developments. *Journal of Forensic Science* 42 (4): 653–661.

[3] Reichs KJ. & Craig, E. 1998 Facial approximation: procedures and pitfalls. In: Reichs (ed) *Forensic Osteology: Advances in the Identification of Human Remains* (2e). Charles C. Thomas, Springfield, pp: 491–513.

[4] Prag J & Neave R. 1997 *Making Faces*. London. British Museum Press.

[5] Wilkinson C & Neave R. 2003 The reconstruction of a face showing a healed wound. *Journal of Archaeological Science* 30: 1343–1348.

[6] Krogman WM. & Iscan MY. 1986 *The human skeleton in forensic medicine* (2e). Springfield, IL Charles C. Thomas.

[7] Auselbrook WA. Iscan MY. Slabbert JH. Becker P. 1995 Superimposition and reconstruction in forensic facial identification: a survey. *Forensic Science International* 75: 101–120.

[8] Gerasimov MM. 1971 The Face Finder. London/Philadelphia.

[9] George RM. 1993 Anatomical and Artistic Guidelines for Forensic Facial Reconstruction. In: Iscan and Helmer (eds) *Forensic Analysis of the skull*. New York, Wiley-Liss. Pp: 215–227.

[10] Iscan MY. 1988 Rise of Forensic Anthropology *Yearbook of Physical Anthropology* 31: 203–230.

[11] Helmer RP. Rohricht S. Peterson D. Mohr F. 1993 Assessment of the reliability of Facial Reconstruction. In: Iscan and Helmer (eds) *Forensic Analysis of the skull*. New York, Wiley-Liss. Pp: 229–246.

[12] Vanezis M. & Vanezis P. 2000 Cranio-Facial Reconstruction in Forensic Identification- Historical Development and a Review of Current Practice. *Medicine. Science and. Law* Vol. 40 No 3: 197–205.

[13] Stephan C & Hennenberg M. 2001 Building faces from dry skull: Are they recognized above chance rates? *Journal of Forensic Science* 46 (3): 432–440.

[14] Aulsebrook WA. 2000 Facial Tissue Thickness in Facial Reconstruction in Siegel JA. Saukko PJ. Knupfer GC. (eds), *Encyclopaedia of Forensic Sciences*. San Diego. Academic Press. Vol II: 779–788.

[15] Nicholson HD & Samalia LD. 2003 Can human tissues embalmed for teaching be successfully used for histology? *Clinical Anatomy* 16: 463.

[16] Samalia LP. 2002 Can human tissues embalmed for teaching purposes be used for histology? In: *Department of Anatomy and Structural Biology. Dunedin: University of Otago*.

[17] Simpson E. & Hennenberg M 2002 Variation in soft-tissue thicknesses on the human face and their relation to craniometric dimensions. *American. Journal of Physical. Anthropology.* 118, 121–133.

[18] Snell RS. & Lemp MA. 1998 Clinical anatomy of the eye (2e). Oxford. Blackwell Science. Inc.

[19] Stephan C. 2002 Facial approximation: Globe projection guideline falsified by exopthalmic literature. *Journal of Forensic Science* 47(4): 730–735.

[20] George RM. 1987 The lateral craniographic method of facial reconstruction. *Journal of Forensic Science* 32: 1305–1330.

[21] Stephan C. 2003 Predicting mouth width from inter-canine width – A 75% rule. *Journal of Forensic Science* 48(4): 1–3.

[22] Manheim MH. Listi GA. Barsly RE. Musselman R. Barrow E. Ubelaker D. 2000 *In vivo* facial tissue depth measurements for children and adults. *Journal of Forensic Science* 45 (1): 48–60.

[23] Simpson E & Henneberg M. 2002 Variation in soft-tissue thicknesses on the human face and their relation to craniometric dimensions. *American Journal of Physical Anthropology* 118: 121–133.

[24] Smith SL & Buschang PH. 2001 Midsagittal facial tissue thicknesses of children and adolescents from the Montreal growth study. *Journal of Forensic Science* 46 (6): 1294–1302.

[25] Wilkinson CM. 2002 *In vivo* facial tissue depth measurements for White British children. *Journal of Forensic Science* 47 (3): 459–465.

[26] Garlie T & Saunders S. 1999 Midline facial tissue thicknesses of subadults from a longitudinal radiographic study *Journal of Forensic Science* 44 (1): 61–67.

[27] Phillips VM & Smuts NA. 1996 Facial reconstruction: utilization of computerized tomography to measure facial tissue thickness in a mixed racial population. *Forensic Science International* 83 (51–59).

[28] Wilkinson CM. Motwani M Chiang E. 2003 The relationship between the soft tissues and the skeletal detail of the mouth. *Journal of Forensic Science* 48 (4): 728–732.

[29] El-Mehallawi IH & Soliman EM. 2001 Ultrasonic assessment of facial soft tissue thicknesses in adult Egyptians. *Forensic Science International* 117 (99–107).

[30] Rhine JS & Moore CE. 1984 Forensic Anthropology. Maxwell Museum Technical Series One.

Imagetrak – Biometric Recognition

Prunău Dan-Cristian

Forensic Science Intitute – General Inspectorate of Romanian Police, Romania

Abstract

In this paper we will present the Imagetrak system that was bought by the Romanian Police, the main features that allows the user to exploit the facial images and individual body marks, scars, and tatoos to identify those persons from the database that have the apropriate phisionogmy.

1 Introduction

The Investigative Image Management System is a photo application that allows law enforcement agencies to capture, store, organize and manage images and descriptor data essential for investigation and identification services. At this moment the workstations of Romanian ImageTrak system are installed and put in operation in all the police districts.

The system has a central data station, placed in the Forensic Science Institute, at the Romanian Police Headquarters in Bucharest. This central unit is linked with all the 42 workstations, one in each of the police districts and one in Capital Police Center. The system's network is independent (named Metropolitan Network), completely separated from other communication lines.

2 Central database

The database of the system is adapted for the police operational needs:

– The maximum storing capacity of the system is 500,000 personal records;

– Digital images can be fed into the system in form of JPEG file, live digital video camera & still digital camera records, scanner or other TWAIN – compliant devices. ImageTrak allows for the management of mug shots, photos of scars, marks, and tattoos (SMT). The system has an interface for feeding in the information and images from the offender's body. The frontal image is the key in every personal record, as it is used in LFA (Local Facial Analysis) search engine for identification;

– The offender can be tracked down from the database using different search filters like: some information about the personal data, biometric data, individual body marks, scars, tattoos etc.

– The snapshot of an unknown person or the robot portrait can be searched into the database and a list of maximum 100 hits will be generated, consisting of persons that have the closest appearance to the searched image.
– The system is easy to install and maintain;
– The digital camera provided with the system allows the feeding at high resolution images of the subjects into the database;
– The system administrator can set user accounts and passwords, define roles and access rights, and forbid other system-level features such as lookup tables and system settings.

3 Imagetrak workstation

We have 42 workstations, one in each of the police districts. The workstation has scanner, ink-jet printer, digital photo camera with 4 Mpixels;

The necessary softwares are: Imagetrak, E-FIT for facial composition and other applications for capturing and video editing.

4 Imagetrak benefits

Imagetrak benefits are far more efficient for our police inquiry purposes than the previous image storage systems:

– The old photo albums with pictures of criminals are replaced by a national digital database in which the pictures are stored together with other very useful information for investigative purposes;
– The database could be rapidly searched against all the information included in the person's registration form, which has been filled out during the initial recording procedure;
– The system can use search criteria like:
  – Person's particular body marks;
  – Biometric data;
  – Informations including person's physical characteristics, criminal record and charge informations;
  – Digital photos – facial image of the person;
  – Police drawings based on witness testimony (the E-FIT software is integrated in IMAGETRAK).

- The Imagetrak system includes standard reports. For specialized reports that are not part of the standard package, Imagetrak includes a report wizard, allowing users to quickly create ad hoc custom reports;
- Imagetrak system is organized as a network, throughout all the police districts, the link between the workstations being provided by secure connections.

5 Importing images

The pictures can be fed into the system through a wide range of digital means:

- Frames from surveillance video tapes;
- TWAIN files;
- Police drawings;
- Image files (in JPEG, TIFF, GIF, or BMP formats);
- The images could be edited by resizing, cut & paste, brightness and contrast adjustments etc.

6 Main screen

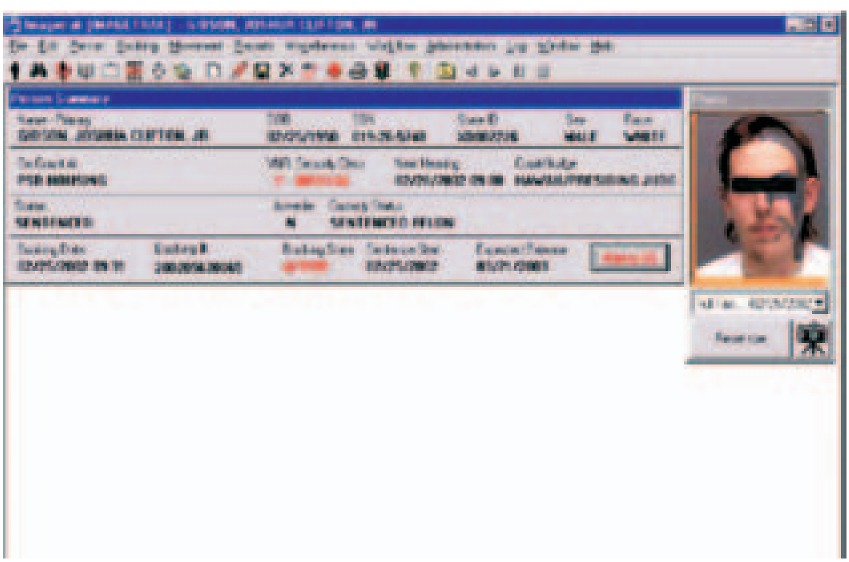

Fig. 1: Graphical User Interface with personal data summary and the person's image.

7 Search results

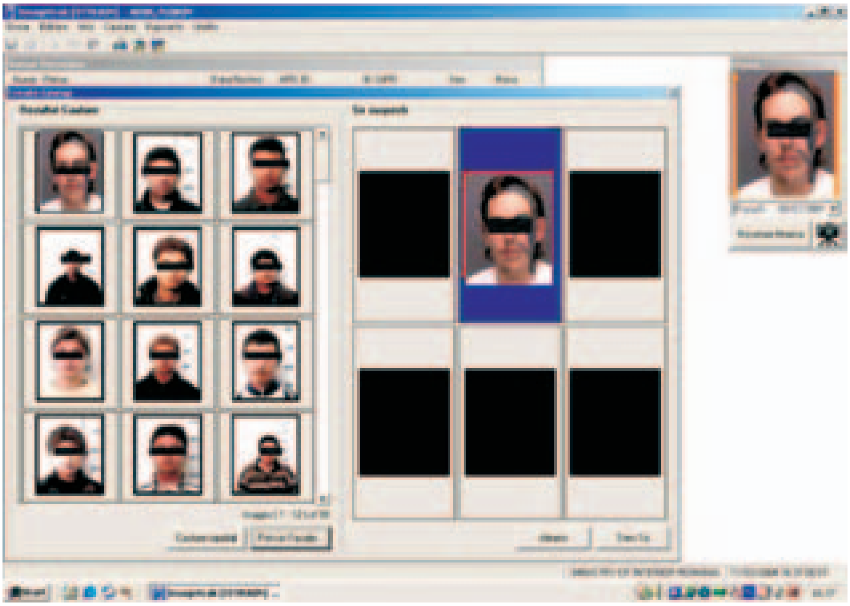

Fig. 2: Allows the visualization of the persons images that could match the subject which is searched in the database.

8 LFA- Local Feature Analysis

The algoritm for facial recognition (LFA) implies processing of some significant facial biometric data like:

- Distance between eyes;
- Nose length;
- Eye socket depth;
- The distance of the facial bones;
- Maxillary shape;
- Chin shape.

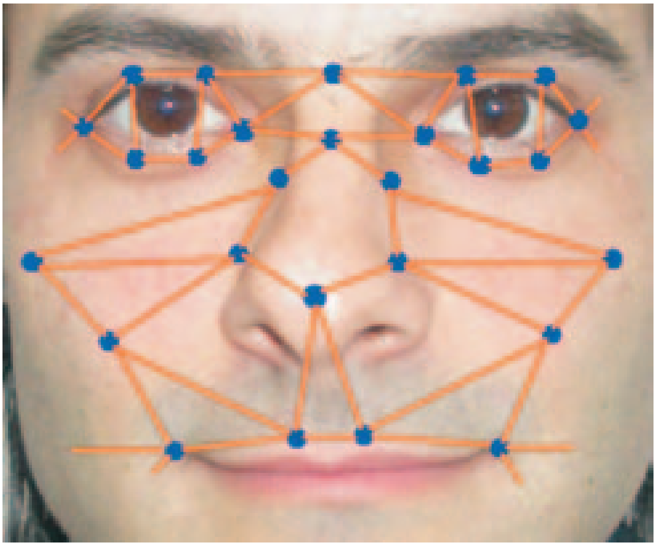

Fig. 3: Faceprint.

The software measures all these elements and generates a file for the processed image (faceprint), consisting of 14–20 such measurements. The file for each measured feature takes no more than 84 bytes.

9 LFA benefits

The face recognition algorithm – LFA matching results are independent from:

- gender, age or race of the subject;
- the source of the file processed (scanner, video camera, etc.);
- other facial details (facial make-up, glasses, facial hair).

10 E-FIT – software for facial composition

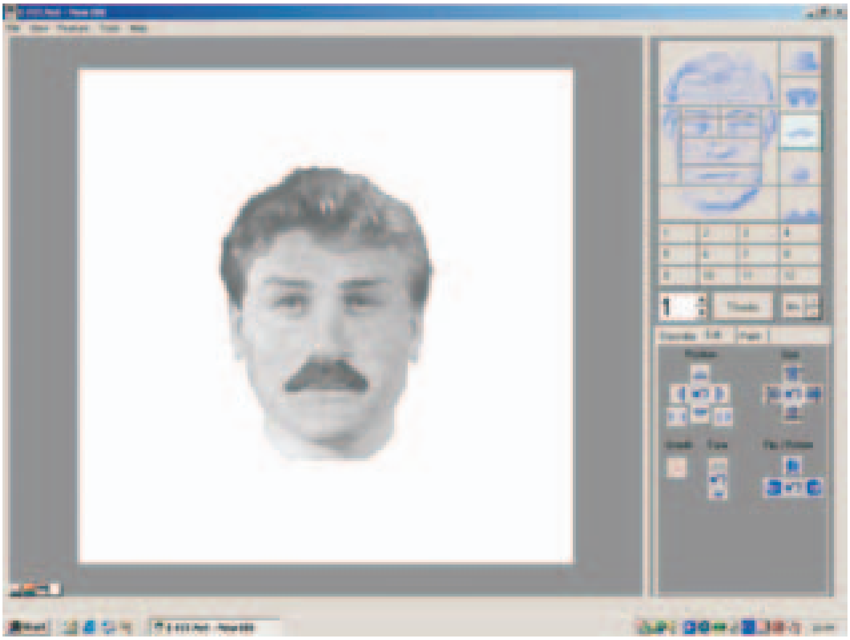

Fig. 4: Robot portrait realised in E-FIT.

E-FIT is an application for composition that uses different parts of faces to allow the realisation of the robot portrait. The user can choose the parts of the face (the eyes, the nose, the shape of the face, hairstyle etc.), then he can adjust the size, color and position of the pieces to realise the image of the person.

Biometroskopie – a new discipline in the facial reconstruction?

Kurt Kindermann

State Criminal Police Office, Baden-Württemberg, Germany

Since thousands of years the humanity is busy in the examination of the human appearance. Pictures of the uniqueness of body and face were found in cave paintings, from the old Egyptians and Greeks to the romans and all worldwide known existing primitive peoples created humans in drawings, sculptures and death masks. In the modern history it was Alphonse Bertillon, who founded in the end of the 19th century a anthropometric system for the identification of people. With the continual progress of capacity development in the medical und criminal technical science and the emergence of technical systems, there are now for us inexhaustible potentialities, which give us insight into the human physiognomy. The scientists in the facial reconstruction claim these elements without giving this an independent and comprehensive term. In a all-embracing direction of thought is the "Biometroskopie" a new possible discipline, which is made up of

- biometry: science of the counting and body measurement at human; biologic statistics, the varied application of the mathematic, particularly the mathematic statistics, in the biologic and similar sciences – the biometric (biometry and informatics) in which the use of the biometry in the informatic sience will be seen in mutual relation to each other,
- biology and medicine with their possibility of academic realization,
- and also anthropology connected with Sociology and in fact of the global mixture of humans with new existing phenotypes.

The chance for the facial reconstruction, which come up from the "Biometroskopie", will be descripted in an all-embracing direction of thought, current technical view and forward-looking situations.

"Biometroskopie" includes the terms "bio" = life, "metro" = measure and that from the greek language descended term "skopein" = examination/to look at and stands for the criminalistic measurment and application from body views. United are here all phenotypical possibilities of human beings. Decisive for the assignment to the categories leading types of humans is the real appearence, that means the recognizable characteristic feature, not a politicle or nationalaccompanying. Also belongs to this case the facial measuring, differences of the ears, the dactyloscopy (finger prints) iris-, retina- and voice-identification, the DNA-analystic, the finger- and handgeometric, the venous structure, the gait and handwritng analysis . There are all criminal technique methods included, which are subsume with human beings and the life.

These methods are not only for the individual characteristic identification for existing humans, they also give sequential insights for the facial reconstruction and identification of unknown dead people.

In a technical presentation it will be shown, how facial reconstructions, like hand-drawings, 2D and 3D-animation, are realized and which technical method includes informative informations and are used for a verification.

A further development of Phantom Professional in order to cover the special requirements for face reconstruction started from a skull.

But instaed of using the remembrance of a witness special characteristics of the skull are used to line up with the database to select matching facial details: it's arcs and bows and angles, the length of the canine teeth or the inclination of the bony nose bottom are typical for skully forms and specific for different ethnic groups. The following demonstration shows the steps.

In the first step all facial dimensions are taken from the skull and from all images of missing persons which are considered to be the matching person in order to set all images to the same proportions and to generate facial dimension values.

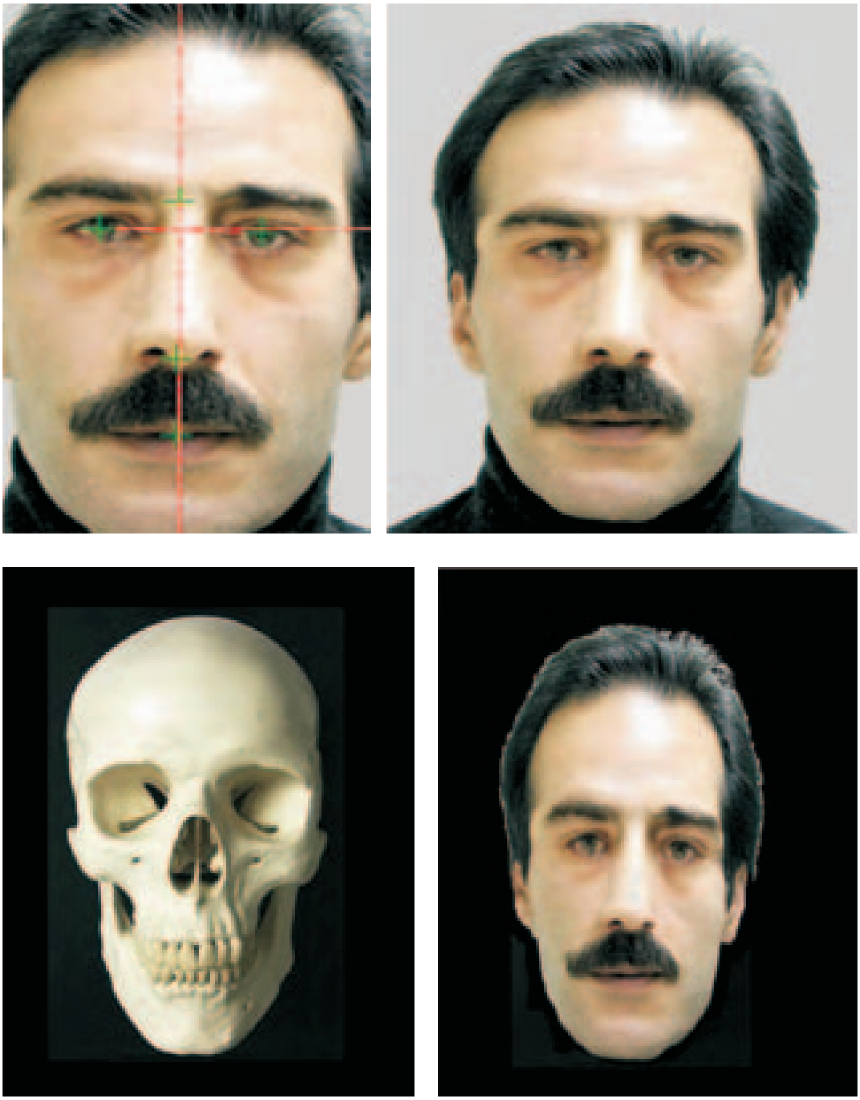

Fig. 1: Image of missed person

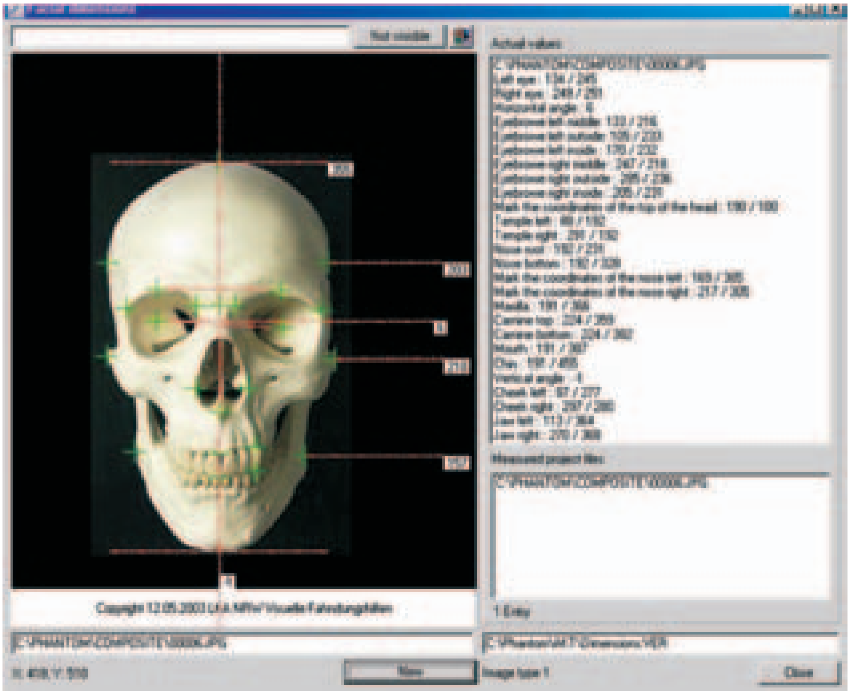

In this stage the skull and images of missing persons are automatically compared to find matching dimensions. These are then displayed in various superimposed steps for visual control.

The reconstruction steps, started from the skull to the fully rebuilded face are shown on this page. Each reconstruction step can be controlled in all stages by superimposing the images.

The system is available from a stand-alone PC or Notebook to a wide area network solution in client-server architecture and utilizes off the-shelf hardware that complies with open industry standards.

2 Expertise

The determination of identity with the aid of photographs is based on the principle of individuality applicable for the entire biology and with it being value for all individuals. All human beings have different appearance and thus distinguishable.

There are more than 100 anatomic characteristics on the human face – from the eyebrows to the double chin. The forehead can be low, middle, high, narrow or wide, wider on the bottom, rectangular shaped- or even wider on the top. The ear, "the fingerprint of photo queries", has over 15 different characteristics. When a suspect has about 15–20 facial characteristics that correspond to a suspect's photo, the police's suspicions are usually verified. Many people have rare and unmistakable birthmarks or scars on the cheek – that even a small number of specific facial characteristics are sufficient in identification. Thus it is possible to definitely determine that a person is not or is identical on the basis of current – or even previously recorded – photo material.

With **Expertise*Pro*ISIS®** UNIDAS offers a state-of-the-art system for the examination of available photo material and to create a guided anthropologic report to be used as an expertise with substantial image documentations. Developed with prominent expert co-authors from German police authorities and forensic laboratories.

The examination applies to a General Comparison and a Detailed Comparison. The general comparison encompasses similarity and optical conformity or the opposite. By detailed comparison identifiable anatomical signs within the face area will be exploited in order to reliably evaluate the identity. This intensive verification can be made with different image modes in order to point out congruence or make edges visible. The result of the evaluation is displayed in a scale where the degree of probability is defined as follows:

- Probable
- With the most utmost probability
- Maximum likelihood

The program is easy to use. The main menu contains only 3 category groups: ***Identification, Official expertise*** and ***Help***.

For an identity check a collection of photos (at least 2 images) can be centralised under a characteristic name e.g. a file reference.

As shown in this illustration below, all images of a file reference appear in a catalogue window on the operator's screen after selecting the file number. Photos can be incorporated from different sources.

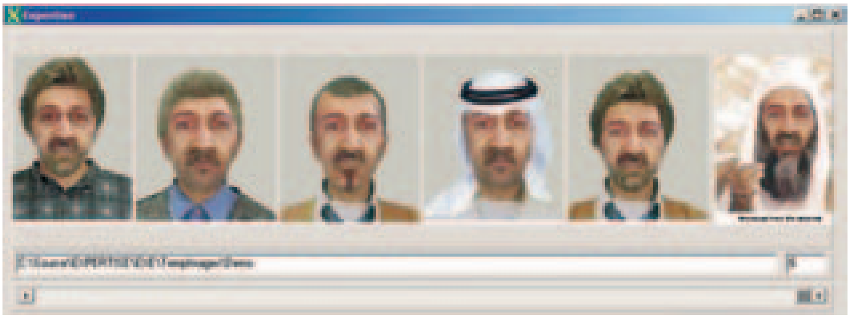

Expertise*Pro*$^{ISIS®}$ supports all available image acquisition systems, transferring pictures to the application. Within the digital range all devices with USB-drivers (1 and 2) and FireWire devices (IEEE1394) can be used. Using the TWAIN-driver selection all scanners as well as all imaging devices (Scanner) with compatible TWAIN drivers (cameras etc.) can be selected.

To select two images from the catalogue for verification the operator can easily use the program's drag-and-drop capability to drag images from the catalogue window to the verification panel.

As a pre-requisite for the verification the photos must be sized to comparable proportions. Therefore the operator must mark five facial positions, which are easily applied. These landmarks are automatically saved and are available for further use.

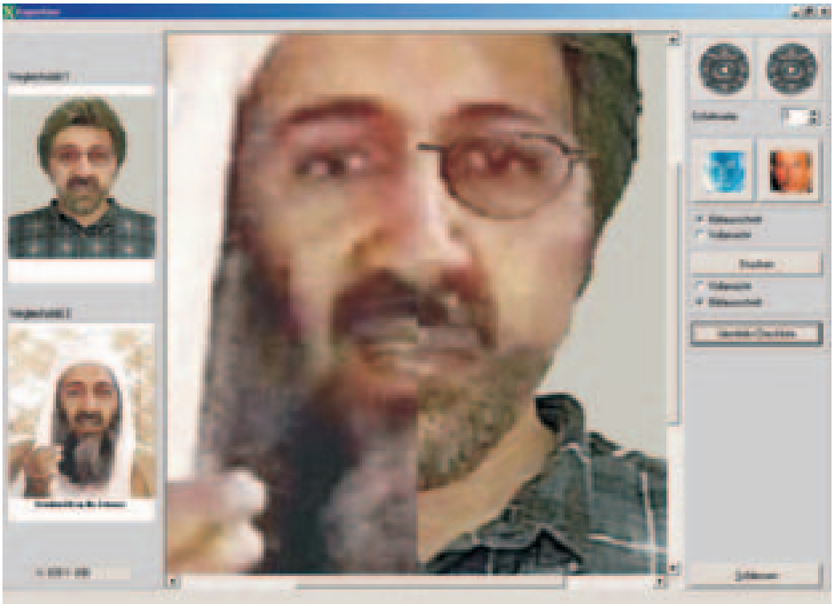

Now both images are sized to comparable proportions, the eye angles are set horizontally to zero, the left eyes are centred and a vertical cut is applied to the two images. The line of intersection can be set to any position – just by dragging the mouse – to determine particular areas of both faces. Aside this, distinctive characteristics like the wings of the nose or the position of the ears (height, type) are definite signs for optical conformity.

General Comparison

With the in-build **Expertise*Pro***ISIS® check list corresponding facts related to the contour of the face and areas of the eyes, nose, mouth and ears can quickly be determined and be made visible.

Detailed Comparison

Using the detailed comparison matching or non-matching anatomical characteristics can be determined. For identifiable anatomical signs within the face area the operator can select special designators from comprehensive forensic catalogues as illustrated on this page.

Using the detailed comparison matching or non-matching anatomical characteristics can be determined. By using special arrows and descriptive labels corresponding facts can quickly be determined and be made visible including substantial image documentations as illustrated in the following example (condensed report).

Image no. 1

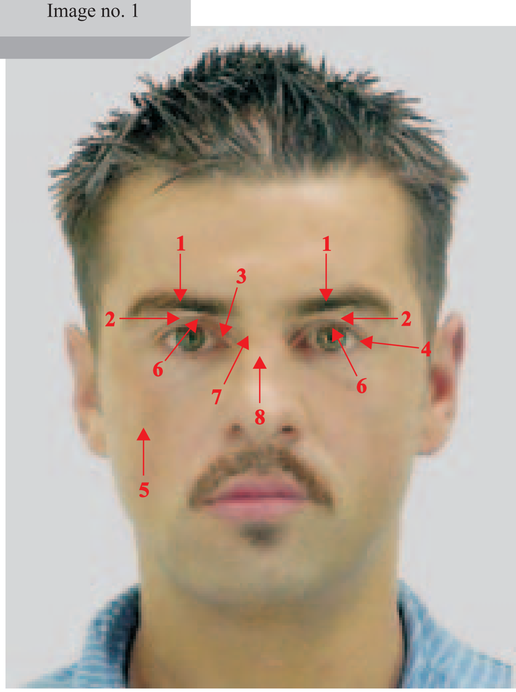

1. Eyebrows
2. Eye Area
3. Upper part of the eye socket
4. Skin folds over the eyelid
5. Pigmentation
6. Eyelashes
7. Base of the nose
8. Bridge of the nose

Image no. 2

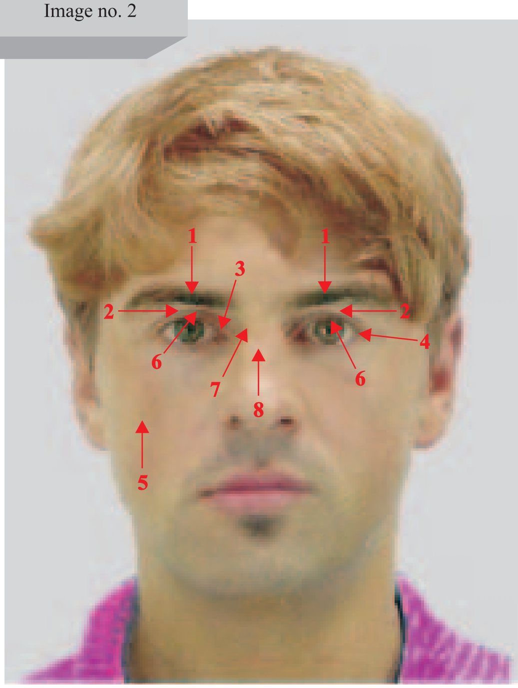

1. Eyebrows
2. Eye Area
3. Upper part of the eye socket
4. Skin folds over the eyelid
5. Pigmentation
6. Eyelashes
7. Base of the nose
8. Bridge of the nose

Anatomic Characteristics

1. Eyebrows
Form: arched; Extension (Width): Extends over the outer corner of the eye;

2. Eye Area
Upper lid area: small

3. Upper Part of the Eye socket
Right upper part of the eye socket: punctuate skin pigmentation in the area of the inner corner of the eye.

4. Skin folds over the eyelid
Skin Folds over the Eyelid: narrow - only visible at the left eyelid.

5. Pigmentation
Left half of the face: skin pigmentation in the area of the cheek.

6. Eyelashes
Slightly placed on the edge of the eyelid.

7. Base of the nose
Base of the Nose: medium-wide.

8. Bridge of the nose
Bridge of the Nose: narrow - no difference.

Deviating anatomic characteristics depending illumination uniformity were not determined.

Result of the Examination:

Due to the determined congruent anatomic characteristics it is assumed that both photos are displaying with

Maximum Likelihood

one and the same person.

3. Face.Net Booking Tracking System

In addition to the "classical" tasks involved in identification service, this system also can offer you true support in fulfilling your other police tasks and duties within this realm. Since FACES comprises a wide spectrum of services, employs modern techniques, and creates positive results, FACES has gained high merit at those investigational centres where it has been implemented and with those people who work in the branch of identification service. The corresponding investigational successes (the success rate of line-up, suspect investigations with the support of police sketches and photo changes) all affirm the efficiency of FACES. The system is available from a stand-alone PC to a wide area network solution in client-server architecture. Operating system Windows NT/ 2000 Professional or XP. The database is independent, e. g. Oracle, SQL-Server or InterBase can be used. The system utilizes off the-shelf hardware that complies with open industry standards and can be interfaced with an agency's records management, livescan fingerprint and AFIS System.

Booking

By using the menu-driven user interface, the data acquired during a booking can be simultaneously recorded and saved. With the use of digital or live camera technique the system eliminates any department's use of film and film development completely. Photos can be automatically integrated with booking records into a corresponding file. You can even supervise the quality of photos, and if necessary, the photos can be reproduced. Photos are immediately available and can be printed out at a designated printer.

Input device support: analog (grabber board), USB and Firewire

Typically a mug-shot, a full body image, fingerprint image and personal data and the complete ten-print record are taken at the point of capture. In addition photos can be taken to collect special physical characteristics such as tattoos, scars etc.

FACES allows also image imports by USB, Firewire or still video cameras (Twain), TV-signals or scanners.

USB and Firewire devices do not need grabber boards or external power supply.

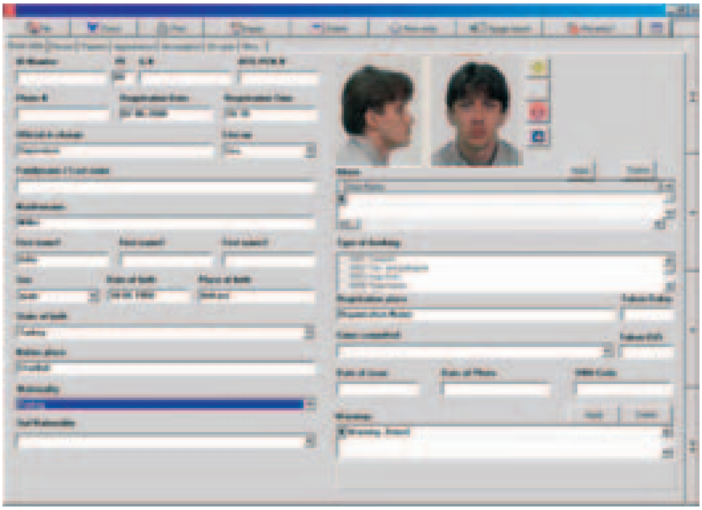

Previous entry search

Each new entry to the database starts a comparison of existing similar data. If comparing data are found, the system displays all found entries including the mug photos. The different entries can be merged to one record for one person. Before starting the merging procedure the operator can determine which data fields should be overwritten or kept.

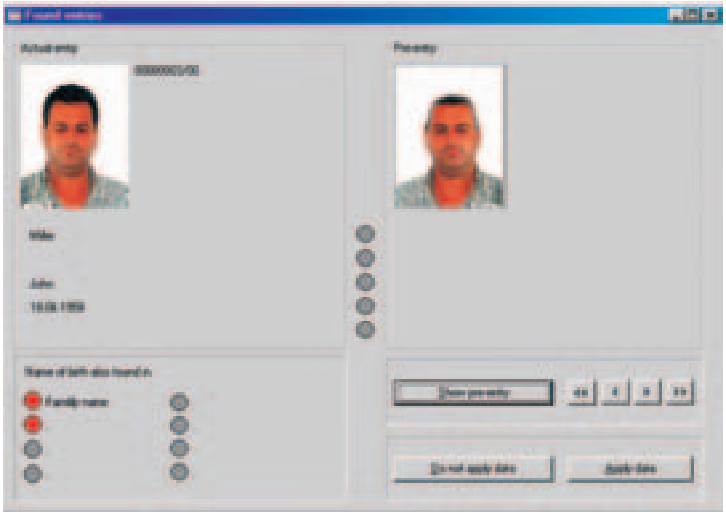

Electronic file & Windows Media Player

The entire booking process, the creation of LIVE video sequences (image and sound e.g. during registration) along with personal data and any measures that have been taken are all an integral part of a designated electronic computer file that can be saved. All common multi-media formats are supported.

International standards

FACES supports all relevant national and international standards, like for the image files the NIST standard type 10.

Image formats

Basically all dimensions of image formats can be processed. With network versions FACES offers different image qualities in a resolution which does not affect the speed of the net. For administrative work pictures can for example be used only in reduced dissolution (106x142). Also user-defined formats can be stored, indicated and processed.

Queries

FACES offers comprehensive search functions, e. g. photo queries or search for physical characteristic data files. In addition to standard queries, the user can create custom queries with unlimited self-defined conditions, using AND/OR/NOT operators. Whenever selecting a filter condition, the preview of the query results will appear on the screen. This enables the user to modify the query conditions without actually having to run a query.

Line Up

FACES enables the detective to obtain a line-up by running a query against the photo database and to project a photo selection onto the witness' monitor (Figs. 2–3) in various line-up formats and it is also possible to show different profiles. For the line-up procedure FACES 9.0 offers the possibility to determine whether 7, 11 or 14 comparison photos should be displayed for the line up.

Fig. 2: Suspect's photo

Fig. 3: Line-up

During detective review versus witness viewing sessions the operator can display descriptive data on his screen. On the witness' monitor, the position of the suspect's photo is changed in different steps and the corresponding witness' statement is also integrated into the respective electronic file. The conducting of a picture line-up on the screen with FACES is fast, more effective and the endurance, patience and power of recollection on the part of the witness is less strenuous.

Printouts

FACES offers various print functions. Aside photos also individual lists can be user defined created and printed.

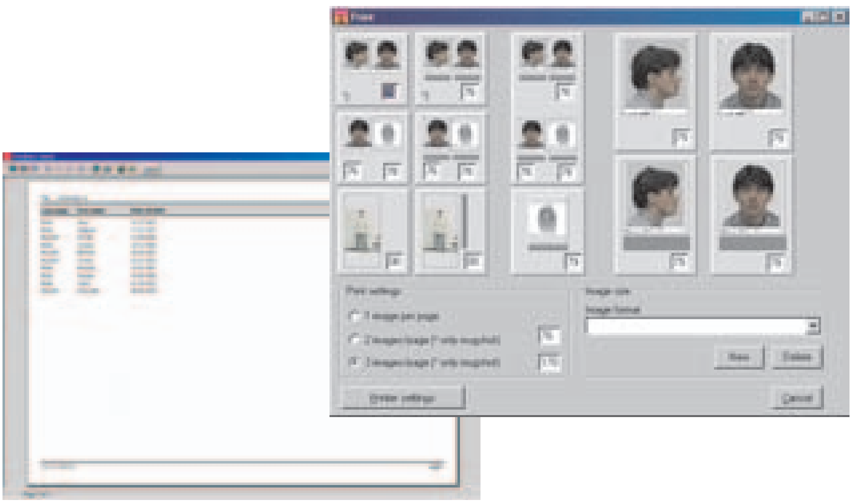

Forms

The workload at any agency, especially follow-ups like the completion of forms is being handled more efficiently. FACES allows create custom forms or letters using MS Word. This feature offers handy tools to supply original forms with data entry forms or to create any number of custom forms. Data fields from the basic data entry form are automatically transferred into the forms. The Supervisor can determine whether a form should be write-protected or not. Together with the personal data also photos can be integrated into an individual created word form.

Statistics

FACES also has an statistics module. By running a query, the detective can for example create the results of the statistic for the actual working month. He can make any statistics with any evaluation type and can also make any statistics a standard statistic by giving it a name. Such a standard evaluation type can be used again and again by opening the statistic by its file name.

Logs

FACES automatically generates a log of all editing steps. The contributor's number, date, time, and edit step (and if applicable, the number of the edited records) are saved in this log. All logs can be printed out. With a selection function selections can be made from the entire file. Several criteria are at the user's disposal.

Mail function

To send photos to other agencies or departments, FACES has a photo-send function. That can be done by mail or – if available – through the Internet or other electronic mail. By simply calling up the electronic file and clicking the appropriate photo(s) the feature will be activated and only the address has to be filled out by the operator.

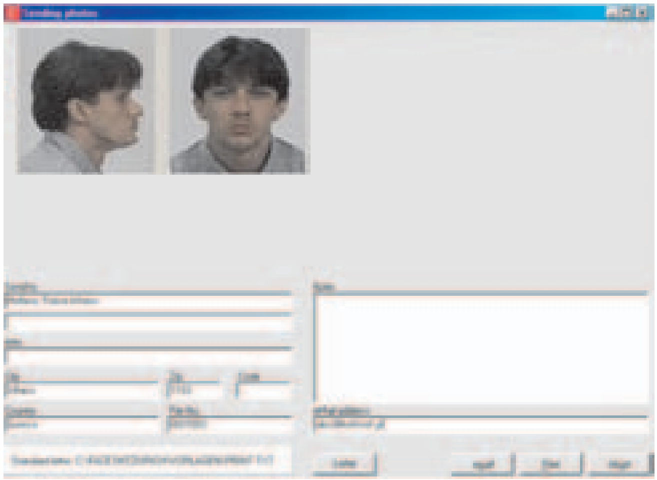

Authorized Personnel

FACES has access rights that can be defined individually. The user can determine different access rights for his personnel depending on the level of confidentiality of the documents and can also determine several levels, e. g., *date from – to*, *time from – to* or *day*. This provides you with the advantage that you can determine which of your co-workers may be granted complete or temporary access to various documents.

WEB Browser

FACES offers an integrated WEB Browser as a gateway to Internet or Intranet sources. This browser can also be used to get access to other user owned WEB-IT applications, e. g. an AFIS system to display data and images or to interact with *www-data or information bases.*

Advanced integration/transfer between Faces and Phantom
After a photo inquiry session with a witness the complete photo inquiry result (multiple images) can be transferred to Phantom and used for a composite creation. Thus created composite can be stored in the electronic file and be used to search for similar photos in the database FIRE_FACECHECK).

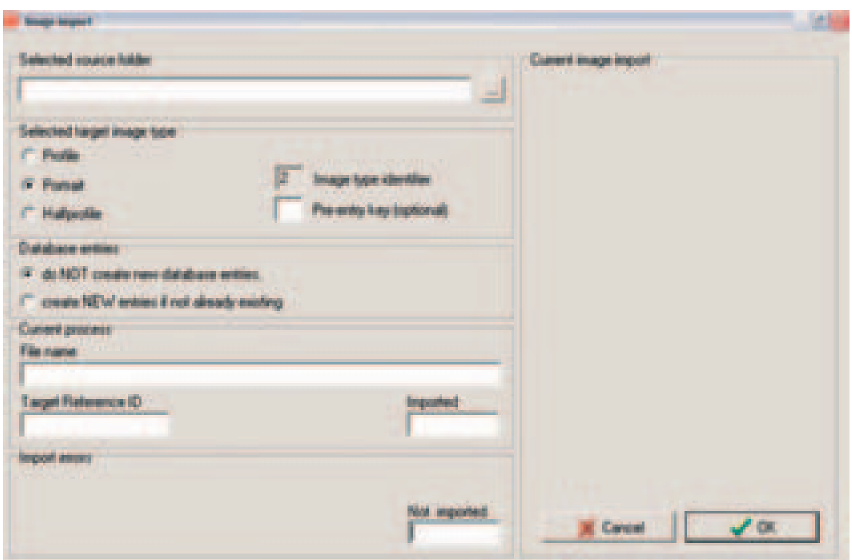

New photo import function
In order to import images to the database FACES 9.0 enables to make a mass image import even when there is not yet an entry in the database.

4. ISIS PHANTOM

All the photos of the basic data are described as attributes, e. g., sex, age, etc. Furthermore, all photos of the basic data are segmented, meaning that all essential parts of the face: eyes, hair, nose, mouth, chin, and any special characteristics of the face, such as scars, etc., are saved as polygons and are available as individual segments. This allows you to quickly and easily create police sketches.

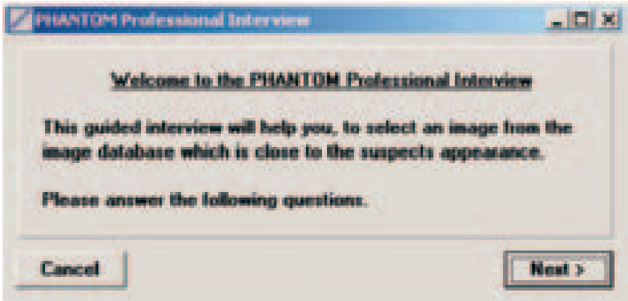

Phantom Professional is a unique photo-based composite software for suspect identification, face reconstruction or up-dating photos from known suspects.

The system is available from a stand-alone PC or Notebook to a wide area network solution in client-server architecture and utilizes off the-shelf hardware that complies with open industry standards.

The archives can store Portrait, Profile or Half-Profile Images.

Phantom Profeessional offers two operation mode: RGB or Greyscale image processing and the option to determine whether full images or facial elements should be displayed to the witness during creation of a composite.

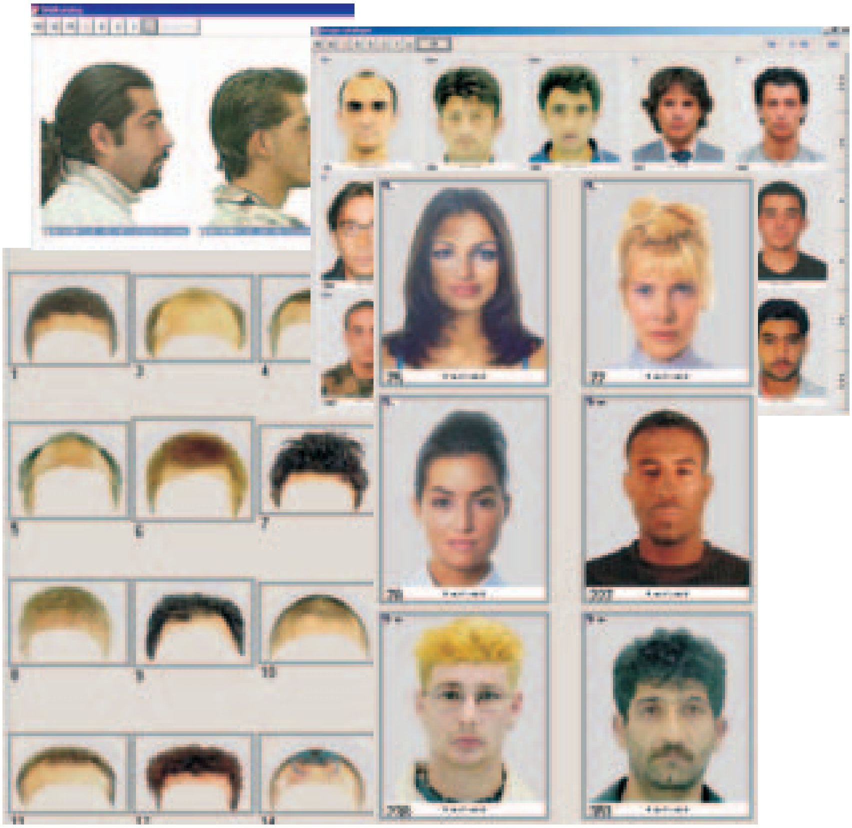

Creation of a Composite

PHANTOM was developed for police work where a witness' statement gives a description of the suspect. Based upon this description, a query can be run according to a given basic photo. This basic photo can be changed in its own segments at any time or by modifying it with segments obtained from reference photos that are not part of the basic photo as illustrated below.

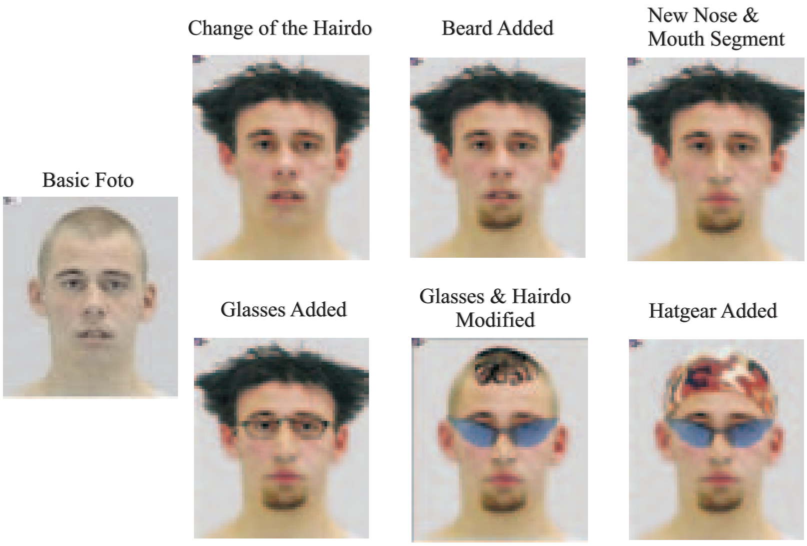

Enhanced tools with multiple options

Enhancement of transparency, blending and magic wand. The blending tool offers an advanced transparency function, which allows any kind of retouching in a fast and very effective way as illustrated alongside.

Clipboard-Switching

Offers placing a particular work state in another Windows based software application, e.g. Photoshop for further processing and when finished this altered state can be transferred back to Phantom.

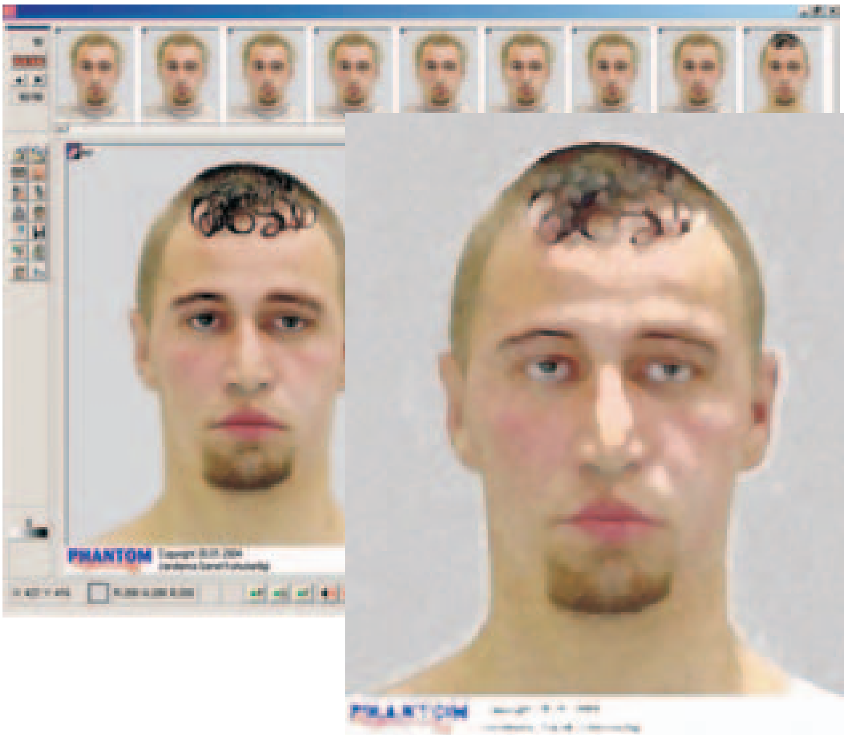

Fig. X Image altered with a Photoshop "artistic" filter

Interactive Work Step Gallery

The Interactive Work Step Gallery allows the operator to jump to any recent state of the image created during the current work session. Each time a change to an image is applied, the new state of that image is added to the gallery.

While copying and/or rotating a part of an image, each of those stages is displayed separately in the gallery. The user can then select any of these stages, and the image will revert to how it looked before the change. The operator can call up this step as current image.

All states are automatically saved and are available for future reference.

Aside this an undo-storage is available, in order to call up any action for- or backwards.

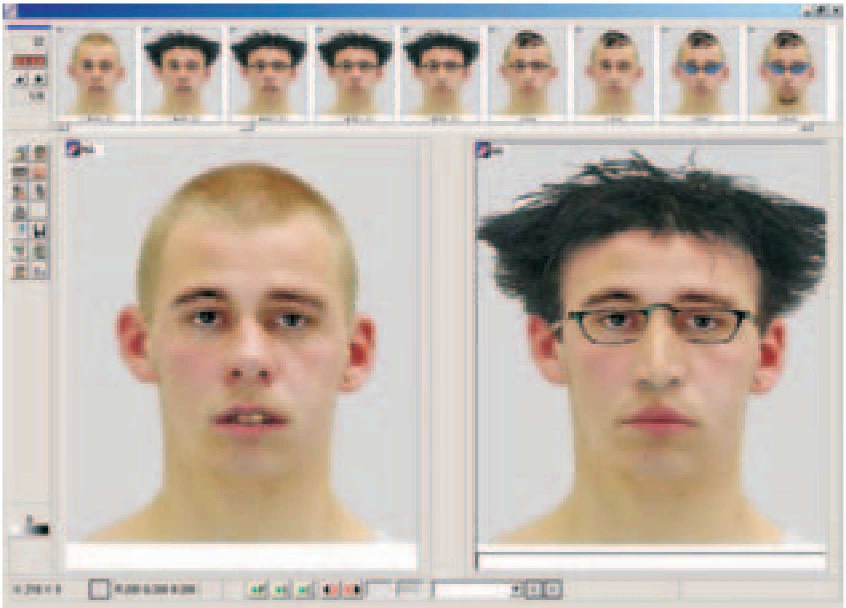

Aging

To age or juvenile a face is one of the specialities of PHANTOM. The XP version offers an unequalled comfort for aging. The system can either create automatically 6 different aging states for on-screen viewing.

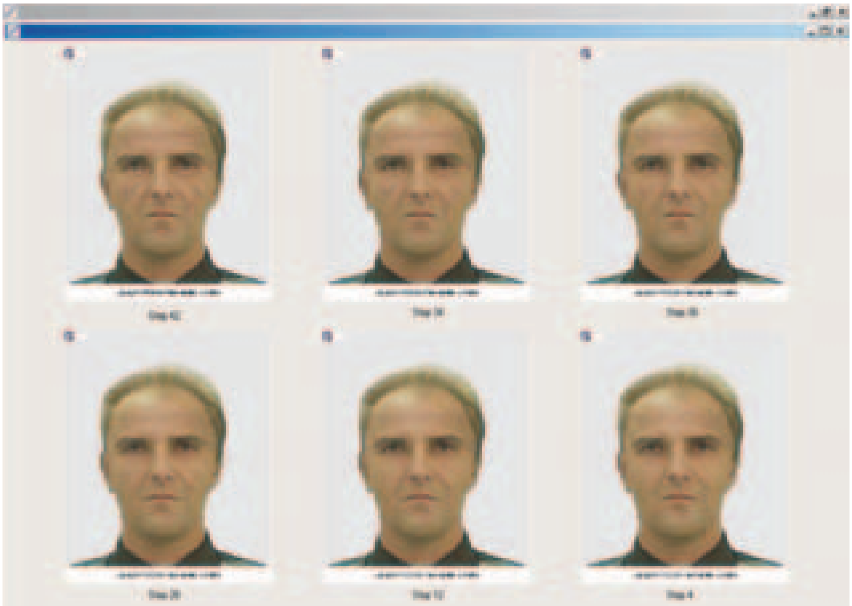

Automatically created aging states.

Original

In addition the operator can call up the aging process

Original Individually created aging states.

Inquiry result management

Together with a chosen basic image the operator is enabled to transfer certain reference pictures to the composite creation in order to obtain particular details from reference photos that are not part of the basic photo.

This selection will remain as start selection during the entire production, even if further searches were accomplished. These queries can be stored under a designator, this enables the officer to change during the production between these selections back and forth without having run another query.

Facial reconstruction

The XP version includes tools to develop facial reconstruction, for instance faces with injuries. The facial reconstruction, especially started from a skull, is one of the extraordinary techniques offered from the optional reconstruction module for Phantom Professional: Phantom Rebuilder as illustrated below.

Creation of virtual line-up collections

PHANTOM 9.0 offers a special function to create a line-up. After importing the suspect's photo 7,11 or 14 other photos for comparison of which the faces are quite similar for the line up can be chosen. These comparison photos can be modified in order to increase the grade of similarity. During the line-up photos can be mixed manually or by randomisation and can be repeated at any time.

If a separate witness station is available the photos can be transferred to the witness' monitor.

When the line up has been completed, a protocol can be printed to document the corresponding witness' statement.

5.

3D Interaction Tools and Haptic Devices

3D-Interaktionswerkzeuge und haptische Vorrichtungen

CAD enhanced soft tissue reconstruction in forensics with Phantom® 3D Touch – an electronic modeling tool with haptic feedback

Subke Jörg, Wittke Michael

University of Applied Sciences Giessen-Friedberg, Biomechanics Lab, Germany

Abstract

Computerized methods gradually gain ground in the field of forensic facial reconstructions (Subke et al. 2000, Subke and Wittke 2004). A new approach to computer enhanced procedures in soft tissue reconstruction is based on the functionalities of the software Freeform® and the touch-based input device Phantom® 3D Touch by SensAble Technologies Inc®.

The combined features of Phantom® 3D Touch and Freeform® allow on the one hand the digital freehand sculpturing and crafting of objects and on the other hand digital 3D construction.

Starting point of the reconstruction is the individual digital model of the scull scanned with the help of Streifenlichttopometrie (SLT) that includes all individual landmarks on the scull's surface that are essential for the accuracy of the reconstruction.

In contrast to other computerized methods, digital construction with Phantom® 3D Touch includes haptics. Digital assemblies, their shapes (curves, edges) or physical properties (softness, smoothness, firmness) representing bones or soft tissue material give a haptic feedback on the input device. The materials' properties can be estimated intuitively while working (e. g. cutting, drilling, sculpting, grinding) contours with the Phantom® input device.

In addition CAD functionalities can be used to improve the reconstruction e. g. cross sections through the layers of material can be used to survey the depth of the modeled tissue.

The computerized models allow in addition the fast and precise creation of variations to compensate the lack of bone structure in areas like nose and ears.

Different examples of the application of the new procedure will be presented.

Introduction

Facial reconstruction is the last resource to identify unknown dead persons whose only remains are fragments of bones.

It is the goal of the reconstruction to give the best possible model of the facial features of the unidentified dead person.

The underlying assumption in facial reconstruction is that the skull plays the major role for the actual shape of the face. The soft tissue is considered only as a layer that covers the bones. The ratio of the soft tissue to the skull has been treated in several anthropological studies, where the thickness of the soft tissue was measured at certain points of the skull that are anatomically important. As a result of these studies, it has become apparent that the thickness of the tissue is conditioned by sex, race and age.

Besides these dependent parameters, there are some inherent difficulties of the facial reconstruction method. There are some parts of the face such as ears, eyes and nose that lack an underlying bone structure for the soft tissue; it is therefore impossible to make a precise reconstruction of their shape. This is also the case for the lips. The place of the reconstruction can be estimated by using certain points of the bone formation as a reference, and the lips' shape can be determined by using knowledge of typical racial features (Helmer [1]).

There are still several difficulties the make-up artist has to deal with, because knowledge of details such as haircut, eye color, hair or skin is lacking.

For a valid facial reconstruction, it is imperative to come up with different facial variants

There are several methods to reconstruct a face [2]. Thanks to technical developments, more and more digital three-dimensional methods are available for facial reconstruction. The advantages of these methods are essentially as follows: the possibility to construct rapidly several facial variants and the measurement functions that are used to objectively evaluate the accuracy of a modeled face.

The digital method requires as a first step to digitalize the skull three-dimensionally. To do so, different surface measuring techniques are used, for example laser scanning [3], the holography technique [4], and an optical surface measuring process called "Streifenlichttopometrie" or SLT [5], [6]. In addition, radiological techniques (CT) can be used for the digitalization of the skull [7].

In case only fragments of the skull are available, they can be digitally joined together in the manner of a three-dimensional puzzle [8], [9].

The face then is reconstructed, using the digitalized skull as a basis. There are several techniques currently available to do so.

The morphing method consists in fitting the predetermined surface of the skin onto the underlying skull structure. The skin surface is made up of a multitude of points that are connected by spatial curbs building a grid. These spatial curbs have the ability to incorporate the change of position of one point in the curb, while still maintaining their rounded course. This is how the points of the skin surface are adjusted to the thickness of the soft tissue according to predetermined measures [3], [10].

Another technique for the facial reconstruction is the use of mathematical equivalence transformations [11], [12]. The geometrical discrepancy between the skull of the unknown dead person and a known person is calculated as a mathematical transformation and then applied to the facial surface of the known person. The facial surface of the dead unknown person is reconstructed in this way.

Another method has been developed in the area of molding where three-dimensional modeling tools are used [13], [14]. The 3D-modeling tool developed by Sensable Technologies opens up a new way of facial reconstruction. It offers the possibility to do free digital sculpturing in combination with computer-based construction techniques (CAD) [15]. As a main topic of this article, the new applications of this system for the reconstruction of faces are shown, together with the possible development of new techniques.

Method

For the reconstruction process, the digital 3D modeling tool made by Sensable Technologies is used. The modeling tool consists of the program Freeform and the input device Phantom 3D with which the virtual workpieces are handled.

The Phantom 3D is conceived to "touch" the digital workpieces. This is called haptic feedback.

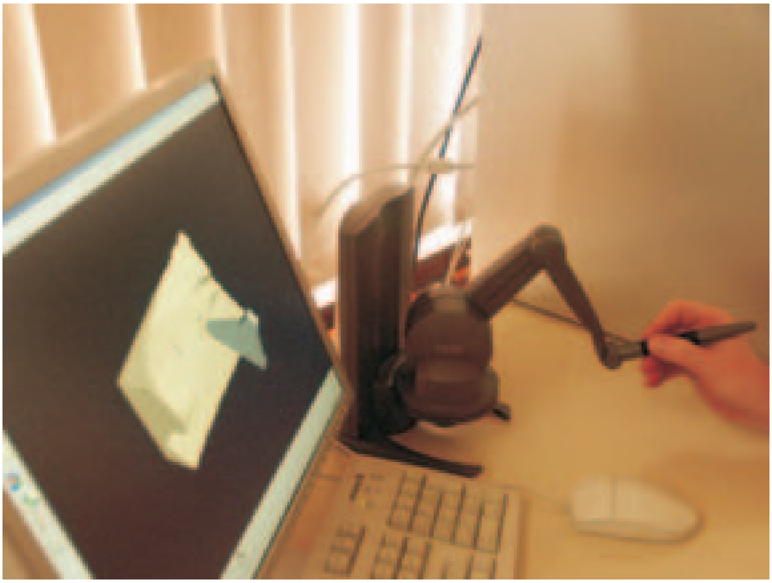

Fig. 1: Phantom 3D tool with the virtually displayed toolhead and clay block.

The Phantom 3D is made of 5 pieces that are connected to each other by 5 swivel joints (fig. 1).

The body that is attached at its end has the shape of a handle that can be moved and turned in space. The position of the handle is measured by the angular positions of the single bodies. This information is transmitted in the digital 3D space and used to illustrate the virtual tool.

A tool head is added to the digital handle, it can be adjusted to different shapes and sizes.

One “touches” the digital work piece in the following way: the distance between the tool attachment and the work piece is continuously measured, and if a contact is made, the Phantom 3D produces the sensation of mechanical resistance.

This resistance is electro-technically produced in the joints, and it blocks further manipulation of the handle, avoiding pushing through the surface of the work-piece. One can only perforate the surface structure of the piece with the tool by using excessive force.

Clay is used as a molding material, its physical qualities such as hardness and granularity are simulated by the program Freeform. It is the resistance towards the Phantom 3D that indicates the digitally simulated hardness of the clay. The granular structure of the clay determines the roughness of the surface that can be “felt” with the Phantom 3D.

The typical tools such as a putty knife, a scraper and modeling tools are available to manually shape the clay. Molding cutters can also be employed.

In addition, it is possible to incorporate CAD-techniques in the modeling process; they work in combination with the manual methods. They allow a metrically accurate manipulation of the clay. As an example, the clay material can be applied in a regular fashion on a predetermined surface using the off-set function.

Several techniques can be used for the visualization of a complex layering of structures. Either one of the following three techniques apply: Certain layers can be faded out, so that only one layer at a time is displayed. It is also possible to show the profile of a structure by cutting it, thus uncovering hidden layers. Another technique is based on the manipulation of the transparency of the layers in order to detect underlying ones. Even the combination of all three techniques is possible.

Several measuring tools for the Freeform program are also available; they can be used for the quality control of the reconstructed layers.

Application

The process of the digital facial reconstruction using Freeform consists in the following steps.

Fig. 2: The clay model of the 3D digitalized skull.

In the beginning of the construction process a skull is modeled in clay, the surface of the skull is recorded using 3-dimensional measuring techniques (SLT, holography) and the data are imported in the Freeform program (fig. 2).

In the next step, the positions of the soft tissue markers are displayed on the skull surface. Since no standard exists currently as to how to apply them, a number of guidelines are used here. For an overview of marker positions and their terminology, see Miller [16].

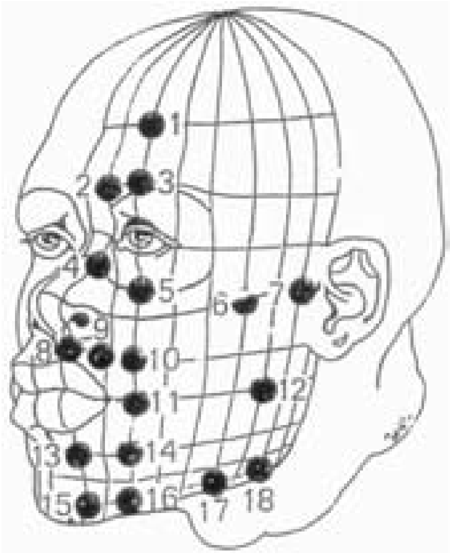

Fig. 3: The position of the markers in accordance with Aulsebrook [17].

Tab. 1: The soft tissue data of El-Mehallawi [18].

Marker	Male			Female		
	Min.	Max.	Mean	Min.	Max.	Mean
1	3,0	5,6	4,18	3,5	5,0	4,24
2	4,2	6,8	5,31	4,0	6,6	5,70
3	3,4	7,1	5,13	4,5	7,2	5,69
4	–	–	–	–	–	–
5	3,3	5,4	4,17	3,6	5,0	4,31
6	5,0	7,8	6,46	6,1	7,8	6,83
7	4,2	7,1	5,75	5,4	6,7	6,07
8	6,0	7,9	7,13	6,6	9,4	7,69
9	4,8	6,7	5,79	5,8	7,8	6,73
10	7,4	11,0	9,33	7,6	11,0	9,19
11	9,2	13,0	10,55	9,4	13,0	10,81
12	10,0	16,0	13,00	13,0	18,0	15,05
13	6,5	8,6	7,55	7,0	9,3	8,21
14	7,0	9,7	8,60	9,7	14,0	11,16
15	4,4	6,2	5,47	6,2	9,0	7,29
16	4,7	8,5	6,78	7,1	8,8	8,00

Marker	Male			Female		
	Min.	Max.	Mean	Min.	Max.	Mean
17	5,9	8,6	7,19	7,3	15,0	8,52
18	9,4	15,0	11,65	11,0	15,0	13,14

Marker positions in this article are based on Aulsebrook [17] (fig. 3), and the thickness of the soft tissue is calculated following El-Mehallawi [18] (tab. 1).

Aulsebrook's method has the distinct advantage that it is based on a grid of coordinates that in turn allows improvements with regard to the positioning of the markers (fig. 3).

El-Mehallawi bases his soft tissue thickness values on the results found for 204 North-African participants in his study (120 men and 84 women), using the positions suggested by Aulsebrook and ultrasound as a measuring technique (fig. 3).

El-Mehallawi notes the smallest values for the front area (M1; men 4.16 mm and women 4.24 mm) and for the infraorbital area (M5; men 4.17 mm and women 4.31 mm); the highest values are found for the cheek area (M12; men 13 mm and women 15.05 mm) (tab. 1).

In the next step of the reconstruction, circular lines are designed around the marker positions using the CAD-function of Freeform. These lines are transformed to markers making use of the emboss function after having entered their height. The markers are placed in a right angle onto the surface. Afterwards, they are numbered following Aulsebrook [17], [18] in order to facilitate their retrieval (fig. 4).

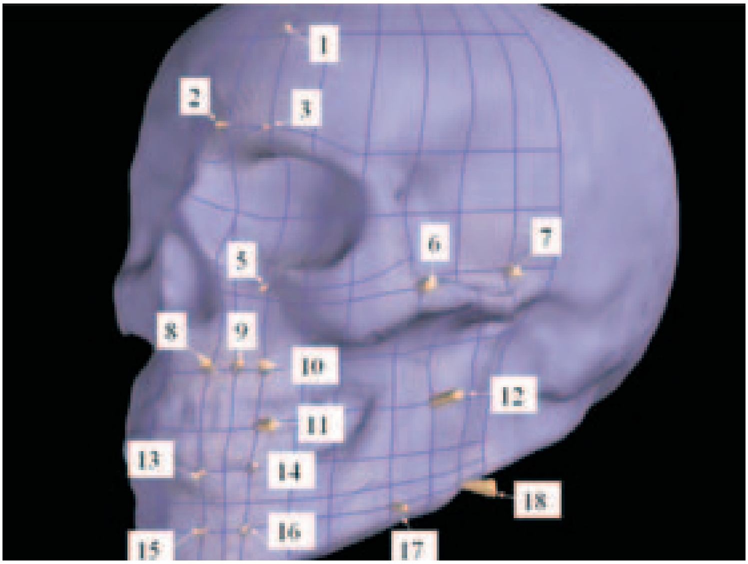

Fig. 4: Applying the grid and the soft tissue markers to the skull surface.

It was impossible to construct marker number 4, since El-Mehallawi did not furnish measurement values for this position [18].

For the reconstruction of the soft tissue layer, the following steps apply:

The facial surface is divided in different areas by the markers. For each area, the soft tissue layers are reconstructed one by one, relying on several CAD functions designed by Freeform.

Then, spatial curbs connect the endpoints of the markers, they serve to delimit a space which than is automatically filled with the soft tissue mass. Since the delineating lines are curbs, the soft tissue mass is somewhat bulged. In case the arching effect is insufficient, one can manipulate the shape of the delineating lines by using markers in between.

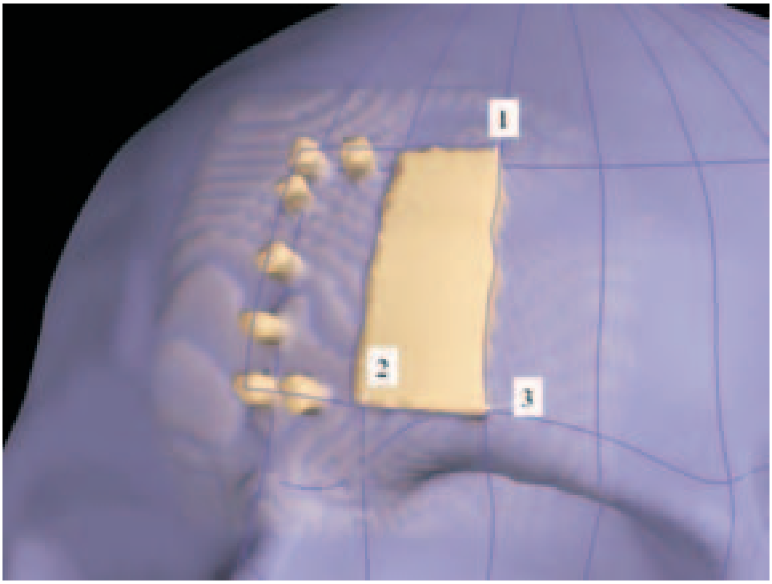

Fig. 5: Construction of the soft tissue layer; soft tissue markers with delineating lines.

Fig. 5 demonstrates the most important steps of the process. Additional markers are created in this area by marker 1 and 2.

Along the horizontal line on which marker 1 (M1) is placed, more markers are placed medially to M1. Since the thickness of the soft tissue layer is essentially the same here, the additional markers have the same height as M1.

The markers that are placed on a horizontal line through marker 2 (M2) and that are positioned medially to M2, are produced in a similar fashion (fig. 5).

The markers between the two horizontal lines along the median-sagittal plane are constructed by using linear interpolation (compare figure 5).

Then, the upper limit of the area to be filled is determined by a spatial curb. This curb is illustrated by a blue-violet color.

In the areas marked 1, 2 and 3, the material has been filled in as described above.

The single parts of the skull are one by one manipulated in this way, from the calotte to the lower jaw (fig. 6–10). To have an overall view, it is possible to make the grid lines visible or invisible, as needed (compare figure 6 and 7).

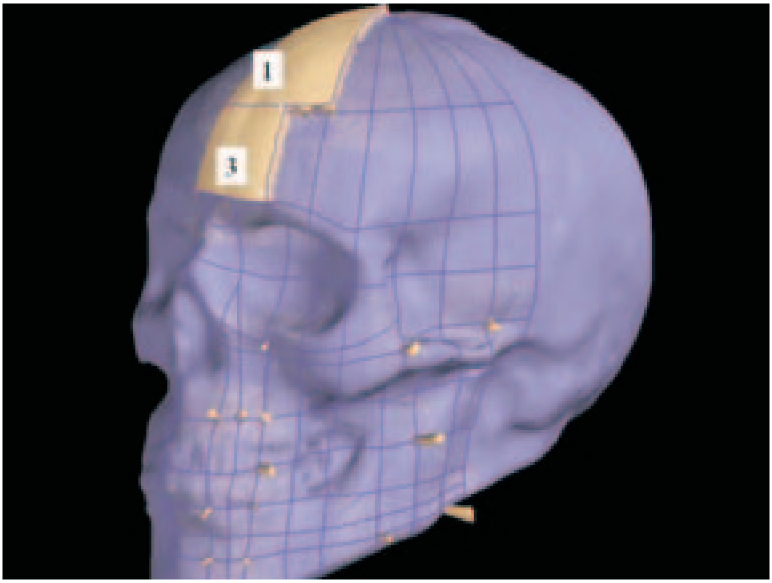

Fig. 6: Construction of the soft tissue layer in the area of the calotte.

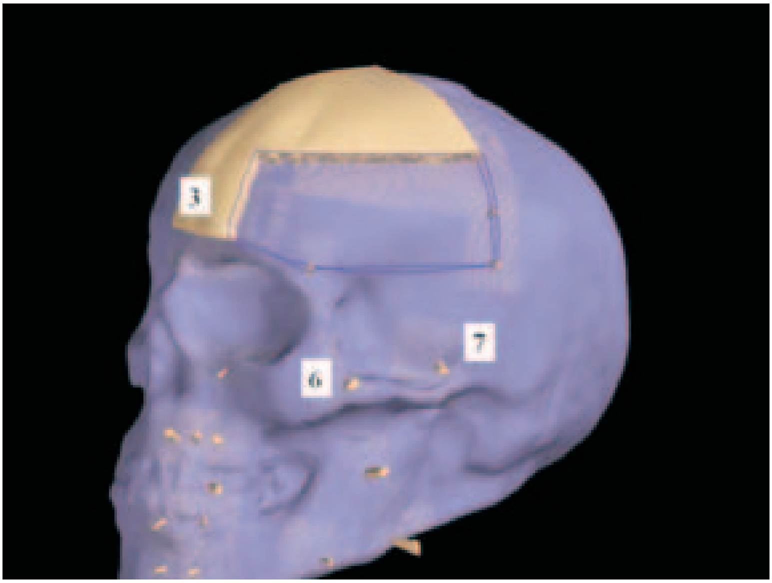

Fig. 7: Construction of the soft tissue layer in the frontal area.

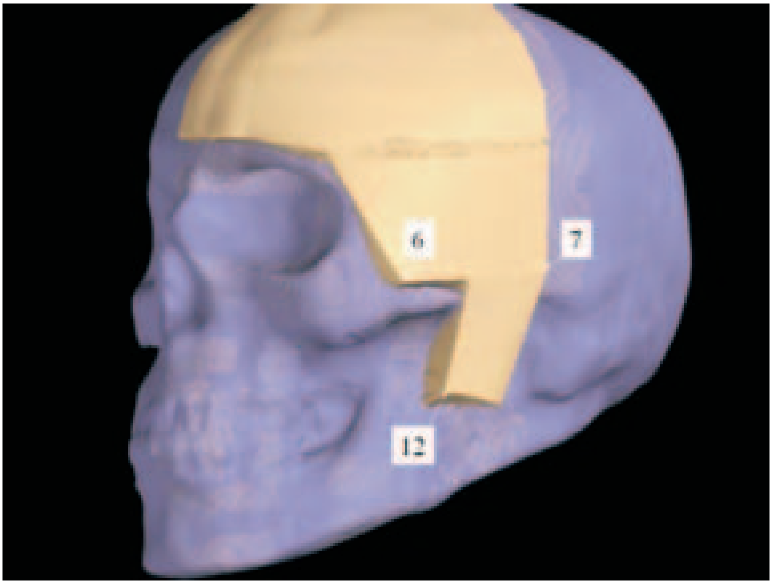

Fig. 8: Construction of the soft tissue layer in the temporal area.

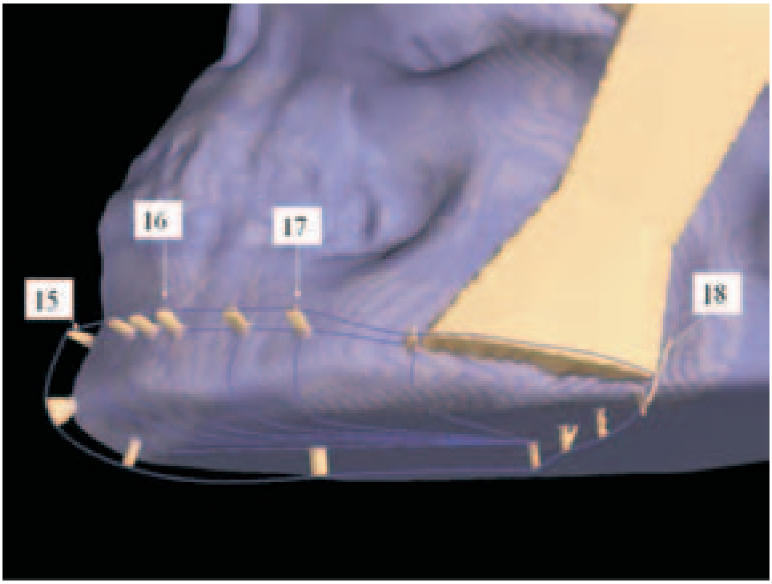

Fig. 9: Construction of the soft tissue layer in the chin area. Shaping of the soft tissue surface by additional soft tissue markers.

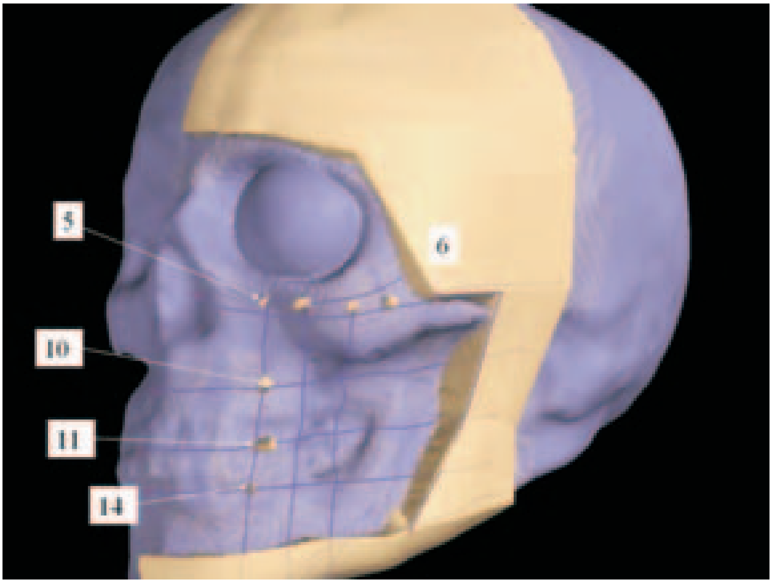

Fig. 10: Construction of the cheek area.

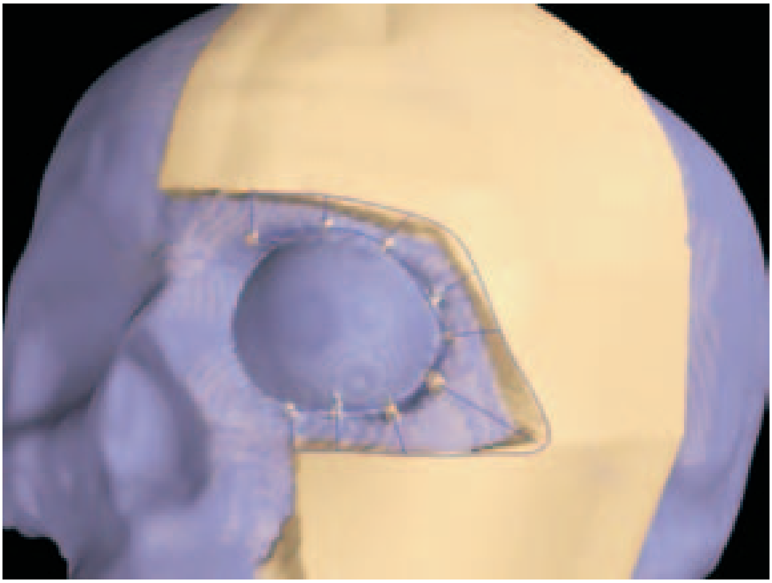

Fig. 11: Construction of the soft tissue area in the orbital area. Subdivision into smaller units.

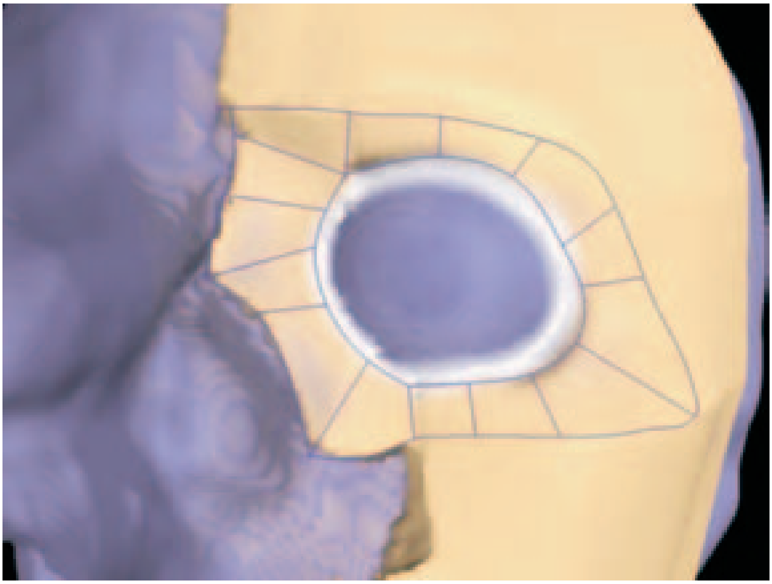

Fig. 12: Units filled with soft tissue in the orbital area.

Fig. 13: Construction of the soft tissue layer in the nose area; modeling of the eyeball.

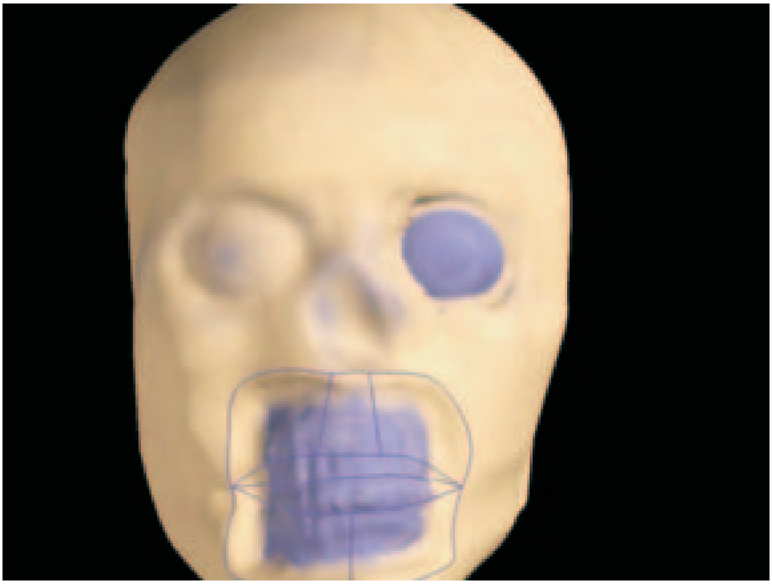

Fig. 14: Construction of the second half of the face.

Fig. 15: Construction of the mouth area. Delineating lines in lip form.

Especially the area around the eyes is divided in smaller units, a method that facilitates the construction of a well-shaped surface (figure 11 and 12). Before doing so, it is recommended to add an eyeball in the orbital area, because this will make it possible to geometrically adjust the soft tissue parts to one another.

Then, the parts around the nose are constructed (fig. 13).

After finishing work on one side of the face, the other side is treated in the same way (fig. 14).

In a next step, the area around the mouth is created. The delineating lines around the subdivided units give the lips their shape. Their profile is constructed using a vertical spatial curb in the median-sagittal plane. Again, it is the arch of this curb that will decide the three-dimensional shape of the lips (fig. 15).

Then, the work on the nose begins. A ready-made nose model is therefore chosen from a 3D library and adjusted to the actual size and proportions of the face by a scaling function. The guidelines designed by Helmer [1] are applied here for the final positioning of the nose.

The simulated clay is used to fill the space in between, which then is sanded with the help of the digital tools. Edges are smoothed down with the molding cutter.

Fig. 16: Modeling of the nose area using a ready-made 3D model.

Fig. 17: Modeling of the ears with ready-made 3D models.

Fig. 18: Adaptation of the ears.

The ears are reconstructed in the same way. Again, some models from the 3D library are chosen and adjusted to the ear canal (figure 17 and 18). No detailed guidelines apply here due to the absence of an underlying bone structure.

It is reasonable to create three different versions of a face for comparative purposes. The shape of the nose is usually modified for each one of them, and two different pairs of ears are used (compare figure 19 and 20).

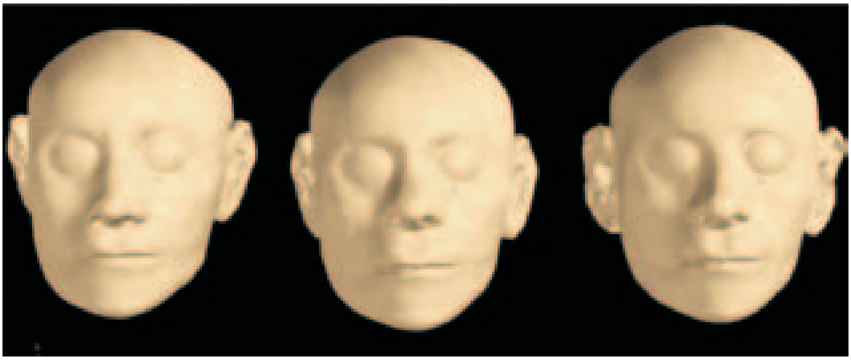

Fig. 19: Facial variants (frontal); 3 different noses and 2 different pairs of ears.

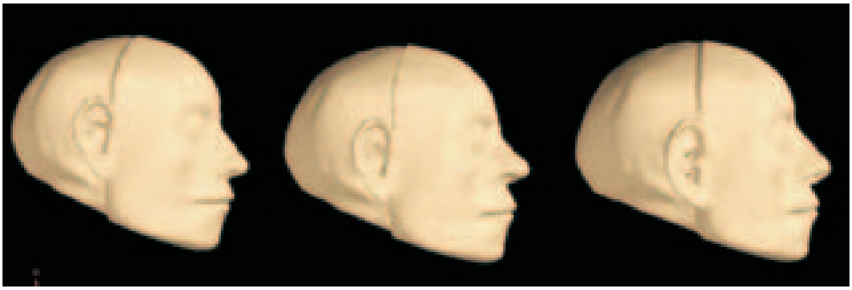

Fig. 20: Facial variants (lateral); 3 different noses and 2 different pairs of ears.

Fig. 21: Modeling of the eyes.

In the final step, the area around the eyes is shaped. A pair of closed eyes is chosen from the digital library, and they are fitted in according to the guidelines of Helmer [1] (fig. 21). Once again, the digital tools are used for covering and smoothing the space in between.

Another case is described below, showing the reconstruction of the face of a middle-age woman.

The skull has been recorded using computer tomography. Due to recording artefacts, the teeth in the front upper jaw area could not be represented in their entirety. The occlusion has been reconstructed based on the lower jaw joint and the molar teeth (fig. 22).

Fig. 22: Model of the skull of a middle-aged woman.

The soft tissue construction also makes use of the markers (Aulsebrook [17]) and takes El-Mehallawi's soft tissue thickness values into account [18]. Two variants of the face are reconstructed. The soft tissue thickness values for women and men are used, as well as sex-specific models of noses, ears, eyes and mouths. The male variant is constructed for a comparison test.

A comparison between the soft tissue data shows that higher values apply for the women as compared to the men (only exception: M10) (tab. 1).

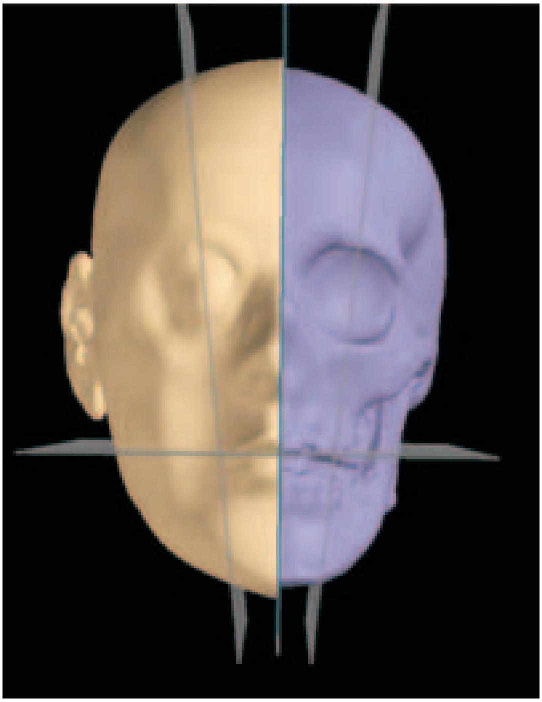

Fig. 23: Reconstruction of the mouth based on Stephan [19].

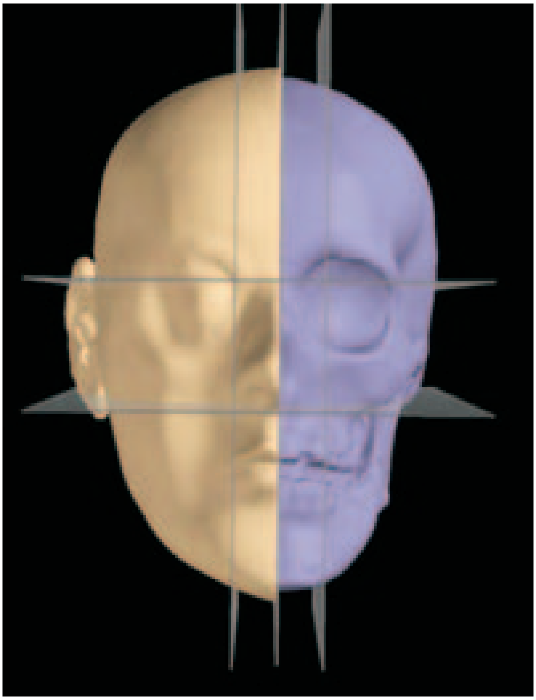

Fig. 24: Reconstruction of nose length based on George [20], nose breadth based on Helmer [1] (frontal view).

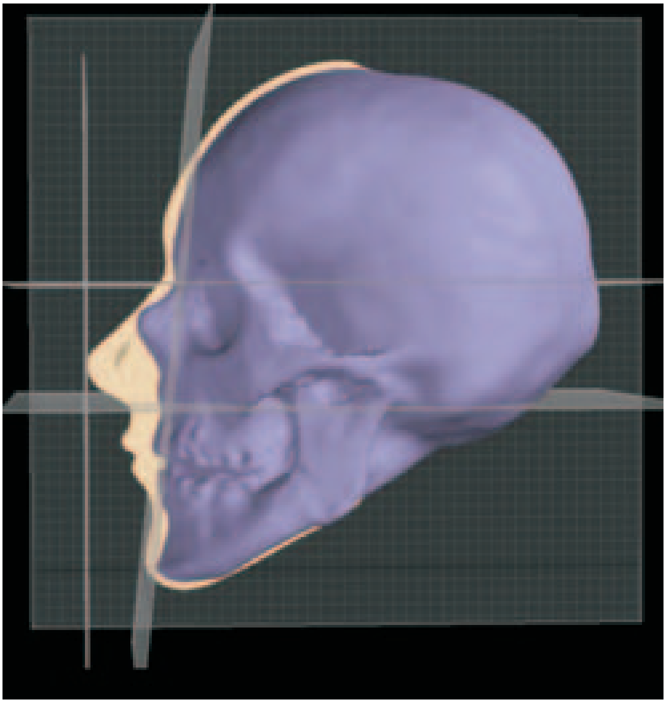

Fig. 25: Reconstruction of nose length based on George [20], nose breadth based on Helmer [1] (lateral view).

For the first facial variant, the data and models for women are employed. A model is used for the reconstruction of the mouth and is scaled and adjusted following the guidelines of Stephan [19] (fig. 23) whose study is based on a survey of 123 participants.

Another model is used for the nose and is adjusted according to George's guidelines [20] that are thought to be more accurate than those of Gerasimov [21], Krogman [22] and Prokopec/Ubelaker [23] (Stephan [24], see figure 24 and 25). The breadth of the nose is adjusted according Helmer [1].

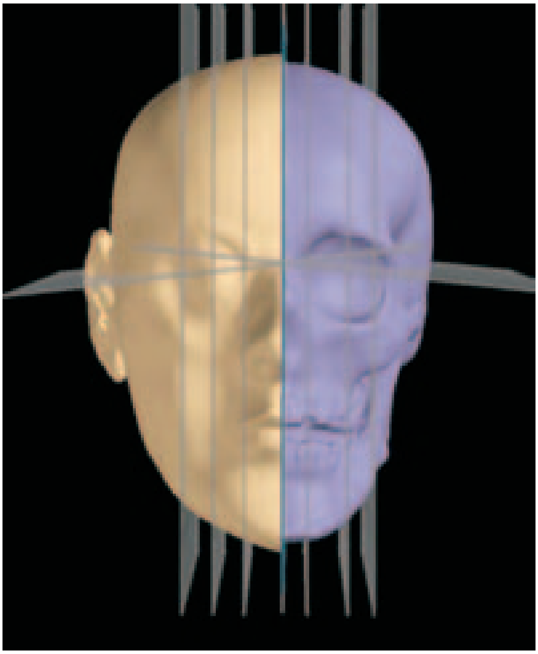

Fig. 26: Reconstruction of the eyes based on Helmer [1].

Fig. 27: Reconstructed female face.

Again, a model from the digital library is used for the reconstruction of the eyes. The chosen pair of eyes is modified following Helmer [1] whose work is based on Gatliff [25] and Rid [26] (fig.26).

The ears are reconstructed using another 3D model, they are fitted into the ear canals (fig. 27).

For the second facial variant, the soft tissue values for men are used (El-Mehallawi [18]). The male models for mouth, nose, ears and eyes are chosen from the 3D library (fig. 28).

Fig. 28: Reconstructed male face.

Discussion and prospect

Several techniques for the facial reconstruction based on the 3D modeling tool Freeform are shown in this article. Two skulls formed the basis for different facial variants that have been constructed for comparative purposes.

The strong impact of the skull bone on the facial surface is clearly seen in the reconstructed face number 1. The skull is characterized in the lower jaw area by a lack of symmetry with regard to the median-sagittal plane, an asymmetry that further projects into the soft tissue area and eventually on the facial surface.

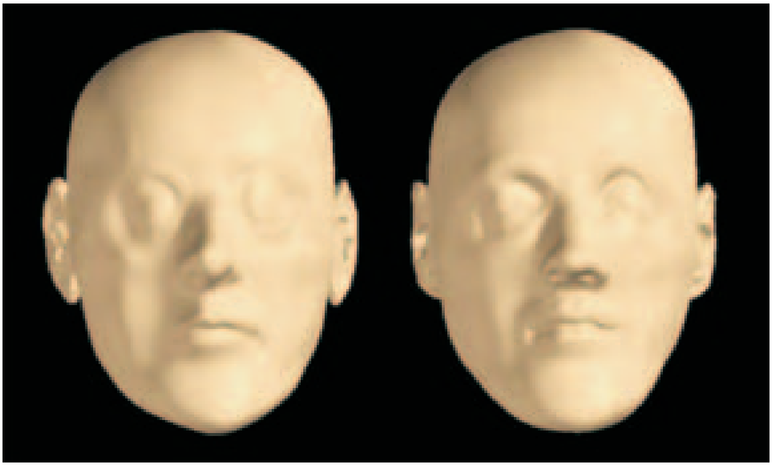

Fig. 29: Comparison of the female face with the male face.

Skull number 2 has a more pointed chin compared to number 1, and a bigger angle in the ramus area (see figure 4 and 25). In addition, the back of the head is more rounded, a feature that is not considered any further in this article.

One can clearly see the effect of differing soft tissue values in the next variant, where female tissue values are applied to skull number 2 (El-Mehallawi [18]). The most important discrepancy is noted in the cheek area. The application of female soft tissue values usually results in a fuller filled and softer face.

The impact of different skull shapes on the facial surface is clearly seen by comparing face number 1 and 2 (fig. 29). In both cases though, the same soft tissue values have been used.

The influence of the form of the nose and ears on the face as a whole is shown in figure 19 and 20, where different male 3D models have been used with little variation as to their shape. Fig. 29 of skull 2 demonstrates the effect of the 3D models that have been chosen according to sex.

The high quality of the reconstruction is readily shown by the comparison of a reconstructed face with the original photographical portrait of the person [27] whose skull data have been used (see figure 30).

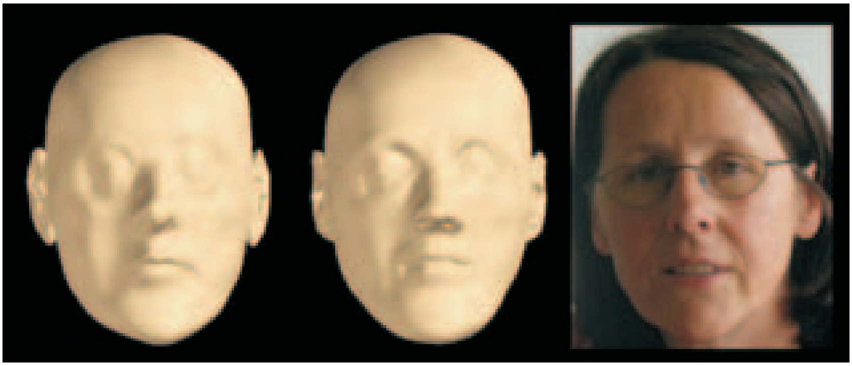

Fig. 30: Comparison of the modeled faces with the original photographical portrait of the person.

To summarize, the digital methods for facial reconstruction have several advantages.

It is possible to immediately copy the constructed facial variants, without further manipulation of the models as required for most other methods.

Each step of the reconstruction process can be directly corrected, since they are recorded separately.

It is also possible to digitally save intermediate stages of the model in order to develop a higher number of facial variants.

Using other digital methods (SLT, holography), one can construct entire 3D libraries containing parts of the face parts that will allow for future use of the corresponding noses, eyes, ears and mouths for the modeling of facial variants. Efficiency of time is a major advantage here.

These methods also apply to make-up work. Freeform can be used to model different types of haircuts that can subsequently be stored in a 3D library.

Virtual methods of measurement can be applied to evaluate the reconstructed faces. They can be employed thanks to the CAD qualities of Freeform.

In figure 25 a profile is shown in the sagittal plane where the modeled soft tissue thickness values can be measured with metrical accuracy. Objective evaluation criteria are thus created.

The proposed modeling technique that consists of a combination of digitalized freehand sculpturing and computer based programs offers new ways for facial reconstruction. Due to its numerous advantages, there is a strong likelihood for its future importance.

References

[1] Helmer R., Identifizierung unbekannter, unkenntlicher Leichen mittels bildtechnischer oder rekonstruktiver Verfahren. In: Identifikation unbekannter Toter. Leopold D., Reihe: Arbeitsmethode der medizinischen und naturwissenschaftlichen Kriminalistik. Band 22, Schmidt-Römhild Verlag, Lübeck, 1998.

[2] Vanezis P., Vanezis M., Cranio-Facial Reconstruction in Forensic Identification – Historical Development and a Review of Current Practice. Medicine, Science and the Law, Vol 40, No. 3 July 2000.

[3] Vanezis, P., Blowes, R. W., Linney, A. D., Tan, A. C., Richards, R. and Neave, R. (1989). Application of 3-D computer graphics for facial reconstruction and comparison with sculpting techniques. Forensic Sci. Int., 42, 69–84.

[4] Ladrière N., Frey S., Thelen A., Hirsch S., Bongartz J., Giel D., Hering P., Ultraschnelle holografische Gesichtsprofilvermessung mit vollautomatischer Hologrammentwicklung. In: Hartman, Kohl-Bareis, Hering, Lonsdale, Bongartz, Buzug (Hrsg.) Aktuelle Methoden der Laser- und Medizinphysik. VDE-Verlag 2004.

[5] Subke, J., Wehner H. D., Wehner F. and Wolf H., Wundtopographie mittels Streifenlichttopometrie. Rechtsmedizin Supplement I zu Band 8, 1998.

[6] Subke, J., Wehner, H. D., Wehner, F. and Szczepaniak, S. (2000). Streifenlichttopometrie (SLT). A New Method for a 3-Dimensional Photorealistic Forensic Documentation in Color. Forensic Sci. Int., 113, 289–295.

[7] Seitz H., Tille R., Rider R., Irsen S., Bermes G., Rapid Prototyping Models for Facial Reonstruction. Presented at 2nd International Conference on Reconstruction of Soft Facial Parts. Remagen, March 2005.

[8] Subke J, Zeller M, Wehner HD, Wolf H (2000): Digital 3D reconstruction of skulls from fragments using Streifenlichttopometrie (SLT) and a special DNA method. 9th Biennial Scientific Meeting of the Craniofacial Identification Association, Washington. Forensic Science Communications Vol. 2, No. 4, Oct. 2000.

[9] Subke J., Digital 3D reconstruction of skulls from fragments using SLT and CAD/CAM tools. In: Computer-Graphic Facial Reconstruction – Ed. By M Marks and J Clement, Elsevier, 2005. In press.

[10] Evison M. P., Presenting Three-Dimensional Forensic Facial Simulations on the Internet Using VRML. Technical Note. J. Forensic Sci, 44(6): 1219–1223, 1999.

[11] Nelson, L. A. and Michael, S. D. (1998). The application of volume deformation to three-dimensional facial reconstruction: A comparison with previous techniques. Forensic Science Int, 94 167–181.

[12] Quatrehomme, G., Cotin, S., Subsol, G., Delingette, H., Garidel, Y., Grévin, G., Fidrich, M., Bailet, P., Ollier, A. (1997). A fully three-dimensional

method for facial reconstruction based on deformable models. J Forensic Sci 42 (4): 649–652.
[13] Knie I., Realisierung eines Messaufbaus zur Annahme und Modellierung von 3D-Modellen mit den Systemen der Firma ABW und Sensable. Studienarbeit, Fachbereich Krankenhaus- und Medizintechnik, Umwelt- und Biotechnologie, Fachhochschule Giessen-Friedberg, 2004.
[14] Moscheik J., Anwendungsmöglichkeiten des 3D-Modellierprogramms Freeform™ für die Orthopädie-Technik an ausgewählten Beispielen. Studienarbeit, Fachbereich Krankenhaus- und Medizintechnik, Umwelt- und Biotechnologie, Fachhochschule Giessen-Friedberg, 2004.
[15] Subke J., Wittke M., Digitale 3D Methoden in der Schädel- und Gesichtsrekonstruktion für die Identifikation unbekannter Toter. 13. Internationales Kriminaltechnik-Seminar, Proceedings, Villingen-Schwenningen Sept. 2004.
[16] Miller K. W. P., Taister M. A., Turner W. D., Tu P., Kelliher T. P., Brown R. E., A Survey of Tissue-Depth Landmarks for Facial Approximation. Forensic Communications Vol. 6, No. 8, 2004.
[17] Aulsebrook W. A., Becker P. J., Iscan M. Y., Facial Soft-Tissue Thickness in the Adult Male Zulu. Forensic Sci. Int. 19, 83–102, 1996.
[18] El-Mehallawi I. H., Soliman E. M., Ultrasonic Assessment of Facial Soft Tissue Thicknesss in Adult Egyptians. Forensic Sci. Int., 117, 99–107, 2001.
[19] Carl N. Stephan. Facial Approximation: An Evaluation of Mouth-Width Determination. Am J Phys Anthropol 121: 48–57, 2003.
[20] George RM. 1987. The Lateral Craniographic Method of Facial Reconstruction. J Forensic Sci 32: 1305–1330.
[21] Gerasimov M. 1971. The Face Finder. London: Hutchinson & Co.
[22] Krogman WM. 1962. The Human Skeleton in Forensic Medicine. Springfield, IL: Charles C. Thomas.
[23] Prokopec M, Ubelaker DH. 2002. Reconstructing the Shape of the Nose According to the Skull. Forensic Sci Commun 4. p 1–4.
[24] Carl N. Stephan, Maciej Henneberg, and Wayne Sampson. Predicting Nose Projection and Pronasale Position in Facial Approximation: A Test of Published Methods and Proposal of New Guidelines. Am J Phys Anthropol 122: 240–250, 2003.
[25] Gatliff B.P, Snow C. C., From Skull to Visage. J. Biocommun. 6, 27–30, 1979.
[26] Rid B., Die Tiefenlage der Augen. Diss. Erlangen 1937.
[27] Hering P., (Private Communication) March 2005.

CAD-gestützte forensische Weichteilrekonstruktion mit Hilfe des Phantom 3D-Touch – ein elektronisches Modellierwerkzeug mit haptivem Feedback

Jörg Subke und Michael Wittke

Fachhochschule Gießen-Friedberg, Biomechanik-Labor, Deutschland

Abstract

In der forensischen Gesichtsrekonstruktion werden immer mehr computergestützte Verfahren eingesetzt. Einen neuen Zugang zur digitalen Gesichtsmodellierung bietet das elektronische Modellierwerkzeug Phantom 3D Touch, das sowohl die handwerkliche Skulpturierung wie auch das CAD-Konstruieren unterstützt.

Auf der Basis der Funktionalitäten des Programms Freeform und der Eigenschaften des handgeführten Werkzeugs Phantom 3D-Touch wurde eine Verfahrensweise für die Weichteilrekonstruktion entwickelt. Dazu wurde ein Schädel mit Hilfe der Streifenlichttopometrie 3-dimensional gescannt und digital bearbeitet.

Freeform unterscheidet sich von anderen digitalen Werkzeugen durch die Einbeziehung der Haptik, mit der digitale Werkstücke „begreifbar" werden. Die Formen (Rundungen und Kanten) und die Festigkeit (Weichheit, Härte) der digitalen Schädel und Weichteilmassen werden mit dem handgeführten Phantom3D-Werkzeug ertastet.

Die Festigkeit der aufgetragenen Weichteilmasse macht sich dabei über die Kraft bemerkbar, die beim Bearbeiten (Schneiden, Bohren, Verformen, Schleifen) der Gesichtskonturen mit dem Werkzeug Phantom3D aufgewendet werden muss.

Zusätzlich werden bei der Rekonstruktion CAD-Funktionen eingesetzt, mit denen beliebige Profilschnitte durchgeführt und die modellierten Weichteildicken geprüft werden können.

Weitere Vorteile der digitalen Verarbeitung ergeben sich bei der Untersuchung von Gesichtsvarianten, die aufgrund der fehlenden knöchernen Strukturen im Nasen- und Ohrenbereich erstellt werden müssen.

Anhand zweier Beispiele wird das entwickelte Verfahren vorgestellt. Im ersten Beispiel werden die Techniken vorgestellt und im zweiten Beispiel werden die Techniken in einem Blindversuch validiert.

Einleitung

Bei unbekannten Toten, von denen nur noch die knöchernen Überreste vorhanden sind, ist die Gesichtsrekonstruktion das letzte Mittel, um eine Identifizierung zu erreichen. Ziel der Rekonstruktion ist es, die Gesichtszüge des unbekannten Toten möglichst genau zu modellieren.

Grundsätzlich wird bei der Rekonstruktion des Gesichtes davon ausgegangen, dass der Schädel den maßgeblichen Anteil an der Formgebung des Gesichtes hat, während das Weichteilgewebe nur noch als eine den Knochen bedeckende Schicht betrachtet wird.

Der Zusammenhang zwischen Weichteilschicht und Schädel war Gegenstand verschiedener anthropologischer Untersuchungen, in denen die Weichteildicke an charakteristischen anatomischen Stellen des Schädels gemessen wurde. Die Untersuchungen ergaben, dass die Weichteildicken geschlechts-, rasse- und altersabhängig sind.

Neben diesen abhängigen Größen gibt es prinzipielle Schwierigkeiten bei der Rekonstruktion des Gesichtes. Überall dort, wo keine knöchernen Strukturen vorhanden sind, fehlen die weichteilprägenden Unterlagen und damit die Möglichkeiten einer genauen Rekonstruktion der Formen. Dies gilt für die Ohren, die Augen und die Nase. Ebenso kann die Form der Lippen nur über die typischen Rassemerkmale bestimmt und die Konstitution anhand der Knochenausbildung an bestimmten Stellen abgeschätzt werden (Helmer [1]).

Darüber hinaus gibt es noch weitere Schwierigkeiten bei der maskenbildnerischen Arbeit, die aufgrund fehlender Informationen über die Frisur und der Farben von Augen, Haar und Haut auftreten.

Die einzige Möglichkeit eine sinnvolle Gesichtsrekonstruktion durchzuführen ist, verschiedene Gesichtsvarianten aufzubauen.

Zur Gesichtsrekonstruktion werden verschiedene Methoden eingesetzt [2]. Aufgrund der technischen Entwicklungen bieten immer mehr digitale 3D Methoden die Möglichkeit, sie für die Gesichtsrekonstruktion einzusetzen. Die Vorteile dieser Methoden sind die schnellere Bildung von Gesichtsvarianten und die messtechnischen Funktionalitäten, die zur objektiven Bewertung der modellierten Gesichter eingesetzt werden können.

Die digitale Vorgehensweise beginnt mit der 3D-Digitalisierung des Schädels. Dazu werden Oberflächenmessverfahren eingesetzt, wie z. B. Laser-Scanner [3], holografische Verfahren [4], die Streifenlichttopometrie [5], [6]. Darüber hinaus lassen sich auch radiologische Verfahren (CT) für die Digitalisierung des Schädels einsetzen [7]. Liegen nur Schädelfragmente vor, so können die digitalisierten Fragmente ähnlich einem 3D-Puzzle zusammengefügt werden, um einen für die Rekonstruktion verwendbaren Schädel zu erhalten [8], [9].

Für die Rekonstruktion des Gesichtes auf der Basis dieser digitalisierten Schädel gibt es verschiedene Vorgehensweisen.

Die Morphing Methode ist die Anpassung vorgegebener Hautoberflächen an die darunter liegende Schädelstruktur. Die Hautoberfläche besteht hier aus einer Vielzahl an Punkten, die über Raumkurven miteinander netzartig verbunden sind. Diese Raumkurven haben die Eigenschaft bei Änderung der Lage einer Kurvenpunktes einen abgerundeten Verlauf der Kurve beizubehalten. Auf diese Weise werden die Punkte der Hautoberfläche an die vorgegebenen Weichteilstärken angepasst [3], [10].

Eine andere Vorgehensweise zur Rekonstruktion des Gesichtes ist der Einsatz mathematischer Ähnlichkeitstransformationen [11], [12]. Hier wird die geometrische Änderung zwischen dem Schädel des unbekannten Toten und einer bekannten Person als mathematische Abbildung berechnet und anschließend auf die Gesichtsoberfläche der bekannten Person angewendet. Auf diese Weise wird die Gesichtsoberfläche des unbekannten Toten erzeugt.

Eine weitere Methode stammt aus dem Bereich des Formenbaus (Molding), in dem 3D-Modellierwerkzeuge eingesetzt werden [13], [14]. Einen neuen Ansatz in der Gesichtsrekonstruktion bietet das 3D-Modellierwerkzeug von Sensable Technologies mit dem das digitale Freihand-Skulpturieren in Kombination mit computergestütztem Konstruieren (CAD) möglich ist [15]. Die Einsatzmöglichkeiten dieses Systems und die Entwicklung von Techniken zur Gesichtsrekonstruktion sind Gegenstand dieser Arbeit.

Methode

Das 3D-Modellierwerkzeug von Sensable Technologies besteht aus dem Programm Freeform und dem Eingabegerät Phantom 3D, mit dem die virtuellen Werkstücke bearbeitet werden. Mit dem Phantom 3D wurde ein Eingabeinstrument realisiert, das ein Ertasten der digitalen Werkstücke möglich macht. Dies wird als haptisches Feedback bezeichnet.

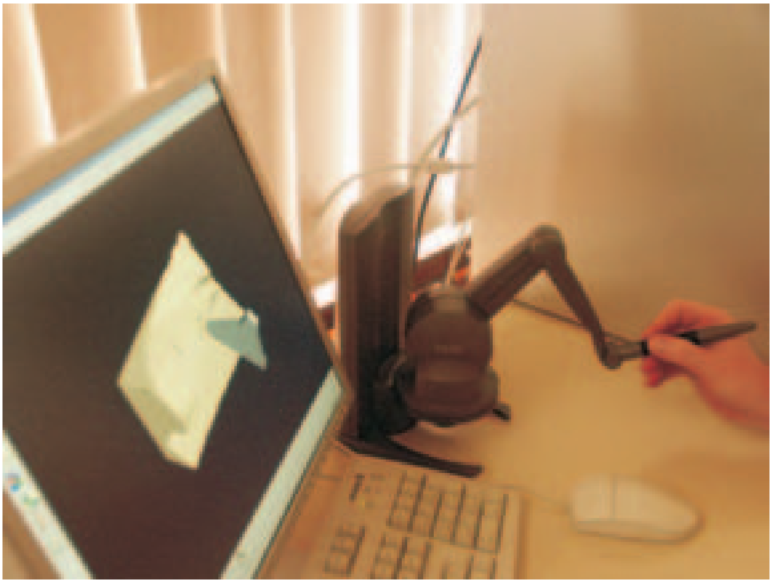

Abb. 1: Phantom 3D-Werkzeug mit virtuell dargestelltem Werkzeugkopf und Tonblock

Das Phantom 3D besteht aus insgesamt 5 Teilen, die über 5 Drehgelenke miteinander verbunden sind (Abb. 1).

Der am Ende befindliche Körper hat die Form eines Werkzeuggriffes, der im Raum verschoben und gedreht werden kann. Über die Winkelstellungen der einzelnen Körper wird die Position des Griffes gemessen und in den digitalen 3D

Raum übertragen und zur Darstellung des virtuellen Werkzeugs verwendet. An diesem digitalen Griff wird ein Werkzeugkopf befestigt, der in Form und Größe variiert werden kann. Das Ertasten der digitalen Werkstücke wird dadurch realisiert, dass der Abstand zwischen dem Werkzeugkopf und dem Werkstück ständig gemessen wird und im Kontaktfall einen mechanischen Widerstand am Phantom 3D auslöst. Dieser Widerstand wird elektrotechnisch in den Gelenken erzeugt, so dass eine weitere Bewegung des Griffes durch die Oberfläche des Werkstücks verhindert wird. Nur mit einem erhöhten Kraftaufwand kann die Oberfläche des Werkstücks mit dem Werkzeug durchstoßen werden.

Als Modellierwerkstoff wird Ton verwendet, dessen Eigenschaften Härte und Körnigkeit programmtechnisch umgesetzt werden. Die Härte des Tons wird über die Höhe des entgegengebrachten Widerstands des Phantom 3D digital simuliert, wenn mit dem Werkzeug der Ton bearbeitet wird. Die Körnigkeit des Tons zeigt sich in der Oberflächenrauhigkeit, die mit dem Phantom 3D ertastet werden kann.

Für die manuelle Bearbeitung des Tons stehen die typischen Werkzeuge wie Spachtel, Schaber und Verformer zur Verfügung mit denen der Ton wie auf herkömmliche Weise bearbeitet werden kann. Ebenso können Fräser für die Bearbeitung der Formen eingesetzt werden.

Darüber hinaus können CAD-Techniken bei der Modellierung in Kombination mit den manuellen Techniken eingesetzt werden, die ein metrisch exaktes Bearbeiten des Tons erlauben. Beispielsweise kann mit Hilfe einer Offset-Funktion gleichmäßig Material auf eine ausgewählte Fläche aufgetragen werden.

Für die Visualisierung komplexer Schichtaufbauten können verschieden Techniken eingesetzt werden. Eine erste Technik ist das Ausblenden einzelner Schichten, so dass nur die wesentlichen Schichten dargestellt werden. Eine zweite Technik ist der Profilschnitt mit der verdeckte Schichten sichtbar gemacht werden. Eine dritte Technik ist die Veränderung der Transparenzeigenschaften der Schichten, um darunter liegende Schichten sichtbar zu machen. Ebenso können die drei Techniken miteinander kombiniert werden.

Darüber hinaus stehen Messwerkzeuge zur Verfügung um den Aufbau der modellierten Schichten zu prüfen.

Anwendung

Das Vorgehen der digitalen Gesichtsrekonstruktion mit Freeform wird im Folgenden anhand zweier Beispiele gezeigt. Im ersten Beispiel werden die Techniken vorgestellt und im zweiten Beispiel werden die Techniken in einem Blindversuch validiert.

Abb. 2: Das Tonmodell des 3D digitalisierten Schädels

Zu Beginn der Gesichtsrekonstruktion wird ein Tonmodell des Schädels erzeugt. Dazu wird die Oberfläche des Schädels mittels 3-dimensinaler Messverfahren (SLT, Holografie) aufgenommen und in das Freeform-Programm importiert (Abb. 2).

Im zweiten Schritt werden die Positionen der Weichteilmarker auf der Oberfläche des Schädels markiert. Da zurzeit kein Standard existiert, wird hier nach unterschiedlichen Richtlinien vorgegangen. Eine Übersicht über die verwendeten Markerpositionen und Bezeichnungen finden sich bei Miller [16].

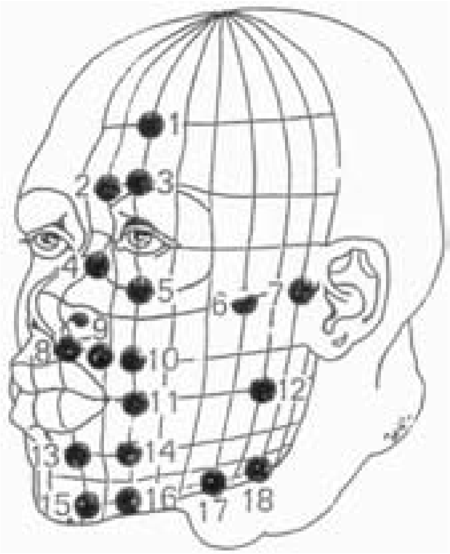

Abb. 3: Die Markerpositionen nach Aulsebrook [17]

Tab. 1: Die Weichteildaten von Männern und von Frauen nach El-Mehallawi [18].

Marker	Männer n=120			Frauen n=84		
	Min.	Max.	Mittelw.	Min.	Max.	Mittelw.
1	3,0	5,6	4,18	3,5	5,0	4,24
2	4,2	6,8	5,31	4,0	6,6	5,70
3	3,4	7,1	5,13	4,5	7,2	5,69
4	–	–	–	–	–	–
5	3,3	5,4	4,17	3,6	5,0	4,31
6	5,0	7,8	6,46	6,1	7,8	6,83
7	4,2	7,1	5,75	5,4	6,7	6,07
8	6,0	7,9	7,13	6,6	9,4	7,69
9	4,8	6,7	5,79	5,8	7,8	6,73
10	7,4	11,0	9,33	7,6	11,0	9,19
11	9,2	13,0	10,55	9,4	13,0	10,81
12	10,0	16,0	13,00	13,0	18,0	15,05
13	6,5	8,6	7,55	7,0	9,3	8,21
14	7,0	9,7	8,60	9,7	14,0	11,16
15	4,4	6,2	5,47	6,2	9,0	7,29
16	4,7	8,5	6,78	7,1	8,8	8,00

Marker	Männer n=120			Frauen n=84		
	Min.	Max.	Mittelw.	Min.	Max.	Mittelw.
17	5,9	8,6	7,19	7,3	15,0	8,52
18	9,4	15,0	11,65	11,0	15,0	13,14

Für die vorliegende Arbeit wurden die Markerpositionen nach Aulsebrook [17] (Abb. 3) und die Weichteildicken nach El-Mehallawi [18] verwendet (Tab. 1), der die Dicke der Weichteilschicht an 17 von Aulsebrook [17] vorgegebenen Stellen bei insgesamt 204 Probanden (120 Männern und 84 Frauen) mit Ultraschall gemessen hat.

Nach Tab. 1 erhält El-Mehallawi die kleinsten Werte im Stirnbereich (M1; Männer 4.16mm und Frauen 4.24mm) und Infraorbital Bereich (M5; Männer 4.17mm und Frauen 4.31mm) und die größten Werte im Backenbereich (M12; Männer 13mm und Frauen 15.05mm).

Im nächsten Schritt werden an den Markerpositionen mit Hilfe einer CAD-Funktion von Freeform kreisförmige Linien eingezeichnet. Diese Linien werden mit Hilfe der Emboss-Funktion und der Eingabe der Höhe zu Markern aufgebaut, die senkrecht zur Oberfläche stehen. Anschließend werden die Marker zur besseren Auffindung nach Aulsebrook [16], [17] nummeriert (Abb. 4). Der Marker Nummer 4 fehlt, da El-Mehallawi [18] keine Messwerte für diese Position angegeben hat.

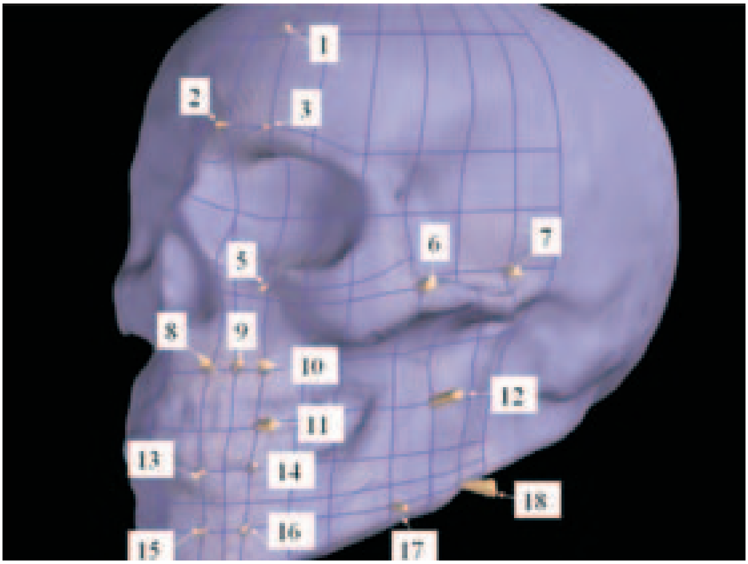

Abb. 4: Aufbringen des Gitternetzes und der Weichteilmarker auf die Schädeloberfläche

Für den Aufbau der Weichteilschicht wird wie folgt vorgegangen:

Es wird die Gesichtsoberfläche mit Hilfe der Marker in einzelne Felder eingeteilt, in denen anschließend die Weichteilschichten mit Hilfe verschiedener CAD-Funktionen von Freeform aufgebaut werden.

Die Technik besteht darin, dass Raumkurven zwischen den Markerendpunkten verspannt und als Begrenzungslinien für das automatische Auffüllen mit Weichteilmasse eingesetzt werden.

Durch die Form der Begrenzungslinien wird eine Wölbung der aufgefüllten Masse erreicht. Ist die Wölbung nicht ausreichend, kann durch den Aufbau von Zwischenmarkern die Form der Begrenzungslinien beeinflusst werden.

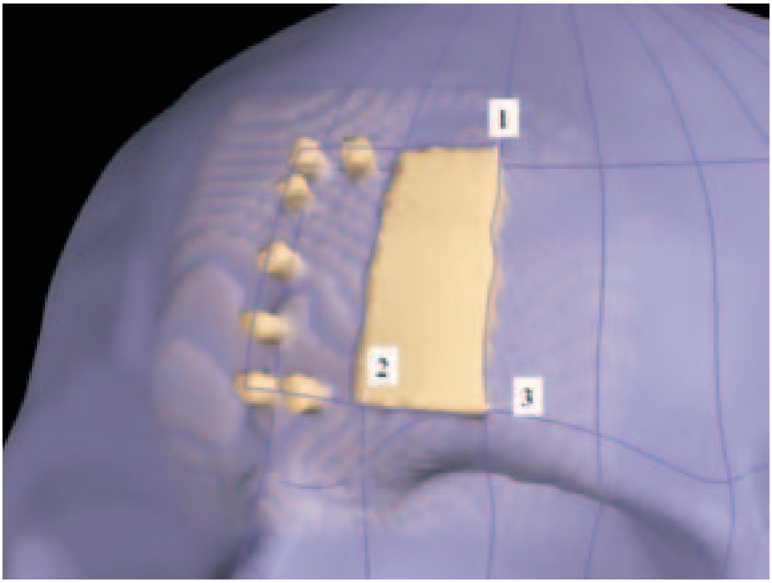

Abb. 5: Aufbau der Weichteilschicht; Weichteilmarker mit Begrenzungslinien

In Abb. 5 ist das prinzipielle Vorgehen dargestellt. Mit Hilfe der Marker 1 und 2 werden zusätzliche Marker in diesem Bereich gebildet. Entlang der Horizontalen, auf die der Marker 1 (M1) liegt werden medial von M1 weitere Marker platziert. Da sich die Dicke der Weichteilschicht in diesem Bereich nur geringfügig ändert, haben diese zusätzlichen Marker dieselbe Höhe wie M1. In gleicher Weise werden die Marker erzeugt, die auf der Horizontalen durch Marker 2 (M2) medial von M2 liegen. Die Höhe der Marker zwischen den beiden Horizontalen entlang der Median-Sagittal-Ebene wird mit Hilfe der linearen Interpolation berechnet (siehe Abb. 5).

Anschließend wird die Obergrenze der Materialantragung mit einer Raumkurve, hier die blauviolette Linie festgelegt. Das Ergebnis einer Materialantragung ist im Feld mit den Markern 1, 2 und 3 zu sehen.

Auf diese Weise werden die einzelnen Teilbereiche des Schädels von der Kalotte bis zum Unterkiefer bearbeitet (Abb. 6 bis 10). Zur übersichtlichen Darstellung können die Gitterlinien im Bedarfsfall ein- und ausgeblendet werden (siehe Abb. 6 und 7).

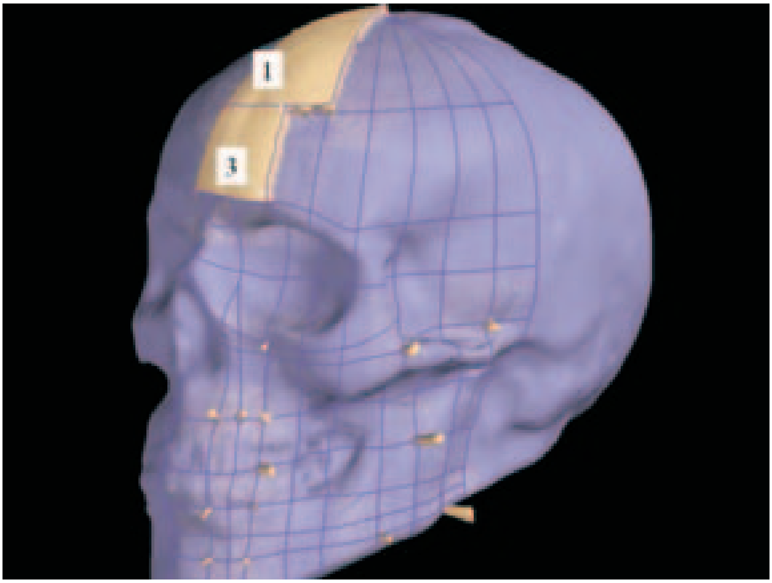

Abb. 6: Aufbau der Weichteilschicht im Bereich der Kalotte

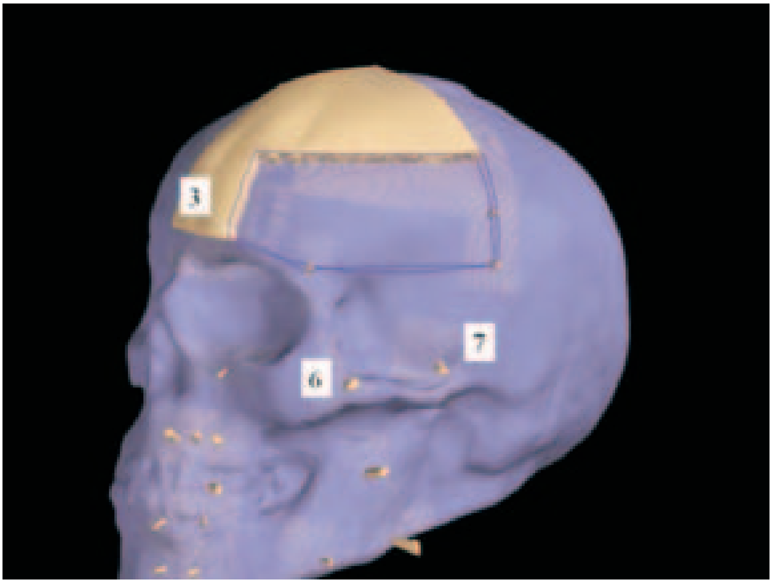

Abb. 7: Aufbau der Weichteilschicht im Stirnbereich

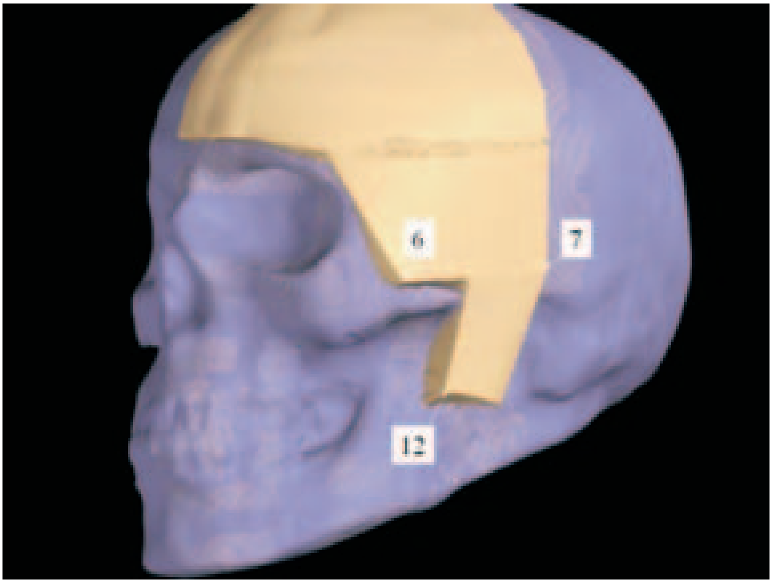

Abb. 8: Aufbau der Weichteilschicht im Schläfenbereich

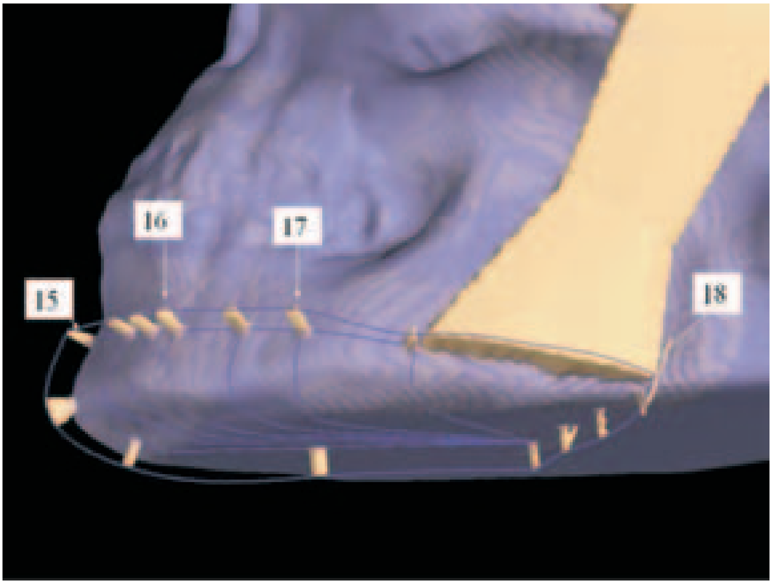

Abb. 9: Aufbau der Weichteilschicht im Kinnbereich. Ausformung der Weichteiloberfläche durch zusätzliche Weichteilmarker

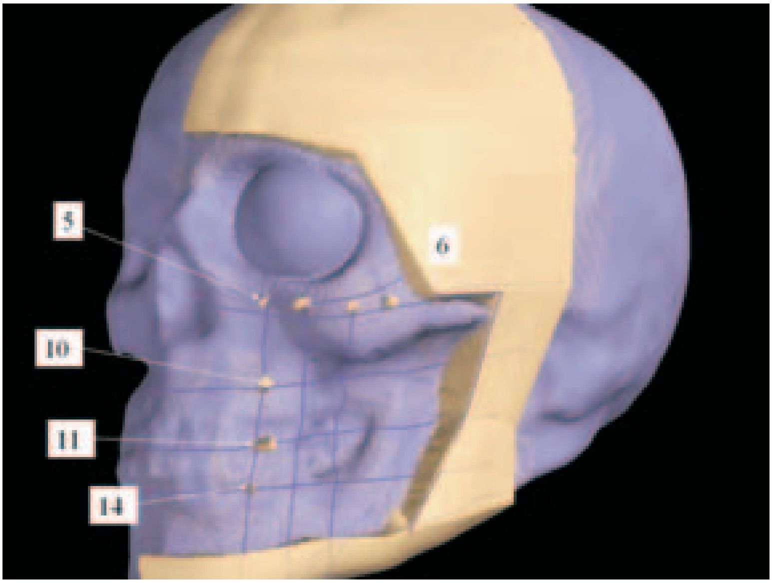

Abb. 10: Aufbau des Wangenbereichs

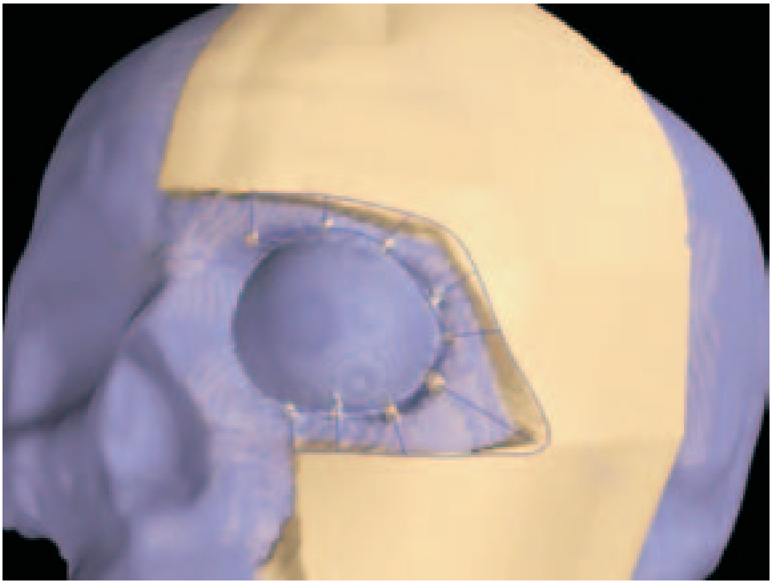

Abb. 11: Aufbau der Weichteilschicht im Augenbereich. Unterteilung in kleinere Felder

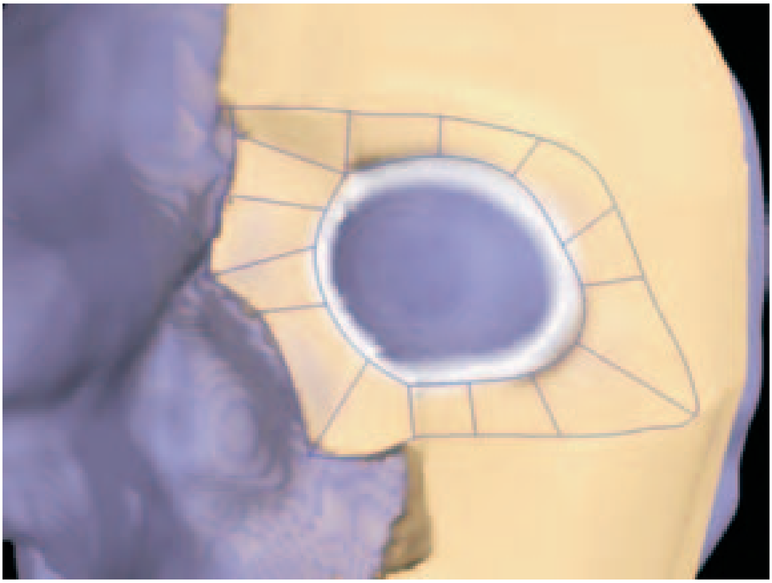

Abb. 12: Mit Weichteil gefüllte Felder im Augenbereich

Abb. 13: Aufbau der Weichteilschicht im Nasenbereich; Modellierung eines Augapfels

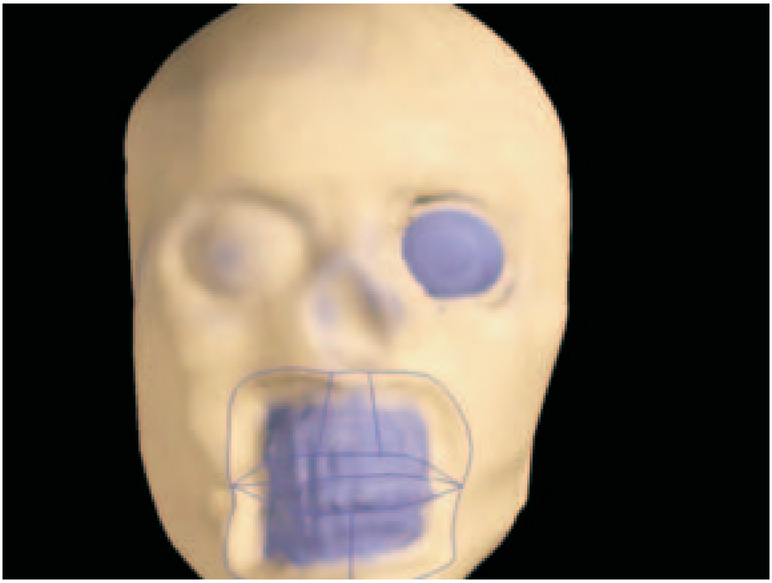

Abb. 14: Aufbau der zweiten Gesichtshälfte

Abb. 15: Aufbau des Mundbereiches. Begrenzungslinien der Felder in Lippenform

Speziell im Bereich der Augen werden die Felder kleiner gewählt um eine wohlgeformte Oberfläche zu erhalten (Abb. 11 und 12). Zuvor ist noch ein Augapfel in die Orbita eingesetzt worden, um die Weichteilübergänge geometrisch abzustimmen.

Danach werden die Bereiche um die Nase bearbeitet (Abb. 13), bevor die andere Gesichtshälfte in gleicher Weise aufgebaut wird (Abb. 14).

Im nächsten Schritt wird der Mundbereich bearbeitet. Bei der Einteilung der Felder wird die Form der Lippen mit Hilfe der Begrenzungslinien aufgebaut. Das Lippenprofil wird durch eine vertikale Raumkurve in der Median-Sagittal-Ebene erzeugt. Die Krümmung dieser Raumkurve hat einen entscheidenden Einfluss auf die Form der Lippenwulst (Abb. 15).

Im weiteren Schritt wird die Nase modelliert. Da hier die knöchernen Unterlagen und somit die Weichteildaten fehlen wird ein fertiges Nasenmodell aus einer 3D-Bibliothek entnommen, die mit 3-dimensional gescannten Gesichtern aufgebaut wurde.

Zuerst wird das Nasenmodell mit Hilfe einer Skalierfunktion auf die Größenverhältnisse des Gesichtes angepasst. Danach erfolgt die genaue Platzierung nach den Richtlinien von Helmer [1] und die Bearbeitung der Übergänge. Die überstehenden Kanten werden mit dem Fräser entfernt, die Lücken mit Ton aufgefüllt und die Übergänge abschließend verschliffen.

Abb. 16: Modellierung des Nasenbereiches mit einem fertigen 3D-Modell

Abb. 17: Modellierung der Ohren mit fertigen 3D-Modellen

Abb. 18: Anpassung der Ohren

In gleicher Weise wird mit den Ohren verfahren. Hier werden ebenfalls fertige Modelle aus der 3D-Bibliothek ausgewählt und mit Hilfe des Gehörkanals eingepasst (Abb. 17 und 18). Aufgrund der fehlenden knöchernen Strukturen im Ohrbereich gibt es keine festen Richtlinien für die Modellierung der Ohren.

Wie bei der Nase wird für die Rekonstruktion der Ohren eine Variantenbildung notwendig. Um die Wirkung unterschiedlicher Nasen- und Ohrenmodelle zu zeigen, werden von dem modellierten Gesicht zwei weitere Varianten aufgebaut und nebeneinander gestellt. Drei der Gesichter unterscheiden sich in der Nasenform und zwei in der Ohrenform (Abb. 19 und 20).

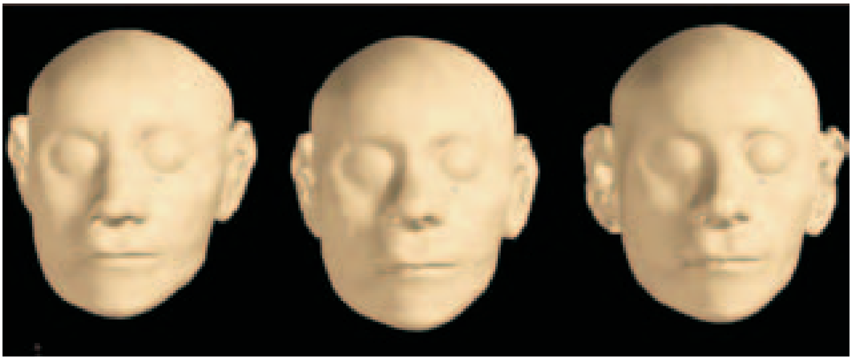

Abb. 19: Gesichtsvarianten (frontal); 3 verschiedene Nasen und 2 verschiedene Ohrenpaare

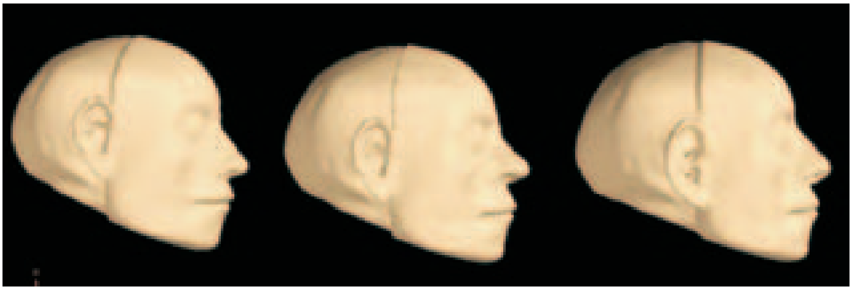

Abb. 20: Gesichtsvarianten (lateral); 3 verschiedene Nasen und 2 verschiedene Ohrenpaare

Abb. 21: Modellierung der Augen

Im letzten Schritt wird der Augenbereich modelliert. Dafür werden aus der 3D-Bibliothek geschlossene Augen ausgewählt und nach den Richtlinien von Helmer [1] eingepasst (Abb. 21). Die Übergänge werden ebenfalls mit den oben beschriebenen Werkzeugen bearbeitet.

Im zweiten Fall wird die Technik validiert, indem das Gesicht einer Frau mittleren Alters rekonstruiert wird. Dazu wurde ein klinischer CT-Datensatz des Schädels von [4], [7] verwendet. Aufgrund von Aufnahmeartefakten liegen im vorderen oberen Zahnbereich keine vollständigen Zähne vor. Die Okklusion wurde mit Hilfe des Unterkiefergelenks und den Backenzähnen rekonstruiert (Abb. 22).

Abb. 22: Schädelmodell einer Frau mittleren Alters

Der Weichteilaufbau erfolgt ebenfalls mit den Markern nach Aulsebrook [17], [18] und den Weichteildaten nach El-Mehallawi [18]. Es werden zwei Gesichtsvarianten aufgebaut, in denen die Weichteildicken von Frauen und die von Männern und fertige nach Geschlecht geordnete 3D Modelle an Nasen, Ohren, Augen und Mündern verwendet werden. Die männliche Gesichtsvariante wird zu Vergleichszwecken angefertigt. Ein Vergleich der Weichteildaten zeigt, dass bei den Frauen im Vergleich zu den Männern höhere Werte (Ausnahme bei M10) vorliegen (Tab. 1).

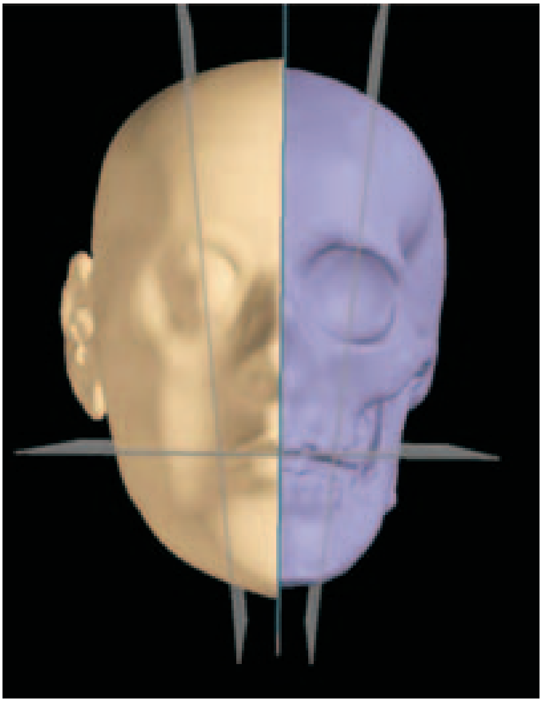

Abb. 23: Rekonstruktion des Mundes nach Richtlinien von Stephan [19]

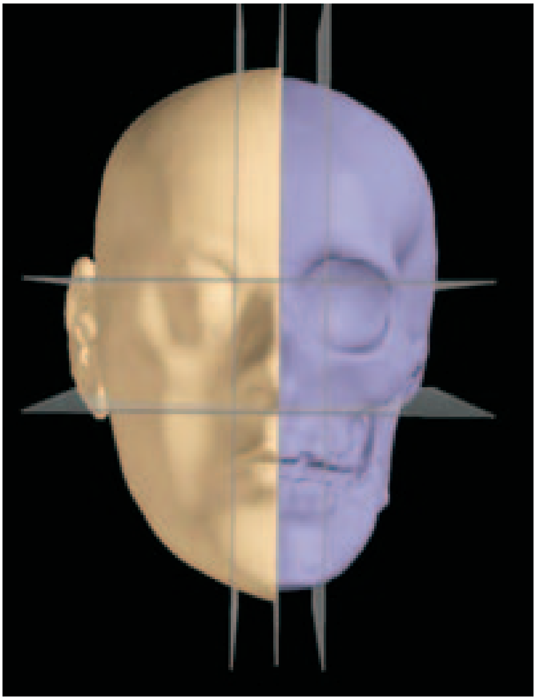

Abb. 24: Rekonstruktion der Nase nach Richtlinien von George (Stephan [19]) und Helmer [1]; Frontalansicht

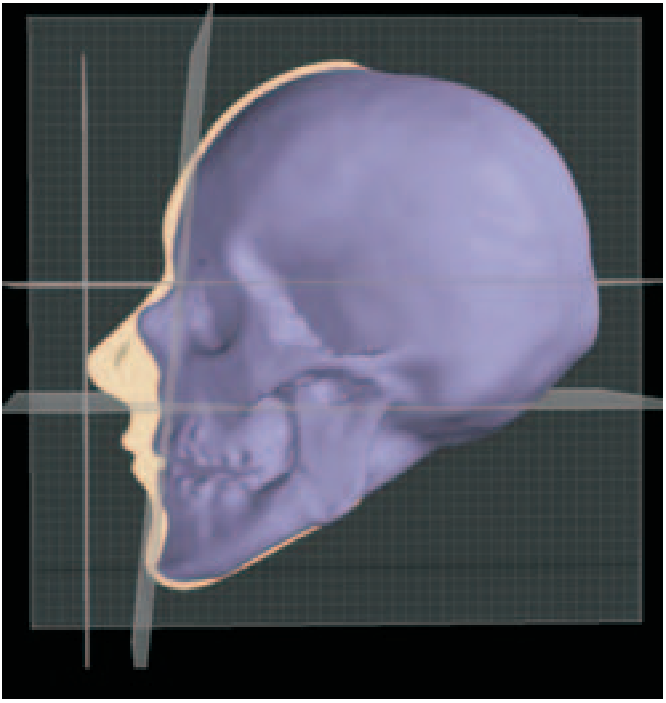

Abb. 25: Rekonstruktion der Nase nach Richtlinien von George (Stephan [19]) und Helmer [1]; laterale Ansicht

In der ersten Gesichtsvariante werden die weiblichen Daten und Modelle verwendet. Für die Rekonstruktion des Mundes wird ein weibliches Modell aus der 3D-Bibliothek entnommen. Das Modell wird nach den Richtlinien von Stephan [19] skaliert und eingefügt (Abb. 23), dessen Studie auf einer Untersuchung von insgesamt 123 Probanden basiert.

Bei der Modellierung der Nase wird ähnlich vorgegangen. Hier wird die Nasenlänge nach den Richtlinien von George [20] eingepasst, da diese Richtlinie im Vergleich zu denen von Gerasimov [21], Krogman [22] und Prokopec/Ubelaker [23] am genauesten ist (Stephan [24], siehe Abb. 24 und 25). Die Nasenbreite wird nach Helmer [1] rekonstruiert.

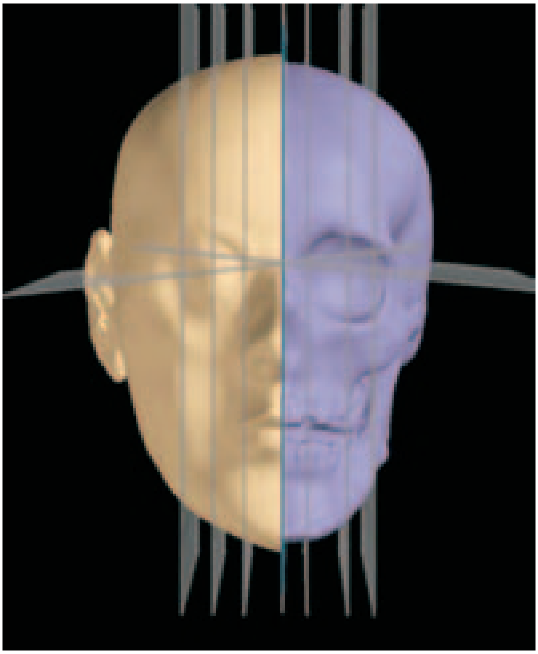

Abb. 26: Rekonstruktion der Augen nach Helmer [1]; Frontalansicht

Abb. 27: Rekonstruiertes Frauengesicht

Für die Rekonstruktion der Augen wird ebenfalls die 3D-Bibliothek genutzt. Die fertigen Augenmodelle werden nach den Richtlinien von Helmer [1] eingepasst, der wiederum auf Gatliff [25] und Rid [26] verweist (Abb. 26). Für die Rekonstruktion der Ohren wurde aus der 3D-Bibliothek ein Paar mittlerer Größe ausgewählt und mit Hilfe der Gehörkanals eingepasst (Abb. 27).

Die zweite Gesichtsvariante wird mit den Weichteildaten von Männern nach [18] aufgebaut. Bei dieser Gesichtsvariante werden männliche 3D-Modelle des Mundes, der Nase, der Ohren und der Augen verwendet (Abb. 28).

Abb. 28: Rekonstruiertes Männergesicht

Diskussion und Ausblick

In dieser Arbeit werden Techniken für die digitale Gesichtsrekonstruktion auf der Basis des 3D-Modellierwerkzeug Freefrom entwickelt. Dazu werden verschiedene Gesichtsvarianten anhand zweier Schädel aufgebaut und miteinander verglichen.

Die prägende Wirkung des Schädelknochens auf die Gesichtsoberfläche sieht man deutlich beim rekonstruierten Gesicht des ersten Falles (Abb. 2 und 21). Der Schädel weist im Unterkieferbereich eine Unsymmetrie bezüglich der Median-Sagittal-Ebene auf, die sich nach der Bedeckung des Knochens mit Weichteilgewebe auf die Gesichtsoberfläche projiziert.

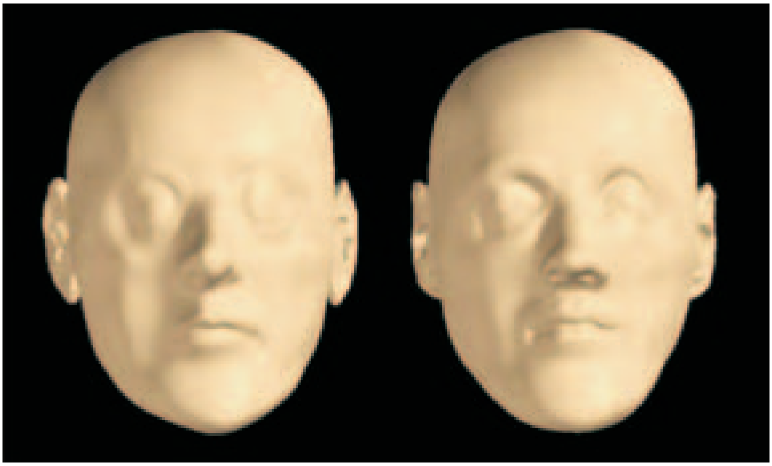

Abb. 29: Vergleich der Gesichter von Fall 2

Der Schädel aus Fall Nr. 2 hat im Vergleich zu Fall Nr. 1 ein spitzeres Kinn und weist einen größeren Winkel im Ramus-Bereich auf (Abb. 4 und 25). Zudem ist der Hinterkopf rundlicher, was für die Rekonstruktion in dieser Arbeit nicht weiter betrachtet wird.

Der Einfluss unterschiedlicher Weichteildicken wird in der nächsten Variante deutlich, bei der auf den Schädel aus Fall Nr. 2 die Weichteile mit den Dickenwerten von Frauen (El-Mehallawi [18]) aufgebaut werden. Die größten Unterschiede machen sich im Backenbereich bemerkbar. Vom Gesamteindruck ergibt sich mit den Weichteildicken der Frauen ein vom Erscheinungsbild etwas volleres Gesicht (Abb. 29).

Der Einfluss der Nasen- und der Ohrenform auf den Gesamteindruck wird in den Abbildungen 19 und 20 deutlich, wobei hier verschiedene männliche 3D-Modelle verwendet wurden, die keine großen Unterschiede in ihrer Form aufweisen.

Die Wirkung der 3D-Modelle in den Gesichtsvarianten von Schädel aus Fall Nr. 2, die nach dem Geschlecht ausgewählt wurden, ist in Abb. 29 zu sehen. Wie gut die digitale Rekonstruktion ist, zeigt sich durch den Vergleich des modellierten Gesichtes mit einer Portraitaufnahme der Person [27], deren Schädeldaten verwendet worden sind. Das Ergebnis der Modellierung ist in der Abb. 30 zu erkennen.

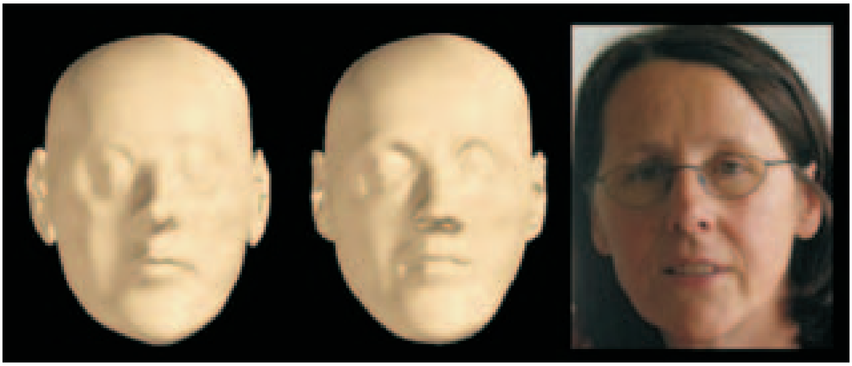

Abb. 30: Vergleich der Modellierung mit einem Foto der Probandin

Der Einsatz digitaler Methoden bei der Rekonstruktion von Gesichtern hat folgende Vorteile:

In der Bildung der Gesichtsvarianten können die erarbeiteten Modelle sofort kopiert werden und bedürfen keinerlei Nachbearbeitung wie sie bei der herkömmlichen Methode erforderlich sind.

Die Bearbeitungsschritte können augenblicklich revidiert werden, da sie einzeln abgespeichert werden.

Die Zwischenzustände der Modellierarbeit können ebenfalls abgespeichert werden, um weitere Gesichtsvarianten zu bilden.

Mit Hilfe digitaler Methoden (Streifenlichttopometrie, Holographie) lassen sich 3D-Bibliotheken an Organteilen aufbauen, aus denen entsprechende Nasen, Augen, Ohren und Münder für die Modellierung von Gesichtsvarianten entnommen werden können.

Mit diesen Möglichkeiten kann die Modellierzeit der Gesichter erheblich herabgesetzt werden.

Bei den maskenbildnerischen Arbeiten kann in ähnlicher Weise verfahren werden. Mit Freeform können verschiedene Frisurtypen modelliert und in einer 3D-Bibliothek abgespeichert werden.

Bei der Beurteilung der rekonstruierten Gesichter können die virtuellen Messmethoden, die aufgrund der CAD Eigenschaften von Freeform möglich sind eingesetzt werden. Damit stehen objektive Bewertungskriterien zur Verfügung.

Die vorgestellte Modelliertechnik, die auf der Kombination von digitalem handwerklichem Skulpturieren mit computergestütztem Konstruieren basiert, bietet neue Möglichkeiten in der computergestützten Gesichtsrekonstruktion und wird aufgrund ihrer Eigenschaften zukünftig immer mehr an Bedeutung gewinnen.

Referenzen

[1] R. Helmer, „Identifizierung unbekannter, unkenntlicher Leichen mittels bildtechnischer oder rekonstruktiver Verfahren“, in Identifikation unbekannter Toter, D. Leopold, Reihe: Arbeitsmethode der medizinischen und naturwissenschaftlichen Kriminalistik. Band 22, Schmidt-Römhild Verlag, Lübeck, 1998.

[2] P. Vanezis, M. Vanezis, „Cranio-Facial Reconstruction in Forensic Identification – Historical Development and a Review of Current Practice,“ Medicine, Science and the Law, Vol 40, No. 3 July 2000.

[3] P. Vanezis, R. W. Blowes, A. D. Linney, A. C. Tan, R. Richards and R. Neave, „Application of 3-D computer graphics for facial reconstruction and comparison with sculpting techniques,“ Forensic Sci. Int., 42, 69–84, 1998.

[4] N. Ladrière, S. Frey, A. Thelen, S. Hirsch, J. Bongartz, D. Giel, P. Hering, „Ultraschnelle holografische Gesichtsprofilvermessung mit vollautomatischer Hologrammentwicklung“, in Aktuelle Methoden der Laser- und Medizinphysik, Hartman, Kohl-Bareis, Hering, Lonsdale, Bongartz, Buzug (Hrsg.), VDE-Verlag 2004.

[5] J. Subke, H. D. Wehner, F. Wehner and H. Wolf, „Wundtopographie mittels Streifenlichttopometrie“, Rechtsmedizin Supplement I zu Band 8, 1998.

[6] J. Subke, H. D. Wehner, F. Wehner, and S. Szczepaniak, „Streifenlichttopometrie (SLT). A New Method for a 3-Dimensional Photorealistic Forensic Documentation in Color,“ Forensic Sci. Int., 113, 289–295, 2000.

[7] H. Seitz, R. Tille, R. Rider, S. Irsen, G. Bermes, „Rapid Prototyping Models for Facial Reonstruction.,“ presented at 2nd International Conference on Reconstruction of Soft Facial Parts. Remagen, March 2005.

[8] J. Subke, M. Zeller, H. D. Wehner and H. Wolf, „Digital 3D Reconstruction of Skulls from Fragments Using Streifenlichttopometrie (SLT) and a Special DNA Method“. 9th Biennial Scientific Meeting of the Craniofacial Identification Association, Washington. Forensic Science Communications Vol. 2, No. 4, Oct. 2000.

[9] J. Subke, „Digital 3D reconstruction of skulls from fragments using SLT and CAD/CAM tools,“ in Computer-Graphic Facial Reconstruction, Ed. By M Marks and J Clement, Elsevier, 2005.

[10] M. P. Evison, „Presenting Three-Dimensional Forensic Facial Simulations on the Internet Using VRML,“ Technical Note. J. Forensic Sci, 44(6): 1219–1223, 1999.

[11] L. A. Nelson and S. D. Michael, „The Application of Volume Deformation to Three-dimensional Facial Reconstruction: A Comparison with Previous Techniques,“ Forensic Sci. Int., 94 167–181, 1998.

[12] G. Quatrehomme, S. Cotin, G. Subsol, H. Delingette, Y. Garidel, G. Grévin, M. Fidrich, P. Bailet and A. Ollier, „A fully three-dimensional method for facial reconstruction based on deformable models,“ J Forensic Sci, 42(4):649–652, 1997.

[13] I. Knie, „Realisierung eines Messaufbaus zur Annahme und Modellierung von 3D-Modellen mit den Systemen der Firma ABW und Sensable," Studienarbeit, Fachbereich Krankenhaus- und Medizintechnik, Umwelt- und Biotechnologie, Fachhochschule Giessen-Friedberg, 2004.

[14] J. Moscheik, „Anwendungsmöglichkeiten des 3D-Modellierprogramms Freeform™ für die Orthopädie-Technik an ausgewählten Beispielen", Studienarbeit, Fachbereich Krankenhaus- und Medizintechnik, Umwelt- und Biotechnologie, Fachhochschule Giessen-Friedberg, 2004.

[15] J. Subke, M. Wittke, „Digitale 3D Methoden in der Schädel- und Gesichtsrekonstruktion für die Identifikation unbekannter Toter", 13. Internationales Kriminaltechnik-Seminar, Proceedings, Villingen-Schwenningen Sept. 2004.

[16] K. W. P. Miller, M. A. Taister, W. D. Turner, P. Tu, T. P. Kelliher, R. E. Brown, „A Survey of Tissue-Depth Landmarks for Facial Approximation," Forensic Communications Vol. 6, No. 8, 2004.

[17] W. A. Aulsebrook, P. J. Becker, M. Y. Iscan, „Facial Soft-Tissue Thickness in the Adult Male Zulu," Forensic Sci. Int. 19, 83–102, 1996.

[18] I. H. El-Mehallawi, E. M. Soliman, „Ultrasonic Assessment of Facial Soft Tissue Thicknesss in Adult Egyptians," Forensic Sci. Int., 117, 99–107, 2001.

[19] C. N. Stephan, „Facial Approximation: An Evaluation of Mouth-Width Determination," Am J Phys Anthropol 121:48–57, 2003.

[20] R. M. George, „The Lateral Craniographic Method of Facial Reconstruction," J Forensic Sci 32:1305–1330, 1987.

[21] M. Gerasimov, The Face Finder. London: Hutchinson & Co, 1971.

[22] W. M. Krogman, The Human Skeleton in Forensic Medicine. Springfield, IL: Charles C. Thomas, 1962.

[23] M. Prokopec, D. H. Ubelaker, „Reconstructing the Shape of the Nose According to the Skull," Forensic Sci Commun 4. pp. 1–4, 2002.

[24] C. N. Stephan, M. Henneberg and W. Sampson, „Predicting Nose Projection and Pronasale Position in Facial Approximation: A Test of Published Methods and Proposal of New Guidelines," Am J Phys Anthropol 122:240–250, 2003.

[25] B. P. Gatliff and C. C. Snow, „From Skull to Visage," J. Biocommun. 6, 27–30, 1979.

[26] B. Rid, „Die Tiefenlage der Augen.", Dissertation Erlangen 1937.

[27] P. Hering (private communication), March 2005.

Landmark Navigation for Forensic Facial Reconstruction

Markus Pung[1], Stephan Theisen[1], Dirk Thomsen[1], Jens Bongartz[1] and Thorsten M. Buzug[2]

[1] Department of Mathematics and Technology, RheinAhrCampus Remagen, Suedallee 2, D-53424 Remagen, Germany
[2] Institute of Medical Engineering, University of Lübeck, Ratzburger Allee 160, 23538 Lübeck, Germany

Abstract

The recent developments in the IT-sector and the implicated improvement of computing power and progress in technologies for visualization, lead to novel ways for computer-aided forensic facial reconstruction. The first part of this work includes the interactive navigation of predefined landmarks, the interpolation of points between these landmarks and a 3D Spline approach. With the help of this method surfaces for the facial reconstruction can be calculated. The visualization of the skull is based on a CT data set. For the placement of the landmarks an optical tracking system is used.

The second part of this work concerns the implementation of a real time system to provide a fast and efficient forensic work frame. For this purpose a PC-system is used, which contains a graphic accelerator manufactured by TeraRecon Company. The visualization toolkit from kitware™ is used as an interface between a Java implementation and the graphic accelerator.

Introduction

The classic facial reconstruction is evolving towards the computer-aided facial reconstruction. The field of computer-based strategies is the source for many projects, which are engaged in the improvement of the existing procedures and working schemes.

In this paper a 3D Spline method is introduced, which calculates the cranial surface based on the defined landmarks. Additionally, a prototyp of a forensic workplace is developed, which enables user interaction in real time. This paper describes the following parts:

- Virtual placement of landmarks on CT skull data
- Brief mathematical basics of the B-Spline method
- First results of a calculated surface of holographic data
- Requirement of a graphic-accelerator
- Basics of rendering
- Technical characteristics of the graphic accelerator
- Implementation of the software into the graphic accelerator

Fig. 1 shows the forensic work place at the RheinAhrCampus Remagen. Essential parts of the system are:

- PC system with graphic accelerator
- Optical tracking system
- Skull with fixed markers
- Skull fixation unit

Fig. 1: Forensic workplace

Composition of soft-tissue landmarks on the virtual skull

In a first step a digital skull data set is acquired using computed tomography (CT). This data set is visualized in 3D on a PC and – guided by a Polaris optical tracking system developed by Northern Digital Inc. (NDI) – landmarks are placed on the virtual skull.

The landmarks are characteristic points of the skull, which are defined by R. P. Helmer [1], reflecting the local soft-tissue thickness. Fundamental elements of the tracking system are the position sensor and the active tracker. Active means in this case that diodes, which are embedded in the Tracker, emit infrared light which is detected by the optical position sensor. However, to allow the virtual composition of landmarks, a registration must be performed first. This means we have to transform the coordinate system of the real skull into the coordinate system of the virtual skull. We use the marker-based registration (with three marker points only). The markers are attached to the real skull prior to the acquisition of the CT data set. After this registration step the coordinates of each marker from the virtual skull given by CT are known in real space.

In a next step the soft-tissue landmarks can be placed onto the virtual skull. This is done with help of the optical pointer tool, which means by navigated placement. The direction of the concerning landmark is defined as the surface normal of the skull at that position. The optical pointer position in the virtual coordinate system yields the spatial origin for the surface normal calculation. For estimation of the normal direction of the virtual skull the surface is analyzed in a *Volume of Interest* (VOI). This means that only surface points, which are located in a small neighbourhood of the pointer tip, are used for this calculation. In that way a $m \times 3$ matrix is obtained comprising the relevant coordinates. The variable m depends on the number of the data points inside the VOI. In the next step the covariance matrix K of these data points is calculated. In statistics, the covariance matrix is a $k \times k$ matrix which includes the variance and covariance of k random variables. The covariance of two random variables is a measure for the common change of them. In our case there are three random variables namely the spatial coordinates of surface points in the VOI. Hence, we obtain the following covariance matrix:

$$K = \begin{pmatrix} \sigma_{xx} & \sigma_{xy} & \sigma_{xz} \\ \sigma_{yx} & \sigma_{yy} & \sigma_{yz} \\ \sigma_{zx} & \sigma_{zy} & \sigma_{zz} \end{pmatrix}, \text{ with } \sigma_{ab} = \frac{1}{m-1} \sum_{i=1}^{m} (a_i - \overline{a})(b_i - \overline{b}) \qquad (1,2)$$

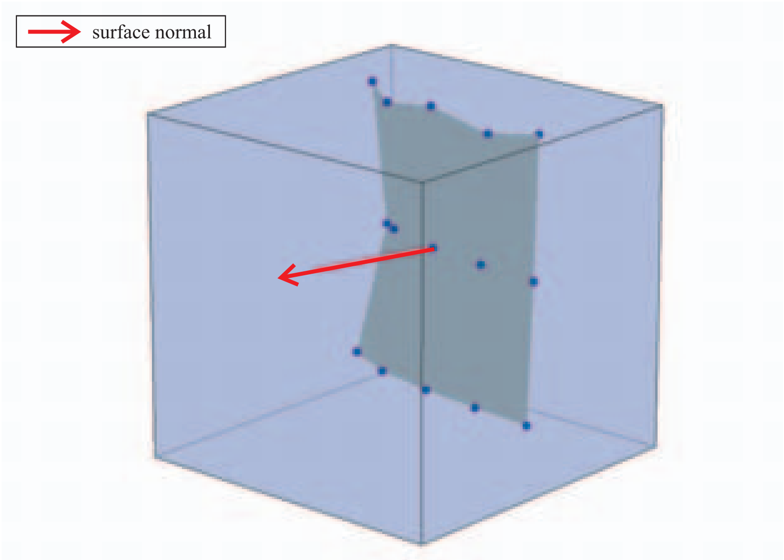

Fig. 2: VOI including surface normal and surface points

The eigenvalues of this covariance matrix define the variance of the data points in the directions of the main axes. These directions of the axes are important for the application presented here. They are defined by the eigenvectors of this covariance matrix K [2].

In figure 2 a VOI is shown, which includes surface points of an area on the mandible and, furthermore, a calculated eigenvector which represents the surface normal. The size of the VOI is approx. 14 mm^3. $\Delta x, \Delta y$ and Δz have a length of 2,4 mm.

The parameters of the landmarks, for example the height or the variance, are obtained from a database. Before the landmarks are visualized, the user can change these parameters manually and save it to the database. 53 landmarks are predefined by R. P. Helmer. In figure 3 the user interface with the virtual skull und some landmarks are shown. The different heights of the landmarks on characteristic positions can clearly be seen. Every landmark consists of three sections. The first interval, starting from the skull, displays the minimal soft tissue thickness. The end of the second interval represents the mean and the end of the third interval the maximal soft tissue thickness.

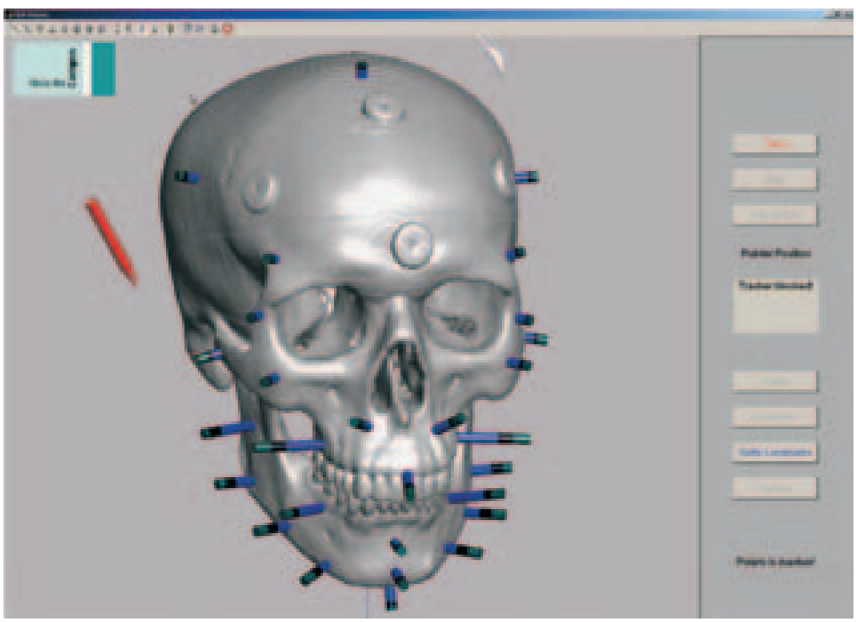

Fig. 3: Skull with landmarks

Mathematical basics of the B-Spline method

B-splines are powerful tools for generating parameterised curves or surfaces which are defined by control points. These curves are piecewise polynomials of arbitrary degree with continuous differentiable interfaces. An advantage of these splines is the possibility of the local control.

Equation (3) shows the general definition of a B-spline curve of arbitrary degree or order, respectively.

$$\vec{q}(u) = \sum_{i=0}^{n} B_{i,k}(u) * \vec{p}_i \qquad (3)$$

With: $\vec{q}(u)$ = parameterised B-spline curve

$B_{i,k}(u)$ = base functions

$\vec{p}_i$ = control points

k = order of the curve

n = number of control points

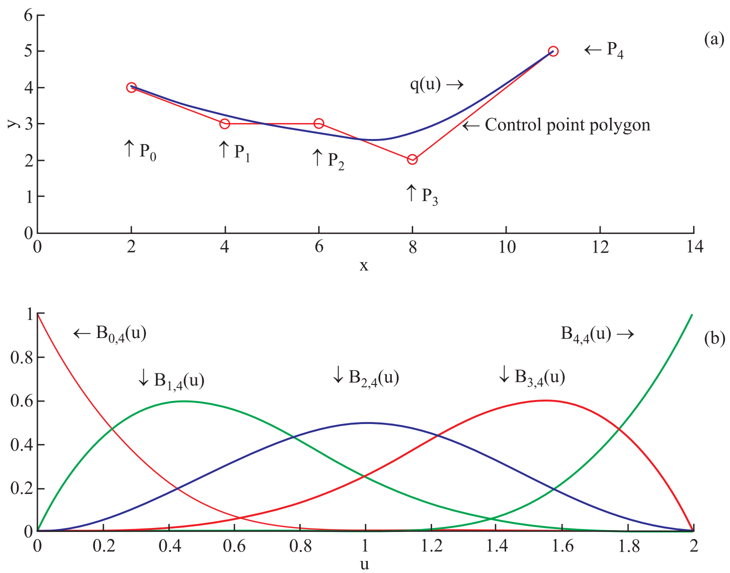

Fig. 4: Degree three B-spline curve with base functions

In figure 4 a a degree three B-spline curve $q(u)$is shown, which consists of five points. Additionally, the control polygon is displayed. The corresponding base functions are shown in Fig. 4b. Generally, one curve is defined or parameterised by n control points and base functions. The degree of the curve is the same as the degree of the base functions. Every control point corresponds to a base function. To determine the base functions we have to define a knot vector $\vec{u}$. This vector includes real numbers $u_i \leq u_{i+1}$. The values of u_i are known as knot values. It is possible to define a knot vector with multiple knots $u_i = u_{i+1} = \cdots = u_{i+j}$, but it has to be ensured that $j \leq k$ (j= multiplicity of the knot). Thus, the differentiability of the base function $B_{i,k}(u)$ at u_i is reduced to C^{k-j}. For example, the knot vector for defining the curve shown in figure 4 a is:

$$\vec{u} = [0,0,0,0,1,2,3,3,3,3] \quad (4)$$

As a result of the multiplicity of factor four at the first and last knots the curve interpolates the end control points. If the single knots are equally spaced the name *uniform B-splines* is used. In that case the base functions are translations of each other. Otherwise the name *nonuniform B-splines* is used. The base functions of all B-splines can be defined by the following recursion formula, known as Cox-de Boor formulation.

$$B_{i,1}(u) = \begin{cases} 1 & if \quad u_i \leq u \leq u_{i+1} \\ 0 & else \end{cases} \quad (5)$$

$$B_{i,k}(u) = \frac{u - u_i}{u_{i+k-1} - u_i} B_{i,k-1}(u) + \frac{u_{i+k} - u}{u_{i+k} - u_{i+1}} B_{i+1,k-1}(u) \quad for \quad k > 1 \quad (6)$$

where k is the order of the desired curve $\vec{q}(u)$. If there are knots with a multiplicity larger than one quotients 0/0 may appear. In that case the common convention 0/0 is equal to zero is used. It can be seen from eq. (5) and (6) that a degree $(k-1)$ base function is at most in k intervals unequal to zero. For that reason the B-splines can be controlled locally, i. e. a shift of a control point will influence only curve parts and not the global curve.

Further characteristics of the base functions are:

- Decomposition of the unit $\sum_{i=0}^{n} B_{i,k}(u) = 1$ (7)
- Positivity: $B_{i,k}(u) \geq 0$ (8)
- Continuity: $B_{i,k}(u)$ is $(k-1)$ times cont. differentiable (9)

Strategy for defining B-spline curves:

- Definition of control points $\vec{p}_0, \vec{p}_1, \cdots, \vec{p}_{n-1}, \vec{p}_n$
- Definition of a knot vector

  The length of the knot vector l is given by the desired curve order k and the number of control points n
  $\rightarrow l = n + k$ (10)
  $\rightarrow \vec{u} = [u_0, u_1, \cdots, u_{l-1}, u_l]$ (11)

- Calculation of the base function using the Cox-de Boor formula
- Calculation of the B-spline curve $\vec{q}(u) = \sum_{i=0}^{n} B_i(u) * \vec{p}_i$

The definition of curves can be easily extended to surfaces:

$$\vec{q}(u,v) = \sum_{i=0}^{n} \sum_{j=0}^{m} B_{i,k}(u) * B_{j,k}(v) * \vec{p}_{i,j} \quad (12)$$

With: $\vec{q}(u,v)$ = parameterised B-spline surface

$B_{i,k}(u)$ = base functions in direction of the parameter u

$B_{j,k}(v)$ = base functions in direction of the parameter v

$\vec{p}_{i,j}$ = control points

k = order of the surface

n = number of control points in $u$direction

m = number of control points in $v$direction

The length of the knot vectors and the resulting base functions are defined, analogue to equations (5, 6, 10, 11), for both parameter directions u,v.

The NURBS (*Non-Uniform-Rational-B-Splines*) are an alternative description of B-Splines. By using NURBS the single control points will be weighted. Consequently, it is possible to calculate an individual approximation for any control point. The general form is:

$$\vec{q}(u) = \frac{\sum_{i=0}^{n} w_i B_{i,k}(u) \vec{p}_i}{\sum_{i=0}^{n} w_i \vec{p}_i} \tag{13}$$

The base functions will be calculated with the recursion formula again, which is described above. Due to the weighting w_i of the control points rational curves are obtained. This is the most popular type of B-Splines.

Surfaces will be calculated with the following equation:

$$\vec{q}(u,v) = \frac{\sum_{i=0}^{n} \sum_{j=0}^{m} w_{i,j} B_{i,k}(u) B_{i,k}(v) \vec{p}_{i,j}}{\sum_{i=0}^{n} \sum_{j=0}^{m} w_{i,j} \vec{p}_{i,j}} \tag{14}$$

B-splines usually do not interpolate their control points. However, it is possible to define interpolating B-splines which pass through all the given control points or data points, respectively. For this situation a tridiagonal linear system of equations must be solved.

Results of a calculated surface of holographic data

The capability of the B-spline methods is shown on a holographic measurement. Fig. 5 shows the measured values of a face scan that consist of 40.000 points. In Fig. 6 the data can be seen as a rendered patch object. In a next step the number of points is reduced by the factor 25 to 1600 points. Based on the reduced measurement points, which are displayed in figure 7, again a surface patch is rendered and shown in figure 8. Even for the reduced number of points the result is acceptable. Only on the chin and at the border area some irregularities are induced by the parameterization of the B-splines.

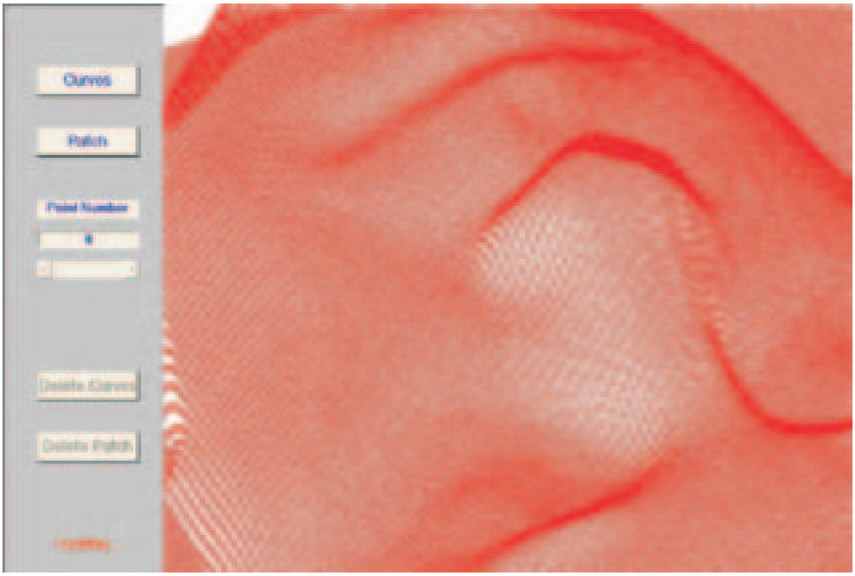

Fig. 5: Holographic measurement with 40.000 points

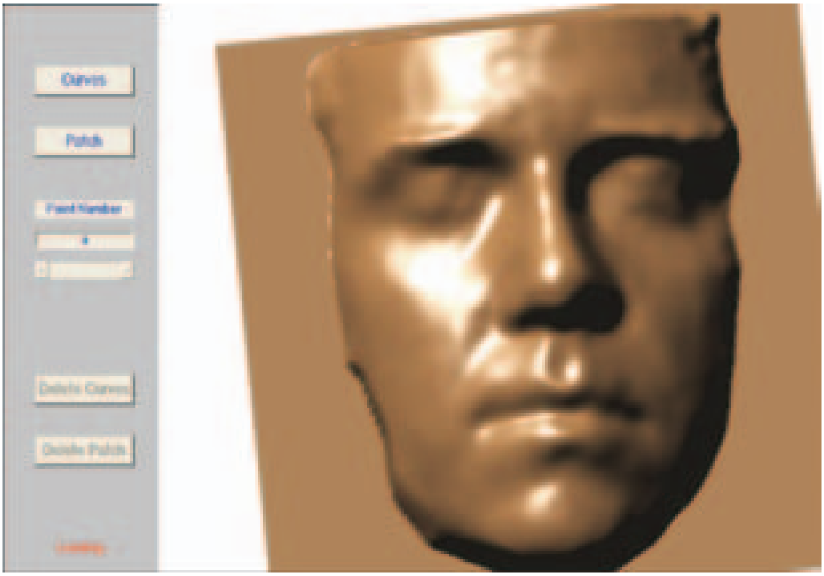

Fig. 6: Rendered surface patch

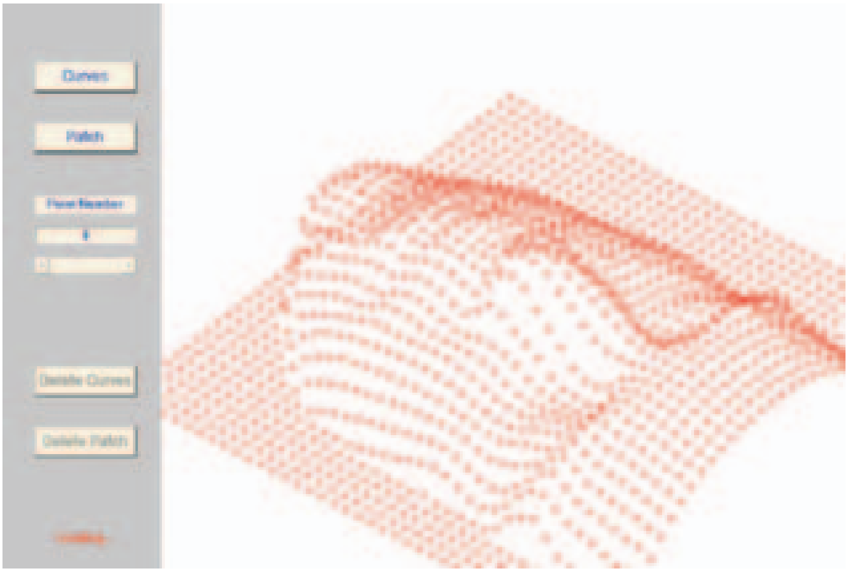

Fig. 7: Reduced number of measurement points

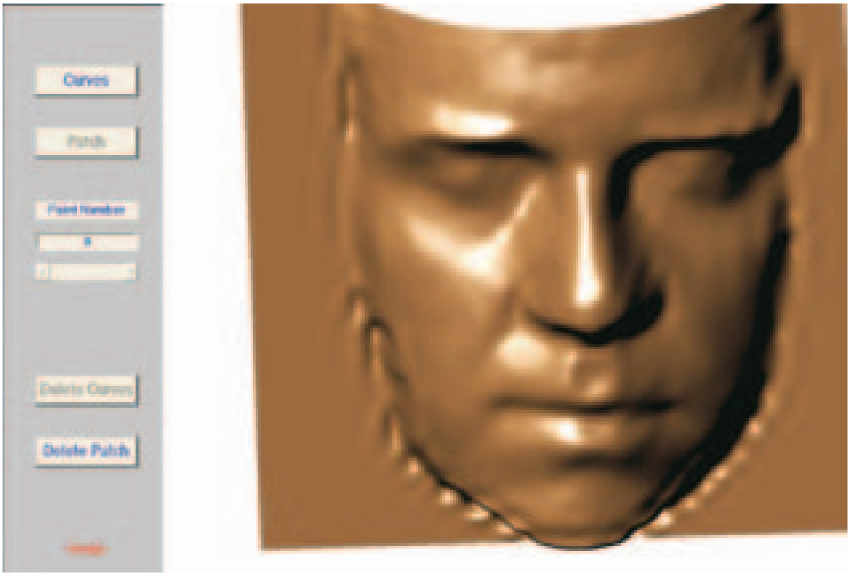

Fig. 8: Rendered patch with reduced number of measurement points

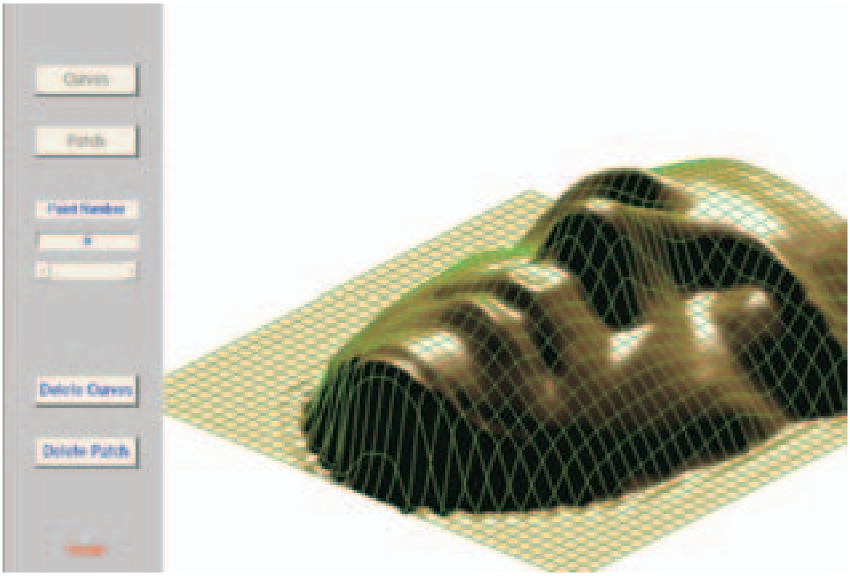

Fig. 9: Shows the spline curves in both parameter directions (*u, v*), which run through the control points (measured points). At the intersection points of the curves in *u* and the curves in *v* direction, the measurement points can be found

It is possible to obtain a better result, if the points used are not chosen equidistantly in x- or y-direction, because regions with high detail need more measured points as regions with low details.

Implementation of a real time system

In the second part of this work, first results of the ongoing implementation of the developed methods and functions into a prototyp real time system are given. This prototype allows an efficient and fast work with the graphical user interface.

Necessity of the graphic-accelerator

To obtain a highly detailed visualization of the skull, data sets from computed tomography are used. The distance between the axial slices should be as small as possible. For the data presented here the slices are acquired with an axial distance of 1 mm.

Due to the huge amount of data the calculation for data visualisation on the main CPU and RAM in normal pc-systems slows down the overall performance. For that reason the assistance of a graphic accelerator is needed, which handles the visualization of the data. The complex calculation is assigned to the CPU of the graphic accelerator.

We have implemented in our pc-system a VolumePro1000 graphic accelerator by TeraRecon Company shown in figure 10.

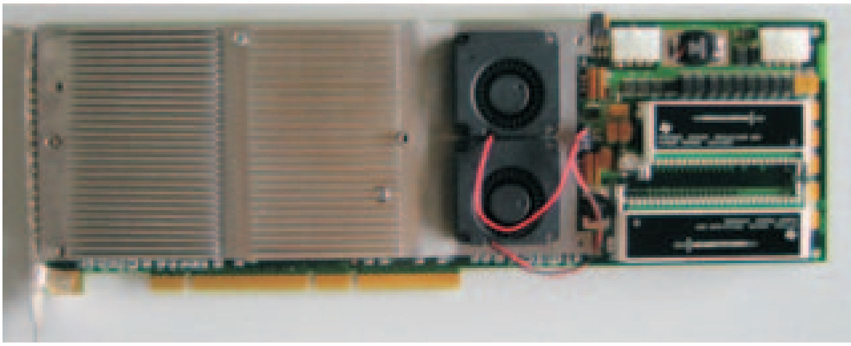

Fig. 10: Graphic accelerator from TeraRecon

Basics of rendering

Volume rendering is the mapping of volumetric data generated by three dimensional scanning techniques to a two dimensional image that can be displayed with a standard graphic card on a computer screen without intermediate processing of surface extraction. 3D scanning techniques that generate volumetric data include magnetic resonance imaging (MRI), computed tomography (CT), and 3D ultrasound. Volume rendering can fully reveal the internal structure of 3D data, including amorphous and semi-transparent features. The VolumePro1000 performs volume rendering by casting rays through a three dimensional volume from an image plane.

The following steps are the key processes required to render the 3D volumes into a 2D image that can be displayed on a computer screen:

– Casting the rays through the volume and defining sample points along the rays

– Assigning colour and opacity values to the sample points

– Interpolating voxel or colour values to new sample points along each ray

– Calculating gradients and assigning lighting to the image

– Accumulating all the colour and opacity values to create the image

Each ray cast through the volume is an imaginary beam of light passing through the center of a pixel on the image plane. As the ray passes through the volume, it samples colour (red, green, and blue) and opacity (a value indicating the opposite of transparency of the point) at points along the ray (called sample points). The VolumePro1000 then accumulates colour and opacity values for each ray passing through the volume and stores the accumulated value in a pixel on the image plane. The image can now be projected onto the computer screen as shown in Fig. 11:

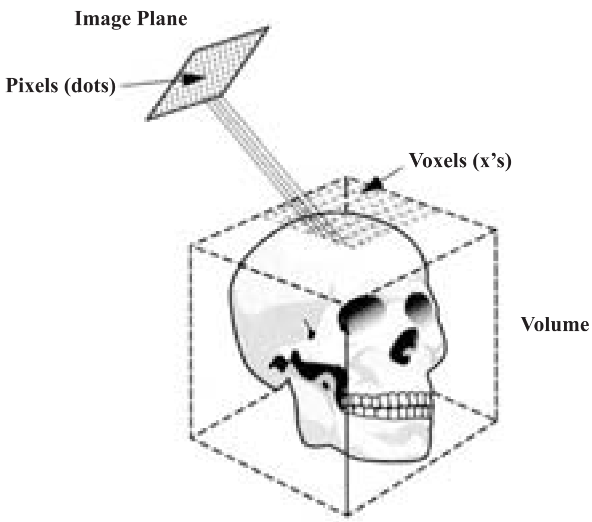

Fig. 11: A Volume and an Image plane [9]

Note that for each new situation, caused by turn over or zoom the volume, the graphic accelerator has to render the new image plane from the volume. The VolumePro1000 accelerator can realize this in real time and without any loss of details and informations in the image plane. The single steps of rendering is shown in figure 12.

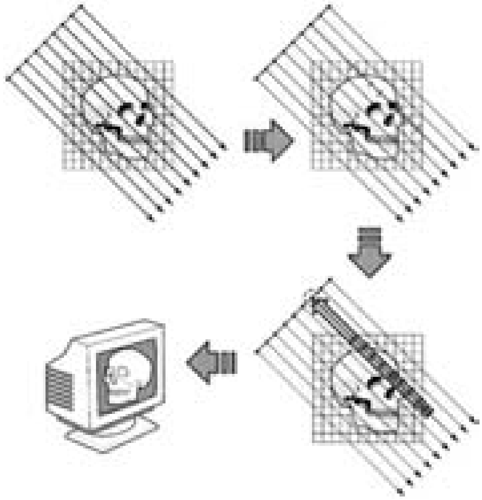

Fig. 12: Single steps of rendering [9]

If the spacing between adjacent voxel points of the rectilinear volume is the same in physical space in each of the three dimensions, the volume data is called *isotropic*. If the spacing between adjacent voxels of the rectilinear volume is not the same in the three dimensions, the volume data set is called *anisotropic*. This is the kind of volume we typically obtain from a computed tomography and used to visualize the skull in the work place presented here. For example, the spacing of the voxels along the x and y axes may be 0.5mm, but the spacing of the voxels along the z axis is 1mm. In this case, the x, y, and z coordinates of a voxel must be multiplied by separate factores, to obtain its positions in physical space.

The third form of volumes is the sheared volume. These are volumes in which the axes of the volume are not right angled in the physical world of object. They occur when the sensor of a CT scanner pass over a body at other than right angles to its longitudinal axis. Fig. 13 shows the different kinds of volume data.

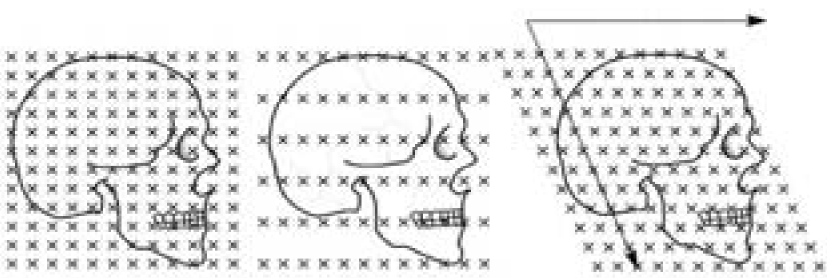

Fig. 13: Different kinds of volume data [9]

The VolumePro1000 graphic accelerator can handle with all of these three different kinds of volume data.

Technical characteristics of the graphic accelerator

This accelerator is able to work in every pc-system, which includes the new 64 bit PCI standard with 66 MHz. It can also be used in a system with 32 bit PCI standard. However, the whole performance of the accelerator is not obtained.

The accelerator supports a Video-RAM from 256 Mbyte up to 1024 Mbyte. The system used here consist of a Video-RAM with a size of 1024 Mbyte.

The large sized Video-RAM is especially used for the so called "z-buffering". This technique applied in computer graphics is used to detect sub-surfaces in the volume. With the information in the z-buffer the accelerator can calculate the elements in a rendering szene which are hidden in the volume data. If the graphic accelerator renders an object, it will first evaluate the depth information of the pixel and save it to the z-buffer. This buffer consist of a two dimensional array, which carries the depth value for every pixel in the image. To display another value at the same pixel, the accelerator compares the two different values of the pixels and selects the point which is nearest to the observer.

Then the depth information of this pixel is saved in the z-buffer and the old value on this position is deleted. By using the z-buffer the graphic accelerator can emulate the natural depth informations of the volume. The memory depth of a z-buffer is important for the quality of the rendering scene.

For example if two objects are very next to each other, a z-buffer with a memory depth of 8 bit can easily produce artefacts. The graphic accelerator used in the system presented here consist of a z-buffer with 32 bit memory depth.

For a new rendering the accelerator must delete the z-buffer by overwriting it with a constant value, which is in most cases zero. On recent graphic accelerators (1999–2003) the z-buffer uses the main part of the available Video-RAM and the bandwidth. There are several methods to reduce the impact of the z-buffer on the accelerators performance. For example the loss-free data compression: Compressing or recompressing the data is not as expensive as upgrading the bandwith. Another method reduces the number of delete steps in the z-buffer: For that the accelerator writes the depth information with an alternating algebraic sign into the z-buffer. Thus, one image is stored with a positive algebraic sign and the next one with a negative sign. However, in the next step the accelerator must delete the z-buffer.

The VolumePro1000 graphic accelerator enables an interactive real time visualization of a data set of $512^3$3 voxels. TeraRecon specifies up to one billion samples per second for the VolumePro1000.

To use the full performance of the graphic accelerator it is necessary to have a high performance pc-system as well. The system build up for the forensic work place includes two Xenon processors with 3.0 GHz from Intel, which are working on a dual processing motherboard with 2 Gbyte RAM. The performance of the AGP graphic card is not relevant, because it only displays the images from the accelerator on the monitor. In figure 14 the different parts of the entire pc-system including the graphic accelerator are shown.

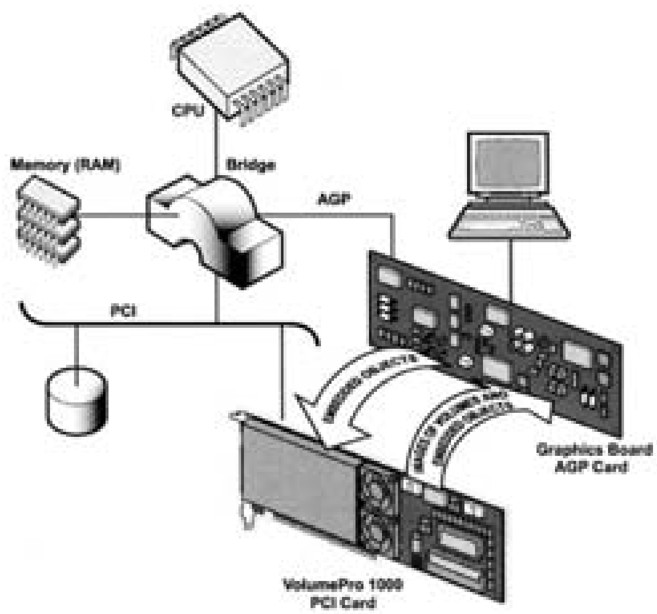

Fig. 14: Shows the different parts of the pc system [9]

Implementation of the software onto the graphic accelerator

To communicate with the graphic accelerator it is necessary to know in which programming language the libraries of the accelerator are developed. These libraries are used to work with the special functions and methods of the accelerator. The libraries of the VolumePro1000 have been developed in C++.

However, the programming language Java ensures a platform independent implementation of the virtual forensic work place. Additionally, Java has been used to build the user interface, because this language is very flexible to design the layout of a GUI (Graphical User Interface). Therefore, an interface which allows to communicate with the libraries of the VolumePro1000 is needed. For that purpose the Visualization Toolkit (VTK) from Kitware is chosen, because it consist of classes for the implementation of the VolumePro hardware. Furthermore, a translator is included which allows to interact with the classes of VTK using Java, phyton and TCL. To use VTK the source code and the data package can be downloaded from the homepage of Kitware. The classes that are needed to communicate with the VolumePro hardware are not implemented in the default package of VTK.

For the rebuild process it is necessary to download a program called Cmake. Cmake builds a C++ project which can be compiled later with a C++ compiler like MS Visual Studio. The *.jar archive must be included in the class path of the Java software development kit. Subsequently, all the VTK classes can be used for development in Java [6].

The main advantage of VTK is that it includes classes and functions, which are espacially designed for the VolumePro hardware. So it is possible to use these classes to render 3D objects with the VolumePro hardware. For example the VTK libraries include a class called vtkVolumeProVP1000Mapper [7]. The input parameters for this class are the volume data obtained from the computed tomography and a piecewise linear function (PLF), which is used to blank out some values.

For instance, with the help of the PLF the value of air can be blanked out, because it will be displayed as black pixels [7]. The VTK-class employs the VolumePro hardware to render the volume data using the piecewise linear function.

All further changes of the volume data caused by the user interface will be detected by the program. The VolumePro hardware will now render and display the new scene in real time. In that way it is possible to work fast and efficient with the accelerated user interface.

The information of the graphical accelerator's technical characteristics, the basics of the rendering technique and the example for using the VTK are from the books [6], [7] and [9]. In Fig. 15 the user interface with a visualized skull is shown.

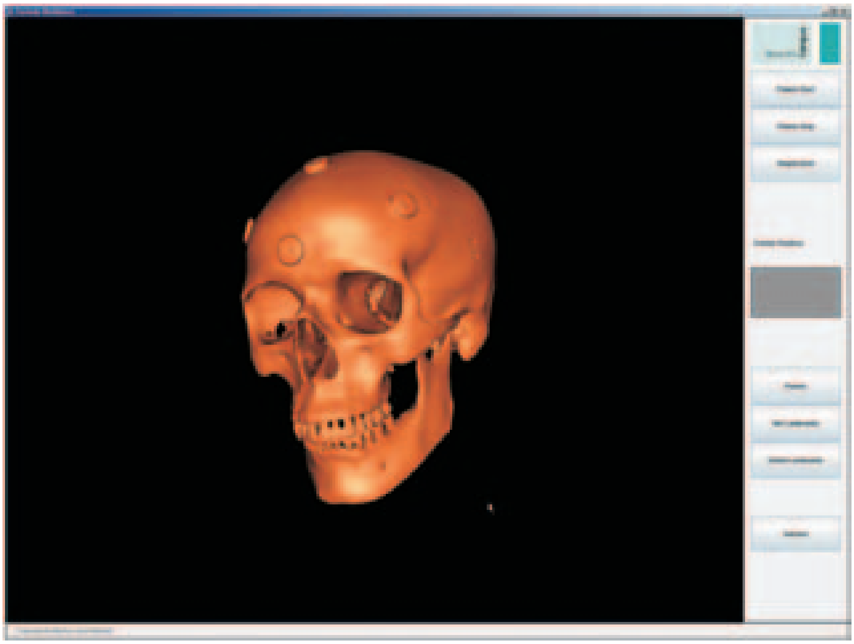

Fig. 15: Screenshot of the user interface (developed in java)

Conclusion

In a first version of the virtual forensic work place, which was implemented in Matlab^{TM}, it is possible to place characteristic landmarks on the skull with the help of an optical tracking system. However, for a precise calculation of the skin surface the number of landmarks is too low. Therefore, values between these landmarks must be interpolated. At the moment we are developing an algorithm, which inserts 200 interpolated points in each half of the face. With different parameterisations the results of the calculated skin surface shown in Fig. 8 must be improved. Another application for interactive landmark setting guided by the optical tracking system is described in [8].

Furthermore, we set up a prototype, which is able to carry out the functions of the forensic work place in real time. We have developed this workplace by using VTK in the frame work of the programming language Java. The main part is to implement a high performance graphic accelerator to improve the performance of the system.

Literature

[1] R. P. Helmer, private communication, 2004.

[2] W. Kleppmann, *Wahrscheinlichkeitsrechnung und Statistik*. Script of the study courses electronics/ computer engineering and informatics. FH Aalen

[3] S. R. Buss, *3-D Computer Graphics*. Cambridge: Cambridge University Press, 2003.

[4] B. Brüderlin, A. Meier, *Computergrafik und geometrisches Modellieren*. Stuttgart: Teubner, 2000.

[5] A. Watt, *3D-Computergrafik*. Bonn: Addison-Wesley-Longman, 2002.

[6] W. Schroeder, L. S. Avila, K. Martin, B. Lorensen, *The VTK user's guide.* Clifton Park, NY: Kitware, 2003.

[7] W. Schroder, K. Martin, B. Lorensen, *Visualization Toolkit*. Clifton Park, NY: Kitware, 2003

[8] J. Müller, A. Mang, D. Thomsen, T. M. Buzug, "Regularized 3D Thin-Plate Splines for Soft-Tissue Reconstruction" in *Biomedizinische Technik*, volume 49, supplementary volume 2, 2004, pp. 134–135.

[9] TeraRecon VolumePro1000 Users Guide, *Principals of Operation*, Tera-Recon Inc., 2001.

Landmarken-Navigation für die forensische Gesichtsrekonstruktion

Markus Pung[1], Stephan Theisen[1], Dirk Thomsen[1], Jens Bongartz[1] and Thorsten M. Buzug[2]

[1] Fachbereich für Mathematik und Technik, RheinAhrCampus Remagen, Suedallee 2, D-53424 Remagen
[2] Institut für Medizintechnik, Universität zu Lübeck, Ratzeburger Allee 160, 23538 Lübeck

Abstract

Mit dem Fortschritt der Technik speziell in der IT-Branche und den damit verbundenen Steigerungen der Rechenleistung und Darstellungsmöglichkeiten eröffnen sich neue Wege für die rechnergestützte forensische Gesichtsrekonstruktion.

Der erste Teil unserer Arbeit beschäftigt sich mit dem interaktiven Einfügen von charakteristischen Landmarken sowie dem Interpolieren von Punkten zwischen diesen Landmarken. Anhand dieser Landmarken sowie den interpolierten Werten, wird mit einem 3D-Spline Verfahren die Gesichtsoberfläche berechnet. Die Visualisierung des Schädels erfolgt auf der Basis eines CT-Datensatzes. Das Setzen der Landmarken wird mit Hilfe eines optischen Trackingsystem vorgenommen. Dazu muss vorab eine Koordinatentransformation zwischen den Koordinatensystemen des reellen bzw. virtuellen Schädels durchgeführt werden.

Der zweite Teil beinhaltet im Wesentlichen die Implementation eines Echt-Zeit-Systems, um ein schnelles und effizientes Arbeiten mit der Benutzeroberfläche zu ermöglichen. Zu diesem Zweck wurde eine Rechnereinheit aufgebaut, die einen aktuellen Grafikbeschleuniger der Firma TeraRecon beinhaltet. Daraus ergibt sich die Frage nach der richtigen Kommunikation mit der Hardware, ausgehend von der Programmsprache Java in Verbindung mit dem Visualization Toolkit VTK von Kitware, um die schnellstmögliche Darstellung der betreffenden Objekte zu gewährleisten.

Einleitung

Die klassische Gesichtsrekonstruktion befindet sich im Übergang zur computergestützten Gesichtsrekonstruktion. Dieser Forschungsbereich ist die Quelle für viele Projekte, welche sich zum einen mit der Verbesserung der bereits bestehenden Verfahren und zum anderen mit der Erprobung neuer Theorien beschäftigt. Inhalt unserer Arbeit ist die Erstellung eines 3D-Spline-Verfahrens, welches auf der Grundlage von Landmarken eine Gesichtsoberfläche berechnet. Darüber hinaus wird ein Prototyp eines forensischen Arbeitsplatzes entwickelt, der eine Interaktion in Echtzeit ermöglicht. Im diesem Paper sind folgende Abschnitte enthalten:

- Setzen der Landmarken auf dem virtuellen Schädel
- Mathematische Grundlagen der B-Spline Verfahren
- Erste Ergebnisse einer berechneten Oberfläche aus einem holographischen Datensatz
- Notwendigkeit des Grafikbeschleunigers

- Grundlagen der Rendertechnik
- Technische Merkmale des Grafik-Beschleunigers
- Implementierung der Software für den Grafik-Beschleuniger

Abb. 1 zeigt den forensischen Arbeitsplatz am RheinAhrCampus Remagen.

Wesentliche Bestandteile des Systems sind hierbei:

- Rechner mit Grafikbeschleuniger
- Optisches Trackingsystem
- Schädel mit aufgeklebten Markern
- Schädelfixierung

Abb. 1: Forensischer Arbeitsplatz

Setzen der Landmarken auf dem virtuellen Schädel

Mit Hilfe der Computertomographie wird eine Aufnahme des Schädels erstellt. Dieser Datensatz wird mit dem Rechner als 3D-Abbild des Schädels visualisiert. Mit dem optischen Trackingsystem Polaris der Firma Northern Digital Inc. (NDI) werden die Landmarken auf dem virtuellen Schädel gesetzt. Die Landmarken beziehen sich auf die von R. P. Helmer definierten charakteristischen Punkte des Schädels und geben die Weichteildicken an den entsprechenden Stellen wieder

[1]. Das Trackingsystem besteht im Wesentlichen aus einem Positionssensor und einem aktiven Zeiger. Aktiv bedeutet hierbei, dass Dioden am Zeigeinstrument infrarotes Licht emittieren, welches dann vom Positionssensor erfasst wird. Um das Setzen der Landmarken zu ermöglichen, muss zunächst eine Registrierung durchgeführt werden. Das bedeutet, das Koordinatensystem des reellen Schädels muss in das Koordinatensystem des virtuellen Abbildes überführt werden. Hier wurde auf die marker-basierte Registrierung mit 3 Punkten zurückgegriffen. Dazu werden dem Schädel vor der Aufnahme mit dem Computertomographen Marker aufgeklebt. Die jeweiligen räumlichen Koordinaten der Marker im Koordinatensystem des visualisierten Schädels werden dann aus dem Datensatz entnommen. Zur Registrierung werden diese Marker mit dem Zeigeinstrument des optischen Trackingsystems nacheinander angefahren. Die Reihenfolge hierbei, wird vom Programm vorgegeben. Das Trackingsystem liefert dann die Position und Orientierung des Zeigers und damit die Position des angefahrenen Markers im Koordinatensystem des Positionssensors an das Programm. Mit Hilfe dieser Daten wird die Koordinatentransformation berechnet. Nach erfolgreicher Registrierung kann das Setzen der Landmarken auf dem virtuellen Schädel erfolgen. Dabei fährt man mit dem Zeigeinstrument die von R. P. Helmer definierten Stellen am reellen Schädel an. Die Richtung der jeweiligen Landmarken entspricht den Flächennormalen des Schädels an diesen Stellen. Bei der Berechnung der Flächennormalen geht man wie folgt vor. Die Zeigerposition im virtuellen Koordinatensystem liefert den räumlichen Ausgangspunkt für die Berechnung. Zur Richtungsbestimmung wird die Oberfläche des virtuellen Schädels in einem bestimmten Volumenbereich um diese Koordinaten, dem so genannten *Volume of Interest* oder kurz VOI, genauer untersucht. Das heißt, alle Oberflächenpunkte, die sich in diesem Volumen befinden, gehen in die Berechnung der Flächennormalen ein. Es entsteht eine $m \times 3$ Matrix in der jeweils die räumlichen Koordinaten der Datenpunkte enthalten sind. Die Variable m gibt die Anzahl der Zeilen dieser Matrix an und ist abhängig davon, wie viele Datenpunkte sich im VOI befinden. Im Anschluss daran wird die Kovarianzmatrix$K$dieser Datenpunkte bestimmt. Als Kovarianzmatrix bezeichnet man in der Statistik eine$k \times k$Matrix, welche die Varianzen bzw. Kovarianzen von k Zufallsvariablen beinhaltet. Die Kovarianz zweier Zufallsvariablen ist ein Maß für die gemeinsame Änderung derselben. In unserem Fall existieren 3 Zufallsvariablen, nämlich die jeweiligen räumlichen Koordinaten der Oberflächenpunkte im VOI.

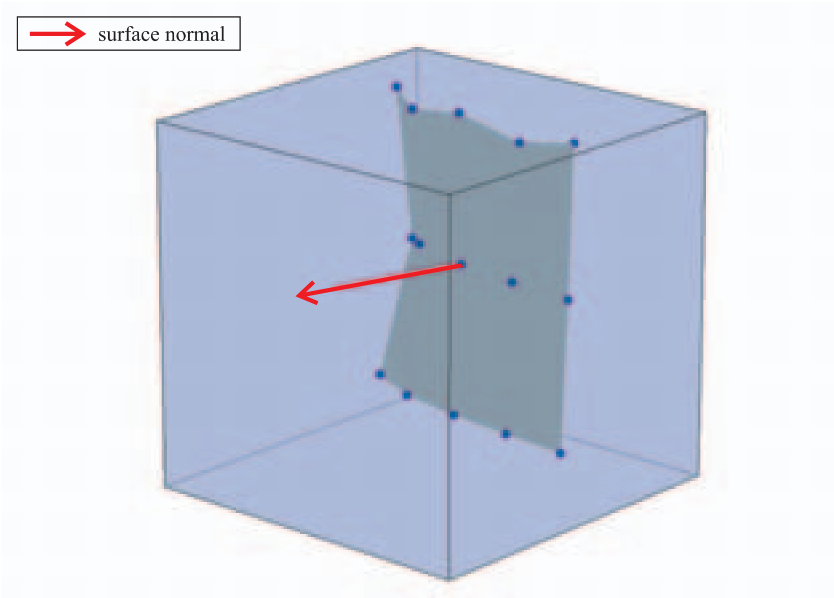

Abb. 2: VOI mit Oberflächenpunkten und Flächennormale

Folglich entsteht eine 3×3 Matrix folgender Gestalt:

$$K = \begin{pmatrix} \sigma_{xx} & \sigma_{xy} & \sigma_{xz} \\ \sigma_{yx} & \sigma_{yy} & \sigma_{yz} \\ \sigma_{zx} & \sigma_{zy} & \sigma_{zz} \end{pmatrix}, \text{ wobei } \quad \sigma_{ab} = \frac{1}{m-1} \sum_{i=1}^{m} (a_i - \overline{a})(b_i - \overline{b}) \qquad (1),(2)$$

Die Eigenwerte dieser Matrix geben die Varianz der Datenpunkte in Richtung der Hauptachsen an. Für unsere Anwendung interessant sind die Richtungen der Hauptachsen, welche durch die Eigenvektoren der Kovarianzmatrix K bestimmt werden [2].

Abb. 2 zeigt ein VOI mit den darin enthaltenen Oberflächenpunkten an einer Stelle des Unterkiefers, sowie einen berechneten Eigenvektor, welcher die Flächennormale darstellt. Das VOI hat hier eine Größe von ca. 14 mm^3, wobei $\Delta x, \Delta y$ und Δz eine Länge von jeweils 2.4 mm haben. Diese Größenordnung hat sich für unsere Anwendungen als sinnvoll erwiesen.

Die Parameter der Landmarken, wie z. B. die Höhe oder Varianz, werden aus einer Datenbank entnommen. Vor dem Darstellen der Landmarken ist es dem Benutzer möglich, diese Parameter manuell zu verändern und in der Datenbank zu speichern. Mit Hilfe der uns zur Verfügung gestellten Landmarkendatenbank werden 53 Punkte auf dem gesamten Schädel gesetzt.

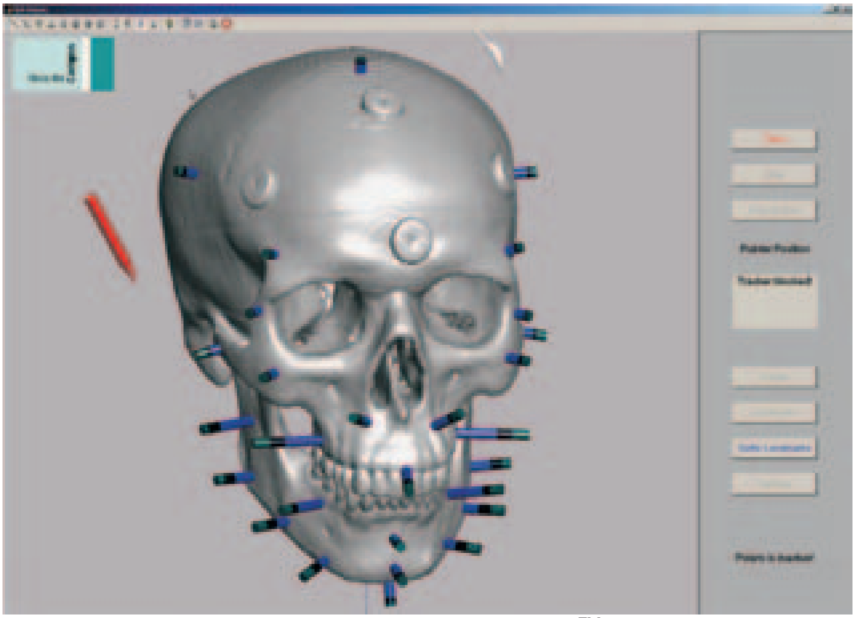

Abb. 3: Screenshot der rudimentären Benutzeroberfläche in Matlab™

Abb. 3 zeigt die Benutzeroberfläche in Matlab™ mit dem visualisierten Schädel und einigen bereits gesetzten Landmarken.

Gut zu erkennen sind die unterschiedlichen Höhen der Landmarken an den markanten Stellen. Jede Landmarke ist in drei Abschnitte unterteilt. Der erste Abschnitt vom Schädel aus betrachtet stellt die minimale Weichteildicke dar. Das Ende des zweiten Abschnitts repräsentiert die mittlere und das Ende des dritten Abschnitts die maximale Weichteildicke.

Mathematische Grundlagen der B-Spline Verfahren

Die Berechnung der Gesichtsoberfläche erfolgt zunächst mit Hilfe von kubischen B-Spline Flächen. Mit diesem Verfahren ist es möglich, wohlgeformte parametrisierte Flächen zu berechnen, welche durch die Kontrollpunkte definiert werden. B-Spline-Kurven sind stückweise Polynome beliebigen Grades mit stetig differenzierbaren Nahtstellen. Sie haben den Vorteil der lokalen Steuerung. Die allgemeine Gleichung zur Berechnung einer B-Spline-Kurve beliebigen Grades (bzw. Ordnung k) ist wie folgt definiert:

$$\overrightarrow{q}(u) = \sum_{i=0}^{n} B_{i,k}(u) * \overrightarrow{p}_i \tag{3}$$

mit: $\overrightarrow{q}(u)$ = gesamte parametrisierte B-Spline-Kurve

$B_{i,k}(u)$ = Basis- oder Vermischungsfunktionen

$\vec{p}_i$ = Kontrollpunkte

k = Ordnung der Kurve bzw. Basisfunktion

n = Anzahl der Kontrollpunkte

Abb. 4 a zeigt eine B-Spline-Kurve 3. Grades $q(u)$, bestehend aus fünf Punkten sowie das Kontrollpolygon. In Abb. 4 b sind die dazugehörigen Basisfunktionen dargestellt. Eine Kurve ist also definiert bzw. parametrisiert durch n Kontrollpunkte und Basisfunktionen. Der Grad der Kurve ist gleich dem Grad der Basisfunktionen. Jeder Kontrollpunkt erhält eine Basisfunktion. Für die Bestimmung der Basisfunktionen wird ein Knotenvektor $\vec{u}$ definiert. Dieser Vektor enthält reelle Zahlen u_i wobei gilt: $u_i \leq u_{i+1}$. Die Werte u_i werden als Knotenwerte bezeichnet. Zu beachten ist, dass auch Mehrfachknoten $u_i = u_{i+1} = \cdots = u_{i+j}$ auftreten können, wobei gelten muss, dass $j \leq k$ (j= Mehrfachheit der Knoten). Dadurch bedingt wird die Differenzierbarkeit der Basisfunktion $B_{i,k}(u)$ im Punkt u_i zu C^{k-j} reduziert. Beispielsweise sieht der Knotenvektor für die oben dargestellten Basisfunktionen bzw. für die dargestellte Kurve wie folgt aus:

$$\vec{u} = [0,0,0,0,1,2,3,3,3,3] \tag{4}$$

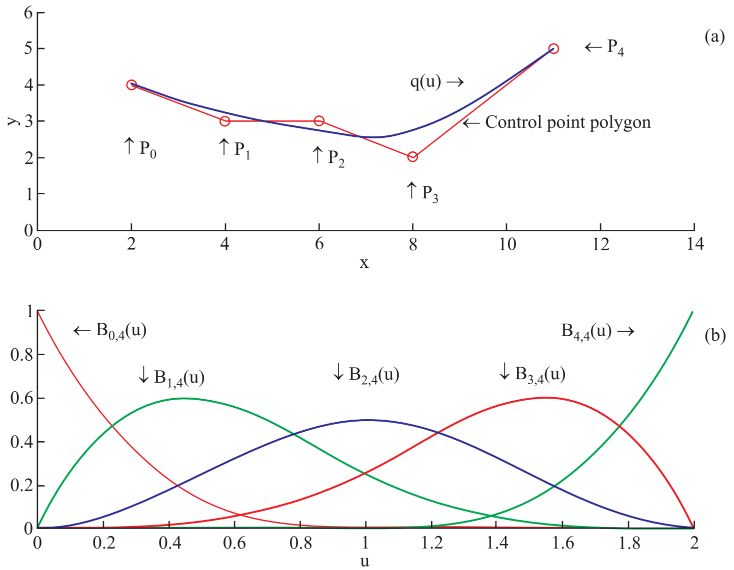

Abb. 4: B-Spline Kurve 3.Grades mit Basisfunktionen

Durch die Mehrfachheit mit dem Faktor vier an den Anfangs- bzw. Endknoten, interpoliert die Kurve die Endkontrollpunkte. Sind die Abstände der einzelnen Knoten äquidistant, verwendet man die Bezeichnung uniforme B-Splines. Die Basisfunktionen sind hierbei Translationen voneinander. Bei nicht äquidistanten Knotenwerten handelt es sich um nicht uniforme B-Splines.

Die Basisfunktionen aller B-Splines können durch folgende Rekursionsformel, bekannt als Cox-de Boor Formulierung, bestimmt werden.

$$B_{i,1}(u) = \begin{cases} 1 & \textit{falls} \quad u_i \le u \le u_{i+1} \\ 0 & \textit{sonst} \end{cases} \tag{5}$$

$$B_{i,k}(u) = \frac{u - u_i}{u_{i+k-1} - u_i} B_{i,k-1}(u) + \frac{u_{i+k} - u}{u_{i+k} - u_{i+1}} B_{i+1,k-1}(u) \quad \textit{für} \quad k > 1 \tag{6}$$

Hierbei entspricht $k$der Ordnung der gewünschten Kurve $\vec{q}(u)$. Sind im Knotenvektor Mehrfachknoten vorhanden, können Quotienten der Form 0/0 entstehen. Deshalb wird beim Auswerten der Formulierung die Konvention 0/0=0 festgelegt. Anhand dieser Rekursionsformel kann man erkennen, dass eine Basisfunktion vom Grad $k-1$ höchstens in k Intervallen ungleich null ist. Beispielsweise ist $B_{i,3}(u)$ in drei Intervallen ungleich null. Das ist der Grund für die lokale Steuerung der B-Spline-Kurven.

Das heißt, das Verschieben eines Kontrollpunktes hat nur Auswirkungen auf bestimmte Kurvenabschnitte und nicht auf die gesamte Kurve.

Weitere Eigenschaften der Basisfunktionen sind:

- Zerlegung der Einheit: $\sum_{i=0}^{n} B_{i,k}(u) = 1$ (7)
- Positivität: $B_{i,k}(u) \ge 0$ (8)
- Stetigkeit: $B_{i,k}(u)$ ist $(k-1)$ mal stetig differenzierbar (9)

Allgemeines Schema zur Bestimmung einer B-Spline-Kurve:

- Kontrollpunkte festlegen: $\vec{p}_0, \vec{p}_1, \cdots, \vec{p}_{n-1}, \vec{p}_n$
- Knotenvektor festlegen:

Die Länge des Knotenvektors ergibt sich aus der gewünschten Ordnung der Kurve und der Anzahl der Kontrollpunkte.

Allgemein gilt für Kontrollpunkte $\vec{p}_0, \vec{p}_1, \cdots, \vec{p}_{n-1}, \vec{p}_n$, Ordnung der Kurve k:
  - $l = n + k$ (10)
  - $u = [u_0, u_1, \cdots, u_{l-1}, u_l]$ (11)

- Berechnung der Basisfunktionen mit Hilfe der Cox-de Boor Formulierung
- Berechnung der B-Spline Kurve $\vec{q}(u) = \sum_{i=0}^{n} B_i(u) * \vec{p}_i$

Diese Definition der Kurven lässt sich leicht auf Flächen erweitern. Es existieren dann zwei Parameterrichtungen (u und v).

$$\vec{q}(u,v) = \sum_{i=0}^{n} \sum_{j=0}^{m} B_{i,k}(u) * B_{j,k}(v) * \vec{p}_{i,j} \tag{12}$$

mit: $\vec{q}(u,v)$ = gesamte parametrisierte B-Spline-Fläche

$B_{i,k}(u)$ = Basis- oder Vermischungsfunktionen in Abhängigkeit des Parameters u

$B_{j,k}(v)$ = Basis- oder Vermischungsfunktionen in Abhängigkeit des Parameters v

$\overrightarrow{p}_{i,j}$ = Kontrollpunkte

k = Ordnung der Kurve bzw. Basisfunktionen

n = Anzahl der Kontrollpunkte in u Richtung

m = Anzahl der Kontrollpunkte in v Richtung

Die Länge der Knotenvektoren und die daraus folgenden Basisfunktionen werden, analog wie in den Gleichungen (5, 6, 10, 11) beschrieben, für beide Parameterrichtungen u,vbestimmt.

Eine weitere Form der B-Splines sind die NURBS (Non-Uniform-Rational-B-Splines). Bei NURBS werden die einzelnen Kontrollpunkte mit verschiedenen oder gleichen Gewichtungsfaktoren behaftet, somit ist eine individuelle Annäherung der Kurve an beliebige Kontrollpunkte möglich. Die allgemeine Form für NURBS Kurven lautet:

$$\overrightarrow{q}(u) = \frac{\sum_{i=0}^{n} w_i B_{i,k}(u) \overrightarrow{p}_i}{\sum_{i=0}^{n} w_i \overrightarrow{p}_i} \tag{13}$$

Die Basisfunktionen werden wieder mit der oben beschriebenen Rekursionsformel bestimmt. Durch die Normierung bzw. Gewichtung w_i eines jeden Kontrollpunktes $\overrightarrow{p}_i$ handelt es sich um rationale Kurven. Diese Form von B-Splines ist wohl die populärste.

Die NURBS Flächen werden analog mit folgender Gleichung bestimmt:

$$\overrightarrow{q}(u,v) = \frac{\sum_{i=0}^{n} \sum_{j=0}^{m} w_{i,j} B_{i,k}(u) B_{i,k}(v) \overrightarrow{p}_{i,j}}{\sum_{i=0}^{n} \sum_{j=0}^{m} w_{i,j} \overrightarrow{p}_{i,j}} \tag{14}$$

Gewöhnlich interpolieren B-Spline-Kurven bzw. -Flächen nicht ihre Kontrollpunkte. Es ist jedoch möglich, interpolierende B-Splines zu berechnen, welche alle vorgegebenen Kontrollpunkte bzw. Datenpunkte durchlaufen. Eine Möglichkeit besteht darin, durch lösen eines tridiagonalen Gleichungssystems auf der Basis der gegebenen Datenpunkte neue Kontrollpunkte zu bestimmen.

Der kurze Überblick über die B-Splines wurde im Wesentlichen mit Hilfe von drei Büchern [3], [4], [5] erarbeitet, welche im Literaturverzeichnis aufgeführt sind.

Erste Ergebnisse einer berechneten Oberfläche aus einem holographischen Datensatz

Die Leistungsfähigkeit der Spline-Verfahren kann an einer holographischen Messung gezeigt werden. Abb. 5 zeigt die vergrößerte Darstellung der Messwerte eines holographischen Gesichtsscans. Der Datensatz besteht aus 40.000 Punkten. In Abb. 6 ist dieser Datensatz als ein gerendertes Patchobjekt zu sehen. Das Gesicht ist gut zu erkennen und weist eine hohe Detailgenauigkeit auf. Die Anzahl der Punkte wurde danach um den Faktor 25 auf 1600 Punkte reduziert. In Abb. 7 sind die in der Anzahl reduzierten Messwerte zu sehen, auf deren Grundlage der entsprechende Oberflächenpatch in Abb. 8 berechnet wurde. Die Oberfläche wurde hierbei mit Hilfe von interpolierenden B-Splines berechnet. Das Ergebnis ist angesichts der verwendeten Anzahl der Punkte durchaus akzeptabel. Beide Bilder in Abb. 6 und 8 weisen eine hohe Ähnlichkeit auf. Mängel sind noch im Kinn- bzw. Randbereich des Gesichts zu finden.

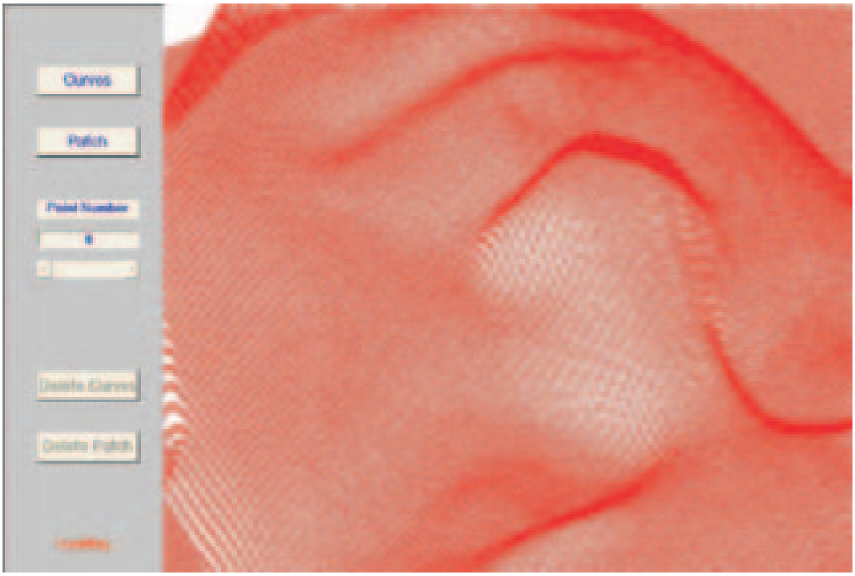

Abb. 5: Messwerte einer holographischen Messung.

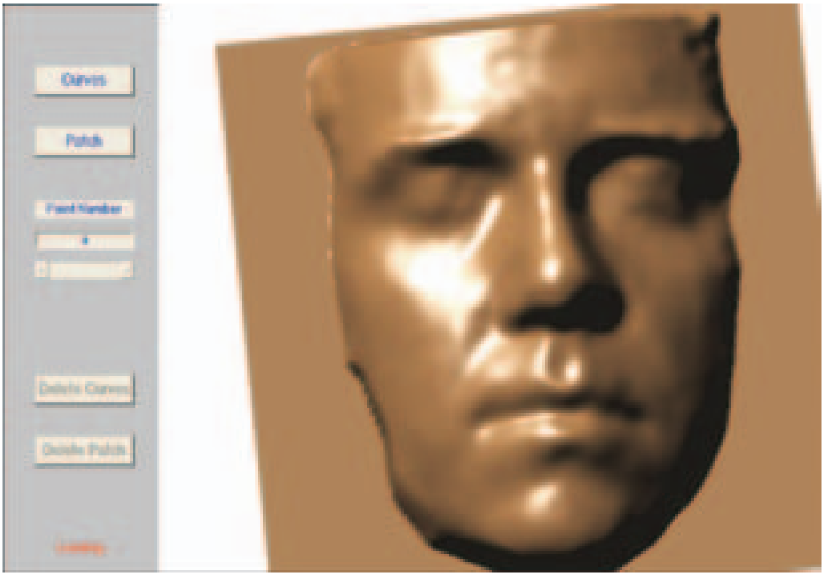

Abb. 6: Gerenderter Oberflächenpatch aus 40000 Punkten.

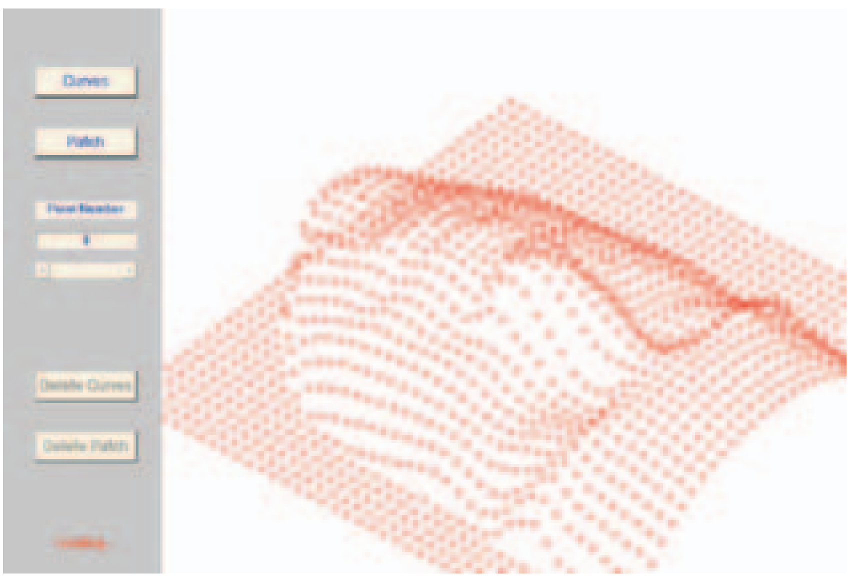

Abb. 7: Reduzierte Anzahl von Messwerten.

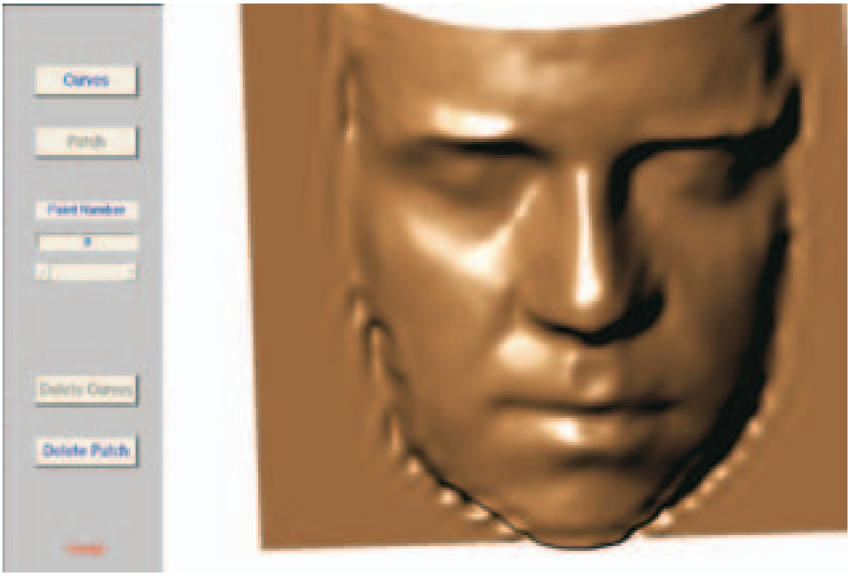

Abb. 8: Oberflächenpatch aus 1600 Punkten.

Abb. 9 zeigt den Verlauf jener Kurven in beiden Parameterrichtungen (u,v), welche die Kontrollpunkte (Messpunkte) durchlaufen. An den Schnittstellen zwischen den Kurven in den u- und den Kurven in v-Richtung befinden sich die Messpunkte. Eine Verbesserung der Ergebnisse ist sicherlich möglich, indem die reduzierten Messpunkte in x- bzw. y-Richtung nicht mehr äquidistant gewählt werden, sondern der Abstand der Messpunkte der jeweiligen Gesichtsregion angepasst wird. Regionen mit hohem Detailreichtum benötigen mehr Messpunkte als Regionen mit geringem Detailreichtum.

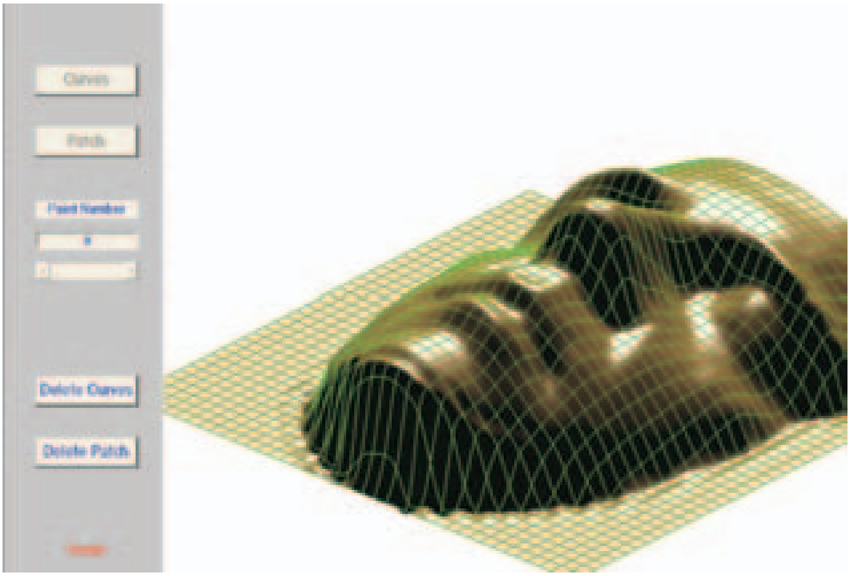

Abb. 9: Eingepasste Kurven durch die Messpunkte in zwei Parameterrichtungen.

Implementierung eines Echtzeit fähigen Systems

Der zweite Teil unserer Arbeit beschäftigt sich damit, die erarbeiteten Methoden und Funktionen in einen Prototyp eines echtzeitfähigen Systems zu überführen. Dadurch soll ein schnelles und effizientes Arbeiten mit der Benutzeroberfläche und allen damit verbundenen Funktionen ermöglicht werden.

Notwendigkeit des Grafikbeschleunigers

Um eine weitestgehend detailgetreue Darstellung des Schädels zu erlangen, sind Schichtaufnahmen mit dem Computertomographen erforderlich, die eine möglichst feine Unterteilung in z-Richtung beinhalten. Hier sind Größenordnungen von 1mm als Standard angesetzt. Dadurch ergibt sich allerdings der Nachteil, dass bedingt durch die entstandenen großen Datensätze der Rechenaufwand sehr hoch und das System langsam wird.

Dies ist dadurch begründet, dass bei normalen PC-Systemen ein Großteil der Berechnungen zur Visualisierung des Datensatzes von der Kern-CPU und dem Hauptspeicher des Systems übernommen werden. So weist allein das Schwenken des Schädels um die eigene Achse erhebliche Verzögerungen auf.

Daher haben wir uns der Unterstützung durch einen Grafikbeschleuniger bedient, der die Aufgabe der Visualisierung und aller damit verbundenen Berechnungen übernehmen soll. Somit verlagern wir die meist komplexen und aufwändigen Berechnungen in den Prozessor des Grafikbeschleunigers. Die Kern-CPU sowie der Hauptspeicher des PC's können dann für andere Operationen verwendet werden.

Bei dem hier verwendeten System handelt es sich um einen Grafikbeschleuniger der Firma TeraRecon mit der Bezeichnung VolumePro1000 der in Abb. 10 dargestellt ist.

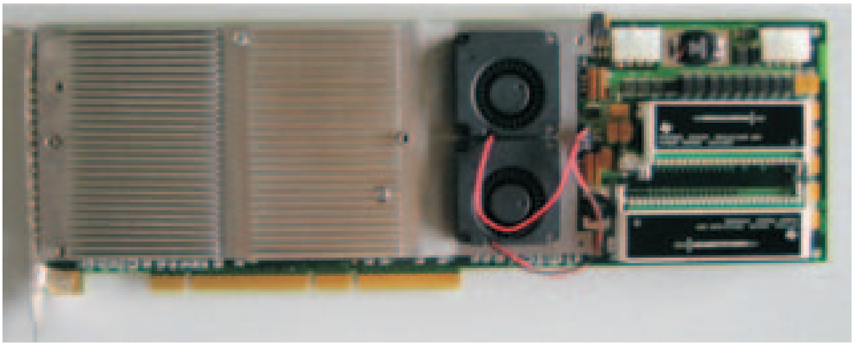

Abb. 10: Grafikbeschleuniger der Firma TeraRecon.

Grundlagen der Rendertechnik

Bevor wir uns den technischen Eigenschaften des Grafikbeschleunigers widmen, sollten wir uns kurz die Vorgehensweise des „Rendern" klarmachen. Hierbei werden Daten, die durch dreidimensionale Aufnahmeverfahren entstanden sind, zum Beispiel durch eine Computertomographie oder MR, in ein zweidimensionales Bild konvertiert, das über eine handelsübliche Grafikkarte auf den Bildschirm der Rechnereinheit ausgegeben werden kann. Dabei geht der Beschleuniger wie folgt vor:

- Strahlenförmiges durchdringen des Volumendatensatzes und definieren so genannter „sample points" entlang dieser Strahlen im Bereich des Objektes
- Ermitteln der Farb- und Transparentwerte an diesen Stellen
- Interpolieren von Voxeln oder Farbwerten an neuen „sample points" entlang der Durchdringungsrichtung
- Berechnung der Gradienten und Lichtwerte für das jeweilige Bild
- Ermitteln aller Farb- und Transparentwerte des gesamten Bildes

Bildlich kann man sich die erwähnten Strahlen als imaginäre Lichtstrahlen vorstellen, die ausgehend von der jeweiligen Bildoberfläche (Betrachtungswinkel und Objektgröße) durch den Volumendatensatz geschickt werden. Abb. 11 zeigt die Entstehung eines Bildes unter einem bestimmten Winkel und einer bestimmten Entfernung zum Objekt:

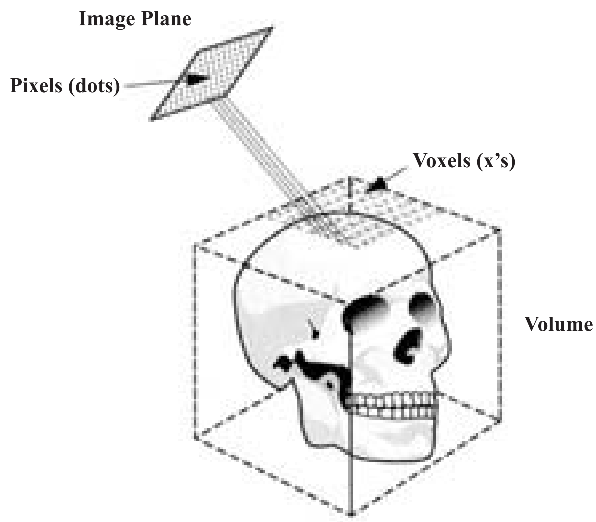

Abb. 11: Zusammenhang zwischen 2D-Bild und Volumen [9].

Dabei werden an bestimmten Punkten entlang der Strahlen, die Farb- und Transparentwerte „abgetastet". Der Grafikbeschleuniger berechnet nun die Farb- und Transparentwerte für jeden Strahl und speichert sie in dem dazugehörigen Pixel für das entsprechende Bild.

Dabei sollte man beachten, dass beim Schwenken und Zoomen des Schädels in der Programmoberfläche für jede Situation möglichst schnell das entsprechende neue Bild generiert werden muss. Durch den von uns verwendeten Grafikbeschleuniger ist die Visualisierung in Echt-Zeit möglich und dies vor allem ohne den merklichen Verlust von Informationen.

In Abb. 12 wird die Vorgehensweise des „Renderns“ verdeutlicht.

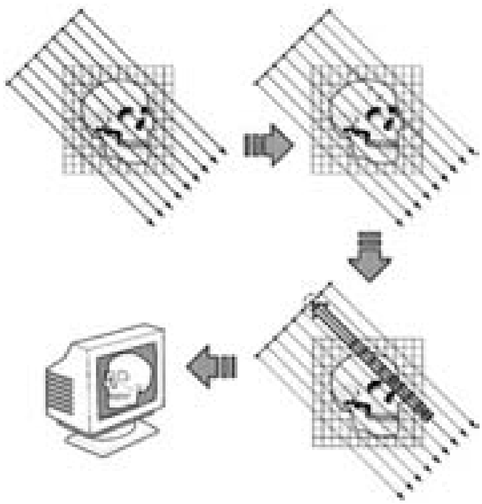

Abb. 12: Vorgehensweise beim Rendern [9].

Wenn wir im vorangegangenen Abschnitt von Volumendatensätzen sprechen, so muss man sich verdeutlichen, dass es große Variationen in der Anordnung von volumetrischen Datensätzen gibt. So können die Daten isotrop (gleicher Abstand der Elemente zueinander), anisotrop (ungleicher Abstand) oder isotrop, aber unter einem bestimmten Winkel zueinander angeordnet sein. Die Volumendatensätze die aus den CT-Schichtbildaufnahmen entstehen, werden typischer Weise der anisotropen Kategorie zugeordnet. Zum Veranschaulichen der anisotropen Anordnung kann man sich ein Volumen mit einem Voxel-Abstand in x- und y-Richtung von 0.5mm vorstellen, in dem die Schichten in z-Richtung einen Abstand von 1mm aufweisen.

In diesem Fall müssen die Koordinaten des entsprechenden Voxels in den jeweiligen Raumrichtungen mit einem, für jede Raumrichtung unterschiedlichen, Faktor multipliziert werden, um an die entsprechende Position im Volumen zu gelangen. Volumendatensätze die zwar isotrop, aber unter einem bestimmten Winkel angeordnet sind, können bei CT-Messungen entstehen, bei denen die sensitive Fläche des Scanners nicht rechtwinklig zur Bewegung in z-Richtung angeordnet ist. Die Grafiken in Abb. 13 verdeutlichen die beschriebenen Unterschiede.

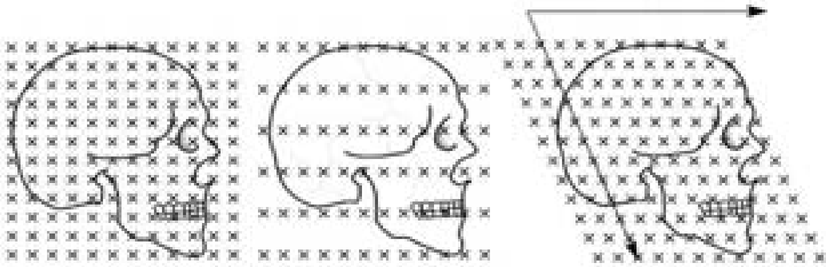

(a) isotropic, rectilinear (b) anisotropic, rectilinear (c) isotropic, gantry-tilted

Abb. 13: Unterschiedliche Volumentypen [9].

Der verwendete Grafikbeschleuniger unterstützt alle diese möglichen Anordnungen von Volumendatensätzen.

Technische Merkmale des Grafik-Beschleunigers

Wenden wir uns nun den technischen Eigenschaften der Beschleunigerkarte zu. Die Karte kann in jedem handelsüblichen PC-System betrieben werden, wobei darauf zu achten ist, dass sie den neuen 64bit PCI Standard mit 66Mhz unterstützt. Dabei ist man auf die größere Bauform der PCI-Slots angewiesen.

Der auf der Karte installierte Videospeicher ist in verschiedenen Abstufungen von 256 bis 1024 Mbyte erhältlich. Der von uns verwendete Beschleuniger verfügt über eine Speichergröße von 1024 Mbyte. Dies ist deshalb von besonderer Bedeutung, da umso größer der Videospeicher ist, desto mehr Informationen darin gespeichert werden können – und umso weniger Daten belasten den Hauptspeicher des Systems. Die in diesem Speicher abgelegten Daten sind darüber hinaus für den Prozessor des Beschleunigers schnell verfügbar, wodurch eine schnellere Generierung neuer Ausgabesequenzen möglich ist. Des Weiteren kommt dieser große Speicher dem sogenannten „z-Buffering" zu Gute. Das z-Buffering wird in der Computergraphik angewandt, um die verdeckten Flächen in einem Volumendatensatz zu ermitteln. Durch die Informationen im z-Buffer kann der Grafikbeschleuniger feststellen, welche Elemente einer Szene gezeichnet werden müssen und welche verdeckt sind.

Wird ein Objekt von einem 3D-Beschleuniger gerendert, so wird die Tiefeninformation der erzeugten Pixel (die z-Koordinate) im so genannten z-Buffer abgelegt. Dieser Buffer, gewöhnlich als zweidimensionales Array aufgebaut, enthält also für jeden Bildschirmpunkt einen Tiefenwert. Wenn ein anderes Objekt im selben Pixel dargestellt werden soll, vergleicht der Beschleuniger die beiden Tiefenwerte und wählt dasjenige Pixel, welches dem Beobachter am nächsten ist. Die Tiefeninformation des ausgewählten Pixels wird dann im z-Buffer gespeichert und ersetzt den alten Wert. Durch den z-Buffer kann der Grafikbeschleuniger die natürliche Tiefenwahrnehmung nachbilden: Ein nahe gelegenes Objekt verdeckt ein fernes Objekt.

Die Speichertiefe eines z-Buffers hat einen großen Einfluss auf die Qualität der Szene. Wenn zum Beispiel zwei Objekte sehr eng beieinander liegen, können beim 8-bit z-Buffer leicht Artefakte entstehen. Ein z-Buffer mit 16 bit oder 32 bit Speichertiefe erzeugt weniger Artefakte. Der verwendete Grafikbeschleuniger besitzt einen z-Buffer mit einer 32-Bit-Speichertiefe. Zum Erstellen einer neuen Szene muss der z-Buffer gelöscht werden, in dem er einen einheitlichen Wert (üblicherweise Null) erhält. Auf aktuellen Grafikkarten (1999–2003) beansprucht dieser z-Buffer einen bedeutenden Teil des verfügbaren Speichers und der Bandbreite. Mit verschiedenen Methoden wird versucht, den Einfluss des z-Buffers auf die Performance des Beschleunigers zu reduzieren. Zum Beispiel durch die verlustfreie Kompression der Daten, da das Komprimieren und Dekomprimieren der Daten kostengünstiger ist, als die Erhöhung der Bandbreite einer Karte. Ein anderes Verfahren spart Löschvorgänge im z-Buffer. Die Tiefeninformation wird dabei mit alternierendem Vorzeichen in den z-Buffer geschrieben. Ein Bild wird mit positiven Vorzeichen gespeichert, das nächste Bild mit negativem, erst dann muss der z-Buffer wieder gelöscht werden. Für den VolumePro1000 Grafikbeschleuniger wird eine Rate von bis zu einer Milliarde Samples pro Sekunde angegeben.

Natürlich sollte das Trägersystem vergleichbar gute Peripheriewerte aufweisen können, da sonst das Potenzial des Beschleunigers nicht vollständig ausgenutzt werden kann. Das von uns verwendete PC-System beinhaltet zwei Xeon 3.0 GHz Prozessoren der Firma Intel die auf einem Dualprozessorboard untergebracht sind. Als Hauptspeicher stehen 2Gbyte RAM zur Verfügung. Die Leistung des Ausgabeelements, also der AGP-Grafikkarte, fällt nicht weiter ins Gewicht, da der Beschleuniger die Berechnung der Sequenzen übernimmt und die Grafikkarte lediglich die generierten Bilder auf dem Monitor ausgeben muss.

Die Skizze in Abb. 14 soll noch einmal das Zusammenspiel der unterschiedlichen Komponenten im System verdeutlichen.

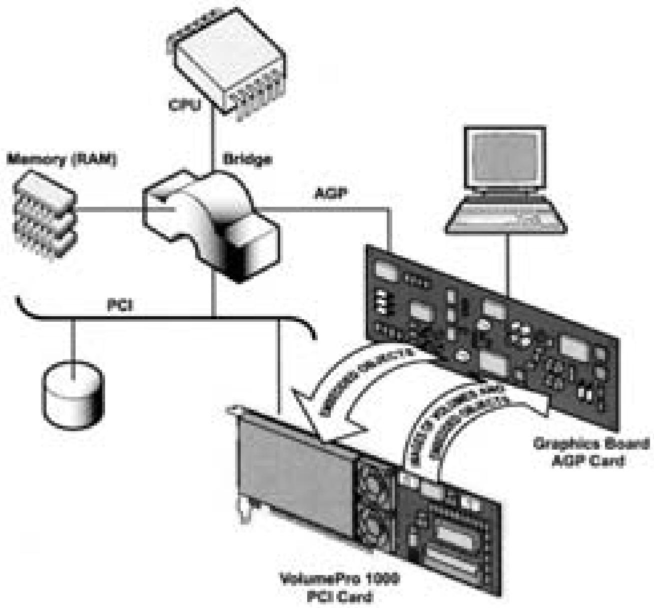

Abb. 14: Aufbau eines PC-Systems mit Grafikbeschleuniger [9].

Implementierung der Software für den Grafik-Beschleuniger

Um mit dem Grafikbeschleuniger kommunizieren zu können, ist es von grundlegender Bedeutung zu wissen, in welcher Programmiersprache die Programmbibliotheken des Beschleunigers realisiert wurden. Diese werden dazu benötigt, um auf die karteneigenen Funktionen zugreifen zu können. Die Firma TeraRecon bediente sich dabei der weit verbreiteten Programmiersprache C++.

Um eine plattformunabhängige Implementierung zu gewährleisten, haben wir uns für eine Javaimplementierung entschieden. Wir benötigten also eine Schnittstelle die unserem Programm den Zugriff auf diese Klassen ermöglicht. Hierbei bietet sich das von der Firma Kitware entwickelte Visualization Toolkit kurz VTK an. Dieses Visualization Toolkit beinhaltet bereits Klassen, die es ermöglichen, auf die VolumePro Hardware zuzugreifen. Die Klassen und Funktionen dieses Toolkit sind ebenfalls in C++ realisiert, jedoch ist hier ein „Übersetzer" enthalten, der es Programmiersprachen wie Java, Phyton und TCl erlaubt, auf die Klassen und Funktionen des VTK zuzugreifen. Der Sourcecode sowie die dazugehörige Dokumentation für VTK sind auf der Internetseite von Kitware erhältlich. Für die Nutzung der VolumePro-Funktionen muss das Softwarepaket allerdings neu erstellt werden. Dies geschieht mit Hilfe des Programms Cmake, welches ebenfalls auf der Internetseite von Kitware erhältlich ist. Dieses Programm bietet eine Reihe von Variablen und Einstellungen die entsprechend des Verwendungszwecks definiert werden müssen. Nähere Angaben zu den Einstellungen finden sich in den Dokumentationen des Programms. Zur Erstellung des neuen VTK Package erzeugt Cmake ein C++ Projekt, das mit einem entsprechenden Compiler (MS VisualStudio) erstellt werden muss. Nach erfolgreichem Kompilieren des Projektes erhält man ein Jar-Archiv, welches in den Classpath des Java-Compilers eingebunden werden kann. Anschließend sind alle Klassen des VTK in Java verfügbar [6].

Von besonderem Interesse sind dabei die Klassen, die speziell für das Rendern mit einem VolumePro Grafikbeschleuniger gestaltet sind. So beinhaltet das VTK zum Beispiel die Klasse vtkVolumeProVP1000Mapper [7]. Dieser Klasse übergibt man beispielsweise den eingelesenen Volumendatensatz der CT-Schichtbildaufnahme und sogenannte Piecewise-Linearfunctions (PLF), die zum Hervorheben oder Ausblenden bestimmter Werte im Datensatz benötigt werden [7]. So kann zum Beispiel der Wert für Luft ausgeblendet werden, da bei einer ersten Visualisierung Luft mit einem Wert von Null interpretiert und folglich schwarz dargestellt wird. Durch die richtige Einstellung der PLF's, wird der Farbwert für Luft ausgeblendet und das eigentliche Objekt dargestellt.

Alle folgenden Änderungen des Volumendatensatzes die zu einer abweichenden Darstellung vom Originalbild führen, werden, bedingt durch einen neuerlichen Aufruf der entsprechenden Klasse, nun von der Beschleunigerkarte in Echtzeit neu berechnet und dargestellt. Somit ist ein schnelles und effizientes Arbeiten mit der Programmoberfläche möglich.

Die Informationen über die technischen Eigenschaften des Grafikbeschleunigers und der Vorgehensweise des „Rendern", sowie das Beispiel zur Erläuterung der Funktionsweise des Visualization Toolkit, sind den Büchern [6], [7] und [9] entnommen. Abb. 15 zeigt die Benutzeroberfläche in Java.

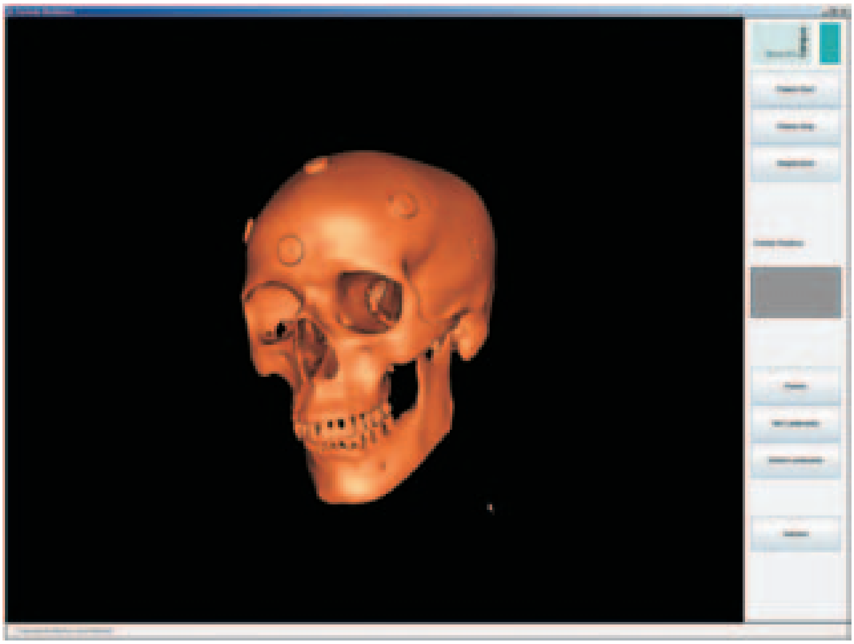

Abb. 15: Screenshot der Java Benutzeroberfläche.

Zusammenfassung

In der ersten Version des forensischen Arbeitsplatzes die in Matlab realisiert wurde, können mit Hilfe des optischen Trackingsystems die charakteristischen Landmarken auf dem visualisierten Schädel interaktiv eingefügt werden. Die Anzahl der gesetzten Landmarken ist für die Berechnung der Gesichtsoberfläche zu gering. Deshalb müssen noch mehrere Zwischenpunkte interpoliert werden. Zurzeit sind wir dabei, einen Algorithmus zu entwickeln, der pro Gesichtshälfte ca. 200 Zwischenpunkte einfügt. Ingesamt erhalten wir dann ca. 450 Punkte zur Berechnung der Oberfläche. Eine andere Anwendungsmöglichkeit für das Setzen mit Hilfe des optischen Trackingsystems stellt die in [8] vorgestellt Methode zur Gesichtsrekonstruktion dar. Ferner wird versucht, mit unterschiedlichen Parametrisierungen und Verfahren die Ergebnisse der berechneten Gesichtsoberfläche in Abb. 8 zu verbessern. Des Weiteren wurde mit der Erstellung eines Prototypen begonnen, der die Funktionen und Methoden des forensischen Arbeitsplatzes in ein echtzeitfähiges System überführt. Die Realisierung wurde unter Verwendung der Programmiersprache Java in Verbindung mit VTK vollzogen. Hierbei steht besonders die Einbindung einer leistungsstarken Beschleunigerkarte im Vordergrund, um die Performance des Systems zu verbessern.

Literatur

[1] R. P. Helmer, private Mitteilung, 2004.

[2] W. Kleppmann, *Wahrscheinlichkeitsrechnung und Statisti*k. Vorlesungsmanuskript der Studiengänge Elektronik/ Technische Informatik und Informatik. FH Aalen.

[3] S. R. Buss, *3-D Computer Graphics*. Cambridge: Cambridge University Press, 2003.

[4] B. Brüderlin, A. Meier, *Computergrafik und geometrisches Modellieren*. Stuttgart: Teubner, 2000.

[5] A. Watt, *3D-Computergrafik*. Bonn: Addison-Wesley-Longman, 2002.

[6] W. Schroeder, L. S. Avila, K. Martin, B. Lorensen, *The VTK user's guide*. Clifton Park, NY: Kitware, 2003.

[7] W. Schroder, K. Martin, B. Lorensen, *Visualization Toolkit*. Clifton Park, NY: Kitware, 2003.

[8] J. Müller, A. Mang, D. Thomsen, T. M. Buzug, *Regularized 3D Thin-Plate Splines for Soft-Tissue Reconstruction.* Biomedizinische Technik, Band 49, Ergänzungsband 2, 2004.

[9] TeraRecon VolumePro1000 Users Guide, *Principals of Operation*, TeraRecon Inc., 2001.

6.

Technical Innovations and Implementations
Technische Innovationen und Implementationen

Ultrafast Holographic 3D Facial Topometry and Digital Reconstruction

S. Hirsch[1,2], S. Frey[1], A. Thelen[1], N. Ladrière[1], J. Bongartz[1,3], and P. Hering[1,4]

[1] Caesar foundation, Ludwig-Erhard-Allee 2, D-53175 Bonn
[2] HFZ, University Hospital Basel, CH-4031 Basel
[3] RheinAhrCampus, Fachhochschule Remagen, Südallee 2, 53424 Remagen
[4] Institute for laser medicine, University of Duesseldorf, Universitaetsstrasse 1, D-40225 Duesseldorf

Abstract

At *caesar* (Center for Advanced European Studies and Research) in Bonn, Germany we are developing a two-step method for topometric measurement using pulsed holography. In a first step we produce a portrait hologram of the person. To achieve this, we designed a mobile holographic system that is able to capture holograms in ambient light situations. Consequent to the recording, the real image is reconstructed optically and digitized slice-by-slice. From this volumetric data set the skin surface of the patient is extracted and transferred into a 3 d surface.

With our method we obtain an accurate (0.4 mm) virtual 3D representation of the face with highly resolved texture information (160µm). In comparison computer tomography yields the bone structure and a coarse facial surface of the person. We utilize the extracted surface to perform the registration of our textured model with the skull. The main application of our method is to provide soft tissue information for planning and documentation of craniofacial surgery.

1 Introduction

Planning, simulation and documentation of interventions in maxillofacial surgery require high-resolution soft tissue information of the human face. Topometric data may be gained with various methods (CT, optical, contact), and these all have their advantages and drawbacks. We developed a topometry system using pulsed holography to capture the surface of objects.

In topometry it is necessary to avoid movement of the object during measurement. For static objects this is hardly of influence, however, movement artifacts are the primary cause of errors in measurements of living or moving objects. In this case, either the recording time needs to be sufficiently short, or the object needs to be immobilized as much as possible.

Most current topometric techniques feature overall capture times ranging around or just below one second. Although their nominal accuracy, which is defined on static objects, might be excellent, the surface quality from moving objects is often questionable. Therefore great efforts are being made to speed up the measurement. Yet in real life situations it is desirable to use shorter acquisition times to avoid movement artifact systematically. In portrait photography usually 1/60 s is well accepted. In pulsed portrait holography we capture the surface of an object in 25 ns, which obviously freezes all movements ([1], [2]).

Fig. 1: Mobile holographic camera HSF-mini developed in cooperation with GEOLA, Lithuania.

2 Mobile holographic camera

During our development of holographic topometry we used a standard GP-2J holographic camera from GEOLA with a Nd:YLF laser (526.5 nm). There we saw the demand for a flexible and mobile recording system. Together with GEOLA, Lithuania we designed a mobile holographic camera based on a pulsed Nd:YAG laser. The system (see **fig. 1**) is currently located at the Universitätsspital Basel in the High-tech Forschungszentrum, which is directed by Prof. H.-F. Zeilhofer. We are adapting the system there for clinical use and pursue first clinical studies for planning of maxillofacial surgery with the holographic data sets. The system is also used to conduct measurement campaigns for data retrieval outside our laboratory.

The laser is built in an oscillator-amplifier arrangement, the second harmonic of this Q-switched laser offers a wavelength of 532 nm with up to 1.4 J pulse energy and with a pulse duration of about 25 ns. The wavelength of the laser in the green is ideal for portrait holography, since it displays a low penetration depth into tissue below 1 mm with a reflectivity of app. 60%.

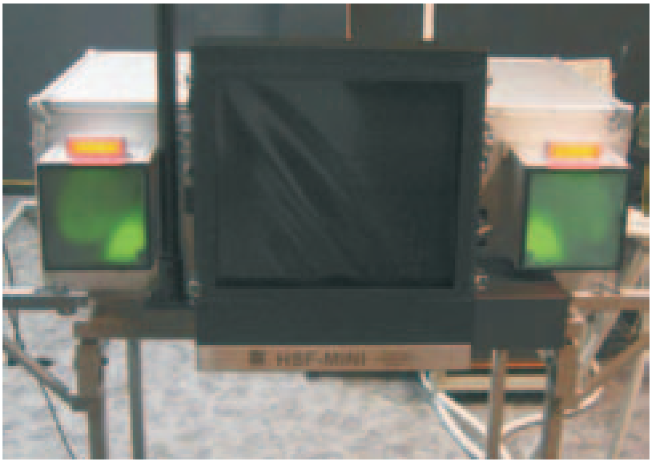

Fig. 2: Holographic camera from the viewpoint of the patient. Left and right are the two illumination ports with the diffuser plates for eyes-safe recording. Centrally located is the mechanical shutter system that covers the holographic plate.

The hologram recording is performed with a single laser pulse of 25 ns and hence does not display any movement artefacts. So even with uncooperative patients, e. g. children, or moving targets it is possible to record a spatial image. The coherence length of 6 m allows for the coverage of a large volume with one exposure.

The recording procedure is usually performed in an upright position of the patient. We use diffuser plates on the illumination ports, which make the hologram capture eyes-safe (see **fig. 2**). The camera features a mechanical shutter system that makes it possible to work at daylight conditions.

The hologram is recorded on standard holographic plates or film VRP-M from Slavich. For the chemical processing of exposed film we adapted an automated film processor ([3]) to the special needs of holograms.

Due do its modular and compact construction the camera is portable and can be set up in the field within 20 minutes. The camera contains the option to engage structured illumination. This feature allows digitizing objects that do not show enough structure on the reflecting surface.

3 Holographic Topometry

Recording

In holography not only the amplitude but as well the phase of an object is recorded. For interferometric measurement with coherent light, this task is performed by superimposing the beam itself with a manipulated copy of the same beam.

The beam from a coherent light source, usually a laser, is split into two parts. The first beam illuminates the object, the light is then scattered back from the object towards the sensor material. The second part of the beam, the reference beam, is expanded to a spherical wave and travels directly to the holographic plate, where it interferes with the object beam (**see fig. 3a**).

The resulting interference pattern carries not only the amplitude of the object beam but as well the phase relative to the reference beam. All of this information is stored in a modulation of the amplitude transmittance of the plate. The emulsion used for holography has a very fine grain size (<3000 lines/mm), which is essential for successfully capturing the fine fringe patterns that form the hologram from an off-axis arrangement. The additional presence of the phase information in the hologram makes it possible to reconstruct the spatial information of the object.

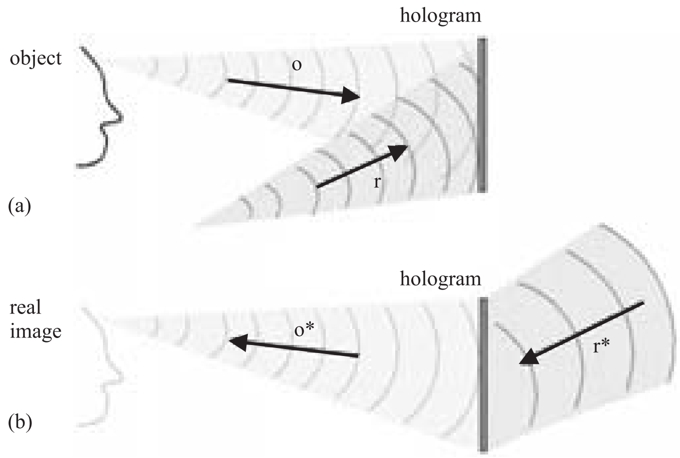

Fig. 3: (a) Recording – Interference between reference and object waves. (b) For the optical reconstruction the hologram is illuminated with the complex conjugate reference beam, forming the real image.

Optical Reconstruction

The second step is the optical reconstruction of the hologram. When illuminating the holographic plate with the conjugate (“time reversed”) reference beam, a light body, the so-called real image, resembles at the place where the scattering object was situated before (**see fig. 3b**). The real image is a one-to-one copy of light field of the illuminated object, maintaining the object dimensions perfectly. The real image shows a theoretical resolution in the range of a few micrometer.

This light body is scanned axially in a series of 2d-projections of equal distance (app. 100µm) with a lateral resolution of 160µm. This procedure is referred to as hologram tomography (**see fig. 4**).

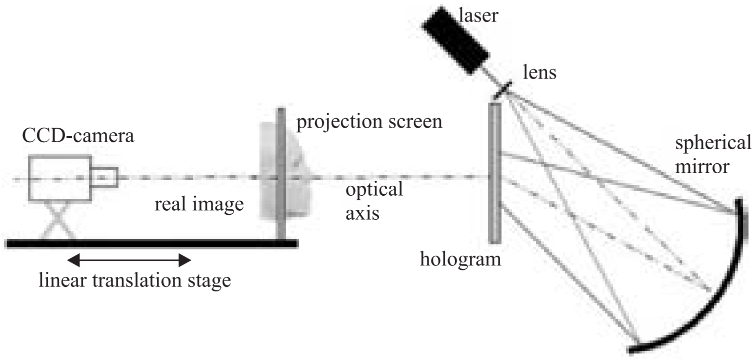

Fig. 4: Set-up for optical reconstruction.

Surface extraction

In the volumetric image stack each slice contains the light information of the focussed regions and the blurred information of all neighbouring regions (see **fig. 5**) as described by the point spread function (PSF). So we face the task to differentiate between focussed and unfocussed regions ([4]). The procedure of finding the regions with the maximal local image contrast uses the local variance of the slices.

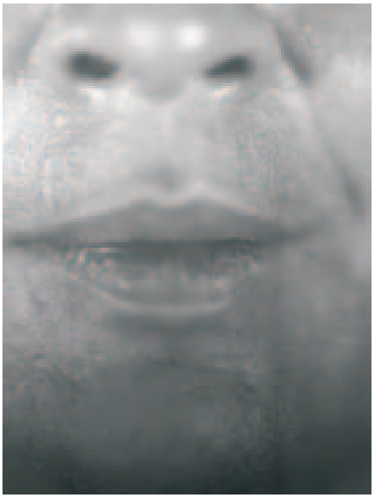

Fig. 5: In the projection of the real image each slice displays focussed and unfocussed areas. Clearly visible is the highly resolved texture information of the hologram.

When being in the focus of the surface, one can extract the surface coordinate as well as the brightness information of this point. Along with the surface one obtains a greyscale representation of the surface texture. The combination of this information yields a textured 3d model with fine details (see **fig. 6**). The accuracy of the surface gained by our method is about 0.4 mm, whereas the highly resolved texture is only limited by the lateral resolution of the real image. It has to be noted that this resolution applies for both, static and dynamic objects.

Fig. 6: The textured 3d model is a combination of the surface with the inherent greyscale texture of the hologram.

With our system, the capture of the face and the optical reconstruction of the textured surface are performed in two separate steps. After processing, the holographic information is permanently stored in the emulsion and can be recalled at any time. This offers the possibility to analyse the hologram again at a later time if technical advances facilitate a more accurate digitisation.

4 Combination with CT datasets

A CT provides a volumetric data set of the skull but no surface texture. By combining this with the soft tissue information of the hologram it is possible to achieve a very precise representation of the patients face along with the face texture and hair representation. Through appropriate threshold it is possible to obtain the bone information of the head and the facial surface. By registering the holographically attained surface (**fig. 6**) to the facial surface from the CT scan, the surface of the holographic method is perfectly aligned with the CT surface (**fig. 7**). For clarity of the representation, the texture information is omitted in this figure.

Fig. 7: Resulting three-dimensional model as a combination of CT data with holographic surface data. The texture information is not shown in this figure.

5 Conclusion

With our technique it is possible to generate digital models of the face/skin, whereas it is not limited to this application. We measure technical objects as well as forensic and archaeological findings (see **fig. 8**) with sub-millimeter accuracy, which offers still potential for improvement. Due to the large measurement volume, the method can be applied to bigger areas, which offers the possibility to perform reconstructions of crime sites. The short exposure time of the hologram capture makes it possible to reconstruct even moving objects.

Fig. 8: Digital model of the skull of the Kripo Celle case.

In a current effort we are exploring the potential and limitations of a complete digital processing of the hologram. It is the goal to capture the hologram with a light sensitive array and perform a digital numerical of the real image ([5]). This is possible by simulating the interference of the conjugate reference beam with the digital hologram. This would eliminate the step of chemical processing and optical reconstruction of the real image, but still require the subsequent step of detecting the focussed surface of the hologram.

Due to technical limitations of current capture hardware the resolution of the image sensors (3–14 µm) is still two orders of a magnitude away from the resolution of the holographic film (50 nm grain size). This restriction imposes certain constraints on the recording set-up and limits the resolution. Yet the persistent popularity of imaging capabilities in consumer electronics proliferates a rapid developments in the field of image sensors, so it can be expected that the pixel pitch will further decrease while the chip dimensions will increase constantly.

We aim to establish a database of soft facial tissue profiles depending on age, gender, and ethnic origin. In combination with CT data it provides information about the soft and hard tissue and can serve for computer based fast craniofacial identification, forensic medicine and archaeology.

Acknowledgements This work is supported by the NCCR CO-ME (Computer Aided and Image Guided Medical Interventions) funded by Swiss National Research Foundation.

6 References

[1] J. Bongartz, “Hochauflösende dreidimensionale Gesichtsprofilvermessung mit kurzgepulster Holographie,” Ph. D. dissertation, Mathematisch Naturwissenschaftliche Fakultät der Heinrich-Heine-Universität Düsseldorf, 2002. http://diss.ub.uni-duesseldorf.de/ebib/diss/file?dissid=192

[2] D. Giel, “Hologram tomography for surface topometry,” Ph. D. dissertation. Mathematisch Naturwissenschaftliche Fakultät der Heinrich-Heine-Universität Düsseldorf, 2002. http://diss.ub.uni-duesseldorf.de/ebib/diss/file?dissid=598

[3] N. Ladrière, “Optische und chemische Aspekte der hochauflösenden, automatischen Hologrammentwicklung,” diploma thesis, Fachhochschule Köln, 2004.

[4] A. Thelen, J. Bongartz, D. Giel, S. Frey and P. Hering, “Iterative focus detection in hologram tomography”, JOSA A, Volume 22, Issue 6, 1176–1180 (2005).

[5] W. Jüptner, U. Schnars, “Direct recording of holograms by a CCD target and numerical reconstruction”, Applied Optics, 33(2):179–181, 1994.

Rapid Prototyping Models for Facial Reconstruction

H. Seitz, C. Tille, W. Rieder, S. H. Irsen, G. Bermes

caesar research center, Ludwig-Erhard-Allee 2, 53175 Bonn, Germany

Abstract

This paper presents the application of rapid prototyping techniques for facial reconstruction. Rapid prototyping techniques allow to manufacture prototypes from complex three-dimensional datasets. Rapid prototyping is well-established nowadays and was originally developed for building technical prototype models based on CAD data. But these techniques show also great potential for non-technical applications like manufacturing of physical models for facial reconstruction. Computer tomography, holographic tomography or other three-dimensional (3D) scanning techniques can be used to acquire raw-data of the object to be built. Usually, these datasets have to be edited and converted into 3D surface data, which can be processed by rapid prototyping machines. Dependent on the application of the models and the required characteristics of the physical models, the appropriate rapid prototyping technique has to be chosen for manufacturing of the models based on 3D datasets. The rapid prototyping processes 3D printing, stereolithography and subsequent vacuum casting have been used to build models for facial reconstruction in forensic, anthropological and medical application areas. Moreover, three-dimensional datasets from computer-aided facial reconstruction can also be used to directly build models based on the generated datasets.

A rapid prototyping process chain was established and optimized for the medical and anthropological field and has been applied in several cases. The results demonstrate the advantages and disadvantages of these techniques for the respective application.

Introduction

Rapid prototyping, also known as solid freeform fabrication (SFF) is a class of techniques to manufacture prototypes from complex three-dimensional datasets. All rapid prototyping processes are based on the same principle of building three-dimensional models layer by layer. There are several rapid prototyping techniques on the market, each having advantages and disadvantages. The most important techniques are stereolithography, fused deposition modeling, selective laser sintering and 3D printing [1]. Rapid prototyping was originally developed for building technical models based on CAD data and was mainly used within the automotive, aerospace and mechanical engineering industries. Nowadays, rapid prototyping processes are not only used in the technical field for making concept models or functional prototypes for engineering test and evaluation issues but also in promising areas like medicine or anthropology. For instance, in cranio-maxillofacial surgery physical anatomical models made from medical imaging data of the patients help surgeons to prepare operations in close detail [2]. Rapid prototyping technology has also been used to build replicas of skull findings for forensic [3] and anthropologic studies [4]. Most of the previous studies report a process chain where CT scans serve as data sources and the models are build by stereolithography. The application of various 3D data scanning methods and rapid prototyping techniques increases the potential of these technologies for forensic, anthropologic and medical applications.

Data Acquisition and Preparation

Rapid prototyping requires 3D datasets for manufacturing physical models. These data can come from various sources. Computer tomography (CT), magnetic resonance imaging (MRI), holographic tomography [5] or other 3D surface scanning techniques can be used to acquire raw-data of the desired object. In holographic tomography, a holographic image of a person is taken by a pulsed laser system. Then, a real image of the hologram is reconstructed, captured and converted in a 3D surface computer model. In case of CT or MRI data, the software MIMICS (Materialise, Belgium) is a suitable tool to transform the 2D medical datasets into 3D surface models (STL file format). Specific object regions can be extracted selecting the corresponding threshold value (Houndsfield units) for segmentation. Raw-data from holographic tomography or other 3D surface scanners can be used directly but have to be converted into the STL file format. Usually, the resulting STL-datasets have to be edited using the software tool MAGICS (Materialise, Belgium) in order to correct errors in the STL-files, to manipulate regions of interest or to define a certain thickness when dealing with 3D surface scans. Furthermore, the STL-files can be imported into the FreeForm modeling system (SensAble Technologies, USA) for special data manipulations. The software operates in conjunction with the PHANTOM Desktop, a haptic device that provides force feedback to the operator. Especially freeform surfaces of body structures can be manipulated intuitively and interactively with the FreeForm software. FreeForm allows to close holes, to connect inner structures and to cut, mirror, carve and smooth the model into the right shape where necessary. Various other software tools are used to modify the original 3D data e. g. to map a texture file on the 3D surface dataset for 3D printing of colored models if necessary. When working with 3D files with texture maps, the VRML-file format has to be chosen, because the STL-file format cannot deal with textures. An emerging field in anthropologic and forensic facial reconstruction is computer-aided facial reconstruction [6]. Three-dimensional datasets generated by this technique can also be used directly or have to be converted in the STL-file format to build models.

Rapid Prototyping Processes

Dependent on the application of the models and the required characteristics of the physical models, the appropriate rapid prototyping technique has to be chosen for manufacturing the models based on 3D datasets. In this study the rapid prototyping processes 3D printing, stereolithography and vacuum casting have been used to build models. These processes allow manufacturing of models with various mechanical and optical characteristics.

3D printing

The 3D printing process is a powder-based process that builds physical 3D models directly from computer data [7]. A box filled with plaster-based material is printed with a binder solution layer by layer (see figure 1, step 1 to 4). Powder is bonded in wetted regions. Unglued powder can be removed after the building process is finished and the printed part remains. Finally, the model is infiltrated with a lacquer for improved strength. The main advantage of this process is the capability of printing in full-color. Thus, it is possible to process for example color facial scans and manufacture full-color models based on these datasets. Furthermore, replicas of skulls made by 3D printing are well suited as models for forensic or anthropological reconstruction of soft facial parts with clay or plasticine.

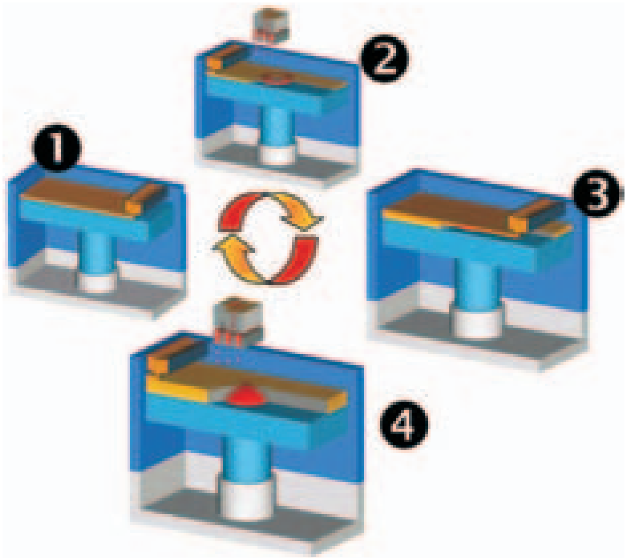

Fig. 1: 3D printing process scheme

Stereolithography

Stereolithography is the most widely used rapid prototyping technology. Stereolithography builds plastic models that can be used directly or as masters for vacuum casting [7]. In stereolithography, a laser draws the cross section of the model onto the surface of a vat containing liquid, photocurable polymeric resin (see figure 2). The laser energy solidifies the resin to create a solid geometry. This process is repeated for every single layer. The resulting models are translucent providing an insight into internal structures of the 3D model. Using special polymers it is also possible to selectively mark regions of interest within the translucent model in a single color. This allows e. g. the improved visualization of anatomical features, such as tumors within an anatomical model made for surgical planning.

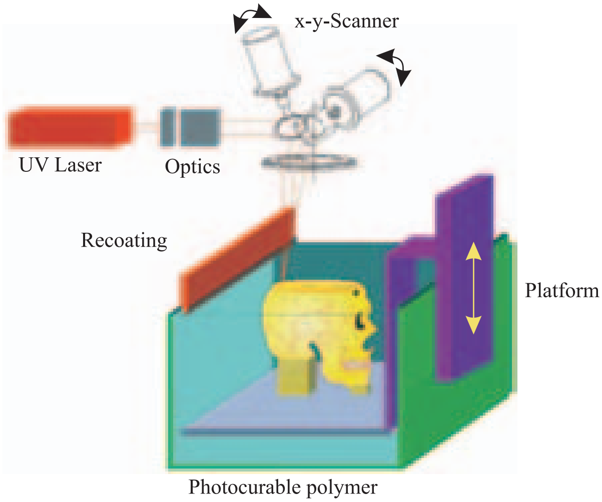

Fig. 2: Stereolithography process scheme

Vacuum casting

Stereolithography models cannot only be used directly but also as masters to produce silicone moulds for vacuum casting. The use of the vacuum casting process allows building replicas of a master in various materials with different material properties and colors [7]. In the first step of the vacuum casting process, silicone is cast around the stereolithography master. After curing, the silicone mould is cut open and the master is removed, leaving a cavity for the cast. The resulting flexible mould is used to cast one ore more copies of the master. Casting is performed in vacuum in order to avoid air bubbles. Although the flexibility of the silicone mould allows to cast models with partial undercuts like the human ear, the complexity of the models is restricted. The cast models must be demouldable from the silicone mould. Cast materials are typically two-component polyurethanes. But it is also possible to use silicones as cast materials. The elasticity and the color of the used resin can be adjusted with different additives to simulate different kinds of tissue. Thus, it is possible to mimic various types of tissue with realistic haptic and optical characteristics.

Applications

The presented manufacturing processes have been applied in several medical and anthropological cases. The 3D models were made based on various data sources and were used for different applications. The respective manufacturing process was chosen dependent on the mechanical and optical characteristics of the models and taking into consideration the manufacturing costs.

Colored 3D portrait model

Colored 3D portrait models of patients were manufactured by 3D printing. 3D datasets of patients were acquired by holographic tomography. The raw-datasets were transformed in the STL-file format and a certain thickness of the surfaces was generated in order to be able to build physical models. Digital photo images of patients were mapped onto the resulting STL-files to get full-color datasets. The resulting VRML-files were imported into the machine software of the 3D printer. The 3D printer generated the full-color models. Fig. 3 shows an example of a full-color 3D printed portrait model of a subject.

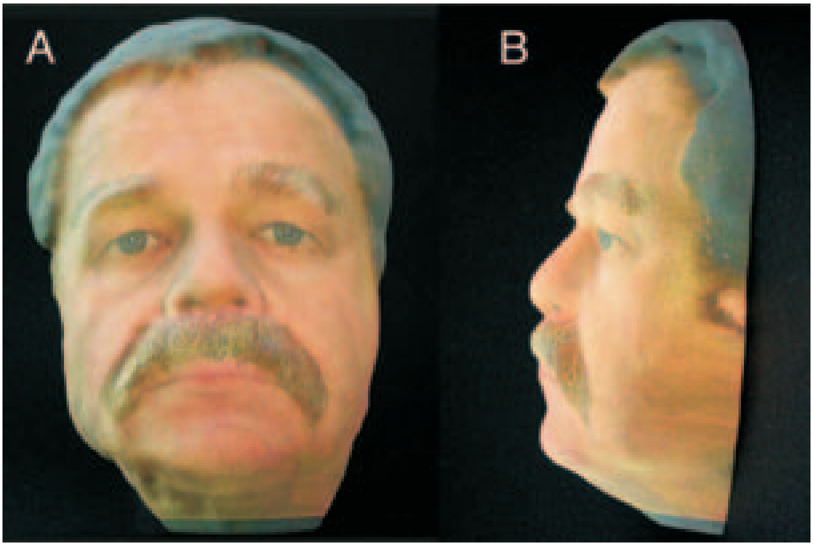

Fig. 3: Colored 3D portrait model of a male subject made by 3D printing; A = front view, B = side view

Skull models for reconstruction of soft facial parts

Rapid prototyping technology is especially suited to build replicas of skull findings e. g. for reconstruction of soft facial parts. Several models have been generated by 3D printing as well as stereolithography. The data were acquired by CT scans and segmented using the software tool MIMICS. Fig. 5 shows a model for facial reconstruction made by 3D printing. The original skull was found in a forest near Celle, Germany in January 2003 (see figure 4). The identity of the person is still unknown. 12 replicas of the skull have been manufactured for a comparative study of facial reconstructions [8]. The models were used as hard tissue basis for soft tissue reconstruction with modeling techniques like clay or similar materials. Results of this ongoing study will be published elsewhere in the near future.

Fig. 4: Original skull found in a forest near Celle, Germany (Polizeiinspektion Celle/RheinAhrCampus Remagen)

Fig. 5: Model for reconstruction of soft facial parts made by 3D printing

A stereolithography replica of a skull finding from the Museum for Hamburg History was also used for reconstruction of soft facial parts. This skull is discussed to belong to Klaus Stoertebeker, a famous pirate, who plundered ships of the Hanseatic League in the North Sea and Baltic Sea. He was executed in Hamburg in 1402 and his head was nailed to a pole as a deterrent to others. Fig. 6 shows the stereolithography replica whereas figure 7 shows the reconstructed face that was formed by French artist Elisabeth Daynes, Paris.

Fig. 6: Stereolithography replica of a skull finding from the Museum for Hamburg History. (©Philippe PLAILLY/Atelier DAYNES/EURELIOS)

Fig. 7: Image of the reconstructed face formed based on a stereolithography replica (©Philippe PLAILLY/Atelier DAYNES/EURELIOS)

Combined soft and hard tissue models

Using multiple rapid prototyping techniques allows building anatomical models with realistic haptic and optical representation of various types of tissue. Based on medical datasets, preferably computer tomography scans of the affected region, both soft and hard tissue structures are reconstructed. A stereolithography apparatus builds the hard tissue models and the masters of the soft tissue structures. The vacuum casting technique allows manufacturing realistic representations of soft tissues. Fig. 8 shows an anatomical model for testing of a new stereoscopic overlay display that supports surgeons during the intervention by displaying 3D stereoscopic anatomical structures over the actual operating situs.

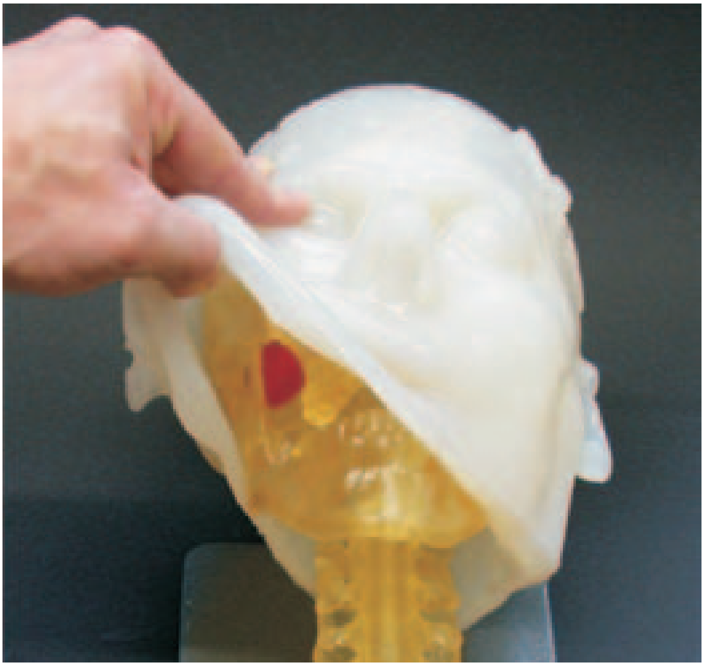

Fig. 8: Anatomical model for testing of a new stereoscopic overlay display

Discussion

The manufacturing of physical models for facial reconstruction using rapid prototyping technologies shows many benefits. These techniques are especially suited for generating replicas of skull findings. Rapid prototyping allows reproducing external and internal morphological details of the original skull. It is possible to reproduce regions of interest in various scales. A further advantage is the possibility to produce multiple replicas to perform investigations or facial reconstructions simultaneously by several people at different places.

Since every rapid prototyping technique has its advantages and disadvantages, various rapid prototyping techniques have been investigated for manufacturing physical models for facial reconstruction.

3D printing is a fast and cost-effective technology for building physical models. The mechanical stability and the geometrical precision of 3D printed models are not as high as achievable with stereolithography. On the other hand, 3D printing is the only technology for building models in full-color. The quality of the color is not true-color but is sufficient to give a good optical impression of the original. Thus, 3D printing is especially suited to manufacture full-color portrait models e. g. for documentation of patients undergoing maxillo-facial surgery. 3D printing is also an appropriate technique for building models based on three-dimensional datasets from computer-aided facial reconstruction. Moreover, 3D printing is especially capable of producing multiple replicas of an original since it is a fast and a cost-effective technology in comparison to stereolithography.

Very precise replicas of an original can be manufactured by stereolithography. It is possible to build models in a translucent material in order to view internal anatomical structures. Stereolithography generally is considered to provide the greatest accuracy and best surface finish of any rapid prototyping technology. Thus, it is the preferred method to fabricate replicas that are used to perform investigations if handling of the usually valuable and sensitive originals should be avoided. Since stereolithographic models are mechanically very stable, they are well suited as templates for reconstruction of soft facial parts with modeling techniques like clay or plasticine. Furthermore, anatomical models made by stereolithography can be sterilized and used in the operating room. As a consequence, stereolithography is the preferred technique to build models used for surgical planning.

The manufacturing of combined anatomical models needs significant technical efforts. Stereolithography as well as vacuum casting have to be used to manufacture anatomical models with realistic haptic and optical representation of different types of tissue. Thus, combined models are applicable for special cases like training models or anatomical models for surgical planning. In surgical planning, these models allow to control aesthetic aspects of the surgery during the surgical planning, because the soft tissue model (e. g. soft facial parts) adapts changes of the modified hard tissue structure (e. g. osseous structure). Generally, the vacuum casting technique allows building various anatomical structures in a wide range of materials with variable material properties and colors from a stereolithographic master.

Conclusion

The main objective of the paper was to present the possibilities of rapid prototyping technologies for manufacturing models for facial reconstruction. Different process chains have been presented to produce such models by different rapid prototyping techniques. Dependent on the application of the models and the required physical characteristics, the appropriate rapid prototyping technique has to be chosen for manufacturing.

Since rapid prototyping industry is a dynamically growing market, further new effective technologies and materials for manufacturing models for soft facial reconstruction will be available in the near future.

References

[1] T. Wohlers, Wohlers Report 2004: Rapid Prototyping & Tooling State of the Industry. Wohlers Associates, Fort Collins, Colorado 2004.

[2] J. F. Arvier, T. M. Barker, Y. Y. Yau, P. S. D'Urso, R. L. Atkinson and G. R. McDermant, (1994), "Maxillofacial biomodelling", British Journal of Oral and Maxillofacial Surgery, vol. 32, pp. 276–283, 1994.

[3] M. S. Dolz, S. J. Cina and R. Smith, "Stereolithography – A Potential New Toll in Forensic Medicine", The American Journal of Forensic Medicine and Pathology, vol. 21, number 2, pp. 119–123, 2000.

[4] C. P. E. Zollikofer, M. S. Ponce de León and R. D. Martin, "Computer-assisted paleoanthropology", Evol. Anthropol., vol. 6, pp. 41–54, 1998.

[5] A. Thelen, S. Frey, S. Hirsch, N. Ladriére, J. Bongartz, D. Giel and P. Hering, "Digitization of holographic recordings for medical applications", in Proceedings of the Remagener Physiktage. Remagen. September 2004.

[6] J. Subke and M. Wittke, "CAD Enhanced Soft-Tissue Reconstruction in Forensics with Phantom 3D Touch – An Electronic Modelling Tool with Haptic Feedback", in Proceedings of the 2nd International Conference on Reconstruction of Soft Facial Parts. Remagen. March 2005.

[7] A. Gebhardt, Rapid prototyping. Munich: Hanser, 2003.

[8] J. Bongartz, T. M. Buzug, P. Hering, C. Tille and H. Seitz, "Introduction to the Comparative Study on Facial Reconstruction", in Proceedings of the 2nd International Conference on Reconstruction of Soft Facial Parts. Remagen. March 2005.

Rapid Prototyping Modelle für die Gesichtsrekonstruktion

H. Seitz, C. Tille, W. Rieder, S. H. Irsen, G. Bermes

Forschungszentrum caesar, Ludwig-Erhard-Allee 2, 53175 Bonn, Germany

Abstract

Dieser Artikel präsentiert die Anwendungsmöglichkeiten von Rapid Prototyping Technologien für die Gesichtsrekonstruktion. Rapid Prototyping Technologien erlauben die Herstellung von Prototypen aus komplexen dreidimensionalen Datensätzen. Rapid Prototyping Verfahren sind heutzutage sehr gut etabliert und wurden ursprünglich entwickelt, um technische Prototypenmodelle direkt aus CAD Daten herzustellen. Darüber hinaus zeigen diese Techniken jedoch auch ein großes Potential für nichttechnische Anwendungen, wie die Herstellung von Modellen für die Gesichtsweichteil-Rekonstruktion. Computertomographie, holographische Tomographie oder andere dreidimensionale (3D) Scan-Verfahren können dazu benutzt werden, Computerdaten des zu fertigenden Originals zu erhalten. Normalerweise müssen diese Datensätze noch bearbeitet und anschließend in 3D-Oberflächendaten umgewandelt werden, welche von den Rapid Prototyping Maschinen verarbeitet werden können. Welche der verschiedenen Rapid Prototyping Techniken für die Herstellung von solchen Modellen gewählt wird, hängt von der späteren Anwendung und der gewünschten Eigenschaften der Modelle ab. In der vorliegenden Arbeit wurden die Rapid Prototyping Prozesse 3D-Drucken, Stereolithographie und Vakuumguss benutzt, um Modelle für Gesichtsrekonstruktionen, für forensische, anthropologische und medizinische Anwendungen herzustellen. Außerdem können dreidimensionale Datensätze aus der computergestützten Gesichtsrekonstruktion zur direkten Herstellung von Modellen verwendet werden.

Eine RP-Prozesskette wurde für medizinische und anthropologische Anwendungsgebiete entwickelt und optimiert und bereits in mehreren Fällen angewendet. Die Ergebnisse demonstrieren die Vorteile und Nachteile der verschiedenen Techniken für die jeweilige Anwendung.

Einleitung

Rapid Prototyping, auch Solid Freeform Fabrication (SFF) genannt, ist eine Klasse von Techniken zur Herstellung von Prototypen aus komplexen dreidimensionalen Datensätzen. Die Rapid Prototyping Prozesse basieren alle auf dem gleichen Prinzip, dem schichtweisen Aufbau dreidimensionaler Modelle. Es sind verschiedene Rapid Prototyping Verfahren am Markt etabliert, wobei jedes Verfahren seine eigenen Vor- und Nachteile besitzt. Die wichtigsten Verfahren sind die Stereolithographie, das Fused Deposition Modeling, das Lasersintern und das 3D-Druckverfahren [1]. Rapid Prototyping wurde ursprünglich entwickelt, um technische Modelle direkt auf Basis von CAD-Daten herzustellen. Der häufigste Einsatz findet in den Bereichen Automobil-Entwicklung, Luftfahrt und Maschinenbau-Industrie statt. Heutzutage werden Rapid Prototyping Verfahren allerdings nicht nur in technischen Bereichen zur Herstellung von Konzept-Modellen oder Prototypen für funktionale Tests einsetzt sondern auch in neuen viel versprechenden Bereichen wie der Medizin oder der Anthropologie. Zum Beispiel werden in der Mund-Kiefer-Gesichtschirurgie anatomische Modelle, die auf Basis von Patientendaten hergestellt werden, verwendet, um dem Chirurgen die Operationsvorbereitung zu erleichtern [2]. Darüber hinaus finden Rapid Prototyping

Verfahren bei der Herstellung von Kopien von Schädelfunden für forensische [3] und anthropologische Studien [4] Verwendung. Die meisten früheren Studien beschreiben eine Prozesskette, bei der Computertomographie-Daten als Datenquelle dienten und die Modelle mittels Stereolithographie erstellt wurden. Gerade jedoch die Kombination verschiedener 3D-Scan-Verfahren und unterschiedlicher Rapid Prototyping Techniken steigern das Potential dieser Technologien für forensische, anthropologische und medizinische Anwendungen.

Datenerfassung und -aufbereitung

Rapid Prototyping setzt 3D-Datensätze zur Herstellung von Modellen voraus. Diese Daten können auf verschiedene Arten generiert werden. Computertomographie (CT), Magnetresonanztomographie (MRT), holographische Tomographie [5] oder andere 3D-oberflächenabtastende Scan-Verfahren können verwendet werden, um Rohdaten des gewünschten Objektes zu erhalten. In der holographischen Tomographie wird mit einem gepulsten Laser ein holographisches Bild einer Person aufgenommen. Danach wird ein reelles Bild des Hologramms rekonstruiert und in ein 3D-Oberflächencomputermodell umgewandelt. Liegen die Daten als CT- oder MRT-Daten vor, so kann der zweidimensionale Datensatz mit Hilfe der Software MIMICS (Materialise, Belgien) in ein 3D-Oberflächenmodell umgewandelt (STL-Datenformat). Die einzelnen Objektregionen können durch Auswahl des entsprechenden Schwellwertes für die Segmentierung unterschieden werden. Rohdaten der holographischen Tomographie oder anderer 3D-oberflächenabtastenden Verfahren lassen sich direkt in das STL-Datenformat umwandeln. Häufig müssen STL-Datensätze mit der Software MAGICS bearbeitet werden, um Fehler in den STL-Daten zu korrigieren, gewünschte Regionen nachzubearbeiten oder eine bestimmte Materialdicke zu definieren, wenn es sich um 3D-Oberflächendaten handelt. Weiterhin können die STL-Daten zur weiteren Datenbearbeitung in die FreeForm Modeling Software (SensAble Technologies, USA) importiert werden. Diese Software wird in Verbindung mit einem haptischen Eingabegerät, dem PHANTOM Desktop verwendet, welches eine Kraftrückkopplung zum Benutzer ermöglicht. Besonders Freiform-Oberflächen von anatomischen Strukturen können mithilfe der FreeForm Software intuitiv und interaktiv bearbeitet werden. FreeForm ermöglicht das Schließen von Löcher im Modell, das Verbinden innerer Strukturen, das Schneiden, Spiegeln und, falls nötig, ein Glätten der Modelle. Verschiedene andere Software-Programme können zur Bearbeitung der Original-3D-Daten verwendet werden, z. B. um eine farbige Textur auf einer 3D-Datenoberfläche für die Verwendung im 3D-Druckverfahren zu definieren. Werden 3D-Daten mit farbigen Texturen bearbeitet, wird das VRML-Datenformat gewählt, da im STL-Format keine Texturinformationen gespeichert werden können. Ein wachsendes Gebiet im Bereich der anthropologischen und forensischen Gesichtsrekonstruktion ist die computerunterstützte Gesichtsrekonstruktion [6]. Die mit dieser Technik erstellten dreidimensionalen Datensätze können direkt oder nach Umwandlung in das STL-Format zum Modellbau verwendet werden.

Rapid Prototyping Prozesse

Abhängig vom Einsatzgebiet der Modelle und den gewünschten Modelleigenschaften muss das geeignete Rapid Prototyping Verfahren für die Modellherstellung aus 3D-Datensätzen ausgesucht werden. In dieser Studie wurden die Rapid Prototyping Verfahren 3D-Drucken, Stereolithographie und Vakuumguss zur Herstellung von Modellen eingesetzt. Diese Verfahren erlauben die Herstellung von Modellen mit vielfältigen mechanischen und optischen Eigenschaften.

3D-Drucken

Beim 3D-Druckverfahren handelt es sich um einen pulverbasierten Prozess zur Herstellung von Modellen direkt aus Computerdaten [7]. Eine mit gipsartigem Pulver gefüllte Box wird Schicht für Schicht mit einer Binderlösung bedruckt. Das Pulver verklebt in den bedruckten Bereichen (siehe Abb. 1, Schritt 1 bis 4). Der Prozess wiederholt sich, bis die letzte Schicht gedruckt wurde. Anschließend wird das lose Pulver entfernt und man erhält das fertige Modell. Zur Erhöhung der Stabilität wird das Modell abschließend mit einem Lack infiltriert.

Der größte Vorteil dieses Verfahrens besteht darin, dass in Farbe gedruckt werden kann. Dadurch ist es möglich, Gesichtsscans mit zusätzlichen Texturen zu verarbeiten und so farbige Modelle herzustellen. Darüber hinaus sind die mit dem 3D-Druckverfahren hergestellten Schädelmodelle sehr gut zur forensischen oder anthropologischen Gesichtsweichteil-Rekonstruktion mit Ton oder Plastilin geeignet.

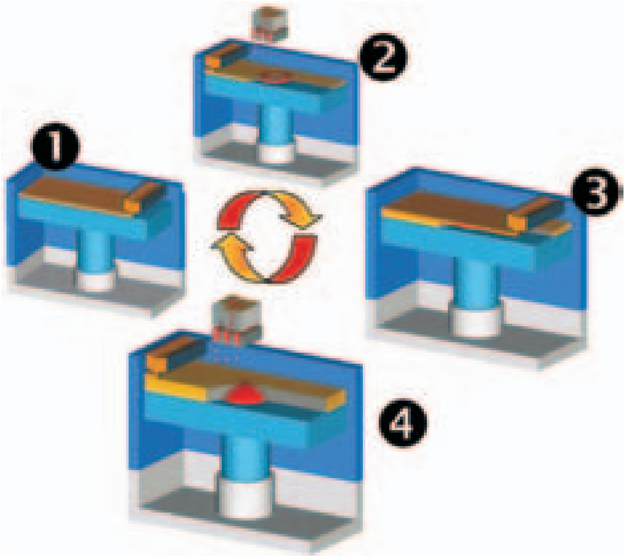

Abb. 1: 3D-Druck-Prozessschema

Stereolithographie

Die Stereolithographie ist das am häufigsten genutzte Rapid Prototyping Verfahren. Die mittels Stereolithographie gebauten Kunststoffmodelle können direkt oder als Urmodell für einen sich anschließenden Vakuumguss eingesetzt werden [7]. In der Stereolithographie schraffiert ein Laser einen Querschnitt des Modells auf der Oberfläche einer mit flüssigem, photosensitivem Harz gefüllten Wanne (siehe Abb. 2). Die Laserenergie verfestigt das Harz und es entsteht eine feste Struktur. Dieser Prozess wird schichtweise wiederholt. Die fertigen Modelle sind transparent und ermöglichen die Ansicht von im Modellinneren liegenden Strukturen. Bei Verwendung spezieller Harze ist es zusätzlich möglich, gewünschte Bereiche im Modell selektiv in einer Farbe zu markieren. Das erlaubt eine verbesserte Visualisierung anatomischer Einzelheiten wie z. B. eines Tumors bei einem Modell für die Operationsplanung.

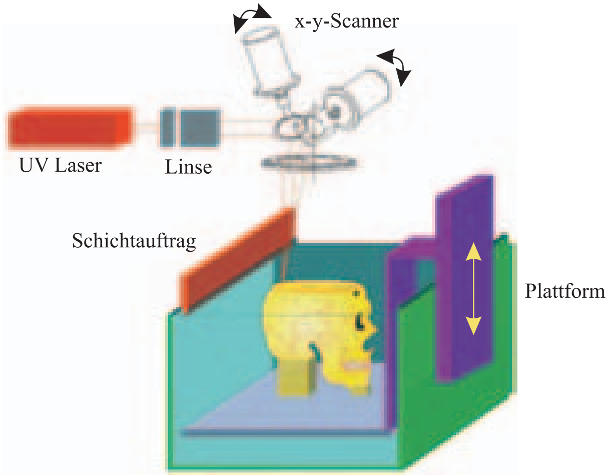

Abb. 2: Stereolithographie-Prozessschema

Vakuumguss

Stereolithographiemodelle können nicht nur direkt sondern auch als Urmodelle zur Herstellung von Silikonformen für den Vakuumguss dienen. Die Verwendung des Vakuumgussverfahrens erlaubt die Herstellung von Abgüssen der Urform mit Materialien mit unterschiedlichen Eigenschaften und Farben [7]. Im ersten Schritt des Vakuumgussverfahrens wird das Stereolithographie Urmodell in Silikon eingebettet. Nach dem Aushärten wird die Silikonform aufgeschnitten und das Urmodell entfernt; zurück bleibt ein Negativ des Urmodells für den Abguss. Diese flexible Silikonform wird für den Abguss einer oder mehrerer Kopien des Urmodells benutzt. Zur Vermeidung von Blasenbildung wird der gesamte Abguss im Vakuum durchgeführt. Obwohl es die Flexibilität der Silikonform erlaubt, Modelle mit partiellen Hinterschneidungen, wie sie z. B. bei einem menschlichen Ohr auftreten, zu fertigen, sind der Komplexität der Modelle Grenzen gesetzt. Die Abgussmodelle müssen sich aus der Silikonform entformen lassen, ohne diese zu zerstören. Als Abgussmaterialien kommen typischerweise Zwei-Komponenten-Polyurethane zum Einsatz. Es ist jedoch auch möglich, andere Materialien, wie Silikone, als Abgussmaterial zu verwenden. Die Elastizität und die Farben der verwendeten Harze kann mit verschiedenen Additiven verändert werden, um so verschiedene Gewebetypen mit realistischen haptischen und visuellen Eigenschaften zu simulieren.

Anwendungsgebiete

Die vorgestellten Herstellungsverfahren wurden schon in verschiedenen medizinischen und anthropologischen Fällen eingesetzt. Die jeweiligen 3D-Modelle wurden unter Nutzung verschiedener Datenquellen für die unterschiedlichen Anwendungen hergestellt. Der jeweils geeignete Herstellungsprozess wurde abhängig von den mechanischen und visuellen Anforderungen an die Modelle und unter Berücksichtigung der Herstellungskosten ausgewählt.

Farbiges 3D-Portraitmodell

Mit einem 3D-Drucker wurden farbige Portraitmodelle von Patienten hergestellt. Die 3D-Datensätze der Patienten wurden mit Hilfe der holographischen Tomographie erstellt. Die Rohdaten wurden in das STL-Format konvertiert und eine Oberflächendicke festgelegt, um das 3D-Modell bauen zu können. Die Computermodelle wurden mit digitalen Patientenphotos überlagert, um so farbige Datensätze zu erhalten. Die Datensätze wurden in das VRML-Format konvertiert und anschließend in die Maschinensoftware des 3D-Druckers geladen. Die farbigen Modelle wurden dann durch den 3D-Drucker generiert. Abb. 3 zeigt ein solches farbiges, im 3D-Druckverfahren hergestelltes Portraitmodell.

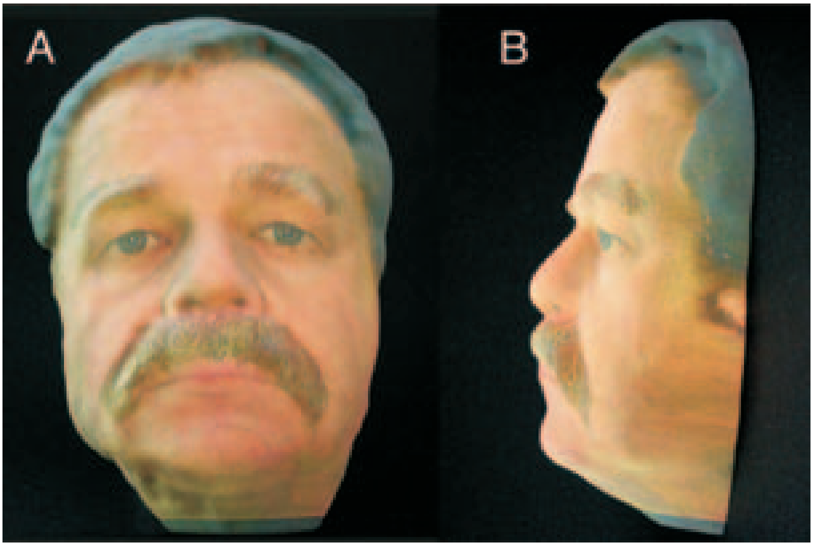

Abb. 3: Farbiges 3D-Portraitmodell einer männlichen Versuchsperson, hergestellt im 3D-Druckverfahren

Schädelmodelle für die Gesichtsweichteil-Rekonstruktion

Die Rapid Prototyping Technologie eignet sich auch sehr gut für die Herstellung von Kopien von Schädelfunden, z. B. für eine Gesichtsweichteil-Rekonstruktion.

Sowohl im 3D-Druckverfahren als auch mit Hilfe der Stereolithographie wurden verschiedene Modelle erzeugt. Die hierzu benötigten Daten wurden mit Hilfe von CT-Aufnahmen erzeugt und mit der Software MIMICS aufbereitet. Abb. 5 zeigt ein im 3D-Druckverfahren hergestelltes Modell für eine Gesichtsrekonstruktion. Der Originalschädel wurde in einem Waldgebiet bei Celle (Deutschland) im Januar 2003 gefunden (siehe Abb. 4). Die Identität der Person ist immer noch ungeklärt. 12 Kopien des Schädels wurden für eine vergleichende Studie zur Gesichtsrekonstruktion hergestellt [8]. Die Modelle wurden als Hartgewebebasis für die Weichgewebsrekonstruktion in modellierender Technik wie Ton oder ähnlichen Materialien verwendet. Die Ergebnisse dieser Studie werden an anderer Stelle in naher Zukunft veröffentlicht.

Abb. 4: Originalschädel, gefunden in einem Wald bei Celle, Deutschland (Polizeiinspektion Celle/RheinAhrCampus Remagen)

Abb. 5: Modell für eine Gesichtsweichteil-Rekonstruktion, hergestellt im 3D-Druckverfahren

Die Stereolithographie-Kopie eines Schädels aus dem Museum für Hamburgische Geschichte wurde ebenfalls zur Gesichtsweichteil-Rekonstruktion verwendet. Es wird diskutiert, ob dieser Schädel von Klaus Störtebeker stammt, einem berüchtigten Piraten, der Schiffe in der Nordsee und im baltischen Meer kaperte. Er wurde in Hamburg im Jahre 1402 hingerichtet. Sein Kopf wurde als Abschreckung für andere auf einen Balken genagelt. Abb. 6 zeigt das Stereolithographiemodell, während Abb. 7 das von der französischen Künstlerin Elisabeth Daynes, Paris rekonstruierte Gesichtsmodell darstellt.

Abb. 6: Stereolithographiekopie eines Schädelfundes des Museums für Hamburgische Geschichte (©Philippe PLAILLY/Atelier DAYNES/EURELIOS)

Abb. 7: Foto des rekonstruierten Gesichtsmodells, das auf Basis eines Stereolithographiemodells hergestellt wurde. (©Philippe PLAILLY/Atelier DAYNES/EURELIOS)

Kombinierte Hart- und Weichgewebemodelle

Die Verwendung verschiedener Rapid Prototyping Verfahren erlaubt die Herstellung von anatomischen Modellen mit einer realistischen haptischen und visuellen Darstellung verschiedener Gewebetypen. Auf Basis medizinischer Datensätze, vorzugsweise Computertomographiedaten der betreffenden Areale, werden sowohl Hart- als auch Weichgewebe rekonstruiert.

Die Hartgewebeteile und die Urformen der Weichgewebe wurden mit Hilfe der Stereolithographie hergestellt. Das Vakuumgussverfahren ermöglicht die Herstellung realistischer Weichgewebemodelle. Abb. 8 zeigt ein anatomisches Modell, das auf diese Art für den Test eines neuen intraoperativen Navigationssystems hergestellt wurde. Das Navigationssystem soll es dem Chirurgen ermöglichen, seine zuvor computergestützt durchgeführte Planung der Operation während des Eingriffs am Patienten räumlich exakt zu verfolgen.

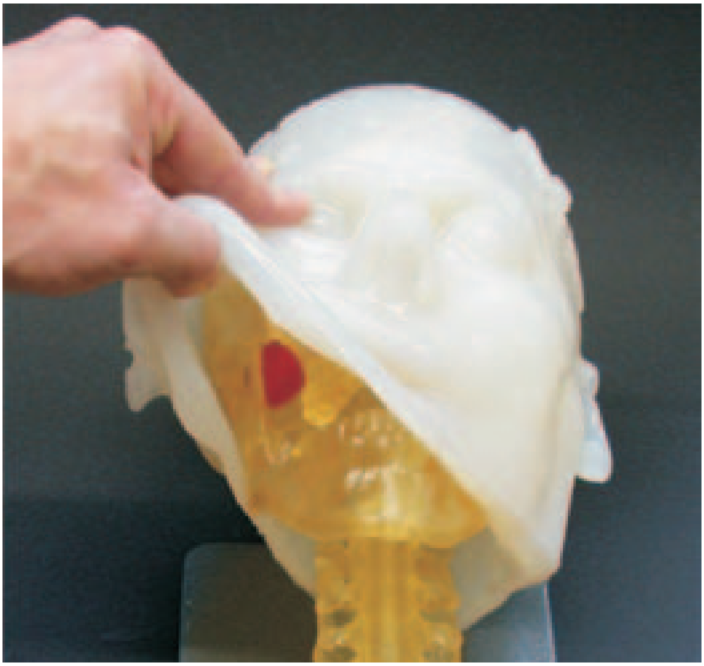

Abb. 8: Anatomisches Modell zum Testen eines neuen intraoperativen Navigationssystems

Diskussion

Die Herstellung von Modellen für die Gesichtsrekonstruktion mittels Rapid Prototyping Verfahren besitzt viele Vorteile. Die Verfahren eignen sich sehr gut zur Generierung von Kopien von Schädelfunden. Rapid Prototyping erlaubt außerdem die Reproduktion innerer und äußerer morphologischer Details eines Originalschädels. Es ist möglich, interessante Bereiche in unterschiedlichen Maßstäben herzustellen. Ein weiterer Vorteil ist die Herstellung mehrerer Kopien, damit Studien zur Gesichtsrekonstruktion von mehren Personen gleichzeitig an verschiedenen Orten durchgeführt werden können.

Da jede Rapid Prototyping Technik ihre Vor- und Nachteile aufweist, wurden unterschiedliche Rapid Prototyping Techniken zur Herstellung von Modellen für die Gesichtsrekonstruktion untersucht.

Das 3D-Druckverfahren ist ein schnelles und kostengünstiges Verfahren zum Bau solcher Modelle. Die mechanische Stabilität und die Abbildungsgenauigkeit 3D-gedruckter Modelle sind nicht so hoch wie sie mit der Stereolithographie erreicht werden können. Auf der anderen Seite bietet das 3D-Druckverfahren als einziges Rapid Prototyping Verfahren die Möglichkeit, farbig zu bauen. Der Farbeindruck erreicht keine Fotoqualität, er ist aber ausreichend, um einen guten optischen Eindruck des Originals zu erhalten. So ist das 3D-Druckverfahren besonders geeignet, farbige Portraitmodelle z. B. zur Dokumentation von Patienten herzustellen, die sich im Bereich der Mund-Kiefer-Gesischtschirurgie einer Operation unterziehen müssen. Das 3D-Druckverfahren ist auch eine geeignete Technik, um Modelle auf Basis dreidimensionaler Datensätze aus dem Bereich der computerunterstützten Gesichtsweichteil-Rekonstruktion herzustellen. Darüber hinaus ist das 3D-Druckverfahren zur Herstellung mehrerer Kopien eines Originals geeignet, da es im Verhältnis zur Stereolithographie schneller und kostengünstiger ist.

Sehr genaue Modelle eines Originals lassen sich mit Hilfe der Stereolithographie erzeugen. Es ist möglich, die Modelle aus transparentem Material herzuerstellen, um so innere anatomische Strukturen sichtbar zu machen. Generell liefert die Stereolithographie von allen Rapid Prototyping Verfahren die genauesten Modelle mit der besten Oberflächenqualität. Somit ist es die bevorzugte Methode, Kopien von Originalen für Untersuchungen herzustellen, wenn die Originale wegen ihres Wertes oder ihrer Empfindlichkeit geschont werden sollen. Da die Stereolithographiemodelle eine hohe mechanische Stabilität aufweisen, sind sie gut als Vorlage für die Gesichtsweichteil-Rekonstruktion mit Modellierungstechniken wie Ton oder Plastilin geeignet. Weiterhin können stereolithographische Modelle sterilisiert und im Operationssaal verwendet werden. Daraus folgt, dass die Stereolithographie die bevorzugte Technik zur Herstellung von Modellen für die Operationsplanung ist.

Die Herstellung kombinierter anatomischer Modelle erfordert einen hohen technischen Einsatz. Sowohl die Stereolithographie als auch der Vakuumguss werden zur Herstellung anatomischer Modelle mit realistischer Wiedergabe haptischer und optischer Eigenschaften der verschiedenen Gewebetypen benötigt. Somit liegen die Einsatzgebiete von mehrteiligen anatomischen Modellen im Trainingsbereich oder bei der Operationsplanung. Die Modelle erlauben eine Kontrolle der ästethischen Aspekte während der Operationsplanung, da sich das Weichgewebemodell (z. B. Gesichtsweichteile) den Änderungen der Hartgewebeteile (z. B. Knochenstrukturen) anpasst. Allgemein bietet das Vakuumgussverfahren die Möglichkeit, Modelle mit verschiedenen anatomischen Strukturen in unterschiedlichen Materialien und Farben einer stereolithographischen Urform herzustellen.

Schlussfolgerung

Hauptanliegen dieses Artikels war es, die Möglichkeiten der Rapid Prototyping Verfahren für die Modellherstellung in der Gesichtsrekonstruktion vorzustellen. Es wurden Prozessketten zur Herstellung solcher Modelle auf Basis verschiedener Rapid Prototyping Techniken präsentiert. Abhängig von der Anwendung der Modelle und der gewünschten Modelleigenschaften muss die geeignete Rapid Prototyping Technik zur Herstellung der Modelle ausgewählt werden.

Da die Rapid Prototyping Industrie ein dynamisch wachsender Markt ist, werden in naher Zukunft weitere neue und effektive Technologien und Materialien zur Herstellung von Modellen für die Weichgewebegesichtsrekonstruktion zur Verfügung stehen.

Literatur

[1] T. Wohlers, Wohlers Report 2004: Rapid Prototyping & Tooling State of the Industry. Wohlers Associates, Fort Collins, Colorado 2004.

[2] J. F. Arvier, T. M. Barker, Y. Y. Yau,, P. S. D'Urso, R. L. Atkinson and G. R. McDermant, (1994), „Maxillofacial biomodelling", British Journal of Oral and Maxillofacial Surgery, vol. 32, pp. 276–283, 1994.

[3] M. S. Dolz, S. J. Cina and R. Smith, „Stereolithography – A Potential New Toll in Forensic Medicine", The American Journal of Forensic Medicine and Pathology, vol. 21, number 2, pp. 119–123, 2000.

[4] C. P. E. Zollikofer, M. S. Ponce de León and R. D. Martin, „Computer-assisted paleoanthropology", Evol. Anthropol., vol. 6, pp. 41–54, 1998.

[5] A. Thelen, S. Frey, S. Hirsch, N. Ladriére, J. Bongartz, D. Giel and P. Hering, „Digitization of holographic recordings for medical applications", in Proceedings of the Remagener Physiktage. Remagen. September 2004.

[6] J. Subke and M. Wittke, „CAD Enhanced Soft-Tissue Reconstruction in Forensics with Phantom 3D Touch – An Electronic Modelling Tool with Haptic Feedback", in Proceedings of the 2nd International Conference on Reconstruction of Soft Facial Parts. Remagen. March 2005.

[7] A. Gebhardt, Rapid prototyping, Munich: Hanser, 2003.

[8] J. Bongartz, T. M. Buzug, P. Hering, C. Tille and H. Seitz, „Introduction to the Comparative Study on Facial Reconstruction", in Proceedings of the 2nd International Conference on Reconstruction of Soft Facial Parts. Remagen. March 2005.

Child pornography: Development of a Method for Identification of Faces as Childish

Hans-Martin Bröker[1], Stefan Gehlen[1], Stefanie Ritz-Timme[2], Janina Tutkuviene[3] and Cristina Cattaneo[4]

[1] Viisage Technology AG, Bochum, Germany
[2] Heinrich-Heine Universität Düsseldorf, Germany
[3] Vilnius University, Lithuania
[4] University of Milan, Italy

Abstract

The age of the victims of child pornography is of great relevance for the investigating authorities. It is the key information for the classification of pornography as child pornography. It is also of great importance for the termination of a continuing abuse and for the identification of the offenders. Today, there is a lack of sufficiently reliable and reproducible methods for age estimation based on the analysis of films or photographs. Another problem is the significant increase in the number of pictures and videos that have to be checked by the investigating authorities with regard to the question "Child pornography?".

To mitigate these problems, the aim of this work is to develop an objective and scientifically reasonable method for age estimation, applicable to films and photographs. The proposed approach is based on the evaluation of age-specific changes of proportions in the face during childhood.

1 Introduction

The increasing abuse of the World Wide Web as a platform for dissemination of child pornographic material is alarming. Investigating authorities cannot cope with the huge number of suspicious images with presumably child pornographic content. An exhaustive scan is psychologically stressing and time consuming. Typically, hard disks with huge storage capacity may carry a tremendous number of images or videos, impractical for exhaustive manual inspection, if not impossible at all.

A sorting of the data according to the probability of containing images of children would be desirable. Thus, the need of a software aid performing this preselection of the relevant portion of the data sets driven by the age of children is evident for the fight against child pornography. Although the facial differences between children and adults are obvious for any human observer, there is a lack of computer-aided systems to take over this task in an automated manner.

In this contribution we show the applicability of established face recognition techniques in order to classify facial images as containing children or adults. Due to the above mentioned goal it is most important that an automatic face finding procedure precedes the classification process. This is a well studied and for many applications satisfactorily solved problem and thus not purpose of this work. See [1] for a survey.

In the next section we sketch the two basic techniques of coding the characteristics of a facial image used in this work, i. e. Graph Matching [2] and Eigenfaces [3]. This will be followed by a description of the classifiers used for identifying a face as childish or adult. Finally we present our results.

2 Graph Matching and Eigenfaces

For nearly a decade the Graph Matching is one of the most powerful techniques to solve face recognition issues. As the name suggests, a critical ingredient of this method is the use of a graph, which is essentially a grid consisting of nodes and edges (see Fig. 2–1). During the matching process the graph is adapted in shape and size, so that it covers the face with the nodes lying on defined positions (so called landmarks). This process runs fully automated and thus solves the face finding problem. Instead of using the raw image pixels, Graph Matching transforms the image information to features more suited for automatic recognition than the gray level information. Graph matching makes use of specialized kernel functions, which are robust against changes in illumination and contrast. For feature generation a set of these filter functions is applied to the original image. The set of all filter responses at a certain point in the image domain describes a feature vector at a certain image location. This vector may directly be used to calculate similarities between different faces.

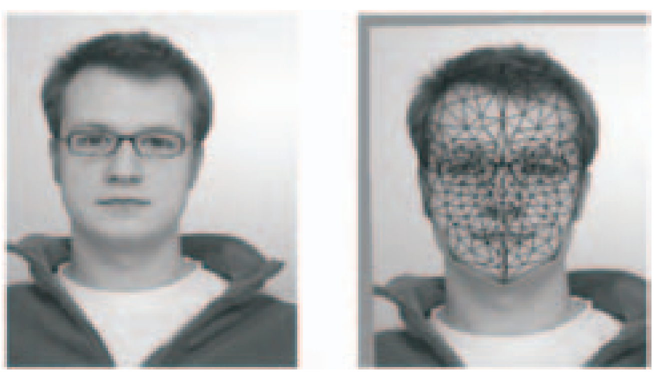

Fig. 2-1: This figure shows a facial image and the graph placement. The matching process runs fully automated and the graph covers exactly the face. This indicates, that the matching process was successful.

The other well established method was introduced in [3] and is known as Eigenface analysis. Based on a large data set of training images one creates a new set of artificial faces, i. e. the principal components of the covariance matrix of the training data, which contain mainly facial information (see Fig. 2–2). Any facial image can be uniquely expanded in a series of these Eigenfaces, under simultaneous suppression of undesired disturbances like noise. This set of coefficients in the series expansion is further used as a description of the considered face.

We used both techniques in order to obtain two independent model descriptions of the facial images, which will presumable complement one another. Note that the transformation of the image into the feature vector diminishes the original data amount over several orders magnitude. Thus the usage of two models reduces the risk of loosing essential information. Even though both methods were developed for face identification tasks we assume and verify by our experiments that they carry also the facial age information, which will be extracted and sorted during the classification process.

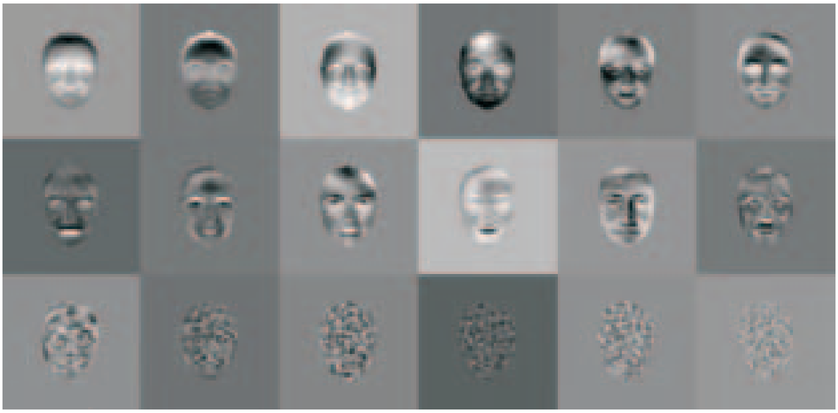

Fig. 2-2: This figure shows an ordered set of Eigenfaces. While the first images in the top row can be easily identified as faces, the last images essentially contain noise.

3 Classification

The basic idea behind all of the classifiers we used lies in the definition of a similarity measure between a given face and the entire training sets of both classes, i. e. the children and the adults. Irrespectively which method is used, Graph Matching or Eigenfaces, any considered face is encoded by a feature vector, i. e. set of real valued numbers. Those vectors do not contain the desired age information explicitly and it is the task of the classifier to assign each probe vector to one of the two classes. Under the constraint of robustness and high processing speed several classifiers were applied.

First of all we tested a nearest neighbor algorithm, which seeks for n representatives in the training set that are closest to the probe and votes for the class with the majority of nearest neighbors. Furthermore we applied the well known Fisher Linear Discriminant Analysis (LDA) [4]. The LDA seeks those directions in the high dimensional feature space that are efficient for discrimination. This leads to a reduction of each feature vector to a single number.

More advanced classifiers require training algorithms to learn the characteristics of the classes and the decision is not based on the similarity to individual class members but to models of the entire class. From this group we tested both linear and non-linear PCA methods [5].

When using several classifiers their potentially contradictory outputs must be fused to a final decision. This fusion of experts again offers different options. During our examinations we used techniques based on majority votes, Bayesian methods and neural networks [4].

The Fig. 3–1 shows the entire scheme of the classification process. Different paths through the subsequent levels lead to slightly different results, offering the option to choose the one that performs best. We saw that the usage of two different feature vectors and several classifiers led in any case to better results than a single solution.

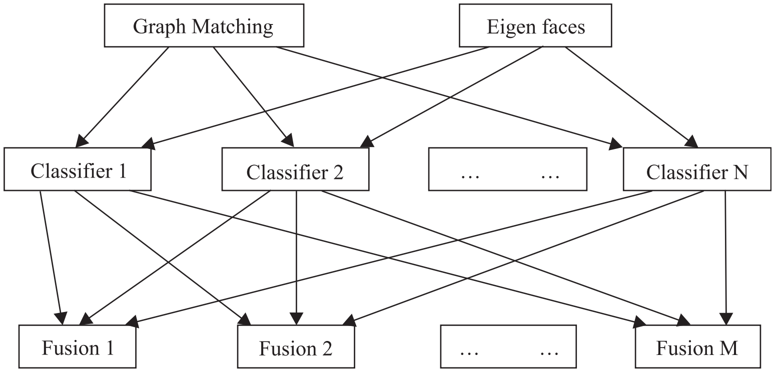

Fig. 3-1: This figure shows the entire classification scheme. The feature vectors result from the Graph Matching and the Eigenface method, respectively. Both of them run through several classifying processes whose results are fused at the bottom level.

4 Experiments and Results

Great effort was done to collect a large data set of childish facial images. Reference data for facial proportions from 600 children in defined age classes (3 to 7 years) were gathered by anthropologists in Germany, Italy and Lithuania. High resolution photographs of the faces in 3 standardized positions, including a frontal pose, as well as detailed anthropological measurements (22 parameters per face) were taken.

Together with a database of adult images of comparable size and quality as the images containing children we trained the classifiers described above. Due to the limited number of images we designed a generalized leave one out test, i. e. the greatest part of the data set was used to train the classifiers. Thus only a small number of probes could be classified simultaneously. In order to get reliable statistics the test set run through the entire data set while the models had to be computed in each step anew.

The output of the fused classifiers is a score between 0 and 1, which can be understood as an estimation of the confidence that a given image shows a children's face. In order to quantify the system's accuracy it is common to introduce two error rates, i. e. the False Acceptance Rate (FAR) and the False Rejection Rate (FRR). For a given threshold *s* the FAR measures the probability that an adult facial image is classified with a score greater than *s*, whereas the FRR measures the probability that a childish face leads to a score less than *s*. Those rates, as shown in Fig. 4–1, tell us immediately the result of an experiment for searching all children's faces in an unsorted data set. In that case the classifier's output is transformed into a binary decision, i. e. all scores lower than *s* are identified with adults and vice versa. It is obvious that with decreasing *s* the chance to find all children increases simultaneously with the number of false labelled adults. We see that the Equal Error Rate (EER), the coincidence of FAR and FRR, is less than 5%. Thus more than 95% of the images were correctly classified. For the considered application it seems advisable to lower the threshold leading to a vanishing FRR, i. e. all children within the data set were correctly identified, with the disadvantage of a slightly increasing probability of classifying adults as children.

But the critical benefit of our system seems us to lie in the option of performing sorting tasks. If a large data set of facial images is sorted according to the classifiers score in a descending order, the children's faces will accumulate at the top of the resulting image list, whereas the adult faces will be shifted to the end of the list.

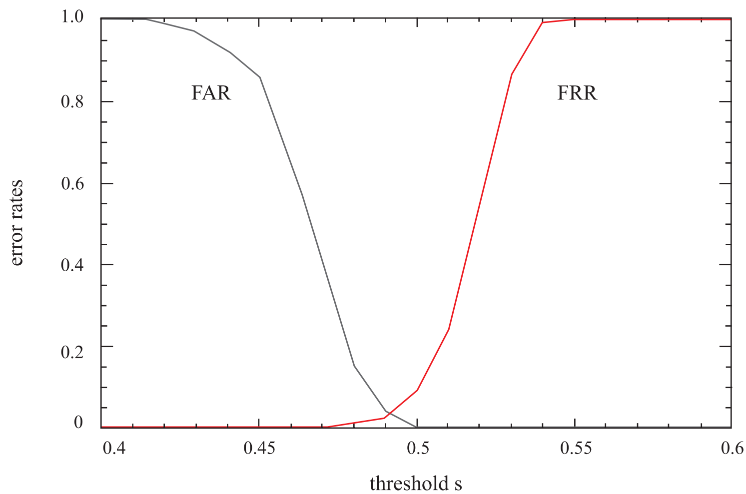

Fig. 4-1: This figure shows the False Acceptance Rate (FAR) and False Rejection Rate (FRR) versus the threshold *s*. When we set s to 0.49 then the error rates are approximately 5%, i. e. 5% of the children were classified as adults and vice versa. Lowering the threshold increases the probability to find all children's faces in the data set.

The anthropological measurements, whose detailed description is beyond the scope of this letter, suggest that there are only slight age-dependent changes in the faces of the children in the considered age range. Nevertheless we tried to estimate the children's age directly with the developed methods. Therefore we divided the children's data into two sets of images consisting of the youngest and the oldest faces, respectively, with a variable age gap between them. We found that in the case of a vanishing gap, i. e. the classes are tangent to each other, the correct classification rate is about 50%, which is equivalent to a random guess. But with increasing gap, up to 30 month, the rate reaches 75%. Note that due to the limited size of the data set, an increasing gap diminishes the training set as well as the test set. Thus the results loose statistical significance and the classifiers become harder to train.

5 Conclusion

We could show that the facial differences between young children and adults are detectable with a face recognition system. We suggested an automatic classifier to categorize the faces as childish or adult. Applied to images of children in the analysed age group and adults not included in the training set, the classification is highly reliable. If the classifiers' parameters are set to classify nearly all children in the images correctly, it classifies approximately 90% of all adults also correctly. Face finding and classification work completely automated and extremely fast (less than 1 s per photo).

Note that our studies were done under controlled lab conditions, i. e. we used exclusively high resolution images, without any disturbances and facial poses. Our aim is to extend the methods towards more realistic scenes and the final goal is a significant reduction of the images to be investigated manually to find child pornographic material, as the classifier is able to exclude a vast amount of images only containing adult faces.

First experiments on a small age range also show that the methods seem to be applicable to direct age estimation. We found that our estimates were comparable to those found by analysing the anthropological measurements. Future work should be also focussed on an extension to the complete range from infant to adult.

Acknowledgement

The authors want to thank M. Hüsken for fruitful discussions and carefully reading the manuscript. This work was supported by the European Union (JAI/2002/STOP/132).

References

[1] M.-H. Yang, D. Kriegman, and N. Ahuja, “Detecting Faces in Images: A Survey”, *IEEE Transactions on Pattern Analysis and Machine Intelligence*, 24(1), pp. 34–58, 2002.

[2] L. Wiskott, J.-M. Fellous, N. Krüger, and C. von der Malsburg, “Face recognition by elastic bunch graph matching”, *IEEE Transactions on Pattern Analysis and Machine Intelligence,* 19, pp. 775–779, 1997.

[3] M. Turk and A. Pentland, “Eigenfaces for recognition”, *Journal of Cognitive Neuroscience* 3(1), 1991.

[4] R. O. Duda, P. E. Hart, and D. G. Stork, “*Pattern Classification*”, John Wiley & Sons, Inc., New York, 2001.

[5] B. Schölkopf, A. Smola, and K.-R. Müller, “Nonlinear Component Analysis as a Kernel Eigenvalue Problem”, Max-Planck-Institut für biologische Kybernetic, Technical Report No. 44, 1996.

Kinderpornographie: Entwicklung eines Verfahrens zur Identifikation von Gesichtern als kindlich

Hans-Martin Bröker[1], Stefan Gehlen[1], Stefanie Ritz-Timme[2], Janina Tutkuviene[3] und Cristina Cattaneo[4]

[1] Viisage Technology AG, Bochum, Germany
[2] Heinrich-Heine Universität Düsseldorf, Germany
[3] Vilnius University, Lithuania
[4] University of Milan, Italy

Abstract

Das Alter der Opfer von Kinderpornographie ist von großer Bedeutung für die Ermittlungsbehörden. Es ist die Schlüsselinformation zur Klassifizierung von Pornographie als Kinderpornographie. Es ist ebenso von großer Wichtigkeit für die Beendigung fortgesetzten Missbrauchs und zur Identifikation der Täter. Bislang fehlt es an hinreichend verlässlichen und reproduzierbaren Methoden zur Altersschätzung auf Grundlage der Analyse von Filmen oder Photographien. Ein weiteres Problem liegt in dem signifikanten Anstieg der Anzahl der Bilder und Videos, die von den Ermittlungsbehörden bezüglich der Frage „Kinderpornographie?“ hin untersucht werden müssen.

Zur Entschärfung dieses Problems war es das Ziel dieser Arbeit, ein objektives und wissenschaftlich begründetes Verfahren zur Altersschätzung zu entwickeln, das auf Filme und Photographien anwendbar ist. Der vorgestellte Ansatz basiert auf der Analyse von altersspezifischen Änderungen der Gesichtsproportionen während der Kindheit.

1 Einleitung

Der ansteigende Missbrauch des Internets als eine Plattform zur Verbreitung kinderpornographischen Materials ist alarmierend. Die Ermittlungsbehörden können die immense Anzahl verdächtigen Bildmaterials mit mutmaßlich kinderpornographischem Inhalt kaum bewältigen. Eine vollständige Sichtung ist psychologisch bedrückend und zeitaufwendig. Typischer Weise können Festplatten mit einer großen Speicherkapazität riesige Mengen von Bildern oder Filmen enthalten, die sich kaum oder gar nicht manuell inspizieren lassen.

Eine Sortierung der Daten gemäß der Wahrscheinlichkeit des Beinhaltens von Kinderbildern wäre wünschenswert. Demnach ist der Bedarf einer softwarebasierten Unterstützung zur Durchführung einer Vorauswahl relevanter Teile der Datenmengen bezüglich des Alters der Kinder für den Kampf gegen die Kinderpornographie evident. Obwohl die gesichts-spezifischen Unterschiede zwischen Kindern und Erwachsenen jedem menschlichen Beobachter offensichtlich sind, herrscht ein Mangel an rechnergestützten Systemen, die diese Aufgabe automatisiert übernehmen können.

In diesem Beitrag demonstrieren wir die Anwendbarkeit etablierter Techniken der Gesichtserkennung auf die Klassifizierung von Gesichtsbildern bezüglich der Darstellung von Kindern oder Erwachsenen. Gemäß der oben beschriebenen Anwendung ist es nötig, dass eine automatische Gesichtsfindung dem Klassifikationsprozess vorangestellt ist. Die Gesichtsfindung ist ein intensiv untersuchtes und für viele Anwendungen hinreichend gelöstes Problem und soll hier nicht weiter untersucht werden. Ein Überblick findet sich in [1].

Im nächsten Abschnitt skizzieren wir die beiden grundlegenden Techniken zur Kodierung der Charakteriska von Gesichtsbildern, nämlich Graph Matching [2] und Eigen Faces [3]. Anschließend folgt eine Beschreibung der zur Identifizierung von Gesichtern als kindlich oder erwachsen benutzten Klassifikatoren. Zuletzt erläutern wir unsere Resultate.

2 Graph Matching und Eigenfaces

Seit nahezu zehn Jahren stellt das Graph Matching eine der leistungsfähigsten Techniken im Bereich der Gesichtserkennung dar. Wie der Name vermuten lässt, liegt ein entscheidender Bestandteil dieser Methode in der Benutzung eines Graphen, der im Wesentlichen ein Gitter, bestehend auf Knoten und Kanten, darstellt (siehe Abbildung 2–1). Während des Matching Prozesses wird der Graph in Form und Größe derart angepasst, dass er das Gesicht bedeckt, wobei die Knoten an definierten Positionen im Gesicht (den sogenannten Landmarken) zu liegen kommen. Dieser Prozess läuft voll automatisch und löst somit auch das Gesichtsfindungsproblem. Anstatt die unverarbeiteten Bildpixel zu nutzen, transformiert das Graph Matching die Bildinformation in ein Muster, das zur automatischen Erkennung besser geeignet ist als die Grauwertinformation. Dabei wird von speziellen Filterkernen Gebrauch gemacht, die sich sehr robust gegen Änderungen in der Beleuchtung und dem Kontrast erweisen. Zur Musterextraktion wird ein Satz dieser Filterkerne mit veränderlichen Parametern auf das Bild angewandt. Die Menge all dieser Filterantworten an den einzelnen Punkten ergibt einen Mustervektor für den betrachteten Bildpunkt. Dieser Vektor kann unmittelbar zur Berechnung einer Ähnlichkeit zwischen unterschiedlichen Gesichtern genutzt werden.

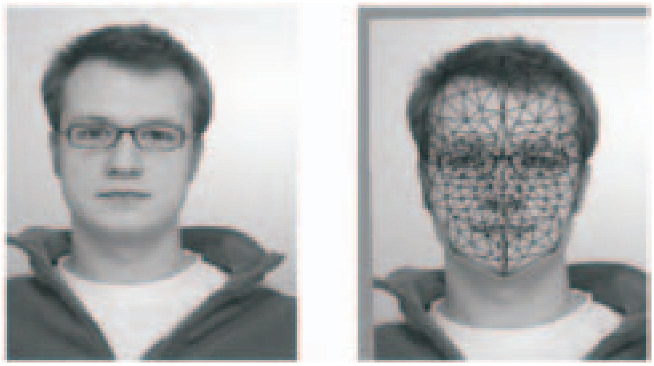

Abb. 2-1: Diese Abbildung zeigt ein Gesichtsbild und die Platzierung des Graphen. Der Matching Prozess läuft voll automatisch und der Graph überdeckt das Gesicht exakt. Dies zeigt, dass der Matching Prozess erfolgreich war.

Die andere etablierte Methode wurde in [3] eingeführt und ist unter dem Namen Eigenface Analyse bekannt. Basierend auf einem großen Datensatz von Trainingsgesichtern wird ein Satz von künstlichen Gesichtern erzeugt, d. h. die Hauptkomponenten der Kovarianzmatrix der Trainingsdaten, die im Wesentlichen die Gesichtsinformationen tragen (siehe Abbildung 2–2). Jedes betrachtete Gesichtsbild kann in eindeutiger Weise in eine Reihe dieser Eigengesichter entwickelt werden, bei gleichzeitiger Unterdrückung unerwünschter Störungen wie Rauschen. Der Satz von Koeffizienten dieser Reihenentwicklung wird im Weiteren als eine Beschreibung des betrachteten Gesichts genutzt.

Wir benutzten beide Techniken, um zwei unabhängige Modellbeschreibungen der Gesichtsbilder zu erhalten, von denen anzunehmen ist, dass sie sich gegenseitig ergänzen. Man beachte, dass die Transformation der Gesichtsbilder in einen Mustervektor die originale Datenmenge um mehrere Größenordnungen verkleinert. Demnach verringert die Nutzung zweier Modelle das Risiko, entscheidende Information zu verlieren. Obwohl beide Methoden zur Gesichtsidentifikation entwickelt wurden, setzen wir voraus und belegen durch unsere Experimente, dass sie ebenso geeignet sind, Altersinformation zu kodieren, die im Klassifikationsschritt extrahiert und sortiert werden kann.

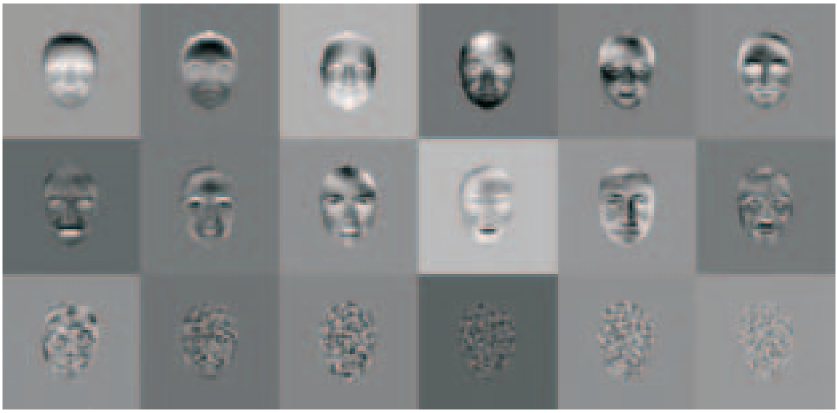

Abb. 2-2: Diese Abbildung zeigt einen sortierten Satz von Eigengesichtern. Das erste Gesicht in der obersten Reihe kann leicht als Gesicht erkannt werden, während die letzten Gesichter im Wesentlichen nur noch Rauschen enthalten.

3 Klassifikation

Die zu Grunde liegende Idee hinter allen Klassifikatoren, die wir benutzten, liegt in der Definition eines Ähnlichkeitsmaßes zwischen einem gegebenen Gesicht und der gesamten Trainingsmenge beider Klassen, d. h. der Kinder und der Erwachsenen. Ungeachtet welcher Methode, Graph Matching oder Eigenfaces, wird jedes betrachtete Gesicht durch einen Mustervektor, d. h. einem Satz reeller Zahlen, beschrieben. Diese Vektoren enthalten die gewünschte Altersinformation nicht explizit und es ist die Aufgabe des Klassifikators, jeden Probenvektor einer der beiden Klassen zuzuordnen. Unter der Nebenbedingung der Robustheit und der Rechengeschwindigkeit wurden einige Klassifikatoren angewandt.

Zunächst testeten wir einen Nächste-Nachbarn Algorithmus, der diejenigen n Repräsentanten jeder Klasse sucht, die der Probe am ähnlichsten sind und diejenige Klasse bestimmt, die die Mehrheit nächster Nachbarn aufweist.

Des Weiteren wandten wir die bekannte Fisher Lineare Diskriminanz Analyse (LDA) [4] an. Die LDA sucht jene Richtungen in dem hochdimensionalen Musterraum, die für die Unterscheidung geeignet sind. Dabei wird der Mustervektor auf eine Zahl reduziert.

Weiter entwickelte Klassifikatoren benötigen einen Trainingsalgorithmus, um die Charakteristika der Klassen zu erlernen und die Entscheidung basiert nicht auf der Ähnlichkeit zu individuellen Klassenelementen, sondern zu Modellen der gesamten Klasse. Aus dieser Gruppe testeten wir sowohl lineare als auch nicht-lineare PCA-Methoden [5].

Wenn mehrere Klassifikatoren benutzt werden, müssen deren möglicherweise widersprüchlichen Ergebnisse zu einer Gesamtentscheidung fusioniert werden.

Diese Fusion der Experten bietet abermals mehrere Möglichkeiten. In unseren Untersuchungen nutzten wir Techniken, die auf Mehrheitsentscheidungen, Bayes'schen Methoden und Neuronalen Netzen beruhen [4].

Die Abbildung 3–1 zeigt das Gesamtschema des Klassifikationsprozesses. Verschiedene Pfade durch die aufeinanderfolgenden Ebenen führen zu leicht verschiedenen Resultaten, von denen dasjenige mit der geringsten Fehlerrate gewählt werden kann. Insgesamt führte die Nutzung beider Mustervektoren und mehrerer Klassifikatoren stets zu besseren Ergebnisse als eine Einzellösung.

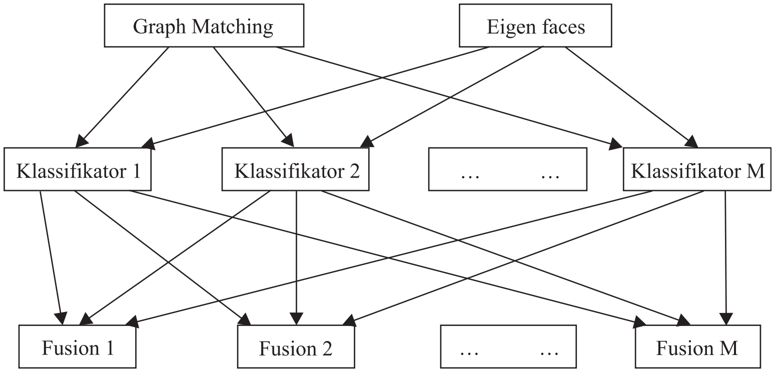

Abb. 3-1: Diese Abbildung zeigt das gesamte Klassifikationsschema. Die Mustervektoren ergaben sich aus dem Graph Matching und der Eigenface Methode. Beide durchliefen mehrere Klassifikatoren, deren Ergebnisse schließlich fusioniert wurden.

4 Experimente und Ergebnisse

Ein großer Aufwand musste betrieben werden, um einen großen Datensatz kindlicher Gesichtsbilder zu akquirieren. Referenzdaten für Gesichtsproportionen von 600 Kindern definierter Altersklasse (3 bis 7 Jahre) wurden von Anthropologen in Deutschland, Italien und Litauen erhoben. Dazu wurden sowohl hochaufgelöste Photographien in drei standardisierten Positionen, einschließlich einer Frontalpose, als auch detaillierte anthropologische Messungen (22 pro Gesicht) aufgenommen.

Zusammen mit einem Datensatz von Erwachsenenbildern vergleichbarer Größe und Qualität wie die der Kinderbilder wurden die oben skizzierten Klassifikatoren trainiert. Auf Grund der begrenzten Anzahl von Bildern musste ein generalisierter „leave one out"-Test entworfen werden, d. h. der größte Teil des Datensatzes wurde zum Training verwendet. Demnach konnte nur eine geringe Anzahl von Proben gleichzeitig klassifiziert werden. Um aber eine verlässliche Statistik zu bekommen, durchlief der Testsatz die gesamte Datenbasis, wobei die Modelle für jeden Test neu berechnet werden mussten.

Das Ergebnis der Fusion der Klassifikationen ist eine Maßzahl zwischen 0 und 1, die als eine Schätzung des Zutrauens, dass ein gegebenes Bild ein Kind zeigt, interpretiert werden kann. Um die Genauigkeit des Systems zu quantifizieren, werden üblicherweise zwei Fehlerraten eingeführt, nämlich die Falschakzeptanzrate (FAR) und die Falschrückweisungsrate (FRR). Bei einem gegebenen Schwellwert *s* misst die FAR die Wahrscheinlichkeit, dass ein Erwachsenenbild mit einer Maßzahl größer als *s* klassifiziert wird, während die FRR die Wahrscheinlichkeit misst, dass ein Kinderbild einen Wert unterhalb von *s* ergibt. Diese Fehlerraten, dargestellt in Abbildung 4–1, geben Auskunft über ein Experiment, bei dem alle Kinderbilder aus einem unsortierten Datensatz herausgesucht werden sollen. In diesem Falle wird das Klassifikationsergebnis in eine binäre Entscheidung umgeformt, d. h. alle Maßzahlen unterhalb von *s* werden mit Erwachsenen identifiziert und umgekehrt. Es ist offensichtlich, dass mit sinkendem *s* sowohl die Wahrscheinlichkeit alle Kinder zu finden, aber auch die Anzahl der falsch klassifizierten Erwachsenen, steigt. Wir sehen, dass die Equal Error Rate (EER), der Schnittpunkt von FAR und FRR, unterhalb von 5% liegt. Demnach sind mehr als 95% aller Bilder richtig klassifiziert worden. Bei der vorliegenden Anwendung scheint es empfehlenswert den Schwellwert zu verringern, was zu einer verschwindenden FRR führt, d. h. alle Kinder in dem Datensatz werden korrekt erkannt, mit dem Nachteil einer leicht steigenden Wahrscheinlichkeit, einen Erwachsenen als Kind zu klassifizieren.

Aber der entscheidende Nutzen unseres Systems scheint uns darin zu liegen, dass es Sortieraufgaben übernehmen kann. Wird ein großer Datensatz von Gesichtsbildern gemäß der Maßzahl der Klassifikation in absteigender Reihenfolge sortiert, so werden sich die Bilder der Kinder am Anfang dieser Bilderliste anhäufen, während die Erwachsenenbilder tendenziell an das Ende der Liste sortiert werden.

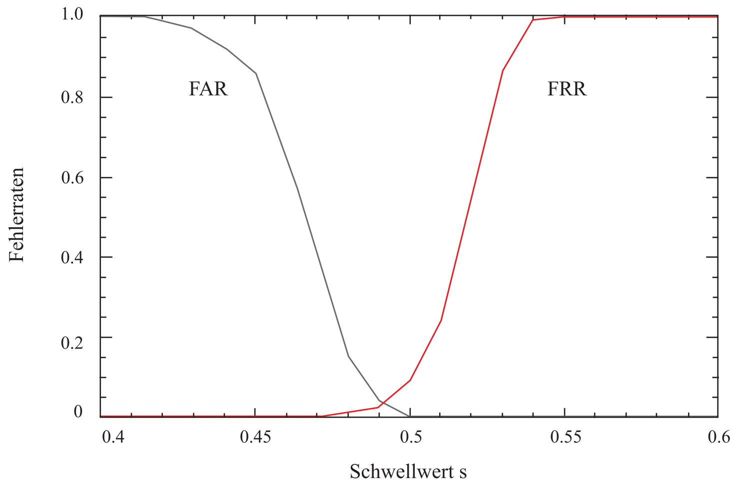

Abb. 4-1: Diese Abbildung zeigt die Falschakzeptanzrate (FAR) und die Falschrückweisungsrate (FRR) in Abhängigkeit vom Schwellwert *s*. Wird *s*=0.49 gesetzt, liegen die Fehlerraten bei ungefähr 5%, d. h. nur 5% der Kinder sind fälschlicherweise als Erwachsene klassifiziert worden, und umgekehrt. Wird der Schwellwert erniedrigt, so steigt die Wahrscheinlichkeit, alle Kinder in dem Datensatz zu finden.

Die anthropologischen Messungen, deren detaillierte Beschreibung über den Rahmen dieses Papiers hinausginge, legen nahe, dass sich nur leichte altersabhängige Änderungen in den Gesichtern von Kindern in dem betrachteten Altersspektrum vollziehen. Dennoch versuchten wir, das Alter der Kinder mit den entwickelten Methoden direkt zu messen. Dazu teilten wir die Kinderdaten in zwei Sätze von Bildern, die jeweils die jüngsten beziehungsweise die ältesten Gesichter enthielten. Dabei ließen wir eine veränderliche Alterslücke zwischen diesen beiden Datensätzen. Wir fanden, dass sich im Falle einer verschwindenden Lücke, d. h. die Klassen berührten sich, eine korrekte Klassifikationsrate von 50% ergab, was einem zufälligen Raten entspricht. Mit Vergrößerung der Lücke, bis hin zu 30 Monaten, stieg aber die Rate auf 75%. Dabei ist zu beachten, dass wegen der begrenzten Datenmenge die Vergrößerung des Klassenabstandes sowohl die Trainingsmenge als auch die Testmenge verkleinert. Daher verlieren die Ergebnisse an statistischer Signifikanz und die Klassifikatoren sind ungenügend zu trainieren.

5 Ausblick

Wir konnten zeigen, dass die Gesichtsunterschiede zwischen Kindern und Erwachsenen mit einem Gesichtserkennungssystem detektierbar sind. Wir schlugen einen automatischen Klassifikator zur Kategorisierung von Gesichtern als kindlich oder erwachsen vor. Angewandt auf Bilder von Kindern der analysierten Altersgruppe und Erwachsene, die nicht der Trainingsmenge angehörten, war die Klassifikation sehr verlässlich. Wurden die Parameter der Klassifikatoren so eingestellt, dass nahezu alle Kinderbilder richtig erkannt wurden, wurden auch 90% der Erwachsenen richtig klassifiziert. Die Gesichtsfindung und die Klassifikation arbeiten voll automatisch und extrem schnell (weniger als 1 s pro Bild).

Man beachte, dass unsere Experimente unter kontrollierten Laborbedingungen durchgeführt wurden, d. h. wir nutzten ausschließlich hochaufgelöste Bilder ohne Störungen und Gesichtsposen. Es ist beabsichtigt, die Methoden auf realistischere Szenen auszuweiten und unser Ziel ist es, die Menge der Bilder, die zur Aufdeckung von Kinderpornographie untersucht werden müssen, signifikant zu verringern, indem der Klassifikator eine große Anzahl von Erwachsenenbildern aussortiert.

Erste Versuche auf einem schmalen Altersspektrum zeigen, dass die Methoden auch zur direkten Altersschätzung einsetzbar sind. Wir fanden, dass unsere Schätzungen vergleichbar mit denen auf Grundlage der anthropologischen Messungen gewonnenen sind. Zukünftige Arbeit sollte auch auf die Erweiterung auf den gesamten Altersbereich vom Kind bis hin zum Erwachsenen fokussiert sein.

Danksagungen

Die Autoren möchten M. Hüsken für die fruchtbaren Diskussionen und die sorgfältige Lektüre des Manuskriptes danken. Diese Arbeit wurde durch die Europäische Union gefördert (JAI/2002/STOP/132).

Literatur

[1] M.-H. Yang, D. Kriegman, and N. Ahuja, „Detecting Faces in Images: A Survey", *IEEE Transactions on Pattern Analysis and Machine Intelligence*, 24(1), pp. 34–58, 2002.

[2] L. Wiskott, J.-M. Fellous, N. Krüger, and C. von der Malsburg, „Face recognition by elastic bunch graph matching", IEEE *Transactions on Pattern Analysis and Machine Intelligence,* 19, pp. 775–779, 1997.

[3] M. Turk and A. Pentland, „Eigenfaces for recognition", *Journal of Cognitive Neuroscience* 3(1), 1991.

[4] R. O. Duda, P. E. Hart, and D. G. Stork, „*Pattern Classification*", John Wiley & Sons, Inc., New York, 2001.

[5] B. Schölkopf, A. Smola, and K.-R. Müller, „Nonlinear Component Analysis as a Kernel Eigenvalue Problem", Max-Planck-Institut für biologische Kybernetic, Technical Report No. 44, 1996.

Digitisation of holographic recordings for medical applications

Andrea Thelen[1], Susanne Frey[1], Sven Hirsch[1], Natalie Ladriere[1], Jens Bongartz[2], Dominik Giel[3] and Peter Hering[1,4]

[1] Stiftung caesar, Ludwig-Erhard-Allee 2, D-53175 Bonn
[2] RheinAhrCampus, Fachhochschule Koblenz, Südallee 2, D-53424 Remagen
[3] Fraunhofer Institut IPM, Heidenhofstraße 8, D-79110 Freiburg
[4] Institut für Lasermedizin, Universität Düsseldorf, Universitätsstraße 1, D-40225 Düsseldorf

Abstract

A hologram contains the entire three-dimensional information of the recorded object with high resolution. In order to utilise this information for medical applications, for example a three-dimensional model of a human face for documentation and planning in maxillofacial surgery, the hologram has to be optically reconstructed and digitised. Illumination of the hologram with the complex conjugate reference beam leads to a three-dimensional real image of the recorded face, which can be digitised into a set of two-dimensional projections and merged to a three-dimensional computer model. A focus measure operator has to be used to separate the focused information from the scattering surface and the unfocused background. The characteristics of the off-axis region in the holographic imaging process are taken into account through an iterative algorithm.

1 Introduction

For planning, simulation and documentation of interventions in maxillofacial surgery high resolving soft tissue information of the human face in upright position is needed. This information can be gained by holographic methods, which allow a recording of the whole face in an extremely short time period, so that no movement artefacts can occur.

The hologram is recorded with a single laser pulse of 35 ns duration and stored in a photosensitive material. After automated wet-chemical processing, the hologram can be optically reconstructed with a cw-laser and digitised. During the optical reconstruction, a light field, which is a one-to-one three-dimensional image of the recorded object, emerges at its original position. By moving a diffuser screen through this so-called real image, a series of 2D images is projected and digitised with a CCD camera. This procedure is called hologram tomography [1]. Each projection shows a focused contour of the patients face as well as an unfocused background. The main problem of locating this contour is therefore to distinguish between focused and unfocused regions in each image slice.

2 The holographic principle

During the holographic recording process, the scattered light wave *o* from the object is superimposed with the so-called reference beam *r*. Due to the coherent properties of the used laser light they form an interference pattern with the intensity distribution

$$I = |o + r|^2 = |o|^2 + |r|^2 + o^* r + o r^*,$$

which is stored in a photosensitive emulsion on the holographic plate (see **figure 1a**). If such a hologram is illuminated with the complex conjugate reference beam *r**, the light is diffracted and forms different wave fronts according to the following equation

$$r^* \cdot I = r^* |o|^2 + r^* |r|^2 + o^* |r|^2 + o r^{*2}.$$

The interesting term is $o^* |r|^2$, which forms, despite a constant factor, the complex conjugate object wave o^*. It can be regarded as the object wave *o*, travelling back in time, which means that it is propagating from the hologram to the original position of the scattering surface and forms a three-dimensional image (see **figure 1b**) [2].

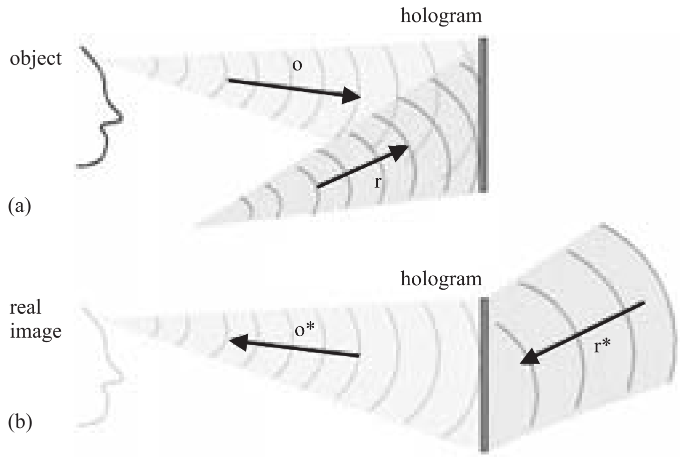

Fig. 1: (a) Recording of the hologram (b) Reconstruction with the complex conjugate reference beam and formation of the real image.

3 Experimental Setup

3.1 Hologram recording and chemical processing

The hologram recording is done with a holographic camera of the type GP-2J from Geola with a Nd:YLF laser in a master-oscillator arrangement and second harmonic generation with a resulting wavelength of 526.5 nm. The high coherence length of approximately 6 m in combination with the high pulse energy of 2 J and the short pulse duration of 35 ns leads to an optimised system for portrait holography. The laser pulse is split into three parts. Two are expanded by concave lenses and diffusor plates and serve as homogeneous illumination of the face. The third part acts as reference beam, which forms an interference pattern with the scattered light from the face. The holographic plate, on which the interference pattern is stored, has to undergo chemical processing to obtain a phase hologram.

3.2 Hologram reconstruction and digitisation

A continuous wave frequency doubled Nd:YAG laser is used as coherent light source for the reconstruction of the hologram. The complex conjugated reference beam is created by the usage of lenses and a spherical mirror and produces, if illuminating the hologram, the real image of the recorded face. 2D projections of the real image are gained at different axial positions with a projection screen and a digital camera, both mounted on a translation stage (see **figure 2**). The inter-slice distance can be chosen arbitrarily down to the axial resolution of the holographic recording in the micrometer range. For medical imaging of the human face, inter-slice distances between 100 µm to 1 mm seem reasonable. A typical data set contains 256 or 512 slices. The lateral resolution is approximately 200 µm (see [1] and [3]).

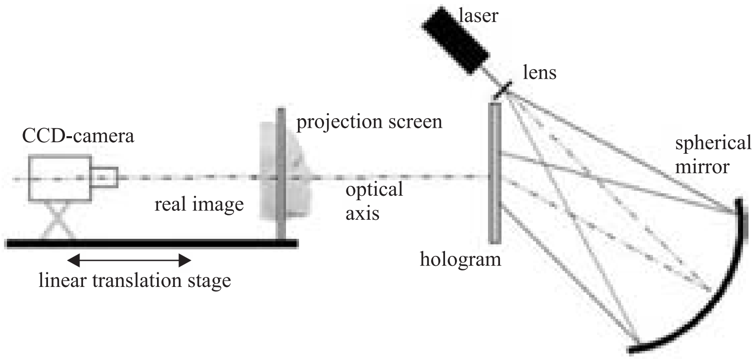

Fig. 2: Reconstruction of the hologram and digitisation of a set of two-dimensional projections of the real image.

4 Surface extraction

The procedure described above leads to a set of two-dimensional images, so-called slices, which contain a focused contour of the face as well as an unfocused background (see **figure 3**).

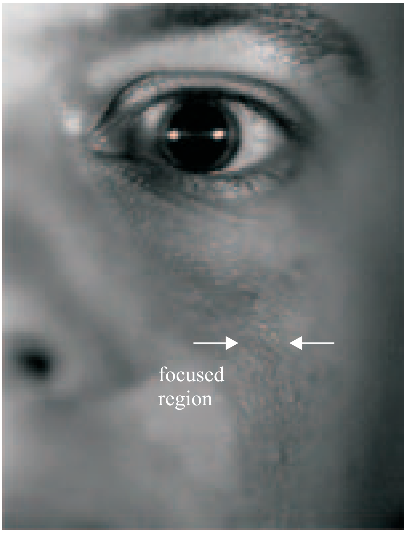

Fig. 3: Section of a two-dimensional projection of the real image at a specific position of the diffuser screen. The focused region is surrounded by an unfocused background.

To obtain the topometry of the face, the focused and unfocused regions have to be separated. In order to achieve this, a focus detection procedure has to be performed. This is done by defining a focus measure operator $F_{xy}(z)$, whose values are compared for different z-positions. Such a comparison causes a curve like the one shown in **figure 4**. The slice position, which is maximal concerning this focus measure operator, leads to the desired z coordinate corresponding to the lateral position (x,y) and therefore to the topometry of the recorded object.

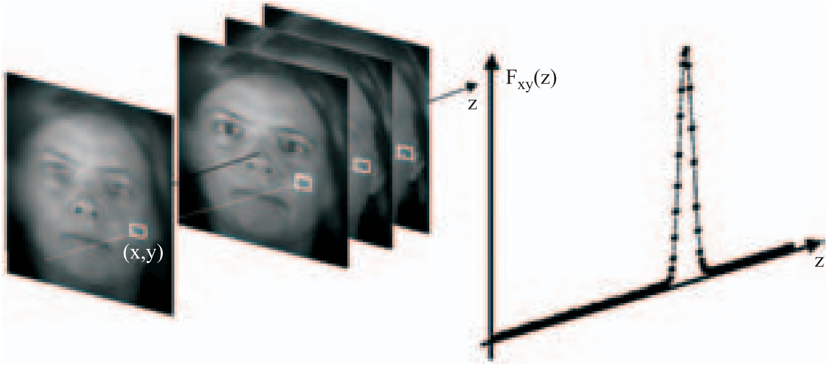

Fig. 4: Evaluation of the focus measure operator $F_{xy}(z)$ for a specific lateral coordinate (x,y) along the z-axis. The z value, for which $F_{xy}(z)$ maximal, delivers the third coordinate of the focus point.

5 Focus measure operator

For the procedure described above, various focus measures have been tested. It was found that the so-called SML-operator invented by *Nayar* [4] for focus detection in microscopy produces the best results in a relatively short amount of time.

Due to the fact that defocusing acts as a low-pass filter, a focus measure operator must high-pass filter the image. One possibility to do this is to determine the second derivative of the intensity *I(x,y)*. In case of two-dimensional images, the *Laplacian* should be used:

$$\Delta I = \frac{\partial^2 I}{\partial x^2} + \frac{\partial^2 I}{\partial y^2} .$$

If the second derivates in x and y directions have opposite signs they tend to cancel each other and the *Laplacian* may have an unstable behaviour. To overcome this problem the modified *Laplacia*n is defined:

$$\Delta_M I = \left|\frac{\partial^2 I}{\partial x^2}\right| + \left|\frac{\partial^2 I}{\partial y^2}\right|.$$

In the discrete approximation of the *Laplacian* the partial derivatives are calculated with a variable spacing *s* to accommodate for possible variations in the size of the texture. This yields to the modified *Laplacian*, which is defined as follows:

$$ML(x,y) = |I(x-s,y) + I(x+s,y) - 2I(x,y)| + |I(x,y-s) + I(x,y-s) - 2I(x,y)|$$

Finally the focus measure at a point (x,y) is defined as the sum of the modified *Laplacian* values over a small neighbourhood U(x,y) of the point (x,y). It is called sum-modified-Laplacian (SML):

$$SML(x,y) = \sum\nolimits_{(i,j)\in U(x,y)} ML(i,j)$$

(see [4]).

The procedure described in section 3 with the SML as focus measure operator, a neighbourhood size of 9x9 pixel and a s-value of 3 produces a resulting three-dimensional model as can be seen in **figure 5**.

Fig. 5: Resulting three-dimensional computer model.

6 Off-axis effects

The captured data contains focused and unfocused images of each object point. These corresponding points lie on a straight line, defined by the position of the actual focus and the centre of the hologram.

For object points in the off-axis region, the line of corresponding pixels cannot be assumed to be parallel to the optical axis (see **figure 6**).

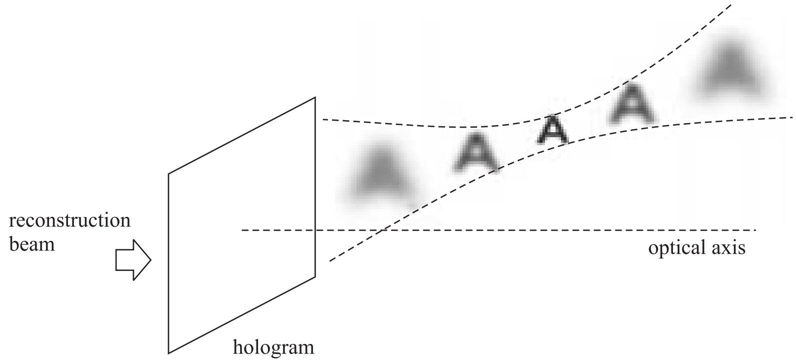

Fig. 6: Schematic illustration of the direction, along which image points form up in off-axis region.

Opposed to this, the maximization of the focus measure operator is performed parallel to the optical axis. By doing so it cannot be guaranteed that focused and unfocused images of one and the same object point are compared. Focused images of object regions with low intrinsic texture can produce a lower focus measure value than unfocused regions with high intrinsic contrast. Such cases cause errors in the surface localisation in off-axis regions.

To overcome this problem, an iterative algorithm was invented (see [5], [6]), which takes the direction of image formation into account and performs the focus detection along this particular direction.

The surface points found in the maximization step parallel to the optical axis deliver a starting dataset for the iteration. The direction of image formation is calculated for each focus point individually out of this first estimation of the focus position and the centre of the hologram. Along this direction a new maximization step is performed, which leads to a new set of focus positions. This process can be repeated until the variation in the found focus coordinates is considerably small. Experiments showed that after approximately ten iterations no further significant changes occur. **Fig. 7** shows the improvement in the three-dimensional computer model. Fig. 7 (a) is produced in an evaluation step parallel to the optical axis, figure 7 (b) shows the result of the direction dependent method after ten iterations.

(a) (b)

Fig. 7: Computer models obtained in a maximisation procedure parallel to the optical axis (a) and for each point along the iteratively calculated direction of image formation (b).

7 Conclusion

Hologram tomography is a new approach towards high resolving facial measurement. Due to the extremely short recording time of 35 ns no movement artefacts occur and a resolution in the sub-mm range can be reached. Analysis of a set of two-dimensional projections produces topometrical data of the recorded face.

To accomplish this analysis, the SML-operator was found to perform best in combination with an iterative procedure for the off-axis region.

8 References

[1] J. Bongartz, "Hochaufloesende dreidimensionale Gesichtsprofilvermessung mit kurzgepulster Holographie," Ph. D. dissertation, Mathematisch naturwissenschaftliche Fakultaet der Heinrich-Heine-Universitaet Duesseldorf, 2002. *http://diss.ub. uni-duesseldorf.de/ebib/diss/file?dissid=192*

[2] R. W. Meier, "Magnification and third-order aberrations in holography," in *Journal of the Optical Society of America,* Vol. 55, pp. 987–992, 1965.

[3] D. Giel, "Hologram tomography for surface topometry," Ph. D. dissertation. Mathematisch naturwissenschaftliche Fakultaet der Heinrich-Heine-Universitaet Duesseldorf, 2002. *http://diss..ub.uni-duesseldorf.de/ebib/diss/file?dissid=598*

[4] S. K. Nayer and Y. Nakagawa, "Shape from Focus," *IEEE transactions on pattern analysis and machine intelligence*, Vol. 16, pp. 824–831, Sep 1994.

[5] A. Thelen, J. Bongartz, D. Giel, S. Frey and P. Hering, "Iterative focus detection in hologram tomography", in *Journal of the Optical Society of America A*, Vol. 22, pp. 1176–1180, 2005.

[6] A. Thelen, "Holographische Topometrie. Off-Axis Effekte in der Digitalisierung holographischer Rekonstruktionen,", M. S. thesis, Rheinische Friedrich-Wilhelms-Universität Bonn, 2003.

Digitalisierung holographischer Aufnahmen für medizinische Anwendungen

Andrea Thelen[1], Susanne Frey[1], Sven Hirsch[1], Natalie Ladriere[1], Jens Bongartz[2], Dominik Giel[3] und Peter Hering[1,4]

[1] Stiftung caesar, Ludwig-Erhard-Allee 2, 53175 Bonn
[2] RheinAhrCampus, Fachhochschule Koblenz, Südallee 2, 53424 Remagen
[3] Fraunhofer Institut IPM, Heidenhofstraße 8, 79110 Freiburg
[4] Institut für Lasermedizin, Universität Düsseldorf, Universitätsstraße 1, 40225 Düsseldorf

Abstract

In einem Hologramm ist die gesamte dreidimensionale Information des aufgezeichneten Objektes mit hoher Auflösung gespeichert. Um diese in digitaler Form für medizinische Anwendungen nutzbar zu machen, z. B. die holographische Aufnahme eines Gesichts zur Dokumentation und Planung von Operationen im Bereich der Mund-, Kiefer- und Gesichtschirurgie, wird das Hologramm optisch rekonstruiert und digitalisiert. Durch Ausleuchtung des Hologramms mit dem phasenkonjugierten Referenzstrahl entsteht ein dreidimensionales reelles Bild, welches scheibenweise digitalisiert und zu einem Computermodell zusammengefügt wird. Hierzu wird durch Maximierung eines Schärfemaßes die fokussierte Information der Gesichtsoberfläche von dem unfokussierten Hintergrund getrennt. Durch ein iteratives Verfahren werden die off-axis-Bereiche der holographischen Abbildung in der Fokusfindung gesondert berücksichtigt.

1 Einleitung

Für die Planung, Simulation und Dokumentation von Eingriffen in der Mund-Kiefer- Gesichtschirurgie ist hochaufgelöste 3D-Information der Gesichtsoberfläche einer Person in aufrechter Position vonnöten. Diese kann mittels gepulster holographischer Methoden gewonnen werden, die extrem kurze Aufnahmezeiten besitzen, und somit die Entstehung von Bewegungsartefakten verhindern.

Das Hologramm wird mit einem einzigen Laserpuls von 35 ns Dauer aufgezeichnet und in einem fotosensitiven Material gespeichert. Nach nasschemischer Entwicklung kann das Hologramm mit Hilfe eines cw-Lasers optisch rekonstruiert und digitalisiert werden. Während der optischen Rekonstruktion entsteht ein Lichtfeld, welches eine orginalgetreue dreidimensionale Abbildung des aufgezeichneten Objektes ist. Indem eine Streuscheibe durch dieses so genannte reelle Bild bewegt wird, kann eine Serie von 2D Bildern projiziert und digitalisiert werden. Diese Prozedur wird als Hologramm-Tomographie bezeichnet [1]. Jede Projektion zeigt eine fokussierte Kontur des Gesichts sowie einen unfokussierten Hintergrund. Die Hauptaufgabe besteht nun in der Lokalisierung dieser Kontur und somit in der Unterscheidung zwischen fokussierten und unfokussierten Regionen in jedem Schnittbild.

2 Das holographische Prinzip

Während des holographischen Aufnahmeprozesses wird die vom Objekt gestreute Lichtwelle o mit dem Referenzstrahl r überlagert. Aufgrund der Kohärenz des verwendeten Laserlichts bildet sich ein Interferenzmuster mit der Intensitätsverteilung

$$I = |o + r|^2 = |o|^2 + |r|^2 + o^*r + or^*,$$

das in der fotosensitiven Schicht auf der Hologrammplatte gespeichert wird (siehe Abbildung 1). Wird ein solches Hologramm mit dem komplex konjugierten Referenzstrahl r^* beleuchtet, so wird dieses Licht gebeugt und erzeugt verschiedene Lichtwellen entsprechend folgender Gleichung:

$$r^* \cdot I = r^*|o|^2 + r^*|r|^2 + o^*|r|^2 + or^{*2}.$$

Der interessierende Term ist $o^*|r|^2$, welcher, abgesehen von einem konstanten Faktor, die komplex konjugierte Objektwelle o^* darstellt. Diese kann als eine sich rückwärts in der Zeit bewegende Objektwelle o angesehen werden. Das bedeutet, dass sie vom Hologramm ausgehend zur ursprünglichen Position der streuenden Oberfläche hin propagiert (siehe Abbildung 1b) [2].

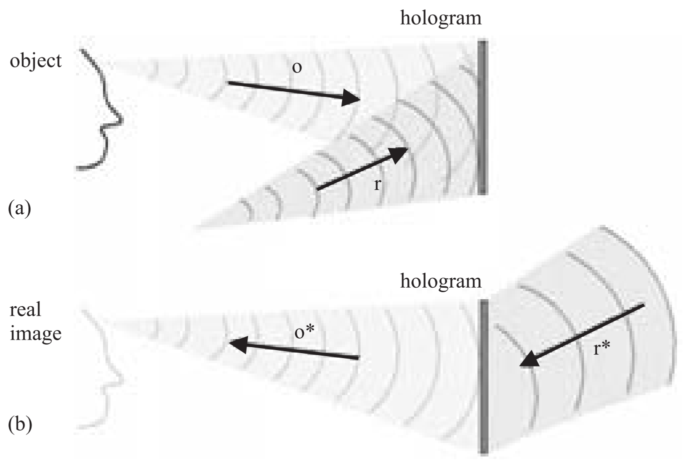

Abb. 1: (a) Aufnahme eines Hologramms (b) Rekonstruktion mit der komplex konjugierten Referenzwelle und Entstehung des reellen Bildes.

3 Experimenteller Aufbau

3.1 Hologrammaufnahme

Das Hologramm wird mit einer holographischen Kamera vom Typ GP-2J der Firma Geola aufgenommen, die einen Nd:YLF Laser in einer Oszillator-Amplifier Anordnung enthält und mittels Erzeugung der zweiten Harmonischen eine Wellenlänge von 526,5 nm erreicht. Die hohe Kohärenzlänge von 6 m in Kombination mit einer hohen Pulsenergie von 2 J und die kurze Pulsdauer von 35 ns machen das System optimal für die Aufnahme von Portrait-Hologrammen. Der Laserpuls wird in drei Teile geteilt. Zwei Teile werden mit Hilfe von Streuscheiben aufgeweitet und dienen der homogenen Ausleuchtung des Gesichts. Der dritte Teil fungiert als Referenzstrahl, der zusammen mit dem von Gesicht gestreutem Licht in der Hologrammebene das Interferenzmuster bildet. Die Hologrammplatte, auf der das Interferenzmuster gespeichert ist, wird chemisch zu einem Phasenhologramm verarbeitet.

3.2 Hologrammrekonstruktion und Digitalisierung

Für die optische Rekonstruktion des Hologramms wird ein frequenzverdoppelter kontinuierlicher Nd:YAG Laser verwendet. Mit Hilfe von Linsen und einem sphärischen Spiegel wird der komplex konjugierte Referenzstrahl erzeugt, so dass bei Beleuchtung des Hologramms das reelle Bild des aufgezeichneten Gesichts entsteht. Zweidimensionale Projektionen des reellen Bildes an verschiedenen axialen Positionen werden mit einer Streuscheibe und einer Digitalkamera aufgenommen, die beide auf einem Verschiebetisch installiert sind (siehe Abbildung 2). Der Schnittbildabstand kann beliebig gewählt werden, bis zur axialen Auflösung des Hologramms im Mikrometerbereich. Für medizinische Anwendungen der Gesichtsdaten hat sich ein Schnittbildabstand von 100 µm bis 1 mm bewährt. Typische Datensätze enthalten 256 oder 512 Schnittbilder. Die laterale Auflösung beträgt ungefähr 200 µm (siehe [1] and [3]).

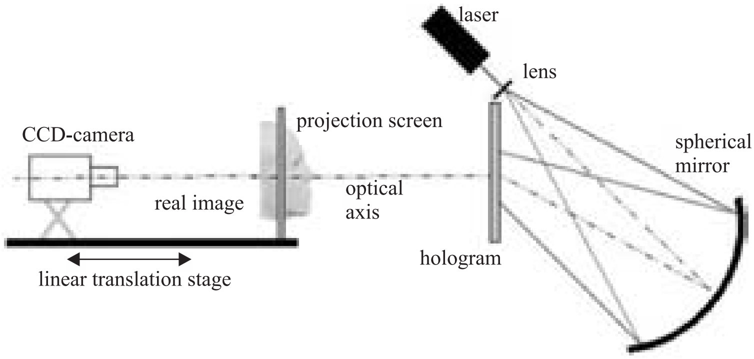

Abb. 2: Optische Rekonstruktion des Hologramms und Digitalisierung mittels eines Satzes zweidimensionaler Projektionen.

4 Oberflächenextraktion

Die oben beschriebene Prozedur führt zu einem Satz von zweidimensionalen Projektionen, den so genannten Schnittbildern. In ihnen ist jeweils eine fokussierte Kontur des Gesichts sowie unfokussierten Hintergrund enthalten (siehe Abbildung 3).

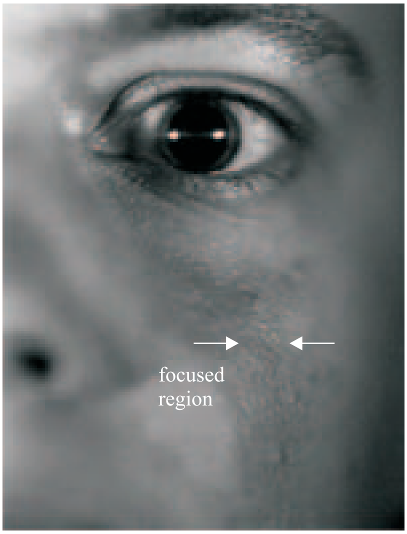

Abb. 3: Ausschnitt einer zweidimensionalen Projektion des reellen Bildes an einer bestimmten Position der Streuscheibe. Der fokussierte Bereich ist umgeben von unfokussiertem Hintergrund.

Um die Topometrie des Gesichts zu extrahieren, müssen die unfokussierten Bereiche von fokussierten separiert werden. Dazu wird eine Fokusmaß $F_{xy}(z)$ definiert, dessen Werte für verschiedene z-Positionen verglichen werden. Ein solcher Vergleich liefert einer Kurve, wie sie in Abbildung 4 zu sehen ist. Die Schnittbildposition, an der das Fokusmaß für jede laterale Koordinate (x,y) maximal ist, bestimmt die gewünschte z-Koordinate dieses Punktes und damit die Topometrie des aufgezeichneten Objektes.

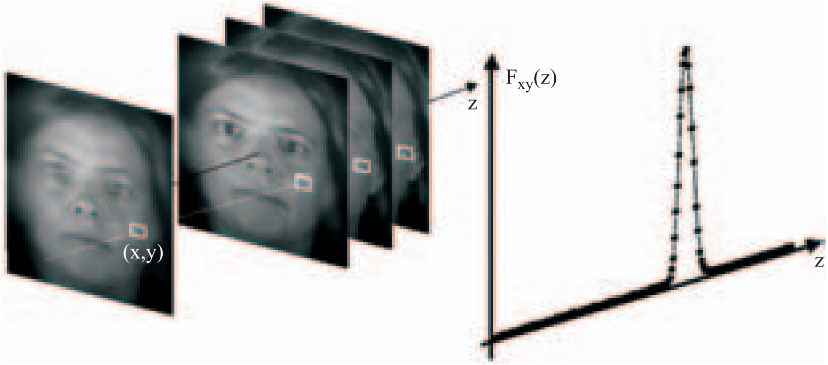

Abb. 4: Vergleich des Fokusmaßes $F_{xy}(z)$ einer spezifischen lateralen Koordinate (x,y) entlang der z-Achse. Der z-Wert, für welchen $F_{xy}(z)$ maximal ist, liefert die gewünschte dritte Koordinate des Fokuspunktes.

5 Fokusmaß

Für die oben beschriebene Prozedur wurden verschiedene Fokusmaße getestet. Dabei hat sich erwiesen, dass der von *Nayar* [4] für die Fokusdetektion in der Mikroskopie eingeführte SML-Operator die besten Ergebnisse mit einem sehr geringem Rechenaufwand liefert.

Da Defokussierung wie ein Tiefpass-Filter wirkt, muss das Fokusmaß als Hochpass-Filter fungieren. Eine Möglichkeit hierzu ist die Verwendung der zweiten Ableitung der Intensität *I(x,y)*. Im Falle eines zweidimensionalen Bildes muss der Laplace-Operator verwendet werden:

$$\Delta I = \frac{\partial^2 I}{\partial x^2} + \frac{\partial^2 I}{\partial y^2} .$$

Haben die zweiten Ableitungen in x- und y-Richtung unterschiedliche Vorzeichen, so können sie sich gegenseitig aufheben und der Laplace-Operator zeigt ein instabiles Verhalten. Um dieses zu verhindern wird der so genannte modifizierte Laplace-Operator definiert:

$$\Delta_M I = \left| \frac{\partial^2 I}{\partial x^2} \right| + \left| \frac{\partial^2 I}{\partial y^2} \right| .$$

Die diskrete Approximation des Laplace-Operators wird mit variabler Diskretisierungsweite s berechnet um Besonderheiten in der Textur des Objektes gerecht zu werden. Dieses führt folgender diskreten Version des modifizierten Laplace-Operators:

$$ML(x,y) = |I(x-s,y) + I(x+s,y) - 2I(x,y)| + |I(x,y-s) + I(x,y-s) - 2I(x,y)|$$

Letztlich wird als Fokusmaß jedes Punktes (x,y) der so genannte als SML-Wert (sum modified Laplacian) als Summe der modifizierten Laplacewerte über eine kleine Umgebung U(x,y) definiert:

$$SML(x,y) = \sum\nolimits_{(i,j) \in U(x,y)} ML(i,j)$$

(siehe [4]).

Die oben beschriebene Prozedur mit dem SML-Fokusmaß, einer Umgebungsgröße von 9x9 Pixeln und einen s-Wert von 3 führt zu einem dreidimensionalen Computermodell, wie in Abbildung 5 zu sehen ist.

Abb. 5: Resultierendes dreidimensionales Computermodell.

6 Off-axis Effekte

Die aufgezeichneten Schnittbilder enthalten fokussierte und unfokussierte Bilder jedes Objektpunktes. Solche korrespondierenden Punkte liegen auf einer Geraden, welche durch die Position des Fokuspunktes und das Zentrum des Hologramms definiert wird. Für Objektpunkte in der off-axis Region kann diese Gerade korrespondierender Punkte nicht als parallel zur optischen Achse angenommen werden (siehe Abbildung 6).

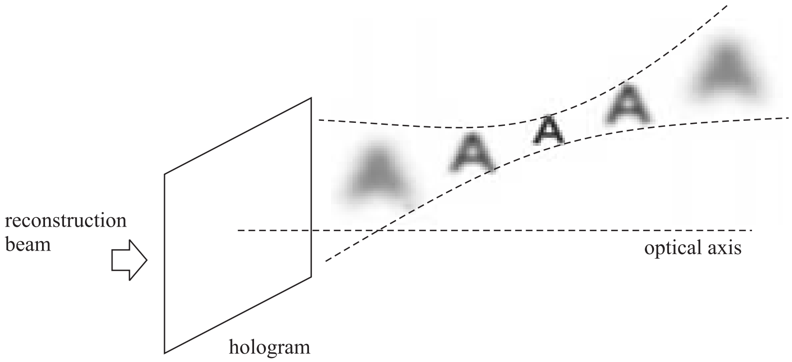

Abb. 6: Schematische Darstellung derjenigen Richtung, entlang welcher sich das Bild eines Punktes in den off-axis-Regionen formiert.

Im Gegensatz dazu wird die Maximierung des Fokusmaßes parallel zur optischen Achse durchgeführt. Hierbei kann jedoch nicht garantiert werden, dass das fokussierte und unfokussierte Bild ein und desselben Objektpunktes miteinander verglichen werden. Fokussierte Bildregionen mit intrinsisch geringem Kontrast können einen niedrigeren Fokuswert erzeugen als unfokussierte Regionen mit intrinsisch hohem Kontrast. Solche Fälle führen in den off-axis-Bereichen zu Fehlern in der lokalisierten Oberfläche.

Um dieses Problem zu umgehen wurde ein iterativer Algorithmus entwickelt (siehe [5], [6]). In diesem wird die individuelle Richtung, in der sich jeder Bildpunkt formiert, einbezogen und die Maximierung des Fokusmaßes wird entlang dieser Richtung vollführt.

Die Oberflächenpunkte, die im Maximierungsschritt parallel zur optischen Achse gefunden werden, liefern die Startdaten für die Iteration. Die Richtung der Bildformierung wird für jeden Bildpunkt individuell aus der im vorherigen Iterationsschritt ermittelten Fokusposition und dem Hologrammzentrum bestimmt. Entlang dieser Richtung wird das Maximum des Fokusmaßes bestimmt, welches zu einem neuen Satz von Fokuspositionen führt. Dieser Prozess wird wiederholt, bis die Änderungen in den Fokuspositionen entsprechend klein werden. Experimentell konnte gezeigt werden, dass nach ungefähr 10 Iterationen keine beträchtlichen Änderungen mehr auftraten. Die erreichten Verbesserungen im dreidimensionalen Computermodell sind in Abbildung 7 dargestellt. Abbildung 7 a zeigt das Modell, das durch Maximierung parallel zur optischen Achse entstanden ist, Abbildung 7 b das Resultat der richtungsabhängigen Maximierung nach zehn Iterationen.

(a) (b)

Abb. 7: Computermodelle entstanden durch Maximierung des Fokusmaßes parallel zur optischen Achse (a) und entlang der für jeden Bildpunkt iterativ bestimmten Richtung der Bildausbreitung (b).

7 Fazit

Hologramm-Tomographie ist ein neuartiger Ansatz zur hochauflösenden Gesichtsprofilvermessung. Aufgrund der extrem kurzen Aufnahmezeit von 35 ns werden Bewegungsartefakte umgangen und eine Auflösung im sub-mm Bereich erreicht. Die Bildanalyse eines Satzes von zweidimensionalen Projektionen führt zu topometrischen Daten des aufgezeichneten Gesichts. Diese Analyse wird mit dem SML-Opterator in Verbindung mit einer iterativen Methode für die off-axis-Bereiche durchgeführt.

8 Literatur

[1] J. Bongartz, „Hochaufloesende dreidimensionale Gesichtsprofilvermessung mit kurzgepulster Holographie," Ph. D. dissertation, Mathematisch naturwissenschaftliche Fakultaet der Heinrich-Heine-Universitaet Duesseldorf, 2002. *http://diss.ub. uni-duesseldorf.de/ebib/diss/file?dissid=192*

[2] R. W. Meier, „Magnification and third-order aberrations in holography," in *Journal of the Optical Society of America,* Vol. 55, pp. 987–992, 1965.

[3] D. Giel, „Hologram tomography for surface topometry," Ph. D. dissertation. Mathematisch naturwissenschaftliche Fakultaet der Heinrich-Heine-Universitaet Duesseldorf, 2002. *http://diss..ub.uni-duesseldorf.de/ebib/diss/file?dissid=598*

[4] S. K. Nayer and Y. Nakagawa, „Shape from Focus," *IEEE transactions on pattern analysis and machine intelligence*, Vol. 16, pp. 824–831, Sep 1994.

[5] A. Thelen, J. Bongartz, D. Giel, S. Frey and P. Hering, „Iterative focus detection in hologram tomography", in *Journal of the Optical Society of America A*, Vol. 22, pp. 1176–1180, 2005.

[6] A. Thelen, „Holographische Topometrie. Off-Axis Effekte in der Digitalisierung holographischer Rekonstruktionen,", M. S. thesis, Rheinische Friedrich-Wilhelms-Universität Bonn, Bonn, 2003.

7.

FEM Principles and Statistical Shape Models

Finite-Elemente-Methoden und statistische Formmodelle

Combined Statistical Modeling of Tissue Depth and 3D Facial Outlook for Computerized Facial Approximation

P. Claes[1] (*), D. Vandermeulen[1], S. De Greef[2], G. Willems[2], P. Suetens[1]

[1] Medical Image Computing (ESAT-Radiology),
[2] Centre of Forensic Odontology
K. U. Leuven, Faculties of Medicine and Engineering, Katholieke Universiteit Leuven, Belgium, U. Z.Gasthuisberg, Herestraat 49, 3000 Leuven

Abstract

In forensic facial reconstruction, facial features of an unknown individual are approximated in order to aid in recognition and identification. The development of software for computerized facial approximations of an individual would be of benefit to various law enforcement agencies, by allowing faster, easier and more efficient generation of multiple representations of an individual.

Current computerized techniques are limited in the model and deformation method used for reconstructing the complete facial outlook. A generic skin surface or a specific best look-alike according to the skull is used as a starting point. Subsequently, the skin surface is inferred based on a generic interpolation and extrapolation of a deformation field in between corresponding interactively placed virtual dowels or skull features.

We address the facial reconstruction problem with a combined statistical deformable model of facial surfaces and tissue-thicknesses at 52 anatomical landmarks, learned from a facial database. This allows us to deform the average face surface and thicknesses from the database to a given skull using correlation ranked face-specific modes of deformation in combination with a more generic deformation, resulting in an unbiased and more realistic facial reconstruction. Additionally, more realism and reconstruction flexibility is gained through the possibility of determining facial deformations originating from changes in age, weight-length ratio and gender.

Experiments are performed on a real-case, where a comparison is made between the proposed method, a manual reconstruction, a typical current computerized reconstruction and an alternative statistical method, that we developed earlier, without incorporation of tissue-thicknesses.

1 Introduction and related work

When confronted with a corpse that is unrecognizable due to its state of decomposition, skeletonisation, mutilation or incineration, where no other identification evidence is available, craniofacial reconstruction can be considered. The goal of craniofacial reconstruction is the attempt to recreate the face of an individual at the time of death. This, hopefully, will trigger recognition so that individuals can be excluded from further investigation and new evidence would lead to a likely candidate to be identified with the remains. Although craniofacial reconstruction is a valuable tool in the initiation of the process of identification, positive identification has to be obtained by classic techniques such as radiographic and dental comparisons or DNA-analysis [1].

Several 3D manual methods for facial reconstruction have been developed and are currently used in practice. The reconstruction consists of modeling a face on a skull by use of clay or plasticine. However, manual reconstruction methods have several fundamental shortcomings, such as being highly subjective, time-consuming and requiring artistic talent. Computer-based methods were developed trying to provide an answer to the shortcomings of manual reconstructions. Computers are consistent and objective so that they are able in a short time to reconstruct a face in a repeatable way and if necessary perform multiple reconstructions from the same skull.

Current computerized techniques are limited in the model used for reconstructing the complete facial outlook. Some techniques [2] – [6] fit a generic skin surface or a specific best look-alike according to the skull to a set of interactively placed virtual dowels on a 3D digitized model of the skull. The dowel lengths represent averages of ancestry-, gender- and age-matched tissue depths at a limited number of predefined cephalometric landmarks. However, there is no direct correlation between the reported measures of tissue depth and skin surface shape of an individual. Furthermore, skin surface shape is directly defined at the dowel positions only, and inferred by generic interpolation (Spline-based, e. g.) in between, in combination with some extra manual modelling of the nose, eyes, e. g. afterwards to improve the result. Finally, the reconstruction is biased by the generic skin surface or specific best look-alike used. Other computer-based techniques deform a reference skull to a skull based on crest lines (lines of maximal local curvature) 7], control data sets [8] or feature points [9]. The calculated skull deformation is then extrapolated and applied to the skin surface associated to the reference skull in order to estimate the facial outlook corresponding to the skull sample. A reference skull is selected based on similarity in ancestry, gender and age. Reference skulls and corresponding facial surfaces are obtained using CT scanning, which limits its use because of the involved irradiation dose. As a result, it is ethically not approved to build a representative database of reference skulls and faces using CT scanning. Furthermore the reconstruction is again biased by the choice of reference skull. A common remark on all current computer-based reconstruction methods is the use of generic interpolations and extrapolations of the deformation fields. All of them are nicely defined mathematically, but are not face-specific as they don't incorporate knowledge about typical human face variations and correlated differences.

The presented work in this paper is similar to [2] – [6], but here we maintain the direct statistical relationship between skin surface shape and tissue depth for each individual and use it explicitly in a combined statistical model or template. This requires the acquisition of skin surfaces and associated tissue depths, measured over a sufficiently large and diverse population and storing them in a database together with the population individual's age, weight-length ratio, gender and race. A combined statistical deformable template, modelling the population-dependent variation and correlation of skin surface shape and tissue depth, is obtained from the database and can be represented as an elastic mask with elastic dowels at particular locations on the inside of the mask. This mask is subsequently fitted to the external surface of the individual craniofacial skeleton and an estimate of the nose tip, such that all the dowels touch the skull at the, currently manually indicated, corresponding skull landmark locations. The elasticity of the mask and the dowels is defined as the statistically allowed correlated variation learned from the database. In order to overcome a lack of elasticity of the mask due to a limited database or limited variation in the database, we combine the face-specific deformations with a more generic Thin-Plate-Spline (TPS) based deformation, resulting in a flexible but constraint deformation of the mask towards a given skull. The average face from the database is used as initialization of the mask and in combination with the face-specific constraints on the deformation no severe bias is introduced into the final reconstruction. Finally in order to incorporate constraints of age, weight-length ratio, gender and race on the final reconstruction, we explicitly determine the facial deformations originating from differences in age, weight-length ratio, gender and race in the database and apply them to the final reconstruction.

The remainder of this paper is organised as follows: In section 2 we shortly describe the acquisition hardware and software for measuring facial surfaces and tissue depths and the current database of individuals used. Section 3 explains the creation of a statistical facial deformable model based on the acquired database. Section 4 presents the fitting procedure of the elastic mask to a given skull. Section 5 will show results and comparisons of the proposed method with other existing methods on a real-case. Finally, in section 6 we finish with a conclusion, shortcomings and future improvements.

2 3D facial database

A 3D facial entry (sample) in the database consists of a 3D skin surface coupled with soft tissue depths measured at 52 (10 midline plus 2 times 21 bilateral) anatomical landmarks and an indication of the nose tip. These landmarks are determined as a combination of landmarks in previous tissue depth studies [10] – [15]. In order to construct 3D facial entries of the database we assembled acquisition hardware and software to capture 3D skin surfaces and to measure tissue depths. Fig. 1 shows a high-level overview of the database acquisition.

The skin surface is measured by a mobile 3D photographic device (ShapeCam, Eyetronics (www.eyetronics.com)). This is an active 3D reconstruction device, which projects a regular grid on the face. At the same time a digital camera (CANON D60) takes an image of the face from a different point of view such that by triangulation the 3D shape of the face can be retrieved. The ShapeCam also captures texture information, which is used to determine the 3D location of the landmarks on the skin surface reconstruction. Indeed, before taking 3D images, the 52 landmarks are marked on the face with a blue eyeliner pencil by a forensic odontologist. The coordinates of these blue points are extracted by simple image processing.

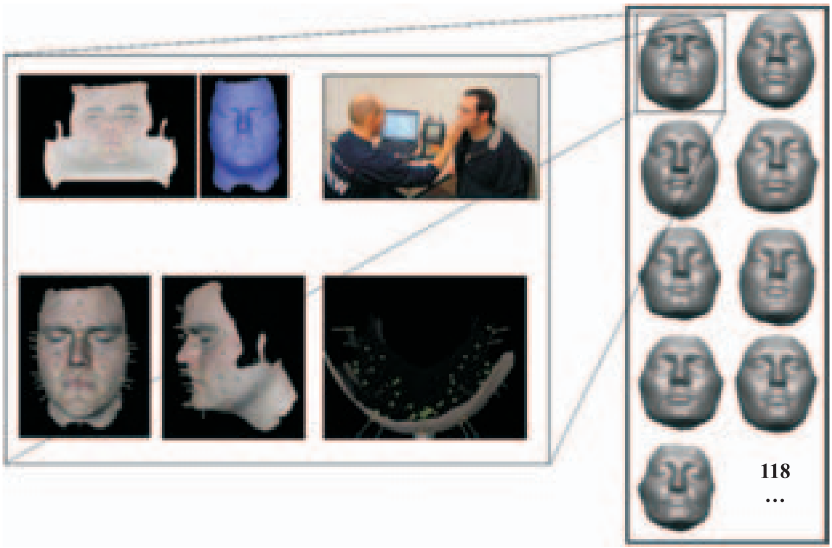

Fig. 1: High level overview of the 3D facial surface and tissue-depth acquisition of an individual in the database. 2D texture and 3D shape are combined with tissue depth measurements. Skull landmarks (green spheres) are created by setting out the corresponding depths along the normal on the skin surface in the skin landmark.

To measure the soft tissue depths a mobile semi-automated ultrasound system enabling in vivo, fast and non-destructive measurements at the 52 anatomical landmarks was constructed. The system is composed of a compact and lightweight mobile digital ultrasound "A-mode" scanner (Epoch 4B with a 10MHz 0.6mm∅ transducer, Panametrics Inc., Waltham, USA), a database (MySQL) and a self-designed interface program. Further details and validation of the system can be found in [16].

The current database consists of 118 facial entries. All individuals are from the Caucasoid race consisting of 48 female and 70 male subjects. Other distributions related to Age and weight-length ratio are plotted in figure 2. We must state that the current database is relatively limited, so that it is important to add extra flexibility to the statistical model constructed from this database.

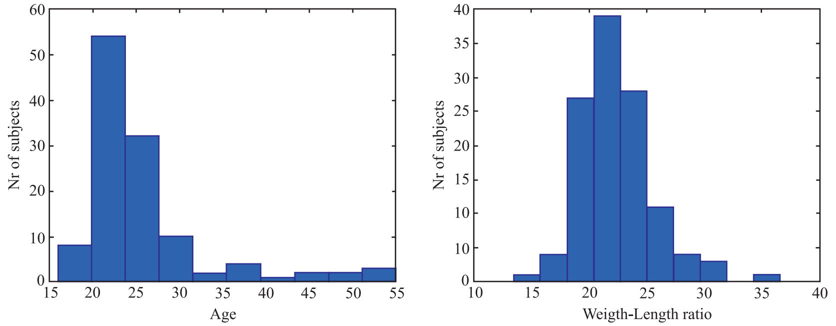

Fig. 2: Age (left) and weight-length ratio (right) distribution of the database

3 Combined statistical deformable model

Statistical deformable models in literature are also known as Active Shape Models (ASM). In [17] a 2D facial ASM is build for image segmentation and in [18] a 3D ASM of facial surfaces is used for the synthesis of 3D faces from 2D images. We construct a combined facial surface and tissue-thickness statistical deformable model, from the acquired database, consisting of a set of densely sampled point representations of the 3D skin surfaces and their corresponding soft-tissue depth measurements at the 52 anatomical landmarks. This is obtained by principal component analysis (PCA) of the inter-subject point correspondences, which leads to a relatively small number of modes describing the principal components of variation within a sample database. The result of the PCA is a geometrically averaged facial template, which is calculated together with a correlation-ranked set of modes of principal variations that capture the major changes between different facial outlooks and their corresponding soft tissue thickness measurements. In order to calculate the combined PCA of skin surfaces and depth measurements, dense point correspondences between skin surfaces and corresponding skull landmarks need to be established. Skull landmarks are constructed by setting out the depth measurement starting from the landmarks on the skin surface perpendicular to the skin surface and are therefore the representation of the tissue depths of a facial entry.

Inter-subject correspondences between landmarks on the skin surfaces are automatically calculated using a non-linear robust point matching procedure [19, 20]. Skull landmark correspondences are then inferred implicitly from these correspondences. The correspondences between the landmarks on the skin surfaces are also used to align the facial entries of the database into one coordinate frame and to automatically label the landmarks so that the correct depth measurement per landmark can be retrieved from the MySQL database. Alignment of the facial data is necessary to exclude extrinsic variations, like pose differences of the person during acquisition of the skin surface and depth measurements e. g.

Dense correspondences of the other, non-landmark, points on the skin surfaces are initialized by TPS interpolation of the inter-subject landmark correspondences and refined using geodesic surface matching based on a combined Euclidean distance and local curvature similarity. By first deforming a reference face to a facial entry, based on a TPS deformation field, calculated from the inter-subject landmark correspondences, the reference face better resembles the facial entry and dense non-landmark correspondences are found as a kind of extrapolation of the landmark correspondences. The deformed reference face resembles the facial entry, but is not equal to it, so an extra refinement step for finding dense non-landmark correspondences is necessary. This is obtained by geodesic surface matching [21]. Corresponding points are points connected through a minimal cost path (geodesic path), going from the reference face to the facial entry, on the 4D cost surface, where the cost is determined based on Euclidian distance and local curvature similarity between the end points of the path.

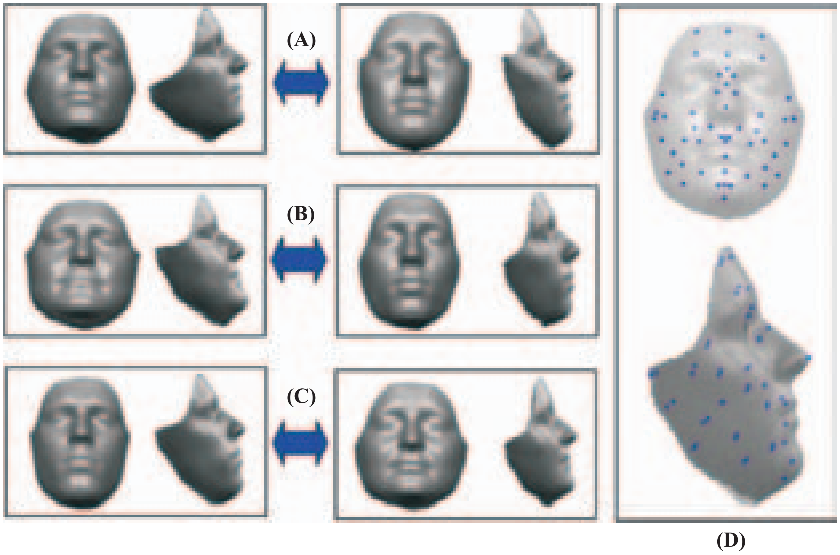

Fig. 3: Visualization of the first three modes of variation, (A) first mode, (B) second mode and (C) third mode. (D) The geometrically average face of the database, where the blue points are the average skull landmarks and nose tip.

A combined statistical deformable model is constructed from the current database consisting of 118 facial samples based on the inter-subject correspondences. In figure 3 the geometrically average face and the effects of the first three modes of variation at –/+ three standard deviations are shown. The first mode models the facial differences between compressed and elongated faces along an axis going from the front to the back of the face. The second mode of variation seems to be characterized by the same variation as the first mode but along the vertical axis of the frontal view (taller and shorter). The third mode also seems to be characterized by the same variation as the two previous ones but along a horizontal axis of the face (thinner and wider faces). A total of 117 modes of variation can be retrieved from a database consisting of 118 entries. Three important points should be kept in mind when viewing these examples in figure 3. First of all, the shape of these modes of variation is entirely dependent on the 118 facial samples in the database. Secondly, the first mode is characterized by the largest degree of variation (freedom) in the sample database, the second mode by the next larger degree of variation in the data that is uncorrelated with the first mode, and so on. And finally, the variations in the sample data characterized by each mode are statistically uncorrelated.

Every facial entry in the database can be parameterized as a function of the statistical model. Instead of using a vector description of densely sampled points and skull landmarks, the facial entry can be modelled as well as the sum of the geometrically averaged face and a weighted linear combination of the modes of principal variation. The parameters describing the facial entry are the weights in the linear combination. By altering the parameters, in between statistically determined boundaries, new valid faces, lying within the statistical boundaries of the model, can be generated based on the average face and a linear combination of face-specific deformations modelled by the modes of variation. This is the key point of using a statistical model in the facial reconstruction process.

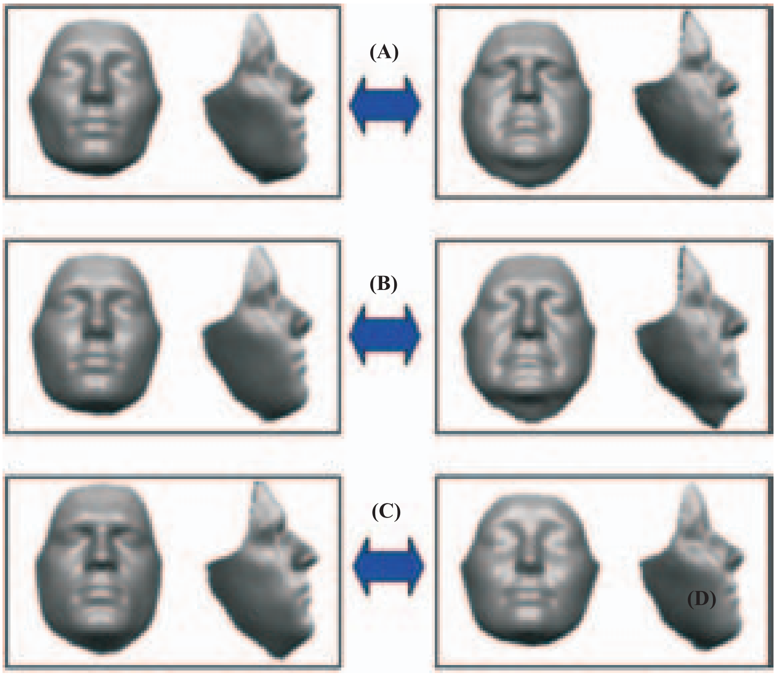

Fig. 4: Attribute related deformations applied on the average face, (A) low and high weight-length ratio, (B) younger and older, (C) more male and more female.

Another interesting point of using a statistical model is the ability to determine the facial deformations originating from differences in attributes like age, weight-length ratio, gender and race in the database and apply them to the final reconstruction. By labeling the facial entries according to their attributes and mapping them to the parameter space of the statistical deformable model, we are able to manipulate a specific attribute of a face while keeping all the other attributes as constant as possible. The mapping consists in finding the linear combination of modes of variation that describe the change in attribute. Fig. 4 shows those attribute related deformations applied on the average face in figure 3.

4 Model fitting procedure

The first step in the facial reconstruction process is digitising the skull, which can be done by scanning the skull with a CT scanner. A forensic odontologist estimates the gender, age, weight-length ratio and race of the skull as good as possible and indicates, currently manually, the 52 anatomical skull landmarks on the skull together with an estimate of the nose tip according to [22].

The combined statistical model obtained in the previous section can be considered as an elastic mask with elastic dowels at particular locations on the inside of the mask. The modes of elastic deformation are the modes of variation while the elasticity of each mode is determined within statistical boundaries and are related with the model parameters. Subsequently, this mask has to be fitted to the external surface of the individual craniofacial skeleton by finding a set of model parameters, such that all the dowels touch the skull at the corresponding indicated skull landmark locations and the estimate of the nose tip. However, a current problem is that our database only consists of 118 facial samples. Using such a limited database is insufficient to create a statistical facial model, which is capable of exactly fitting the skull landmarks of the model on the indicated skull landmarks. There is a lack of elasticity in the mask due to the limited database or limited variation in the database. In a worst-case scenario, when there is no correlation between the 52 different skull landmarks and the nose tip, 159 (53*3) degrees of freedom are needed to describe the 53 points. A statistical facial model based on 118 samples has a maximum of 117 degrees of freedom (modes of variation), which are mostly insufficient to cover the 159 degrees of freedom of the skull landmarks. Note that it may be possible to have an exact fit with a limited database, but it is unlikely.

In order to overcome a lack of elasticity in the mask one could increase the number of samples and variation in the database or allowing additional elasticity (freedom) in the mask. In [17] two approaches are given for adding extra elasticity to a statistical model.

The first approach is obtained by adding modes of vibration of a finite element model based on the samples in the database. The second approach is to introduce additional variance and covariance in the covariance matrix of the samples in the database. This is done by adding some values directly to the appropriate elements of the covariance matrix. However both methods require some notion of neighbouring points in order to guarantee extra smooth deformations, which is easily to define in 2D but less trivial in 3D. They also assume the explicit calculation of the covariance matrix of the samples in the database. This matrix can be huge and computational impractical when using densely sampled point representations of the 3D skin surfaces. Furthermore it is difficult to determine the additional needed vibration modes or values added to the covariance matrix in order to insure enough flexibility of the mask to fit the external surface of the individual craniofacial skeleton. Therefore we developed a novel approach combining the face-specific deformations with a more generic Thin-Plate-Spline (TPS) deformation based on the 52 skull landmarks and the estimate of the nose tip, resulting in a flexible enough but constraint deformation of the mask towards a given skull.

Combining face-specific variations or deformations with a more generic deformation is done with the following iterative updating scheme: We start with the average face and deform it with a TPS deformation such that the skull landmarks and the tip of the nose of the average face are mapped onto the corresponding indicated skull landmarks and tip of the nose. The remaining facial surface of the average face is also mapped through the TPS interpolation of the deformation field in between the landmarks. This is comparable with a facial reconstruction based on current computerized methods starting from a generic facial surface with that difference that we map skull points instead of estimated facial points created by setting out average thicknesses on a skull. Then we project the facial outcome of the TPS deformation back into the statistical model space by finding a set of model parameters such that the projection describes as good as possible (within model boundaries) the facial outcome. This back projection is now the starting point for a new TPS deformation. Alternation of the TPS deformation and the back projecting into the model space is iteratively done until convergence, resulting in a TPS deformed facial surface solution close to or constraint by the facial model space.

5 Experiments and results

In this section some comparative reconstruction results are shown based on a real-case skull found in Belgium. The anthropological examination estimated the age at the time of dead being 35 and the origin of the skull being from White Russia. No further details were given. The original skull during CT scanning and the digitised model of the skull are shown in figure 5. The purpose of this section is to compare our combined tissue-depth and facial surface statistical method with a manual reconstruction, a typical current computerized reconstruction and an alternative statistical method, that we developed earlier and does not incorporate tissue-thicknesses with facial surfaces.

The first reconstruction of the skull is a manual reconstruction made by the Forensic Facial Imaging department of the federal police Belgium. The landmarks definitions and tissue depth tables from [23] were used during reconstruction. The final result looks rather skinny and corps-alike, because the used tables of tissue-depths are based on corps measurements. A 3D model made with the ShapeCam from the reconstruction result is shown in figure 6. Despite the very nice results obtained by manual reconstruction methods it is difficult and time consuming to generate multiple reconstructions, other weight-length ratio, older or younger e. g.

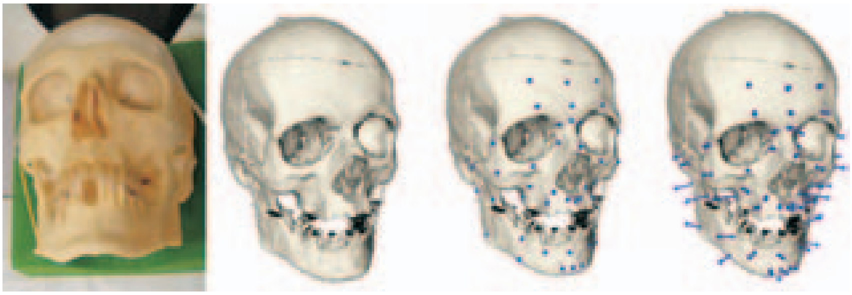

Fig. 5: The real-case skull. (A) During CT scanning, (B) Digitized model, (C) skull landmarks indicated, (D) with 52 facial surface point estimates by setting out average tissue thicknesses.

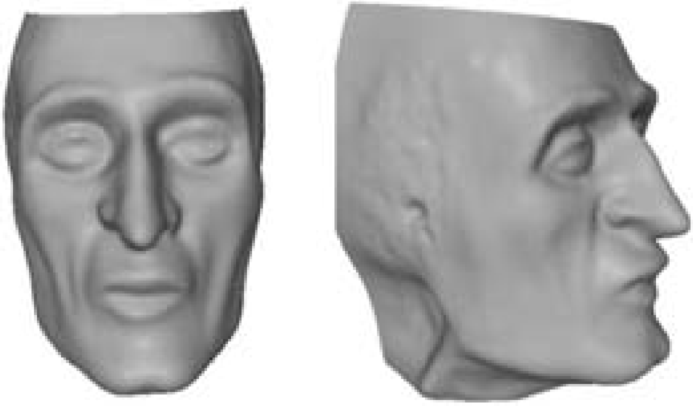

Fig. 6: ShapeCam model of the manual reconstruction made by the Forensic Facial Imaging department of the federal police Belgium.

The second reconstruction of the skull is made by a typical current computerized reconstruction method. In a first step a forensic odontologist sets out mean tissue thicknesses in the 52 skull landmarks (figure 5 (d)) defined in [16] and used in our database. An estimate of the nose tip is made according to [22]. This gives an estimate of the facial surface in 53 points or landmarks. Using the average facial surface of our database as input or generic face, the remaining skin surface shape of the skull is inferred by generic interpolation of the deformation (Spline-based) in between the 53 facial point estimates and deforming the average face accordingly. The result is shown in figure 7 together with a result generated when a different (more specific) face than the average face was used as input. As can be seen in the figure this typical reconstruction method is severely biased by the facial input surface used. The result from the average face is very smooth and contains no specific facial characteristics just like the average face itself. When using a specific face, facial characteristics of the input face remain in the final reconstruction. Furthermore local surface inconsistencies are visible in the final reconstructions in the form of small dips and bumps in the neighbourhood of the 53 facial point estimates. This originates from the fact that the 53 corresponding facial landmarks of the mean face or the specific face are too different from the estimated facial landmarks. The sharp unrealistic nose reconstruction is another example of the fact that the nose tip of the average face or the specific face differ too much from the estimated nose tip. However the TPS deformation forces the 53 corresponding facial landmarks of the input faces to map on the 53 estimated landmarks.

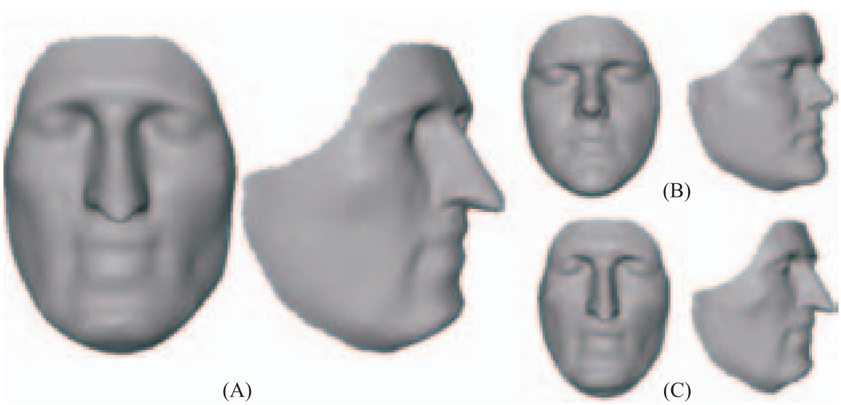

Fig. 7: Reconstruction made by a typical current computer-based technique. (A) final reconstruction starting from the average face, (B) A more specific face used as starting point for the reconstruction seen in (C).

The third reconstruction of the skull is done by using a statistical facial deformable model that models facial surfaces without incorporation of tissue-thicknesses. The same 53 facial point or landmark estimates from the previous method are used as input representation of the skull to the fitting procedure (figure 5 (d)). The fitting procedure itself is very similar to the fitting procedure described in section 5, with the differences that we use 52 facial surface point and tip of the nose estimates instead of 52 skull landmarks and the tip of the nose estimate and that the tissue thicknesses indirectly are kept fixed during fitting, because the facial surface model used is not able to change them like the combined statistical model. The result is shown in figure 8. The final reconstruction does not experience any severe bias of the average face being the starting point of the fitting procedure. Even more, we can use a different face as starting point, but we observed that the final reconstruction remains the same because of the deformable model and fitting procedure used. During the fitting procedure the back projection into the model space changes the starting face (average or another) into a face more likely to belong to the configuration of the 53 facial point estimates within the model boundaries and by making use of the face-specific deformations. As such, a more specific and correct face is generated as input for the final TPS deformation before convergence of the fitting procedure, resulting in lesser local surface inconsistencies of the final reconstruction, which is also more characteristic, but unbiased, than the result of the previous typical computerized method. However some local surface inconsistencies can remain because of a bad estimated facial landmark by making use of inconsistent average tissue thicknesses according to the skull. A small dip remains in the right cheek and left to the nose, while a small bump is visible under the left eye. The location of these dips and bump corresponds to the location of facial point estimates indicating that they are not consistent with neighbouring facial point estimates. During a manual reconstruction these wrong estimates are changed or are simply discarded.

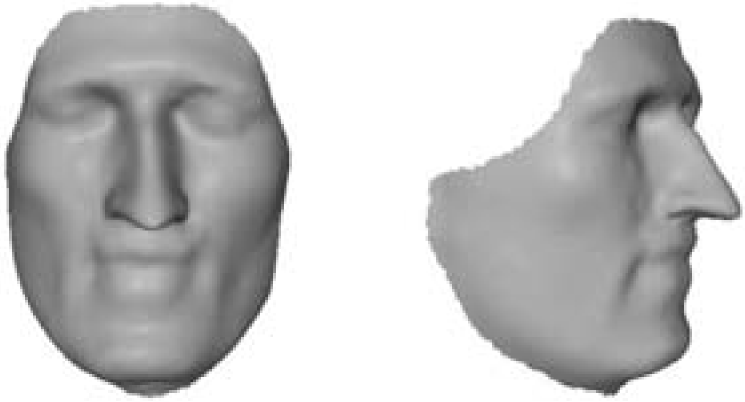

Fig. 8: The reconstruction made by using a statistical facial deformable model that models facial surfaces without incorporation of tissue-thicknesses.

The last reconstruction is made with the method described in this paper, making use of a combined facial surface and tissue thickness statistical model and 52 skull landmark indications (figure 5 (c)) in combination with an estimate of the tip of the nose. The result is depicted in figure 9. The final reconstruction resembles the reconstruction of the previous method and has the same positive properties. However no local surface inconsistencies are observed, because the combined statistical method was able to change tissue thicknesses statistically during the fitting procedure in order to produce a more consistent solution. The nose is also more realistic than all the other computer-based reconstructions. Fig. 10 shows attribute related deformations of the final reconstruction to show the ability of the method to incorporate attribute constraints like age, gender and weight-length ratio into the final reconstruction.

5 Conclusion and discussion

We proposed a combined statistical facial model, which can be used for 3D computerized forensic facial reconstructions. The difference with other models and techniques for facial reconstruction is that we maintain the direct statistical relationship between skin surface shape and tissue depth, represented as skull landmarks, for each individual and use it explicitly in a combined statistical template of skin surface shape and tissue depth. A system was developed for the acquisition of skin surfaces and associated tissue depths at 52 anatomical landmarks. This system is currently used in practise to build a database of facial samples. Based on a database of 118 faces a first statistical facial template that models population-dependent variation and correlation of skin surface shape and tissue depth was build and can be represented as an elastic mask with elastic dowels at particular locations on the inside of the mask. The elasticity of the mask and the dowels was defined as the statistically allowed variation learned from the database. This mask was subsequently fitted by an iterative fitting procedure to the external surface of the individual craniofacial skeleton and an estimate of the nose tip, using face-specific deformations in combination with a more generic deformation in order to overcome a lack in elasticity due to a limited database. Finally, constraints of age, weight-length ratio, gender and race were incorporated by determining explicitly the facial deformations originating from differences in age, weight-length ratio and gender in the database and applying them to the final reconstruction.

Fig. 9: The reconstruction made by the proposed combined facial surface and soft-tissue thicknesses statistical deformable model.

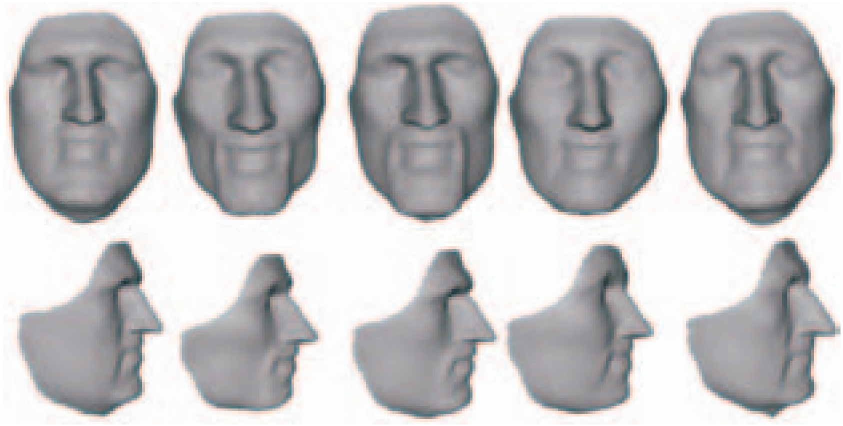

Fig. 10: Attribute changes of the final reconstruction in figure 9. (A) higher weight-length ratio, (B) lower weight-length ratio, (C) more male characteristics, (D) more female characteristics, (E) older.

We conclude from the comparisons of the reconstruction method with other reconstruction techniques on a real-case that the combined statistical modelling of facial surfaces and tissue depths can be used for 3D forensic facial reconstruction. However, two further improvements are to be made. Firstly a more expanded database is preferable such that the elasticity of the mask becomes more flexible in order to limit the contribution of the generic non-face specific TPS deformation in the final reconstruction. Secondly representing tissue depths in the combined model by converting them into skull landmarks based on the depth measurement and the skin surface normal is error prone. Especially in attribute outlier cases compared to the average face, like high age or weight-length ratio of the individual, the skin surface normal is often erroneously for using it to estimate a skull landmark, which is used as the depth representation. This is the main reason why attribute constraints are not incorporated during the fitting procedure, but applied afterwards. By not incorporating attribute constraints during the fitting procedure we reconstruct a face with attribute values comparable with the attribute values of the average face. As a result, parameters calculated during back projection into the model space lie well within the statistical boundaries and close to the average face were the skull landmarks are good representations of tissue-depths. Incorporating outlier attribute values during fitting will lead to calculated model parameters near the statistical boundaries of the model where the skull landmarks are a more erroneously representation of tissue depth. The skin surface on the other hand compared to the skull landmarks will change more correctly when changing the attributes towards outlier values, because the attribute related skin surface deformation only depends on the establishment of the dens inter-subject correspondences described in section 4, which is less erroneously. This is why we still can incorporate attribute constraints by deforming the facial surface accordingly after the fitting procedure.

Future work will concentrate on expanding the database. We will also explore alternative representations of tissue depths into the combined model, such that attribute related constraints can be incorporated into the fitting procedure, resulting in better reconstructions. Furthermore the possibility of texturing the final reconstruction will also be investigated.

References

[1] B. P. Gatliff, “Facial sculpture on the skull for identification.” *American Journal of Forensic Medicine and Pathology* 1984; vol 5(4): pp. 327–332.

[2] P. Vanezis, “Application of 3-D computer graphics for facial reconstruction and comparison with sculpting techniques.” *Forensic Science International* 1989; vol 42: pp. 69–84.

[3] P. Vanezis, M. Vanezis, G. McCombe, T. Niblet, “Facial reconstruction using 3-D computer graphics.” *Forensic Science International* 2000; vol 108: pp. 81–95.

[4] R. Evenhouse, M. Rasmussen, L. Sadler, “Computer-aided Forensic facial reconstruction.” *Journal of BioCommunication* 1992; vol 19(2): pp. 22–28.

[5] A. W. Shahrom, P. Vanezis, R. C. Chapman, A. Gonzales, C. Blenkinsop, M. L. Rossi, “Techniques in facial identification: computer-aided facial reconstruction using laser scanner and video superimposition.” *Int. J. Legal Med*. 1996; vol 108: pp. 194–200.

[6] A. J. Tyrell, M. P. Evison, A. T. Chamberlain, M. A. Green, “Forensic three-dimensional facial reconstruction: historical review and contemporary developments.” *Journal of Forensic Science* 1997; vol 42(4): pp. 653–661.

[7] G. Quatrehomme et al, “A fully three-dimensional method for facial reconstruction based on deformable models.” *Journal of Forensic Science* 1997; vol 42(4): pp. 649–652.

[8] L. A. Nelson, S. D. Michael, “The application of volume deformation to three-dimensional facial reconstruction: a comparison with previous techniques.” *Forensic Science International* 1998; vol 94: pp. 167–181.

[9] M. W. Jones, “Facial reconstruction using volumetric data.” *Proceedings of the 6th International Vision Modeling and Visualisation Conference*; 2001 Nov pp. 21–23; Stuttgart.

[10] E. R. Dumont, “Mid-facial tissue depth of white children: An aid in facial feature reconstruction.” *Journal of Forensic Science* 1986; vol 31(4): pp. 1463–1469.

[11] G. Hodson, L. S. Lieberman, P. Wright, “In vivo measurements of facial tissue thicknesses in American Caucasoid Children.” *Journal of Forensic Sciences* 1985 Oct; vol 30(4): pp. 1100–1112.

[12] W. A. Aulsebrook, P. J. Becker, M. Yasar Iscan, “Facial soft-tissue thicknesses in the adult male Zulu.” *Forensic Science International* 1996; vol 79: pp. 83–102.

[13] I. H. El-Mehallawi, E. M. Soliman, "Ultrasonic assessment of facial soft tissue thicknesses in adult Egyptians." *Forensic Science International* 2001; vol 117: pp. 99–107.

[14] M. H. Manhein, G. A. Listi, R. E. Barsley, R. Musselman, N. E. Barrow, D. H. Ubelbaker, "In vivo facial tissue depth measurements for children and adults." *Journal of Forensic Science* 2000; vol 45(1): pp. 48–60.

[15] C. M. Wilkinson, "In vivo facial tissue depth measurements for White Britsh children." *Journal of Forensic Science* 2002; vol 47(3): pp. 459–465.

[16] S. De Greef, P. Claes, W. Mollemans, D. Vandermeulen, P.Suetens, G. Willems, "Semi-automated ultrasound soft-tissue depth registration: method, validation ans preliminary results," *In proceedings RSFP 2005*, March 17–18, 2005, Remagen, Germany.

[17] T. F. Cootes and C. J. Taylor, "Statistical Models of Appearance for Computer Vision." Technical Report October 26, 2001.

[18] V. Blanz, T. Vetter, "A Morphable Model for the Synthesis of 3D Faces." *SIGGRAPH* 1999 Conference Proceedings, pp. 187–194 (1999).

[19] H. Chui, A. Rangarajan, "A New Algorithm for Non-Rigid Point Matching," *IEEE Conference on Computer Vision and Pattern Recognition* (CVPR) 2000, vol 2, pp. 44–51.

[20] H. Chui and A. Rangarajan, "A Feature Registration Framework using Mixture Models." *IEEE Workshop on Mathematical Methods in Biomedical Image Analysis* (MMBIA) 2000, pp. 190–197.

[21] E. Huot, H. Yahia, I. Cohen, I. Herlin, "Matching Structures by Computing Minimal Paths on a Manifold." INRIA, Air Project France, Universaty of Southern California, USA.

[22] K. T. Taylor, "Forensic art and illustration." New York: CRC Press, 2001.

[23] J. S. Rhine, C. E. Moore, "Tables of facial tissue thickness of American Caucasoids in forensic anthropology." Maxwell Museum Technical series 1984;1. In: Taylor KT. Forensic art and illustration. New York: CRC Press, 2001; pp. 326–359.

Statistically Motivated 3D Faces Reconstruction

C. Basso and T. Vetter

University of Basel, Computer Science Department, Swizerland

Abstract

Facial surgeons require a vast amount of knowledge about the human face, in order to decide how to reconstruct an injured or traumatized part. Does this knowledge consist only of explicit notions about face anatomy, or is there also an implicit knowledge of the normal appearance of a face? And if the answer to the latter question is affirmative, is there a way for a computer to automatically learn this implicit knowledge and exploit it to predict the optimal reconstruction of part of a face? A set of examples of human faces, acquired as 3D surfaces, can be used to build a statistical model, which can generate synthetic faces or analyze novel ones. Such a model is also able to reconstruct the missing part of a face in a statistically meaningful way: any face which can be generated by such a model has a certain probability, and the optimal reconstruction can be defined as the one which maximizes it, given the available data. However, since the model is built from a finite set of examples, it cannot generate any possible face, and therefore the purely statistical reconstruction will not perfectly fit the available data, leading to discontinuities at the boundary between the missing and the available data. In order to avoid this, we look for the surface that explicitly satisfies the continuity constraints at the boundary, and at the same time approximates the first derivatives of the statistical prediction. This leads to a partial differential equation, which can be solved numerically as a linear system. As an example, we show how this method performs reconstructing the noses of a set of test faces.

1 Introduction

We define the problem of surface reconstruction as the one of estimating the optimal shape of a three-dimensional surface's region, which for some reason is not considered trustworthy, or is altogether missing. In Computer Graphics, this problem often arises in the context of post-processing three-dimensional surfaces acquired with range scanning devices, in order to remove artifacts due to errors or limitations of the acquisition process. However, the problem has a more general application scope than just post-processing raw acquisition data, and is especially interesting for medical applications, e. g. to reconstruct the shape of a traumatized region.

The optimality of a given reconstruction is set by two requirements:

- Continuity (or smoothness) at the boundaries of the reconstruction;
- Minimal distance from the true surface (known as reconstruction error).

Variational approaches typically satisfy the first requirement: the optimal reconstruction is defined as the one which satisfies the given boundary conditions and minimizes a certain functional (e. g. membrane or thin-plate energy) of the surface over the invalid region. With respect to the second requirement, these methods work well if the energy to be minimized captures some of the properties of the surface, for example when modeling a surface resulting from a well-understood physical phenomenon. But in case we want to reconstruct something with a more complex structure, like the nose of a face, a variational approach, by itself, is not sufficient, as shown in fig.1(a,b).

The minimization of the reconstruction error, on the other hand, is the explicit goal of statistical reconstruction methods. In the case of faces, since the surface belongs to a specific

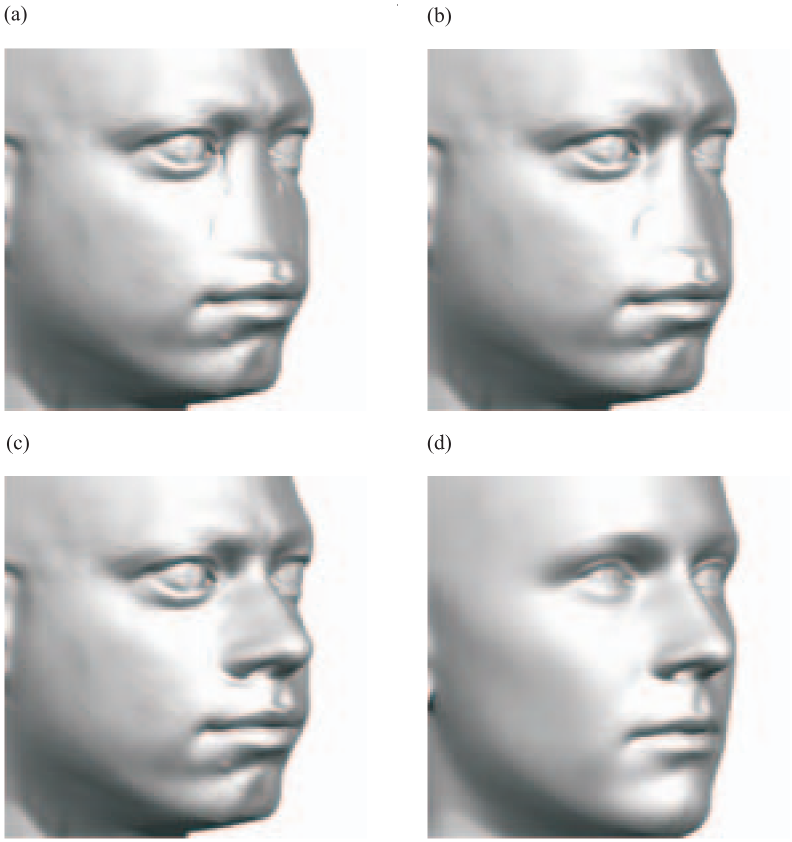

Fig. 1: Examples of variational reconstruction applied to the nose. (a)-(b) Reconstructions obtained by minimization of the membrane and the thin-plate energy, respectively. Note that the former results in continuity, while the latter in smoothness at the boundaries. In both cases the shape of the nose is not recovered. (c) Result of a Poisson reconstruction using (d) as a guidance surface.

class of objects, we can build an example-based statistical model in order to infer a realistic nose from the known portion of the face. The disadvantage of this approach is that it works globally, reconstructing a full face that is generally different from the input. Trying to cut the nose from the reconstruction and paste it into the input face will result in discontinuities at the boundaries.

To summarize, each of the two approaches satisfies one of the two requirements: our goal is to combine them into a method that satisfies both. As we will see, the statistical reconstruction can be further refined solving a variational problem, so that it also achieves continuity at the boundaries.

1.1 Previous Works

We formalize the problem by explicitly defining the three-dimensional surface as a function from a parameterization domain S to R^3, where S is a closed subset of R^2. Part of this surface is invalid or unknown, and we denote by $\Omega \subset S$ the corresponding of the parameterization domain. The subset of S outside Ω is denoted by $\partial\Omega$, and on this subset the surface is known. We denote by f^* the valid surface defined only on $\partial\Omega$, and by f the unknown, full surface defined on the whole S. The problem consists in finding the function f satisfying the two requirements mentioned in the previous section: (1) continuity, which we can write as $f|_{\partial\Omega} = f^*$, and (2) minimal reconstruction error. However, we will first consider a class of methods that address the problem by minimizing various kinds of surface energies rather than the reconstruction error.

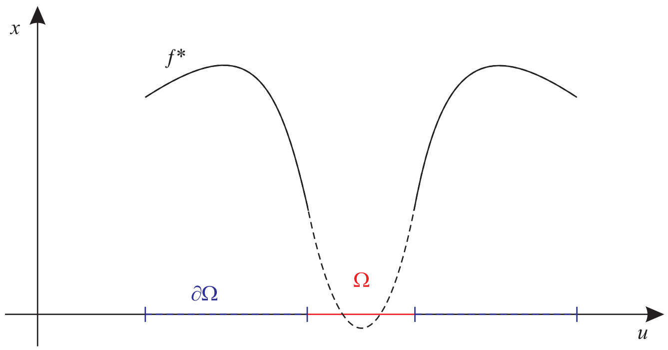

Fig. 2: A schematic representation of the continuous formulation for a one-dimensional surface embedded in R^2. We denote by $\partial\Omega$ not just the boundaries of Ω, but also the whole subset of S that is outside $\partial\Omega$, so that $S = \Omega \cup \partial\Omega$. The solid line is the known part of the surface f^*, while the dashed line is the unknown part which has to be reconstructed.

Variational methods define the optimal f as the one minimizing a given functional as well as satisfying the boundary constraints. Typical choices for the functional of the surface are the membrane and the thin-plate energy, and depending on the choice more strict constraints can be imposed on the boundary, requiring for instance C^1-continuity (smoothness). The variational problem is transformed to a partial differential equation (PDE), which is discretized over a polygonal mesh and solved as a sparse (typically non-symmetric) linear system. Examples are the methods of [1], which uses a simple discretization of the thin-plate energy, and of [2], using the Willmore energy. Both methods ensure C^1-continuity at the boundaries.

Note that the discretization of the PDE requires the topology of the polygonal mesh in Ω to be defined, which is not true if Ω corresponds to an actual hole in the data; in such a case, a necessary preprocessing step is the identification and triangulation of the hole. However, this is not necessary if the surface f has been registered against a template surface g as in [3], where the author makes use of the difference $(f-g)$ to obtain f as a deformation of g, using volume splines.

The problem of the missing topology can also be avoided by defining the surface implicitly rather than explicitly. In this case S and Ω are subset of R^3, and the surface is defined by a level set of the function f from S to R. The invalid regions have still to be identified, but since the topology of the surface is implicitly defined in f, the reconstruction of the latter yields both the shape and the topology of the surface. In [4] the authors use as f a clamped signed distance function, and define a function discriminating the valid regions from the invalid ones. The reconstruction is obtained by a diffusion of both functions in the invalid regions. A more sophisticated approach uses anisotropic diffusion ([5], an extension to surfaces of the image inpainting method presented in [6]). Also using implicit functions is the method of [7], which minimizes the L^1-norm, measured on the implicit surface, of a distance function from the valid data. The method is in fact intended for surface reconstruction, but hole filling descends as a side effect.

All the methods discussed so far do not try to explicitly minimize the reconstruction error in the invalid region; in fact, the solution depends only on a small region surrounding the hole, if not simply on its boundary. Since all other information about f is discarded, it is difficult for such a method to obtain convincing results if the invalid surface has a complex structure. Sharf et al. ([8]) propose a method that uses the valid surface to predict the structure of the invalid region: using an implicit representation for the surface, the invalid voxels are filled in a multi-resolution approach with examples extracted from the available surface. The choice depends on the context of the voxel, defined by its valid neighboring voxels. This is an interesting approach, in that it makes use of the information provided by the whole valid surface, but it would still be unable to solve the nose problem we mentioned previously.

Our method is based on [9] and [10]. The first work shows how, given a surface registered with a 3D morphable model ([11]), the reconstruction problem can be formulated in a statistical framework. As previously mentioned, since the surface is registered, the topology of the mesh in the invalid region is known even in the case of a hole. This method however does not ensure a solution continuous at the boundaries. In the second work a variational method for image editing is presented, by which the gradient of an image can be used as a guidance field for reconstructing part of another image: as a result the reconstruction has the appearance of the guiding image, but is continuous at the boundaries. This method has also been applied to polygonal meshes in [12], but only to the aim of editing the shape of the meshes, rather than to the reconstruct their surface.

We will show how the statistical reconstruction of [9] can be used as guidance in a variational problem that yields a reconstruction close to the statistical one but continuous at the boundaries. We will first describe in detail the statistical reconstruction method (section 2); then, in section 3, we will describe the variational method of [10] applied to a polygonal 3D mesh, and show how to use it for refining the results of the statistical method.

2 Statistical Reconstruction

In order to approach the problem from a statistical point of view, we assume that the surfaces we want to reconstruct belong to a specific object class (e. g. human faces, teeth, cars), which can be modeled statistically. That is, we assume there exist a parameterized class of functions f_α, where α is a vector holding the parameters of the surface, such as for any surface f of this class there is a choice of α for which $f = f_\alpha$. Moreover, not all choices of the parameters α are equally probable, but rather α follows a certain probability distribution $P(\alpha)$, which depends on the type of model used. We will use a linear model

$$f_\alpha = \sum_{i=0}^{k} \alpha_i f_i,$$

where the surfaces are a linear combination of $k+1$ registered examples f_i. By registered we mean that: (1) all the exemplar surfaces share a common parameterization domain S, and (2) that every point (u,v) of the common domain corresponds to a unique physical point in all examples (e. g. the tip of the nose). Of course, when 3D models of faces are acquired, they are not registered, and they have to be processed in order to be used for building such a linear model. We refer to [11] and [13] for methods on how to register 3D models of faces, and we will assume in the following that we have access to such a database of registered examples.

Given such a model and a partial measurement f^* of an unknown complete surface $\hat{f}$, our goal is to obtain a reconstruction f_α as close as possible to $\hat{f}$ (for the moment we will not consider the continuity at the boundaries). More precisely, we want to minimize the generalization error defined as the mean reconstruction error over the whole objects class:

$$E = \left\langle \iint \left\| f_\alpha - \hat{f} \right\|^2 \right\rangle$$

given a certain probability distribution $P(\hat{f})$ of the surfaces. Note that this equation sets the goal, but that it cannot be explicitly used for estimating the reconstruction since $\hat{f}$ is unknown; what can be done is to minimize the error over the known surface $\left\| f_\alpha|_{\partial\Omega} - f^* \right\|^2$, but it is well known that this method may lead to overfitting. In the following section we describe a statistical approach that reduces this problem.

2.1 3D Morphable Models

We will now proceed to define the linear model in discrete terms, in order to apply it to the case where the surfaces are actually described by triangular (or in general polygonal) meshes. Remember that such a mesh consists of an ordered list of vertices in R^3 connected by edges: we denote by $\mathbf{p}_i$ the i-th vertex of the mesh, and by i^* the set of indices of its neighboring vertices. In the discrete formulation we denote by S, $\Omega$and $\partial\Omega$ the sets of indices of, respectively, all the vertices of the mesh, the invalid vertices, and the valid vertices. If $i \in \partial\Omega$, the i-th vertex is valid, and we denote its known position by $\mathbf{p}_i^*$, in analogy with f^*.

If the mesh has N vertices, we can represent its full shape (the positions of all the vertices) in two different ways, which we will use depending on the context. One way is to put all vertices positions in a $3 \times N$ matrix $\mathbf{P}$, where the i-th column of $\mathbf{P}$ corresponds to the i-th vertex $\mathbf{p}_i$:

$$\mathbf{P} = (\mathbf{p}_1, \ldots, \mathbf{p}_N) \in R^{3\times N}$$

Alternatively, we can use a $3N$-dimensional vector $\mathbf{v}$, where the vertices positions are stacked one after the other:

$$\mathbf{v} = (\mathbf{p}_1^T, \ldots, \mathbf{p}_N^T)^T \in R^{3N\times 1}$$

The two forms are obviously related, and when necessary we can convert one to the other by rearranging their elements. In particular, we denote the conversion from $\mathbf{P}$ to $\mathbf{v}$ as $\mathbf{v} = vec(\mathbf{P})$, where the vec operator stacks the columns of $\mathbf{P}$ one after the other into a single column vector. The opposite conversion is denoted by $\mathbf{P} = \mathbf{v}^{(3)}$: given an n-dimensional vector $\mathbf{x}$, we denote by $\mathbf{x}^{(m)}$ the $m \times (n/m)$ matrix obtained by splitting $\mathbf{x}$ in contiguous blocks of m elements, and rearranging them in (n/m) columns.

The term 3D Morphable Model was introduced by [11] to denote a statistical linear model for 3D meshes, learned from a set of registered examples: a generic surface shape $\mathbf{v}$ is modeled as

$$\begin{aligned} \mathbf{v} &= \bar{\mathbf{v}} + \mathbf{C}\cdot\alpha + \varepsilon \\ \alpha &\propto N(0,\mathbf{I}) \\ \varepsilon &\propto N(0,\sigma^2\mathbf{I}) \end{aligned}$$

where $\bar{\mathbf{v}}$ is the mean of the model, $\mathbf{C}$ is the $3N \times k$ generative matrix, $\alpha \in R^k$ is the vector holding the coefficients of the model, and ε is a gaussian noise (this last term expresses the fact that in general our model will not be able to generate any possible shape $\mathbf{v}$). Both α and ε are normally distributed, and the model parameters $(\bar{\mathbf{v}},\mathbf{C},\sigma)$ are estimated from the set of examples (see subsection 4.1).

Assume now an incomplete vector $\mathbf{v}^*$ is given, built with the known vertices positions $\mathbf{p}_i^*$: the reconstruction problem consists of inferring, given a model defined by the parameters $(\bar{\mathbf{v}},\mathbf{C},\sigma)$, the optimal model coefficients α for $\mathbf{v}^*$, where the optimality is defined in terms of the posterior probability:

$$P(\alpha|\mathbf{v}^*) = \frac{P(\alpha)P(\alpha|\mathbf{v}^*)}{P(\mathbf{v}^*)} \propto P(\alpha)P(\mathbf{v}^*|\alpha)$$

That is, the optimal model coefficients will be the one with maximal probability, conditioned to $\mathbf{v}^*$. The two terms on the right hand side of the equation can be derived from the definition of the model. We know that the probability distribution of the model coefficients is normal with covariance equal to the identity, and therefore we have the following expression:

$\sigma^2 = 0$ $\sigma^2 = 10^{12}$ $\sigma^2 = 10^{20}$

Fig. 3: The nose is statistically reconstructed with different values of σ. Without noise the reconstruction correspond to an orthogonal projection into the subspace of the linear model; increasing the value of the noise regularizes the reconstruction until, for high values, the reconstruction is equal to the model mean. Note also the evident discontinuities at the boundary of the reconstructed region.

$$P(\alpha) = (2\pi)^{-k/2} \exp\left\{ -\frac{\|\alpha\|^2}{2} \right\}$$

The second component of the posterior probability, $P(\mathbf{v}^*|\alpha)$, is the likelihood of the observed data given the estimate, and we can derive it again from the definition of the model, taking into account the invalid dimensions by a matrix $\mathbf{L}$ which maps them to zero:

$$P(\mathbf{v}^*|\alpha) = (2\pi\sigma^2)^{-3l/2} \exp\left\{ -\frac{\|\mathbf{L}(\mathbf{v}^* - \bar{\mathbf{v}} - \mathbf{C}\cdot\alpha)\|^2}{2\sigma^2} \right\}$$

The matrix $\mathbf{L}$ is a diagonal $3N \times 3N$ matrix, with element equal to one if it correspond to the x, y or z coordinate of a known vertex, and zero otherwise. It is convenient to maximize the posterior probability $P(\alpha|\mathbf{v}^*)$ by minimizing its log-inverse. Defining the matrix $\mathbf{Q} = \mathbf{LC}$, the log-inverse is

$$E = -\log \mathrm{P}(\alpha|\mathbf{v}^*) \propto -\log \mathrm{P}(\alpha) - \log \mathrm{P}(\mathbf{v}^*|\alpha) =$$
$$= \|\alpha\|^2/2 + \|\mathbf{L}\cdot(\mathbf{v}^* - \bar{\mathbf{v}}) - \mathbf{Q}\cdot\alpha\|^2/2\sigma^2$$

The effect of the first term of E is to penalize choices of α which, according to the model, have low probabilities; the second term is a cost that depends on how well $\mathbf{v}$ fits the available data. Observe that the parameter σ is practically weighting the importance of a good fit to the data with respect to the likelihood of it: for very low values of σ, the likelihood will have no influence on the result, and the model will be very flexible; on the contrary, for very high values, the original data will have no importance and the likelihood will be maximized by setting all the model coefficients to zero.

It can be shown (see appendix A for details) that decomposing the matrix **Q** via Singular Value Decomposition (SVD) as

$$\mathbf{Q} = \mathbf{U}\,\mathbf{W}\,\mathbf{V}^T$$

the global minimum of E is given by

$$\alpha = \mathbf{V}(\mathbf{W}^2 + \sigma^2\mathbf{I})^{-1}\mathbf{W}\mathbf{U}^T\mathbf{L}(\mathbf{v}^* - \bar{\mathbf{v}})$$

A complete reconstruction of $\mathbf{v}^*$ is therefore

$$\mathbf{v} = \bar{\mathbf{v}} + \mathbf{C}\cdot\mathbf{V}(\mathbf{W}^2 + \sigma^2\mathbf{I})^{-1}\mathbf{W}\mathbf{U}^T\mathbf{L}(\mathbf{v}^* - \bar{\mathbf{v}})$$

Here again we can note how the noise parameter acts as a regularization factor, smoothly constraining the degrees of freedom of the model. If the noise of the model were null, the equation above would reduce to the familiar orthogonal projection onto the subspace spanned by the columns of **C:**

$$\mathbf{v} = \bar{\mathbf{v}} + \mathbf{C}\cdot\mathbf{Q}^+\cdot\mathbf{L}(\mathbf{v}^* - \bar{\mathbf{v}}),\ \text{with}\ \mathbf{Q}^+ = \mathbf{V}\cdot\mathbf{W}^{-1}\cdot\mathbf{U}^T$$

where $\mathbf{Q}^+$ is called the pseudoinverse of **Q**. But as the noise value increases the reconstruction gets closer to the mean of the model, as shown in fig. 3.

3 Refinement via Variational Methods

The statistical reconstruction described in the previous section is global, in the sense that provides an estimate not only for the positions of the invalid vertices, but also for the valid ones. Since in general the statistical model will not be able to achieve a perfect reconstruction of the valid vertices, the constraint $f|_{\partial\Omega} = f^*$ used throughout the introduction is not respected, and therefore the method cannot guarantee continuity at the boundaries of Ω. We will now examine a variational method by which the problem can be overcome.

3.1 Laplacian Reconstruction

As noted in the introduction, variational methods reconstruct the surface f in the invalid region Ω by minimizing a functional, and an often used one is the membrane energy, in which case the variational problem is

$$\min_f \iint_\Omega \|\nabla f\|^2 \ \text{with}\ f|_{\partial\Omega} = f^*.$$

Thinking to the surface in terms of an elastic membrane, the minimization of the integral on the left ensures a surface with minimal tension, while the conditions on the right ensure the continuity of f at the boundaries of Ω. The solution of the above problem is defined by its Euler-Lagrange equation, a PDE of simple form (a Laplace equation with Dirichlet boundary conditions):

$$\Delta f|_{\Omega} = 0 \text{ with } f|_{\partial\Omega} = f^*.$$

To solve the problem numerically we define a discrete approximation of the Laplacian operator and rewrite the above equation as a system of linear equations. With the notation introduced in the previous section, we define a discretization of Δf known in Computer Graphics as the umbrella-operator ([14], [15]):

$$U(\mathbf{p}_i) = \frac{1}{|i^*|} \sum_{j \in i^*} (\mathbf{p}_j - \mathbf{p}_i)$$

where $|i^*|$ is the valence (the number of neighbors) of $\mathbf{p}_i$. $U(\mathbf{p}_i)$ is the average of the distance vectors between $\mathbf{p}_i$ and its neighbors. By representing the shape of the mesh with the matrix $\mathbf{P}$ introduced in the previous section, the action of U on the whole mesh can be compactly represented in matrix form; the discrete approximation of the Laplacian for all the vertices of the mesh can be written as

$$U(\mathbf{P}) = \mathbf{K}\mathbf{P}^T$$

where $\mathbf{K} \in R^{N \times N}$ is a sparse matrix, with

$$(\mathbf{K})_{ii} = -1 \text{ and } (\mathbf{K})_{ij} = 1/|i^*| \forall j \in i^*$$

which depends on the connectivity of the mesh. As an example, let us consider a tetrahedron. Each vertex has three neighbors, so that $|i^*| = 3$ for any vertex, and

$$\mathbf{K} = \frac{1}{3} \begin{pmatrix} -3 & 1 & 1 & 1 \\ 1 & -3 & 1 & 1 \\ 1 & 1 & -3 & 1 \\ 1 & 1 & 1 & -3 \end{pmatrix}$$

Note that some of the rows of $\mathbf{K}$ would be typically discarded, since they operate on vertices outside Ω. Without changing the shape of the matrix $\mathbf{K}$, the same effect can be obtained defining a diagonal matrix $\mathbf{\Lambda} \in R^{N \times N}$, with elements $\lambda_i = \{0,1\}$ whose values depend on whether $i \in \Omega$ or not. Using $\mathbf{\Lambda}$ the Euler-Lagrange equation can be written in matrix form, together with the boundary conditions, as

$$(\mathbf{\Lambda} + (\mathbf{I} - \mathbf{\Lambda})\mathbf{K})\mathbf{P}^T = \mathbf{\Lambda}\mathbf{P}^{*T},$$

where $\mathbf{P}^*$ is as $\mathbf{P}$ a $3 \times N$ matrix, where the i-th column is either $\mathbf{p}_i^*$ if the i-th vertex was valid, or a zero vector otherwise. If the vertex is outside, then $\lambda_i = 1$, and its linear equation will reduce to

$$\mathbf{p}_i = \mathbf{p}_i^*$$

On the other hand, if the vertex is inside, then $\lambda_i = 0$ and the corresponding equation will be

$$\frac{1}{n} \sum_{j \in i^*} (\mathbf{p}_j - \mathbf{p}_i) = 0$$

The linear system is sparse, separable in the *x,y,z* coordinates, and efficiently solvable by LU decomposition (e. g. using the UMFPACK library, see [16]).

3.2 Poisson Reconstruction

We show in fig. 1(a) the results of solving the linear system for one of our test cases: as we would have expected the minimization of the membrane energy only cares about continuity at the boundaries. Trying to use a different functional does not improve the situation either: see the result obtained with a thin-plate energy, in fig. 1(b).

The method for image editing presented in [10] offers a simple way to improve the results: if we know something about the gradient of f in Ω, we can use this information along with the boundary conditions. Let $\mathbf{w}=(u,v)$ be an R^2 vector field, called guidance field, defined on Ω. If we modify the membrane energy to take $\mathbf{w}$ into account, the variational problem becomes

$$\min_f \iint_\Omega \|\nabla f - \mathbf{w}\|^2 \text{ with } f|_{\partial\Omega} = f^*,$$

and the Euler-Lagrange equation becomes a Poisson equation with Dirichlet boundary conditions

$$\Delta f|_\Omega = \nabla \cdot \mathbf{w} = \frac{\partial u}{\partial x} + \frac{\partial v}{\partial y} \text{ with } f|_{\partial\Omega} = f^*.$$

where $\nabla \cdot \mathbf{w}$ is the divergence of the field.

This equation can be further simplified in the case where the guidance field is itself the gradient of a known function g, and we have therefore $\nabla \cdot \mathbf{w} = \nabla \cdot \nabla g = \Delta g$. The above Poisson equation reduces again to a Laplace equation:

$$\Delta(f - g)|_\Omega = 0 \text{ with } f|_{\partial\Omega} = f^*,$$

which can be solved as shown above. It is useful to reformulate the problem by defining the displacement function $h = f - g$:

$$\Delta h|_\Omega = 0 \text{ with } h|_{\partial\Omega} = f^* - g|_{\partial\Omega},$$

(a) (b)

Fig. 4: The nose is first reconstructed statistically, shown in (a). To remove the evident discontinuities the statistical reconstruction can be used as guidance surface by the Poisson reconstruction, yielding the result in (b).

from which is evident that the reconstruction will be the sum of the function g (which provides the structure) and of h (which provides continuity at the boundary of Ω). In a discrete formulation the reconstruction will given by $\mathbf{P}$=$\mathbf{G}$+$\mathbf{H}$, where $\mathbf{H}$ is the solution to

$$(\mathbf{\Lambda} + (\mathbf{I} - \mathbf{\Lambda})\mathbf{K})\mathbf{H}^T = \mathbf{\Lambda}\mathbf{H}^{*T} \text{ with } \mathbf{H}^* = \mathbf{P}^* - \mathbf{G}.$$

Fig. 1(c) shows how the solution follows the shape of the guidance function, while at the same time respecting the boundary constraints.

As already mentioned, in [10] the method was used for image editing rather than reconstruction, since for this latter use a good guess of the guidance function g from the known surface would be needed. In our case, this can be provided by the result of the statistical reconstruction.

The combination of the two methods yields the following scheme:

- given a model defined by the parameters ($\bar{\mathbf{v}}$,$\mathbf{C}$,σ), the statistical reconstruction $\mathbf{v}$ of $\mathbf{v}^*$ is computed, as in shown in section 2.1;
- setting $\mathbf{G}$=$\mathbf{v}^{(3)}$, the solution $\mathbf{H}$ of the above sparse linear system is computed;
- the final reconstruction is given by $\mathbf{P}$=$\mathbf{v}^{(3)}$+$\mathbf{H}$

This method has all the advantages of the statistical reconstruction, while at the same time removing the discontinuities at the boundary of Ω. Moreover, results show an improvement of the performance in terms of generalization error (see section 5).

4 Technical Aspects

Before examining the results, we want to describe more in detail two technical issues:

- In section 4.1 we explain how the three parameters ($\bar{\mathbf{v}}$,$\mathbf{C}$,σ) of the model are estimated, in particular the noise level;
- In section 4.2 we examine a more general definition for a discrete Laplacian operator than the umbrella operator, and consider if it can yield any advantage.

4.1 Model Estimation

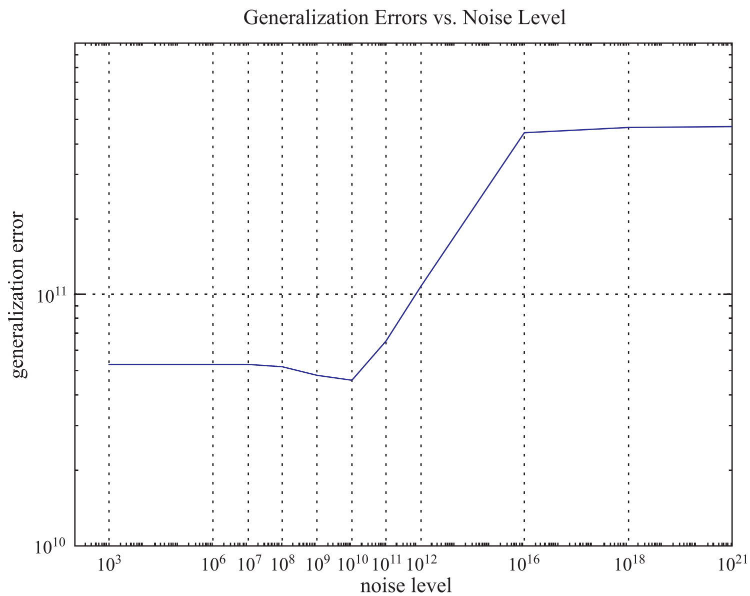

Fig. 5: Variation of the generalization error with respect to different values of the noise variance. The error is computed by 5-fold cross validation on the reconstruction of the invalid vertices, given the valid ones. The global minimum is at about 10^{10}.

The optimal model parameters are estimated from a set of training examples $\{\mathbf{v}_i|i=1\ldots m\}$, arranged into a data matrix $\mathbf{A}=(\mathbf{v}_1,\ldots,\mathbf{v}_m)$. The optimal estimate of $\bar{\mathbf{v}}$ is always the sample mean:

$$\bar{\mathbf{v}} = \frac{1}{m}\sum_i \mathbf{v}_i.$$

The other two parameters $\mathbf{C}$ and σ can be estimated from the centered data matrix

$$\tilde{\mathbf{A}} = (\mathbf{v}_1 - \bar{\mathbf{v}}, \ldots, \mathbf{v}_m - \bar{\mathbf{v}})$$

using an EM-algorithm as shown in [17] and [18]. However, in the case of $m<3N$ the estimation is simplified by the fact that the estimated value for σ will always be zero: in this particular case the matrix **C** can be estimated by Principal Component Analysis (PCA). In practice, given an SVD of the centered data matrix $\tilde{\mathbf{A}} = \mathbf{UWV}^T$, the optimal estimate of **C** is:

$$\mathbf{C} = \mathbf{UW}.$$

Our training set has $m=200$ examples, but $3N$ is of the order of 10^6, and therefore we estimated **C** as above. It must be clear however that, although the optimal estimate of the noise variance is zero, this is due to the relatively small number of training vectors with respect to their dimensionality, and not because the model can generate any possible shape. Therefore we estimated the optimal value for σ by performing a 5-fold cross-validation (see [19]) of the model with different values of σ and choosing as optimal the value for which the reconstruction error of the invalid vertices is minimal. As shown in fig. 5, the reconstruction error has a minimum when the noise variance is equal to 10^{10}, and we will use this value for the experiments detailed in section 5.

4.2 Discrete Laplacian Design

As shown in [15], there is a more general form of the umbrella operator by which the Laplacian operator can be discretized over a polygonal mesh:

$$\Delta(\mathbf{p}_i) = \sum_{j \in i^*} w_{ij}(\mathbf{p}_j - \mathbf{p}_i)$$

where the coefficients w_{ij} weight the contribution from the different neighbors to the Laplacian of each vertex, and are constrained to sum up to one for a given vertex, that is $\sum_{j \in i^*} w_{ij} = 1$. The weighting coefficients can be derived from a set of positive values $\phi_{ij} = \phi_{ji}$ defined over the edges of the mesh as

$$w_{ij} = \frac{\phi_{ij}}{\sum_{h \in j^*} \phi_{ih}}$$

It is easy to see that by setting $\phi_{ij} = 1$ for every edge we obtain the same discretization of the umbrella operator; another sensible choice is $\phi_{ij} = \left\| \mathbf{p}_i - \mathbf{p}_j \right\|^{-1}$, which weights the contribution of a given neighbor with the inverse of its distance from the vertex. Note in passing that in general **K** is not symmetric since we could have

$$\sum_{h \in i^*} \phi_{ih} = \sum_{h \in j^*} \phi_{jh}$$

even for simple choices of ϕ (like for the umbrella operator if the vertices have different valence).

The question we want to address now is the following: given that our goal is not to approximate the Laplacian of the continuous surface, but rather to minimize the generalization error, is there a better choice for the discrete Laplacian than the umbrella-operator?

In order to answer to this question it helps to note that the condition on the invalid vertices $\mathbf{KP}^T$=0 defines the global minimum of the energy

$$E = \mathbf{P} \cdot \mathbf{K} \cdot \mathbf{P}^T = \sum w_{ij} \left\| \mathbf{p}_i - \mathbf{p}_j \right\|^2,$$

which can be seen as a discrete formulation of the membrane energy in terms of edges elongations. From the above equation we can observe that the values w_{ij} determine the stiffness of each edge: edges with a low value will deform more easily than others with a higher one, since their contribution to the overall energy will also be lower.

We argue that this property can be used, by learning the values w_{ij} from the set of training examples that we used to estimate the statistical model. In fact, the most sensible choice is to set

$$\phi_{ij} = \frac{1}{\sigma_{ij}^2}$$

where σ_{ij} is the standard deviation of the edge length in our example set. We will investigate in the next section if this choice yields any improvement to the reconstruction performance.

5 Results

In order to prove the validity of our method we have to verify the following points:

- Let alone the issue of the continuity at the boundaries, does our method perform better than the statistical reconstruction alone?
- Does it perform better than a variational scheme using as guidance the mean shape $\bar{\mathbf{v}}$, rather than the statistical reconstruction?
- Does the particular choice of the discrete Laplacian operator, described in the previous section, improve the results?

We answer to these questions by comparing the generalization errors of the different reconstruction methods, not only in terms of vertex positions, but also of normals directions. The tests are carried on by 5-fold cross validation on a set of 200 examples: for each method the examples set is split in 5 groups, and each group is used in turn as test set, while the other groups are used as training set. With the training set we estimate the model parameters, apart from the noise variance, which is set to 10^{10}; then, for the examples in the test set, the vertices of the nose are reconstructed. For each method, the error on the vertices positions is computed as

$$e_p = \left(\frac{1}{200 \cdot N} \sum \|\mathbf{p}_i - \hat{\mathbf{p}}_i\|^2 \right)^{1/2},$$

while the error on the normals directions is computed as

$$e_n = \left(\frac{1}{200 \cdot N} \sum \arccos^2(\mathbf{n}_i \cdot \hat{\mathbf{n}}_i) \right)^{1/2}$$

The results are shown in the histograms of fig. 6–7. With respect to the first question, we can observe that our method improves the performance of the statistical reconstruction both in terms of positions and normals errors. It is also clear that using the mean shape as guidance for the variational method yields the worse results. However, with respect to the last question, the advantage of the operator described in section 4.2 with respect to the umbrella operator is less evident: especially for the position error, the improvement is marginal. Finally, we have to qualify the results by saying that we did these tests only on the reconstruction of the nose, and it may be that on other regions the results would be different.

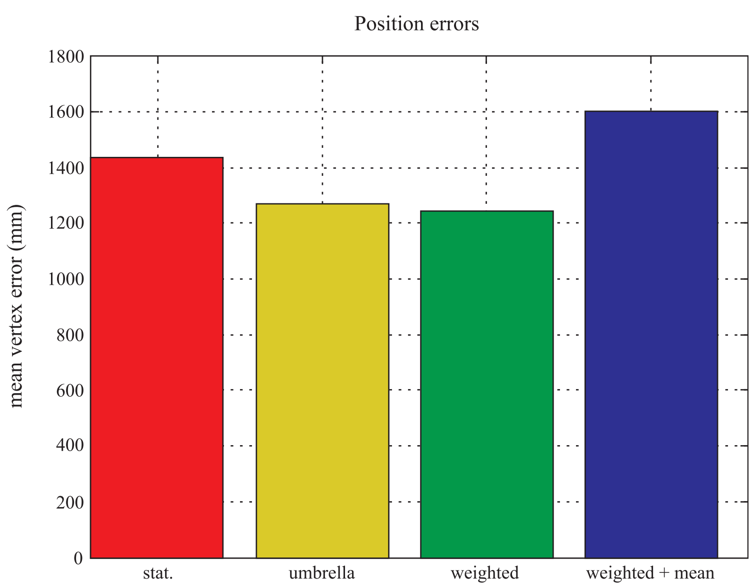

Fig. 6: Comparison of the error in generalizing the vertices positions, for the different reconstruction methods: statistical ($1.43 \cdot 10^3$), Poisson using the umbrella operator ($1.27 \cdot 10^3$), Poisson using the operator described in section 4.2 ($1.24 \cdot 10^3$), and the Poisson using the latter operator but the mean as guidance ($1.61 \cdot 10^3$).

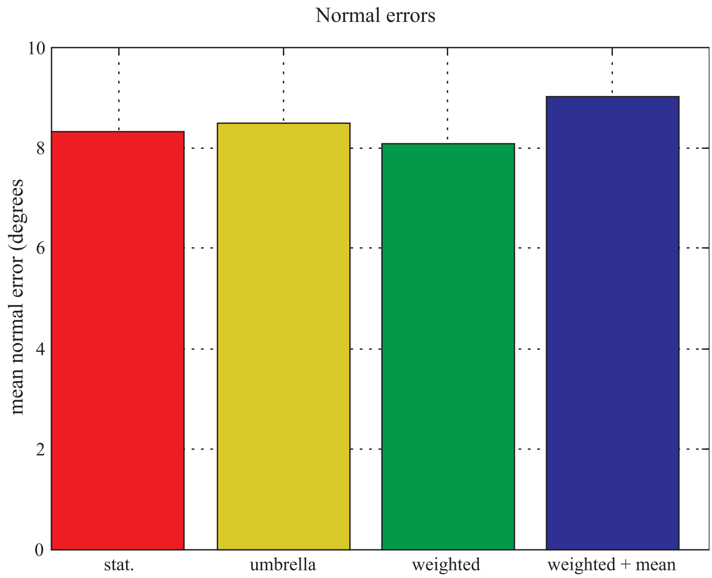

Fig. 7: Comparison of the error in generalizing the normals directions, for the different reconstruction methods: statistical (8.30 degrees), Poisson using the umbrella operator (8.44), Poisson using the operator described in section 4.2 (8.06), and the Poisson using the latter operator but the mean as guidance (9.00).

A sample of the results obtained during the tests are in fig. 8, where we selected the four examples with maximum and minimum error, both in terms of vertex positions and normal directions. Visually, the reconstructions with minimum error are very close to the original shape of the nose. The reconstructions with maximum error are in fact different from the originals; note however how they still fits very well with the overall shape of the face.

6 Conclusions

We presented a method to reconstruct invalid or missing areas of a surface by first computing an approximation via a statistical approach, and then refining it by solving a variational problem. The results satisfy the two requirements we set at the beginning: they are smooth at the boundaries and minimize the generalization error. The performance in terms of two different measures of the error between the reconstructed surface and the ground truth, prove that the method does not only remove the discontinuities from the statistical reconstruction, but also that it improves the results of the latter.

The method could be improved from two sides: first, by substituting the membrane energy with a functional that would yield a smooth solution at the boundaries (rather than only a continuous one), and second, by reducing the generalization error of the statistical reconstruction. Regarding the first point, we are currently investigating the possibility of using a guidance field in conjunction with a thin-plate energy; this should directly provide a smooth solution. With respect to the second point, we assume that choosing a subset of the known vertices to drive the statistical reconstruction could reduce its generalization error; in particular, it seems reasonable to select only the vertices that are highly correlated with the missing ones.

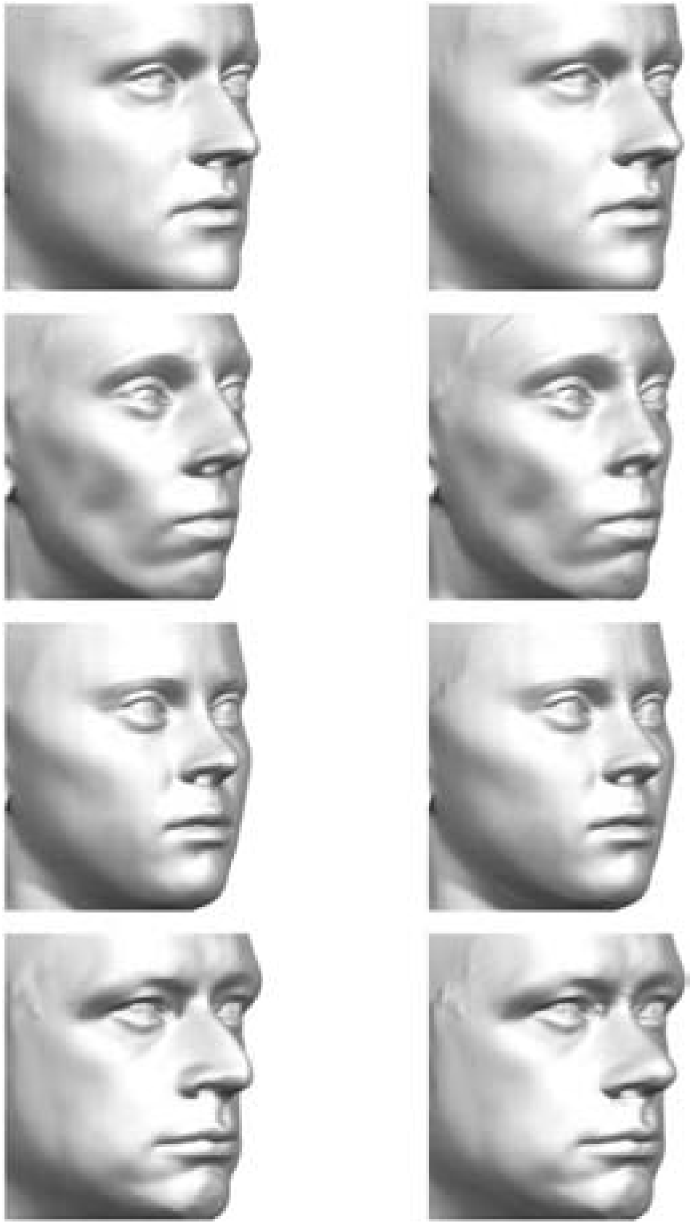

Fig. 8: Some results of the experiments: in the left column are the originals, in the right column the reconstructions. The first two rows shows the examples with minimum and maximum average error on the vertices positions ($6.49 \cdot 10^2$ and $2.84 \cdot 10^3$ micrometers respectively), the last two rows are the examples with minimum and maximum average error on the normals directions (5.21 and 11.3 degrees respectively).

Appendix A. Optimal PPCA reconstruction

In section 2.1 we have shown how the optimal model coefficients α given an incomplete vector $\mathbf{v}^*$ are obtained from the minimization of the following energy:

$$E = \|\alpha\|^2/2 + \|\mathbf{L} \cdot (\mathbf{v}^* - \bar{\mathbf{v}}) - \mathbf{Q} \cdot \alpha\|^2/2\sigma^2.$$

Deriving E with respect to α, we can find the global minimum as the solution of the following linear system:

$$(\mathbf{Q}^T\mathbf{Q} + \sigma^2\mathbf{I}) \cdot \alpha = \mathbf{Q}^T \cdot \mathbf{L}(\mathbf{v}^* - \bar{\mathbf{v}}),$$

Let $\mathbf{Q}=\mathbf{XWV}^T$ be the singular value decomposition of the matrix $\mathbf{Q}$, where W is a diagonal matrix. The equation above can be then rewritten as

$$(\mathbf{VWX}^T\mathbf{XWV}^T + \sigma^2\mathbf{I}) \cdot \alpha = \mathbf{VWX}^T \cdot \mathbf{L}(\mathbf{v}^* - \bar{\mathbf{v}})$$

Remembering that $\mathbf{X}^T\mathbf{X}=\mathbf{I}$ and $\mathbf{V}^T\mathbf{V}=\mathbf{VV}^T=\mathbf{I}$, we can manipulate the equation further:

$$(\mathbf{VW}^2\mathbf{V}^T + \sigma^2\mathbf{VV}^T) \cdot \alpha = \mathbf{VWX}^T \cdot \mathbf{L}(\mathbf{v}^* - \bar{\mathbf{v}}),$$

and finally:

$$\mathbf{V}(\mathbf{W}^2 + \sigma^2\mathbf{I})\mathbf{V}^T \cdot \alpha = \mathbf{VWX}^T \cdot \mathbf{L}(\mathbf{v}^* - \bar{\mathbf{v}}).$$

The matrix on the left hand side can be inverted and brought to the right hand side, yielding the equation for the optimal coefficients α:

$$\alpha = \mathbf{V}(\mathbf{W}^2 + \sigma^2\mathbf{I})^{-1}\mathbf{WX}^T \cdot \mathbf{L}(\mathbf{v}^* - \bar{\mathbf{v}})$$

References

[1] P. Liepa, "Filling holes in meshes", in *Symposium on Geometry Processing*, 2003, pp. 200–205.

[2] U. Clarenz, U. Diewald, G. Dziuk, M. Rumpf, and R. Rusu, "A finite element method for surface restoration with smooth boundary conditions", *Computer Aided Geometric Design*, vol. 21, pp. 427–445, May 2004.

[3] V. Savchenko and N. Kojekine, "An approach to blend surfaces", in *Proceedings of CGI'2002 Conference, Advances in Modeling, Animation and Rendering*, 2002, pp. 139–150.

[4] J. Davis, S. R. Marschner, M. Garr, and M. Levoy, "Filling holes in complex surfaces using volumetric diffusion", in *Proceedings of the 1st International Symposium on 3D Data Processing Visualization and Transmission (3DPVT-02)*, 2002, pp. 428–438.

[5] J. Verdera, V. Caselles, M. Bertalmio, and G. Sapiro, "Inpainting surface holes", in *Proceedings of the IEEE International Conference on Image Processing (ICIP 2003)*, 2003.

[6] M. Bertalmio, G. Sapiro, V. Caselles, and C. Ballester, "Image inpainting", in *Proceedings of SIGGRAPH'00*, 2000.

[7] H.-K. Zhao, S. Osher, and R. Fedkiw, "Fast surface reconstruction using the level set method", in *Proceedings of the IEEE Workshop on Variational and Level Set Methods (VLSM'01)*, 2001.

[8] A. Sharf, M. Alexa, and D. Cohen-Or, "Context-based surface completion", in *Proceedings of SIGGRAPH'04*, 2004.

[9] V. Blanz, A. Mehl, T. Vetter, and H. P. Seidel, "A statistical method for robust 3 d surface reconstruction from sparse data", in *Int. Symp. on 3D Data Processing, Visualization and Transmission*, Thessaloniki, Greece, 2004.

[10] P. Perez, M. Gangnet, and A. Blake, "Poisson image editing", in *Proceedings of SIGGRAPH'03*, 2003.

[11] V. Blanz and T. Vetter, "A morphable model for the synthesis of 3 d faces", in *Proceedings of SIGGRAPH'99*, 1999, pp. 187–194.

[12] Y. Yu et al., "Mesh editing with Poisson-based gradient field manipulation", in *Proceedings of SIGGRAPH'04*, 2004.

[13] C. Basso, T. Vetter, and V. Blanz, "Regularized 3D Morphable Models", in *Proceedings of the 1st IEEE International Workshop on Higher-Level Knowledge in 3D Modeling and Motion Analysis (HLK2003)*, 2003.

[14] L. Kobbelt, S. Campagna, J. Vorsatz, and H.-P. Seidel, "Interactive multi-resolution modeling on arbitrary meshes", in *Proceedings of SIGGRAPH '98*, 1998.

[15] G. Taubin, "A signal processing approach to fair surface design", in *Proceedings of SIGGRAPH'95*, 1995.

[16] T. A. Davis, UMFPACK version 4.3, 2004, unterstrichen>http://www.cise.ufl.edu/research/sparse/umfpack/W.

[17] S. Roweis, "EM algorithms for PCA and SPCA", in *Advances in Neural Information Processing Systems (NIPS)*, 1997.

[18] M. E. Tipping and C. M. Bishop, "Probabilistic principal component analysis", *Journal of the Royal Statistical Society, Series B*, vol. 21, pp. 611–622, 1999.

[19] M. Stone, "Cross-validatory choice and assessment of statistical predictions", *Journal of the Royal Statistical Society,* vol. 36, pp. 111–147, 1974.

Statistical skull models from 3D X-ray images

M. Bérar [1], M. Desvignes [1], G. Bailly[2], & Y. Payan[3]

[1] LIS, CNRS/INPG/UJF, 961 rue de la Houille Blanche, 38402 St. Martin d'Hères
[2] ICP, CNRS/INPG/U3, 46, av. Félix Viallet – 38031 Grenoble France
[3] TIM-C, Faculté de Médecine, 38706 La Tronche France

Abstract

We present 2 statistical models of the skull and mandible built upon an elastic registration method of 3D meshes. The aim of this work is to relate degrees of freedom of skull anatomy, as static relations are of main interest for anthropology and legal medicine. Statistical models can effectively provide reconstructions together with statistical precision.

In our applications, patient-specific meshes of the skull and the mandible are high-density meshes, extracted from 3D CT scans. All our patient-specific meshes are registrated in a subject-shared reference system using our 3D-to-3D elastic matching algorithm. Registration is based upon the minimization of a distance between the high density mesh and a shared low density mesh, defined on the vertexes, in a multi resolution approach.

A Principal Component analysis is performed on the normalised registrated data to build a statistical linear model of the skull and mandible shape variation. The accuracy of the reconstruction is under the millimetre in the shape space (after rigid registration). Reconstruction errors for Scan data of tests individuals are below registration noise. To take in count the articulated aspect of the skull in our model, Kernel Principal Component Analysis is applied, extracting a non-linear parameter associated with mandible position, therefore building a statistical articulated 3D model of the skull. Another aim of this work is to relate these detailed shape models to feature points – such as cephalometric points (e. g. glabella, porion for the skull) or motion capture data of patients.

Introduction

This paper describes an approach for building shape models by adapting a static generic model to patient-specific static raw X-ray tomography. Section 1 describes how we obtain normalized patient-specific skull and mandible using a 3D-to-3D matching procedure. Section 2 explores the free dimensions of skull and mandible shape models using CT-scans from 12 subjects. Section 3 presents an articulated model based on Kernel method.

(a) (b) (c)

Fig. 1: (a) raw scan data, (b) shape reconstructed using the marching cube algorithm; (c) generic mesh obtained from the Visible Woman Project®.

1 Building normalized shapes for the skull

In order to quantify the anatomical differences between patients, we would like to construct a statistical model of the variability of the morphology of the skull. As each skull shape should share the same mesh structure with the same number of vertices, all our meshes need to be registrated in a subject-shared reference system. In our system, the triangles for a region of the skull are the same for all subjects, while the variability of the position of the vertices will reflect the anatomical characteristics of each subject. The vertex of these shared mesh can be considered as semi-landmarks, i. e. as points that do not have names but that correspond across all the cases of a data set under a reasonable model of deformation from their common mean [1]. This shared meshes were obtained by matching generic meshes of the skull and the mandible (see Fig. 1c) to several patient-specific meshes (see § 1.3 and Fig. 1b) using our 3D-to-3D matching algorithm.

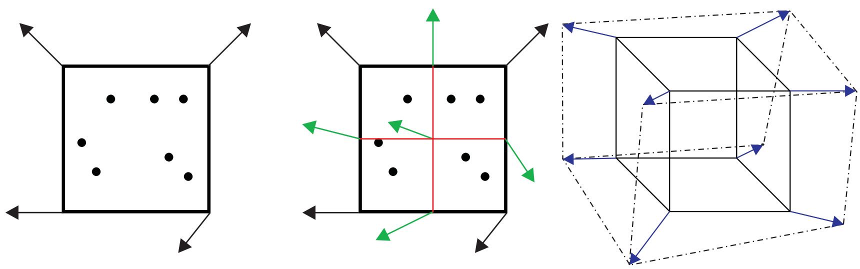

(a) (b)

Fig. 2: Applying a trilinear transformation to a cube. (a) 2D simplification of a subdivision of n elementary volume of the original space and new transformation vectors; (b) elementary 3D transformation within a cube.

1.1 3D-to-3D matching

The basic principle of the 3D-to-3D matching procedure developed by [2] consists basically of the deformation of the initial 3D space by a series of trilinear transformations *Tl* (see Wolberg 1990, for more details) applied to all vertices *qi* of elementary cubes (see also Fig. 2):

$$T_l(q_i,p) = \begin{bmatrix} p_{00} & p_{01} & & p_{07} \\ p_{10} & p_{11} & \dots & p_{17} \\ p_{20} & p_{21} & & p_{27} \end{bmatrix} . [1 \quad x_i \quad y_i \quad z_i \quad x_i y_i \quad y_i z_i \quad z_i x_i \quad x_i y_i z_i]^T \quad (Eq.\ 1)$$

The parameters *p* of each trilinear transformation *Tl* are computed iteratively using the minimization of a cost function (see Eq. 2 below). The elementary cubes are determined by iteratively subdividing the input space (see Fig. 2) in order to minimize the Euclidian distance between the 3D surfaces:

$$\min_{p}\left[\sum_{i=1;i\notin Paired(S_S,S_T)}^{card(S_S)}[d(T(t_i,p),S_S)]^2+Rw.\sum_{k\in Paired(S_S,S_T)}[d(T(t_k,p),s_k)]^2+P(p)\right] \quad \textit{(Eq. 2)}$$

where *SS* is the source surface to be adjusted to the set of points $\{ti\}$ of the target surface *ST*, *p* the parameters of the transformations *T* (6 parameters of the initial rototranslation of the reference coordinate system plus 3x8 parameters for each embedded trilinear transformation) applied to the set of points $\{si\}$ of *SS*. *P(p)* is a regularization function that guaranties the continuity of the transformations at the limits of each subdivision of the 3D space and that allows larger deformations for smaller subdivisions. The second term weighted by the factor *Rw* deals with feature points and was added for this study. *Rw* compensates for the few paired points usually available. Its value is set with a high value at the first mapping for forcing pairing. It can be then be decreased once transformed and target surfaces are close enough. In Eq. 2, the first term deals with the distance between the points and the surface (considering the projection of each point onto the deformed surface). The second term deals with point-to-point distance: a set of 3D feature points $\{tk\}$ of the target surface *ST* are identified and paired with $\{sk\}$ vertices of the source surface *SS*. The minimization is performed using the Levenberg-Marquardt algorithm [3].

1.2 Matching Symmetry

The problem of matching symmetry [4] is encountered, due to the necessary difference of density between the source and target meshes (number of vertices respectively 30 and 70 times larger in the source meshes than in the target meshes). In our case, the distance from the transformed source to the target $d(T(s_i,p),S_T)$ is very low whereas the adaptation of the target to the source may result in a much larger distance $d(T(t_i,p),S_S)$.

The problem of matching symmetry can better be observed using very different synthetic shapes. In Fig. 3, our mismatched cone is well-matched considering the first distance but is flattened on one border of the sphere. We therefore symmetrize the minimization function of (Eq. 2) as in [5] by adding a term that computes also the distance of the target mesh to the transformed source mesh using the pseudo-inverse transform T^{-1} in the following way:

$$\min_{p}\left[\sum_{i=1;i\notin Paired(S_T)}^{card(S_T)}[d(T(t_i,p),S_S)]^2+\right.$$

$$\sum_{j=1;j\notin Paired(S_S)}^{card(S_S)}\left[d\left(T^{-1}\left(t_j,p\right),S_T\right)\right]^2+Rw.$$

$$\left.\sum_{k\in Paired(S_S,S_T)}[d(T(t_k,p),s_k)]^2+P(p)\right] \quad \textit{(Eq. 3)}$$

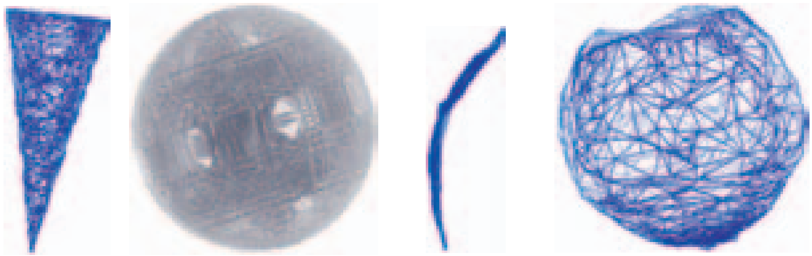

(a) source one (b) target sphere (c) standard distance (d) symmetric distance

Fig. 3: Matching a cone (a) to a sphere (b). (c) Mismatched cone using the single distance method. (d) Matched cone using the symmetric distance method.

1.3 Data collection protocol

1.3.1 Data collection

Coronal CT slices (see Fig. 1a) were collected for the partial skulls of 12 subjects (helical scan with a 1-mm pitch and slices reconstructed every 0.31 mm or 0.48 mm). The Marching Cubes algorithm [6] has been implemented to reconstruct the skull from CT slices on isosurfaces (see Fig. 1b). The mandible and the skull are separated before the beginning of the matching process, our subjects having different mandible apertures. Patient-specific meshes for the skull and jaw have around 180000 and 30000 vertices. The respective generic meshes from the Visible Woman Project have 3473 and 1100 vertices (see Fig. 1c). Our 3D-to-3D matching algorithm is used to separate normalized meshes of these organs.

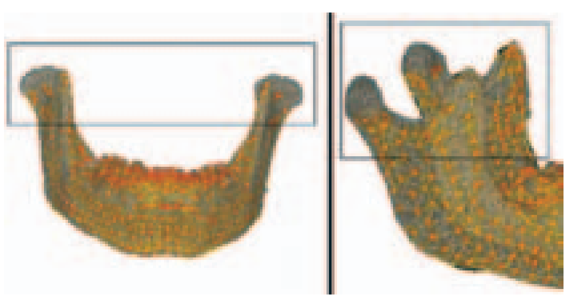

Fig. 4: Mandible Registration Projection of the transformed mesh on the original data. Except in the condylar region, each part of the mesh is well matched (red and orange less than 1 and 2 mm).

The transformed mandible is well-matched to the closest surface but the correspondence between the two surfaces is false (see Fig. 4). The "single distance" approach leads to many mismatches in the condyle and gonial angle regions: this is due to the necessary difference of density between the source and target meshes (number of vertices respectively 30 and 70 times larger in the source meshes than in the target. Part of this mismatch is due to the problem of identification of the internal vs. external surfaces from CT scans. This could be solved by exploiting more intensively surface normals if reliable. Paired feature points could also have been used but the dramatic disproportion between the number of vertices and feature points cause for instance too many problems of convergence: point-to-point pairing in this case should be replaced by the association of a target point with an entire region of the source. However this point-to-region pairing should be adapted during the matching process and often results in too many local deformations.

Using a "symmetric matching" to mandible meshes (see Fig. 5), the maximal distances are located now on the teeth and on the coronoid process. The mean distances can be considered as the registration noise, due to the difference of density (see Tab. 1).

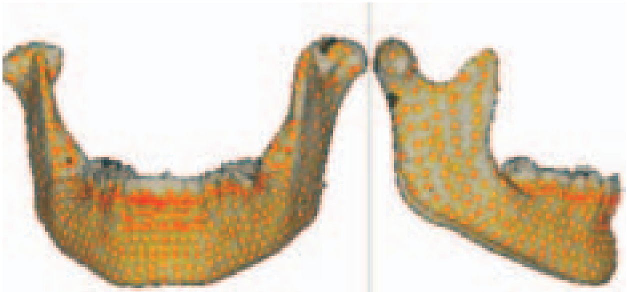

Fig. 5: Projection of the transformed mesh on the original data using the symmetric distance.

Tab. 1: Mean distances between transformed and target jaw meshes.

Distances (mm)	Generic → Scan		Scan → Generic	
	mean	max.	mean	max
Single	1.27	9.28	5.80	56.87
Symmetric	1.33	8.42	2.57	22.78

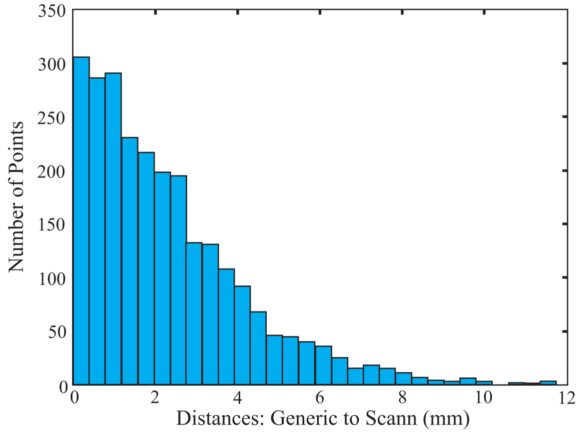

Fig. 6: Histogram of distances between points of the transform mesh to target scan surface.

1.3.2 Skull registration

Most of our subject are partial skull data. So, first a partial mesh of the skull (using cutting planes adjusted by hand) is registrated using the "symmetric matching" insuring better registration, as the partial mesh and the original data have equivalent shapes.

Then, our whole mesh is registrated to his transformed part insuring a transformation with low noise as each vertex of the transformed partial mesh has an equivalent in the whole mesh. During this step, the cranial vault is (most of the time) inferred from the border of the skull, using the continuity of the transformation and so it cannot be considered accurate.

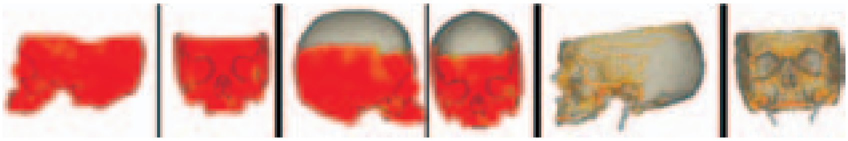

(a) (b) (c)

Fig. 7: (a) partial transformed mesh; (b) final transformed mesh with its distance to the original data; (c) projection of the transformed mesh on the original data (red less than 1 mm, orange less than 2 mm, yellow, less than 5 mm. The location of the styloid processes is emphasized.

The maximal distances found in the resulting mesh are situated in the spikes beneath the skull, where the individual variability is too high and the noise important (some spikes are only partially recovered from the scans) to be fitted even elastically. The nasal bone and the back of the skull are often matched to the internal contour (which should be corrected using normal information). At the end of the process, the mean and maximum absolute distance between the target and transformed meshes are respectively 2 and 8 mm for the jaw and 4 and 36 mm for the skull (see Fig. 6). The mean noise level at the end of the process is 5 mm. The large maximal error for the skull is due to the high variable shape (or more exactly the length) of the styloid processes (see Fig. 7). This part of the skull is too small and thin – like the anterior nasal spine and teeth – to be exactly morphed by a trilinear transformation of the space without any further surface pairing. When discarding these regions, the maximum error is less than 6mm.

2 A generic shape model for the skull

Our twelve matched skulls and jaws are fitted on mean configurations using Procrustes normalization [7]. 7 degrees of freedom due to initial location and scale are retrieved by this fit (three due to translation along three axes, three due to rotations about three axes, one for scale adjustment). Then a Principal Component analysis is performed on the normalized data to build a linear model of shape variation. The model is then compressed to a few principal modes of deformation. These principal modes of deformation represent 95% of the variance of the data and explain a large amount of shape variation.

2.1 Skull

Six principal dimensions explain over 95% of the variability of the shapes (see Tab. 2). Fig. 8 displays these dimensions. The first parameter influences variations of the volume of the skull (this should be not be considered since part of this skull is obtained by extrapolation using the T transform outside of the fitting volume) together with the advance of the lacrimal and nasal bones. The second parameter act upon the relative width of the skull and the prominence of the maxilla. The third parameter is linked to the size of the temporal bones. The fourth parameter is correlated to the height of the orbita. The fifth parameter is linked to the shape of the forehead. The sixth parameter deals with an asymmetry of the left part of the skull (temporal bone and orbita).

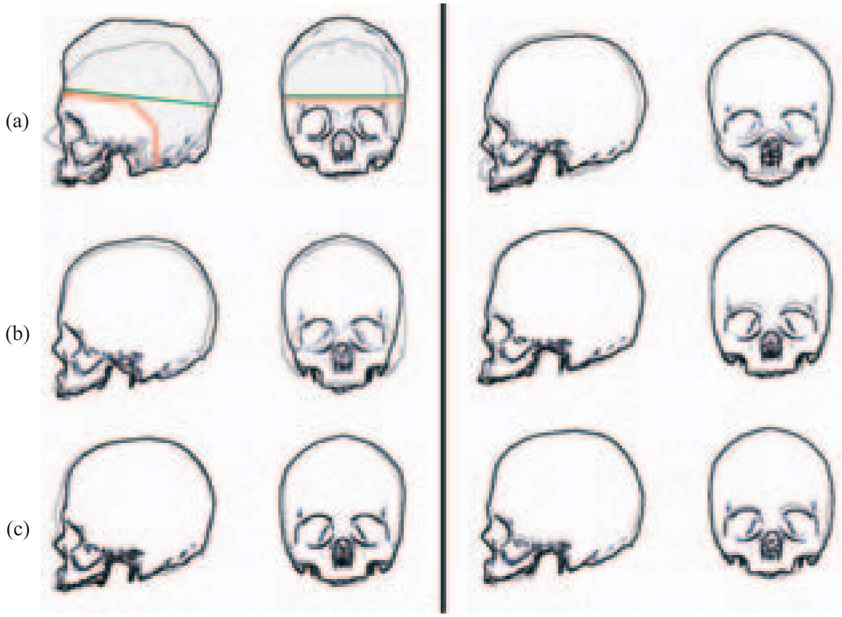

Fig. 8: Variations of the skull shape according to our six modes for parameters varying between +3 and –3 standard deviation. From left to right: (a) first two modes (b) third and fourth mode; (c) fifth and sixth mode. Maximum and minimum fitting volume (that depends on available CT scan data) is indicated on the first mode.

The accuracy of the reconstruction (see Fig. 9) is under the millimetre in the shape space (after rigid registration) even for the "worst" individual. Before Procrustes registration, the mean reconstruction accuracy is also under 1 mm but the worst individual is at 3 mm.

Tab. 2: Percentage (cumulated) of variance of the 3D skull and jaw data explained.

Factors	F1	F2	F3	F4	F5	F6	F7
Skull	46.1	19.9(66.0)	14.4(80.4)	6.2(86.6)	4.8(91.4)	3.7(95.1)	
Jaw	28.4	25.3(53.7)	14.8(68.5)	9.2(77.7)	8.0(85.7)	6.3(91.9)	4.2(96.1)
Jaw by skull factors	5.7	10.8(16.5)	19.8(36.2)	22.6(58.9)	9.5(68.4)	10.1(78.5)	

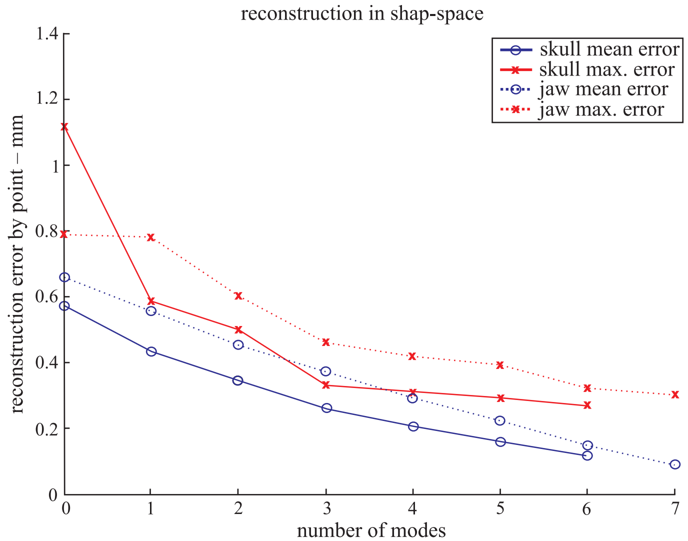

Fig. 9: Mean and max reconstruction errors of the skull and jaw using an increasing number of modes.

Scan data are processed from two test individuals not included in the training database. Mode values obtained by regression are under 3 times standard deviation (see Tab. 3) and for most of them under standard deviation. The mean accuracy of their reconstruction is 4 mm for the skull which is still less than our registration noise.

Tab. 3: mode values of two test subjects (normalized by standard deviation)

Factors	F1	F2	F3	F4	F5	F6	F7
Skull	-1.2/-0.7	0.4/-0.5	0.4/ 0.0	0.3/-3,0	0.6/-0.7	0.6/-0.3	
Mandible	0.1/ 0.4	0.3/-0.4	0.1/-0.8	0.2/-1.8	1.3/ 0.3	0.0/-0.1	0.9/-0.1

2.2 Mandible

Seven principal modes (see Tab. 2) emerge from Principal Component analysis performed on the mandible data. Fig. 10 displays these dimensions. The first parameter explains the variation of the goniac angle and size of the alveolar part while the second parameter controls the relative size of the condylar and coronoid process and correction of the goniac angle.

(a) (b) (c)

Fig. 10: Variations of the mandible shape according to our six modes for parameters varying between +3 and –3 standards deviation.

2.3 Co-dependency of mandible and skull

If regression analysis is performed on our mandible data using the shape coefficient found for their skull counterparts, up to 78 % of the variability of the shape of our mandibles is explained (see Tab. 2). The parameters with strong influences are the third and first skull parameters, which are responsible for the relative width of the skull and the shape and size of the maxilla.

3 A generic articulated model for the skull

In order to separate anatomy from control, we would like to estimate the position of the mandible independently from its shape. This would take in count the articulated aspect of our model. The position of the jaw is a non-linear parameter, so we choose to apply Kernel Principal Component Analysis (KPCA) to separate the position of the jaw from its shape.

3.1 Mandible Movement

The mandible movement is a free hanging movement, restricted by the structure of the muscles, the ligaments, the bone and the morphology of the teeth. In both speech and mastication, jaw motion involves a combination of rotation and translation, which can be described by only four degree of freedom [7] (sagittal plane orientation, horizontal position, vertical position, and coronal plane orientation). During jaw opening, the jaw rotates downward and translates both forward and downward. During closing, the pattern is reversed. Significant lateral movements are observed, primarily in jaw closing movements during mastication. As it can be described by four linear parameters, we hope to determine a non-linear parameter describing jaw movement reducing the degree of freedom to one non-linear parameter. As our real test data is limited, synthesis data is generated, using our linear model for anatomical variation. A simplified jaw motion is produced and this motion is composed of rotation in the midsagittal plane, horizontal translation and vertical translation, respecting the Posselt figure [9].

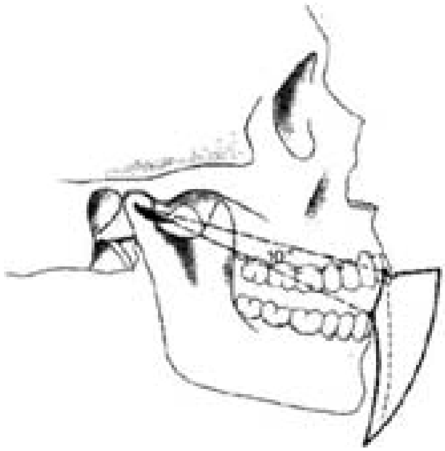

Fig. 11: Posselt figure, sagittal after [8]

3.2 Kernel Principal Component Analysis

Kernel principal component analysis [10] is a technique for non-linear feature extraction, closely related to methods applied in Support Vector Machines. It has proved useful for various applications, such as de-noising [11] and reconstruction [12]. The non-linearity is introduced via a mapping of the data from an input space **I** to a feature space Φ. Linear principal component analysis is then performed in the feature space.; this can be expressed solely in terms of dot products in the feature space. Hence, the non-linear mapping need not to be explicitly constructed, but can be specified by defining the form of the dot products in term of a Mercer Kernel function **K** on **IxI**. In the following, a Gaussian kernel function is always used.

Consider data points $\vec{x}$ and $\vec{y}$ in the input space $\mathbf{I} = R^n$

. The non-linear mapping $\Phi : R^n \rightarrow \Phi : R^n \rightarrow \Phi$ is defined such that:

$$\Phi(\vec{x}) \bullet \Phi(\vec{y}) \equiv k(\vec{x},\vec{y}) = \exp\left(-\frac{1}{2\sigma^2} \|(\vec{x}-\vec{y})\|^2\right) \forall \vec{x},\vec{y} \in R^n$$

where $\bullet$ is the vector dot product in the infinite dimensional feature space Φ, and σ is the width of the kernel. For a data set $\{\vec{x}_i$ i=1 to N$\}$, the corresponding set of mapped data points is noticed $\{\Phi_i = \Phi(\vec{x}_i)$: i =1 to N $\}$in the feature space

To perform PCA in feature space, Eigenvalues $\lambda > 0$ and Eigenvectors $V \in \Phi \setminus \mathbf{\{0\}}$ satisfying $\lambda V = \tilde{C}V$' must be found. The problem becomes in terms of dot products: solve

$$N\lambda\alpha = \tilde{K}\alpha$$

To extract non-linear principal components for the Φ-image of a test point $\vec{x}$, the projection onto the k-th component is computed by:

$$\beta_k = (V^k \bullet \tilde{\Phi}(\vec{x})) = \sum_{i=1}^{N} \alpha_i^k k(\vec{x},\vec{x}_i)$$

For feature extraction, N kernel functions have to evaluated instead of a dot product in Φ, which is expensive if Φ is high dimensional (and for Gaussian kernels infinite dimensional). To reconstruct the Φ-image of a vector $\vec{x}$ from its projections β_k onto the first n principal component in Φ "assuming that the Eigenvectors are ordered by decreasing Eigenvalue size), a projection operator P_n is defined by

$$P_n\tilde{\Phi}(\vec{x}) = \sum_{k=1}^{n} \beta_k V^k$$

3.3 Results on a real example: Finding the pre-image

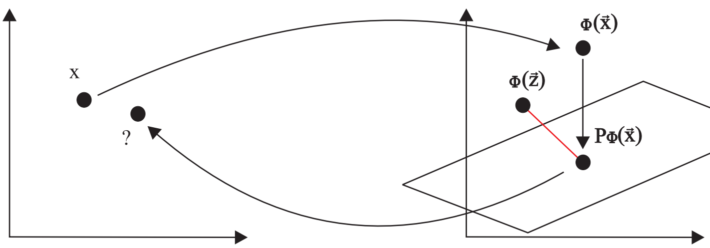

Fig. 12: The Pre-Image Problem in KPCA, extract from [13]

In our application, however, we are interested in a reconstruction in input space rather than in the feature space Φ. So, the pre-image z satisfying $\tilde{\Phi}(\vec{z}) = P_n\tilde{\Phi}(\vec{x})$, must be found but:

1. such a z will not always exist
2. if it exists, it need be not unique.

One way to achieve this is to approximated it by minimising:

$$\rho(\vec{z}) = \left\|\tilde{\Phi}(\vec{z}) - P_n\tilde{\Phi}(\vec{x})\right\|$$

This is a non linear optimisation problem, it is plagued by the problem of local minimum and is sensitive to the initial guess of z [13]. For a Gaussian kernel, this nonlinear optimisation can be solved by a fixed point iteration method:

$$\vec{z}_{t+1} = \frac{\sum_{i=1}^{N} \gamma_i k(\vec{z},\vec{x}_i)\vec{x}_i}{\sum_{i=1}^{N} \gamma_i k(\vec{z},\vec{x}_i)} \text{ with } \gamma_i = \sum_{k=1}^{n} \beta_k \alpha_i^k$$

.

In our example, one of our patient is chosen and we try to find the pre-image reconstructed from the first two parameters associated to the global scaling factor and the jaw angle.

The obtained mesh ($\vec{z}$) presents the same skull as the mean mesh of our learning database as seen in figure 9 and a jaw position similar to $\vec{x}$. With this method, all mandible positions on all our patient data are obtained and this method creates articulated and animated avatars.

3.5 Building a statistical model

A learning base of 12 synthesis data is generated with 4 different anatomies and 3 different jaw apertures. Standard deviation of the parameters in the KPCA space is associated to anatomical variations and jaw aperture regrouping data with identical anatomy. For data with the same anatomy, movement parameters must have a large standard deviation whereas anatomy parameters must have quasi-null standard deviation.

Only 7 modes are necessary to represent more than 95 % of the standard deviation in the feature space. The first three parameters are linked to skull anatomical variations whereas the next 3 parameters seems to represent the anatomical variations of the mandible. However small movements are sometimes describe by this parameter, because small movements of the same jaw can be confused with two jaws with little anatomic differences in the learning dataset.

Parameter 7 describes jaw movement, without anatomical variations. Variations of the last parameter can be observed in Fig. 13a. The movement generated by parameter 7 is close to the simplified aperture movement introduced in 3.1. This method provides separated parameters for anatomy and movement. This is also a way to represent complex spatial relations between two objects the skull and the mandible.

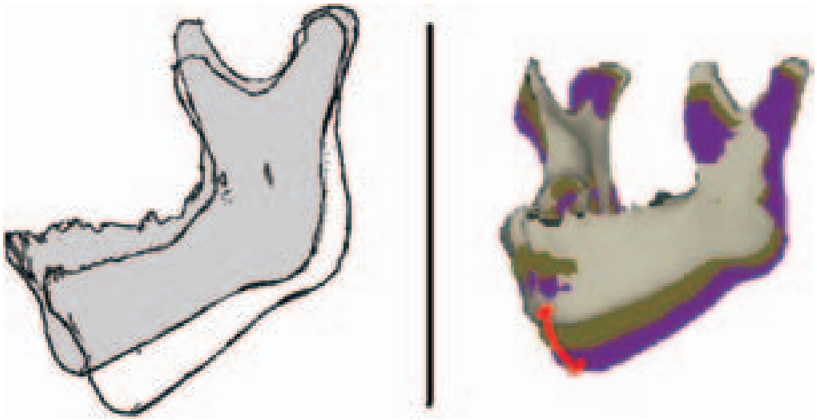

(a) (b)

Fig. 13: Variations of the mandible position according to our last parameter. (a) sagittal view (b) superposed meshes for 3,2and 0 times standard deviation.

Conclusions & Comments

In this paper, skull statistical models are build upon an enhanced matching procedure. This enhanced 3D-to-3D matching procedure has been used for regularizing and morphing a generic mesh to patient data meshes in the context of medical applications. Linear statistical models of the skull and the mandible have been defined. This model can't represent the complex movement of the jaw. Thus, a non-linear statistical method based upon Kernel PCA has been defined to represent this movement. It is applied to synthesis articulated data and it shows good qualitative results.

As this method is a convenient way to represent complex spatial relations between objects, one aim of our future work is to morph generic models of rigid and soft tissues to a target patient. We propose to build generic models of soft tissues, following the same procedure. Then to represent the relation between soft tissues and the skull using the same statistical non-linear method. Knowing the skull we will be able to reconstruct soft tissues.

References

[1] F. L Bookstein. "Landmark methods for forms without landmarks: morphometrics of group differences in outline shape." *Medical Image Analysis*, vol. 1, pp. 225–243, April 1997.

[2] B. Couteau, Y. Payan and S. Lavallée. "The Mesh-Matching algorithm: an automatic 3D mesh generator for finite element structures." *Journal of Biomechanics*, vol. 33, pp. 1005–1009, August 2000.

[3] R. Szeliski and S. Lavallée. "Matching 3-D anatomical surfaces with non-rigid deformations using octree-splines." *International Journal of Computer Vision*, vol. 18, pp. 171–186, May 1996.

[4] M. Berar, M. Desvignes, G. Bailly, Y. Payan, "3D meshes registration: application to skull model", in *Proceedings of the International Conference on Image Analysis and Recognition (ICIAR),(2),* pp 100–107, 2004.

[5] M. Moshfeghi. "Elastic Matching of Multimodality Images." *Graphical models and Processing*, vol. 53, pp. 271–282, May 1991.

[6] W. E. Lorensen and H. E. Cline. "Marching cubes: A high resolution 3D surface construction algorithm." *Computer Graphics*, vol. 21, pp. 163–169. July 1987.

[7] I. L. Dryden. and K. V. Mardia; *Statistical Shape Analysis*. London, United Kingdom, John Wiley and Sons. 1998.

[8] D. J. Ostry, E. Vatikiotis-Bateson and P. L Gribble."An Examination of the Degrees of Freedom of Human Jaw Motion in Speech and Mastication." *Journal of Speech, Language and Hearing Research*, vol. 40, pp. 1341–1351. December 1997.

[9] T. Weingärtner and R. Dillmann. "Simulation of jaw-movements for the musculoskeletal diagnoses". In *Medicine Meets Virtual Reality 5*, San Diego, Jan. 1997. IOS Press and Ohmsha.

[10] B. Schölkopf, A. Smola, and K. R. Müller. "Nonlinear component analysis as a kernel eigenvalue problem". *Neural Computation*, vol. 10, pp. 1299–1319, July 1998.

[11] S. Mika, B. Schölkopf, A. Smola, K. R. Müller, M. Scholz, and G. Rätsch. "Kernel pca and de-noising in feature spaces". In *Advances in Neural Information Processing Systems 11*, M. S. Kearns, S. A. Solla, and D. A.Cohn, editors, Cambridge, MA.: MIT Press., 1999, pp. 536–542.

[12] B. Romaniuk, M. Desvignes, M. Revenu, M.-J. Deshayes. "Shape Variability and Spatial Relationships Modeling in Statistical Pattern Recognition", *Pattern Recognition Letters*, vol. 25, pp. 239–247, (2004).

[13] J. T. Kwok and Ivor W. Tsang. "The Pre-Image Problem in Kernel Methods." in *Proceedings of the Twentieth International Conference on Machine Learning (ICML-2003)*, 2003, pp. 408–415.

Flexible Mesh Generation for Segmented 2D and 3D Images Containing Multiple Materials

G. Berti, J. G. Schmidt und J. Fingberg

NEC C&C Research Laboratories, St. Augustin, Germany

Abstract

We present a hierarchical, dimension-independent approach to mesh generation from segmented images, based on adaptive spacetree subdivision. The central algorithm is extended to generate non-uniform tetrahedral meshes or hybrid meshes containing hexahedra, pyramids, and tetrahedra. We present a volumetric marching tetrahedra algorithm permitting vertices to lie on the separating surface, enabling d-linear separating functions and vertex snapping. This algorithm is extended to multiple material, and a new separating function based on solid angles is proposed. Finally, smoothing in the presence of internal boundaries is discussed.

1 Introduction

Building a geometric representation (that is, a volume mesh) from a medical image is a necessary prerequisite for many interesting numerical analyzes like computational structural mechanics or fluid dynamics, which use finite element or finite volume algorithms [1].

A segmented (or labeled) medical image can already be regarded as such a geometric model by viewing the individual voxels as cells (elements) of a (subset of a) structured mesh. However, such a mesh gives us a fixed resolution and a non-smooth axis-aligned boundary approximation. While this is appropriate for some problems, often one needs meshes that are better adapted to the geometry, for instance by providing smooth approximations of the boundary or permitting local cell spacing in order to control resolution and problem size.

In this paper, we show how to refine the basic structured mesh represented by a multi-material segmented image into a non-uniform unstructured mesh with smooth internal and external boundaries. The algorithms are essentially dimension independent, except some parts of the marching simplices method which have to be adapted for each image dimension. The algorithms can be controlled in a flexible way, allowing one e. g. to treat different materials, interfaces or locations differently.

The meshing paradigm used in this paper we have called volume-oriented meshing, as it directly operates on a volumetric representation of the geometry, and a boundary surface approximation is created in the course of the volume meshing process. It has been used by a number of researchers in the context of medical image data, for instance [2, 3]. Similar approaches have been used at least since 1983 [4].

A competing meshing approach is surface-oriented meshing, where first a surface mesh is generated and used as a starting point for volume meshing. Well-known examples are Delaunay triangulation and the advancing front method, see [5] for an overview. We feel that in the context of geometries represented by segmented volume images, the volume-oriented approach has some advantages over the surface oriented approach. It is fast, stable, and easy to implement. It also seems to be more natural for volumetric data that do not contain an explicit and unambiguous boundary definition. The latter is found as a by-product. whereas the surface-oriented approach needs a surface mesh as starting point. However, in the volume-oriented approach, special attention has to be paid to mesh quality near the boundary.

This paper is composed as follows: In the first section, we give an overview on the work flow of the volumetric meshing approach, going from segmented images to spacetrees to non-uniform simplicial or hybrid meshes and finally to smoothed boundary approximations. Here, we introduce a generalization of the volumetric marching simplices algorithm to permit vertices lying on the separating surface, and discuss smoothing in the presence of internal boundaries. In Section 3, we present an extension of marching simplices to the case of multiple materials. Finally, we discuss the methods presented and point to further research.

2 The Volume-oriented Meshing Pipeline

The volume-oriented meshing approach operates in stages (cf. fig. 1), described briefly in the sequel. More detail can be found in [6]. We start with a segmented d-dimensional image, which has been obtained by assigning material labels to the voxels of a raw (gray-scale) image. Here, we do not consider the segmentation process itself part of the meshing. We only note that the segmented image may result in a loss of geometric precision, which may make it advantageous to use the initial raw image as additional source of information in later meshing stages, for instance for boundary approximation.

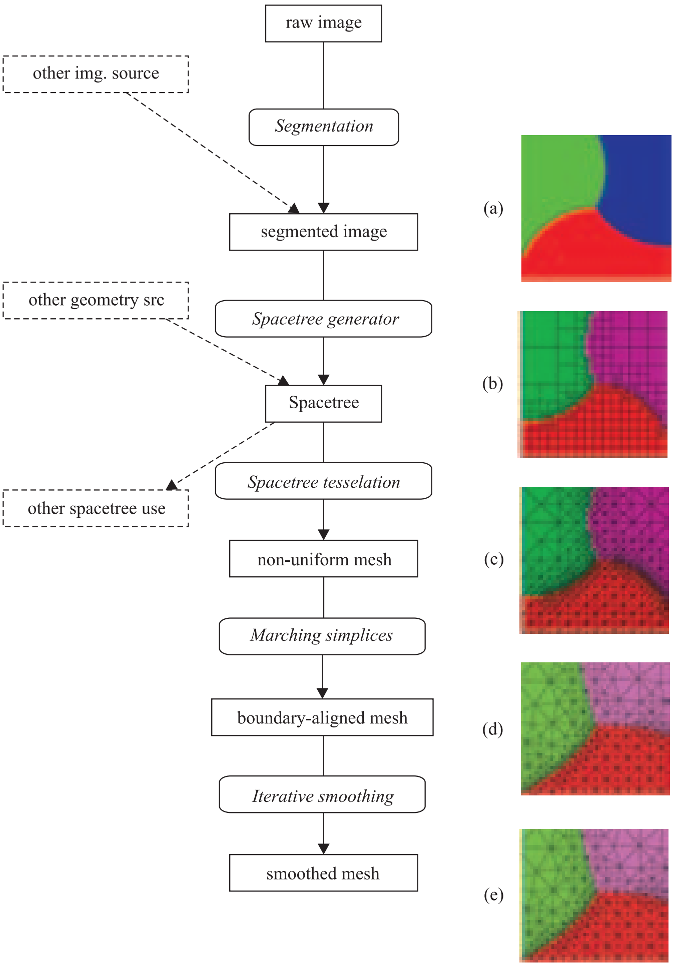

Fig. 1: The volume-oriented mesh generation pipeline. (a) The segmented image, consisting of 3 materials. (b) First a spacetree is constructed from the image. Here, each material and each interface has its own resolution. (c) Next, a non-uniform simplicial (or hybrid) mesh is generated, by using midpoint-based subdivision. Most of the uniformly sized cells in the bottom region are subdivided by a template. (d) A variant of the volumetric marching simplices algorithm is applied to obtain smoother boundaries (zoom). (e) Finally, additional iterative smoothing gives better boundaries (zoom).

Spacetree generation

The next step transforms the segmented image, which may be regarded as a Cartesian grid, into a hierarchical structure called spacetree [7] (known as quadtree in 2D and octree in 3D). We may use different refinement patterns besides the classical bisection pattern. This transformation allows to adapt mesh size locally, e. g. according to material and interfaces. The spacetree may be balanced allowing arbitrary levels of imbalance. See fig. 2 for examples.

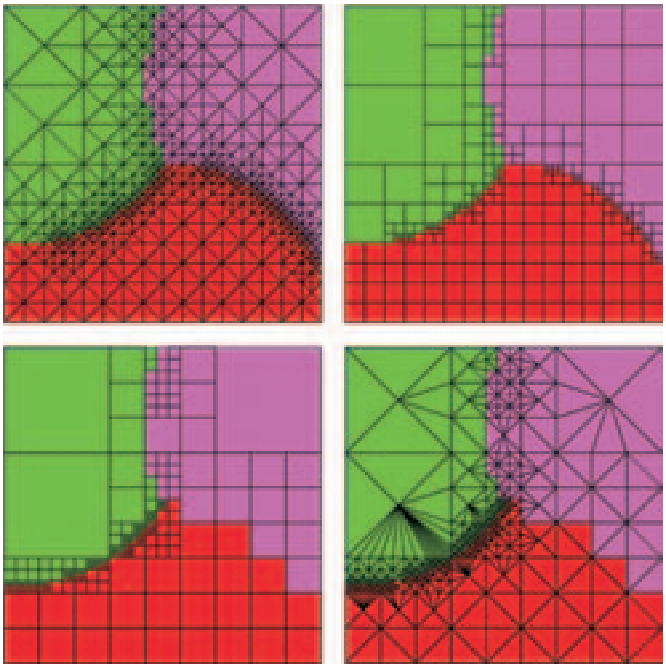

Fig. 2: Different options for spacetree generation.
(a) 2 × 2 pattern, 1 level balancing.
(b) 2 × 2 pattern, 2 levels balancing.
(c) 3 × 3 pattern, no balancing. The interfaces and materials are meshed with different resolutions.
(d) Non-uniform mesh resulting from (c). Imbalanced spacetrees result in skinny simplices.

Non-uniform conforming meshing

So far, the mesh consists of axis-aligned cubes of different sizes (fig. 1 (b)). While this may already be usable for some simulation algorithms [7], most numerical methods require conforming interfaces, i. e. without so-called hanging nodes. Therefore, we now tessellate the spacetree in order to obtain a conforming mesh, consisting either of simplices only or containing simplices, pyramids and cubes. In order to achieve a conforming tessellation into simplices, we apply a recursive midpoint-rule: First, each boundary facet of a cube is subdivided into *d -1*-dimensional simplices, and then, each boundary simplex is connected to the midpoint of the cube, creating a d-dimensional simplex. For cubes which are regular (that is, have no hanging nodes on their boundary), we use a template tessellation which produces much less simplices. See fig. 1 (c) for a 2D example and fig. 3 for a 3D example. This approach can easily extended to hybrid mesh generation, leaving regular cubes and generating pyramids as transition elements between cubes and simplices.

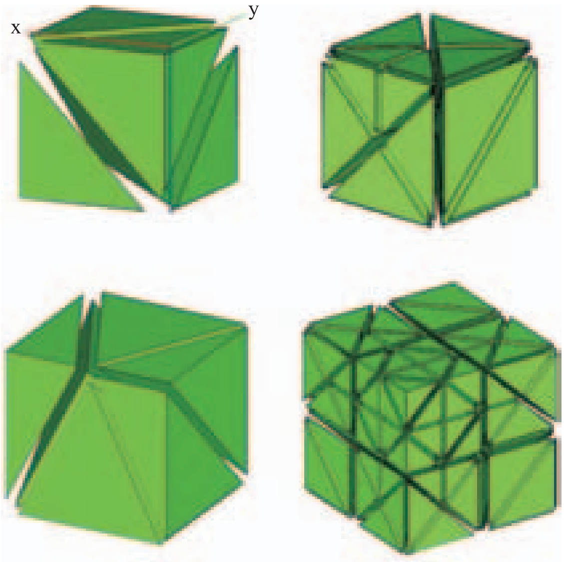

Fig. 3: The non-uniform meshing algorithm in 3D.
(a) Template subdivision of a cube (regular spacetree cell) into 5 tetrahedra.
(b) Midpoint subdivision of a non-regular spacetree cell. The left and the top facets are subdivided according to the midpoint rule, whereas the subdivision of the right facet uses a template. The rule for choosing the diagonal uses only information associated to the facet in order to guarantee a consistent triangulation of two adjacent cells.
(c) Extended template for the case in (b), which avoids the generation of additional nodes.
(d) Full 3D example.

Marching simplices

The resulting mesh is conforming, but still lacks boundary smoothness. The basic idea of marching simplices is to define a separating surface between two regions and split each simplex intersecting this surface. The problems which have to be solved are the following:

1. How to ensure a conforming triangulation after splitting?
2. How to define a smooth separating surface?
3. How to cope with vertices very close to or on the separating surface?
4. How to cope with multiple materials?

In [3], the authors present a volumetric marching tetrahedra algorithm which solves problem 1 by using a vertex ordering rule to disambiguate the splitting process.

A general approach to obtain a separating surface is to define a scalar function f on the image domain and use the zero isosurface of *f*. Probably the simplest way to define *f* is to use *d*-linear interpolation of the binary voxel values. This produces visible staircase artefacts (cf. fig. 6 left), which can be smoothed afterwards. Other possibilities are the use of the gray values in the original raw image, or some higher-order interpolation.

A problem may be vertices which are close to or even on the separating surface. For example, when using d-linear interpolation, we obtain only a finite number of different function values for f; thus, a number of vertices lie on the surface. Also, for arbitrary separating functions, it may happen that a vertex is very close to the surface, resulting in very thin simplices. In such a case, it is preferable to move ("snap") the vertex to the surface. Therefore, the simplex splitting patterns in [3] has been extended to handle the "degenerate" case of vertices lying on the surface.

Finally, the separating surface approach does not directly extend from the binary case to the multi-material case. In the following section, we present a simple iterative technique using a new separating function which can be derived from arbitrary unstructured meshes. case 1: *(1,0,3)/(3,0,1)* case 2: *(2,0,2)* case 3: *(1,1,2)/(2,1,1)* case 4: *(1,2,1)*

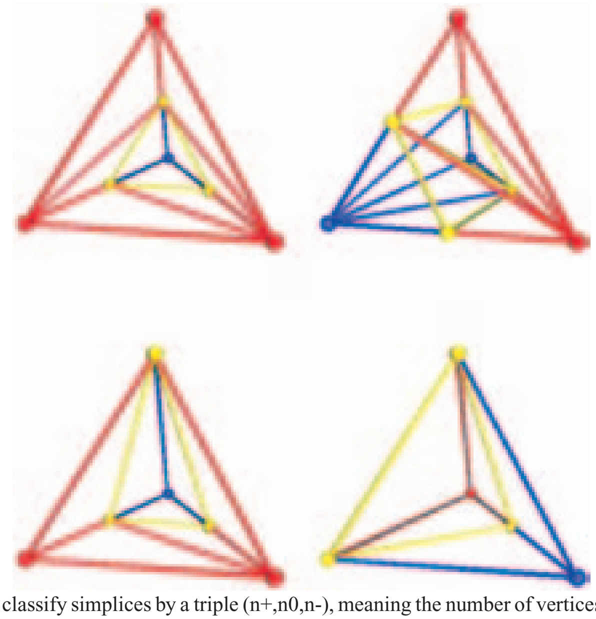

Fig. 4: We can classify simplices by a triple (n+,n0,n-), meaning the number of vertices v with $f(v) > 0$, $f(v) = 0$, and $f(v) < 0$. There are 4 essential cases for vertex signs 3D. Blue (dark gray) is positive, red (medium gray) is negative, yellow (light gray) is zero. The new triangulation edges are also shown, assuming the "smallest" vertex is always the right front one. The real intersection points are found be linear interpolation of *f* along each edge.

Mesh smoothing

Depending on the smoothness of the separating surface used, the boundaries of the mesh produced by the marching simplices algorithm still contain visible staircase artefacts stemming from the non-smooth approximation of the geometry in the underlying segmented image. These artefacts can be reduced significantly by smoothing the boundary surfaces. The basic idea here is to use Laplacian smoothing of boundary vertices. However, Laplacian smoothing will shrink a surface towards its barycenter [8]. Thus, vertex movement has to be constrained, or at least the shrinking effect has to be reduced by a clever use of parameters based on signal processing theory [8].

Smoothing the surface may have an adverse effect on the quality of incident volume element. To mitigate this effect, we first smooth the surface vertices, and then perform a volumetric Laplacian smoothing, keeping surface vertices fixed. In 3D, we first perform smoothing on material edges, that is, on vertices where 3 interior surfaces meet, then surface smoothing, and finally volume smoothing. For each stage, only neighbor vertices in the same subset (material edge, interface or interior) are considered; vertices in lower-dimension subsets (which have already been smoothed) are kept fixed (cf. fig. 5).

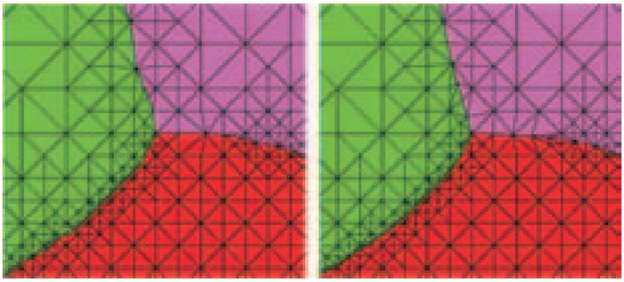

Fig. 5: Different stages of surface smoothing: (a) Only marching simplices, no iterative smoothing (b) Smoothing on material interfaces only.

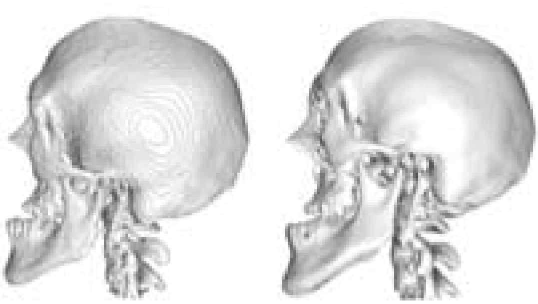

Fig. 6: Surface mesh of a human skull. Left: Result of the marching simplices with 3-linear interpolation. The staircase artefacts resulting from the binary classification are still clearly visible. Right: Same mesh after additional smoothing has been applied.

3 Multiple Materials and Solid Angles as Separating Function

The approaches presented in the preceding section to not generalize directly to the case where $n > 2$ materials are present. If we view an image as a Cartesian grid with the voxels playing the role of cells, we may classify the vertices according to the number of different materials present in the incident cells. Two-material point lie on a material surface and can be handled by the algorithms presented before. However, three-material points lie on material edges and are more difficult to deal with. A basic idea is to replace the scalar separating function f with a vector $(f_1, \ldots, f_n)$ of material inclusion ratios or probabilities summing up to 1.

Several possibilities to handle multiple materials were suggested. Nielson and Franke [9] present a simple extension of the two-material scheme [3]. They assume a labeling of the vertices with an (integer or fractional) inclusion probability. The interfaces are reported to lack smoothness, especially in irregular meshes. This may be due to the use of integer probabilities stemming from assigning vertices to materials.

Bonnell et al [10] consider material interface reconstruction in the context of computational fluid dynamics. They interpret material-inclusion ratios on vertices as barycentric coordinates in a higher-dimensional space and project the intersection with a corresponding Voronoi tessellation back to the physical space to obtain material boundaries. However, they do not treat the splitting of volume cells. Hege et al [11] extend the Marching Cubes algorithm to handle multiple materials. They assign a material-inclusion ratio vector to vertices (assumed integer for efficiency, that is, the probability fm equals 1 for some m) and use a sub-voxel Cartesian subdivision plus a detailed case analysis to subdivide each cube (voxel). Thus, their method is restricted to Cartesian grids.

None of the research cited above considers the case of separating surfaces passing through vertices.

Our basic idea for generalizing the marching simplices algorithm to multiple materials is to apply it iteratively: If we have a set of material $M = \{m_1, \ldots, m_n\}$, we first form the sets $M_1 = \{m_1\}$ and $M_2 = M \setminus M_1$, and apply the two-material algorithm. We repeat this for each material m_j instead of m_1. Thus, each material interface is visited twice. If we use the iterated approach, we have to operate on an unstructured mesh. In order to get a smooth separating function defined for the internal boundaries of an unstructured mesh partitioned into several materials, we have to assign the material inclusion probabilities for each vertex to each material.

When a vertex is surrounded by cells of a single material m, its inclusion probability $f_m(v)$ is 1 with respect to this material and 0 with respect to all other materials. When a vertex is surrounded by cells of different materials, we use the solid angle of these cells to measure the contribution of each material. We define the solid angle ratio $a_c(v)$ of a vertex v of a polytope c as the ratio S_c / S_s of the surface S_c

which the cone at that vertex cuts out on a small sphere surrounding the vertex to the surface S_s of the sphere. We have $0 \leq a_c(v) < 1$ and

$$\sum_{\text{Cells } c \text{ incident to } v} a_c(v) = 1 \tag{1}$$

for interior vertices *v*. Setting

$$f_m(v) = \sum_{\text{Cells } c \text{ with material } m \text{ incident to } v} a_c(v) \tag{2}$$

we use the iso-value $f_m = 1/2$ to separate M_1 from M_2 in the *m*th iteration.

When using the iterative approach, a problem occurs when splitting a cell which is part of the single material set M_1. In this case, one part of the split cell belongs to the multi-material set M_2, and the question arises which material should be assigned to the new cell(s) of this part. We propose a simple but sufficient approach which uses the material of the majority of cell neighbors, weighted by the corresponding facet area.

A problem with the iterated approach is its dependence on the ordering of the materials, which may lead to non-optimal results at material edges in 3D (three or more material interfaces meeting). Also, while it works quite well in 2D (cf. Fig. 1 (d) and (e)), there are some problems with material edges in 3D. Perhaps a combination of the template approach in [9] with our smoother vertex probabilities would be appropriate. However, in order to continue the special treatment of "degenerate" vertices (lying on material surfaces or even edges), a considerable number of cases would have to be treated. A complete treatment of configurations for arbitrary inclusion properties entails a large number of cases, as the maximum probability for *n* materials may change *n* times along an edge. Giving a special treatment to "degenerate" vertices (lying on material surfaces or even edges) would further increase the number of cases. Therefore, a consistent way of reducing the needed cases is preferable.

4 Conclusion

We have outlined a flexible approach for volume-oriented mesh generation, applying different independent steps in a pipelined workflow. The non-uniform meshing algorithm and the marching simplices algorithm with d-linear separating function can guarantee a minimum mesh quality [6]. Subsequent mesh smoothing allows to get smoother boundaries, yet the impact on mesh quality has to be investigated more thoroughly. The iterative extension of the volumetric marching simplices algorithm to multiple materials looks promising, but more work has to be put into the issue of material edges where three or more material interfaces meet. In the future, we will investigate additional subdivision templates for the multi-material case.

Acknowledgments

I thank my current and former colleagues at NEC C&C Research Laboratories, Jochen Fingberg, Jens Georg Schmidt and Ulrich Hartmann, for their ongoing support and constructive discussions. An earlier version of the meshing software was implemented by U. Hartmann and F. Kruggel at the Max-Planck-Institute of Cognitive Neuroscience at Leipzig and continued by U. Hartmann and the author at C&C Research Laboratories and is available at [12]. A CT image used for the meshes displayed in Fig. 6 was kindly provided by Dr. Hierl, Department of Oral and Maxillofacial Surgery, University Clinic Leipzig, and was segmented using software from F. Kruggel, MPI CNS, Leipzig. The author was partially supported by the European Union under research grants IST-1999–10378 and IST-2001–37153 (IST projects SimBio and GEMSS).

References

[1] Jens Georg Schmidt, Guntram Berti, Jochen Fingberg, Gert Wollny, and Junwei Cao. A finite-element based tool chain for the planning and simulation of maxillo-facial surgery. In P. Neittaanmäki, T. Rossi, K. Majava, and O. Pironneau, editors, European Congress on Computational Methods in Applied Sciences and Engineering ECCOMAS 2004. University of Jyväskylä, Department of Mathematical Information Technology, 2004. CDROM.

[2] R. Müller and P. Rüegsegger. Three-dimensional finite element modelling of non-invasively assessed trabecular bone structure. Med. Eng. Phys, 17(2), pp. 126133, 1995.

[3] Gregory M. Nielson and Junwon Sung. Interval volume tetrahedrization. In IEEE Visualization ’97 (VIS ’97), pp. 221228, Washington – Brussels – Tokyo, October 1997. IEEE.

[4] Mark A. Yerry and Mark S. Shephard. A modified quadtree approach to finite element mesh generation. IEEE Computer Graphics and Applications, 3(1), pp. 3946, January – February 1983.

[5] Mark S. Shephard, Hugues L. de Cougny, Robert M. O’Bara, and Mark W. Beall. Handbook of grid generation. CRC Press, 1999.

[6] Guntram Berti. Image-based unstructured 3 d mesh generation for medical applications. In P. Neittaanmäki, T. Rossi, K. Majava, and O. Pironneau, editors, European Congress on Computational Methods in Applied Sciences and Engineering ECCOMAS 2004. University of Jyväskylä, Department of Mathematical Information Technology, 2004. CDROM.

[7] Michael Bader, Hans-Joachim Bungartz, Anton Frank, and Ralf Mundani. Space tree structures for PDE solution. In Peter M. A. Sloot, C. J. Kenneth Tan, Jack J. Dongarra, and Alfons G. Hoekstra, editors, Proceedings of ICCS 2002, part 3, volume 2331 of LNCS. Springer, 2002.

[8] Gabriel Taubin. Geometric signal processing on polygonal meshes. In Eurographics 2000 State of the Art Report, 2000.

[9] Gregory Nielson and Richard Franke. Computing segmented volumes. In Hagen, Nielson, and Post, editors, Proceedings of Dagstuhl Seminar, Scientific Visualization 1997, pp. 251256, 1997.

[10] Kathleen S. Bonnell, Mark A. Duchaineau, Daniel A. Schikore, Bernd Hamann, and Kenneth I. Joy. Material interface reconstruction. In IEEE Transactions on Visualization and Computer Graphics. IEEE, 2003.

[11] Hans C. Hege, Martin Seebaß, Detlev Stalling, and Malte Zöckler. A generalized marching cubes algorithm based on non-binary classifications. Technical Report SC-97–05, Konrad-Zuse-Zentrum für Informationstechnik Berlin (ZIB), 1997.

[12] The SimBio-Vgrid mesh generator homepage. http://www.ccrl-nece.de/vgrid, 2004.

8.

Cranial Reconstructive Surgery and Surgical for Prediction Systems

Rekonstruktive Chirurgie und chirurgische Simulationssysteme

3D-Analysis of Soft Tissue Changes following Maxillary Distraction Osteogenesis

Thomas Hierl [1], Gerd Wollny [2], Jörg Hendricks [1], Guntram Berti [3], Jens Georg Schmidt [3], Jochen Fingberg [3], Alexander Hemprich [1]

[1] Dept. of Oral and Maxillofacial Plastic Surgery, University of Leipzig
[2] MPI for Human Cognitive and Brain Sciences, Leipzig
[3] C&C Research Laboratories, NEC Europe; St. Augustin

Abstract

Maxillary distraction osteogenesis is a new procedure in the treatment of severe maxillary hypoplasia and retrusion. By now most investigations have focused on questions regarding the procedure, bony changes, and dental occlusion . Therefore an investigation was started to look after the concomitant soft tissue changes associated with large bony maxillary advancements. Methods: 20 patients were analyzed, most of them suffering from cleft lip and palate. Pre- and posttreatment CT scans were compared using a novel tool chain based on rigid and non-rigid registration. This tool chain allows to extract data for individual anatomical landmarks and displays changes in a colour pattern. Furthermore soft tissue and bony changes could be compared. In addition to time-series analysis, a 3D cephalometric tool is integrated into the tool chain which permits pre- and post-operative comparison to control groups. To assess precision of the tool chain, cadaver studies were carried out.

Results: Our novel tool chain permits an excellent overview over bony and soft tissue changes. Looking at the soft tissue after an average bony advancement of 8 mm in the malar prominence region, similar changes could be seen. Facial appearance was altered towards a harmonic relation. Cadaver studies showed that the tool chain works well within the limitations of the CT-data.

Introduction

In the treatment of severe maxillary and midfacial retrusion and hypoplasia, distraction osteogenesis (DOG) has evolved as the method of choice. DOG offers the unique option to lengthen bone and soft tissue almost unlimited and has opened new dimensions in orthognathic surgery. By now most investigations on maxillary DOG have focused on questions regarding technical aspects which device to use or how to perform DOG. Further stress has been laid on postoperative stability with respect to dental occlusion and some 2D cephalometric landmarks. By now, however, no investigations have been carried out with respect to 3D hard and soft tissue changes, which was the incentive for this work. With the aid of a novel tool chain for the 3D analysis, the relation between soft and hard tissue changes was to be investigated in a group of patients treated at the Leipzig University Department of Oral and Maxillofacial Plastic Surgery.

Methods

Patient Group

From 2002 to 2004, 20 patients were treated by way of maxillary DOG. 18 suffered from cleft lip and palate, age ranged from 10 to 63 yrs (Ø 24 yrs). In all cases an external, halo-frame based distractor and a miniplate system for bony anchorage were used (RED II and Leipzig Retention Plate; Martin Medizintechnik, Tuttlingen, Germany). After a subtotal modified quadrangular osteotomy, the distraction procedure started on the 4^{th} – 5^{th} day after surgery. Advancement was 1mm/day until an overcorrection of 15–20 % was achieved. The consolidation period lasted 4–8 weeks depending on age and dentition. Then the distractor was removed [1].

Time Series Analysis

All measurements performed were based on pre- and postoperative CT scans. Data acqusition at time point 1 was 3–5 weeks before surgery. Postoperative scanning was performed 2–4 weeks after removal of the distraction device. Scanning was performed on a Siemens Volume Zoom plus scanner. Slice thickness was 1 mm without overlapping. The data was transferred in DICOM format and all computation was performed on a conventional PC.

Analysis Software

The tool chain for 3D-analysis consists of two programs which were developed by G. Wollny.

All programs run on LINUX platform and use the VISTA-format for data input. Therefore all data had to be converted first from DICOM into VISTA. The first program is a tool to assess 3D landmark coordinates of a given volume data set. The data is loaded and can be shown by way of volume rendering. Soft and hard tissue display is possible via adjusting a Hounsfield units slider. Futhermore, zooming, pan and rotate options can be performed with mouse buttons. After importing the data, a landmark table has to be created. Then, by simply clicking on the surface (bone or soft tissue, as adjusted) landmarks are located. X, y, and z coordinates are allocated to the landmarks which serve as the basis for the cephalometric analysis. For better performance, the position, zoom, and Hounsfield units of all landmarks are saved in the landmark table, thus when proceeding through the analysis on the next patient, the area of the subsequent landmarks is presented. Thus almost no zooming or rotating of the skull is necessary on the following data sets. Furthermore, snapshots of the landmarks can be taken to show the exact position of an ideal landmark (figs. 1, 2).

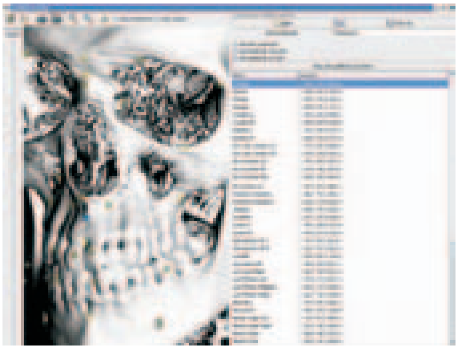

Fig. 1: Screenshot of the 3D cephalometric tool. Here the slider on the left has been adjusted to bone. Dots mark the landmarks seen in the table. The active landmark is highlighted. Changing the position is simply done ba a mousclick. The x, y, and z coordinates are displayed in the table and saved in a spreadsheet for further calculations.

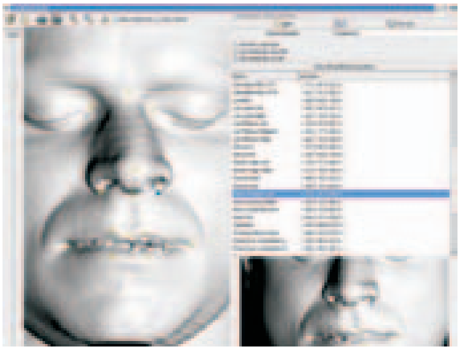

Fig. 2: Screenshot of the 3D cephalometric tool with soft tissue display. If required, the position of an "ideal" landmark can be demonstrated in the window below the landmark table.

The second program consists of a toolchain to segment, register and show the displacement of corresponding areas in pre- and postoperative CT-scans. First, both data sets are segmented using an intensity filter. According to the chosen Hounsfield units, bone or soft tissue changes will be analyzed. Next step is a linear registration of the the postoperative scan to the preoperative one to adjust position and head orientation. To quantify the structural changes of the skull, a non-linear registration based on a visco-elastic approach is performed last [2]. For visualizing the shape changes, two ways are implemented. After creating surfaces from the volume data, the deformation vectors are shown as arrows ending at the surface. Alternatively, deformation is displayed by a colouring scale. Here colour intensity reflects deformation magnitude (figs. 3, 4). A more detailed description of the toolchain may be looked up in the literature [3].

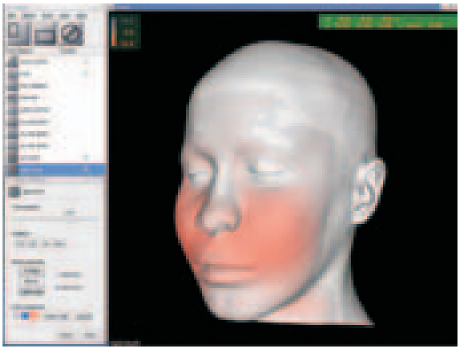

Fig. 3: Soft tissue changes in the midface of a 21-ys-old female patient. The relevant areas are colour-coded, colour intensity resembles the amount of displacement.

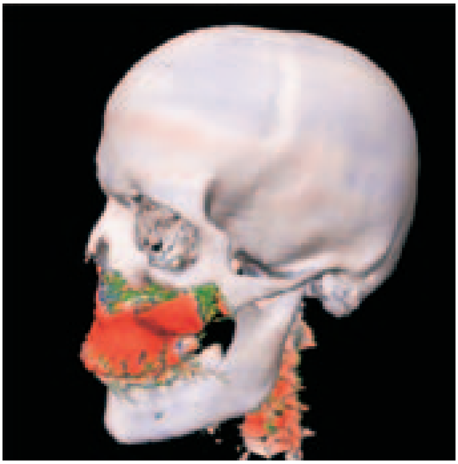

Fig. 4: Bony displacements in an 23-ys-old male patient. Colour-coded display of bony changes, furthermore the displacement vectors are shown. The movement in an anterior-kaudal direction is easily recognisable.

Study Protocol

To investigate the relationship between hard and soft tissue changes, pre- and postoperative CT-scans were evaluated in the following manner. First, pre- and posttreatment CT scans were registered (see above) and the displacement vectors of hard and soft tissue landmarks calculated. Therefore a limited number of easy to locate landmarks was chosen (Table 1). Landmarks, which proved to be difficult to locate were omitted [4]. By way of Wilcoxon test, the interdependence of soft and hard tissue changes was evaluated (program: PC-Medas, Fa. Grund, Margetshöchheim).

Tab. 1: Anatomical landmarks used in this study

Landmark	Definition
Anterior nasal spine	most anterior point of the anterior nasal spine
Columella base	turning point of the columella and upper lip
Nasion (bone)	deepest point of the nasofrontal suture
Nasion (soft tissue)	point in the soft tissue concavity above the nasofrontal suture
Piriforme aperture left	most lateral-kaudal bony point of the left piriforme aperture
Piriforme aperture right	most lateral-kaudal bony point of the right piriforme aperture
Alar base (nose) left	soft tissue point of the most lateral-kaudal point of the nasal alar base left
Alar base (nose) right	soft tissue point of the most lateral-kaudal point of the nasal alar base right
Zygomatic prominence left	bony point of the zygoma, most anterior-lateral point left
Zygomatic prominence right	bony point of the zygoma, most anterior-lateral point right
Zygomatic prominence left (soft tissue)	soft tissue cheek prominence left
Zygomatic prominence right	soft tissue cheek prominence right (soft tissue)

Furthermore, soft tissue thickness was measured on these bony landmarks directly using the landmark location tool. Here corresponding soft and hard tissue landmarks could be easily detected by just moving the Hounsfield unit slider. Then the distance could be computed. This data served as a control measurement for the displacement vectors as again pre- and post data were statistically compared with the Wilcoxon test.

As the novel toolchain had to be validated, cadaver studies were performed. First, micro titanium screws (1.5 mm) were implanted in five skulls in the position of medical cephalometric landmarks (fig. 5). Then the distance could be measured with precision calipers and the skulls were scanned. Now these distances could be compared with those measured in the 3D-landmark tool. 162 distances were calculated that way.

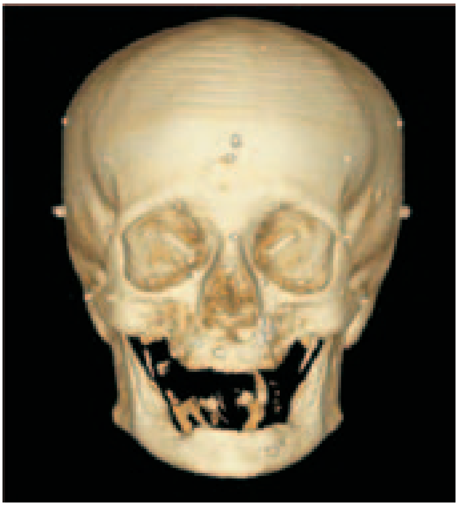

Fig. 5: Validation study: CT scan of a cadaver specimen with titanium microscrews.

Afterwards, maxillary osteotomies of the skulls were performed and the advanced maxillae were fixated with titanium miniplates. Now a second CT scan was acquisitioned and again, directly measured distances were compared with the displacements computed by the registration software. Now the maxillae were fixated in more advanced position and the procedure was repeated.

Results

The results of the validation studies showed, that the landmark location tool worked well with deviations ranging from 0.1–1.8 mm (mean deviation 0.7 mm) between directly measured and computed distances. Keeping in mind that slice thickness was 1 mm, these results proved excellent. Looking at the registration tool, deviations lay between 0.1–3.5 mm with a mean deviation of 1.3 mm (32 measurements of 162 showed deviations of 2.0 mm or more). As CT slice thickness was 1 mm differences up to 2 mm are withhin the accuracy of the scans. Thus the registration tool showed in over 80 % of the landmarks acceptable results. The crucial question is now, whether valid and invalid displacement vectors can be discerned. As starting and ending points of all vectors are located on the appropriate pre- and postoperative surface, a visual quality check is easy. Regarding displacement vectors of anatomical landmarks, erroneous vectors can be easily recognized.

Patient data analysis showed an average bony displacement in the piriforme aperture region (equals Le-Fort-I plane) of 8.1 mm with a soft tissue displacement of 8.0 mm. Regarding cheek prominence displacement distances lay at 8.6 mm (bone) and 8.3 mm (soft tissue). No statistical significant difference could be noted. Looking at directly measured soft tissue thickness, no significant difference between pre- and posttreatment data was seen, too (average soft tissue depth over bony landmarks ranged between 13–16 mm).

Figs. 6 and 7 show a typical displacement result. In all patients a clinically significant improvement in facial harmony was seen and posttreatment 2-dimensional cephalometric data

showed “normal” values [5]. A typical pre- and posttherapeutical situation is given in fig. 8.

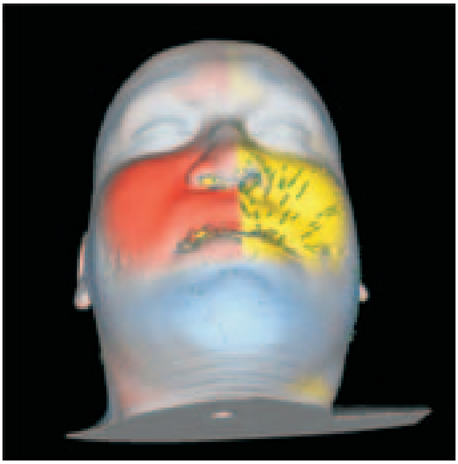

Fig. 6: Pre-post comparison of soft tissue changes in another study patient. The postoperative situation is shown on the right, whereas the left side resembles the preoperative appearance. Areas of change are colour coded, displacement vectors are visible.

Fig. 7: Soft tissue analysis of the patient seen in Fig. 3. Colour-coded display with vectors.

Fig. 8: Pre- and posttreatment clinical situation of a 21-ys-old female (cf. fig. 3). Marked midfacial hypoplasia and unilateral cleft lip and palate preoperatively. Below the posttreatment situation is given.

Discussion and Conclusion

We present a novel tool chain to evaluate 3D changes of hard and soft tissue. By now most studies working with 3D data have focused on soft tissue, aquisitioned with surface scanning or CT analysis [6–11]. Simultaneous 3D evaluations of soft and hard tissue are not known to have been performed so far to our knowledge.

The novel tool chain proved to lead to clinically acceptable results. The landmark location tool worked accurate, whereas 20 % of the registration tool landmark data was clinically inacceptable. Reasons for that are not known but may lie in specific geometry problems of the intricate bony structure of the human skull. Therefore, until the reasons for these mistakes have been found, a second method to evaluated the data has to be performed like in this study.

On the other hand, this is the first software to our knowledge which allows time series analysis of CT data in 3D. By showing changes graphically and giving the displacement vectors, the impact of surgical therapies can be evaluated quickly. Furthermore the software works on normal PCs at the clinicians desktop and needs no special knowledge in programming, a point which is extremly important in our opinion.

In our patient group, the analysis of the results is extremely important. Besides correcting dental occlusion, a "perfect" look is the main goal in correcting dentofacial deformities. The problem is, however, that surgery is planned on the underlying bony structures and concomitant soft tissue changes are solely expected if the bony deformity is corrected. Here the results help to define the level of osteotomy (where has the bone to be cut to lead to soft tissue changes) and the amount of hard tissue displacement needed for soft tissue changes. In this study similar displacements of soft and hard tissue in the esthetically important cheek area were found. This implies that osteotomy lines can be planned according to the preoperative soft tissue situation.

Of course, further investigations are needed to evaluate long-term results which will be affected be remodeling and aging. Here surface scanning is thought to be the method of choice and will be performed in regular instances. Therefore our analysis software will be adapted to that data format.

References

[1] T. Hierl, N. Klisch, R. Klöppel, and A. Hemprich, "Therapie ausgeprägter Mittelgesichtsrücklagen mit Hilfe der Distraktionsosteogenese", *Mund Kiefer GesichtsChir*, vol. 7, pp. 7–13, 2003.

[2] P. Thévenanz, U. E. Ruttimann, and M. Unser, "A pyramid approach to subpixel registration based on intensity", *IEEE Transact Image Process*, vol. 7, pp. 27–41, 1998.

[3] G. Wollny, *Analysis of changes in temporal series of medical images*, MPI Series for Human Cognitive and Brain Sciences No 43. Leipzig, 2004.

[4] J. Hendricks, *Analyse der Mittelgesichtsdistraktion an Hand von CT-Untersuchungen*, Med. Diss., Leipzig, in press.

[5] Th. Hierl, *Untersuchungen zur Distraktionsosteogenese des Mittelgesichts*, Med. Habil. Universität Leipzig, 2002.

[6] S. E. Bishara, D. M. Cummins, G. J. Jorgensen, and J. R. Jakobsen, "A computer assisted photogrammetric analysis of soft tissue changes after orthodontic treatment. Part I: Methodology and reliability", *Am J Orthod Dentofac Orthop*, vol. 107, pp. 633–639, 1995.

[7] G. Bhatia, M. W. Vannier, K. E. Smith, P. K. Commean, J. Riolo, and V. L. Young, "Quantification of facial surface change using a structured light scanner", *Plast Reconstr Surg*, vol. 94, pp. 768–774, 1994.

[8] T. J. Coward, R. M. Watson, and B. J. J. Scott, "Laser scanning for the identification of repeatable landmarks of the ears and face", *Br J Plast Surg*, vol. 50, pp. 308–314, 1994.

[9] M. Y. Hajeer, D. T. Millett, A. F. Ayoub, and J. P. Siebert, "Applications of 3D imaging in orthodontics: Part I", *J Orthod*, vol. 31, pp. 62–70, 2004.

[10] A. M. McCance, J. P. Moss, W. R. Fright, A. D. Linney, and D. R. James, "A three-dimensional soft tissue analysis of 16 skeletal class III patients following bimaxillary surgery", *Br J Oral Maxillofac Surg*, vol. 30, pp. 221–232, 1992.

[11] P. Techalertpaisarn, and T. Kuroda, "Three-dimensional computer-graphic demonstration of facial soft tissue changes in mandibular prognathic patients after mandibular sagittal ramus osteotomy", *Int J Adult Orthod Orthognath Surg*, vol. 13, pp. 217–225, 1998.

3D-Analyse der Weichgewebsveränderungen nach Distraktionsosteogenese des Oberkiefers

Thomas Hierl[1], Gerd Wollny[2], Jörg Hendricks[1], Guntram Berti[3], Jens Georg Schmidt[3], Jochen Fingberg[3], Alexander Hemprich[1]

[1] Klinik und Poliklinik für Mund-, Kiefer- und Plastische Gesichtschirurgie, Universitätsklinikum Leipzig AöR
[2] Max-Planck-Institut für Kognitions- und Neurowissenschaften, Leipzig
[3] C&C Research Laboratories, NEC Europe Ltd, St. Augustin

Abstract

Die Oberkieferdistraktion ist ein neues Verfahren in der Behandlung ausgeprägter Mittelgesichtsrücklagen. Bisherige Untersuchungen konzentrierten sich auf Fragen zur Durchführung, auf knöcherne Veränderungen und das Erreichen einer akzeptablen Zahnbeziehung. Aus diesem Grund wurde eine Studie entworfen, die auch die dazugehörigen Weichteilveränderungen berücksichtigen sollte. Bei 20 Patienten wurden prä- und postoperative CT-Daten mit Hilfe einer neuen Software verglichen. Nach rigider und nicht-rigider Registrierung wurden die Veränderungen anatomischer Landmarken verglichen; zugleich wurden die Strecken farbskaliert dargestellt. Dies galt sowohl für Hart-, wie auch für Weichgewebsparameter. Zusätzlich wurde eine 3D-Kephalometriesoftware entwickelt, die einen Vergleich von prä- und postoperativen Daten erlaubt. Um die Analyse zu validieren wurden zusätzlich Kadaverstudien durchgeführt. Die hier vorgestellte Software ermöglicht einen exzellenten Überblick über Hart- und Weichgewebsveränderungen. Im Vergleich zu der durchschnittlichen knöchernen Verlagerung um ca. 8 mm im Bereich der Wangenprominenz ergaben sich ähnliche Veränderungen der Weichgewebe. Die Kadaverstudien zeigten unter Berücksichtigung der Auflösung der CT-Datenaquisition eine klinisch akzeptable Genauigkeit der Software.

Einleitung

In der Behandlung einer ausgeprägten Oberkiefer- und Mittelgesichtsrücklage bzw. -hypoplasie stellt die Distraktionsosteogenese (DOG) heute die Methode der Wahl dar. Die DOG bietet die einzigartige Möglichkeit, Knochen und Weichgewebe fast uneingeschränkt zu verlängern. Bisherige Studien haben sich hauptsächlich mit technischen Fragestellungen beschäftigt (welches Gerät sollte eingesetzt werden, wie ist der Ablauf des Verfahrens). Darüberhinaus wurde die postoperative Stabilität der Kieferverlagerung mit Hinblick auf die Zahnbeziehung von Ober- zu Unterkiefer und zweidimensionaler kephalometrischer Parameter untersucht. Bisher erfolgten keine Studien zu den dreidimensionalen Veränderungen von Hart- und Weichgewebe, was der Anlaß dieser Untersuchung war. Mit

Hilfe einer neuen Software zur 3D-Analyse wurde das Verhältnis von Weich- zu Hartgewebsveränderung in einer Gruppe von am Universitätsklinikum Leipzig behandelten Patienten untersucht.

Methoden

Patienten

Im Zeitraum 2002–2004 wurden 20 Patienten mit ausgeprägter Mittelgesichtsrücklage behandelt. 18 litten dabei an einer Lippen-Kiefer-Gaumen-Spalte, das Alter lag zwischen 10 und 63 Jahren (Ø 24 J.). In allen Fällen kamen ein externer, Halobogen-verankerter Distraktor und ein Miniplattensystem zur Verbindung mit dem osteotomierten Mittelgesicht zum Einsatz (RED II und Leipzig Retention Plate; Martin Medizintechnik, Tuttlingen). Nach einer subtotalen modifizierten quadrangulären Mittelgesichtsosteotomie begann die Distraktoraktivierung am 4. – 5. postoperativen Tag. Die Distraktionsrate betrug 1mm/Tag bis eine Überkorrektur um 15–20 % erzielt wurde. Die Konsolidierungsphase dauerte in Abhängigkeit vom Alter und dem Zahnstatus 4–8 Wochen. Anschließend wurden Distraktor und Verankerungssystem entfernt [1].

Zeitreihenanalyse

Alle Untersuchungen basierten auf prä- und postoperativen CT-Daten. Präoperativ erfolgte die Untersuchung drei bis fünf Wochen vor dem Eingriff. Die zweite Untersuchung lag zwei bis vier Wochen nach der Abnahme des Distraktors. Als CT-Scanner diente ein Gerät vom Typ Volume Zoom plus der Fa. Siemens. Die Schichtdicke betrug 1 mm ohne Überlappung. Nach der Untersuchung wurde der Datensatz im DICOM-Format überspielt und anschließend auf einem Standard-PC weiterverarbeitet.

Analysesoftware

Die Auswertesoftware besteht aus zwei Programmen die von G. Wollny entwickelt wurden. Als Plattform dient LINUX, der Dateninput erfolgt im VISTA-Format. Aus diesem Grund müssen die DICOM-Daten initial nach VISTA exportiert werden. Die erste Analysesoftware dient zur dreidimensionalen Bestimmung der Koordinaten von anatomischen Landmarken. Nach Laden des Datensatzes wird er via Volumenrendering dargestellt. Sowohl Weich- wie auch Hartgewebe können durch Anpassung der Hounsfieldeinheiten visualisiert werden. Weiterhin sind Zoom, Verschieben und Rotation über Mausbewegungen möglich. Nach Import des Datensatzes wird eine Landmarkentabelle erstellt, die die Basis der kephalometrischen Analyse darstellt. Anschließend werden die Landmarken durch einfaches Anklicken (Weich- bzw. Hartgewebe) lokalisiert. Die X, Y und Z-Koordinaten werden bestimmt und stellen die Grundlage für die weiteren Berechnungen dar. Zur einfacheren Durchführung werden die Hounsfield Einheiten, die Position und der Zoomfaktor aller Landmarken gespeichert, so daß beim Durchführen weiterer Analysen nur minimale Veränderungen notwendig sind. Darüberhinaus können Screenshots von Ideallandmarken aufgenommen werden, die zum Vergleich eingeblendet werden können (Abb. 1 und 2).

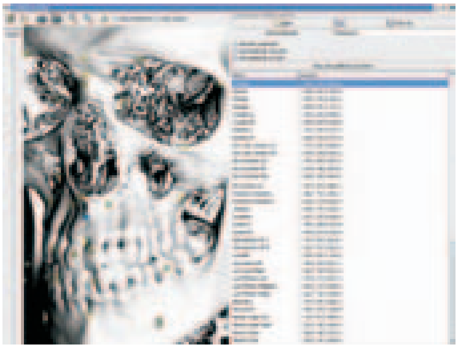

Abb. 1: 3-D Kephalometriesoftware. Dargestellt ist eine typische Analyse, der Hounsfield- Schieber links ist auf Knochen eingestellt. Die Landmarken der Tabelle sind durch gelbe Punkte dargestellt, die aktive Landmarke ist blau. X-, Y- und Z-Werte sind in der Tabelle abgebildet und dienen als Grundlage für die Analyse.

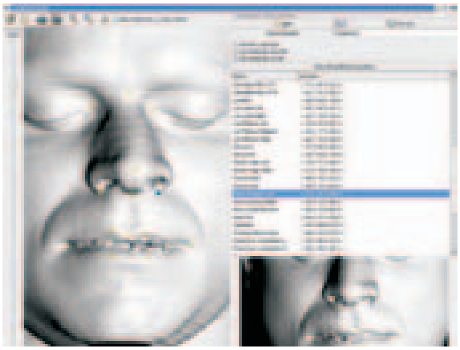

Abb. 2: Gleicher Patient, nun im Weichteilfenster dargestellt. Je nach Bedarf kann ein Screenshot einer Ideallage der betreffenden anatomischen Landmarke eingeblendet werden (rechts unten im Bild).

Das zweite Programm ermittelt Veränderungen der beiden Datensätze nach rigider und nicht-rigider Registrierung. Zuerst werden die CT-Datensätze unter Verwendung eines Intensitätsfilters segmentiert. Hierbei wird entschieden, ob eine knöcherne oder Weichgewebsanalyse erfolgen soll. Anschließend erfolgt eine lineare Registrierung des postooperativen Datensatzes auf den präoperativen, um Lageunterschiede während der Aufnahme zu eliminieren. Um die strukturellen Veränderungen des Schädels zu quantifizieren, wird anschließend eine auf Viskoelastizität basierende nicht-lineare Registrierung durchgeführt [2]. Nach erfolgter Registrierung wird nun zur Darstellung eine interaktive Visualisierung eingesetzt. Dazu werden zuerst aus den Volumendatensätzen Oberflächen generiert. Die Verschiebungsvektoren werden dann als Pfeile auf der Oberfläche dargestellt, wobei die Koordinaten und Beträge einzelner Vektoren ausgewählt werden können. Alternativ kann die Veränderung auch durch ein Farbschema visualisiert werden, die Farbintensität gibt dann den Betrag der Strecke wieder (Abb. 3 und 4). Da dies nur eine sehr vereinfachte und verkürzte Beschreibung des Programmes sein kann, ist eine ausführliche Erläuterung in der angegebenen Literatur zu finden [3].

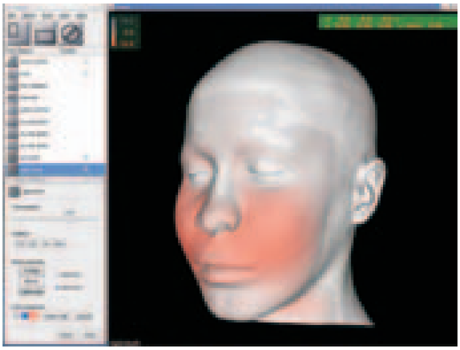

Abb. 3: Darstellung der Weichteilveränderung im Mittelgesicht einer 21-jährigen Patientin. Die betreffenden Areale sind farbkodiert, je tiefer der Rotton, desto größer ist die Veränderung.

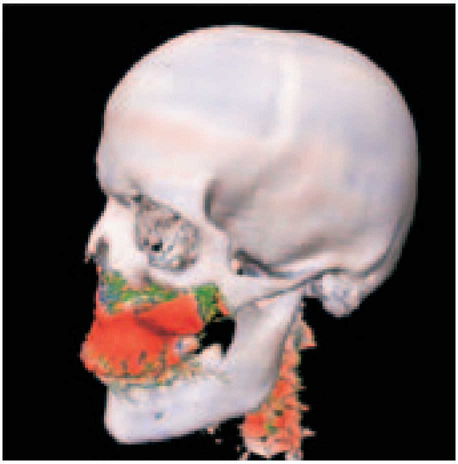

Abb. 4: Hier wird die knöcherne Verlagerung des Mittelgesichts eines 23-jährigen Studienpatienten wiedergegeben. Die Verlagerungsstrecken sind farbkodiert, zusätzlich sind die Verlagerungsvektoren eingeblendet. Gut ist die Verschiebung nach anterior-kaudal zu erkennen.

Studienaufbau

Um die Veränderungen von Hart- und Weichgeweben zu bewerten, wurden die Datensätze wie folgt untersucht. Zuerst wurden die prä- und postoperativen CT-Datensätze registriert und die Verschiebungsvektoren von Hart- und Weichgewebslandmarken berechnet (s. oben). Es wurden einfach zu erkennende anatomische Landmarken ausgewählt (Tab. 1), schwierig zu bestimmende Landmarken wurden weggelassen [4]. Mittels des Wilcoxon-Tests wurde dann der Zusammenhang zwischen Hart- und Weichgewebsveränderungen evaluiert (Statistikprogramm PC-Medas, Fa. Grund, Margetshöchheim). Darüberhinaus wurde die Dicke des Weichteilmantels über den knöchernen anatomischen Landmarken mit der Landmarkensoftware direkt bestimmt. Dies war durch Verschiebung des Hounsfields-Schiebers problemlos möglich. Diese Daten dienten dann als Kontrolle für die Berechnung der Verschiebungsvektoren, wobei auch der Wilcoxon-Test zur Anwendung kam.

Tab. 1: Anatomische Landmarken der Studie.

Landmarke	**Definition**
Anterior nasal spine	vorderer Nasenstachel
Columellabasis	Umkehrpunkt zwischen Nasensteg und Oberlippe
Nasion (Knochen)	tiefste Einziehung der Sutura nasofrontalis
Nasion (Weichgewebe)	tiefste Einziehung der Weichgewebe über der Sutura nasofrontalis
Apertura piriformis links	linker kaudal-lateralster Punkt der Apertura piriformis
Apertura piriformis rechts	rechter kaudal-lateralster Punkt der Apertura piriformis
Alarbasis (Nase) links	linker kaudal-lateralster Punkt des Übergangs Nasenflügel-Wange/Oberlippe
Alarbasis (Nase) rechts	rechter kaudal-lateralster Punkt des Übergangs Nasenflügel-Wange/Oberlippe
Zygoma Prominenz links	köcherne Wangenprominenz des Jochbeins links
Zygoma Prominenz rechts	köcherne Wangenprominenz des Jochbeins rechts
Zygoma Prominenz links (Weichgewebe)	Wangenprominenz links
Zygoma Prominenz rechts (Weichgewebe)	Wangenprominenz rechts

Da die Analyse validiert werden sollte, wurden Validierungsstudien durchgeführt. In fünf Schädeln wurden Mikrotitanschrauben (Ø 1,5 mm) im Bereich anatomischer Landmarken eingebracht (Abb. 5). Anschließend wurden die Abstände mit einer Präzisionsschiebelehre bestimmt und eine CT-Untersuchung durchgeführt. Je 162 Strecken wurden so mit den Werten aus der Landmarkensoftware verglichen.

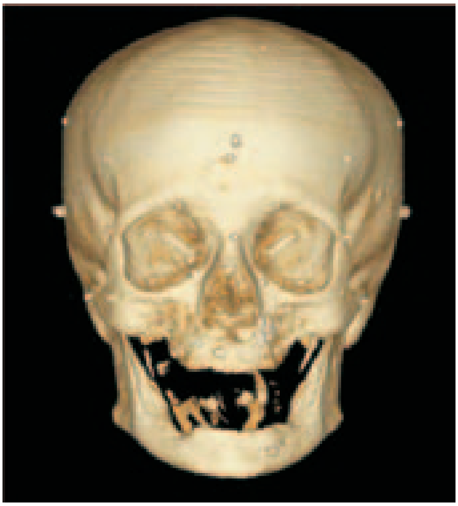

Abb. 5: CT-Darstellung eines Kopfes der Validierungsstudie mit eingebrachten Mikro-Titanschrauben.

Nun wurde der Oberkiefer osteotomiert und in einer neuen Position mit Minititanplatten fixiert. Es erfolgte eine erneute CT-Untersuchung und die direkt gemessenen Strecken wurden mit den Beträgen der Verschiebungsvektoren verglichen. Anschließend wurde der Oberkiefer in einer noch weiter anterioren Position fixiert und das Vorgehen wiederholt.

Ergebnisse

Die Ergebnisse der Validierungsstudie zeigten, daß die Werte der Landmarkenbestimmung hervorragend mit den direkt gemessenen übereinstimmten. Die Unterschiede lagen dabei zwischen 0,1 und 1,8 mm (Ø 0,7 mm). In Anbetracht der Schichtdicke von 1 mm ist diese Übereinstimmung als exzellent zu betrachten. Die Registrierungssoftware zeigte Abweichungen von 0,1 bis 3,5 mm mit einer durchschnittlichen Abweichung von 1,3 mm. 32 von 162 Meßstrecken wiesen dabei eine größere Abweichung als 2,0 mm auf. Bei einer Schichtdicke der CT-Untersuchung von 1mm liegen Abweichungen bis 2 mm innerhalb der Genauigkeit der Ausgangsdaten. So gesehen zeigten 80 % der Messungen der Registrierungssoftware ein akzeptables Ergebnis. Die Frage ist nun, ob zwischen validen und nicht-validen Vektoren unterschieden werden kann, was für die Aussagekraft der Methode von großer Bedeutung ist. Da die Anfangs- und Endpunkte der Verschiebungsvektoren auf den Oberflächen lokalisiert werden können, ist eine visuelle Plausibilitätskontrolle jederzeit möglich. So sind Ausreißer im Bereich anatomischer Landmarken, bei denen die Registrierung fehlgeschlagen ist, leicht zu erkennen.

Die Auswertung der Patientendaten zeigte eine durchschnittliche knöcherne Verlagerung im Bereich der Apertura piriformis (entspricht ca. der Le Fort-I Ebene) um 8,1 mm sowie der darüber liegenden Weichgewebe um 8,0 mm. Für die Wangenprominenz waren die Verlagerungsstrecken 8,6 mm (Knochen) bzw. 8,3 mm (Weichgewebe). Knöcherne und Weichgewebsverlagerung zeigten dabei keinen statistisch signifikanten Unterschied. Die Analyse der Weichteildicke entsprach diesen Werten, da ebenfalls kein statistisch signifikanter Unterschied zwischen prä- und posttherapeutischen Werten gefunden werden konnte (die durchschnittliche Weichteildicke lag je nach Landmarke zwischen 13 –16 mm).

In Abb. 6 und 7 ist eine typische grafische Darstellung wiedergeben. Bei allen Patienten war eine klinisch signifikante Verbesserung des Gesichtsaufbaus festzustellen, wobei die postoperativen Werte der zweidimensionalen Kephalometrie „Durchschnittswerten“ entsprachen [5]. Eine typische prä- und postoperative Situation ist in Abb. 8 wiedergegeben.

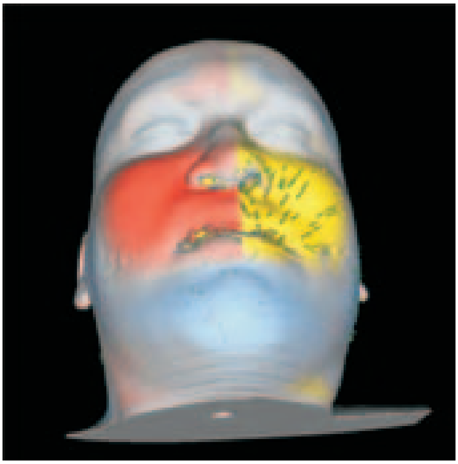

Abb. 6: Prä-post Vergleich der Weichteilveränderung eines weiteren Patienten. Die rechte Hälfte zeigt die postoperative Situation, links ist der Ausgangszustand zu sehen. Die Bereiche der Weichteilveränderung sind jeweils farbkodiert. Zusätzlich sind ausgewählte Verlagerungsvektoren dargestellt.

Abb. 7: Weichteilvergleich der Patientin aus Abb. 3. Die Hautbezirke sind farbkodiert, zusätzlich sind Vektoren dargestellt.

Abb. 8: Oben im Bild die Ausgangssituation einer 21-jährigen jungen Frau (s. Abb. 3). Es liegt eine ausgeprägte Mittelgesichtshypoplasie bei einseitiger Lippen-Kiefer-Gaumen-Spalte vor. Unten der postoperative Zustand nach Distraktionsosteogenese.

Diskussion und Schlussfolgerung

In dieser Studie wird eine neues Verfahren zur Evaluierung von dreidimensionalen Veränderungen von Hart- und Weichgewebe vorgestellt. Bisher haben sich die meisten Untersuchungen mit 3D-Daten auf Weichgewebsveränderungen beschränkt, wobei als Ausgangsmaterial CT-Daten bzw. durch Oberflächenscanner gewonnene Daten dienten [6–11]. Die gleichzeitige dreidimensionale Analyse von Hart- und Weichgewebe ist uns bisher nicht bekannt.

Die neue Bearbeitungssoftware erwies sich insgesamt als klinisch akzeptabel. Die Landmarkenbestimmung wies eine ausgezeichnete Genauigkeit auf, während 20 % der Meßwerte in der Registrierungssoftware klinisch nicht annehmbar waren. Gründe hierfür sind bisher nicht bekannt, Ursachen könnten z. B. in der komplizierten Struktur des menschlichen Mittelgesichts liegen. Aus diesem Grund sollte, bis die Ausreißer minimiert sind, jeweils eine Kontrollstudie für die wichtigsten Landmarken mitgeführt werden. Darüber hinaus ist eine visuelle Kontrolle der berechneten Verlagerungsvektoren immer möglich, so dass grobe Fehler vermieden werden können. Auf der anderen Seite ist dies unseres Wissens die erste Software zur dreidimensionalen Zeitreihenanalyse von CT-Daten. Die grafische Ausgabe ermöglicht einen hervorragenden Überblick über Hart- und Weichgewebsveränderungen. Dank der Darstellung der Verlagerungsvektoren kann die Auswirkung chirurgischer Maßnahmen sofort erkannt werden. Ein wichtiger Punkt ist, dass die Software auf handelsüblichen PCs läuft und keine speziellen Programmierkenntnisse benötigt. Dies bedeutet, dass die Analyse, wie hier, auch durch den Kliniker erfolgen kann.

Für unsere Patienten ist die Analyse der Ergebnisse von großer Bedeutung. Neben der Korrektur der fehlerhaften dentalen Okklusion stellt ein harmonischer Gesichtsaufbau das Hauptziel in der Korrektur dentofazialer Abweichungen dar. Das Problem der Korrektur liegt jedoch darin, dass operative Maßnahmen an Hand der knöchernen Situation geplant werden und entsprechende Weichgewebsveränderungen angenommen werden. Hier helfen die Ergebnisse dieser Studie die knöcherne Veränderung zu definieren, die zum Erreichen der beabsichtigten Weichgewebssituation notwendig sind. In dieser Studie wurde eine gleichmäßige Hart- und Weichgewebsveränderung im ästhetisch wichtigen Wangenbereich gefunden, so dass die Osteotomielinien entsprechend der präoperativen Weichgewebssituation geplant werden können.

Weitere Untersuchungen sind notwendig, um Langzeitveränderungen zu beobachten. Hier sind vor allem die Einflüsse der knöchernen Remodellierung und des Alterns zu nennen. Regelmäßige Datenerfassung via Oberflächenscanning ist hierfür die Methode der Wahl und ist bei allen Patienten vorgesehen. Eine logische Weiterentwicklung wird daher die Anpassung der Analysesoftware für diesen Datentyp sein.

Literatur

[1] T. Hierl, N. Klisch, R. Klöppel, und A. Hemprich, „Therapie ausgeprägter Mittelgesichtsrücklagen mit Hilfe der Distraktionsosteogenese“, *Mund Kiefer GesichtsChir*, vol. 7, pp. 7–13, 2003.

[2] P. Thévenanz, U. E. Ruttimann, and M. Unser, „A pyramid approach to subpixel registration based on intensity“, *IEEE Transact Image Process*, vol. 7, pp. 27–41, 1998.

[3] G. Wollny, *Analysis of changes in temporal series of medical images*, MPI Series for Human Cognitive and Brain Sciences No 43. Leipzig, 2004.

[4] J. Hendricks, *Analyse der Mittelgesichtsdistraktion an Hand von CT-Untersuchungen*, Med. Diss., Leipzig, in press.

[5] Th. Hierl, *Untersuchungen zur Distraktionsosteogenese des Mittelgesichts*, Med. Habil. Universität Leipzig, 2002.

[6] S. E. Bishara, D. M. Cummins, G. J. Jorgensen, and J. R. Jakobsen, „A computer assisted photogrammetric analysis of soft tissue changes after orthodontic treatment. Part I: Methodology and reliability“, *Am J Orthod Dentofac Orthop*, vol. 107, pp. 633–639, 1995.

[7] G. Bhatia, M. W. Vannier, K. E. Smith, P. K. Commean, J. Riolo, and V. L. Young, „Quantification of facial surface change using a structured light scanner“, *Plast Reconstr Surg*, vol. 94, pp. 768–774, 1994.

[8] T. J. Coward, R. M. Watson, and B. J. J. Scott, „Laser scanning for the identification of repeatable landmarks of the ears and face“, *Br J Plast Surg*, vol. 50, pp. 308–314, 1994.

[9] M. Y. Hajeer, D. T. Millett, A. F. Ayoub, and J. P. Siebert, „Applications of 3D imaging in orthodontics: Part I“, *J Orthod*, vol. 31, pp. 62–70, 2004.

[10] A. M. McCance, J. P. Moss, W. R. Fright, A. D. Linney, and D. R. James, „A three-dimensional soft tissue analysis of 16 skeletal class III patients following bimaxillary surgery“, *Br J Oral Maxillofac Surg*, vol. 30, pp. 221–232, 1992.

[11] P. Techalertpaisarn, and T. Kuroda, „Three-dimensional computer-graphic demonstration of facial soft tissue changes in mandibular prognathic patients after mandibular sagittal ramus osteotomy“, *Int J Adult Orthod Orthognath Surg*, vol. 13, pp. 217–225, 1998.

Computer assisted reconstruction of face and skull

[1]A. Schramm, [1]M. Rücker, [1]D. Grotzer, [2]Ch. Zizelmann, [2]R. Schön, [1]N.-C. Gellrich

[1] Department of Cranio-Maxillofacial Surgery, Medical University of Hannover, Carl-Neuberg-Str. 1, D-30625 Hannover, Germany
[2] Department of Cranio-Maxillofacial Surgery, Universityhospital Freiburg, Hugstetterstr. 55, D-79106 Freiburg, Germany

Abstract

Ablative tumor surgery, orbital and mid face reconstruction as much as skull base surgery requires detailed planning using CT or MRI. Reconstruction is depending on reliable information to choose correct type of grafts and to predict the outcome. This study evaluates the benefit and the indications of computer assisted surgery in the treatment of cranio-maxillofacial surgery.Based on a CT or MRI data set an optical navigation system was used for preoperative planning, intraoperative navigation and postoperative control. Surgery was preoperatively planned and intraoperatively navigated. Preoperatively required soft and hard tissue was measured using the mirrored data set of the unaffected side; size and location of the graft were chosen virtually. Intraoperatively contours of transplanted tissues were navigated to the preoperatively simulated reconstructive result.Computer assisted treatment was successfully completed in all cases (107). Preoperatively outlined safety margins could be exactly controlled during tumor resection. Reconstruction was designed and performed precisely as virtually planned. Image guided treatment improves preoperative planning by visualization of the individual anatomy, intended reconstructive outcome and by objectivation the effect of adjuvant therapy. Intraoperative navigation makes tumor and reconstructive surgery more reliable by showing the safety margins, saving vital structures and leading reconstruction to preplanned objectives.

Introduction

Computer assisted technology was initially developed to provide neurosurgeons with accurate guidance during surgical procedures. Stereotactic procedures were introduced to neuro surgery in the early 1980s, and currently systems with and without robotic navigation are in use for specific medical indications. For oral and maxillofacial surgery nowadays mechanical, electro-magnetic and optic systems are available to perform navigational surgery by frameless stereotaxy. In the following pages function and indications for frameless stereotaxy and computer assisted treatment in oral and maxillofacial surgery are described.

Computer Assisted Treatment

Clinical application of computer assisted treatment is performed in three steps. The first step is the analysis of the problem, planning of treatment and simulation of surgical procedures. Part two is the navigational surgery performed as frameless stereotaxy. Step three consists of posttherapeutic control. Indications in traumatology are primary and secondary recon-struction of the orbit and the decompression of the optical nerve [Gellrich et al., 1999a].

Indications in tumor surgery are minimal invasive biopsies, resections of extensive tumors of the midface and skull base – especially following adjuvant chemo- or radiotherapy – and primary and secondary reconstruction of the facial skeletton [Schramm et al., 2000a]. Although it is possible to navigate the insertion of dental implants in the maxilla and mandible, the indication is limited to insertion of zygomatic fixtures or extremely specific anatomical demands [Schramm et al., 2000b].

Frameless stereotaxy

In fig. 1 function of an optic navigation system is described. Infrared localization of the tip of a surgical tool allows correlation of anatomic situation and patient's spiral CT or MRI data set. Defined reference points exposable in the anatomic situation and visible in the data set of the patient are needed for registration of the system.

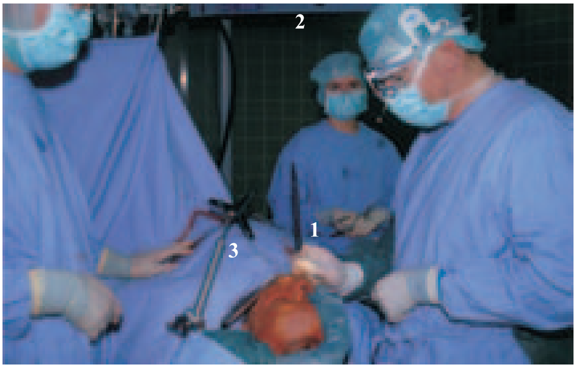

Fig. 1: Surgical Navigation Tool (Stryker-Leibinger, Germany): the infrared LED's of the pointer (1) are detected by the infrared cameras (2). Patient's head is fixed to a Mayfield clamp and movement is tracked by the dynamic referrence frame (3).

Registration with anatomical landmarks or skin fiducial markers lack of accuracy, registration with devices fixed within the oral cavity interfere with surgical procedures. Fiducial markers fixed to bone screws is invasive and limited to one surgical intervention few days after data acquisition.

Non invasive registration for multiple use in the same patient can be achieved fixing markers for CT or MRI scans to an individually performed occlusal splint (fig. 2) with high accuracy (approximately 1 mm). Only in edentulous patients there is still a need for invasive markers fixed to intra- end extraoral temporary implants. Referencing of the navigation system is done by correlation of the outlined markers in the CT/MRI to the markers in the anatomic situs by the tracked tip of the pointer.

The head of the patient is normally fixed to a Mayfield clamp wich is tracked by an dynamic reference frame to allow changing of the position during operation. Non invasive tracking can be achieved fixing this dynamic reference frame to the occlusal splint. With this technique also navigational surgery of the mobile mandible can be performed. With frameless stereotaxy the surgeon is able to localize any desired anatomical structure with the pointer and lead the surgical intervention to the preplanned and simulated result. With specific technique he is also able to guide the tip of any tracked surgical tool (drill, fraise, chisel or endoscope) or to lokalize the focus of a surgical mikroscope [Schramm et al., 1999b].

Fig. 2: Occlusal splint with markers for data acquisition in the CT (for MRI scans gadolinium filled markers are available).

Periorbital reconstruction

In craniomaxillofacial surgery advances in imaging techniques (spiral-CT, 3D-imaging) and associated technologies (stereolithographic models, CAD/ CAM) have led to improved preoperative planning within the past years. Stereolithography models are suitable to resemble the actual situation of the patient three-dimensionaly situation of hard tissue defects and allow to some degree pre- or intraoperative manufacutring of individual prostheses; all they do not fulfill the requirements for craniomaxillofacial plastic and reconstructive procedures i. e. preoperative planning with virtual correction, intraoperative navigation and postoperative control. Stereolithographic models resemble just one given situation within the greyscale of the acquired spiral-CT data set. They always imply the mistake of "pseudoforamina" in thin bony structures, which are widely present in the (peri-) orbital region.

In contrast, a spiral-CT data set allows information on a variety of either soft and hard tissue questions, which is just limited by the way of transformation of the information from the radiologist to the craniomaxillofacial surgeon. However, to get sufficient information on the preoperative situation the surgeon himself has to get familiar with the so called surgical anatomy. Modern navigation systems provide the possibility to handle easily the natively acquired CT-data set, so that the surgeon can adapt the greyscale and the reconstructions to his demands. This is very important especially in cases of enophthalmus to assess exactly the displacement of orbital contents. Furthermore, the spiral-CT/MRI data set can be used for measuring and virtual correction. The following procedures can be achieved:

1. Measurement of distances allows for exact intraindividual comparison of form.
2. Volume measuring allows for precise judgement on orbital contents.
3. Mirroring parts of the data set to an individually created treatment aim allows exact restoration of form in defined dimensions.
4. Virtual insertion and positioning of autologous bone grafts realizes preoperative simulation of augmenting defects within and around the orbit.
5. Outlining of vital and important anatomical structures like the optic nerve is easily possible.
6. Intraoperative navigation allows to check on anatomy online and to compare preoperatively planned contours with present situation before, during and after correction.
7. In cases where postoperative control spiral-CT/MRI are performed (extended craniofacial reconstructive surgery) changes between the preceding and the actual CT/MRI are easily assessable.

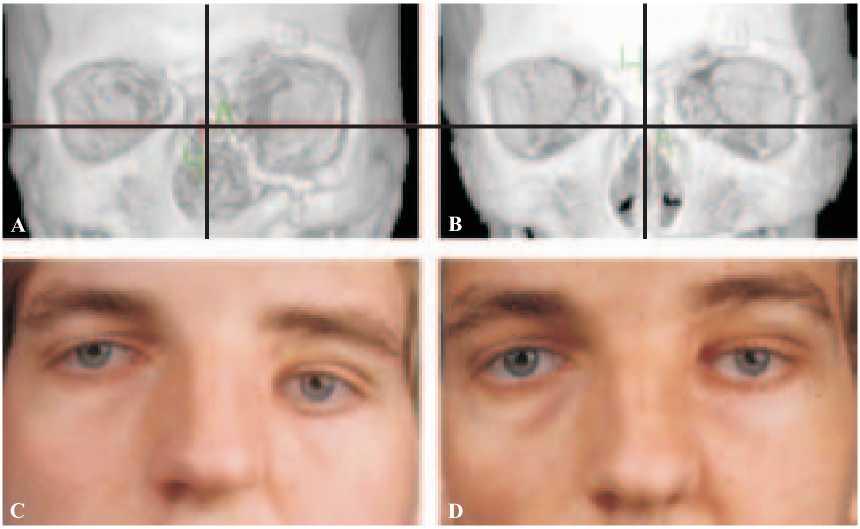

Fig. 3: Periorbital deformation: preoperative 3D reconstruction view (A) and clinical view (C). The simulationof the intended reconstruction result is performed mirroring the uneffected side in the CT data set (B). Orbital reconstruction was performed using navigational surgery. The clinical view 6 month after surgery is shown (D).

Especially in en- or exophthalmus cases measurement of the sagittal projection can be done in the same position on the workstation like the patient will be on the operating table. The sagittal projection of the eyeball can virtually be marked and corrected. To assess asymmtery proper measurement of distances between anatomic structures will help to determine the severity of a deformation. Within the orbit transverse, cranio-caudal and posterior-anterior measurement allow to determine areas of deficient bone and to evaluate how much grafted bone volume or reconfiguration of periorbital bone is necessary. By this procedure the surgeon himself is not limited to an subjective clinical etsimation of the asymmetry but he get's familiar with the individual discrepancies in all three dimensions. The diagnostic value of the multiplanar assessment including the 3D-images is one of the most important features of the system.

Additionally to measuring functions the volume rendering tool allows evaluation of affected and non affected orbital contents with individual $mm^3$3-figures. By this method the orbit can be directly compared to the other side. The majority of orbital deformities is unilateral, so that most of cases can be approached by this side to side comparison. A further development of the idea to compare one side to the other is the mirroring tool (fig. 3). The surgeon has to define the individual level, to which the data set shall be mirrored from the unaffected to the deformed side, an has to set the range, within which the mirroring process shall be performed. The software guides the operator step by step through this procedure. The optimal virtual reconstruction can be done and stored. During the operation these new contours can be navigated and serve as a control of the ongoing orbital reconstruction.

Furthermore outlining of anatomical structures can be performed before the operation, so that during the corrective procedure structures like the optic nerve can be avoided. Additionally virtual limits for bone graft positions can be marked, so that calvarian split grats are not placed beyond these marks. Intraoperatively either the native CT-data set or the modified CT-data set can be used, so that navigation of intraoperatively achieved reconstruction in comparison to preoperative virtual correction is possible at any step of the operation. This means a real innovation in planning and correction especially of orbital deformities [Gellrich et al., 1999].

Optic nerve decompression

Traumatic optic neuropathy in severe skullbase trauma cases requires decompression of the optic nerve if there is loss of vision due to dislocated bony fragments or if the vision decreases under drug therapy with high dose steroids. The operation is performed with a surgical microscope. Preoperative planning of the surgical approach can be transformed into the monitor of the microscope to navigate the surgeon to the optic canal (fig. 4).

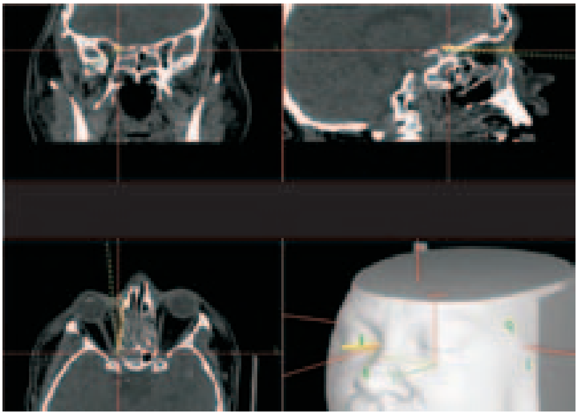

Fig. 4: Decompression of the optic nerve (intraoperative monitoring). The center of the cross shows the focus of the operation microscope. With this technique the surgeon is able to localize any structure of the anatomic situation.

The focus of the microscope is correlated to the CT data set, so the surgeon is able to identify the anatomic structures he sees through the lens by watching the CT scan at any time. Using frameless stereotaxy the decompression of the optic nerve in trauma or tumor cases becomes a safe and predictable as well as a minimal invasive procedure [Schramm et al., 2000a].

Tumor surgery

Frameless stereotaxy allows minimal invasive approaches for biopsy of suspected tumors of the midface and skull base (fig. 5) by guiding the surgeon for example via an intraoral approach to the pathologic process. Therefore the safety of minimal invasive surgical procedures such as endoscopic surgery of paranasal sinuses or skull base, biopsy of suspicious tissues and tumor resections through an intraoral approach are increased by intraoperative navigation.

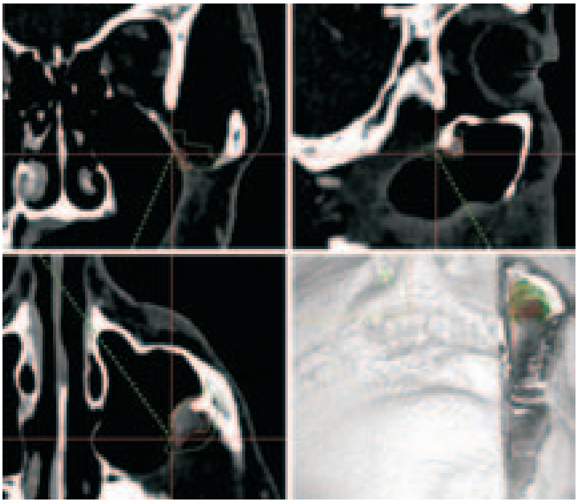

Fig. 5: Image guided biopsy (intraoperative view). The center of the cross shows the tip of the tongue on the posterior wallrt of the left maxillary sinus.

Treatment of malignancies in cranio maxillofacial surgery however requires more than exact localization of anatomical structures. Ablative tumor surgery requires detailed and exact planning using computed tomography (CT) and/or magnetic resonance imaging (MRI) to show extension of the malignoma, to define intended safety margins and to point out relevant structures. Adjuvant pre-, intra- or post-operative chemo- and radiotherapy requires the informations also. Reconstruction following tumor resection especially in the midface and orbit region demand reliable information also to choose correct type and volume of grafts and to predict the outcome.

Computer assisted treatment improves preoperative analyzing by combining CT and MRI data for valid 3D visualization of the anatomiy position. Pre- and post-therapeutic tumor volume (surgery, chemotherapy, radiotherapy) can be assessed precisely in three dimensions to prove the efficiency of adjuvant therapies and to detect recurrences. The pretherapeutic tumor volume can be transfered to the latest dataset to perform resection within the pretherapeutic borderlines (fig. 6) increasing radicality of treatment. Immediate reconstruction of severe cranio maxillofacial deformities after tumor resection can be easily performed by navigational surgery using the pretherapeutic CT scan as a perfect simulation of the intended reconstruction result).

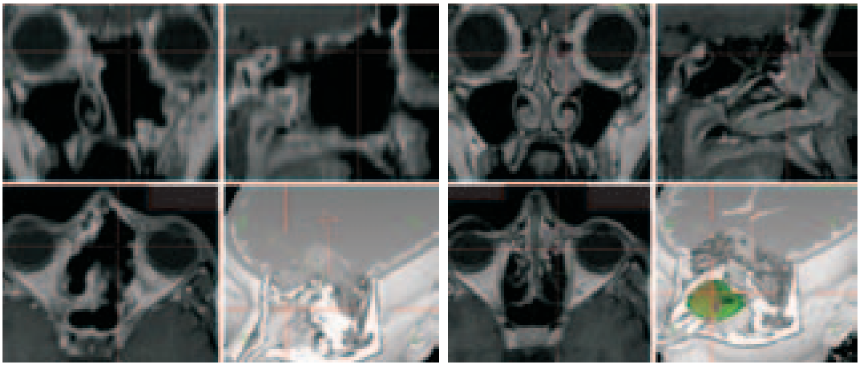

Fig. 6: Esthesioneuroblastoma after adjuvant chemotherapy (A). The original tumor (outer margin) volume before chemotherapy was transferred to the data set to faciliate resection inside the prethera-peu-thic margins. The postoperative control (B) demon-strates radical resection and adequate immediate reconstruction of the left orbit.

Intraoperative navigation makes radical tumor surgery more reliable by facilitating the safety margins, saving vital structures, guiding the radiation tube especially in intraoperative irradiation and primary reconstruction according to the preoperative situs. In secondary reconstruction cases the needed size and shape of the graft can be assessed preoperatively and their position intraoperatively controlled precisely [Schramm et al., 2000a].

Oral implantation

Installation of fixtures for prosthetic reconstruction in the upper jaw in patients with extensive bone and soft tissue defects is still a challenge. These situations usually require the support of vascularized bone or composit grafts and secondary insertion of endosseous implants. The zygomatic fixture (Brånemark System, Nobel Biocare, Köln, Germany) provides additional support in the above described situations by anchoraging implants in the zygomatic bone. The dimension of these zygomaticus fixtures and the complex anatomy due to previous surgical procedures demand specific treatment for a precise and safe insertion of the implants. Preoperative planning and intraoperative monitoring of the navigational guided position of zygomaticus fixtures after subtotal maxillectomy seems to be a helpfull device. Bilateral insertion of zygomaticus fixtures additional to standard Brånemark fixtures placed in the remaining anterior maxillary bone or inilateral insertion of two parallel zygomatic implants after partial resection of the maxilla are faciliated for navigational surgery (fig. 7). The use of zygomatic fixtures after ablative tumor surgery with resection of the maxillary bone provides immediate prosthetic reconstruction without additional bone grafting. Computer assisted insertion of these implants improves preoperative planning by 3D visualization of the anatomic situs and virtually positioning of the fixture and faciliates clinical procedure by guiding the drill to the intended position.

In case of extensive preprosthetic bone grafting procedures the computer assisted planning of insertion of dental implants allows the preoperative comparison between prosthetic demands for the implant axis and bony tissue. The intraoperative navigation of the insertion of standard dental implants in the maxilla and in the mandible has no benefits compared to standard insertion techniques. The higher radiation dose for using CT scans instead of panoramic X-rays demands restrictive use for navigation in oral implantation [Schramm et al., 2000b].

Fig. 7: Computer assisted insertion of two zygomatic implants (intraoperative view). The center of the cross shows the tip of the drill, the dotted line shows the angulation of the drill. The clinical view after prosthodontic restauration demonstrates the suficcient esthetic result.

Conclusion

The higher radiation dose of the CT scan demands restrictive use of navigation systems. Precise registration of the system is the mean precondition to reach acceptable accuracy. For the described indications in cranio maxillofacial surgery navigational surgery is a helpfull tool for minimal invasive surgery, increasing radicality of tumor treatment, preventing damaging of vital structures and leading the reconstruction to preplanned, defined results. Indications are tumors of the midface and skull base, orbital and midface reconstruction, optic nerve decompression, complex orthognathic and cranio-facial surgery and the insertion of zygomatic fixtures. Future perspectives are simulation of multiple osteotomies and moving various fragments to achieve virtual surgery for any kind of oral and cranio-maxillofacial surgery [Schmelzeisen et al., 2000, Schmelzeisen et al., 2003, Schramm et al., 2001a, Schramm et al., 2001b].

References

Gellrich, NC, Schramm, A, Gutwald, R, Schön, R, Husstedt, H, Schmelzeisen, R (1999), "Computer assisted planning and surgery in orbital reconstruction", *CARS '99,* ELSEVIER, New York p 1042.

Gellrich, NC., Schramm, A, Hammer, B, Rojas, S, Cufi, D, Lagrèze, W, Schmelzeisen, R (2003), "Computer-assisted reconstruction of unilateral posttraumatic orbital deformities", *J Plast Reconstr Surg*, (in press).

Schmelzeisen, R, Schramm, A, Schön, R (2000), "Future perspectives in cranio-maxillofacial reconstruction", *Asian Dentech Proc*, Vol. 1, No. 1, pp. 7–12.

Schmelzeisen, R, Schramm, A, Gellrich, NC, Schön, R, Otten, JE (2003), "Navigation-guided resection of temporomandibular joint ankylosis promotes safety in skull base surgery", *J Oral Maxillofac Surg*, (in press).

Schramm, A., Gellrich, NC, Schimming, R, Glaeser, R, Schneider, U, Schmelzeisen, R (1999a), "Computer assisted insertion of zygomaticus fixtures (Brånemark System®) after ablative tumor surgery", *Int Poster J Dent Oral Med,* Vol. 1, No. 4, p. 25.

Schramm, A, Gellrich, NC, Schön, R, Naumann, S, Bühner, U, Schmelzeisen, R (1999b), "Non-invasive referencing in computer assisted surgery", *Comput Biol Med,* Vol. 37, No. 2, pp. 644–645.

Schramm, A, Gellrich, NC, Gutwald, R, Schipper, J, Bloss, HG, Hustedt, H, Schmelzeisen, R, Otten, JE (2000a), "Indications for computer assisted treatment of cranio-maxillofacial tumors", *Comp Aid Surg* Vol. 5, No. 5, pp. 343–352.

Schramm, A, Gellrich, NC, Randelzhofer, P, Schneider, U, Gläser, R, Schmelzeisen, R (2000b), "Use and abuse of navigational surgery in oral implantation", *CARS 2000*, ELSEVIER, New York, pp. 923–926.

Schramm, A, Gellrich, NC, Stricker, A, Schön, R, Gutwald, R, Schmelzeisen, R (2001a), "Computer aided cranio-maxillofacial distraction", *2001 Distraction Odyssey,* Monduzzi Editore, Bologna, pp. 221–227.

Schramm, A (2001b), "Navigational procedures in orthognathic surgery", *J Kor Assoc Oral Maxillofac Surg,* Vol. 27, No. 1, pp. 24–26.

Schramm, A, Stricker, A, Gellrich, NC, Schmelzeisen, R (2002), "Computer assisted insertion of oral implants",*Mediterranean Dental Implant Congress 2002,* Monduzzi Editore, Bologna, pp. 57–60.

Assessment of image quality of low-dose multi-slice spiral CT and cone beam CT imaging for 3D image based maxillofacial surgery simulation

Miet Loubele[1], Filip Schutyser[1,2], Siddharth Srivastava[1], Frederik Maes[1], Dirk Vandermeulen[1], Robert Hermans[3], Reinhilde Jacobs[4], Guy Marchal[3], Paul Suetens[1]

[1] Medical Image Computing (ESAT+Radiology), Faculties of Engineering and Medicine, UZ Gasthuisberg, Leuven, Belgium
[2] Medicim NV, Sint-Niklaas, Belgium
[3] Department Of Radiology, UZ Leuven, Belgium
[4] Oral Imaging Center, Faculty of Medicine, KU Leuven, Belgium

Abstract

In this study the accuracy of bone segmentation by global thresholding on low-dose CT images acquired with multi-slice and cone beam CT-scanners is investigated.

With an image registration-based method the image quality was assessed. The principle of this new validation method is comparing thickness measurements across measure lines, defined perpendicular to the bone surface at corresponding points in the test image and an 'ground truth' image. First the method was applied to clinical and low-dose multi-slice CT-images of the European Spine Phantom (ESP) and a skull phantom. Next, the method is applied on multi-slice CT-images and cone beam CT-images of a skull phantom.

The tests on the clinical image (1) of the ESP, the low-dose images (2) of the ESP, the low-dose images (3) of the skull phantom and the cone beam CT-images (4) of the skull phantom gave a mean difference and standard deviation (SD) of the thickness measurements of: 0.2 mm and 0.3 mm (1), 0.3 mm and 0.5 mm (2), 0.11 mm and 0.48 mm (3) and 0.5 mm and 0.5 mm (4).

The clinical image can be used as a ground-truth image for validation purposes. The images acquired with the lower radiation dose can be used for image-based surgical planning.

Introduction

For the planning of maxillofacial [1] and oral implant surgery [2], multi-slice CT imaging is commonly used. Since conventional CT protocols are generally associated with high radiation dose levels, a big research effort was spent in lowering the effective radiation dose for the patient [3], [4], [5], [6] and [7].

The radiation dose can be lowered by using a modified protocol on a multi-slice CT-scanner [3], [4], [5] and [6] or by using Cone Beam Computed Tomography (CBCT) [7], [8] and [9]. CBCT has short acquisition times (about 20 s) with a significantly lower effective radiation dose [7], [8] and [9]. However, the use of the lower acquisition dose results in an increased noise level in the images. Therefore the image quality of these images has been investigated for low-dose protocols on Multi-Slice CT [3] and [6] and for CBCT [7], [10], [12]. The literature describes different methods for the validation of image quality. A first method is comparing thickness measurements of the bone of a skull on the images by a human observer at a small number of points with ground-truth measurements acquired in vivo [10], [13]. A second method defines important landmarks for the pathology under investigation and then scores the visibility of these landmarks in the images based on a group of observers [3] and [11]. Finally [12] describes a way for assessing the geometrical accuracy of the NewTom 9000 for the use in implant based planning, based on a geometrical object with known accuracy and 216 measure points of which the geometry is exactly known.

In surgery simulations, bone models are used for oral implant planning or planning osteotomies in maxillofacial surgery. For high success rates of these types of surgery it is important that the accuracy of the bone models is known. This requires a new way of assessing the image quality. Therefore the aim of this research was to evaluate the accuracy of bone models generated with marching cubes based on a global threshold in these low-dose images.

The problem for rating the segmentation is the availability of a ground-truth. In [14] the European Spine Phantom is used for validating the segmentation algorithm. In [15] automatic bone thickness measurements at six points were performed for some different HU. We preferred to use a registration-based approach for evaluating the quality of bone segmentation based on a global threshold value. The CT images obtained with lower acquisition dose are registered with a CAD description or a clinical CT-image of the imaged object. The accuracy was performed by comparing thickness measurements of the bone measured in both images at regions of interest at corresponding places [16].

Material and Methods

Image Data Acquisition

Three different types of datasets were used. Each dataset consists of a reference image and an object image of a phantom. The reference image is a geometrical description of the phantom or a CT-image acquired with a clinical protocol. The object image is a CT-image of which the segmentation accuracy is assessed.

European Spine Phantom

The first dataset consists of CT-images of the European Spine Phantom (ESP) [17]. The ESP is a geometrically defined semi-anthropomorphic phantom. It contains a spine insert consisting of three vertebrae of increasing bone mineral density and thicknesses of cortical structures. It is made of water- and bone-equivalent solid materials. Furthermore the manufacturing accuracy of the ESP is below 0.1 mm. The high geometrical accuracy makes this phantom very attractive for assessing image quality of CT images. The reference image of these dataset is a CAD-model of the ESP. The CT-images were acquired with the clinical protocol and the low-dose protocol, which is defined in Table 1 [18]. In [18] the effective radiation of the low-dose protocol was measured at 0.18 mSv, which is 12.7% of the radiation dose of the clinical protocol being 1.5 mSv.

Tab. 1: Parameters of a clinical used protocol and the low-dose protocol for maxillofacial imaging on the Somatom Sensation 16, (Siemens, Erlangen, Germany)

Parameter	**Clinical protocol**	**Low-dose protocol**
Slice thickness [mm]	0.75	0.75
Slice collimation [mm]	0.75	0.75
Slice increment [mm]	0.4	0.4
Table feed [mm/s]	6	12
Pitch p	0.5	1
Current x time [mAs]	90	28
Potential [kV]	120	80
Rotation time [s]	0.75	0.75
Scan length [mm]	225	227
Scan time [s]	29.48	14.19
$CTDI_{vol}$ (mGy)	20.16	2.5

Skull phantom I

The second study object is a skull phantom. It consists of a complete dry skull embedded in a soft tissue simulating material. Because there is no geometrical description of the skull phantom available, the reference image is the image obtained with the clinical protocol. The reference image and the object image of this phantom were obtained respectively with the clinical protocol and the low-dose protocol defined in Table 1.

Skull phantom II

The third study object is also a skull phantom. It is similar to skull phantom I, but with another skull. The references image was acquired with the Somatom VolumeZoom (Siemens, Erlangen Germany) operated at 90 mAs and 120 kV. The object image was acquired with the NewTom 9000 CBCT (Quantitative Radiology, Verona, Italy) operated at 2.3 mA (mean) and 110 kV.

Segmentation

Noise reduction

The noise level of the low-dose images is higher than with images acquired with a clinical protocol. For that reason, the usefulness of anisotropic diffusion filtering for noise reduction was tested. For this purpose five iterations of the curvature flow anisotropic diffusion filter are performed. For the implementation of this filter, the Insight Segmentation Toolkit (ITK) [19] has been used.

Determination of the threshold value

For bone segmentation a global threshold was used. Two methods for the determination of a global threshold value were considered.

For the first method the 50% threshold value is used [20]. This threshold value is defined in the following way: if the intensity profile of a measure line perpendicular to a bone edge of an image is considered, the intensity of the point on the edge is the average of the maximum and the minimum value of the profile being considered. This threshold value was calculated for the ESP for the mean intensity profile for the different anatomical structures.

Because the 50% threshold value only can be calculated when the position of the edges is already known, this is not the ideal strategy for defining a threshold value. Therefore also another way for defining the threshold value was used. The distribution of the intensity values of the images can also be considered as a mixture of Gaussian functions. Here, the histogram is modeled as the sum of two Gaussians. These Gaussians were fitted with the Stochastic Expectation Maximization algorithm like suggested in [21]. The threshold value for bone was defined as the intersection of the two Gaussian curves.

Validation Method

The principle of the validation method is comparing thickness measurements across measure lines, defined perpendicular to the bone surface at corresponding points in the reference image and the bone image. Below, the different steps for the validation method are explained.

Registration from the reference image to the object image

The reference image is registered to the object image with multi-modality registration by maximisation of mutual information [22]. This method computes a rigid transformation (á) that maps every location in the reference image volume space to the object image volume space. As a result, measure lines, defined at particular positions of interest in the phantom description, can be mapped through the transformation (á) from the reference image on the object image. The registration step is illustrated in fig. 1.

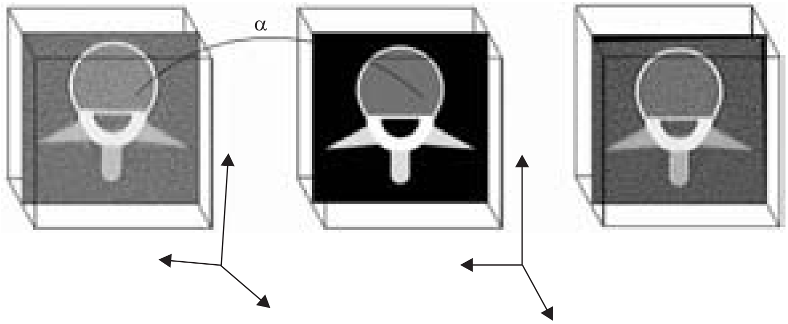

Fig. 1: Illustration of the registration from the reference image to the object image. The reference image is a CAD-model of the ESP and the object image is a CT-image of the ESP.

Definition of the Measure lines

The measure lines are defined perpendicular to the bone surface. In case the reference image is a geometrical description, these measure lines are part of the geometrical description. In case the reference image is a CT-image, the starting point and the direction of the measure lines are selected from the normal vectors of a triangulated model of a "filled" bone segmentation of the image. This filled bone segmentation is calculated with a global threshold operation followed by a special closing operation like suggested in [14]. This special closing operation consists of a 3D dilatation, a 2D close holes operation for each slice and finally a 3D erosion.

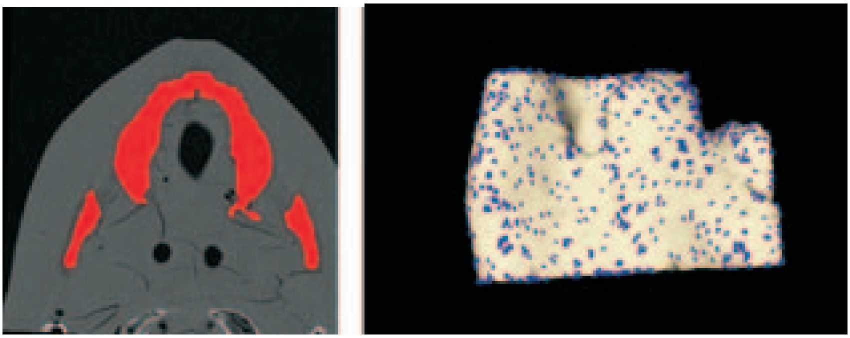

(a) (b)

Fig. 2: Illustration of the "filled" bone segmentation (a) in a slice of a CT-image of the skull phantom on the Somatom VolumeZoom (Siemens, Erlangen, Germany) and of a part of the triangulated model of the filled bone segmentation (b). The starting points of the measure lines are indicated with blue dots.

Thickness measurements

Along the measure lines intensity profiles are calculated for the reference image, for the filled bone segmentation of for the reference image and of the object image with the use of trilinear interpolation. The thickness measurements are performed in the regions of interest. For each region of interest, the begin point, the endpoint and the length of the measure lines is determined based on the bone thickness in that region.

For the reference image and the object image, the position of the bone surface is calculated along the measure line based on a global 1D threshold operation. If more candidates are found for the position of the bone surface, the two positions the smallest distance to the begin point and the end point are selected. More candidates can occur when the bone consists of two cortical structures surrounding a spongiosa part. In fig. 3 the method for the thickness measurement is illustrated.

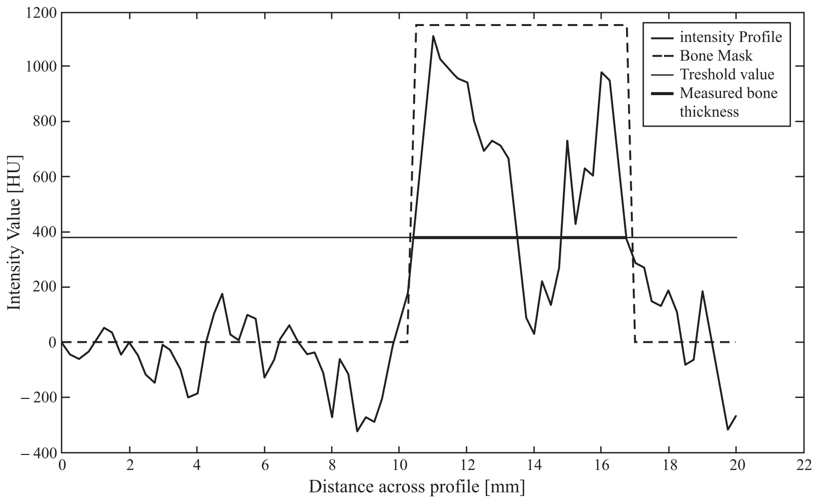

Fig. 3: Illustration of the thickness measurement along a measure line.

Results

European Spine Phantom

In fig. 4 CT-slices acquired with the clinical protocol, the low-dose protocol and the low-dose image that was smoothed with the curvature flow filter are shown.

(a) (b) (c)

Fig. 4: Three CT-slices of the ESP acquired with the Somatom Sensation 16 (Siemens, Erlangen, Germany). Image (a) is acquired with the clinical protocol; image (b) is acquired with the low-dose protocol and image (c) is the low-dose image to which the curvature flow filter has been applied.

Segmentation

Five iterations of the curvature flow diffusion filter were performed to the low-dose image for reducing the image noise. The threshold value was calculated with the two methods described above. The 50% threshold value was searched for the three types of images; the threshold value, determined by the intersection of the two Gaussian functions, was only calculated for the clinical protocol. The calculation of the threshold values is shown in fig. 5.

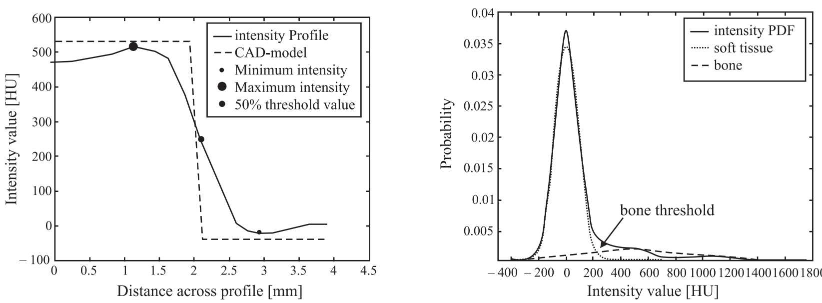

(a) (b)

Fig. 5: Illustration of the two methods for the calculation for the threshold value for bone of the ESP imaged with the clinical protocol. Figure (a) shows the calculation of the 50% threshold value for the transverse direction of the first spinous. Figure (b) shows the calculation of the bone threshold value as the intersection of two Gaussians fitted to the histogram.

Thickness measurements

Based on the two types of calculated threshold values, the diameter and length of the three bodies, and the thickness and the length of the three spinous processi were calculated. The positions of the measure lines perpendicular to the bone on the CAD-model are shown in fig. 6. In Table 2 a summary for the thickness measurements for the 50% threshold value is listed. Table 3 shows the difference in thickness measurements between both threshold determination methods for the clinical protocol. Because the ESP consists of different materials, for each material the density is given.

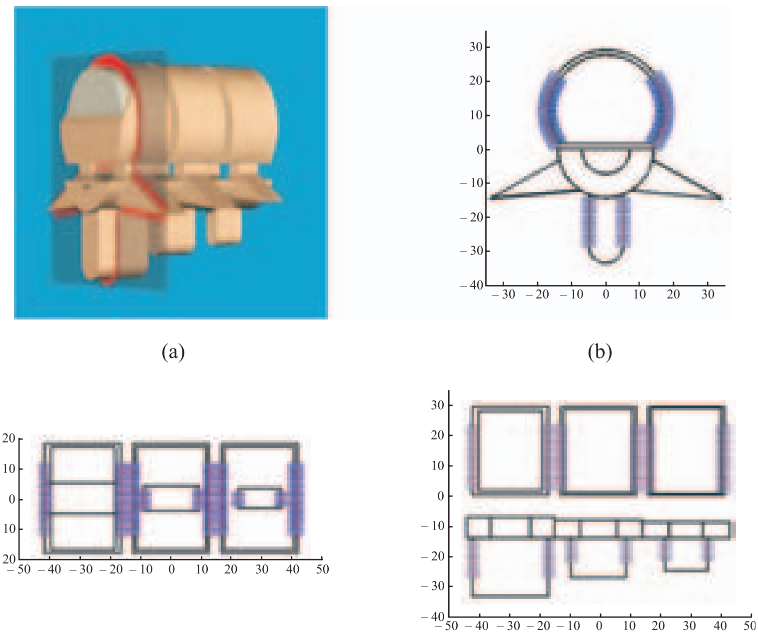

(a) (b) (c) (d)

Fig. 6: Images representing the ESP-phantom. In the first picture, a CAD-model of the ESP is The other pictures show the transverse, the coronal and the sagittal view of the CAD-model of the ESP. The start points of the measure lines are indicated with red dots and the direction of the measure lines is indicated with thin blue lines. The units on the axis are measured in mm.

Tab. 2: Results of the thickness measurements of the bone in the ESP for images obtained with the clinical protocol and the low-dose protocol on the Siemens Senstation 16 (Erlangen, Germany).

Anatomical structure	**Variable**	**ESP specification [mm]**	**Number of measure lines**	**Measured Bone Thicknesses (mean ± SD) [mm]**		
				Clinical Protocol	**Low Dose protocol**	**Low Dose protocol + filtering**
Body 1	**Diameter**	36.0	21 × 75	35.97 ± 0.06	35.98 ± 0.43	36.04 ± 0.18
	Length	25.0	22 × 48	25.15 ± 0.18	25.02 ± 1.06	25.12 ± 0.55
Body 2	**Diameter**	36.0	23 × 75	36.12 ± 0.06	36.23 ± 0.45	36.33 ± 0.20
	Length	25.0	22 × 48	25.69 ± 0.25	25.80 ± 1.11	25.78 ± 0.70
Body 3	**Diameter**	36.0	23 × 75	36.50 ± 0.11	36.54 ± 0.89	36.76 ± 0.56
	Length	25.0	23 × 48	25.82 ± 0.53	26.13 ± 1.50	26.04 ± 1.16

Anatomical structure	Variable	ESP specification [mm]	Number of measure lines	Measured Bone Thicknesses (mean ± SD) [mm]		
				Clinical Protocol	Low Dose protocol	Low Dose protocol + filtering
Spinous 1	**Thickness**	10.0	30 × 25	10.04 ± 0.14	10.00 ± 0.53	9.99 ± 0.42
	Length	25.0	13 × 18	24.73 ± 0.29	24.85 ± 1.01	24.65 ± 0.55
Spinous 2	**Thickness**	8.0	20 × 17	7.97 ± 0 .12	7.95 ± 0.53	7.92 ± 0.38
	Length	18.0	8 × 14	17.82 ± 0.28	18.02 ± 0.85	17.96 ± 0.59
Spinous 3	**thickness**	6.0	16 × 14	5.82 ± 0.76	5.79 ± 0.86	5.73 ± 0.88
	Length	14.0	7 × 10	13.76 ± 0.24	13.86 ± 1.02	13.78 ± 0.61

Tab. 3: Comparison of the use of the two different methods for defining the bone threshold.

Anatomical Structure	Variable	ESP specification [mm]	Material Hydroxa-patitie densities [mg/cm³]	50 % threshold Value[1] [HU]	Measured Bone thickness (mean±SD) [mm]	
					50% threshold	threshold value 225 HU
Body 1	**Diameter**	36.0	800	757	35.97 ± 0.06	35.97 ± 0.06
	Length	25.0		440	25.15 ± 0.18	26.02 ± 0.22
				451		
Body 2	**Diameter**	36.0	800	615	36.12 ± 0.06	36.12 ± 0.06
	Length	25.0		298	25.69 ± 0.25	26.02 ± 0.26
				276		
Body 3	**Diameter**	36.0	400	374	36.50 ± 0.11	36.48 ± 0.10
	Length	25.0		156	25.82 ± 0.53	25.65 ± 0.80
				178		
Spinous 1	**Thickness**	10.0	400	243	10.04 ± 0.14	10.10 ± 0.13
	Length	5.0		243	24.73 ± 0.29	24.90 ± 0.29
				243		
Spinous 2	**Thickness**	8.0	400	254	7.97 ± 0.12	8.06 ± 0.12
	Length	18.0		265	17.82 ± 0.28	18.04 ± 0.28
				243		
Spinous 3	**Thickness**	6.0	400	254	5.82 ± 0.76	5.07 ± 0.51
	Length	14.0		265	13.76 ± 0.24	14.02 ± 0.25
				254		

Skull Phantom I

In fig. 7 CT-slices acquired with the clinical protocol, the low-dose protocol and the low-dose image that was smoothed with the curvature flow filter are shown.

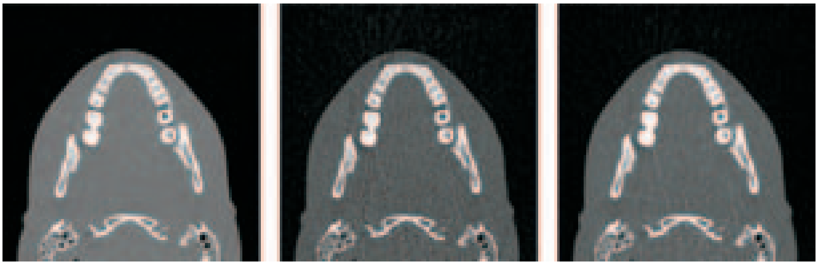

(a) (b) (c)

Fig. 7: Three CT-slices of the skull phantom I acquired with the Somatom Sensation 16 (Siemens, Erlangen, Germany). Image (a) is acquired with the clinical protocol; image (b) is acquired with the low-dose protocol and image (c) is the low-dose image to which the curvature flow filter has been applied.

Segmentation

Again the noise has been reduced by the use of 5 iterations of the curvature flow diffusion filter. The threshold value has been searched for the three images by fitting two Gaussians to the intensity histogram. For the CT-image obtained with the clinical protocol, the CT-image obtained with the low-dose protocol and the CT-image obtained with the smoothed version of the low-dose protocol the threshold value for bone was respectively, 404 HU, 835 HU and 586 HU.

Thickness Measurements

The differences of bone thicknesses were measured on the mandibula. The positions of the starting points of the measure lines are shown in fig. 8: Positions of the start points for the measure lines along the left ascending ramus, the right ascending ramus and the maxilla for skull phantom II.

The thicknesses were measured at 1525 measure lines. The histogram of the differences between the bone thicknesses measured in the images obtained with the clinical protocol and the images obtained with the low-dose protocol and the smoothed low-dose protocol are shown in fig. 9.

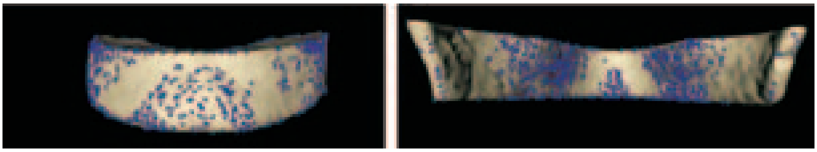

(a) (b)

Fig. 8: Positions of the start points for the measure lines along the left ascending ramus, the right ascending ramus and the maxilla for skull phantom II.

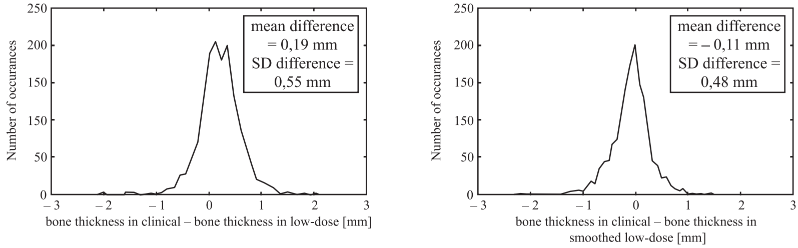

(a) (b)

Fig. 9: Histograms of the differences of the bone thickness measurements on the mandibula of skull phantom I, imaged with the clinical protocol and the low-dose protocol (a) and the low-dose protocol with smoothing (b) on the Somatom Sensation 16 (Siemens, Erlangen Germany).

Skull Phantom II

(a) (b) (c)

Fig. 10: Images of the skull phantom II. Image (a) is acquired with a clinical protocol at the Somatom VolumeZoom (Siemens, Erlangen, Germany); image (b) is acquired with NewTom 9000 CBCT (Quantitative Radiology, Verona, Italy); image (c) is image (b) to which the curvature flow filter has been applied.

Segmentation

The threshold value was calculated by fitting two Gaussians to the probability density function of the intensity values. As a result, the threshold value for the CT-image was 380 HU, for the NewTom-image 312 HU and for the smoothed NewTom image 297 HU.

Thickness Measurements

The thicknesses of the right ascending ramus, the left ascending ramus and the maxilla were calculated. Fig. 11 shows the position of the starting points of the measure lines. The results of the thickness measurements are summarized in Table 4.

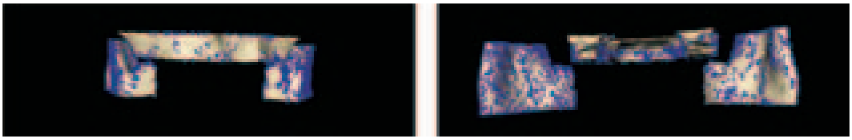

(a) (b)

Fig. 11: Positions of the start points for the measure lines

Tab. 4: Results of comparison of thickness measurements in the third dataset containing the images of a skull phantom

	Siemens thickness (threshold 380 [HU]) – Newtom thickness (threshold 312 [HU]) [mm]		**Siemens thickness (threshold 380 [HU] – smoothed Newtom thickness (threshold 297 [HU]) [mm]**	
Anatomical Structure	Number of measure lines	Difference in measured thickness (mean ± SD)[mm]	Number of measure lines	Difference in measured thickness (mean ± SD)[mm]
Left ascending ramus	1391	– 0.14 ± 0.38	1420	– 0.20 ± 0.41
Right ascending ramus	934	– 0.50 ± 0.60	938	– 0.66 ± 0.66
Maxilla	1165	– 0.47 ± 0.44	1185	– 0.58 ± 0.44

Discussion

The results of the validation method on the ESP with the clinical protocol show that the three bodies and the first two spinous processi can be segmented with global thresholding. The 50% threshold value is within the accuracy of the specification of the ESP in the transverse direction. The accuracy in the sagittal direction is worse but the standard deviation remains under 0.5 mm except for the structures of the third body. Because the 50% threshold value can only be applied when the position of the object edges is a priori known, we also investigated the accuracy of the threshold value defined as the intersection of two Gaussian functions fitted to the histogram. Table 3 shows similar results compared with the 50% threshold value, except for the sagittal direction of the two bodies. Three densities of hydroxyapatite used for simulating the bone structures in the ESP. These three materials have different intensity characteristics. This means that the assumption that the intensity histogram only consists of two Gaussians, one representing the soft tissue intensity distribution and the other representing the bone intensity distribution is not completely correct. Because the first two bodies have the highest intensity, the deviation of the 50% threshold value for these structures is the largest. By consequence, the deviation between the ESP-specification and the measured thickness is the largest for these structures. However, this problem is only observed in the sagittal direction and not in the transverse direction. As a result, we can conclude that the threshold value defined by the intersection of the Gaussian functions is acceptable. A segmentation accuracy close to the specification of the ESP was obtained. This means that this method is applicable as a ground-truth for comparing bone segmentation algorithms on images acquired with a protocol with lower acquisition dose.

The reduction of the radiation dose lowers the accuracy for bone segmentation. This is shown in Table 4 by a difference between the mean measured bone thickness and the ESP specification and by the higher standard deviation of the measured bone thickness. The usage of curvature flow diffusion filter reduces the standard deviation and enables a mean measured thickness that only differs a little bit from the ESP specifications.

To move towards the anatomy of interest, a skull phantom was used to test bone segmentation on CT-images acquired according the low-dose CT-protocol on the multi-slice CT-scanner. Based on the test results shown in Fig. 9, we again can see that there is a good correspondence between the two threshold values calculated by fitting two Gaussians through the image histogram because the mean difference of thickness measurements is 0.11 mm and the standard deviation is smaller than 0.5 mm. Based on figure 9 we also can see that there is also a good accuracy of the bone in the smoothed low-dose image.

Finally, the accuracy of the bone segmentation of the NewTom scanner was investigated with a skull phantom. The use of a curvature flow anisotropic filter for improving the segmentation accuracy was also investigated. Based on the results of the NewTom images we can conclude that the segmentation accuracy for the NewTom scanner doesn't improve by the use of curvature flow filtering, and so the segmentation accuracy is influenced by other factors. So for the NewTom images, a better segmentation algorithm than thresholding may be needed.

Conclusions

From the accuracy results with our validation method, we conclude that the low-dose images can be used for image-based surgical planning.

Acknowledgments

This research is part of IWT/GBOU/020195. We thank Johan Van Cleynenbreugel with his contribution to this research. We thank Walter Coudyzer for the technical assistance. We thank Pieter De Groeve and Wouter Mollemans for the use of their software.

References

[1] F. Schutyser, J. Van Cleynenbreugel, M. Ferrant, J. Schoenaers and P. Suetens, "Image-based 3D planning of maxillofacial distraction procedures including soft tissue implication" in *Lecture notes in computer science 1935, Proceedings 3rd international conference on Medical Image Computing and Computer-Assisted Intervention – MICCAI 2000, October 11–14, 2000, Pittsburgh, Pennsylvania, USA*, 2000, pp. 999–1007.

[2] D. van Steenberghe, I. Naert, M. Anderson, I. Brajnovic, J. Van Cleynenbreugel, P. Suetens. "A custom template and definitive prosthesis allowing immediate implant loading in the maxilla: a clinical report", *International Journal of Oral Maxillofacial Implants*, vol. 17, pp. 663–670, 2002.

[3] T. Hagtvedt, T. M. Aaløkken, J. Nøtthellen and Kolbenstvedt "A new low-dose CT examination compared with standard-dose CT in the diagnosis of acute sinusitis." *European Radiology*, vol. 3, pp. 976–980, 2003.

[4] H. Imhof, Chr. Czerny, A. Dirisamer "Head and Neck imaging with MDCT", *European Journal of Radiology*, vol. 45, pp. S23-S31, 2003.

[5] H. Imhof, N. Schibany, A. Ba-Ssalamahm, C. Czerny, A. Hojreh, F. Kainberger, C. Krestan, H. Kudler, I. Nöbauer and R. Nowotny. "Spiral CT and radiation dose". *European Journal of Radiology*, vol. 47, pp. 29–37, 2003.

[6] E. Hein, P. Rogalla, K. Randolph, and B. Hamm"Low-dose CT of the paranasal sinuses with eye lens protection: effect on image quality and radiation." *European Radiology* vol. 12, pp. 1693–1696, 2002.

[7] P. Mozzo, C. Procacci, A. Tacconi, P. Tinazzi Martini, I. A. Bergamo Andreis, "A new volumetric CT machine for dental imaging based on the cone-beam technique: preliminary results," *European Radiology*, vol. 8, pp. 1558–1564, 1998.

[8] D. Schulze, M. Heiland, H. Thurmann and G. Adam, "Radiation exposure during midfacial imaging using 4-slice and 16-slice computed tomography, cone beam computed tomography systems and conventional radiography", *Dentomaxillofacial Radiology*, vol. 33, pp. 83–86, 2004.

[9] J. B. Ludlow, L. E. Davies-Ludlow, S. L. Brooks, "Dosimetry of two extraoral direct digital imaging devices: NewTom cone beam CT and Orthopos Plus DS panoramic unit" *Dentomaxillofacial Radiology*, vol. 32, pp. 239–234, 2003.

[10] C. A. Lascala, J. Panella, M. M. Marques, "Analysis or the accuracy of linear measurements obtained by cone beam computed tomography (CBCT-NewTom)", *Dentomaxillofacial Radiology*, vol 33, pp. 291–294, September 2004.

[11] D. Schulze, M. Heiland, F. Blake, U. Rother, R. Schmelzle, "Evaluation of quality of reformatted images from two cone-beam computed tomographic systems", *Journal of Cranio-Maxillofacial Surgery*, vol. 33, pp. 19–23.

[12] R. Marmulla, R. Wörtche, J. Mühling and S. Hassfeld, "Geometric accuracy of the NewTom 9000 Cone Beam CT", *Dentomaxillofacial Radiology*, vol. 34, pp. 28–31, 2005.

[13] M. G. P. Cavalcanti, S. S. Rocha, M. W. Vannier, "Craniofacial measurements based on 3D-CT volume rendering: implications for clinical applications", *Dentomaxillofacial Radiology*, vol. 33 pp. 170–176, 2004.

[14] Yang Kang, K. Engelke, W. A. Kalender, "A new accurate and precise 3-D segmentation method for skeletal structures in volumetric CT data" *IEEE Transactions on Medical Imaging*, vol. 22, pp. 586–598.

[15] G. Eggers, W. Korb, T. Welzel, S. Däuber, R. Marmulla, S. Hassfeld, "The accuracy of CT based cranial models for robotic surgery", *Proceedings Surgetica-2005*, Chambéry, France January 19–21, 2005, p 399–403.

[16] J. Van Cleynenbreugel, F. Haven, F. Maes, M.-H, Sment, G. Marchal, P. Suetens, "An image registration based approach to assess the geometrical accuracy obtainable from spiral CT imaging the European Spine Phantom." presented at 3rd International Workshop on Rapid Prototyping in Medicine & Computer Assisted Surgery, Erlangen, Germany, October 19–21, 1995.

[17] W. A. Kalender, D. Felsenberg, H. K. Genant, M, Fischer, J. Dequeker, and J. Reeve, "The European Spine Phantom – a tool for standardization and quality control in spiral bone mineral measurements by DX and QCT", *European Journal of Radiology*, vol. 20, pp. 83–92, 1995.

[18] M. Loubele, F. Schutyser, D. Debaveye, R. Jacobs, D. Vandermeulen, G. Marchal, P. Suetens, "Radiation dose versus image quality for low-dose CT protocols of the head for maxillofacial surgery and dental implant planning", presented at International Workshop on Optimisation of Dose and Performance in Interventional and Digital Imaging- DIMOND III, Leuven, Belgium, March 25–27, 2004.

[19] L. Ibáñez, W. Schroeder and the Insight Consortium NLM Insight Segmentation & Registration Toolkit, April 2003.

[20] Prevrhal, S., Engelke, K., and Kalender, W. A. "Accuracy limits for the determination of cortical width and density: The influence of object size and CT imaging parameters." *Physyics in Medicine and Biology*, vol. 44, pp. 751–764, 1999.

[21] C. Baillard and C. Barillot, "Robust 3D Segmentation of Anatomical Structures with Level Sets", in *Lecture notes in computer science 1935, Proceedings 3rd international conference on Medical Image Computing and Computer-Assisted Intervention – MICCAI2000, October 11–14, 2000, Pittsburgh, Pennsylvania, USA*, 2000, pp. 236–245.

[22] Maes, F., Collignon, A., Vandermeulen, D., Marchal and Suetens, P. Multimodality image registration by maximization of mutual information. *IEEE Transactions on Medical Imaging*, vol. 16, pp. 187–198, 1997.

[23] W. E. Lorenson and H. E. Cline, "A high resolution 3D surface construction algorithm", in Computer Graphics (Proceedings of SIGGRAPH '87), vol. 21, pp. 163–169, 1987.

9.

Case Studies
Fallstudien

A case study of threedimensional facial reconstruction: which problems can occur if no further information about the status of health and nutrition is given for the skull that has to be reconstructed?

Sabine Assmann[1], Kerrin Christiansen[1], Jörg Orschiedt[2]

[1] University of Hamburg; Institute for Human Biology; BioZ Grindel; Martin-Luther-King-Platz 3; D-20146 Hamburg

[2] University of Hamburg; Institute for Archaeology; Johnsallee 35; D-20148 Hamburg

Abstract

The presented work should pursue the question, which bandwith the variability of expressivity a face can assume if no helpful information about the anonymous skull can be given to the reconstructeur in a theoretical and practical way.

It is not visible on the skull, if the person was cachectic, in a normal condititon or adipous in lifetime. It is the same thing with diseases which have an effect on the soft tissue or external influences for example alcohol.

The person to whom the skull belonged in lifetime was known by the police, also some photographs exist. After having finished the reconstructions, a comparison of the reconstructions and the photographs should point out if one of the works is that similar to the person in lifetime in spite of missing information that a positive identification is possible by one of the reconstructions. Further, one will decide, if a positive identification would also have been possible under the wrong condition.

Introduction

The fascination of human faces was and still is unbroken. Each face has its characteristic form of the nose, the eyes, the lips, the chin and each face is unique.

During the observation of skeletons and especially skulls in museums, osteologic collections, historic burial grounds or other sites, one is inevitably forced on the question what the person might have looked like in lifetime, his name was, his story of life and the circumstances of his or her death. In old findings, one will get thrusted upon a mystic, scary or romantic fantasy about the deceased person, but he or she will not be found in any card index of dismissed persons.

Also actual cases are not free of guess and speculation, and the more, the less is known about the finding. But contrary to old findings, the case leads one to the question, if there are family members who are missing the person, who are waiting and who are in sorrow. If a human osteologic finding will be identified, whatever the circumstances might have been, there is a chance to give sureness to the members and might clear up the circumstances of death.

If this is not the case, the person has to stay face- and nameless.

A threedimensional reconstruction can help to give back a face to the dead and, in the best case, an identity.

If there is scanty information about the finding, which can give advice about a disease or a certain condition, a reconstruction can become difficult. If an index for a disease is found, which also occurs at the soft tissue, this information can help to come closer to the face in lifetime.

The question arises, if and how well it is possible to identify a person, even if no information is given.

This question gave reason to a case-study on a skull. It will be described in the following and is the content of my thesis.

The skull, which has been made available for this study, comes from the Institute of Legal Medicine at the University Hospital of Hamburg-Eppendorf (Germany). Because the person was known by the police, some neutral photographs exist, not only snapshots.

It was planned to look by the help of this skull, if it is possible to come that close to the appearance of the person in lifetime if neither the postcranial skeleton nor any information about the person is given. This question should be worked out in five reconstructions on the skull, respectively on a replication, in different expressions of health and nutrition.

After having finished the five reconstructions, one should look if the faces are similar among each other and if it would have been possible to identify the person with the help of one or more of the reconstructions. Further, one should look, if the person could have also been identified under a different condition than the one in lifetime. This comparison will have been done by members of Legal Medicine, of the police and such persons who are not educated in the work with faces.

It was planned to reconstruct the face five times, in the following expressions. For the different statuses of nutrition, one normal expression, one adipous, what means a fat person and a cachectic one, what means a slim person but not under the symptoms of anorexia.

For the statuses of health, two diseases would be chosen which occur in the soft tissue, but not on the facial bones.

Material and Methods

It was planned to produce all the reconstructions after the 'Manchester Method', also named 'Combined Method', which has been founded by Richard Neave [1].

This method indicates to cast every single muscle of the face, which will be coated with a layer of skin. The elaboration of the eyes, the nose, the mouth and the ears, further the expression of the chin would be worked out after anatomical guidelines.

Following these defaults, it should be possible, that every reconstruction looks like the other, only with differences, which depend on the status.

The used data are based on the tables of Richard Helmer [2]. These give 34 landmarks on the bony skull and the mandible, which are well-defined and findable on every skull.

For both sex and different age-ranges, these data give variable thicknesses, which cover the skull at the mentioned areas. For each range of age and sex and for every single landmark, an average is given; further a minimal and a maximal value.

For the different skulls, these data should have to be used as follows. For the reconstruction, which would show a healthy and normally constutioned person, the averages of the mean range would be consulted. For the adipose expression the maximal value and according to this, the minimal values for the cachectic expression. The choice of the data for the pathologic expressions would depend on the disease.

Total overview of the skull.

The most eye-catching feature of the available skull was the extremely bad condition of the teeth. In fact an extensive dental restoration was visible, but some teeth were damaged, untreated or without filling.

During the first view, the skull made a relatively durable and intact impression, which proved however as fallacy. It was nearly complete but fragile, because great parts of the spongiosa was missing, only the compacta was left but thin. So, little areas around the foramina were damaged.

The occipital bone exhibited a clearly minted exit hole, the area around the entrance hole in the sphenoid bone was damaged, so it could not be described after the guidelines.

Also the dental appearance was not complete any longer, but judged by the alveolars, there was a post-mortem loss of the teeth.

The orbitae were missing and great parts of the inner structure of the skull were extremely fragile. A detailed opinion of the orbita can be seen in fig. 1.

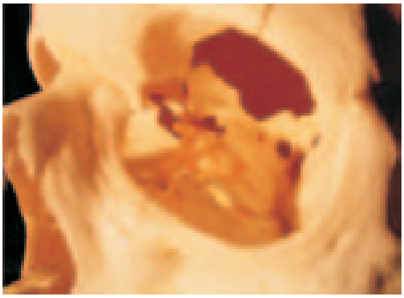

Fig. 1: Detailed opinion of the left orbita. The concave cavern was nearly completely away-broken. By the reasons of this, the inner structures became visible, which had been very filigran.

The area for the incisors was extremely broken at the mandible, not that much at the maxilla. Fig. 2 shows an impression of the mandible.

Fig. 2: A view of the mandible shows the bad dental condition, that continues at the maxilla. All quadrants show an extensive dental work, but not every single damages tooth. The alveolar area around the incisors is not intact anymore.

Also the cranial floor was not intact any longer, it exhibited small holes in numerous places, the left styloid process was missing.

In order to be able to avail itself of the values from the tables of Helmer [2], an aging and sexing of the skull is needed before starting the reconstruction. The available skull was classified as following.

For the determination of the sex one worked with tables of classification of Herrmann et al. [3]. This indicates regions, or characteristics, which exhibit that different developments at the male and female skull that they can be assigned to the respective sex with high accuracy. All given characteristics up to one showed a male development, so it could be assumed it had to concern a man.

For the determination of the age several methods were consulted. By the reasons of a missing postcranial skeleton, the age had to be defined only at the skull, other features for an ensured classification like the symphysis, the epiphyseals and the sternal end of the ribs could not be consulted.

As output criterion the tooth status was taken, at the skull the surely most meaningful criterion. Here in detail the third molar. After its status of development it could be assumed after Ubeleker [4] that that it must have concerned a young adulte person, older than 28 years. This first ageing was supported by consultation with a dentist.

This first classification let two techniques of the regulation separate for the further organization, in detail the one of Lamendin [5] and the one of Norris [6]. In the following, different techniques were used, which permit partly everyone isolated regarded only a more or less rough classification, however together a rather close allocation to a certain age. In detail, it concerned techniques, which are used in different way at teeth, namely the ones being described by Ubelaker [4] and Bass [7]. The moreover, on different places of the skull, the degree of obliteration of the suturae were regarded both ektocranial and endocranial. Further, the angle of the gonion [8] and the ramus hight were regarded. Some of the methods permitted only a rough classification in 'juvenil adult senile', but therefore they should not be ignored, they could underline/confirm the results of the other techniques. After view and evaluation of all determined possible age groups and a means from all, the skull could be assigned to an age- range from 28–33 years at the time of death.

Since at a three-dimensional facial reconstruction on the original skull does not work, it is inevitable to replicate it first. In order to ensure the intactness of the original, a pre-treating is necessary, whose extent depends on the condition of the skull.

In principle, all physiological openings are sealed, in order to receive a closed form. This is necessary, so that no casting material, which is still of a highly liquid consistency during the processing, will flow into the skull. In the available case, also the lesions at the skull base were sealed. Furthermore it was necessary to stabilize the filigrane bone remains bone inside the head so that they would get over the pre-cast. In the following, the skull was replicated in the needed number with an ordinary plaster of Paris, whereby it got a polystyrene ball for the reduction of weight into the cave of the skull.

The preparation for the actual reconstruction followed the 'Manchester method' in all five cases, likewise the correct positioning of the eyes and the structure of the cartilageous part of the nose. Here, the missing parts had to be replaced by guesswork. Also the missing incisors and canines were substituted, whereby their direction followed that one of the empty alveoles. By this replacement, a re-establishment of the upper edge of the mandible was possible, so that landmark 13 could be placed. Also the proceeding when placing the landmarks was always the same, their length differed by the planned condition in each case.

The processing steps, which would be identical in all reconstructions, will be described in the following section. The eyes, handmade ones of glass, were always fit into the orbitae after the anatomical guidelines of Wilkinson [9]. One had to pay attention for a straight and parallel view, each small deviation would be visible as a slightly, but nevertheless visible squinting.

Also the structure of the cartilageous nose was always worked out after the same process. Since the Spina nasalis was fractured, the missing part had to be replaced by guesswork. For each individual reconstruction, the data which determine the nose, were taken again and transferred upon the skull. In the comparison, the result of the nose was always the same, only varying a little.

Also the missing teeth were replaced after the same procedure upon each skull. No replacement of the molars was done, because there is no substantial relevance for a reconstruction, also they are not visible in a reconstruction with an open-represented mouth. Plastic teeth were chosen, which also find use in the building of prostheses. These teeth were taken as guide for dental defaults. Normally formed teeth were taken, no extreme developments. Following the direction of the empty alveoles, the teeth were fastened in the upper and lower jaw. All alveoles for the incisors permitted only very narrow teeth, which, particularly in the mandible, partly overlayed each other. This rather narrow development of the incisors during lifetime implied a relatively narrow lip.

Two osteologic features, mentioned in the following, would also become visible in the face. On the one hand a very well developed mentum with crests, that would be visible as a massive chin in the reconstructions. On the other hand impressions of blood vessels on both sides of the frontal bone, which let assume that during lifetime, it would have been visible under the skin.

Also the form of the eyebrows could be defined by the skull, in the detail by the upper margin of the orbitae. It would be the same in each reconstruction.

It should also be mentioned, that all faces would be represented with a slightly opened mouth, so one could orient oneself at the teeth until having completed the reconstruction.

The basic structure of the ears is always the same, however, the representation of the forms varies from ear to ear. It should be mentioned that this is not the case in the pair of ears of one person, which physiological is push-pull. No extreme forms were taken, they can supply a wrong picture from a person in lifetime and, in the worst case, prevent a positive identification.

For the ear length and ear width, the data of Weerda [10] were taken, who gives a dependency of age and a body height for these parameters. Because nothing was known about the body height, this factor had to fall out of the determination. From the classification of age, the resulting ear length was 67 mm and ear width 35 mm. These measuring data were applied to each skull.

Results

The first reconstruction should show the deceased person in healthy and normally condition. Therefor, the average values of Helmers tables were consulted. By the reasons of the age determination in the span of 28–33 years, two age-ranges coming into question overlapped. The average values of those two did not differ at all or only minimum. At deviating values of more than 2mm, the means of both were taken.

One began with the insertion of the eyes into the orbitae, followed by the reconstruction of the cartilageous structures of the nose, made of wax. By the reasons that some osteologic guidelines for the accurate structure of the nose no longer were present, it had to be replaced in best discretion. The Spina nasalis was fractured, but with the help of the existing part, a rather exact length of the nose could be defined. The form and height of the nostrils could not be fastened at the bone any more, but did result more or less from the given structure.

The procedure of the reconstruction was the same as described in the previous section. After setting the landmarks, one began with the reconstruction of the muscular structure. Already in the stadium of laying the muscles, a very much minted mentum became visible, due to the bone architecture. Occasionally, the chin seemed to have a wrong proportion, so one wanted to adjust this alleged defectiveness. In the following, this alleged wrong proportion adjusted itself. Since all the muscles were worked out embarrassingly exactly, each still existing place was reserved for a certain muscle, so that at the end they were a good match.

The complete facial musculature was covered with a layer of skin, which locked exactly with the ends of the wooden landmarks. A subsequent coloring of the finished face became redundant because the modelling mass already was colored. This gave the face a more natural appearance. On the right forehead, the vessel was visible.

After the complete drying process the developed face received lashes and was treated in such a way that the skin received a damp impression. The figures 3 and 4 show the first finished reconstruction from two different perspectives.

Fig. 3: Opinion on the first reconstruction, which shows the person in healthy and normal condition. On the right forehead, the vessel can be seen under the skin

Fig. 4: This figure shows the finished face in a frontal view. The mouth was represented in slightly opened form, so that during the whole work one could orient itself at the teeth.

The second reconstruction should represent the same face in an adipose condition. For this, the maximum values of the two age ranges were taken, with a tendency to the higher one.

Already the comparison with the preceding reconstruction let suspect that the face would clearly be more fully minted. The differences were most clearly within the ranges, where most of subcutaneous fat is settled, mainly in the region of the cheeks, especially at the location of points 21/ms (first upper molar), point 22/ mi (first lower molar) and point 32/m2 (middle of masseter, between gonion and zygion). The difference at point 21 was with 6.0 mm, at point 22 with 5 mm and at point with 4.0 mm. These differences could be recognized with the eyes. With a frontal view on the head, which had been worked under normal constitution, the ends of point 21 and point 22 did not come to the lateral end of the zygomatic arch, it was not to be assumed that a cheek bone would appear in the finished face. This was not the case in the second reconstruction. The points 21 and 22 did exceed in a frontal view, which let rounded cheeks move in the field of vision, no bone would appear under the skin.

The proceeding was the same as already described and completely resembled the first in the muscular phase, with the difference that muscles had to be prepared more thickly, in the places described above. The chin seemed to be still substantially more oversized in this reconstruction, but adapted itself to the overall view in the further process. Not all developing cavities could be filled out only with muscles, it was necessary to under-feed some muscles with fat. The heads of the wooden landmarks were still visible after the completion of the muscular phase and did show the thickness of the skin. Also this was thicker than in the previous reconstruction. There, it had been sufficient to prepare two parts of modelling mass for the skin in the available reconstruction, almost the double quantity was needed.

After according the skin, it was arranged in a way to show an adipose person. In detail, the rounded cheeks already mentioned, which defined themselves clearly to the nose in shape wrinkle and the same for the lower end of the mandible. Furthermore, more strongly minted lower eyelids as a consequence of more increased subcutaneous fat. Also increased fat in the mentum had to become visible in the face. For this, a more rounded chin and also double chin was worked out. Also a darker color was assigned to the second face. In this reconstruction the representation of the vessels on the forehead was not done, since it could be assumed that it would be embedded in fat and thus not visible.

Also the completed second face was finaltreated, so it got a damp and more alive impression. In the following figures 5 and 6, two impressions of the finished adipose face can be seen.

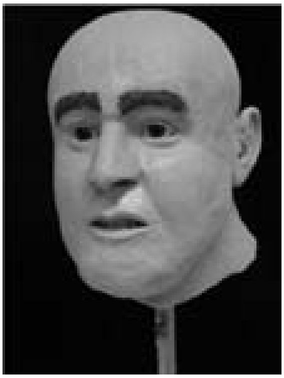

Fig. 5: The adipouse person in a frontal view. The rounded cheeks and the more distinctive lower eyelids are visible.

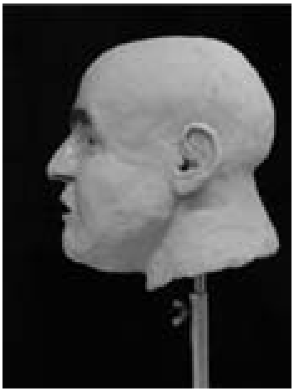

Fig. 6: The adipouse reconstruction can be seen in profile. As in fig. 5 the well-developed chin and the double-chin are visible. Also in the profile view, the cheeks seem to be rounded.

The third reconstruction should become the complement of the previous, showing the person in a cachectic condition, however not with the symptoms of anorexia. Consequentially, the minimum values of the two age ranges were taken. The differences were that small at the separate points of the two groups that they nearly could be ignored. The differences to the second reconstruction were substantial, mainly in the region of the cheeks being already mentioned. The difference of maximum and minimum of point 21 was with 12.0 mm, at point 22 with 9.0 mm, likewise at point 33. In a frontal view on the head with the landmarks it was to be seen that no zygomatic arch would appear in the finished face.

The proceeding was the same as already described. By the orientation of the landmarks, very little space for muscles remained, subcutaneous fat could hardly be used, since the remaining free areas were completely filled out by still missing muscles. Here, the skin was coated in a very thin layer and, contrary to the first reconstruction, two parts of the modelling mass were too much. In this reconstruction, vessels should be resented at both sides of the frontal bone since it was to be assumed that, as a consequence of missing subcutaneous fat substantially more structures would appear. The appearance was adapted to a person in a cadaverous condition. That means eyes laying apparently more deeply in the caves, what is a consequence of decreased subcutaneous fat, that surrounds the eyeballs. This slimmer form indicated a nose sticking out much more. The cheek bones were visible under the skin and the cheeks seemed to be shrunken. Also the mentum, which seemed to have the correct proportion for the first time during the reconstruction, did stick out.

The third face was worked out in a brighter colour, so it became a slightly palely appearance. It can be been in the figures 7 and 8.

Fig. 7: The third reconstruction is to be seen in a frontal view.

The eyes seem to lie deep in the holes, caused by missing subcutaneous fat. The cheeks appear to be shrunken, the nose seems to be bigger.

Fig. 8: The same reconstruction can be seen in the half profile. The contures of the gonion are visible under the skin. Vessels werde worked out at both sides of the Os frontale, two ones at the right side, because a slighter second one was present on the skull. This one should have been visible only at the cachectic reconstruction.

The fourth reconstruction should present the first pathologic case.

The disease should be well-considered. It should not show a clinical picture, which manifests only at the soft tissue, not at bones. Another criterion for the decision should be that the disease does not lead to death too fast, so there could have been a chance for nearbys to see the person with the symptoms of the disease. Furthermore, it should not concern an unusual or rarely occurring disease, whose symptoms at the soft tissue are nearly unknown. Following these presettings, one decided to represent the fourth person in an addiction to alcohol, but not at the final stage.

For this, an average of the minimum and average value of two age ranks was consulted. For this, the four values were added and a new average was calculated, which should represent the used value.

The casting of the muscles was the same as in the cases before. The representation of the disease would start with the casting of the skin. For this representation, no unique colour was taken, contrary to the others. The cranial bone and the ears were represented in a normal and healthy color. The face however got a reddish color with burst vessels and an eczema at the left angle of the mouth. It required some artistically skill to adapt the two colours each other in such a way that no abrupt transition would be visible. It had to be considered thus exactly, in which places of the face the two colours should turn one into the other. The lower eyelid became underlayed with a thin layer of red modelling material before being coated with skin, thus, the finished reconstruction would show an inflammed conjunctiva. The impression of the eyes was completed with lacrymal sacks.

In order to get a glassy gloss for the eyes, they were covered with lacquer, thereby also the conjunctiva received its intensive red color. For the finishing of the eyes, a layer of glue was placed on the conjunctiva, in order to give a slightly aqueous expression to the eyes. For giving the face a neglected expression, a thin and unevenly cut chin beard was worked out.

The result of the first pathological representation is to be seen in the figures 9 and 10:

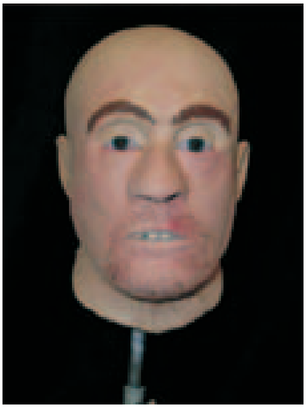

Fig. 9: This reconstuction shows the person under the marked clinical picture of the alcohol disease, but not at the final stadium.
The skin of the cheeks and of the nose is nerved with burst vessels. The inflamed conjunctuva is clearly visible, and so are the lachrymal sacks. The view seems to be sick by the reasons of missing subcutaneous fat at the upper eyelids.

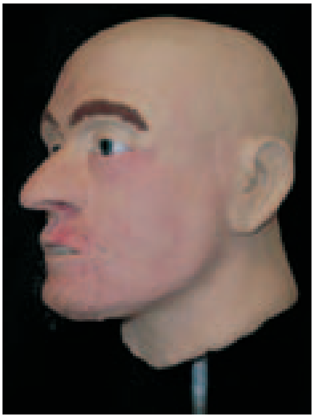

Fig. 10: The ill person can be seen in the profile. Here, the burst vessels are visible again, also the lachrymal sacks and the eczema at the left angle of the mouth.
In fig. 9 and in the actual one, the chin beard is visible, which underlines the neglected appearance.

Future work

At the time of the production of this paper the work was not yet been completely finished. The fifth face had to be reconstructed, which should represent the second pathological case.

A disease was picked out, which has to effect to the body, but only to the skin and especially to the skin of the face. The fifth face should represent the face in the marked clinical picture of the Acne vulgaris, which is a common skin disease that affects 85–100% of people during their lives [11]. The disease is characterized by noninflammatory follicular papules and comedones and inflammatory pustules or nodules in a more or less distinctive form. The acne affects those areas of the skin with the highest frequency of subcutaneous follicules, what is the neck and the face. The mean time for this disease is the adolescence, but this does not mean that an occurrence in the adulthood is impossible.

The face should be represented in normal constitution, thus using the average values, but with numerous inflammatory and nonflammatory papules and pustules, vox populi "zit". Furthermore, scars of earlier features and inappropriately treated flammatory processes.

After the completion of all reconstructions, they would be brought to the Institut for Legal Medicine of the University Hospital of Hamburg-Eppendorf. A number of persons would attend to the ceremony, amongst others members of the police, who did handle the case of the person being unknown for the reconstructeur. They would show photographs of the person in lifetime, which would then be compared with the reconstructions.

The present group would consist of persons, who are educated in the recognition of faces and those, who normally do not work with faces. All these persons should decide whether they could have identified the person in a positive way with the help of the photos of one or more of the reconstructions. The similarities and deviations would be discussed, furthermore a discussion would make sense, on the basis of which of the features the person had been recognized or why this was not the case at all.

In a written form, how this case-study can be helpful for the future work of the reconstructeur. Where and why mistakes were done, why those develop whether and how they could have been avoided and how one could use the acquired knowledge in further reconstructions.

Acknowledgements

This work would not exist in the presenting form without the help of some persons.

Special thanks to:

My tutors Professor Dr. Kerrin Christiansen and Dr. Joerg Orschiedt for an outstanding support.

Professor Dr. Klaus Pueschel for its large readiness to place to me material and consultant and his interest in my work.

Particularly my parents Otto and Erika Assmann for their unconditional benefit during the entire study and especially in the final time.

My sister, Dipl.-Ing. Gabriele Assmann and Dipl.-Ing. Ronnie Schmidt for assistance, whenever I needed assistance.

My great and best friend Elisabeth Neumann for private lector work and the honour to be my best friend.

My friend for all circumstances in life, Dipl. Biol. Dorothea Schütte for their large readiness to divide their scientific knowledge with me and for uncounted scientific and unscientific discussions.

My fantastic Mentor Ronn Taylor from Melbourne for its assistance and pieces of advice by mail, whenever I asked him for his technical advice.

Nils Mertens for dental discussion.

Literature

[1] "Making faces"/Prag, John; Neave. – Richard, Texas: A & M, 1997.
[2] "Schädelidentifizierung durch elektronische Bildmischung"/Helmer, Richard. – Heidelberg: Kriminalistik Verlag, 1984.
[3] "Prähistorische Anthropologie" Leitfaden der Feld- und Labormethoden/Herrmann, Bernd; Gruppe, Gisela; Hummel, Susanne; Piepenbrink, Hermann; Schutkowski, Holger. – Berlin: Springer, 1990.
[4] "Human skeletal remains" Exvacation, analysis, Interpretation/Ubelaker, Douglas H. – 3rd ed., Washington: Taraxacum, 1999.
[5] "A simple technique for age estimation in adult corpses: the two criteria method"/Lamendin, H. et al. – Journal of Forensic Sciences, JFSCA, Vol. 37, No. 5, 1992, pp. 1373–1379.
[6] "Mandibular Ramus Height as an Indicator of Human Infant Age"/Norris, Sean P. – Journal of Forensic Sciences 2002, 47 (1), pp. 8–11.
[7] "Human Osteology"/Bass, William M. – 4th ed., Columbia: Missouri Archaeological Society, Inc., 1995.
[8] "Anatomie" Makroskopische und mikroskopische Anatomie des Menschen; Band 1: Cytologie, Histologie, allgemeine Anatomie und Anatomie des Bewegungsapparates/Benninghoff, Alfred (Begr.). – 14., völlig neu bearb. Aufl., München: Urban & Schwarzenberg, 1985.
[9] "Forensic facial reconstruction"./ Wilkinson, Caroline. – Cambridge: University Press, 2004.
[10] "Chirurgie der Ohrmuschel"./ Weerda, Hilko. – Stuttgart: Thieme, 2004.
[11] Harper, Julie C, MD University of Alabama at Birmingham and Fulton Jr, James, MD PhD, Medical Director, Fulton Skin Institute "Acne Vulgaris", July 2004, http://www.emedicine.com/DERM/topic2.htm (last access: 03. 03. 2005).

Eine Fallstudie zur dreidimensionalen Gesichtsrekonstruktion

Sabine Assmann[1], Kerrin Christiansen[1], Jörg Orschiedt[2]

[1] Universität Hamburg; Institut für Humanbiologie; BioZ Grindel; Martin-Luther-King-Platz 3; D-20146 Hamburg
[2] Universität Hamburg; Archäologisches Institut; Johnsallee 35; D-20148 Hamburg

Abstract

In der vorliegenden Arbeit soll in Theorie und Praxis der Frage nachgegangen werden, welche Bandbreite der Ausprägungsvariabilität an ein Gesicht annehmen kann, wenn keine hilfreichen Informationen zu einem anonymen Schädel dem Rekonstrukteur Anhaltspunkte für die Arbeit liefern können.

Dem Schädel allein kann man nicht ansehen, ob eine Person zu Lebzeiten kachektisch, normal genährt oder adipös war, ob sie unter Krankheiten litt, die sich auch auf das Gesicht auswirken oder ob ihr Gesicht durch äußere Einflüsse (z. B. Alkoholgenuss) verändert war.

Da die Person, deren Schädel für die Arbeit verwandt wird, identifiziert und polizeibekannt ist und daher auch ein Foto existiert, soll nach Fertigstellung der Rekonstruktionen ein Vergleich mit dem Foto vorgenommen und geschaut werden, ob trotz fehlender Informationen eine der unterschiedlichen Darstellungen der Person zu Lebzeiten so nahe kommt, dass mit Hilfe der Rekonstruktion eine Identifizierung möglich wird. Ferner soll ermittelt werden, ob man die Person auch in einem anderen Konstitutionszustand hätte identifizieren können.

Einleitung

Die Faszination an menschlichen Gesichtern war und ist ungebrochen. Jedes Gesicht hat seine besondere Ausprägung der Nase, der Augen, der Lippen, des Kinnes und jedes Gesicht ist einmalig.

Bei der Betrachtung von Skeletten und im Besonderen von Schädeln in Museen, osteologischen Sammlungen, alten Gräberfeldern oder anderen Stätten drängt sich einem meist unweigerlich die Frage auf, wie der Mensch wohl zu Lebzeiten ausgesehen haben mag, wie sein Name gewesen ist, seine Geschichte und die Umstände seines Todes. Bei alten Funden mag sich einem eine mystische, schaurige oder gar romantische Phantasie um die verstorbene Person aufdrängen, doch er wird mit ziemlicher Sicherheit in keiner Vermisstenkartei geführt werden. Auch aktuelle Fälle sind nicht frei von Mutmaßungen und Spekulationen, umso mehr, je weniger über den Fund bekannt ist. Hier stellt sich im Gegensatz zu alten Funden aber eher die Frage, ob es Angehörige gibt, die die unbekannte Person vermissen, auf sie warten und sich sorgen. Wird ein humaner osteologischer Fund, durch welche Umstände auch immer, identifiziert, so besteht eine Möglichkeit, Angehörigen Gewissheit zu verschaffen und vielleicht sogar die Umstände des Todes zu klären.

Ist dies nicht der Fall, so muss die verstorbene Person vielleicht für immer gesichts- und namenlos bleiben.

Hier kann eine plastische Rekonstruktion helfen, dem Toten ein Gesicht und im besten Falle seine Identität zurückzugeben. Liegt jedoch nur ein spärlicher Fund vor, der Rückschlüsse auf eine eventuelle Krankheit oder einen bestimmten körperlichen Zustand nicht zulässt, so kann sich eine Rekonstruktion schwierig gestalten. Werden bei dem Verstorbenen Hinweise auf eine Krankheit gefunden, die sich auch an den Weichteilen des Gesichtes äußert, so kann diese Information helfen, mit der Rekonstruktion näher an das mögliche Aussehen zu Lebzeiten zu gelangen.

Hier stellt sich nun die Frage, ob und wie gut es möglich ist, eine Person auch dann positiv zu identifizieren, wenn derlei Informationen nicht vorhanden sind.

Diese Frage bot Anlass für eine Fallstudie an einem Schädel, die im Nachfolgenden beschrieben werden soll und den Inhalt meiner Magisterarbeit darstellt.

Der Schädel, der für diese Studie zur Verfügung gestellt wurde, kommt aus dem Institut für Rechtsmedizin des Universitätsklinikums Eppendorf/Hamburg (Germany). Da die Person polizeibekannt war, existieren fotographisch neutrale Aufnahmen des Gesichtes, nicht nur Schnappschüsse.

An ihm sollte der Frage nachgegangen werden, wie nahe man mit einer dreidimensionalen Gesichtsrekonstruktion dem Aussehen der Person zu Lebzeiten kommen kann, wenn weder das postcraniale Skelett noch Informationen über die verstorbene Person vorliegen. Bearbeitet werden sollte das Thema in fünf Rekonstruktionen auf dem Schädel bzw. dessen Replikation in immer verschiedener Ausprägung des Ernährungs- und Gesundheitszustandes.

Nach der Fertigstellung aller fünf Rekonstruktionen sollte geschaut werden, ob sich die entstandenen Gesichter untereinander gleichen und ob es möglich wäre, die verstorbene Person mit Hilfe einer oder mehrerer der Rekonstruktionen zu identifizieren. Ferner sollte geschaut werden, ob man die Person auch unter einem anderen Ernährungs- oder Gesundheitszustand als dem zu Lebzeiten vorherrschenden hätte positiv hätte identifizieren können. Für diesen Vergleich würden Mitarbeiter der Rechtsmedizin, der Polizei und solche, die nicht mit ausgebildeter Erkennung vertraut sind, zugegen sein.

Es war geplant, fünf Rekonstruktionen zu fertigen, und zwar in folgenden Ausprägungen. Für die unterschiedlichen Ernährungszustände eine normale Ausprägung, eine adipöse, also fettleibige Darstellung und eine kachektische, also sehr dünne, jedoch nicht unter dem Krankheitsbild der Anorexie. Für die Gesundheitszustände sollen zwei Krankheitsbilder gewählt werden, die sich nur an den Weichteilen manifestieren, jedoch nicht am Gesichtsknochen.

Material und Methoden

Es war vorgesehen, alle Rekonstruktionen nach der ‚Manchester Methode', auch ‚Kombinierte Methode' genannt, zu arbeiten, welche von Richard Neave begründet wurde [1]. Diese Methode sieht den genauen Aufbau aller Facialmuskeln vor, welche dann mit einer Schicht Haut überzogen werden. Die Ausarbeitung der Augen, Nase, Mund und Ohren, ferner die Ausprägung des Kinns würde nach anatomischen Richtlinien gearbeitet werden.

So sollte es theoretisch möglich sein, dass sich diese Bereiche bei allen fünf Gesichtern sehr ähneln, trotz ihrer unterschiedlichen Ausprägungen aufgrund der verschiedenen Ernährungs- und Gesundheitszustände.

Als Grundlage für die Weichteildicken würden die Tabellen von Richard Helmer [2] zugrunde gelegt werden. Diese Datensätze geben 34 Punkte am knöchernen Schädel und an der Mandibel an, welche genau definiert und an jedem Schädel auszumachen sind.

Für beide Geschlechter und verschiedene Altersränge sehen diese Datensätze unterschiedliche Dicken vor, die den Schädel an den erwähnten Stellen bedecken. Es ist jeweils ein maximaler, ein minimaler und ein Mittelwert für jeden Punkt jedes Ranges und jedes Geschlechtes gegeben.

Für den zu bearbeitenden Schädel sollten die Datensätze folgendermaßen verwendet werden. Für die Rekonstruktion, die eine gesunde und normal gebaute Person zeigen würde, sollten die Mittelwerte des entsprechenden Ranges konsultiert werden. Für jene in adipöser Ausführung die Maximalwerte und für die kachektische Ausführung entsprechend die Minimalwerte. Bei den beiden pathologischen Rekonstruktionen würde die Wahl der Werte von dem Krankheitsbild abhängig gemacht werden.

Genereller Überblick über den Schädel. Am auffälligsten an dem vorliegenden Schädel war der extrem schlechte Zustand der Zähne. Es lag zwar eine umfangreiche dentale Restauration vor, einige Zähne jedoch waren beschädigt und unbehandelt oder ohne Füllung.

Bei der ersten Betrachtung machte der Schädel einen relativ robusten und intakten Eindruck, was sich aber als Trugschluss erwies. Er war zwar fast vollständig, aber sehr fragil, da über große Gebiete die Spongiosa fehlte und die Compacta zwar vorhanden, jedoch ausgesprochen dünn war. Daher waren auch Bereiche um die kleineren Foramina versehrt.

Das Hinterhaupt wies kurz über der Lambdanaht ein deutlich ausgeprägtes Ausschussloch auf, der Bereich des Einschussloches im Os Sphenoidale war weiter ausgebrochen, so dass es nicht nach den Richtlinien beschrieben werden konnte.

Auch das dentale Erscheinungsbild war nicht mehr komplett, nach der Form der leeren Alveolen zu urteilen, waren die entsprechenden Zähne aber erst postmortal ausgefallen.

Die Orbitae fehlten und weite Teile der inneren Schädelstruktur waren von äußerster Zerbrechlichkeit.

Eine Detailansicht der Orbita ist in Abb. 1 zu sehen.

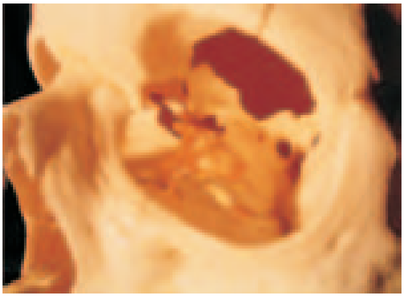

Abb. 1: Detailansicht auf die linke Orbita. Die konkave Höhlung beider Orbitae war fast vollständig weggebrochen. Durch das Fehlen waren die hinterliegenden knöchernen Strukturen sichtbar geworden, welche sehr filigran waren.

Der Bereich der Incisivi war an der Mandibel extrem, an der Maxilla eher verhalten weggebrochen. Abb. 2 zeigt einen Eindruck der Mandibel.

Abb. 2: Eine Ansicht der Mandibel zeigt den schlechten dentalen Zustand, der sich an der Maxilla fortsetzt. Alle Quadranten sind einer umfangreichen dentalen Restauration unterworfen, jedoch nicht jeder beschädigte Zahn. Der alveolare Bereich der Incisivi ist nicht mehr intakt.

Auch die Schädelbasis war nicht mehr intakt, sie wies an zahlreichen Stellen Läsionen oder gar kleine Löcher auf, der linke Processus styloideus fehlte ganz.

Um sich der Werte aus Helmers Tabellen [2] bedienen zu können, ist es unerlässlich, vor Beginn der eigentlichen Rekonstruktion eine Alters- und Geschlechtsbestimmung am Schädel vorzunehmen. Der vorliegende Schädel wurde wie folgt klassifiziert.

Für die Bestimmung des Geschlechtes wurde mit der Zuordnungstabelle von Herrmann et al. [3] gearbeitet. Diese gibt am Schädel Regionen, bzw. Merkmale an, die am männlichen und weiblichen Schädel so unterschiedliche Ausprägungen aufweisen, dass sie mit hoher Genauigkeit dem jeweiligen Geschlecht zugeordnet werden können. Alle vorgegebenen Merkmale bis auf eines zeigten eine männliche Ausprägung, sodass davon ausgegangen werden konnte, dass es sich bei dem Individuum um einen Mann handeln müsse.

Für die Bestimmung des Alters wurden mehrere Methoden konsultiert.

Aufgrund des fehlenden postcranialen Skelettes konnten die relativ gesicherten Merkmale wie Symphyse, Epiphysenfugen und das sternale Ende der Rippen als Indikatoren zwangsläufig nicht verwendet werden.

Das Alter musste einzig und allein am Schädel festgemacht werden.

Als Ausgangskriterium wurde der Zahnstatus genommen, am Schädel das sicher aussagekräftigste Kriterium. Hier im Detail der dritte Molar. Nach dessen Entwicklungsstatus konnte nach Ubelaker [4] davon ausgegangen werden, dass es sich um eine junge adulte Person gehandelt haben musste, älter als 28 Jahre. Diese erste altersmäßige Einteilung wurde durch Rücksprache mit einem Zahnmediziner unterstützt. Diese erste Klassifikation ließ für die weitere Einteilung zwei Techniken der Bestimmung ausscheiden, nämlich jene von Lamendin [5] und von Norris [6]. Im Folgenden kamen verschiedene Techniken zum Einsatz, die zwar teilweise jede für sich betrachtet nur eine mehr oder minder grobe Klassifikation zulassen, wenn jedoch alle Resultate zusammen betrachtet eine ziemlich enge Zuordnung zu einem bestimmten Alter erlauben. Im Detail handelte es sich um Techniken, die in verschiedener Weise an Zähnen angewendet werden, und zwar jene, die von Ubelaker [4] und Bass [7] beschrieben werden. Des Weiteren wurde an unterschiedlichen Stellen des Schädels der Obliterationsgrad der Nähte betrachtet und zwar sowohl ektocranial als auch endocranial. Ferner wurden der Gonionwinkel [8] und die Unterkieferhöhe betrachtet. Einige der Methoden ließen zwar nur eine grobe Unterteilung in „juvenil-adult-senil“ zu, doch sollten sie deshalb nicht außer Acht gelassen werden, sondern die Ergebnisse der anderen Techniken unterstreichen/bestätigen.

Nach Betrachtung und Auswertung aller ermittelten möglichen Altersgruppen und einem Mittel aus allen konnte der Schädel einer Altersspanne von 28–33 Jahren zum Zeitpunkt des Todes zugeordnet werden.

Da bei einer dreidimensionalen Gesichtsrekonstruktion nicht auf dem Originalschädel gearbeitet wird, ist es unumgänglich, diesen vorher abzuformen. Um die Unversehrtheit des Originales zu wahren, ist eine Vorbehandelung nötig, dessen Umfang sich nach dem Zustand des Schädels richtet.

Grundsätzlich werden alle physiologischen Öffnungen versiegelt, um eine geschlossene Form zu erhalten. Dieses ist nötig, damit kein Abformmaterial, was bei der Verarbeitung noch von relativ dünnflüssiger Konsistenz ist, in das Schädelinnere laufen kann. In dem vorliegenden Fall mussten zudem die Läsionen an der Schädelbasis versiegelt werden. Ferner war es notwendig, die filigranen Knochenreste im Schädelinneren zu stabilisieren, damit sie überhaupt die Vorbehandlung überstehen würden. Im Anschluss wurde der Schädel in benötigter Anzahl mit normalem Bau- und Hobbygips vervielfältigt, wobei er zur Gewichtsreduktion eine Styroporkugel in die Höhle des Hirnschädels bekam.

Die Vorbereitung für die eigentliche Rekonstruktion folgte bei allen fünf Arbeiten der ‚Manchester Methode', ebenso die korrekte Positionierung der Augen und der Aufbau des knorpeligen Nasenanteiles. Hierbei mussten die fehlenden Teile durch Schätzarbeit ersetzt werden. Auch die fehlenden Incisivi und Canini wurden substituiert, wobei ihr Verlauf dem der Alveolen folgte. Durch diesen Ersatz war auch eine Wiederherstellung des oberen Mandibelabschlusses möglich, sodass Punkt 13 gesetzt werden konnte. Auch die Vorgehensweise beim Setzen der Landmarken war immer übereinstimmend, deren Länge unterschied sich aber nach der jeweils geplanten Darstellung des Gesichtes.

Die Arbeitsgänge, die bei allen Rekonstruktionen identisch sein würden, sollen in dem folgenden Abschnitt erläutert werden. Die Augen, handgearbeitete Glasaugen, wurden stets nach den anatomischen Vorgaben von Wilkinson [9] in die Orbitae eingepasst. Es musste peinlich genau auf einen geraden und parallelen Blick geachtet werden, jede kleine Abweichung würde sich ansonsten später als leichtes, aber doch sichtbares Schielen bemerkbar machen.

Auch der Aufbau des knorpeligen Nasenanteiles wurde stets nach der gleichen Vorgehensweise gearbeitet. Da die Spina nasalis frakturiert war, musste der fehlende Teil durch Schätzarbeit ersetzt werden. Für jede einzelne Rekonstruktion wurden die Massen, die die Nase bestimmen, neu erfasst und auf den Schädel übertragen. Im Vergleich ergab sich immer die gleiche Nase, nur leicht variierend.

Auch die nicht vorhandenen Zähne wurden bei jedem Schädel nach der gleichen Prozedur ersetzt. Es wurde darauf verzichtet, Molaren zu ersetzen, da sie für eine Rekonstruktion von nicht erheblicher Relevanz und auch bei geöffnet dargestelltem Mund nicht sichtbar sind. Gewählt wurden Kunststoffzähne aus dem Dentalbedarf, welche auch beim Prothesenbau Verwendung finden. Diese Zähne wurden als Richtschnur für dentale Vorgaben genommen. Bedient wurde sich normal geformter Zähne, keine Extremausprägungen. Dem Verlauf der leeren Alveolen folgend, wurden die Zähne an Ober- und Unterkiefer befestigt. Anzumerken sei hierzu, dass sämtliche Alveolen für die Incisivi nur sehr schmale Zähne zuließen, welche sich, speziell in der Mandibel, teilweise überlagerten. Diese folglich eher schlanke Ausprägung der Insicivi zu Lebzeiten implizierte eine relativ schmale Lippe.

Zwei zu erwähnende osteologische Erscheinungen würden auch in dem werdenden Gesicht zum Ausdruck kommen. Zum einen eine sehr ausgeprägte Mentumregion mit knöchernen Ausziehungen würde als massives Kinn in die Rekonstruktionen Einzug halten. Ferner waren auf den Frontalia Aderimpressionen deutlich sichtbar, welche vermuten ließen, dass sich zu Lebzeiten unter der Haut ein Gefäß abgezeichnet hatte.

Gleichermaßen ließ sich auch der Verlauf der Augenbrauen am Schädel, im Detail an dem Verlauf des oberen Orbitarandes definieren. Jener würde ebenfalls bei allen Rekonstruktionen identisch sein.

Anzumerken sei auch, dass alle werdenden Gesichter mit leicht geöffnetem Mund dargestellt werden würden, damit man sich bis zur völligen Vollendung an den Zähnen orientieren könne.

Der Grundaufbau der Ohren ist immer der gleiche, die Darstellung der Formen variiert jedoch von Ohr zu Ohr. Hierzu sei anzumerken, dass dieses nicht für das Ohrenpaar einer Person gilt, welches physiologischerweise spiegelgleich ist. Auch hier wurde auf Exremdarstellungen verzichtet, da solche ein falsches Bild von einer Person zu Lebzeiten liefern kann und im negativsten Fall eine positive Identifikation verhindern. Für die Ohrlänge und Ohrbreite wurde sich der Angaben von Weerda bedient [10], welcher für diese Parameter eine Alters- und Körperhöhenabhängigkeit vorgibt. Da über die Körperhöhe nichts bekannt war, musste dieser Faktor aus der Ermittlung herausfallen. Für die Altersklassifikation ergab sich eine Ohrlänge von 67 mm und eine Ohrbreite von 35 mm. Diese Messdaten wurden auf jeden Schädel angewendet.

Ergebnisse

Die erste Rekonstruktion sollte die verstorbene Person in gesundem und normal genährtem Zustand zeigen. Dafür wurden die Mittelwerte der entsprechenden Altersklasse aus Helmers Tabellen konsultiert. Durch die Altersbestimmung in der Spanne von 28–33 Jahren überlappten sich zwei in Frage kommende Tabellen. Die Mittelwerte jener beiden unterschieden sich jedoch gar nicht oder nur minimal. Bei abweichenden Werten von mehr als 2mm wurde das Mittel aus beiden verwendet.

Die Rekonstruktion verlief wie in dem vorherigen Abschnitt beschrieben.

Begonnen wurde mit dem Einsetzen der Augen in die Orbitae, gefolgt von dem Aufbau des knorpeligen Nasenanteiles, was mit Wachs erfolgte. Da einige knöcherne Leitlinien für den exakten Aufbau der Nase nicht mehr vorhanden waren, mussten diese nach bestem Ermessen ersetzt werden. Die Spina nasalis war zwar frakturiert, doch ließ sich mit dem noch vorhandenen Part eine ziemlich genaue Länge der Nase definieren. Die Form und Höhe der Nasenflügel konnte zwar nicht mehr am Knochen festgemacht werden, doch ergab sich eine Form mehr oder minder aus dem Aufbau an sich.

Die Rekonstruktion verlief wie in dem vorherigen Abschnitt beschrieben. Nach dem Setzen der Landmarken wurde mit dem muskulären Aufbau begonnen. Schon bei dem Auftragen der Muskeln manifestierte sich eine sehr ausgeprägte Mentumregion, bedingt durch die Knochenarchitektur. Zeitweise wirkte das Kinn sogar überproportioniert, sodass die Versuchung nahe lag, diese vermeintliche Fehlerhaftigkeit auszugleichen. In der folgenden Entwicklung glich sich diese vermeintliche Unproportioniertheit von allein wieder aus. Da bei den Muskeln peinlich genau gearbeitet wurde, war stets jeder noch vorhandene Platz für einen Muskel reserviert, sodass sich am Ende alle zusammenfügten.

Die komplette Gesichtsmuskulatur wurde nachfolgend mit einer Schicht Haut überzogen, welche genau mit den Enden der hölzernen Landmarken abschloss. Eine Colorierung der Modelliermasse ließ ein nachträgliches Einfärben des Gesichtes überflüssig werden und verlieh ihm zudem ein natürlicheres Aussehen. Auf der Stirn wurde rechts das sich abzeichnende Gefäß wiedergegeben.

Nach der vollständigen Trocknung erhielt das entstandene Gesicht Wimpern und wurde dergestalt behandelt, dass die Haut wieder einen feuchten Eindruck machte. Die Abbildungen 3 und 4 zeigen die erste fertige Rekonstruktion aus zwei unterschiedlichen Perspektiven.

Abb. 3: Ansicht auf die erste Rekonstruktion, welche die Person in gesundem und normal genährtem Zustand zeigt.
Auf der rechten Stirnseite ist das sich unter der Haut abzeichnende Gefäß zu sehen.

Abb. 4: Diese Figur zeigt eine Frontalaufsicht auf das fertige Gesicht. Der Mund wurde in leicht geöffneter Form dargestellt, damit sich die ganze Arbeit hindurch an den Zähnen orientiert werden konnte.

Die zweite Rekonstruktion sollte das gleiche Gesicht in adipöser Verfassung darstellen. Hierfür wurde sich der Maximalwerte der beiden in Frage kommenden Altersränge bedient, mit einer Tendenz zu dem höheren Wert.

Schon der Vergleich zur der vorangegangenen Rekonstruktion ließ erahnen, dass das Gesicht deutlich voller ausgeprägt sein würde. Die Unterschiede waren am deutlichsten in den Bereichen zu erkennen, wo das meiste subcutane Fett angesiedelt ist, namentlich in der Wangenregion, welche hauptsächlich durch die Punkte 21/ms (oberer erster Molar), Punkt 22/mi (unterer erster Molar) und Punkt 32/m2 (Massetermitte zwischen Gonion und Zygion) bestimmt wird. Die Differenz bei Punkt 21 lag bei 6,0 mm, bei Punkt 22 bei 5 mm und bei Punkt bei 4,0 mm. Diese Unterschiede waren mit dem Auge gut zu erkennen. Bei einer Frontalaufsicht auf den Schädel, der unter normaler Konstitution bearbeitet worden war, erreichten Punkt 21 und Punkt 22 das äußere Ende des Jochbogens nicht, es war zu vermuten, dass sich in dem fertigen Gesicht ein Wangenknochen abzeichnen würde. Anders bei der zweiten Rekonstruktion. Die Punkte 21 und 22 ragten bei einer Frontalaufsicht etwa 0,5 cm über die weiteste Stelle des Jochbogens (Zygion) hinaus, was dermaßen gerundete Wangen ins Blickfeld rücken ließ, unter denen sich kein Knochen mehr abzeichnen würde.

Die Vorgehensweise verlief wie bereits beschrieben und glich in der muskulären Phase der ersten, mit dem Unterschied, dass schon die Muskeln dicker ausgearbeitet werden mussten, ganz besonders an den oben beschriebenen Stellen. Das Kinn wirkte in dieser Rekonstruktion noch wesentlich überdimensionierter als in der ersten Rekonstruktion, glich sich aber im weiteren Verlauf wieder dem Gesamtbild an. Auch konnten hier nicht alle entstehenden Hohlräume nur mit Muskelmasse ausgefüllt werden, es war notwendig, einige Muskeln mit Fett zu unterfüttern. Die nach Fertigstellung des muskulären Gesichtsanteiles noch herausschauenden Köpfe der hölzernen Landmarken gaben die Dicke der Haut vor. Auch diese lag eindeutig höher als bei der vorherigen Rekonstruktion. So war es dort ausreichend gewesen, zwei Teile Modelliermasse für die Haut zu bereiten, in der vorliegenden Rekonstruktion war nahezu die doppelte Menge erforderlich. Nach dem Auflegen der Haut wurde diese entsprechend der Veränderungen bei adipösen Personen gestaltet. Im Detail die bereits erwähnten gerundeten Wangen, die sich zur Nase hin deutlich in Gestalt einer Falte abgrenzten und sich auch zum unteren Ende der Mandibel zogen. Ferner stärker ausgeprägte Unterlider als Folge vermehrten subcutanen Fettes. Auch das erhöhte Fettaufkommen in der Mentumregion musste an dem Gesicht sichtbar werden. Dies tat es als insgesamt gerundeteres Kinn und als Doppelkinn. Auch wurde dem zweiten Gesicht eine rosigere Gesichtsfarbe zugeteilt. Bei dieser Rekonstruktion wurde auf die Darstellung der Gefäße auf der Stirn verzichtet, da davon ausgegangen werden konnte, dass jenes hier in Fett eingebettet und damit nicht sichtbar sein würde.

Auch das vollendete zweite Gesicht wurde endbehandelt, sodass es einen feuchten und lebendigeren Eindruck gewann. In den folgenden Abbildungen 5 und 6 sind zwei Eindrücke des fertig gestellten adipösen Gesichtes zu sehen.

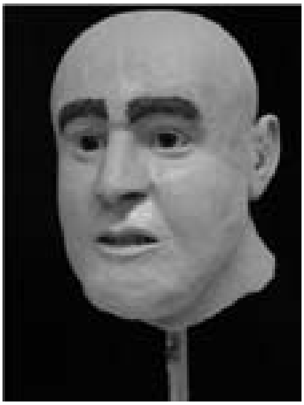

Abb. 5: Zu sehen ist die zweite Rekonstruktion, welche das Gesicht in stark adipöser Konstitution darstellt. Hierfür wurden die Maximalwerte aus den entsprechenden Altersrängen verwendet, mit einer Tendenz zum höheren Wert.
Deutlich sind die stark ausgeprägten Unterlider zu erkennen und die sich zur Nase abgrenzende gerundete Wange. Das Kinn wirkt rund und fleischig.

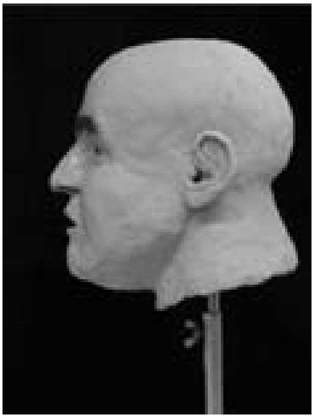

Abb. 6: Hier wird die adipöse Rekonstruktion im Profil gezeigt. Klar zu erkennen ist auch hier wie in Fig. 5 das fleischige Kinn und das Doppelkinn. Auch im Profil wirken die Wangen voll und damit gerundet.

Die dritte Rekonstruktion sollte das Gegenstück zu der vorherigen werden, die Person in kachektischer Darstellung, jedoch nicht unter dem Krankheitsbild der Anorexie. Folgerichtig wurde sich hier der Minimalwerte der beiden Altersklassen bedient. Auch hier hielten sich die Differenzen in einem zu vernachlässigenden Rahmen.

Die Unterschiede zu der zweiten Rekonstruktion waren jedoch augenscheinlich, und zwar hauptsächlich in der bereits mehrfach erwähnten Wangenregion. Die Differenz zwischen Maximal- und Minamalwert bei Punkt 21 lag bei 12,0 mm, bei Punkt 22 bei 9,0 mm, ebenso bei Punkt 33. In der Frontalaufsicht auf den mit den Landmarken versetzten Schädel war ausgesprochen deutlich zu sehen, dass sich deutlich der Jochbogen im fertigen Gesicht abzeichnen würde.

Auch hier war die Vorgehensweise wie bereits beschrieben. Es blieb nach der Orientierung an den Landmarken sehr wenig Spielraum für die Muskeln, subcutanes Fettgewebe konnte kaum bis gar nicht zum Einsatz kommen, da die verbleibenden freien Räume komplett von noch fehlenden Muskeln ausgefüllt wurden. Die Haut wurde hier in einer sehr dünnen Lage aufgetragen und verbrauchte im Gegensatz zu der ersten Rekonstruktion nicht einmal zwei Teile Modelliermasse. Es wurde entschieden, bei dieser Rekonstruktion auf beiden Stirnseiten sich abzeichnende Gefäße darzustellen, da zu vermuten war, dass sich bei fehlendem Unterhautfettgewebe wesentlich mehr Strukturen abzeichnen. Ebenfalls wurde hier das Erscheinungsbild dem einer Person in ausgezehrtem Zustand angeglichen. Dies bedeutete, dass die Augen scheinbar tiefer in den Höhlen lagen, was als Folge des verminderten subcutanen Fettgewebes eintritt, welches die Augäpfel umgibt. Durch die insgesamt schlankere Form wirkte zudem die Nase viel hervorstechender. Die Wangenknochen zeichneten sich wie erwartet unter der Haut ab, die Wangen selber wirkten eingefallen. Auch die Mentumregion, welche hier zum ersten Mal nicht falsch dimensioniert wirkte, stach wieder einprägsam hervor.

Auch wurde das dritte Gesicht in einem helleren Farbton gearbeitet, sodass es leicht blass wirkte. Zu sehen ist es in den Abbildungen 7 und 8.

Abb. 7: Die dritte Rekonstruktion ist hier in der Frontalaufsicht zu sehen. Die Augen wirken hier tief in den Höhlen liegend, was durch fehlendes Unterhautfettgewebe bedingt wird. Die Wangen wirken eingefallen, und dadurch die Nase größer.

Abb. 8: Die gleiche Rekonstruktion kann hier aus dem halben Profil angeschaut werden. Die Konturen des Gonions zeichnen sich deutlich unter der Haut ab. Hier wurden auf der Stirn auf beiden Seiten Gefäße unter der Haut angedeutet, auf der rechten Seite zwei, da auf dem Schädel noch eine etwas gemässigtere zweite Impression vorhanden war, von welcher sich das Gefäß aber nur in diesem kachektischen Konstitutionszustand abzeichnen würde.

Bei der vierten Rekonstruktion sollte es sich um den ersten pathologisch dargestellten Fall handeln.

Die Auswahl des selbigen sollte jedoch mit Bedacht gewählt werden. So sollte es sich um ein Krankheitsbild handeln, welches sich nur an den Weichteilen manifestiert, nicht aber am Knochen. Ein weiteres Kriterium sollte sein, dass die Krankheit nicht oder nicht schnell zum Tode führt, damit sichergestellt wäre, dass die Umwelt die Person noch im Bilde dieser Krankheit erlebt haben könnte. Ferner sollte es sich nicht um eine außergewöhnliche oder selten vorkommende Krankheit handeln, deren Symptomatik an den Weichteilen weitestgehend unbekannt ist. Unter Berücksichtigung all dieser Voraussetzungen wurde entschieden, die vierte Rekonstruktion im Krankheitsbild der Alkoholabhängigkeit darzustellen, jedoch nicht im Finalstadium.

Konsultiert wurde hierfür ein Durchschnittswert aus Minimal- und Mittelwert der beiden Altersränge. Hierfür wurden in diesem Falle alle vier Werte addiert und daraus das Mittel gebildet, welches den verwendeten Wert darstellen sollte.

Auch hier war die Vorgehensweise bei der muskulären Ausarbeitung wie in den Fällen zuvor, die Darstellung der Krankheit würde erst mit der Haut beginnen. Jenes geschah wie folgt. Für diese Darstellung wurde kein einheitlicher Farbton verwendet, vielmehr wurde mit dreien gearbeitet. Der komplette Hirnschädel und die Ohren wurden in einer normalen gesunden Farbe dargestellt. Das Gesicht jedoch bekam eine rötliche Colorierung mit geplatzten Äderchen und einem Ekzem am linken Mundwinkel. Es erforderte einige Kunst, die beiden Farbtöne einander so anzugleichen, dass kein abrupter Übergang sichtbar sein würde. Es musste also genau überlegt werden, an welchen Stellen des Gesichtes die beiden Farbtöne in-einander übergehen sollten. Das Unterlid wurde vor dem Auftragen der Haut an dieser Stelle mit einer dünnen Lage roten Modellierstoffes unterlegt, nach Auftragen und Ausarbeiten der Haut entstand der Eindruck einer entzündeten Bindehaut. Unterstützt wurde der krankhafte Eindruck der Augen noch durch Tränensäcke.

Um den Augen einen glasigen Glanz zu vermitteln, wurden sie mit Lack überzogen, hierdurch erhielt auch die Bindehaut ihre intensive rote Farbe zurück. Zur Abrundung der Augen wurde nach der Trocknung des Lackes auf die Bindehaut eine Schicht Kleber aufgetragen, um den Augen einen leicht wässerigen Ausdruck zu verleihen.

Um dem Gesicht zudem einen vernachlässigten Ausdruck zu geben, bekam es einen dünnen und ungleichmäßig geschnittenen Kinnbart.

Das Ergebnis der Ausarbeitung der ersten pathologischen Darstellung ist in den nachfolgenden Abbildungen 9 und 10 zu sehen.

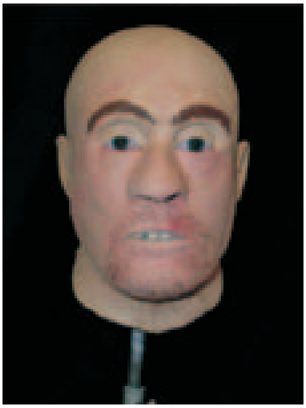

Abb. 9: Diese Figur zeigt die Person im Vollbild der Alkoholkrankheit, jedoch nicht im finalen Stadium.
Die Haut auf den Wangen und der Nase ist mit geplatzten Äderchen durchzogen, deutlich sind die entzündeten Bindehautsäcke und die darunter liegenden Tränensäcke zu erkennen. Den Augen fehlt an den Oberlidern subcutanes Fett, wodurch der Blick krank wirkt.

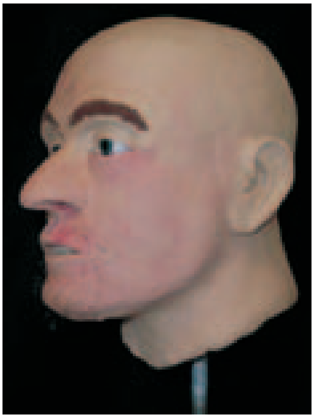

Abb. 10: Die alkoholkranke Person ist hier im halben Profil zu sehen. Deutlich erkennbar hier nochmals die geplatzten Äderchen auf den Wangen und die Tränensäcke. Ebenfalls das Ekzem am linken Mundwinkel. Sowohl in Abb. 9 als auch in der nebenstehenden ist der Kinnbart sichtbar, welcher den vernachlässigten Zustand der Erscheinung noch unterstreicht.

Ausstehende Resultate

Zum Zeitpunkt der Erstellung dieses Papers war die Arbeit noch nicht komplett abgeschlossen. Es stand noch die fünfte Rekonstruktion aus, welche den zweiten pathologischen Fall darstellen sollte. Geplant war hierfür eine Krankheit, die sich nicht weiter auf den Körper auswirkt, nur auf die Haut und dabei speziell auf die des Gesichtes. Das fünfte Gesicht sollte im Vollstadium der Acne vulgaris dargestellt, werden, da es sich hierbei um eine Krankheit handelt, die 85–100% aller Leute im Leben befällt [11]. Das Krankheitsbild äußert sich in nichtinflammatorischen follikulären Papeln oder Comedomen oder in flammatorischen Papeln, Pusteln und Knötchen in mehr oder minder ausgeprägter Form. Die Acne befällt jene Areale der Haut, die die größte Dichte an Talgdrüsen aufweisen, welche das Gesicht, das Dekoltee und der Nacken sind. Die bevorzugte Zeit für das Auftreten der Acne vulgaris wird zwar mit der Pubertät angegeben, doch schließt dieses ein Vorkommen im Erwachsenenalter nicht aus.

Das Gesicht sollte zwar in normaler Konstitution, also unter Verwendung der Mittelwerte, dargestellt werden, doch würde es zahlreiche flammatorische und inflammatorische Papeln und Pusteln, im Volksmund „Pickel“ genannt, bekommen. Ferner Narben von früheren Erscheinungen und unsachgemäß behandelten flammatorischen Prozessen.

Nach Fertigstellung aller Rekonstruktionen würden sie in das Institut für Rechtsmedizin des Universitätskrankenhauses Hamburg-Eppendorf gebracht werden. Dort würde sich eine Reihe Personen einfinden, unter anderem Beamte der Polizei, welche den Fall des für die Rekonstrukteurin bildlich unbekannten Suizidanten bearbeitet hatten. Sie würden Fotos der Person zu Lebzeiten zeigen, welche dann mit den Rekonstruktionen verglichen werden würden.

Die anwesende Gruppe würde sich zusammensetzen aus Personen, welche von Berufs wegen ausgebildet sind in der Wiedererkennung von Gesichtern und solchen, die normalerweise nicht damit arbeiten. All diese Personen sollten dann entscheiden, ob sie die Person auf den Fotos mit Hilfe einer oder mehrerer der Rekonstruktionen hätten positiv identifizieren können. Es würden gemeinsam die Ähnlichkeiten und Abweichungen besprochen werden, ferner wäre eine Diskussion angebracht, anhand welcher Merkmale die Person wieder erkannt worden war oder warum dies nicht der Fall war.

In schriftlicher Form würde festgehalten werden, welche Vorteile die Arbeit der Rekonstrukteurin für weitere Arbeiten gebracht hat. Wo Fehlerquellen lagen, warum jene aufgetreten sind, ob und wie sie hätten vermieden werden können und wie man das erworbene Wissen in weiteren Rekonstruktionen anwenden könne.

Danksagung

Diese Arbeit würde nicht in der vorliegenden Form bestehen ohne die Hilfe einiger Leute. Mein Dank gilt:

Meinen Betreuern Prof. Dr. Kerrin Christiansen und Dr. Jörg Orschiedt für eine hervorragende Betreuung.

Prof. Dr. Klaus Püschel für seine große Bereitschaft, mir Material und Gutachter zu stellen sowie für Interesse an meiner Arbeit.

Meinen Eltern Otto und Erika Assmann für ihre bedingungslose Unterstützung während des gesamten Studiums und besonders in der Abschlusszeit.

Meiner Schwester, Dipl.-Ing. Gabriele Assmann und Dipl.-Ing. Ronnie Schmidt für Hilfe, wann immer ich Hilfe brauchte.

Meiner großartigen und besten Freundin Elisabeth Neumann für private Lektoratsarbeit und die Ehre, ihre Freundin sein zu dürfen.

Meiner Freundin für alle Lebenslagen, Dipl. Biol. Dorothea Schütte für ihre große Bereitschaft, ihr wissenschaftliches Wissen mit mir zu teilen und für ungezählte wissenschaftliche und unwissenschaftliche Diskussionen.

Meinem phantastischen Mentor Ronn Taylor aus Melbourne für seine Hilfe und Ratschläge per Mail, wann immer ich ihn um seinen fachlichen Rat gebeten habe.

Nils Mertens für die dentale Diskussion.

Literatur

[1] „Making faces"/Prag, John; Neave. – Richard, Texas: A & M, 1997.
[2] „Schädelidentifizierung durch elektronische Bildmischung"/Helmer, Richard. – Heidelberg: Kriminalistik Verlag, 1984.
[3] „Prähistorische Anthropologie" Leitfaden der Feld- und Labormethoden/Herrmann, Bernd; Gruppe, Gisela; Hummel, Susanne; Piepenbrink, Hermann; Schutkowski, Holger. – Berlin: Springer, 1990.
[4] „Human skeletal remains" Exvacation, analysis, Interpretation/Ubelaker, Douglas H. – 3rd ed., Washington: Taraxacum, 1999.
[5] „A simple technique for age estimation in adult corpses: the two criteria method"/Lamendin, H. et al. – Journal of Forensic Sciences, JFSCA, Vol. 37, No. 5, 1992, pp. 1373–1379.
[6] „Mandibular Ramus Height as an Indicator of Human Infant Age"/Norris, Sean P. – Journal of Forensic Sciences 2002, 47 (1), pp. 8–11.
[7] „Human Osteology"/Bass, William M. – 4th ed., Columbia: Missouri Archaeological Society, Inc., 1995.
[8] „Anatomie" Makroskopische und mikroskopische Anatomie des Menschen; Band 1: Cytologie, Histologie, allgemeine Anatomie und Anatomie des Bewegungsapparates/Benninghoff, Alfred (Begr.). – 14., völlig neu bearb. Aufl., München: Urban & Schwarzenberg, 1985.
[9] „Forensic facial reconstruction"./ Wilkinson, Caroline. – Cambridge: University Press, 2004.
[10] „Chirurgie der Ohrmuschel"./ Weerda, Hilko.- Stuttgart: Thieme, 2004.
[11] Harper, Julie C, MD University of Alabama at Birmingham and Fulton Jr, James, MD PhD, Medical Director, Fulton Skin Institute „Acne Vulgaris", July 2004, http://www.emedicine.com/DERM/topic2.htm (letzter Zugriff: 03.03.2005).

Stone Age people in Hospital

M. L. d'Hollosy (Archaeology/Physical Anthropology). Researcher of Ancient Bones/Skullpting – Consultant to the NFI (Dutch Forensic Institute)

Abstract

There are some differences between archaeological and forensic facial reconstructions. One difference is the preservation of the skull. In most archaeological cases the preservation is poor, resulting in damaged, fragile and incomplete skulls. The resolution to this problem lies within 3-D scanning techniques, e. g. CT-scanning. After the shape of the skull is transformed into digital data, one can reconstruct the skull on the computer. Rapid prototyping, a three-dimensional printing technique, is used to build the working copy of the skull from the digital data.

The other essential difference is the reason for making them. With forensic cases the aim is identification, where as the goal for an archaeological case is primarily education and illustration. This means that the methods to establish the basic shape of the face and its features are the same, but that after this point, the two methods can diverge. The reconstructionist of archaeological cases has more freedom to fill in the blank spots, within certain boundaries of course.

Three cases of facial reconstructions of Stone Age skulls from the Netherlands are put forward, together with the problems we have encountered.

Differences between forensic and archaeological three-dimensional facial reconstructions

There are some differences between archaeological and forensic facial reconstructions. One of the main differences is the *post-mortem* time, the period of time that has lapsed after the occurrence of death. In forensic cases this time lapse varies from years to hours (in the case of burn-victims). In archaeological cases this lapse differs between thousands of years and hundreds of years.

This space of time can have a big influence on the skull. Biological, e. g. animal, vegetational, bacterial and fungal activities, just as chemical and physical processes all play a roll in the decay en decomposition of the bone [1]. The longer a skeleton is interred, the longer all these factors can affect the quality of the bone. Though the equation "the older the skeleton, the worse its preservation", does not hold in all cases, archaeological skulls tend to be in a less than optimal state compared to contemporary specimens. Bone decomposition can result in very fragile, delicate skulls. Because of the loss of organic and inorganic material, the weight of an ancient skull may be a fraction of a modern one. More often than not, archaeologists also have to deal with incomplete, fragmented and damaged skulls. In combination with the fragility of the bones this makes the handling of the skulls very risky.

All this means that the skull has to be replicated and reconstructed, repaired if you will, before a facial reconstruction can begin. Though some forensic facial reconstruction procedures involve casting the skull prior to building the face (for example the Manchester method [2]), other methods omit this because of its attendant time loss (the American method [4]). If the skull is solid enough, and that is usually the case with forensic specimens, a cast may be made directly from the skull using alginate or silicone rubber as moulding-material. Some archaeological skulls can also be casted in this way, but often the fragility of ancient skulls prohibits taking a mould from it directly, so the skull has to be reproduced in a manner that involves the least handling and thus the least possible amount of damage. The solution to this problem is three-dimensional scanning and three-dimensional printing.

3-D scanning, e. g. CT-scanning (computed tomography scanning) can be used to transform the shape of the skull into digital data [5]. This is a non-destructive technique which ensures that the skull will not be damaged. An additional advantage of having the skull CT scanned (figure 1) is that the data can then be manipulated. Missing parts may be replaced by mirroring their counterparts. Surrounding matrix that sticks to the skull can be digitally removed.

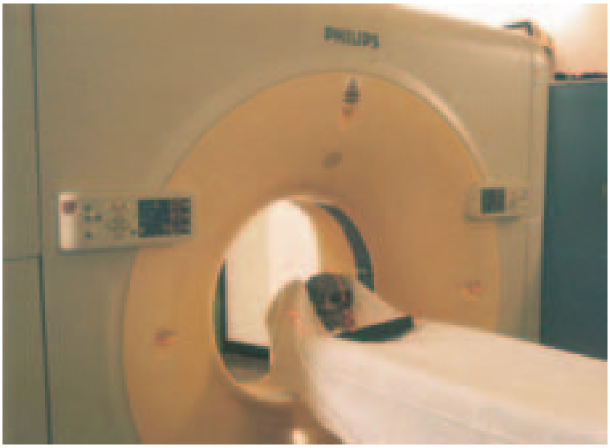

Fig. 1: An archaeological skull ready to be scanned in the CT scanner, at the University Medical Center Utrecht

Furthermore it can be used as a diagnostic tool in the pathological research. After digitizing the skull and checking the computer data for digital artifacts, we have created a virtual skull. In order to make a sculptured, 3-D facial reconstruction, this virtual skull has to become tangible.The technique to establish this is rapid prototyping, a three-dimensional printing technique. This technique can build the working copy of the skull in a synthetic material from the digital data. A disadvantage of duplicating the skull by means of CT scanning is that the copy is not as detailed as the original skull because the CT scan has a resolution of 0,67 mm. Other 3-D scanning techniques, for example some of the laser scans, can reach higher resolutions, but have other disadvantages.

So the preservation level of the skulls can be one difference. Another essential difference between archaeological and forensic facial reconstructions lies in its purpose.

Look at the two pictures (figure 2): which one is the real Stone Age woman from the Netherlands?

Fig. 2: Which one is the real Stone Age woman?

Many people believe that the dumb-looking person with the big brow ridges is the Stone Age woman. In fact, it is the other woman who lived in the Netherlands more than 5000 years ago. This is a facial reconstruction to show the public what Stone Age people may have looked like and, surprisingly, they look just like you and me. They were not ape-like people who dragged their wives into their caves by the hair, they were modern looking humans. And this also illustrates the main reasons why archaeological facial reconstructions are being made: to educate and to illustrate. These are the same reasons why museums exist: to educate, to illustrate and to show. And maybe to entertain as well.

The reason behind forensic facial reconstructions is obvious: identification of the unknown victim in order to solve a crime. This is an essentially different goal from that of archaeological reconstructions.

Similarities and differences in the facial reconstruction procedures

The similarities in reconstructing procedures are clear: the fundamentals are the same, first one has to gather the biological data (sex, age, ethnic group, health, state of nourishment etc.), and maybe some social/cultural data as well (lifestyle, geographical area, occupation). The skull has to be examined for its characteristics. Then the methods and the table of average tissue thicknesses which are the most appropriate for this person must be selected. For instance, if the skull is missing its *spina nasalis anterior* (a small protruding bone at the base of the nasal aperture), it would not be logical to select a method of nose reconstruction which needs the total length of this tiny bone.

The remodelling phase can take place during or after the skull assessment and examining phase. Missing parts can be reconstructed, by hand or on the computer. In the case of 3-D printing the task to combine all the loose parts can also be done after the replica is made. When the skull is completed and duplicated, by casting or by 3-D scanning and 3-D printing, the practical reconstruction procedure can commence. The similarities between forensic and archaeological facial reconstructions lie in the methods and techniques. The used methods to get to the basic shape of the face and its features are the same in both procedures.

Because the goal of the two kinds of reconstructions is different, after some point the procedures may be different. When the shape of the face is established using all the rules, guidelines and tissue thickness tables from literature, the reconstructionist of archaeological cases can begin filling in the blank spots, within certain boundaries of course. You just do not give a Caucasian person a big black afro hairdo. Blank spots are for example eye- and hair-colour. Unless the reconstruction will be monochrome, one has to choose. In these cases it is best to use an average eye- and hair colour for that period and that area. For faces from historic times, the reconstructionist can fall back on paintings or documents. This applies to the hairstyle as well, for example we gave this man a popular haircut for mediaeval times. (figure 3). In figure 4 you can see that we have cheated a little bit by giving this old mediaeval man a cap that was appropriate to his occupation and period of time. If absolutely no data is available, e. g. the reconstruction is from prehistoric times, one most opt for the most plausible solution.

Fig. 3: When no data is available for hairstyle, the reconstructionist of archaeological cases can choose the most likely hairdo. We have given this mediaeval man a popular mediaeval haircut.

Fig. 4: Hiding the hairstyle altogether by putting on a cap on the head of this reconstruction of a very old mediaeval man.

The more realistic a face appears to be, the more interesting it is for the public. So when making an archaeological facial reconstruction, the reconstructionist is allowed to make the face very lifelike. This asks for much detailed sculpting, painting and hair work.

The wrinkles, matching the age and keeping in mind the lifestyle of the subject of course, have to be painstakingly sculpted (figure 5). Skin structure has to be added. This is all very time-consuming but the result is very rewarding. If it is the intention to put the reconstruction on display, the finished clay sculpture has to be reproduced in a less vulnerable material. For this purpose a mould is made of the completed reconstruction so that it may be cast in a synthetic material that is durable and resembles human skin. This cast is then painted, after which real hair is punched in to create the eyebrows, eyelashes, moustache and beard. A wig can be used for the scalp. Glass eyes completed the reconstruction.

Fig. 5: This is a detail of a facial reconstruction which shows the sculpted wrinkles.

For forensic cases such detail is not necessary, or even desirable and too time-consuming. The purpose here is identification. Adding details for which there is no real evidence lessens the chance of recognition. False information can put people who knew the victim on a wrong track so that they exclude the person who has to be identified [3].

When the shape and the features of the face are established, along with the sex and a general suggestion of its age, this alone can trigger the memory of a missing person. So if eye- and hair colour are unknown, the reconstruction should be made monochrome. After all, it is not a portrait, but more an approximation.

The question whether or not to give forensic reconstructions hair when the hairstyle is unknown, remains an issue of some debate among reconstructionists. Most people, especially children and women, do have hair. But hairstyle is so important for the recognition of faces that the following question arises: is it worse to show a bald head (basically also a hairstyle) and in doing so signalling that the hairstyle is unknown, or is it worse to show hair, albeit most likely with a wrong hairstyle, and in doing so giving wrong information? Luckily the chance of finding remains of hair is greater with modern skulls as is with archaeological specimens

If the finished forensic reconstruction does not need to last or to be transported, there is no reason to copy the clay sculpture in a more durable material, so the whole casting procedure can be left out.

Three archaeological cases from the Stone Age

This skull dates from ca. 6000 years ago. In the Netherlands this is the era of the New Stone Age. The skull is from an adult man, *homo sapiens sapiens*, age 25–45 years. His skull was almost complete, but preserved badly and in pieces. The skull was taken to a hospital, where it was scanned in the CT scanner. Little pieces, like parts of the jaw-joint, could be cast using dental alginate. Because the right zygomatic bone was missing, the left cheekbone was mirrored on the computer to complete the skull, see figure 6.

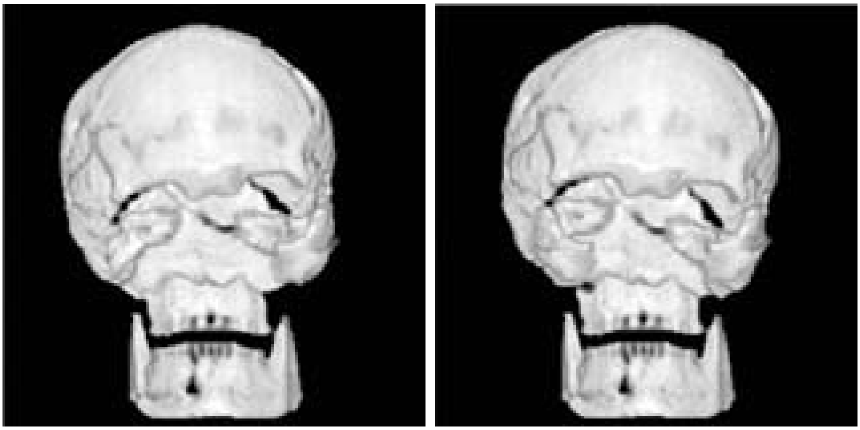

Fig. 6: Two low resolution visualisations of the "exploded", digital skull. Only the big parts were scanned. Left: the skull with the right cheekbone missing. Right: the skull is completed with a mirrored left cheekbone. (Courtesy of K. Vincken, Image Sciences Institute, University Medical Center Utrecht).

Some of the nasal bones were missing too, so the shape of the nose had to be deducted from the surrounding bones and the dimensions of the skull. For this purpose we used guidelines from literature [4], [6]. According to research, remodelling missing parts can be done relatively accurately [7]. As one can see in figure 7 here we have used the anatomical method, first building the facial musculature, and then, with the aid of the average tissue thicknesses, applying the subcutaneous fat and skin layers.

Fig. 7: Halfway the reconstruction. On the right side of the face a stylised representation of the facial musculature is still visible. On the left side the subcutaneous fat and the skin layers have already been applied.

When working on a 3-D printed copy from CT scan data, the skull is not as detailed as the original skull. Only the attachments of the big muscles (e. g. *musculus masseter* and *musculus temporalis)* can be seen. Details on this skull in particular were obscure in any case because of erosion. So building the facial musculature on this skull is merely done for the public. In this way people can get an understanding of how the face emerges from the skull, which is more interesting for educational purposes.

Obviously an other problem with archaeological reconstructions is that there is no tissue data available for ancient people. So we are forced to use the tissue data that hopefully resembles the people living at that time the most. For this reconstruction we have selected the table for West-European males, between 35–39 years of age [8].

Because the people in the New Stone Age were outdoors more, we chose to give him a weather-beaten face. And because archaeologists have never found any evidence of stone-age shaving equipment, a beard seemed a plausible addition, though the fact that something is never found does not mean that it never existed. We have even given this man a facial expression: he is squinting, trying to see something in the distance (figure 8).

Fig. 8: This is the finished reconstruction of the Stone Age man who lived in the Netherlands, some 6000 years ago.

Another example involves the oldest burial site ever found in the Netherlands, dating from 7000 years ago, from the Middle Stone Age, see figure 9. This person was reconstructed in the same position as she was found in her grave, i. e. lying on her left side, with her eyes closed. She was somewhere between 40–60 years old. Because of the fragility and delicacy of the skull, it too was brought to the hospital to be scanned.

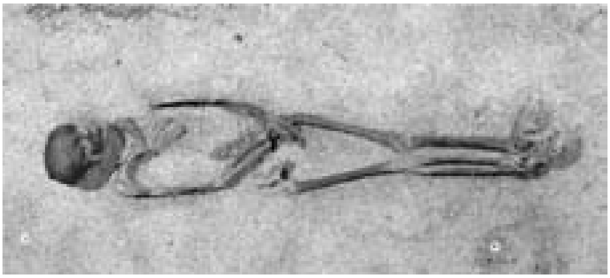

Fig. 9: The skeleton as it was found during excavation. This represents the oldest burial ever found in the Netherlands, dating from 7000 years before present (courtesy of Projectgroep Archeologie Betuweroute).

The left part of her braincase was caved in, so we used the computer to mirror her right side, see figure 10.

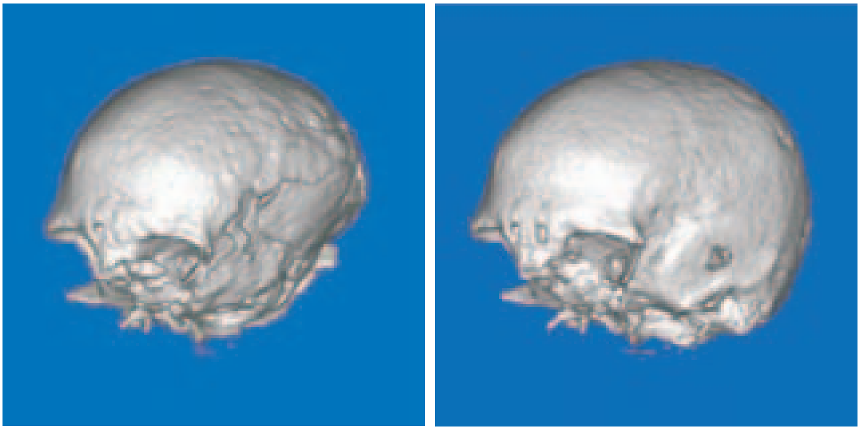

Fig. 10: Left: the left part of the brain case was caved in. Right: on the computer the right side was mirrored over the left side. (Courtesy of K. Vincken, Image Sciences Institute, University Medical Center Utrecht).

Mirroring makes a skull symmetrical, and it is a well known fact that nobody is perfectly symmetrical. But if this is all you have, this is what you will have to work with.

Another problem was that part of her jaw was slightly bent, so after the jaw was 3-D printed in its distorted state, the jaw was cast in a temporarily pliable material in order to correct this.

Because this reconstruction depicts a recently deceased woman, we have used the tissue thickness table derived from cadaver measurements [9]. Her age suggested that she probably had grey hair and as the eyes are closed, no eye colour had to be selected (figure 11).

Fig. 11: A facial reconstruction of the Stone Age woman, in the same position as she was laid out at her burial.

This is another facial reconstruction from the New Stone Age. The reconstruction of this young woman, age 25–34, from 5000 years ago, posed other problems. Because of certain conservation methods, the skull was partly incrusted with the surrounding matrix. The jaw was displaced and also imbedded in this dirt (figure 12).

Fig. 12: The cranium of a Stone Age woman, partly incrusted with the surrounding dirt with an also incrusted displaced lower jaw.

Because of this crust and the fragility of the bones it was impossible to take a cast directly from the skull. Therefore this skull too was CT scanned. Unfortunately the density of the matrix was almost the same as the density of the bone, so it could not be removed automatically from the digital data, but had to be removed manually voxel by voxel (a voxel is a spatial pixel). After some data wrangling the skull was clean. See figure 13 for the result. These data could then be 3-D printed and the reconstruction could commence.

Fig. 13: The skull of figure 12 after the encrusted dirt has been digitally removed. (Courtesy of K. Vincken, Image Sciences Institute, University Medical Center Utrecht).

Principally this facial reconstruction was made following the guidelines of a German method (figure 14) [8], [10]. In figure 15 you can see what this woman may have looked like.

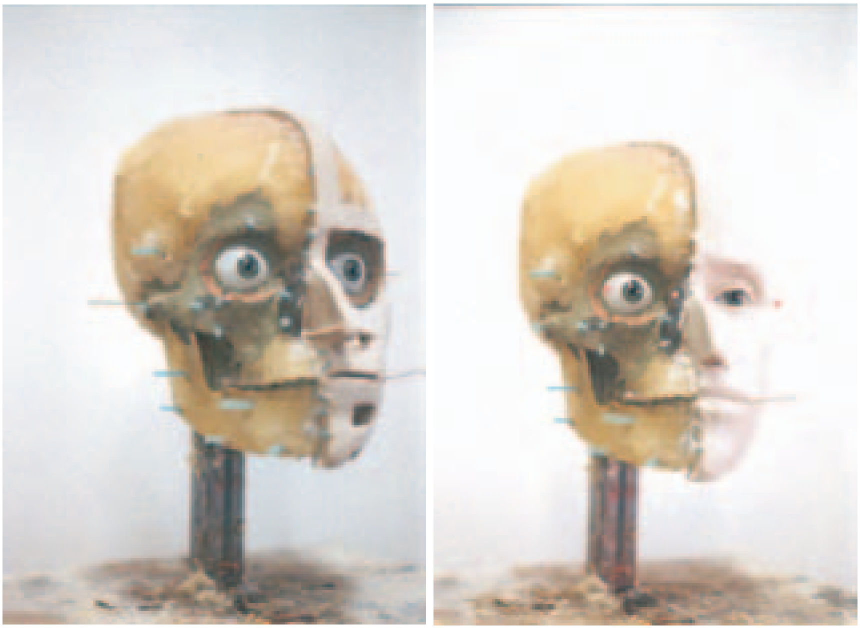

Fig. 14: During the reconstruction.

Fig. 15: The finished reconstruction. This is how this young woman from the Stone Age could have looked like.

And so, by using new techniques, 21st- century man can meet these Stone Age people face to face, thousands of years after their demise.

Whether or not these reconstructions closely resemble the original faces, we will never know. But they surely are spectacular aids in bringing the distant past to life.

References

[1] J. Henderson, "Factors determining the state of preservation of human remains," in *Death, Decay and Reconstruction*, A. Boddington, A. N. Garland and R. C. Janaway, Eds. Manchester: Manchester University Press, 1987, pp. 43–54.

[2] J. Prag and R A. H. Neave, *Making Faces*. London: British Museum Press, 1997.

[3] C. Wilkinson, *Forensic Facial Reconstruction*. Cambridge: University Press, 2004.

[4] K. T. Taylor, *Forensic Art and Illustration*. Boca Raton: CRC Press, 2001.

[5] T. M. Buzug, P. Hering and R. P. Helmer, "3D tomography as a basis for anthropological and forensic facial reconstruction," in *1. International Conference on Reconstruction of Soft Facial Parts in Potsdam/Germany from 10 to 12 November 2003*, pp. 91–108.

[6] R. M. George, "Anatomical and artistic guidelines for forensic facial reconstruction," in *Forensic Analysis of the Skull*, M. Y. Işcan and R. P. Helmer Eds. New York: Wiley- Liss, 1993, pp. 215–227.

[7] H. Colledge, "Loss of face? The effect on the outcome of craniofacial reconstruction when part of the skull is missing," M.Sc. thesis. University of Manchester, Manchester, Great Britain, 1996, in: C. Wilkinson, *Forensic Facial Reconstruction*. Cambridge: University Press, 2004.

[8] R. Helmer, *Schädelidentifizierung durch Elektronische Bildmischung*. Heidelberg: Kriminalistik Verlag, 1984.

[9] J. S. Rhine, C. E. Moore and J. T. Westin, Ed. "Tables of facial tissue thickness of American Gaucasoids in forensic anthropology," in *Maxwell Museum Technical Series*, vol. 1, 1982.

[10] R. Helmer, "Identifizierung unbekannter, unkenntlicher Leichen mittels bildtechnischer oder rekonstruktiver Verfahren," in Identifikation Unbekannter Tote, D. Leopold, Ed. *Arbeitsmethoden der medizinischen und naturwissenschaftlichen Kriminalistik*, Vol. 22. Lübeck: Schmidt-Römhild Verlag, 1998, pp. 449–501.

One man with many faces. Facial reconstruction of Man X.

P. Mala, V. Novotny and H. Eliasova

Abstract

We arranged an experimental study (double-blind experiment) to examine the most common methods of facial reconstruction, especially prediction guidelines both in context of the whole face and separately. Material used in this study was a skull of recently deceased individual, white male, 63 years old. We made eight drawings and three sculptural facial reconstructions according to guidelines of various authors. Using various techniques and guidelines for facial approximation we created more or less different faces based on one and the same skull. The approximative superprojections and partial comparisons of faces (Fig. 6–10) show similarities and differences. The greatest differences were found in size and morphology of the nose and the mouth. In this case the most "accurate" (the nearest to the reality) prediction guideline applied to the facial reconstructions we made are those of Lebedinskaya [6] in both cases, nevertheless the width of mouth still differs about 1 cm.

Introduction

Anthropological facial reconstruction concerns a study and practical application of knowledge about the relation between morphology of face and morphology of its skull. It is a technique used to rebuild lost or unknown features of person's face over the skull. The aim of this process, especially in forensic area, is to promote recognition and identification of the unknown individual.

Contemporaneous principles of the facial reconstruction methods stand on two not too stiff pillars. The first of them is based on average values of soft tissue depths measured at defined points of the face. The second pillar is constituted of several guidelines to determine the size and shape of facial features. It is obvious that knowledge of the thickness of facial soft tissues without knowledge of the prediction guidelines lose its sense for the facial approximation and vice versa. But the crucial question is the accuracy of the techniques of facial reconstruction.

There is quite a limited number of the prediction guidelines regarding the complexity of the human face and only a few of them have been empirically tested to estimate their accuracy (for example [1]). Even if anybody follows them exactly, many other unclear anatomical and morphological characteristics emerge. These are left on intuition of the person who approximates the face. In fact just recent examination has revealed a great inaccuracy of some prediction guidelines.

Design of the study

We arranged an experimental study (a double-blind experiment) to examine the most common methods of facial reconstruction and we tried to evaluate the accuracy of the published prediction guidelines. To realize this objective we have to choose appropriate material. Material used in this study was one skull of recently deceased individual. The skull was provided by The Institute of Criminalistics Prague, Police of the Czech Republic. The identification of this skull was corroborated by scientific and circumstantial evidence. Then it was also positively identified as the presumed person using a photo to skull superimposition (fig. 1). So a photo of that person when alive (frontal view) was available, which allowed a subsequent mutual comparison with a real appearance. But the real appearance of that individual was unknown to the author of the facial reconstructions. It was revealed just after the reconstructions had been completely finished and submitted to the independent evaluation of the forensic expert. We were given only the skull without any other information about the age, sex, health, social status, style of the life . . . of that person.

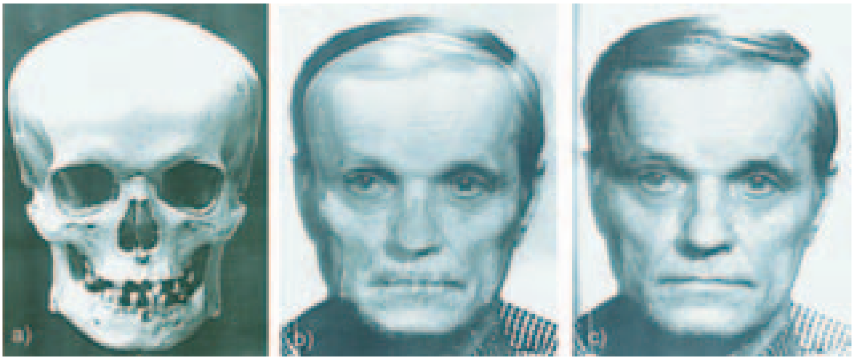

Fig. 1: (a) A photograph of the unidentified skull used for the purpose of skull to photo superimposition, (b) the skull to photo superimposition made by forensic anthropologist Dr. Hana Eliášová from the Institute of Criminalistics Prague, which led to identification of skeletal remains, (c) a photo of the Man X.

Material

The anthropometric and morphoscopic examination of the skull which became a base for the facial approximation was made. It belongs to a white male [2–4]. Age at the time of death was estimated between 45–55 years [5]. With regards to the strongly developed muscle insertion places we supposed that the muscles of the face were developed very well. And we tried to bring this presumption into the approximated face.

Methods

To realize the facial approximation we followed the instructions published in well-known books and articles about the facial reconstructions [6–10]. We made eight drawings (five of them were profiles – according to Lebedinskaya [6], Neave [7], Taylor [8], George [9], Stephan [10]; and three were en faces – according to Lebedinskaya [6], Neave [7], Taylor [8]). Stephan [10] provides a guideline only for the approximation of the nose, so the mouth we approximated according to George [9]. To create three sculptural facial reconstructions we used three classical techniques, the Russian one [6], the British one [7] and the American technique [8] (fig. 2–4). The Russian technique is often called as the anatomical method, which refers to the process of building a face muscle by muscle, developed by Gerasimov. We should mention that the Gerasimov's method was modified by his followers (Lebedinskaya, Balueva, Veselovskaya) and at present only musculus masseter and musculus temporalis are modelled. The next procedure is very similar to that, what is called the American technique, it means putting down strips of clay and filling space between them.

To enable comparison between the reconstructions we used only one and the same set of soft tissue values [6, 16] in each case. Author of the facial approximations is Pavla Malá.

Fig. 2: Sculptural facial reconstructions according to (a) Lebedinskaya [6], (b) Taylor [8] and (c) Neave [7].

Fig. 3: Drawing facial reconstructions according to (a) Lebedinskaya [6], (b) Taylor [8] and (c) Neave [7].

Fig. 4: Drawing reconstructions of profile according to (a) Lebedinskaya [6], (b) Taylor [8], (c) Neave [7], (d) George [9] and (e) Stephan [10].

Results

Using various techniques and guidelines for the facial approximation we created more or less different faces based on one and the same skull (fig. 1–4). In context of other researches similar results were obtained also by Stephan and Henneberg [11]. The greates differences were found in the size and morphology of the nose and the mouth.

We used five several prediction guidelines to approximate the nose from the lateral view. As the nose is an important feature of the face viewed from profile, these differences are reflected also at type of the whole face. Mutual comparison made by overlapping outlines of five drawings revealed that we can distinguish three types of the profile of Man X (fig. 5).

Fig. 5: The overlap of reconstructed profiles according to Neave (red colour), Taylor (green colour), Lebedinskaya (blue colour), George (black colour), Stephan (yellow colour).

Similar couples consist of noses approximated according to Neave [7] and Taylor [8], then George [9] and Stephan [10], and the third type is represented by nose reconstructed following instructions of Lebedinskaya [6]. It should be mentioned that the only technique for prediction of the "exact" shape of nose profile from these selected guidelines is that of Lebedinskaya [6], or generally the Russian technique, while other methods predict only a position of pronasale point. Unfortunately it was not possible to make a comparison with the real appearance of the face profile of Man X, because only photo of en face was available.

Then we chose the published prediction guidelines for determination the width of the mouth, the width of the nose and the height of the lips and we applied them to the skull of the Man X. The results are summarized in the Tables 1 and 2. Determining the width of the mouth we obtained several values ranging from 42 mm to 63 mm. So two extreme values differ about 21 mm! Results of the estimated width of the nose extend from 29,5 mm to 42,2 mm. It indicates the difference about 12,7 mm. Also the height of the red part of lips was different because of diverse positioning of the point stomion refered by several authors [7, 9, 10]. If we consider the size of Man X's face photograph used for identification by superimposition as representing exactly the living size, then his mouth was 59 mm wide and the nose 39 mm wide (measured on the photograph). In this case of the skull of Man X the most "accurate" (the nearest to the reality) guideline among the guidelines selected by us (Tables 1, 2) are those of Fedosyutkin and Nainys [13] and Hoffman, McConathy, Coward and Saddler [18] for the width of the nose and that of Veselovskaya [16] for the width of the mouth. Otherwise, the nearest to the reality prediction guideline from those which we really used to create the facial reconstructions are the guidelines of Lebedinskaya [6] in both cases, nevertheless the width of mouth still differs about 1 cm. Lebedinskaya presents the principles and results of all followers of Gerasimov in her book [6]. However, a development of the reconstruction methods and prediction guidelines quickly continues. That is a brief quantitative evaluation of facial approximations.

Tab. 1: The width of the mouth of Man X estimated according to several prediction guidelines

guideline – the width of the mouth is equal to:	**value [mm]**	**author**	**notes**
the corner of the mouth is situated between the first and the second maxillary premolar	**51***	[6]	* approximately because of the missing crown of the first right premolar
the distance between the medial borders of irises	**50***	[7]	* the position and the size of the eyeballs and irises according to [9]
the corner of the mouth is situated at lateral margin of maxillary canine	**42***	[8]	* approximately because of the missing canines, measured as the distance between the lateral borders of their alveoli
the distance between the midpoints of the pupils	**63***	[12]	* the position and the size of the eyeballs and pupils according to [9]
the distance between the second maxillary molars	**54***	[13]	* approximately because of the missing second molar

guideline – the width of the mouth is equal to:	**value [mm]**	**author**	**notes**
the corner of the mouth is equal to the point of intersection of the line connecting *foramen infraorbitale* and *foramen mentale* and the line of the mouth fissure	**53**	[14]	
the distance between the lateral margines of canines/0,75	**56***	[15]	* approximately because of the missing canines, measured as the distance between the lateral borders of their alveoli
21,817 + 0,7 × dental arch width at the level of the second upper premolars	**57,9**	[16]	

Guidelines and values in italics were applied to sculptural facial reconstruction

Tab. 2: The width of the nose of Man X estimated according to several prediction guidelines

guideline – the width of the nose is equal to:	**value [mm]**	**author**	**notes**
the distance between *juga alveolaria* of canines at the level of *subnasale* point	*37*	[6]	
the distance between the midpoints of alveoli of maxillary canines	**38,5**	[13]	
the width of *apertura piriformis* + 9,9 mm	**35,4**	[17]	
the width of *apertura piriformis* + 10 mm	*35,5*	[8]	
the width of *apertura piriformis* = 3/5 of the width of the nose (the width of the nose = 5/3 of the width of the *apertura piriformis*)	*42,2*	[7]	
the width of *apertura piriformis* +12,2 mm	**37,7**	[18]	
the width of *apertura piriformis* x 1,51	**38,5**	[18]	
the nostrils are about 2–3 mm lateral to a border of *apertura piriformis* on each side	**29,5–31,5**	[14]	
3/5 of the distance between the irises	**37,8***	[19]	* the position of an eyeball according to [9]
the distance between the distal surfaces of maxillary canines	**42***	[20]	* approximately because of missing canines

Guidelines and values in italics were applied to sculptural facial reconstruction

Then we made visual comparison of reconstructions (fig. 6–10). Here we present the images of approximative superimposition and partial comparisons of faces to promote ideas and impressions of the observers about the similarities and the differences. As a visual perception is naturally subjective, we leave the evaluation of the "accuracy" on you, observers. Some discrepancies of compared images are caused by a slightly different orientation of the skull on the photo used for identification by superimposition and the position of the skull used as a base for the reconstructions (fig. 6). We plan to examine obtained results from the other points if view and also to realize face pool comparison in near future.

Fig. 6: White skull is oriented in position appropriate for superimposition made for identification. Coloured skull is photographed in Frankfurter horizontal and it became the base for graphic reconstructions. This slightly different orientation causes a shift of facial features of compared images in following figures.

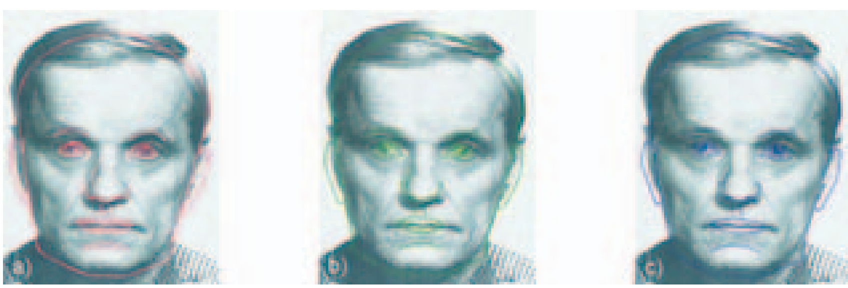

Fig. 7: The overlap of the photo of Man X and scheme of en face according to (a) Neave [7], (b) Taylor [8], (c) Lebedinskaya [6].

Fig. 8: The overlap of reconstructed en faces according to Neave (red colour), Taylor (green colour), Lebedinskaya (blue colour) and the photograph of Man X.

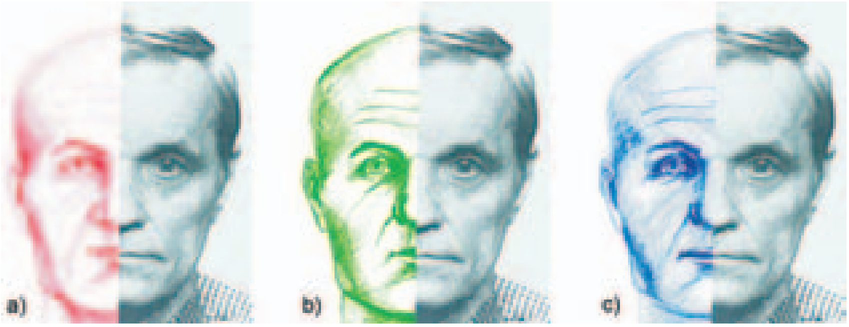

Fig. 9: A comparison of the real face of Man X and the drawing according to (a) Neave [7], (b) Taylor [8], (c) Lebedinskaya [6].

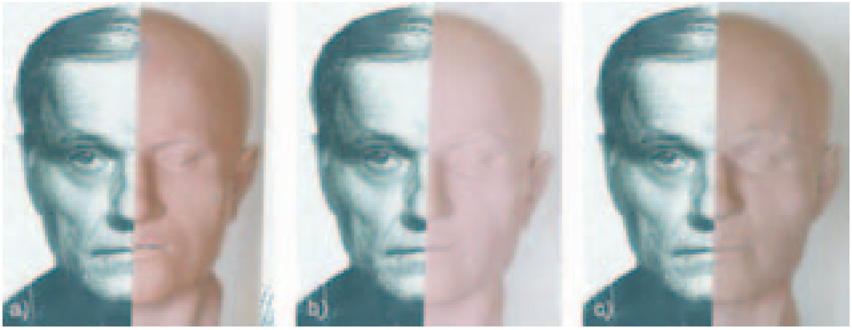

Fig. 10: A comparison of the real face of Man X with the sculptural facial reconstruction according to (a) Neave [7], (b) Taylor [8], (c) Lebedinskaya [6].

The accuracy of the sculptural facial reconstructions was evaluated by the independent expert, the forensic anthropologist Dr. Hana Eliášová from The Institute of Criminalistics Prague, Police of the Czech Republic. The real skull/real face and three facial approximations were considered and their differences and similarities were found out (Fig. 11). Following summary of the results was made:

1. The correspondence between the set of points measured on the skull, and their equivalent points measured on the approximation portrait, is evident.

2. The metric vertical and horizontal proportions of the upper face of skull correspond to the proportions of the facial approximations.

3. The consistency was proved: between the outline of the vault of the skull and all facial approximations, between the outline of the mandible of the skull and all facial approximations.

4. The width and height of forehead (of the skull/face and facial approximations) are coincident in all cases.

5. The position, size and shape of eyes correspond to the reality.

6. The accepted differences were evident in size and morphology of the nose in norma frontalis.

7. The most significat differences between the real skull and facial approximations were found in the shape and size (especially width) of the mouth. The similarity of the width of the mouth is visible only in the case of facial approximation according to Lebedinskaya.

8. Remarkable divergences were found in the low marginal area of mandible (inappropriaetally applied soft tissue).

9. The compared mouth lines show only the approximation.

10. The discrepancies between real mouth ouline and reconstructed results are evident.

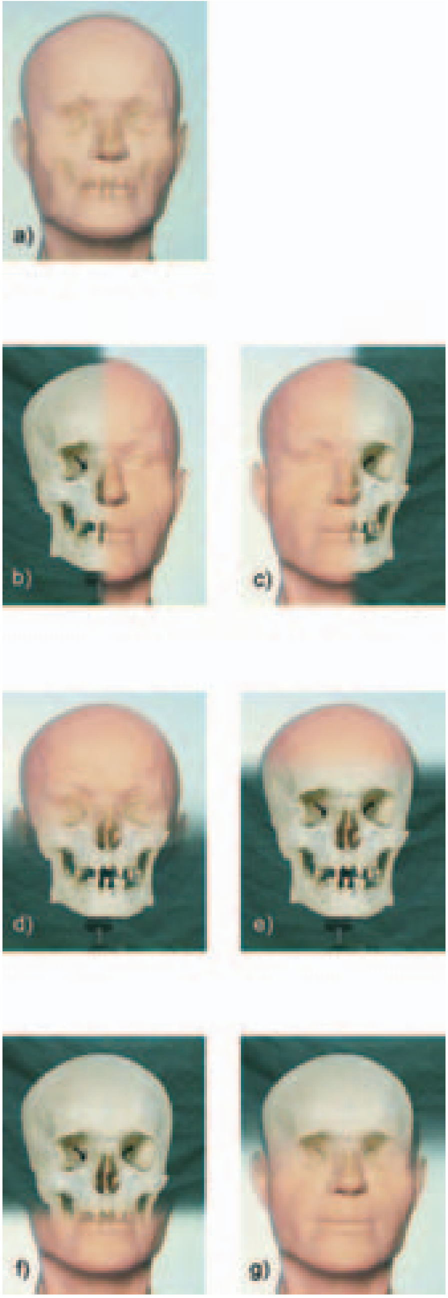

Fig. 11: Presented superimposition showing comparison between the skull and facial approximation (according to Lebedinskaya [6]), (a) superimposition (in frontal view) showing total mixing image of the skull and the reconstructed face (the facial approximation), (b)-(f) the horizontal and vertical wipe images facilitating the comparison of positional relationships between the skull and face approximation.

Apart from the differencies within the whole group of the approximations, we have to mention differences between individual reconstructions and the real face, particularly the age marks of faces. This is due to inaccurate age estimation made by the author (45–55 years), while the real age of Man X was 63. Because of absence of the great number of the teeth and a fixed attachement of mandible to the rest of the skull, what made more detailed view at teeth masticatory surface impossible, the age estimation was difficult. It caused that age marks were not approximated well.

Discussion

In this study we focused on examination of several facial reconstruction methods, especially prediction guidelines in context of the whole face and also separately. Our effort has resulted in eight approximated faces of the one man (drawings of the profile and enface which match together we consider as one face). All of them belong to Man X. Which of them is the right? Does it mean that each human skull can have as many approximated faces as reconstruction methods exist? (or even as many as different scientists and forensic artists do such facial approximation?) As a help to answer these questions we offer to you images of approximative superprojections and partial comparisons of faces.

One of the reasons, why the approximated faces are more or less different form each other, is the use of various reconstructive techniques and different prediction guidelines. Other aspect, which influence is obvious, is a dependability of the author of the reconstructions as well as drawing and sculptural skills. And many other factors contribute to the result. But the most important thing is that there exist several guidelines to determine the same facial feature which give diverse results, so it is logically impossible to be correct all of them [11]. That is one of the reasons, why another tests of facial approximation principles is needed. This study was a test of the methods but also a test of the author herself.

Conclusion

In this study we tried to examine several facial reconstruction methods. Even if reconstructed faces of Man X vary more or less from each other, they represent one similar type. The aim of this study was to reveal a base of facial reconstruction method, to indicate to some problems, inaccuracies and great deal of subjectivity, which is integral part of this method at the present state of knowledge. This is one man "case study", the results cannot be generalized to all cases, but it has revealed interesting findings, which should be borne in mind.

Acknowledgement

I would like to thank all people and institutions that assisted me in working out this study, which was a part of my M. S. thesis.

Referencies

[1] C. N. Stephan, "Facial approximation: an evaluation of mouth width determination," *American Journal of Physical Anthropology*, vol. 121, pp. 48–57, 2003.
[2] W. M. Krogman and M. Y. Iscan, *The Human Skeleton in Forensic Medicine*. Illinois: Charles C. Thomas Publishers, 1986.
[3] J. S. Rhine, "Non-metric skull racing," in *Skeletal Attribution of Race. Methods for Forensic Antropology,* G. W. Gill and S. Rhine, Eds. Maxwell Museum of Anthropology, University of New Mexico, Alburqueque, 1990, pp. 9–21.
[4] G. Acsadi and J. Nemeskeri, *History of Human Life Span and Mortality.* Budapest: Akadémiai Kiadó, 1970.
[5] C. O. Lovejoy, "Dental Wear in the Libben Populations: Its Pattern and Role in the Determination of Adult Skeletal Age at Death," *American Journal of Physical Anthropology,* vol. 68, pp. 473–485, 1985.
[6] G. V. Lebedinskaya, *Rekonstrukcija Lica po Cerepu*. Moskva: Staryj Sad, 1998.
[7] R. Neave and J. Prag, *Making Faces: Using Forensic and Archeological Evidence*. London: British Museum Press, 1997.
[8] K. T. Taylor, *Forensic Art and Illustration*. Boca Raton: CRC Press, 2001.
[9] R. M. George, "The lateral craniographic method of facial reconstruction," *Journal of Forensic Science,* vol. 32, pp. 1305–1330, 1987.
[10] C. N. Stephan, M. Henneberg, and W. Sampson, "Predicting nose projection and pronasale position in facial approximation: A test of published methods and proposal of new guidelines," *American Journal of Physical Anthropology,* vol. 122, pp. 240–250, 2003.
[11] C. N. Stephan and M. Henneberg, "Building faces from dry skulls: are the recognized above chance rates?" *Journal of Forensic Sciences*, vol. 46, pp. 432–440, 2001.
[12] W. M. Krogman, *The Human Skeleton in Forensic Medicine*. Springfield: Charles C. Thomas, 1962.
[13] B. A. Fedosyutkin and J. V. Nainys, "The relationship of skull morphology to facial features," in *Forensic Analysis of the Skull. Craniofacial Analysis, Reconstruction and Identification,* M. Y. Iscan and R. P. Helmer, Eds. New York: Wiley-Liss, 1993, pp. 199–213.
[14] J. Angel, "Restoration of head and face for identification," presented at 30th Annual Meeting of the American Academy of Forensic Sciences, St. Louis, MO, 1978.

[15] C. N. Stephan and M. Henneberg, "Predicting mouth width from inter-canine width – A 75% rule," *Journal of Forensic Sciences*, vol. 48, pp. 1–3, 2003.

[16] E. V. Veselovskaya (private communication), 2004.

[17] A. Schultz, "Relation of the external nose to the bony nose and nasal cartilages in whites and negroes," *American Journal of Physical Anthropology,* vol. 1, pp. 329–338, 1918.

[18] B. E. Hoffman, D. A. McConathy, M. Coward, and L. Saddler, "Relationship between the piriform aperture and interalar nasal widths in adult Males," *Journal of Forensic Science,* vol. 36, pp. 1152–1161, 1991.

[19] L. G. Farkas and I. R. Monro, *Anthropometric Facial Proportions in Medicine*. Springfield: Charles C Thomas, 1987.

[20] C. F. Picard, "Complete denture aesthetics," *Journal of Prosthetic Dentistry,* vol. 8, p. 252, 1958.

Ancient Faces – Facial Reconstruction in Archaeology: 3 – Dimensional Facial Reconstruction in Pre- and Early Historical Archaeology. Development, Methodology and Current Stocktaking

Annika Lampe, Renate Rolle, Jörg Orschiedt

Universität Hamburg, Archäologisches Institut, Abteilung I, Vor- und Frühgeschichtliche Archäologie, Johnsallee 35, D-20148 Hamburg (Germany)

Abstract

The diploma paper "3 – dimensional Facial Reconstruction in Pre and Early Historical Archaeology. Development, Methodology and Current Stocktaking" represents the basis for this Abstract.

The discourse deals with facial reconstructions and their applications and provides a historical overview in the scope of anthropology and archaeology as well as forensics.

The different ways of measuring tissue depths on the human face, as well as the guidelines for reconstructing the facial organs and the reconstruction methods are explained. Additionally, the lack of standardizations in measuring the tissue depths are pointed out. The social meaning of the face in the past and the present represents a further aspect of investigation. In archaeology the facial reconstruction can be of great didactical value.

The archaeologic facial reconstructon plays an important role in understanding mankind's history, because it virtually illustrates the physiological development of the skull and the postcranial skeleton. Another possibility is to show important historic personalities.Bog bodies and mummies are also a suitable subject of facial reconstruction in order to bring us nearer to our past.

The facial reconstructions have changed regarding to the methods and their importance since the first reconstruction in 1898. This is shown clearly by the actual stocktaking of the 176 archaeological facial reconstructions, which were made skulls of the pre- and early historical men, as well as of historical personalities from the european and american region.

Already small differences in the methodical bases and in the individual conceptions are sufficient, in order to produce completely different expression. Finally each reconstruction attempt, and in particular of hominids, is subject to a huge number of imponderables. These get to be eliminated by further background information in today's facial reconstructions.

Facial Reconstruction in Archaeology

The face fascinates the human being since the Neolithic Period at least. This is shown with the so-called "over-modelled heads" from the Neolithic Period (Early Neolithic Period in the Levante, approx. 7500–5500 B. P., fig. 1) and the Bronze Age (Katakombengrabkultur in the area of the north Caucasus, 2100–1700 B. P., fig. 2) [1], [2]. In 5 different sites in israel, skulls were found, which bear signs of post-mortem plaster remodelling recreating soft tissue features in clay.

Supplementary, the death masks made since the Egyptian and Greek Antique Period (approx. 1500 B. P.).give us the chance to get connected to individuals from ancient times [3].

Fig. 1: Plastered skull from Jericho, Israel. (Excavation: 1952–1958 K. Kenyon). In: MSN Encarta (2004): Plaster Skull from Jericho. http://encarta.msn.com/media_461550215_761555928_-1_1/Plaster_Skull_from_Jericho.html (June 2, 2004).

Fig. 2: Modelled face on a skull from the catacombsgraveculture, Northcaucasus. In: Kruc et al. 1991: 52, Abb. 1

Heads of the deceased were treated in the Pre- and Early History in different cultures and periods with special rituals.

The common intention for the death masks and the "over-modelled heads", which are taken as the first Facial Reconstructions in history, is for reasons of keeping the individual face visible beyond it's waste away.

Today's application of the scientifically manufactured facial reconstruction is to try to follow this interest again with a connection to our past, by looking directly into the individual faces.

Today the appearance of former humans still inspires us and in particular the archaeologists.

Especially lifelike death masks can mediate an individual picture of the appearance of the ancient humans.

Tissue depth measurements and guidelines for facial organs

At least in the 18th century scientists started to recognize relationships between particular points at the skull surface to the overlaying soft facial parts of the face. In the year 1792 the physiognomist Camper posited, that the soft facial parts would overlay the skull surface in a regular way.

Since the 19th century we try to approach the appearance of humans on the basis of the skull. The knowledge of soft facial parts and their relations with the skull morphology allows us to reconstruct the face. Research of anatomists, anthropologists, archaeologists, forensics and medicines created a database of standardized tissue thicknesses and guidelines for the reconstruction of the face organs.

Secured data to the conditions of the soft facial parts are required, in order to reconstruct the face on the basis of the skull.

Tissue depth data was won by direct measuring at the beginning of the 20th century [4]. Relationships between the skull surface and the overlaying soft tissues were subject to investigations by Gerasimov since the 1930 s [5], [6]. Soon the Roentgen-method was developed, but it could not be used for tissue depth measuring until the 1950 s [7], [8], [9]. The ultrasonic measuring procedure and the CT-scanning followed [10], [11].

Until today, over 40 different anatomical points for the measuring of the tissue depths were selected. The measurements are based on different conditions and therefore limit comparison of different investigations. Thus, standard tables are missing. Newer results could not revise old ones, that is why there is a lack of universal tissue depth data [10].

Due to this non-standards facial reconstructions are often based on many different data from different investigations. The comparison problems are expressed in following aspects:

1. Difference in the number of examined individuals (sample size),
2. different measuring points,
3. different causes of death,
4. data from corpses and living persons,
5. different populations and
6. different subdivisions into age, sex, constitution, nutritional condition.

The following table seizes some of these aspects together and functions as an overview of the most important data ascertainments and their dimensions.

Tab. 1: The most important tissue depth measurements from adults, subdevided into author, year, measuring method, sample seize and population. (Sample seize: m: male, f: female).

Author	**Year**	**Sample seize**	**Measuring method**	**Population**
Welcker	1883	13 (m: 13)	Direct	Europids
His	1895	37 (m: 33, f: 4)	Direct	Europids
Kollmann/ Büchly	1898	29 (m: 22, f: 7)	Direct	Europids
Birkner	1903–1907	6 (m: 6)	Direct/x-ray	Mongolids: chinese
Fischer	1905	2 (m: 2)	Direct	Mongolids: papua
Czekanowski	1907	115 (m: 64, f: 51)	Direct	Europids: (swiss)
v. Eggeling	1909	3 (m: 3)	Direct	Negroids: (hereros)
Stadtmüller	1923–1925	18 (m: 13,fw: 3)	Direct	Caucasians, mongolids, negroids
Köstler	1940	20 (m: 20)	X-ray	Caucasians
Weißer	1940	20 (m: 20)	X-ray	Caucasians?
Suzuki	1948	55 (m: 48, f: 7)	Direct	Mongoloids: japanese
Gerasimov	1955	Direct method: 71 orientation values (m: 71), x-ray: 19	Skull-soft tissue relationship/x-ray	Mongoloids, caucasians
Bankowski	1958	24 (m: 15,f: 9)	X-ray	Caucasians
Weining	1958	120 (m: 99, f: 21)	X-ray	Americans
Berger	1965	20–32 (m: 20–32)	Direct	Caucasians
Leopold	1968	154 (m: 102, f: 52)	Direct/x-ray	Caucasians
Helwin	1969	50 (?)	X-ray	Caucasians
Rhine/Campbell	1980	91 (m: 68, f: 23)	Direct	Negroids, mongolids: (americans)
Rhine/Moore/ Weston	1982/84	103 (m: 78, f: 25)	Direct	Caucasians (americans)
Helmer	1984	123 (m: 61, f: 62)	Ultrasonic	Caucasians
Lebedinskaya	1993	1695 (m: 845, f: 850)	Ultrasonic	Mongolids
Philipps/Smuts	1996	32 (m:16, f: 16)	CT	Mixed populations, southafrica
Dumont	1986	194 (m: 93, f: 101) youths	X-ray	Caucasians: (weiße Amerikaner)

Author	Year	Sample seize	Measuring method	Population
Manhein et al.	2000	197 (m: 70,f: 127) adults, 515 children (m: 234, f: 281)	Ultrasonic	Adults: caucasians, negroids children: caucasians, (hispano-americans), negroids

The first point reflects the criticism at the initial investigations. The disadvantage of the measurments of the soft facial parts of the old anatomists exists particularly in the investigation of very small collectives from 2 to 37 persons, as Leopold thinks [11]. Later investigations still relied on very small numbers. Thus, in 1940 the measurements from Kostler and Weisser were based on a sample of only 20 persons [7], [8]. As the table shows, Weining is the first who worked with a sample on a larger scale in 1958 (120 persons) [9]. Referring to this, Lebedinskaya et al. reached a sample seize of about 1000 individuals, which seems to be quite representative [12].

Some listings of tissue depth data show a lack of important measuring point. The 3rd aspect refers to the possible distortions of the soft facial parts, which come from different causes of death. Deceased persons, who have suffered long, wearing diseases for example, show other facial tissue thicknesses than accident victims do [13]. Since the investigation material was not easy to get, the possibilities of selecting under the investigation objects were very small.

Differences between the values of corpses and living persons trace back to postmortal changes in the soft tissue. These are caused by the decrease of the Turgor and the loss of the tonus of the musculature. Generally, ultrasonic measurements and CT-data of living persons are to be preferred, otherwise the face of a dead person would be reconstructed [10]. The populations were considered, as that usually only regional investigation objects were at the disposal. Thus Rhine and Campbell examined the tissue depths of black Americans in 1980, Rhine, Moore, and Weston (1982/84) determined values of white Americans and Gerasimov collected data from diverse Eastern European groups [14], [15], [16], [5], [6].

Also Lebedinskaya et al. determined data of various Eastern European subpopulations [12].

It must be noted that variabilities between the populations can not be seized with small data. But early data ascertainments are partly based on very small sample seizes. Among others, Leopold criticizes Gerasimov, who speaks of non-prominent differences between the different populations, though his sample covered however only a very small extent of the representatives of europids and mongolids [11]. Nevertheless, Gerasimov summarized both, europids and mongolids to one group. Ullrich agrees with the criticism, but stressed out, that the tissue depth data from Gerasimov are to be seen as orientation values only [13], [17]. These keep their practical use, since the characteristics of the respective bone surface are finally decisive for reconstructing the soft facial parts.

The latter aspect means particulary the problematic subdivision into the individual characteristics. Since no uniform pattern is present for organization, the data are usually overall. Their comparability is connected with difficulties. The age is often merely described as "adult". Weining for example examined "american adults" [9].

General influences as nutritional condition and constitution were evaluated and considered differently. While Kollmann and Buechly, as well as Gerasimov, Weining among others regarded to the nutritional state with great importance, Helwin ignored this factor completely or did not pay any attention to it [18], [6], [9], [19].

These different criteria let appear a comparison of results of measurement of different investigations critical. As Helmer states, such a unification of the results from different measurements is precarious, but it seems to be necessary for a comparison of all values [10]. Only a direct comparison can make sense, which takes place between the measuring data of persons of the same age, the same constitution, the same nutritional condition, the same sex and the same ethnic origin.

The resulting average values would be of use for a differentiated choice of the tissue thicknesses. The lack of standardized tables makes the selection more difficult for facial reconstructors. Usually, the reconstructor selects the most current data regarding to the probable ethnic origin. Generally, there is a lack of both, the methods and measurements.

Reconstruction methods

Methods developed due to this database are not only in the range of forensics, but also in anthropology and archaeology. These methods experienced many modifications over the time. While the forensics saw a possibility of identifying unknown and unrecognizable dead persons, to archaeology the facial reconstruction meant a possibility to represent early people in a lifelike form. From this interest the american and the russian method of the facial reconstruction was developed, while the anatomical method and the Manchester- combination method were modifications of the two [20], [5], [21], [22].

The methods differ particularly in the muscle reconstruction and in the use of the tissue depth measurements.

The efficiency of the different methods can not be clearly evaluated, because the percentage of successfully identified persons in forensics are not reliable, as Helmer already ascertains [23]. The american method seems to be based rather on the artistic abilities of the reconstructor, since the structure of the skull is not considered [20], [24]. The anatomical method could be favourable for the facial reconstruction of prehistoric men, especially of hominids, since it works without soft tissue thicknesses. Thus one factor of uncertainty can be eliminated, because we do not have any knowledge about the characteristics of their soft facial parts.

Factors of uncertainty

However, the technique of Facial Reconstruction is subject to continuous criticism, because different reconstructions based on the same skull often showed large differences. Control attempts in forensics were made to point out this problem and settle the criticism.

In general it shows that an "approximate to large similarity" can be achieved to the original face, if the conditions are fulfilled [23], [25]. This requires to obey all reconstruction guidelines, the knowledge of the correlations of the soft facial parts to the bone structure, the anthropologic data to age, sex, population, constitution, pathologies and nutritional status, a certain modelling technology as well as general knowledge of face anatomy, anthropology and physiology.

To reconstruct an authentic face, information is also necessary about makeup-artistic details such as hair style, hair color, eye color, skin color, scars, folds, expression and mimics. These elements can not be seen from the skull [23].

In some forensic cases these details can be seen due to the state of decay. Whereas in archaeological reconstructions one has to rely on historical or figurative sources, which is often the case with well-known historical persons. Another possibility to reconstruct features like hair from ancient people is the conservation from bog bodies or mummies.

If these characteristics are to be reconstructed despite missing information, the reconstructor works inevitably with probabilities. Nevertheless, the reconstuction of superficial features is especially suitable for exhibition purposes of archaeological reconstructions.

Particulary the Facial Reconstructions of hominids seem to be problematic. For there does not exist any knowledge about the soft facial thickness. Such reconstructions will always be only approximations to the probable appearance. With the reconstruction of australopithecines one tries to adjust this deficiency by using the tissue depth measurements of chimpanzees. However this interpolations between human and ape data are only based on probabilities.

The soft part thickness data, the guidelines of the facial organs as well as the anthropologic data try to limit and describe the variability of the human face. However, a hundred percent agreement can not be expected by any reconstruction method, since all variabilities of a face can never be seized [23].

Results for the archaeological facial reconstruction

In forensics the Facial Reconstruction is already used as an integral part of the identification process. But Facial Reconstruction is only taken into consideration when other possibilities to identify a person have failed.

As a presupposition for the identification of a person the presence of certain information, concerning anthropologic data such as age, constitution, nutritional condition, personal characteristics (like scars) and superficial characteristics are required.

If there is no information about these details, a successful identification is difficult [23], [26].

In archaeology and anthropology however a general interpretation of the individual is pursued, for which also background information are consulted. These information consist of biological-functional aspects, environmental influences, diseases, origin areas, etc.

These general background information fill the gaps, which exist with the superficial features (hair style, hair color, eye color, skin color, scars, folds, expression and mimics).

Since authenticity and aliveness can be only obtained by these details, they are to be reconstructed in particular for exhibition purposes and for illustration of the evolution process [25].

The representation of Facial Reconstructions in public and private buildings as well as in media is very popular today. Recently the Complete Body Reconstruction as an extension to the Facial Reconstruction is a proper possibility for exhibition presentations. It can illustrate the development of the postcranial skeleton during the morphologic history of the humans in evolution and is frequently on display in dioramas. In this way object-bound single statements are connected in a historical context.

The complete body reconstruction helps the viewer to recognize, that the process of hominisation did not seize all body sections at the same time, but ran rather mosaically [27].

Thus Facial and Complete Body Reconstructions are increasingly used as exhibition objects, which function as “eyecatchers”.

A broad social class is addressed on the one hand by the scientific way and on the other hand by the illustration of former personalities. History is being displayed and teached to help finding his own identity in human history.

Such didactical purposes however hold the danger to persuade the viewer of certain characteristics, which can go back to personal and subjective conceptions of the reconstructor as well as to ideological influences.

For a critical evaluation of the archaeological acial reconstructions of the last century the detailed view of the example the most often reconstructed skull of the Neanderthal man from La Chapelle-aux-Saints has shown, that it is necessary to differentiate the reconstructions due to different backgrounds. Already small differences in the individual conceptions and in the methodical bases are sufficient to produce completely different expressions.

Thus, each reconstruction, in particular reconstructions of hominids, is subject to a multiplicity of imponderables, which are influenced by personal conceptions and intentions [28].

The specialism of the reconstructor can form for example a certain factor of influence for the reconstruction result. While the early reconstructions from the first half of the 20th century were mainly formed from co-operations between anatomists respectively anthropologists and sculptors, today's face reconstructions are often developed as a different interdisciplinary work. Thus, anthropologists, archaeologists, medical Illustrators, palaeoanthropologists, forensics, anatomists, computer experts, artists, and sculptors can be involved.

Approximations to the probable appearance of the pre- and earlyhistorical humans should be marked for the uncritical viewer.

Finally each face causes an unconscious evaluation, based on association of already well-known characteristic samples.

Particulary the mimics of today's Facial Research, represents an elementary component with the personal evaluation. The personal evaluation is a subconscious process [29], [30].

If no mimics are present, the individual or the reconstructed face is even sensed as "dull" [31]. The quality of these facial reconstructions varies substantially by the differences in the scientific basis regarding the method and the anthropologic data, the objective and intention as well as the personal influences. While some reconstructions represent an ethnical portrait, others aim to be an individual copy of the face of famous personalities or even serve with neutral expression for identification purposes. All these criteria are to be considered with the evaluation.

Further research will work up the scientific basis – especially correlations between skull structur and soft facial parts and tissue depth measurements – the imponderables remain if no superficial details are available. The possibility of the computer-generated reconstructions, which already increased in the field of the forensic, are surely working more economical in contrary to the traditional Facial Reconstruction. Though computer-generated 3D-reconstructions are suitable also for exhibition purposes in archaeology, the traditionally manufactured reconstructions will stay as an integral part of museums for reasons of presentation possibilities.

The current presence of the 3-dimensional facial reconstructions in archaeology is shown in the diagram (table 2). The diagram represents the 176 facial reconstructions, which form the actual stocktaking. The distribution of archaeological facial reconstrucitons is summed up in the time period from 1898 to 2004. This compilation lays however no claim on completeness, since only published and documented reconstructions from the region of Europe and America were taken up. Altogether, the number of archaeological reconstruction will be far larger than documented here. But the diagram will show general tendencies of the development of archaeological facial reconstructions in the last 106 years.

Three phases with a high number of reconstructions are to be recognized. In the 1930 s appears a first rise of the number, which abruptly is interrupted by the first World War. The number of the reconstructions increased then into the 1950 s again drastically. The interest continued into the 1960s. The current period exceeds however the previous phases by far, thus over 100 facial reconstructions were made in the last 15 years. After five years. the current decade reached already the value of the previous decade and surely will continue to rise further in the next 5 years.

Tab. 2: The Distribution of archaeological facial reconstructions in one century (1898–2004), shown in decades.

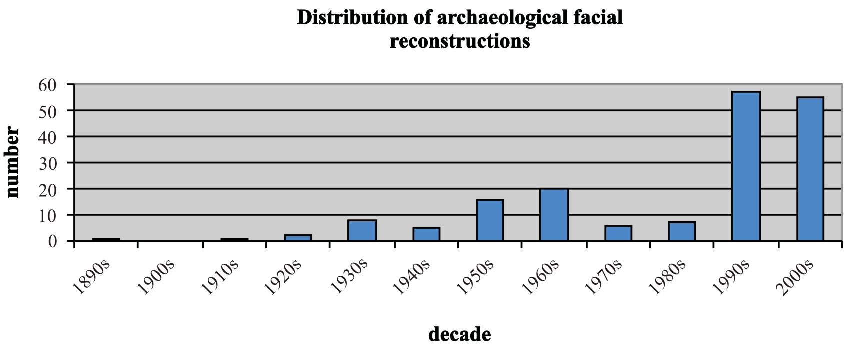

Archaeology can learn from the Facial Reconstruction and co-operation with forensics and anthropologists, in order to bring us nearer to our past. The general interest of connecting history and the names from the past with faces has made the Facial Reconstruction an integral part of archaeology.

References

[1] K. Kenyon, “Jericho,” in *Encyclopedia of Archaeological Excavations in the Holy Land* [Ed.]: Michael Avi Yonah, London, 1976, II.

[2] S. I. Kruc et al., “Das menschliche Gesicht der Bronzezeit,” in *Gold der Steppe. Archäologie der Ukraine*, (Eds.): R. Rolle; M. Müller-Wille; K. Schietzel, Archäologisches Museum der Christian-Albrechts-Universität, Schleswig, 1991.

[3] F. Behn, “Vorgeschichtliches Maskenbrauchtum” Berlin, 1955.

[4] H. Welcker, “Schillers Schädel und Totenmaske nebst Mitteilungen über Schädel und Totenmaske Kants,” Fr. Viehweg u. Sohn, Braunschweig, 1883.

[5] M. M. Gerasimov, “Vosstanovlenie lica po cerepu. (Wiederherstellung des Gesichts aufgrund des Schädels),” in *Izdat. Akad. Nauk SSSR*, Moskau, 1955, pp. 585.

[6] M. M. Gerasimov, “Ich suchte Gesichter. Schädel erhalten ihr Antlitz zurück,” Wissenschaft auf neuen Wegen, Gütersloh, 1968.

[7] J. Köstler, “Röntgenstereoskopische Messungen der Weichteildicken an 20 jungen weiblichen Personen,” Ph. D. dissertation, Erlangen, 1940.

[8] D. Weisser, “Röntgenstereoskopische Messungen der Weichteildicken in der Medianebene des Gesichts an 20 jungen Männern,” Ph. D. dissertation Erlangen, 1940.

[9] W. Weining, “Röntgenologische Untersuchungen zur Bestimmung der Weichteildickenmaße des Gesichts,” Ph. D. dissertation, Frankfurt/Main, 1958.

[10] R. Helmer, “Schädelidentifizierung durch elektronische Bildmischung. Zugleich ein Beitrag zur Konstitutionsbiometrie und Dickenmessung der Gesichtsweichteile,” Kriminalistik-Wissenschaft & Praxis, Band 16, Heidelberg, 1984.

[11] D. Leopold, “Identifikation durch Schädeluntersuchung unter besonderer Berücksichtigung der Superprojektion,” Ph. D. dissertation, Leipzig, 1968.

[12] G. V. Lebedinskaya et al., “Principles of facial reconstruction,” in *Forensic Analysis of the Skull*, Wiley-Liss; 183–198, 1993.

[13] H. Ullrich, “Kritische Bemerkungen zur plastischen Rekonstruktionsmethode nach Gerassimov auf Grund persönlicher Erfahrungen,” in *Ethnogr.-Archäol.*, Vol. 7, 1966, Berlin, pp. 111–123.

[14] J. S. Rhine, H. R. Campbell, “Thickness of facial tissues in the American Blacks,” in *Journal of Forensic Science*, Vol. 25, 1980, pp. 847–858.

[15] J. S. Rhine, C. E, Moore, J. T. Weston, “Facial Reproduction. Tables of Facial Tissue Thickness of American Caucasoids in Forensic Anthropology,” *Maxwell Museum Technical Series*, Nr. 1. 1982.

[16] J. S. Rhine, C. E, Moore, J. T. Weston, “Facial Reproduction. Tables of Facial Tissue Thickness of American Caucasoids in Forensic Anthropology,” *Maxwell Museum Technical Series*, Nr. 1, 1984.

[17] H. Ullrich, "Die methodischen Grundlagen des plastische Rekonstruktionsverfahren nach Gerassimov," in *Zeitschrift für Morphologie und Anthropologie*, 1959, pp. 245–258.
[18] J. Kollmann, W. Büchly, "Die Persistenz der Rassen und die Rekonstruction der Physiognomie prähistorischer Schädel," in *Arch. Anthrop*., Vol. 25, 1898, pp. 329–359.
[19] H. Helwin, "Problematik der Weichteilrekonstruktion auf dem menschlichen Schädel," in *Gegenbaurs morph. Jb*. 116, 1971, pp. 503–513.
[20] W. M. Krogman, "The reconstruction of the living head from the skull". *FBI Law Enforcement Bull*. 15/7, 1946, pp. 11–18.
[21] J. Gurche (jgurche@DMNS.org), "Gurche Main Menu", http://www.gurche.com/main_frameset.htm, Mai 4,2004.
[22] R. Neave, J. Prag, "Making Faces. Using forensic and archaeological evidence," London, 1997.
[23] R. Helmer et al., "Assessment of Reliability of Facial Reconstruction," in *Forensic Analysis of the Skull,* Wiley-Liss., 1993, pp. 229–246.
[24] K. T. Taylor, "Forensic art and illustration," London, New York, Washington D. C., 2001.
[25] C. Wilkinson "Forensic Facial Reconstruction," Cambridge, 2004.
[26] R. Helmer, "Identifizierung unbekannter und unkenntlicher Leichen mittels bildtechnischer oder rekonstruktiver Verfahren," in *Identifikation unbekannter Toter: interdisziplinäre Methodik, forensische Osteologie. Schriftenreihe: Arbeitsmethoden der medizinischen und naturwissenschaftlichen Kriminalistik*; 22. [Eds.]: D. Leopold, S. Berg, B. Brinkmann, Lübeck, 1998, pp. 449–502.
[27] W. Henke, N. Kieser, W. Schnaubelt, "Die Neandertalerin. Botschafterin der Vorzeit," Gelsenkirchen/Schwelm, 1996.
[28] E. Trinkaus, P. Shipman, "Neandertals: Images of Ourselves," in *Evolutionary Anthropology*, Vol. 6, 1993, pp. 189–226.
[29] P. Ekman, "Darwin and facial expression. A century of research in review," New York, London, 1973.
[30] P. Ekman, "Gesichtsausdruck und Gefühl: 20 Jahre Forschung von Paul Ekman," 1988.
[31] J. Cole, "Über das Gesicht. Naturgeschichte des Gesichts und unnatürliche Geschichte derer, die es verloren haben," München, 1999.

Ancient Faces – Facial Reconstruction in Archaeology: Plastische Gesichtsrekonstruktion in der vor- und frühgeschichtlichen Archäologie. Entwicklung, Methodik und aktuelle Bestandsaufnahme

Annika Lampe, Renate Rolle, Jörg Orschiedt

Universität Hamburg, Archäologisches Institut, Abteilung I, Vor- und Frühgeschichtliche Archäologie, Johnsallee 35, D-20148 Hamburg (Germany)

Abstract

Die Magisterarbeit „Plastische Gesichtsrekonstruktion in der vor- und frühgeschichtlichen Archäologie. Entwicklung, Methodik und aktuelle Bestandsaufnahme" bildet die Basis für dieses Abstract.

Die Arbeit beschäftigt sich mit der Gesichtsrekonstruktion und ihrer Anwendung im historischen Überblick auf den Gebieten der Anthropologie und Archäologie sowie der Forensik. Die verschiedenen Ermittlungsmethoden zur Weichteildicke des menschlichen Gesichts, die Richtlinien für die Schädel-Weichteil-Korrelationen sowie die Rekonstruktionsmethoden werden aufgezeigt. Herausgearbeitet werden insbesondere fehlende Standards bei der Weichteildickenermittlung.

Die gesellschaftliche Bedeutung des Gesichts in der Vergangenheit und der Gegenwart stellt einen weiteren Untersuchungsaspekt dar.

Für die Archäologie kann die Gesichtsrekonstruktion eine wertvolle didaktische Arbeit leisten. Der virtuellen Vermittlung von der physiologischen Entwicklung des Schädels- und des postcranialen Skeletts in der Menschheitsgeschichte, sowie der Illustration historisch bedeutsamer Persönlichkeiten kann gar nicht genug Bedeutung beigemessen werden. Auch Moor- und Mumienfunde eignen sich sehr, um der Vergangenheit mittels der Gesichtsrekonstruktion näher zu rücken.

Aufgrund der aktuellen Bestandsaufnahme von 176 plastischen Gesichtsrekonstruktionen auf Schädeln des vor- und frühgeschichtlichen Menschen sowie von historischen Persönlichkeiten aus dem Großraum Europa und Amerika kann ein allgemeiner Methoden- und Bedeutungswandel abgelesen werden. Es stellt sich heraus, dass bereits geringe Unterschiede in den methodischen Grundlagen und in den individuellen Vorstellungen ausreichen, um einen gänzlich anderen Gesamtausdruck zu erzeugen. Jeder Rekonstruktionsversuch, insbesondere der von Hominiden, unterliegt letztendlich einer Vielzahl von Unwägbarkeiten, die aber bei heutigen Gesichtsrekonstruktionen durch weitere Hintergrundinformationen immer besser ausgeräumt werden können.

Gesichtsrekonstruktion in der Archäologie

Das Gesicht übt eine anhaltende Faszination auf den Menschen aus, die mindestens seit dem Neolithikum vorhanden ist. Dies belegen die sogenannten „übermodellierten Schädel" aus dem Neolithikum (Frühneolithikum der Levante, ca. 7500–5500 v. Chr., Abb. 1) und der Bronzezeit (Katakombengrabkultur im Gebiet des Nordkaukasus, 2100–1700 v. Chr., Abb. 2) [1, [2]. Daneben bieten uns die in der ägyptischen und griechischen Antike angefertigten Totenmasken (ab ca. 1500 v. Chr.) die Möglichkeit, Zugang zu einzelnen Individuen aus antiker Zeit herzustellen [3].

Abb. 1: Übermodellierter Schädel von Jericho. (Ausgrabung: 1952–1958 K. Kenyon). In: MSN Encarta (2004): Plaster Skull from Jericho. http://encarta.msn.com/media_461550215_761555928_-1_1/Plaster_Skull_from_Jericho.html (abgerufen am 02.06.2004).

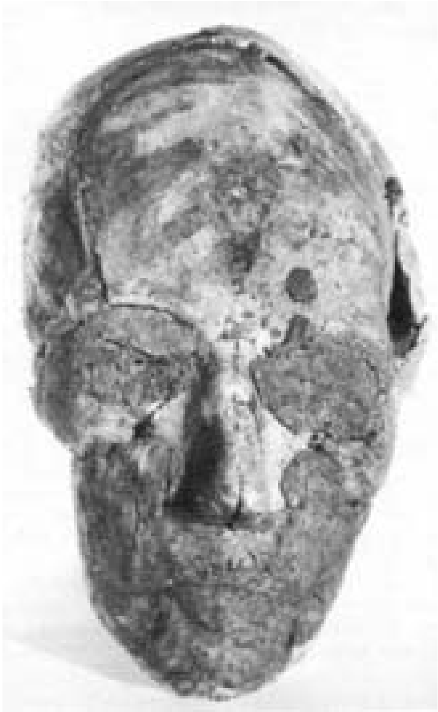

Abb. 2: Modelliertes Gesicht auf einem Schädel der Katakombengrab-Kultur. In: Kruc et al. 1991: 52, Abb. 1.

Schädel Verstorbener wurden in der Vor- und Frühgeschichte in verschiedenen Kulturen und Perioden mit besonderen Ritualen behandelt. Den Totenmasken und den „übermodellierten Schädeln“, die als die ersten Gesichtsrekonstruktionen in der Geschichte gesehen werden, liegt die gemeinsame Intention zu Grunde, das Individuum durch das Gesicht über die Zeit hinaus sichtbar zu machen bzw. zu erhalten.

Durch die heutige Anwendung der wissenschaftlich hergestellten plastischen Gesichtsrekonstruktion versuchen wir diesem Interesse erneut nachzukommen und eine Verbindung zu unserer Vergangenheit aufzubauen, indem wir direkt in die individuellen Gesichter schauen. Das Aussehen früher Menschen begeistert uns und insbesondere den Archäologen noch heute. So können naturgetreue Totenmasken ein individuelles Bild vom Aussehen des vor- und frühgeschichtlichen Menschen vermitteln.

Weichteildickenermittlung und Schädel-Weichteil-Korrelationen

Spätestens ab dem 18. Jahrhundert erkannten Wissenschaftler anatomisch-topographische Beziehungen zwischen Punkten der Schädeloberfläche und den aufliegenden Weichteilen des Gesichtes. Der Physiognom Camper stellte 1792 das

Postulat auf, es gäbe eine gesetzmäßige Beziehung von Knochenoberfläche zur darüber befindlichen Weichteildicke.

Im Zuge der erlangten Kenntnisse über Weichteildicken und deren Beziehungen zur Schädelmorphologie wird seit Ende des 19. Jahrhunderts versucht, sich von wissenschaftlicher Seite dem Aussehen der Menschen auf der Grundlage des Schädels zu nähern.

Die Rekonstruktion des Gesichts auf Grundlage des Schädels erfordert gesicherte Angaben zu den Verhältnissen der Weichteile und der großen Gesichtsorgane.

Die Weichteildicken des menschlichen Gesichts wurden zu Anfang des 20. Jahrhunderts durch Direktmessungen an Leichen gewonnen [4]. Ab den 1930er Jahren sind Untersuchungen der Weichteil-Schädelkonturen insbesondere durch Gerasimov vorgenommen worden [5], [6]. Bereits früh wurde auch die Röntgenmethode entwickelt, doch für die Ermittlung von Weichteildicken konnte sie erst ab den 1950er Jahren verwendet werden [7], [8], [9]. Es folgten das Ultraschall-Messverfahren und die Computertomographie [10], [11].

Bis heute sind über 40 unterschiedliche Messpunkte für die Dicke der Weichteilermittlung gewählt worden. Dabei beruhen die Messungen auf unterschiedlichen Voraussetzungen und begrenzen damit größere Vergleichsmöglichkeiten der Daten untereinander. Fehlende Standardtabellen und Werte sind die Folge. Neuere Ergebnisse konnten dadurch ältere nicht revidieren und es entstanden nie allgemein gültige, universelle Messdaten [10]. Den Gesichtsrekonstruktionen liegen stattdessen häufig viele unterschiedliche Daten von verschiedenen Untersuchungen zu Grunde. Die Vergleichsprobleme äußern sich in den folgenden Aspekten:

1. Differenz in der Anzahl der untersuchten Individuen (Stichprobengröße),

2. unterschiedliche Messpunkte,

3. unterschiedliche Todesursachen,

4. an Leichen und an Lebenden gewonnene Daten,

5. unterschiedliche Populationen und

6. unterschiedliche Unterordnungen nach Alter, Geschlecht, Konstitution, Ernährungszustand.

Die folgende Tabelle fasst einige der o. g. Aspekte zusammen und soll einen Überblick über die wichtigsten Datenerhebungen und ihre Dimension vermitteln.

Tab. 1: Die wichtigsten Weichteildickenuntersuchungen an Erwachsenen, nach Autor, Jahreszahl, Methode, Stichprobengröße und Herkunft bzw. Population gegliedert. (Stichprobengröße: m: männlich, w: weiblich).

Autor	Jahr	Stichprobengröße	Mess-Methode	Population
Welcker	1883	13 (m: 13)	Direkt	Europide
His	1895	37 (m: 33, w: 4)	Direkt	Europide
Kollmann/ Büchly	1898	29 (m: 22, w: 7)	Direkt	Europide
Birkner	1903–1907	6 (m: 6)	Direkt/ Röntgen	Mongolide: Chinesen
Fischer	1905	2 (m: 2)	Direkt	Mongolide: Papua
Czekanowski	1907	115 (m: 64, w: 51)	Direkt	Europide: (Schweizer)
v. Eggeling	1909	3 (m: 3)	Direkt	Negride: (Hereros)
Stadtmüller	1923–1925	18 (m: 13, w: 3)	Direkt	Europide, Mongolide, Negride
Köstler	1940	20 (m: 20)	Röntgen	Europide
Weißer	1940	20 (m: 20)	Röntgen	Europide?
Suzuki	1948	55 (m: 48, w: 7)	Direkt	Mongolide: Japaner
Gerasimov	1955	Direkt: 71 Normwerte (m: 71), Röntgen: 19	Weichteil-Schädel-konturen/Röntgen	Mongolide, Europide
Bankowski	1958	24 (m: 15, w: 9)	Röntgen	Europide
Weining	1958	120 (m: 99, w: 21)	Röntgen	Amerikaner
Berger	1965	20–32 (m: 20–32)	Direkt	Europide
Leopold	1968	154 (m: 102, w: 52)	Direkt/Röntgen	Europide
Helwin	1969	50 (?)	Röntgen	Europide
Rhine/Campbell	1980	91 (m: 68, w: 23)	Direkt	Negride, Mongolide: (Amerikaner)
Rhine/Moore/ Weston	1982/84	103 (m: 78, w: 25)	Direkt	Europide (Amerikaner)
Helmer	1984	123 (m: 61, w: 62)	Ultraschall	Europide
Lebedinskaya	1993	1695 (m: 845, w: 850)	Ultraschall	Mongolide
Philipps/Smuts	1996	32 (m:16, w: 16)	CT	Gemischte Population, Südafrika
Dumont	1986	194 (m: 93, w: 101) Jugendliche	Röntgen	Europide: (weiße Amerikaner)

Autor	Jahr	Stichprobengröße	Mess-Methode	Population
Manhein et al.	2000	197 (m: 70, w: 127) Erwachsene, 515 Kinder (m: 234, w: 281)	Ultraschall	Erwachsene: Europide, Negride Kinder: Europide, (Hispano-Amerikaner), Negride

Der erste Punkt spiegelt die Kritik an den anfänglichen Untersuchungen wider. Der Nachteil der Weichteildickenmessungen einiger alter Anatomen besteht nach Leopold vor allem in der Untersuchung von sehr kleinen Kollektiven von 2 bis 37 Personen. [11] Auch spätere Untersuchungen stützen sich nur auf geringe Zahlen. Köstler und Weisser stützen sich noch 1940 auf eine Stichprobe von nur 20 Personen [7], [8]. Wie die Tabelle zeigt, ermittelt erstmals Weining 1958 in größerem Umfang (120 Personen) [9]. Eine diesbezüglich repräsentative Aussage ist von Lebedinskaya et al. erreicht, die eine Stichprobengröße von über 1000 Individuen herangezogen haben [12].

Bei manchen Auflistungen der Weichteildickenwerte fehlen einige wichtige Messpunkte, so dass nähere Vergleiche nicht immer möglich sind.

Der unter Punkt 3 genannte Aspekt bezieht sich auf die möglichen Verzerrungen der Weichteildicke, hervorgerufen durch verschiedene Todesursachen. Verstorbene Personen, die beispielsweise lange, auszehrende Krankheiten hinter sich haben, weisen andere Weichteildicken auf als Unfallopfer [13]. Da aber oft das Untersuchungsmaterial nicht in großem Umfang vorliegt, waren die Möglichkeiten, unter den Untersuchungsobjekten auszuwählen, sehr gering.

Unterschiede zwischen den Werten, die an Leichen und Lebenden gewonnen wurden beruhen auf postmortalen Veränderungen des Weichteilgewebes. Diese werden durch Abnahme des Turgors und Verlustes des Tonus der Muskulatur hervorgerufen. Insgesamt sind Ultraschallmessungen bzw. CT-Daten von Lebenden für die Gesichtsrekonstruktion vorzuziehen, da sonst das Gesicht eines Toten wiedergegeben würde [10].

Die Populationen wurden insofern berücksichtigt, als dass meist dem Untersucher nur regionale Untersuchungsobjekte zur Verfügung standen. So ermittelten Rhine und Campbell 1980 Werte von schwarzen Amerikanern, Rhine, Moore, und Weston (1982/84) Werte an weißen Amerikanern und Gerasimov an verschiedensten osteuropäischen Ethnien [14], [15], [16], [5], [6]. Auch Lebedinskaya et al. ermittelten Daten von diversen osteuropäischen Bevölkerungsgruppen [12].

Dabei muss beachtet werden, dass Variabilitäten zwischen den Populationen nicht bei geringem Datenmaterial erfasst werden können. Die frühen Datenerhebungen beruhen teilweise auf sehr kleinen Stichproben. Leopold u. a. kritisieren in diesem Zusammenhang Gerasimov, der von nicht markanten Unterschieden zwischen den verschiedenen Populationen ausgeht [11]. Seine Stichprobe umfasste allerdings nur einen sehr geringen Umfang der Vertreter der europiden und mongoliden Merkmalsausprägung. Dennoch hat Gerasimov die europid-mongolide Gruppe zusammengefasst. Ullrich stimmt der Kritik zwar zu, betont jedoch, dass Gerasimovs Weichteildickenwerte als Orientierungswerte zu sehen sind [13], [17]. Diese behalten ihren praktischen Nutzen, da der Ausprägungsgrad des jeweiligen Knochenreliefs letztendlich entscheidend ist.

Der letztgenannte Aspekt meint insbesondere die problembehaftete Untergliederung nach den individuellen Merkmalen. Da kein einheitliches Schema zur Einteilung vorliegt, sind die Angaben meist pauschal bzw. schwer vereinbar.

Das Alter wird des öfteren nur als „erwachsen“ bzw. „adult“ beschrieben. Weining beispielsweise untersuchte „erwachsene Amerikaner“ [9].

Die allgemeinen Einflüsse Ernährungszustand und Konstitution wurden nur bedingt und unterschiedlich bewertet und berücksichtigt. Während Kollmann und Büchly sowie Gerasimov, Weining u. a. dem Ernährungszustand große Bedeutung zukommen lassen, missachtet Helwin diesen Faktor bzw. geht nicht näher darauf ein [18], [6], [9], [19].

Diese unterschiedlichen Kriterien lassen einen Vergleich von Messergebnissen verschiedener Untersuchungen kritisch erscheinen. Nach Helmer ist eine derartige Vereinheitlichung der Messergebnisse zwar bedenklich, jedoch erforderlich für einen Vergleich aller Werte [10]. Ein unmittelbarer Vergleich kann nur sinnvoll zwischen den Messdaten erfolgen, die an Personen von gleicher Konstitution, gleichen Ernährungszustandes, gleichen Geschlechts und gleichen Alters gewonnen wurden. Die daraus resultierenden Mittelwerte wären von Nutzen für eine differenzierte Wahl der Weichteildicken bei der Gesichtsrekonstruktion. Das Fehlen von Standardwerten und Tabellen erschwert die Auswahl geeigneter Weichteildickenwerte für eine bestimmte Gesichtsrekonstruktion. Meist wählen die Rekonstrukteure die aktuellsten Daten nach der anzunehmenden Population. Insgesamt zeigt sich ein Fehlen von Standards in den Methoden und Messungen.

Rekonstruktionsmethoden

Aufgrund dieser Datenbasis sind nicht nur im Bereich der Forensik, sondern auch in der Anthropologie und Archäologie verschiedene Methoden zur Rekonstruktion eines Gesichts auf Grundlage des Schädels entwickelt worden, die wiederum in der Zwischenzeit viele Modifikationen erfahren haben. Während die Forensik in der Gesichtsrekonstruktion eine Möglichkeit sah, unbekannte und unkenntliche Tote zu identifizieren, haben die Archäologie und die Anthropologie insbesondere die Intention, frühe Menschenformen darzustellen.

Aus diesem Interesse heraus entstanden die amerikanische und die russische Methode der plastischen Gesichtsrekonstruktion, während die anatomische Methode und die Manchester-Kombinationsmethode aus Modifikationen der beiden erstgenannten entwickelt worden sind [20], [5], [21], [22].

Die verschiedenen Methoden unterscheiden sich vor allem in der Muskelrekonstruktion und in der Verwendung der Weichteildickenwerte. Die Leistungsfähigkeit der verschiedenen Methoden ist nicht eindeutig zu bewerten, da beispielsweise die Prozentangaben über erfolgreich identifizierte Personen in der Forensik nicht aussagekräftig sind, wie Helmer schon anmerkt [23]. Die amerikanische Methode scheint nach dem technischen Ablauf allerdings eher auf den künstlerischen Fähigkeiten des Rekonstrukteurs zu basieren, da hier weniger die Struktur des knöchernen Schädels berücksichtigt wird [20], [24]. Die anatomische Methode könnte für die Gesichtsrekonstruktion früher Hominiden vorteilhaft sein, da sie ohne Weichteildicken arbeitet und somit den Unsicherheitsfaktor der unbekannten Weichteilausprägung ausgrenzt.

Unsicherheitsfaktoren

Die plastische Gesichtsrekonstruktion unterliegt allerdings bis heute anhaltender Kritik vonseiten der Wissenschaft, da wiederholte Rekonstruktionen auf Basis desselben Schädels oftmals große Unterschiede aufweisen. Durch Kontrollversuche seitens der Forensik wurde versucht, diese Problematik aufzuzeigen und die Kritik beizulegen.

Insgesamt zeigt sich, dass eine „annähernde bis große Ähnlichkeit" zum Originalgesicht erreicht werden kann, wenn die Voraussetzungen erfüllt sind [23], [25]. Erforderlich für ein solches Ergebnis ist die Einhaltung aller Rekonstruktionsrichtlinien, die Kenntnis der Korrelationen der Weichteile zu der knöchernen Unterlage, die anthropologischen Daten zu Alter, Geschlecht, Population, Konstitution, Pathologien und evtl. Ernährungszustand, das Vorhandensein einer gewissen Modelliertechnik sowie allgemeine Kenntnisse der Gesichtsanatomie, Anthropologie und Physiologie.

Für eine detailgetreue Rekonstruktion des Gesichts sind auch Informationen zu maskenbildnerischen Elementen wie Haartracht, Haarfarbe, Augenfarbe, Hautfarbe, Narben, Falten, Ausdruck und Mimik erforderlich, für die es keine Hinweise am Schädel gibt [23]. Bei forensischen Rekonstruktionsfällen sind derartige Informationen unter Umständen noch eher vorhanden, wohingegen es bei archäologischen Rekonstruktionen nur ausnahmsweise dann der Fall ist, wenn es sich um bekannte historische Personen handelt, über die schriftliche oder auch bildliche Quellen existieren, die Aussagen zu den maskenbildnerischen Elementen machen können oder wenn es sich um Moorleichen oder Mumienfunde handelt.

Sollen diese Merkmale trotz fehlender Informationen in die Gesichtsrekonstruktion eingearbeitet werden, wie es sich für Ausstellungszwecke archäologischer Rekonstruktionen anbietet, arbeitet der Rekonstrukteur unweigerlich mit Wahrscheinlichkeiten.

Als problematisch sind insbesondere archäologische Gesichtsrekonstruktionen von Hominiden anzusehen, da von diesen vorgeschichtlichen Menschen keine Weichteildickenwerte bzw. Schädel-Weichteil-Korrelationen bekannt sind. Daher können solche Rekonstruktionen auch in Zukunft nur Annäherungen an das wahrscheinliche Aussehen sein. Bei der Rekonstruktion von Australopithecinen versucht man zwar, dieses Manko durch Zuhilfenahme der Weichteildickendaten von Schimpansen auszugleichen, jedoch beruhen die Interpolationen zwischen den menschlichen Daten und denen von Primaten ebenfalls lediglich auf Wahrscheinlichkeiten.

Die Weichteildickendaten, die Kenntnis der Schädel- Weichteilkorrelationen sowie die anthropologischen Daten versuchen die Variabilität des menschlichen Gesichts einzugrenzen und zu beschreiben. Jedoch kann von keiner Rekonstruktionsmethode eine hundertprozentige Übereinstimmung erwartet werden, da nie alle Variabilitäten eines Gesichts erfasst werden können [23].

Ergebnisse für die archäologische Gesichtsrekonstruktion

Für die Gerichtsmedizin ist die plastische Gesichtsrekonstruktion bereits ein integraler Bestandteil bei Identifizierungsfragen. Jedoch bedient man sich dieses Versuchs erst dann, wenn alle anderen Möglichkeiten fehlgeschlagen sind. Die Identifizierung einer bestimmten Person setzt allerdings das Vorhandensein gewisser Informationen voraus, die anthropologische Daten wie Alter, Konstitution, Ernährungszustand, persönliche Merkmale (wie Narben) und maskenbildnerische Merkmale betreffen. Sind diese Details nicht bekannt, ist eine erfolgreiche Identifizierung schwierig [23], [26].

In der Archäologie und Anthropologie hingegen wird eine allgemeine Interpretation des Individuums verfolgt, wofür auch Hintergrundinformationen zu biologisch-funktionellen Aspekten, Umwelteinflüssen, Krankheiten, Herkunftsgebiete, etc. herangezogen werden. Diese Informationen füllen die Lücken, die in den maskenbildnerischen Elementen bestehen (Haartracht, Haarfarbe, Augenfarbe, Hautfarbe, Narben, Falten, Ausdruck und Mimik), so dass hier mit Wahrscheinlichkeiten gearbeitet wird. Insbesondere für Ausstellungszwecke und zur Veranschaulichung der Hominisation bietet sich dies jedoch sehr an, da Authentizität und Lebendigkeit nur durch sie erzielt werden können [25].

Besonderer Beliebtheit erfreut sich heute besonders die Darstellung von Gesichtsrekonstruktionen in öffentlichen und privaten Einrichtungen sowie in den Medien. Als Erweiterung zu der Gesichtsrekonstruktion bietet sich neuerdings die Ganzkörperrekonstruktion für die museale Präsentation an. Sie kann bei der Darstellung der morphologischen Entwicklungsgeschichte des Menschen die Ausbildung des postcranialen Skeletts veranschaulichen und findet besonders häufig in Dioramen ihren Platz. Auf diese Weise können objektgebundene Einzelaussagen in einem historischen Zusammenhang verbunden werden. Die Ganzkörperrekonstruktion hilft dem Museumsbesucher zu erkennen, dass der Hominisationsprozess nicht alle Körperabschnitte gleichzeitig erfasste, sondern mosaikartig und unregelmäßig verlief [27].

So werden plastische Gesichts- und Ganzkörperrekonstruktionen vermehrt als museale Objekte genutzt, die als „Blickfang" in den Ausstellungen fungieren sollen. Dabei wird versucht eine möglichst breite Bevölkerungsschicht einerseits durch die Wissenschaftlichkeit und andererseits durch die Anschaulichkeit anzusprechen und die Geschichte im Sinne von Identitätsbildung zu vermitteln.

Gerade für solche didaktischen Zwecke besteht allerdings die Gefahr der Suggestion von bestimmten Formmerkmalen, die auf persönliche und subjektive Vorstellungen der Rekonstrukteure sowie auf ideologische Einflüsse zurückgehen können.

Für eine kritische Beurteilung hat die detaillierte Betrachtung der archäologischen Gesichtsrekonstruktionen am Beispiel des Neandertalers von La Chapelle-aux-Saints gezeigt, dass es aufgrund der unterschiedlichen Hintergründe grundsätzlich zu differenzieren gilt. Es reichen bereits geringe Unterschiede in den individuellen Vorstellungen und in den methodischen Grundlagen aus, um einen gänzlich anderen Gesamtausdruck zu erzeugen. So unterliegt jeder Rekonstruktionsversuch, insbesondere der von Hominiden, einer Vielzahl von Unwägbarkeiten, durch die verstärkt persönliche Vorstellungen und Intentionen einfließen können [28].

Das Fachgebiet des Rekonstrukteurs kann z. B. einen gewissen Einflussfaktor auf das Rekonstruktionsergebnis bilden. Während die frühen Rekonstruktionen aus der ersten Hälfte des 20. Jahrhunderts hauptsächlich aus der Zusammenarbeit zwischen Anatomen bzw. Anthropologen und Bildhauern entstanden sind, entstammen heutige Gesichtsrekonstruktionen oftmals interdisziplinärer Arbeit. So können Anthropologen, Archäologen, Medizinische Illustratoren, Paläoanthropologen, Forensiker, Anatomen, Informatiker, Künstler, Bildhauer sowie Experten aus der Computeranimation an einer Rekonstruktion beteiligt sein.

Sind lediglich Annährungen an das wahrscheinliche Aussehen vor- und frühgeschichtlicher Menschen möglich, sollte dies für den unkritischen Betrachter kenntlich gemacht werden. Schließlich ruft jedes Gesicht beim Betrachter unbewusst eine Beurteilung hervor, die auf den Vergleich mit bereits bekannten Merkmalsmustern zurückgeht. Insbesondere die Mimik, mit der sich die heutige Gesichtsforschung beschäftigt, stellt einen elementaren Bestandteil bei der persönlichen Beurteilung dar, die oftmals nur im Unterbewusstsein abläuft [29], [30]. Ist gar keine Mimik vorhanden, kann das Individuum bzw. das rekonstruierte Gesicht sogar als „dumpf" empfunden werden [31].

Die Qualität der Gesichtsrekonstruktion variiert demzufolge erheblich durch die Unterschiede in der wissenschaftlichen Grundlage hinsichtlich der Methode und des anthropologischen Befundes, der Zielsetzung und Intention sowie der persönlichen Einflüsse. Während einige Rekonstruktionen ein ethnisches Portrait darstellen sollen, zielen andere darauf ab, die individuellen Gesichtszüge berühmter Persönlichkeiten nachzuahmen oder gar mit neutralem Ausdruck der Identifikation zu dienen. All diese Gesichtspunkte sind bei der Beurteilung zu berücksichtigen.

Obwohl in Zukunft mit einer weiteren Aufbereitung der wissenschaftlichen Basis – die Schädel-Weichteil-Korrelationen und die Weichteildickenwerte – gerechnet werden kann, bleiben die angesprochenen Ungewissheiten bei jeder archäologischen Rekonstruktion bestehen.

Die Möglichkeit der computergenerierten Rekonstruktionen, die bereits vermehrt in der Forensik zu beobachten sind, sind im Gegensatz zu den traditionellen Gesichtsrekonstruktionen sicherlich ökonomischer. Auch für museale Zwecke in der Archäologie eignen sich die computergenerierten 3D-Rekonstruktionen, jedoch werden sie die traditionell hergestellten Rekonstruktionen alleine aus Gründen der Präsentationsmöglichkeiten in naher Zukunft noch nicht ablösen.

Wie aktuell die plastischen Gesichtsrekonstruktionen in der Archäologie sind, zeigt das Diagramm (Tab. 2). Es gibt die Verteilung der 176 Gesichtsrekonstruktionen aus dem Zeitraum von 1898 bis 2004 wieder, die aus der aktuellen Bestandsaufnahme hervorgehen. Diese Zusammenstellung erhebt jedoch keinen Anspruch auf Vollständigkeit, da nur publizierte und dokumentierte Rekonstruktionen aus dem Großraum Europa und Amerika aufgenommen wurden. Insgesamt dürfte dementsprechend mit einer weitaus größeren Anzahl an angefertigten Rekonstruktionen zu rechnen sein.

Drei Phasen mit einem hohen Rekonstruktionsanteil sind zu erkennen. In den 1930er Jahren zeichnet sich ein erster Anstieg der Anzahl ab, der von dem ersten Weltkrieg abrupt unterbrochen wurde. Die Zahl der angefertigten Rekonstruktionen nahm dann in den 1950er Jahren wieder drastisch zu. Das Interesse hielt bis in die 1960er Jahre an. Die jetzige Periode übertrifft jedoch die vorigen Phasen bei weitem, mit über 100 angefertigten Gesichtsrekonstruktionen in den letzten 15 Jahren. Die jetzige Dekade hat schon nach fünf Jahren den Wert der vorigen Dekade erreicht und wird sicherlich noch weiter ansteigen.

Tab. 2: Die Verteilung der archäologischen Gesichtsrekonstruktionen über ein Jahrhundert (1898–2004) in Dekaden dargestellt.

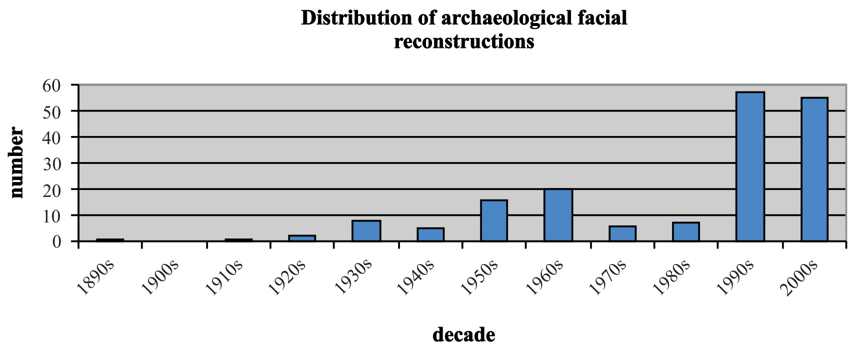

Die Archäologie kann aus der Gesichtsrekonstruktion und der Zusammenarbeit mit Forensikern und Anthropologen lernen, um uns unsere Vergangenheit ein wenig näher zu bringen. Dabei hat das allgemeine Interesse, die Geschichte und die Namen aus der Vergangenheit mit Gesichtern zu verbinden, die Gesichtsrekonstruktion zum integralen Bestandteil der Archäologie gemacht.

Literatur

[1] K. Kenyon, „Jericho," in *Encyclopedia of Archaeological Excavations in the Holy Land* [Ed.]: Michael Avi Yonah, London, 1976, II.

[2] S. I. Kruc et al., „Das menschliche Gesicht der Bronzezeit," in *Gold der Steppe. Archäologie der Ukraine*, (Eds.): R. Rolle; M. Müller-Wille; K. Schietzel, Archäologisches Museum der Christian-Albrechts-Universität, Schleswig, 1991.

[3] F. Behn, „Vorgeschichtliches Maskenbrauchtum" Berlin, 1955.

[4] H. Welcker, „Schillers Schädel und Totenmaske nebst Mitteilungen über Schädel und Totenmaske Kants," Fr. Viehweg u. Sohn, Braunschweig, 1883.

[5] M. M. Gerasimov, „Vosstanovlenie lica po cerepu. (Wiederherstellung des Gesichts aufgrund des Schädels)," in *Izdat. Akad. Nauk SSSR*, Moskau, 1955, pp. 585.

[6] M. M. Gerasimov, „Ich suchte Gesichter. Schädel erhalten ihr Antlitz zurück," Wissenschaft auf neuen Wegen, Gütersloh, 1968.

[7] J. Köstler, „Röntgenstereoskopische Messungen der Weichteildicken an 20 jungen weiblichen Personen," Ph.D. dissertation, Erlangen, 1940.

[8] D. Weisser, „Röntgenstereoskopische Messungen der Weichteildicken in der Medianebene des Gesichts an 20 jungen Männern," Ph. D. dissertation Erlangen, 1940.

[9] W. Weining, „Röntgenologische Untersuchungen zur Bestimmung der Weichteildickenmaße des Gesichts," Ph. D. dissertation, Frankfurt/Main, 1958.

[10] R. Helmer, „Schädelidentifizierung durch elektronische Bildmischung. Zugleich ein Beitrag zur Konstitutionsbiometrie und Dickenmessung der Gesichtsweichteile," Kriminalistik-Wissenschaft & Praxis, Band 16, Heidelberg, 1984.

[11] D. Leopold, „Identifikation durch Schädeluntersuchung unter besonderer Berücksichtigung der Superprojektion," Ph. D, dissertation, Leipzig, 1968.

[12] G. V. Lebedinskaya et al., „Principles of facial reconstruction," in *Forensic Analysis of the Skull*, Wiley-Liss; 183–198, 1993.

[13] H. Ullrich, „Kritische Bemerkungen zur plastischen Rekonstruktionsmethode nach Gerassimov auf Grund persönlicher Erfahrungen," in *Ethnogr.-Archäol.*, Vol. 7, 1966, Berlin, pp. 111–123.

[14] J. S. Rhine, H. R. Campbell, „Thickness of facial tissues in the American Blacks," in *Journal of Forensic Science*, Vol. 25, 1980, pp. 847–858.

[15] J. S. Rhine, C. E, Moore, J. T. Weston, „Facial Reproduction. Tables of Facial Tissue Thickness of American Caucasoids in Forensic Anthropology," *Maxwell Museum Technical Series*, Nr. 1. 1982.

[16] J. S. Rhine, C. E, Moore, J. T. Weston, „Facial Reproduction. Tables of Facial Tissue Thickness of American Caucasoids in Forensic Anthropology," *Maxwell Museum Technical Series*, Nr. 1, 1984.

[17] H. Ullrich, „Die methodischen Grundlagen des plastische Rekonstruktionsverfahren nach Gerassimov," in *Zeitschrift für Morphologie und Anthropologie*, 1959, pp. 245–258.

[18] J. Kollmann, W. Büchly, „Die Persistenz der Rassen und die Rekonstruction der Physiognomie prähistorischer Schädel," in *Arch. Anthrop.*, Vol. 25, 1898, pp. 329–359.

[19] H. Helwin, „Problematik der Weichteilrekonstruktion auf dem menschlichen Schädel," in *Gegenbaurs morph. Jb.* 116, 1971, pp. 503–513.

[20] W. M. Krogman, „The reconstruction of the living head from the skull." *FBI Law Enforcement Bull*. 15/7, 1946, pp. 11–18.

[21] J. Gurche (jgurche@DMNS.org), „Gurche Main Menu", http://www.gurche.com/main_frameset.htm, Mai 4,2004.

[22] R. Neave, J. Prag, „Making Faces. Using forensic and archaeological evidence," London, 1997.

[23] R. Helmer et al., „Assessment of Reliability of Facial Reconstruction," in *Forensic Analysis of the Skull,* Wiley – Liss., 1993, pp. 229–246.

[24] K. T. Taylor, „Forensic art and illustration," London, New York, Washington D. C., 2001.

[25] C. Wilkinson, „Forensic Facial Reconstruction," Cambridge, 2004.

[26] R. Helmer, „Identifizierung unbekannter und unkenntlicher Leichen mittels bildtechnischer oder rekonstruktiver Verfahren," in *Identifikation unbekannter Toter: interdisziplinäre Methodik, forensische Osteologie. Schriftenreihe: Arbeitsmethoden der medizinischen und naturwissenschaftlichen Kriminalistik*; 22. [Eds.]: D. Leopold, S. Berg, B. Brinkmann, Lübeck, 1998, pp. 449–502.

[27] W. Henke, N. Kieser, W. Schnaubelt, „Die Neandertalerin. Botschafterin der Vorzeit," Gelsenkirchen/Schwelm, 1996.

[28] E. Trinkaus, P. Shipman, „Neandertals: Images of Ourselves," in *Evolutionary Anthropology*, Vol. 6, 1993, pp. 189–226.

[29] P. Ekman, „Darwin and facial expression. A century of research in review," New York, London, 1973.

[30] P. Ekman, „Gesichtsausdruck und Gefühl: 20 Jahre Forschung von Paul Ekman," 1988.

[31] J. Cole, „Über das Gesicht. Naturgeschichte des Gesichts und unnatürliche Geschichte derer, die es verloren haben," München, 1999.

10.

CVs of Authors
Vitae der Autoren

Assmann, Sabine

Sabine Assmann wurde 1976 in Hamburg, Deutschland geboren. Nachdem sie 2000 die Prüfung zur staatlich examinierten Krankenschwester an der Uniklinik Lübeck abgelegt hatte, begann sie im Oktober 2000 das Studium der Anthropologie an der Universität Hamburg. Von 2003 bis 2004 studierte sie am Anthropologischen Institut der Universität Zürich in der Schweiz. Sie ist Mitglied der GfA/AGFA und der IALM/FASE. Sie nahm an einigen forensischen workshops inner- und ausserhalb Deutschlands teil, wo sie sich gute Kenntnisse über eine nicht unerhebliche Anzahl forensischer Techniken und deren Umgang erwarb.

Sabine Assmann was born in Hamburg, Germany in 1976. After the education as a nurse at the University Hospital of Lübeck in 2000, she started studying Anthropology at the University of Hamburg in October 2000. From 2003 to 2004, she did study at the Unit of Anthropology at the University of Zurich in Switzerland. She is member of the GfA/AGFA and of the IALM/FASE. She took part at a number of forensic workshops and internships in and outside Germany where she became familiar with a number of forensic techniques about ageing, sexing and how to deal with these techniques.

Basso, Curzio

PhD student in Computer Science, University of Basel

Curzio Basso received the diploma-degree in Physics from the University of Genova, Italy, in 1999 with a thesis on Support Vector Machines applied to regression. Since 2000 he is a PhD student in Computer Science, first at the University of Freiburg, Germany, and currently at the University of Basel, Switzerland. His research activity focuses on the application of statistical learning to the modeling of human faces and expressions.

Berar, Maxime

Doctoral student at LIS, Grenoble

Maxime Berar is a doctoral student at LIS, Grenoble. He received an engineer degree in electronics form the "Ecole NationaleSupérieure d'Electronique et de Radioélectricité de Grenoble (ENSERG)" in 2002. His scientific interests include face and skull statistical modeling and Kernel methods.

Berti, Guntram, Dr.

Senior Scientist, NEC C&C Research Laboratories in St. Augustin

Guntram Berti ist seit 2001 bei den NEC C&C Research Laboratories in St. Augustin tätig. Seine Forschungsinteressen umfassen generische Programmierung im Zusammenhang mit Gittern, Gittererzeugung und numerische Simulation im Bereich der Biomechanik.

Er hat einen Abschluß in Mathematik der Universität Dortmund und promovierte 2000 an der Technischen Universität Cottbus über *Generic software components for scientific computing*.

Guntram Berti obtained a Diploma in mathematics from the University of Dortmund in 1994 and a PhD in mathematics from the Technical University of Cottbus in 2000. Since 2001, he is affiliated with the NEC C&C Research Laboratories in St. Augustin. His current research interests include generic programming for geometric problems, mesh generation and computational biomechanics.

Dr. Guntram Berti
C&C Research Laboratories, NEC Europe Ltd.
Rathausallee 10
D-53757 St. Augustin
Tel. ++49 (0)2242-92 52 32
Fax. ++49 (0)2242-92 52 99
E-Mail: berti@ccrl-nece.de

Bongartz, Jens, Prof. Dr.

Jens Bongartz studierte Physik an der Heinrich-Heine-Universität Düsseldorf und darauf aufbauend Medizinische Physik und Technik an der Technischen Universität Kaiserslautern. 2002 promovierte er über das Thema *„Hochauflösende dreidimensionale Gesichtsprofilvermessung mit kurzgepulster Holographie“*. Nach Tätigkeiten am Institut für Lasermedizin der Universität Düsseldorf und dem *center for advanced european studies and research (caesar)* in Bonn ist er seit Anfang 2004 Professor für Medizintechnik am RheinAhrCampus Remagen.

Prof. Dr. Jens Bongartz
RheinAhrCampus Remagen
Südallee 2
53424 Remagen

Bröker, Martin, Dr.

Senior Engineer for the Viisage Technology AG in Bochum

Hans-Martin Bröker studied physics at the University of Wuppertal in Germany and received his Diploma in 1995. At the same university he received the PhD in Theoretical Physics in 1999. His research activities were concentrated on complex systems showing self organised criticality. After his PhD he gathered two years of professional experience in industrial image processing. Since 2001 he serves as a senior engineer for the Viisage Technology AG in Bochum. His main field of activity lies in the development of algorithms for face recognition tasks.

Buzug, Thorsten M., Prof. Dr. rer. nat.

Direktor des Instituts für Medizintechnik an der Universität zu Lübeck

Thorsten M. Buzug erlangte 1989 sein Diplom im Fach Physik an der Christian-Albrechts-Universität zu Kiel. Im Mai 1993 promovierte er mit dem Thema Analyse Chaotischer Systeme und arbeitete danach als wissenschaftlicher Mitarbeiter bei der Forschungsanstalt der Bundeswehr für Wasserschall- und Geophysik (FWG). Schwerpunkt seiner Forschungstätigkeit dort war die Signalverarbeitung für SONAR-Systeme. Ende 1994 wechselte Buzug dann zu den Philips GmbH Forschungslaboratorien Hamburg. Als Clusterleiter war er verantwortlich für die Projekte der medizinischen Bildverarbeitung. 1998 nahm er den Ruf auf eine Professur für Physik und Medizintechnik am RheinAhrCampus Remagen an. Seit 2006 ist er Direktor des Instituts für Medizintechnik an der Universität zu Lübeck.

Prof. Dr. Thorsten M. Buzug
Direktor des
Instituts für Medizintechnik
Universität zu Lübeck
Ratzeburger Allee 160
23538 Lübeck
Tel. +49 (0) 451 / 500–5400
Fax +49 (0) 451 / 500–5403
E-Mail: buzug@imt.uni-luebeck.de

Claes, Peter

Ph. D. Student, Department ESAT/PSI/ Medical Image Computing of the K. U. Leuven (Belgium)

Peter Claes is currently doing a Ph. D. at the department ESAT/PSI/ Medical Image Computing of the K. U. Leuven (Belgium). The main topic of his research is surface-based cranio-facial statistical modeling and reconstruction. He obtained his M.Sc. in Engineering (Electro-Technical) in 2002 at the same university. Before that he has done three projects as a job student concerning software development at Siemens Mobile in Herentals (Belgium).

Davy, Stephanie L., BA (Hons), BSc (Hons) Education PhD,

Davy, BA (Hons), BSc (Hons) Education PhD, Forensic Facial Reconstruction and Craniofacial Identification. University of Sheffield (UK). Anticipated award date, November 2005. Professional Affiliations Forensic Science Society (FSSoc)**,** British Association of Biological Anthropology and Osteoarchaeology (BABAO), Member, British Association of Human Identification (BAHID), Member, European Association of Archaeologists (EAA) selected publications and presentations *Forensic Facial Reconstruction using Computer Modeling Software*. Davy, S. L. *et al.* Computer-Graphic Facial Reconstruction. Academic Press, *In Press. Computational Forensic Facial Reconstruction.* Evison, M. P.; Davy, S.L; March, J; Schofield, D. Conference Proceedings, International Conference of Reconstruction of Soft Facial Parts, November 2003.

d'Hollosy, Maja Liduina, M.Sc

M. L. d'Hollosy M.Sc. (Archaeology / Physical Anthropology). Researcher of Ancient Bones / Skullpting – Consultant to the NFI (Dutch Forensic Institute)

Education and qualification

1983–1990	University of Amsterdam
1990	M.Sc. Archaeology/Physical Anthropology

Occupation:

1990–1993	Self-employed researcher (archaeology / physical anthropology)
1993–1996	researcher in Physical Anthropology at the University of Amsterdam, department of European Archaeology,
from 1996	Physical anthropological researcher for Ancient Bones
from 1999	Facial reconstruction practitioner for Skullpting
from 2003	Consultant to the Dutch Forensic Institute

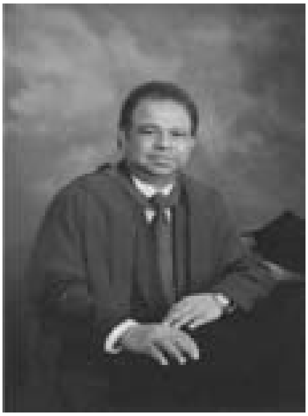

Dias, George J., Dr.

Lecturer in the Department of Anatomy and Structural Biology at the Otago School of Medical Sciences, University of Otago

George J. Dias received his B. D.S in 1977, and his M.S (Dental Surgery) in 1985 and obtained his Ph.D from the University of Otago in 2003. He is currently a lecturer in the Department of Anatomy and Structural Biology at the Otago School of Medical Sciences, University of Otago. His main areas of research are Biomaterials, Clinical Anatomy of head and neck region, Paleopathology, and Biological and Forensic Anthropology.

Helmer, Richard, Prof. Dr.

Professor für Experimentelle Rechtsmedizin an der Universität Bonn

Dr. Richard Helmer gründete im Jahr 1996 das private Institut für „Angewandte Forensische Medizin und Anthropologie".

Er studierte Medizin in Kiel und promovierte 1969. Ab 1975 war er als Facharzt für Rechtsmedizin tätig, anschließend Oberassistent und Stellvertretender Direktor des Instituts für Rechtsmedizin der Universität Kiel. 1982 habilitierte er in der Fachrichtung Rechtsmedizin. Seit 1990 ist er Professor für Experimentelle Rechtsmedizin an der Universität Bonn. Von 1992 bis 2000 fungierte er als 1. Präsident der International Association for Cranio-Facial Identification. Im Jahr 1996 gründete er das private Institut für „Angewandte Forensische Medizin und Anthropologie".

Hering, Peter, Prof. Dr. rer. nat.

Geboren in Messkirch/Baden. Studium der Physik und Mathematik zuerst in Freiburg und Bristol, danach an der neu gegründeten Universität Kaiserslautern. Diplomarbeit und Promotion auf dem Gebiet der Laserentwicklung und Laserspektroskopie. Längerer Forschungsaufenthalt in Houston, Texas an der renommierten Rice University bei Phil Brooks und Nobelpreisträger Bob Curl. Danach 12 Jahre Forschungstätigkeit bei der Max-Planck-Gesellschaft am Institut für Quantenoptik in Garching bei München auf dem Gebiet der Laserchemie und Entwicklung neuer nichtlinearer Methoden der Laserspektroskopie und Laseranalytik.

Seit 1991 ordentlicher Professor am interdisziplinären Institut für Lasermedizin an der Universität Düsseldorf. Schwerpunkt der Forschung sind neue Methoden des analytischen, diagnostischen und therapeutischen Einsatzes des Lasers in Medizin, Umwelt und Life Science. Seit 1999 gleichzeitig bei caesar (center of advanced european studies and research) in Bonn als unabhängiger Projektleiter im Triplet "Laser und Computerunterstützte Chirurgie". Bei caesar werden vor allem neue bildgebende Verfahren auf der Basis von kurzgepulster Holographie und berührungslose Methoden der Knochenbearbeitung weiterentwickelt. Neuere Anwendungsgebiete sind die Bearbeitung von extrem wärmeempfindlichen Materialien mit gepulsten Lasern und die Entwicklung und der Einsatz einer mobilen holographischen Kamera für Medizin (Mund-, Kiefer- und Gesichtschirurgie, plastische Chirurgie), Archäologie, Kriminalistik und Forensik.

E-Mail: hering@uni-duesseldorf.de

www.ilm.uni-duesseldorf.de, www.ilm.uni-duesseldorf/tracegas/,
www.caesar.de

Dr. Peter Hering, Professor of Physics

Peter Hering was born in Messkirch/Baden, Germany. He studied physics and mathematics in Freiburg, Bristol and at the newly founded University of Kaiserslautern, where he received his diploma and Ph. D. degree in physics. From 1978–79 he worked as a DFG research associate at the well-known Rice Quantum Institute in Houston/Texas with Phil Brooks and Bob Curl (Nobel Prize 1996) on transition state spectroscopy. From 1979–1991 he was with the Max-Planck-Institute for Quantum Optics in Garching, Germany, mainly working in laser chemistry with emphasis on nonadiabatic collision processes and the development of new nonlinear laser spectroscopic techniques.

Since 1991 he is Professor of Physics at the interdisciplinary institute of Laser Medicine at the University of Düsseldorf. His work there is devoted to basic research in analytical and diagnostical laser application in biomedicine and environmental research. In October 1999 he got additionally an appointment at caesar (center of advanced european studies and research) in Bonn as an external independent project leader in the triplet "Laser and Computer Aided Surgery". The focus there is on the development of new imaging methods based on short-pulsed holography and on contact less methods for bone treatment. Recent areas of application are the treatment of extremely temperature-sensitive materials with pulsed lasers and the development and implementation of a mobile holographic camera in medicine (craniofacial surgery, plastic surgery), archaeology, criminology and forensic medicine.

www.ilm.uni-duesseldorf.de, www.ilm.uni-duesseldorf/tracegas/,
www.caesar.de

Hierl, Thomas, PD Dr. Dr.

Facharzt für Mund-Kiefer-Gesichtschirurgie/Plastische Operationen Leiter der 3D-Labors der Klinik und Poliklinik für Mund-, Kiefer- und Plastische Gesichtschirurgie am Universitätsklinikum Leipzig

Thomas Hierl leitet seit 1994 die 3D-Labors der Klinik und Poliklinik für Mund-, Kiefer- und Plastische Gesichtschirurgie am Universitätsklinikum Leipzig AöR.

Er wurde am 12. 03. 1963 in München geboren und ist Facharzt für Mund-Kiefer-Gesichtschirurgie/Plastische Operationen. Seine Spezialgebiete sind Lippen-Kiefer-Gaumen-Spalten, orthognathe Chirurgie sowie Computer-aided Surgery

Thomas Hierl: * 12. 03. 1963 in Munich. Specialist in oral and maxillofacial surgery; working at Leipzig University Clinic since 1994. Head of 3D-laboratory of the Dept. of Oral and Maxillofacial Plastic Surgery.

Specialities: cleft lip and palate; orthognathic surgery, computer aided surgery

Hirsch, Sven

Physicist at the centre of advanced european studies and research (Caesar)

Sven Hirsch received his diploma in Physics from the University of Heidelberg in 1999 for a work in medical image processing. In 2003 he received a postgraduate degree from the Academy of Media Arts, in Cologne. Under the name Sven Mann he actively produces works in various artistc forms. In 2004 he joined the holography research group at caesar, working with the University Hospital in Basel to make the holographic topometry technology available for medical applications. His research focus is the digital capture and reconstruction of holograms.

Kindermann, Kurt P., Kriminalhauptkommissar

Landesfachkoordinator für visuelle Fahndungshilfen und digitale Phantombildanwendungen in Baden-Württemberg.

Kurt Kindermann wurde am 24. August 1957 in Meriden /Connecticut/USA geboren und verrichtet seinen Dienst beim Landeskriminalamt Baden-Württemberg. Seit 1983 ist er Phantombildersteller bei der Landespolizeidirektion Stuttgart II und gehört seit 1995 der Projektgruppe für die Umsetzung des Bildfahndungssystems in Baden-Württemberg an.

Seit 1996 beschäftigt er sich mit Systemen zur biometrischen Gesichtsvermessung und biometrischen Erkennungssystemen, Identifizierungsmethoden sowie Gesichtsrekonstruktionen. Dabei führte er interne und externe Versuchsreihen (Gerichtsmedizin Tübingen) zur Gesichtsweichteilrekonstruktion durch.

Nach Einführung eines landesweiten Systems an der Akademie der Polizei Baden-Württemberg in Freiburg und Wertheim im Jahr 1997 bildet er Phantombildanwender aus und koordiniert ab 2001 Phantombildanwendungen im System I. S. I. S. Zugleich wirkt er mit an der Erstellung einer „Virtuellen Datenbank" für die Länder Baden-Württemberg, Nordrhein-Westfalen, Hessen und Hamburg. Im Juni 2003 richtete er die 2. Bundesfachtagung für visuelle Fahndungshilfen und Phantombilderstellung aus und bereitet die folgende vor. Er ist auch im Projekt neues Informations- und Kommunikationsnetz (Februar 2003) der Polizei Baden-Württemberg – Teilprojekt Digitaler Erkennungsdienstarbeitsplatz beteiligt.

Seit September 2003 arbeitet er mit dem Max-Planck-Institut für biologische Kybernetik in Tübingen und dem Psychologischen Institut der Universität Zürich in einem Projket zur Erstellung eines face-modellers zur dreidimensionalen Rekonstruktion von Gesichtern und Erstellung von visuellen Fahndungshilfen wie Phantombilder oder der Aktualisierung von Fahndungsbildern durch – „aging" – Gesichtsalterung zusammen.

Lampe, Annika

Annika Lampe wurde 1977 in Hamburg, Deutschland geboren. Nach ihrem Abitur im Jahre 1997 begann sie ihr Studium der Vor- und Frühgeschichte, Anthropologie und Geographie an der Universität Hamburg. In mehreren Praktika und musealer Tätigkeit gewann sie einen guten Einblick in die Arbeitsweise der Vor- und Frühgeschichtsforschung. Mit einer Tätigkeit im sozialen Bereich finanzierte sie größtenteils ihr Studium. Ihr Thema zur Erlangung des Grades des Magister Artium behandelte die plastische Gesichtsrekonstruktion in der vor- und frühgeschichtlichen Archäologie.

Annika Lampe was born 1977 in Hamburg, Germany. After her university-entrance diploma in 1997 she started studying Pre- and Early Historical Archaeology, Anthropology and Geography at the University of Hamburg. In several practical courses and activities in some museums, she got a good overview of the functioning of the prehistorical Research. With an activity within the social range, she financed its study to a large extent. Her topic for the acquisition of the degree of the Magister Artium treated the term of the Facial Reconstruction in Pre- an Early Historical Archaeology.

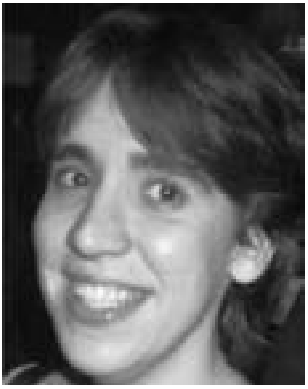

Loubele, Miet

Ph.D at the laboratory for Medical Image Computing (ESAT/PSI + Radiology) at the K. U. Leuven

Miet Loubele received her Masters degree in Engineering in 2002 (Computer Science) from the K. U. Leuven. Currently she is making her Ph.D at the laboratory for Medical Image Computing (ESAT/PSI + Radiology) at the K. U. Leuven. Her research is about geometrical and dosimetric aspects of low-dose CT of the head. The focus of her research is assessing the quality of these images for bone segmentation in these low-dose CT-images for the use in 3D image-based planning environments for oral and maxillofacial surgery.

Malá, Pavla, Mgr.

Postgraduate student of Charles University in Prague, Faculty of Natural Science, Department of Anthropology and Human genetics

Anthropologist

Born 7. 8. 1979 in Ostrava, Czech Republic.

1998–2004: Masaryk University in Brno, Faculty of Natural Science, Department of Anthropology, state examination of anthropology, (Mgr.)

2002–2003: six month study at The University of Florence, Italy, Department of Anthropology.

Currently a postgraduate student of Charles University in Prague, Faculty of Natural Science, Department of Anthropology and Human genetics.

Her interests are focused on historical and forensic facial reconstruction.

Mang, Andreas

Wissenschaftlicher Mitarbeiter am Institut für Medizintechnik der Universität Lübeck

Seit 2006 ist er wissenschaftlicher Mitarbeiter am Institut für Medizintechnik der Universität Lübeck.

Andreas Mang ist 1981 in Illertissen/Deutschland geboren, studierte 2002–2006 am RheinAhrCampus Remagen Medizinische Technik. Im Jahr 2003 trat er der Arbeitsgruppe von Prof. T. M. Buzug im Bereich Bildverarbeitung für die Gesichtsrekonstruktion zur postmortalen Identifizierung von Leichen bei. 2004/2005 arbeitete er sieben Monate bei der Compumedics Germany GmbH an dem medizinischen Quellrekonstruktions-Softwarepaket CURRY. Seine Diplomarbeit *Medical Image Registration To Improve The Understanding of Disease Progression of Glioma Tumours* fertigte er als Stipendiat des DAAD am University College London an. Er ist Mitglied in der DGBMT (Deutsche Gesellschaft für Biomedizinische Technik) des VDE.

Andreas Mang was born in Illertissen, Germany, in 1981. 2002–2006 he studied Medical Engineering at the RheinAhrCampus Remagen. In the year 2003 he joined the Research Group of Prof. T. M. Buzug in the field of image processing for craniofacial reconstruction. He has been working on the medical source reconstruction software package CURRY at Compumedics Germany GmbH for seven month in 2004/2005. For his diploma thesis *Medical Image Registration To Improve The Understanding of Disease Progression of Glioma Tumors* he worked at University College London partially financed by a DAAD grant. Since 2006 he is Ph. D. student at the Institute of Medical Engineering at the University of Lübeck. He is member of the DGBMT (German Society of Biomedical Engineering) of VDE.

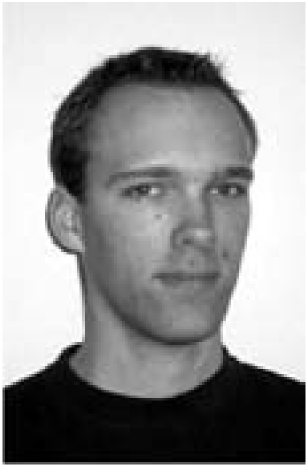

Müller, Jan

Wissenschaftlicher Mitarbeiter am Institut für Medizintechnik der Universität Lübeck

Seit 2006 ist er wissenschaftlicher Mitarbeiter am Institut für Medizintechnik der Universität Lübeck.

Er wurde 1982 in Bonn/Deutschland geboren. 2002–2006 studierte er Medizintechnik am RheinAhrCampus Remagen. Im Jahre 2003 trat er einer Projektgruppe unter Leitung von Prof. T. M. Buzug bei, die sich mit der forensischen Gesichtsrekonstruktion beschäftigt. Während eines 7monatigen Praxissemesters 2004/2005 arbeitete er an dem Softwarepaket CURRY der Firma Compumedics Germany GmbH in Hamburg, das für Quellrekonstruktionen eingesetzt wird. Seine Diplomarbeit über Artefaktreduktion bei der Computertomographie fertigte er im Philips Forschungslabor Hamburg an. Er ist Mitglied der Deutschen Gesellschaft für Biomedizinische Technik des VDE.

Jan Müller was born in 1982, in Bonn, Germany. 2002–2006 he studied Medical Engineering at the RheinAhrCampus Remagen. In the year 2003 he joined a research group of Prof. T. M. Buzug in the field of image processing for craniofacial reconstruction. During his practical term he has been working on the source reconstruction software package CURRY at Compumedics Germany GmbH for about seven months in 2004/2005. His diploma thesis on artefact reduction for computed tomography has been carried out at the Philips research lab Hamburg. Since 2006 he is Ph. D. student at the Institute of Medical Engineering at the University of Lübeck. He is member of the DGBMT (German Society of Biomedical Engineering) of VDE.

Neave, Richard

Richard Neave trained as an artist, and joined the Middlesex Hospital, London, in 1957 to study as a Medical Artist, taking a full-time appointment at the University of Manchester as a Medical Artist in 1959. Since 1989, Richard has been a leader in the field of forensic photo comparison. Following his retirement from academic life in 2000, he has remained closely involved in the running and the activities of a number of organisations relating to both his forensic work and his artistic endeavours, and has continued his work in the field of facial reconstruction. He maintains a number of teaching commitments, both in the UK and overseas, and continues to lecture at meetings throughout the world.

Niinimäki, Sirpa Taina Johanna

Post-graduate student in Oulu University, Finland

Niinimäki Sirpa Taina Johanna, 061178, nationality Finnish

Education
University of Oulu 1998–2002, Bachelor of Arts degree 2002.

University of Oulu 2002–2005, Master of Arts degree 2005,

title of Master's dissertation: Possibilities of facial reconstructions in Finland's archaelogy.

Merits
Presentation in 22. Nordic Archaeology conference by the subject of Finnish facial tissue thickness study.

Present position:
Post-graduate student in Oulu University by the subject of Optional means for reconstructing facial tissue thickness.

Ponce de León, Marcia S.

Senior research assistant at the Anthropological Institute of the University of Zurich

Marcia S. Ponce de León studied civil engineering in La Paz, Bolivia, and biology at the University of Zurich, Switzerland, where she received a PhD in anthropology. She is currently senior research assistant at the Anthropological Institute of the University of Zurich. Her research focuses on the evolutionary developmental biology of fossil and modern humans and apes, and on new methods for morphometric analysis of three-dimensional patterns of craniofacial shape variation.

Prüfer, Klaus, Kriminalhauptkommissar

Kriminalvollzugsbeamter im Bundeskriminalamt

Er ist seit 1977 als Krimnalvollzugsbeamter im Bundeskriminalamt.

Klaus Prüfer trat 1974 in das Bundeskriminalamt ein. Von 1974 bis 1977 absolvierte er die Ausbildung zum gehobenen Kriminaldienst des Bundes. Seit dem Jahr 2000 war er Mitarbeiter des Fachbereichs „Nationale-Internationale Zusammenarbeit/Neue Technologien" bis er im März 2006 in den Fachbereich „Bildungsmanagement/Personalentwicklung" im Kriminalistischen Institut des Bundeskriminalamtes wechselte.

BKA – KI 31
65173 Wiesbaden
klaus.pruefer@bka.bund.de

Prunău, Dan-Cristian

Forensic Science Institute – General Inspectorate of Romanian Police

Studies
1999–2004 Police Academy "Al. I. Cuza" – Bucharest;
1995–1996 The College for Police Agents "Vasile Lascar" – Campina.

Workplace
2000 – present
Forensic Science Institute – General Inspectorate of Romanian Police;
1996–2000 Forensic Science Service – General Directorate of Bucharest Police.

Pung, Markus

Student der Medizintechnik am RheinAhr-Campus Remagen

Derzeit studiert Herr Pung im Fachbereich Mathematik und Technik am RheinAhrCampus Remagen.

Er wurde am 17. 11. 1977 in Neuwied geboren. Nach dem Abschluss der Realschule im Jahre 1995 durchlief er eine Ausbildung zum Energieelektroniker Fachrichtung Betriebstechnik bei der Veitsch-Radex Urmitz GmbH. Anschließend erwarb er seine Fachhochschulreife an der Berufsbildenden Schule Technik in Koblenz. Zum Sommersemester 2001 nahm er sein Studium der Medizintechnik RheinAhrCampus Remagen auf. Er befasst sich als Mitarbeiter der Arbeitsgruppe von Prof. Dr. Buzug zur Zeit mit seiner Diplomarbeit.

Markus Pung was born in Neuwied, Germany, in 1977. He is a student at the department of Mathematics and Technology, RheinAhrCampus Remagen. After the secondary school in the year 1995, he made an apprenticeship as an electronic installer at the Veitsch-Radex Urmitz Ltd. Following he get the advanced technical college entrance qualification at a technical school in Coblenz. In the summer term 2001 he has started his studies of medical engineering at RheinAhrCampus Remagen. At the moment he writes his diploma thesis in the research group of Prof. T. M. Buzug.

Ruifrok, A. C. C.

Forensic Scientist, Department of Digital Technology, Netherlands Forensics Institute, The Hague, The Netherlands

Primary education: University of Groningen, Ph. D., 1987, Philosophy, Radiobiology. University of Groningen. M. S., 1982, Molecular Genetics, Radiobiology, Animal Physiology. University of Groningen, B. S., 1979, Biology

Job experience:

2002–present	Forensic Scientist, Department of Digital Technology, Netherlands Forensics Institute, The Hague, The Netherlands
1999–2002	Assistant Professor, Departments of Pathology, The University of Texas, M. D. Anderson Cancer Center, Houston, Texas
1994–1999	Assistant Professor, Departments of Biomathematics and Experimental Radiotherapy, The University of Texas, M. D. Anderson Cancer Center, Houston, Texas

Seitz, Hermann, Dr.

Leiter der Forschungsgruppe Rapid Prototyping bei der Stiftung caesar

Hermann Seitz studierte Elektro- und Informationstechnik an der Technischen Universität München und erhielt 1997 sein Diplom. Von 1997 bis 2001 forschte er an der Fakultät für Maschinenbau der Technischen Universität München. Er arbeitete an piezoelektrischen Tropfenerzeugern und deren vielfältigen Anwendungsmöglichkeiten. Ein weiteres Forschungsgebiet war die Entwicklung neuer tropfenbasierter Rapid Prototyping Systeme (3D-Druckverfahren). Er erwarb 2002 den Doktorgrad für seine Arbeit über die Modellierung und Simulation von Tropfenerzeugern mit piezoelektrischen Aktoren (Institut für Feingerätebau und Mikrotechnik, Prof. J. Heinzl, TU München). Seit 2001 leitet er zusammen mit Carsten Tille die Forschungsgruppe Rapid Prototyping bei der Stiftung caesar. Schwerpunkte der laufenden Forschung sind innovative Rapid Prototyping Technologien und

Materialien für medizinische Anwendungen mit dem besonderen Fokus auf den Bereich der 3D-Druckverfahren.

Hermann Seitz studied electrical engineering and information technology at the Technical University of Munich and received his diploma in 1997. From 1997 to 2001 he was a research associate at the Faculty of Mechanical Engineering, TU Munich. He worked on piezoelectric ink-jet printheads and their use for various applications. A further research area was on the development of new ink-jet based Rapid Prototyping systems (3D printing technologies). He earned his doctorate for his work on the modeling and simulation of a printhead with piezoelectric actuators (Institute for Precision Engineering and Micromechanics, Prof. J. Heinzl, TU Munich) in 2002. Since 2001 he is leading the research group Rapid Prototyping together with Carsten Tille. His major focus of his current research is on innovative Rapid Prototyping techniques and materials for medical applications with emphasis on the 3D printing technology.

Dr. Hermann Seitz
Universität Rostock
Fakultät für Maschinenbau und Schiffstechnik
Lehrstuhl Fluidtechnik/Mikrofluidtechnik
18051 Rostock

Sigl, Karl-Michael, Diplomverwaltungswirt und Kriminalhauptkommissar

Kriminalvollzugsbeamter im Bundeskriminalamt

Er ist seit 1983 Kriminalvollzugsbeamter im Bundeskriminalamt.

Karl-Michael Sigl begann seine Laufbahn 1978 als Polizeivollzugsbeamter bei der Bayerischen Bereitschaftspolizei in Würzburg. 1980 wechselte er zum Bundeskriminalamt, studierte an der Fachhochschule des Bundes in Köln und schloss 1983 das Studium als Diplomverwaltungswirt ab.

In der Zeit von 1983–2000 verrichtete er seinen Dienst in operativen Bereichen des Bundeskriminalamtes, wechselte dann zum Kriminalistischen Institut. Dort ist er im Fachbereich „Neue Technologien“ Sachgebietsleiter „Bewertung/Analyse“.

BKA – KI 21–1
65173 Wiesbaden
karl.sigl@bka.bund.de

Subke, Jörg, Prof. Dr.

Professor für Biomechanik und medizinische Messtechnik, FH Gießen

Im Jahr 2002 erhielt Herr Dr. Subke den Ruf an die Fachhochschule Gießen-Friedberg als Professor für Biomechanik und medizinische Messtechnik in den Studiengängen Medizintechnik/Biomechanik, Orthopädie- und Rehatechnik.

1989 erwarb er sein Physik-Diplom an der Universität Tübingen, promovierte 1995 an der Biomechanischen Abteilung der Theoretischen Astrophysik ebenfalls an der Universität Tübingen.

Von 1995 bis 1998 arbeitete er dort als Wissenschaftlicher Mitarbeiter in verschiedenen Forschungsprojekten in den Bereichen Rechtsmedizin und Sportmedizin mit, bevor er 1999 Wissenschaftlicher Assistent in der Rechtsmedizin wurde.

1989 Physik-Diplom, Universität Tübingen

1995 Promotion, Biomechanische Abteilung der Theoretischen Astrophysik, Universität Tübingen

1995–1998 Wissenschaftlicher Mitarbeiter in verschiedenen Forschungsprojekten in den Bereichen Rechtsmedizin und Sportmedizin der Universität Tübingen

1999–2002 Wissenschaftlicher Assistent in der Rechtsmedizin, Universität Tübingen

2002 Ruf an die Fachhochschule Gießen-Friedberg, Professur für Biomechanik und medizinische Messtechnik in den Studiengängen Medizintechnik/Biomechanik und Orthopädie- und Rehatechnik.

1989 Diploma of Physics, University of Tuebingen, Germany.

1995 PhD; Biomechanics division of the department of Theoretical Astrophysics, University of Tuebingen, Germany.

1995–1998 Scientific work in different research projects at the institute of legal medicine and the division of sports medicine of the medical clinic, University of Tuebingen, Germany.

1999–2002 Scientific assistant at the institute of legal medicine, University of Tuebingen, Germany.

2002 Offering of a professorship in biomechanics and medical measurement engineering at the University of Applied Sciences Giessen-Friedberg; study courses medical engineering / biomechanics and orthopaedic / rehabilitation technology.

Thelen, Andrea

Physikerin, Stiftung caesar, Ludwig-Erhard-Allee 2, 53175 Bonn

Andrea Thelen studied physics at the University of Bonn. She received her diploma in 2003 working on holographic topometry. In October 2003 she joined the project group holography at caesar where she is developing reconstruction algorithms for holographic surface measurement.

Vandermeulen, Dirk

Associate professor at the department ESAT/PSI (Center for Processing Speech and Images) of the K. U. Leuven

Dirk Vandermeulen received a M.Sc. in Engineering (Computer Science) from the K. U. Leuven (1983) and obtained his Ph. D. in Computer Science from the same university in 1991. He is currently associate professor at the department ESAT/PSI (Center for Processing Speech and Images) of the K. U. Leuven and member of the Medical Image Computing (ESAT/PSI + Radiology) research group at the same university. His research focuses on biomedical image analysis and biometric systems with a particular emphasis on image registration and object modeling.

Vignal, Jean Noel, Dr.

Ph. D., Head of the Department of Anthropology-Thanatology-Odontology Criminal research institut of the french gendarmerie

Position: Head of the Department of Anthropology-Thanatology-Odontology Criminal research institut of the french gendarmerie

Qualifications:

– 2003	University of Paris/France PhD – Paleopathology
– 1998	University of Bordeaux 1/France PhD – Physical Anthropology
– 1995	University of Paris/France MS – Paleopathology
– 1994	University of Lyon 1/France MS – Anthropology

Wang, Li Jun

Chief of Jinzhou Police Department, with Postgraduate degree and EMBA of Northeast University of Finance and Economics

Male, Meng Gu Minority, born on December 26^{th}, 1959. He is acting as Deputy Mayor of Jinzhou People's Municipal government cum Chief of Jinzhou Police Department, with Postgraduate degree and EMBA of Northeast University of Finance and Economics. He is also Executive Chairman to the 11^{th} scientific meeting of IACI (International Association of Craniofacial Identification) and Deputy Chairman of IACI. On the other hand, he is elected as a representative to the 14^{th} and 16^{th} National Party's Congress of the National Communist Party of China (CPC) respectively, a member of All-China Youth Federation and Deputy Chairman to Liaoning Provincial Youth Federation. He is the director of China On-scene Psychology Research Center and Social Psychology Research Center of the Northeast University of Finance and Economics, MBA College.

Weidenbusch, André

Doktorand, Institut für Rechtsmedizin der Universität des Saarlandes

Seit Oktober 2003 ist André Weidenbusch im Rahmen seiner Dissertation Mitglied der Arbeitsgruppe für Morphologie/Gesichtsweichteilrekonstruktion des Institutes für Rechtsmedizin der Universität des Saarlandes und beschäftigt sich mit Fragestellungen zur Gesichtsweichteildicke bei lebenden und verstorbenen Personen.

Nach seinem Studium an den Universitäten Homburg/Saar und Rennes/Frankreich steht er kurz vor dem Abschluss als Humanmediziner.

After his studies at the University of Rennes/France and Homburg-Saar/Germany, he is close to finish his studies as a doctor of human medicine. Since 2003 he is part of the workgroup morphology/facial reconstruction at the University of Saarland/ Homburg.

Wittwer-Backofen, Ursula, Prof. Dr.

Professorin für Biologische Anthropologie an der Medizinischen Fakultät der Universität Freiburg

Ursula Wittwer-Backofen ist seit 2002 Professorin für Biologische Anthropologie an der Medizinischen Fakultät der Universität Freiburg. Sie war vorher als Research Scientist am Max-Planck-Institut für demografische Forschung in Rostock beschäftigt, nachdem sie Mitarbeiterstellen an den Anthropologischen Instituten der Universitäten Mainz und Gießen hatte. 1998 hat sie sich für die Fächerkombination Anthropologie/Humanbiologie in Gießen habilitiert. Sie studierte Biologie, Chemie und Ur- und Frühgeschichte an den Universitäten FU Berlin, Mainz und Heidelberg. Ihre wissenschaftlichen Schwerpunkte sind Prähistorische Anthropologie, Biomarker am Skelett, Biodemographie und Forensische Anthropologie. Zahlreiche Veröffentlichungen auf dem Gebiet der Biologischen Anthropologie und Demographie.

Positions
From may 2002 University of Freiburg/Germany

Professor
Head of the Department of Anthropology, Institute for Human Genetics and Anthropology, University of Freiburg.
July 2000 – Dec.2002Max-Planck-Institute for Demographic Research, Rostock/ Germany

Research Scientist
Head of the Tooth Laboratory.
1990–1998 University of Giessen/Germany

Research Scientist/Associate Professor
Lecturer in Anthropology.
Research, in Anthropology
1982–1988 University of Mainz/Germany

Zollikofer, Christoph, P. E.

Professor of Anthropology, Anthropological Institute of the University of Zurich

Christoph P. E. Zollikofer studied biology at the University of Zurich, Switzerland, where he received a PhD in neurobiology. After studying music ('cello), he returned to science for a postdoc in computer science and anthropology. He is currently Professor of Anthropology at the Anthropological Institute of the University of Zurich. His main research field is computer-assisted anthropology, encompassing the investigation of patterns of morphological variability and evolutionary diversification in fossil and extant primates, computational modeling of morphogenetic processes, and development of image-based analytical tools for anthropology.